University of Maribor

UNIVERSITY OF THE WEST *of* SCOTLAND
UWS

10^{TH} International Conference on Sustainable Energy and Environmental Protection:

Energy Efficiency

(June 27^{TH} - 30^{TH}, 2017, Bled, Slovenia)

(Conference Proceedings)

Editors:
Emeritus Prof. dr. Jurij Krope
Prof. dr. Abdul Ghani Olabi
Prof. dr. Darko Goričanec
Prof. dr. Stanislav Božičnik

University of Maribor Press

University of Maribor Press

University of Maribor Press

10TH International Conference on Sustainable Energy and Environmental Protection

Energy Efficiency

(June 27TH – 30TH, 2017, Bled, Slovenia)

(Conference Proceedings)

Editors:
Emeritus Prof. dr. Jurij Krope
Prof. dr. Abdul Ghani Olabi
Prof. dr. Darko Goričanec
Prof. dr. Stanislav Božičnik

June 2017

Title: 10TH International Conference on Sustainable Energy and Environmental Protection (June 27TH – 30TH, 2017, Bled, Slovenia) (Conference Proceedings)

Subtitle: Energy Efficiency

Editors: Emeritus Prof. Jurij Krope, Ph.D. (University of Maribor, Slovenia),
Prof. Abdul Ghani Olabi, Ph.D. (University of the West of Scotland, UK),
Asso. Prof. Darko Goričanec, Ph.D. (University of Maribor, Slovenia),
Asso. Prof. Stanislav Božičnik (University of Maribor, Slovenia).

Review: Prof. Željko Knez, Ph.D. (University of Maribor, Slovenia),
Prof. Niko Samec, Ph.D. (University of Maribor, Slovenia).

Tehnical editors : Jan Perša (University of Maribor Press),
Armin Turanović (University of Maribor Press).

Design and layout: University of Maribor Press

Conference: 10TH International Conference on Sustainable Energy and Environmental Protection

D.G.Simeonov (Bulgaria), Prof. Abdelakder Outzourhit (Morocco), Prof. Bilge Albayrak Çeper (Turkey), Prof. Bekir Zühtü Uysal (Turkey), Prof. D. Bradley (UK), Dr. Silvia Tedesco (UK), Dr. Valentin Ivanov (Germany), Dr. Vincent Lawlor (Austria), Prof. Yonghua Cheng (Belgium), Prof. Yasufumi Yoshimoto (Japan), Prof. Yahya Erkan Akansu (Turkey), Prof. Yunus Ali Çengel (Turkey), Prof. Zeljko Knez (Slovenia), Prof. Zoltan Magyar (Hungary), Dr. William Smith (Ireland), Dr. Abed Alaswad (UK).

First published in 2017 by
University of Maribor Press
Slomškov trg 15, 2000 Maribor, Slovenia
tel. +386 2 250 42 42, fax +386 2 252 32 45
http://press.um.si, zalozba@um.si

Co-published by
University of Maribor, Faculty of Chemistry and Chemical Engineering
Smetanova ulica 17,2000 Maribor, Slovenia
tel. +386 (0)2 22 94 400, faks + 386 (0)2 25 27 774
http://www.fkkt.um.si, fkkt@um.si

Published: 5. July 2017

CIP - Kataložni zapis o publikaciji
Univerzitetna knjižnica Maribor

620.92/.98:502.131.1(082)(0.034.2)

INTERNATIONAL Conference on Sustainable Energy and Environmental Protection (10 ; 2017 ; Bled)
Energy efficiency [Elektronski vir] : (Conference proceedings) / 10th International Conference on Sustainable Energy and Environmental Protection, (June 27th-30th, 2017, Bled, Slovenia) ; [organised by] University of Maribor [and] University of the West of Scotland ; editors Jurij Krope ... [et al.]. - El. zbornik. - Maribor : University of Maribor Press, 2017

Način dostopa (URL): http://press.um.si/index.php/ump/catalog/book/241

ISBN 978-961-286-050-9 (pdf)

doi: 10.18690/978-961-286-050-9
1. Gl. stv. nasl. 2. Krope, Jurij 3. Univerza (Maribor)
COBISS.SI-ID 92426753

ISBN 978-961-286-050-9

DOI: https://doi.org/10.18690/978-961-286-050-9

Price: Free copy

For publisher: Prof. Igor Tičar, Ph.D., rector (University of Maribor)

University of Maribor Press

Preface

The 10th International Conference on Sustainable Energy and environmental Protection – SEEP 2017 was organised on June 27th – 30th 2017 in Bled, Slovenia, by:

- Faculty of Chemistry and Chemical Engineering, University of Maribor, Slovenia,
- University of the West of Scotland, School of Engineering and

The aim of SEEP2017 is to bring together the researches within the field of sustainable energy and environmental protection from all over the world.

The contributed papers are grouped in 18 sessions in order to provide access to readers out of 300 contributions prepared by authors from 52 countries.

We thank the distinguished plenary and keynote speakers and chairs who have kindly consented to participate at this conference. We are also grateful to all the authors for their papers and to all committee members.

We believe that scientific results and professional debates shall not only be an incentive for development, but also for making new friendships and possible future scientific development projects.

General chair
Emeritus Prof. dr. Jurij Krope

Plenary Talk on The Relation between Renewable Energy and Circular Economy

ABDUL GHANI OLABI - BIBLIOGRAPHY

Prof Olabi is director and founding member of the Institute of Engineering and Energy Technologies (www.uws.ac.uk\ieet) at the University of the West of Scotland. He received his M.Eng and Ph.D. from Dublin City University, since 1984 he worked at SSRC, HIAST, CNR, CRF, DCU and UWS. Prof Olabi has supervised postgraduate research students (10 M.Eng and 30PhD) to successful completion. Prof Olabi has edited 12 proceedings, and has published more than 135 papers in peer-reviewed international journals and about 135 papers in international conferences, in addition to 30 book chapters. In the last 12 months Prof Olabi has patented 2 innovative projects. Prof Olabi is the founder of the International Conference on Sustainable Energy and Environmental Protection SEEP, www.seepconference.co.uk

He is the Subject Editor of the Elsevier Energy Journal https://www.journals.elsevier.com/energy/editorial-board/abdul-ghani-olabi, also Subject editor of the Reference Module in Materials Science and Materials Engineering http://scitechconnect.elsevier.com/reference-module-material-science/ and board member of a few other journals. Prof Olabi has coordinated different National, EU and International Projects. He has produced different reports to the Irish Gov. regarding: Hydrogen and Fuel Cells and Solar Energy.

CORRESPONDENCE ADDRESS: Abdul Ghani Olabi, Ph.D., Professor, University of the West of Scotland, School of Engineering and Computing, D163a, McLachlan Building, Paisley, United Kingdom, e-mail: Abdul.Olabi@uws.ac.uk.

https://doi.org/10.18690/978-961-286-050-9 ISBN 978-961-286-050-9

Available at: http://press.um.si.

10TH INTERNATIONAL CONFERENCE ON SUSTAINABLE ENERGY AND ENVIRONMENTAL PROTECTION (JUNE 27TH – 30TH, 2017, BLED, SLOVENIA), ENERGY EFFICIENCY
J. Krope, A.Ghani Olabi, D. Goričanec & S. Božičnik

Plenary Talk on Energy Footprints Reduction and Virtual Footprints Interactions

JIŘÍ JAROMÍR KLEMEŠ & PETAR SABEV VARBANOV

Increasing efforts and resources have been devoted to research during environmental studies, including the assessment of various harmful impacts from industrial, civic, business, transportation and other economy activities. Environmental impacts are usually quantified through Life Cycle Assessment (LCA). In recent years, footprints have emerged as efficient and useful indicators to use within LCA. The footprint assessment techniques has provided a set of tools enabling the evaluation of Greenhouse Gas (GHG) – including CO_2, emissions and the corresponding effective flows on the world scale. From all such indicators, the energy footprint represents the area of forest that would be required to absorb the GHG emissions resulting from the energy consumption required for a certain activity, excluding the proportion absorbed by the oceans, and the area occupied by hydroelectric dams and reservoirs for hydropower.

An overview of the virtual GHG flow trends in the international trade, associating the GHG and water footprints with the consumption of goods and services is performed. Several important indications have been obtained: (a) There are significant GHG gaps between producer's and consumer's emissions – US and EU have high absolute net imports GHG budget. (b) China is an exporting country and increasingly carries a load of GHG emission and virtual water export associated with consumption in the relevant importing countries. (c) International trade can reduce global environmental pressure by redirecting import to products produced with lower intensity of GHG emissions and lower water footprints, or producing them domestically.

To develop self-sufficient regions based on more efficient processes by combining neighbouring countries can be a promising development. A future direction should be focused on two main areas: (1) To provide the self-sufficient regions based on more efficient processes by combining production of surrounding countries. (2) To develop the shared mechanism and market share of virtual carbon between trading partners regionally and internationally.

CORRESPONDENCE ADDRESS: Jiří Jaromír Klemeš, DSc, Professor, Brno University of Technology - VUT Brno, Faculty of Mechanical Engineering, NETME Centre, Sustainable Process Integration Laboratory – SPIL, Technická 2896/2, 616 69 Brno, Czech Republic, e-mail: klemes@fme.vutbr.cz. Petar Sabev Varbanov, Ph.D., Associate Professor, Brno University of Technology - VUT Brno, Faculty of Mechanical Engineering, NETME Centre, Sustainable Process Integration Laboratory – SPIL, Technická 2896/2, 616 69 Brno, Czech Republic, e-mail: varbanov@fme.vutbr.cz.

https://doi.org/10.18690/978-961-286-050-9 ISBN 978-961-286-050-9

Available at: http://press.um.si.

JIŘÍ JAROMÍR KLEMEŠ - BIBLIOGRAPHY

Head of "Sustainable Process Integration Laboratory – SPIL", NETME Centre, Faculty of Mechanical Engineering, Brno University of Technology - VUT Brno, Czech Republic and Emeritus Professor at "Centre for Process Systems Engineering and Sustainability", Pázmány Péter Catholic University, Budapest, Hungary.

Previously the Project Director, Senior Project Officer and Hon Reader at Department of Process Integration at UMIST, The University of Manchester and University of Edinburgh, UK. Founder and a long term Head of the Centre for Process Integration and Intensification – CPI2, University of Pannonia, Veszprém, Hungary. Awarded by the EC with Marie Curies Chair of Excellence (EXC). Track record of managing and coordinating 91 major EC, NATO and UK Know-How projects. Research funding attracted over 21 M€.

Co-Editor-in-Chief of Journal of Cleaner Production (IF=4.959). The founder and President for 20 y of PRES (Process Integration for Energy Saving and Pollution Reduction) conferences. Chairperson of CAPE Working Party of EFCE, a member of WP on Process Intensification and of the EFCE Sustainability platform.

He authored nearly 400 papers, h-index 40. A number of books published by McGraw-Hill; Woodhead; Elsevier; Ashgate Publishing Cambridge; Springer; WILEY-VCH; Taylor & Francis).

Several times Distinguished Visiting Professor for Universiti Teknologi Malaysia, Xi'an Jiaotong University; South China University of Technology, Guangzhou; Tianjin University in China; University of Maribor, Slovenia; University Technology Petronas, Malaysia; Brno University of Technology and the Russian Mendeleev University of Chemical Technology, Moscow. Doctor Honoris Causa of Kharkiv National University "Kharkiv Polytechnic Institute" in Ukraine, the University of Maribor in Slovenia, University POLITEHNICA Bucharest, Romania. "Honorary Doctor of Engineering Universiti Teknologi Malaysia", "Honorary Membership of Czech Society of Chemical Engineering", "European Federation of Chemical Engineering (EFCE) Life-Time Achievements Award" and "Pro Universitaire Pannonica" Gold Medal.

CORRESPONDENCE ADDRESS: Jiří Jaromír Klemeš, DSc, Professor, Brno University of Technology - VUT Brno, Faculty of Mechanical Engineering, NETME Centre, Sustainable Process Integration Laboratory – SPIL, Technická 2896/2, 616 69 Brno, Czech Republic, e-mail: klemes@fme.vutbr.cz.

https://doi.org/10.18690/978-961-286-050-9 ISBN 978-961-286-050-9

Available at: http://press.um.si.

10TH INTERNATIONAL CONFERENCE ON SUSTAINABLE ENERGY AND ENVIRONMENTAL PROTECTION (JUNE 27TH – 30TH, 2017, BLED, SLOVENIA), ENERGY EFFICIENCY
J. Krope, A.Ghani Olabi, D. Goričanec & S. Božičnik

Plenary Talk on
Renewable energy sources for environmental protection

HAKAN SERHAD SOYHAN

Development in energy sector, technological advancements, production and consumption amounts in the countries and environmental awareness give shape to industry of energy. When the dependency is taken into account in terms of natural resources and energy, there are many risks for countries having no fossil energy sources. Renewable and clean sources of energy and optimal use of these resources minimize environmental impacts, produce minimum secondary wastes and are sustainable based on current and future economic and social societal needs. Sun is one of the main energy sources in recent years. Light and heat of sun are used in many ways to renewable energy. Other commonly used are biomass and wind energy. To be able to use these sources efficiently national energy and natural resources policies should be evaluated together with the global developments and they should be compatible with technological improvements. Strategic plans with regard to energy are needed more intensively and they must be in the qualification of a road map, taking into account the developments related to natural resources and energy, its specific needs and defining the sources owned by countries. In this presentation, the role of supply security was evaluated in term of energy policies. In this talk, new technologies in renewable energy production will be shown and the importance of supply security in strategic energy plan will be explained.

CORRESPONDENCE ADDRESS: Hakan Serhad Soyhan, Ph.D., Professor, Sakarya University, Engineering Faculty, Esentepe Campus, M7 Building, 54187 - Esentepe /Sakarya, Turkey, e-mail: hsoyhan@sakarya.edu.tr.

https://doi.org/10.18690/978-961-286-050-9 ISBN 978-961-286-050-9

Available at: http://press.um.si.

HAKAN SERHAD SOYHAN- BIBLIOGRAPHY

Professor at Sakarya University, Engineering Faculty. 50 % fot teaching and the rest for reasearch activities.

Teaching, courses taught:

Graduate courses:

- Combustion technology;
- Modelling techniques;

Undergraduate courses:

- Combustion techniques;
- Internal combustion engines;
- Fire safety.

Tehnical skills and competences professional societies:

- 25 jurnal papers in SCI Index. 23 conference papers;
- Editor at FCE journal. Co-editor at J of Sakarya University;
- Head of Local Energy Research Society (YETA);
- Member od American Society of Mechanical engineers (ASME);
- Member of Turkish Society of Mechanical Engineers (TSME).

CORRESPONDENCE ADDRESS: Hakan Serhad Soyhan, Ph.D., Professor, Sakarya University, Engineering Faculty, Esentepe Campus, M7 Building, 54187 - Esentepe /Sakarya, Turkey, e-mail: hsoyhan@sakarya.edu.tr.

https://doi.org/10.18690/978-961-286-050-9 ISBN 978-961-286-050-9

Available at: http://press.um.si.

Table of Contents

CONFERENCE PROCEEDINGS

Energy Simulation and Analysis of an Intermittent Ventilation System Under Two Climates 1
Alan Kabanshi, Arman Ameen, Bin Yang, Hans Wigö & Mats Sandberg

Refurbishment of Multi-Family Buildings with the Application of Timber-Glass Upgrade Modules: Influence of the Building Volume Ratio on Energy Efficiency 11
Vesna Žegarac Leskovar, Maja Žigart, Miroslav Premrov & Maja Lešnik

Influence of Building Shape on Energy Performance of Timber-Glass Buildings Located in Warm Climatic Regions 25
Maja Žigart, Miroslav Premrov & Vesna Žegarac Leskovar

Phase-Changing Materials for Thermal Stabilization of Buildings 37
Marjan Krasna & Samo Kralj

Electrocaloric Effect in Nematic Liquid Crystal Phase 45
Eva Klemenčič, Maja Trček, Zdravko Kutnjak & Samo Kralj

Comparative Study on the Thermal Performance and Environmental Footprint of Traditional and Contemporary Masonry Systems Used in Southern Europe 57
Andreas Kyriakidis, Aimilios Michael, Rogiros Illampas, Dimos C. Charmpis & Ioannis Ioannou

Ldm Compact – a Highly Efficient Method for Developing Gas Engines for Use with Low Environmental Impact Non-Natural Gas 69
Gerhard Pirker, Eduard Schneßl, Igor Šauperl & Andreas Wimmer

A Review on Analysis on Cooling Technologies of Concentrated Solar Power System 79
Manxuan Xiao, Llewellyn Tang, Xingxing Zhang, Isaac Yu Fat Lun & Guozhen Li

On the Incidence of Occupant's Behavior in the Evaluation of Energy Efficiency in Buildings 91
Lamberto Tronchin & Massimiliano Manfren

Controlled Mechanical Ventilation: Comparison of Energy Use and Primary Applied to 20 Different Devices in a Testing Room 105
Kristian Fabbri, Chiara Bertolli & Lamberto Tronchin

Investigation of Performance and Emissions in a SI Engine Fuelled by Gasoline - Acetylene Mixtures 117
Mehmet İlhan İlhak, Selahaddin Orhan Akansu, Nafiz Kahraman & Sebahattin Ünalan

Investigation of Performance and Emissions of an SI Engine Powered with Oxygenated Fuel Blends 129
H.Enes Fil, Paolo Sementa, S.Orhan Akansu, Michela Costa & Nafiz Kahraman

Numerical and Experimental Investigations on Improving the Efficiency of Clean-in-Place Procedures in Closed Processing Systems: A Review 141
Guozhen Li, Llewellyn Tang, Xingxing Zhang, Jing Hao, Manxuan Xiao & Jie Dong

Comparative Evaluation Model for Smart Envelope Systems 153
Marko Jaušovec & Metka Sitar

Practical Approach for Energy Consumption Optimisation in Educational and Research Buildings - Case Study Cluster Computers and Data Room 165
Boris Sucic, Sandi Cimerman, Marko Peckaj & Fouad Al-Mansour

Energy Efficiency of Camelina and Crambe Biomass Production Under Different Cultivation Conditions 175
Mariusz Jerzy Stolarski & Michał Krzyżaniak

Climate Change and Thermal Comfort in Educational Buildings of Southern Europe: the Case of Cyprus 183
Chryso. Heracleous & Aimilios. Michael

An experimental study on heat transfer of CO_2 at supercritical conditions 195
Gregor Kravanja, Gašper Zajc, Željko Knez, Mojca Škerget & Maša Hrnčič Knez

Critical Review of Micro-Nano Scale Surface Modification for Phase Change Heat Transfer 207
Shoukat Alim Khan, Adnan Ali, Muataz A. Hussien & Muammer Koc

Stochastic Model for Prediction of Photovoltaic Production Uncertainty Based on Measured Data 219
Marinko Barukčić, Miralem Hadžiselimović & Sebastijan Seme

Shaping the Envelope of Buildings by Looking at Both Architectural Layout and Technical Performance in Order to Maximize the Energy Efficiency of the Whole Ensemble 235
Eugen Mandric, Mugurel-Florin Tălpigă & Florin Iordache

Performance Evaluation of a Mobile Air Conditioning Unit: An Exergetic Approach 247
Huseyin Gunhan Ozcan, Huseyin Gunerhan & Arif Hepbasli

Cycle of Power and Steam Generation in Sugar-Energy Industries 261
Maykon Cesar Spolti Ferreira, Joao Marcos Roncarci Mari, Marcus Vinicius Roncari Mari, W. A. S. Conceição & Cid Marcos Goncalves Andrade

Informatics Solution for Energy Efficiency Improvement and Consumption Management 271
Simona Vasilica Oprea, Adela Bâra & Adriana Reveiu

Changes on Building Energy Consumption Using Future High Spatial Resolution Climate Data 279
Roberto San José, Juan L. Pérez, Libia Pérez & Rosa Maria Gonzalez Barras

Development of an Energy Simulation-Occupant Behavior Coupling Model to Reduce Building Energy Consumption 289
Taehoon Hong, Chan-joong Kim, Jimin Kim, Myeonghwi Lee & Jaemin Jeong

Exergetic Analysis of Cogeneration Processes: Study of Case 299
Marcus Vinicius Roncari Mari, João Marcos Roncari Mari, Maykon Cesar Spolti Ferreira, Etiene Nataniel Pedro Dundão, Danilo Toledo Ribeiro da Silva, Anderson Rodrigo Visconcini, Eugênia Leandro Almeida, Fernando Castro Vieira Filho & Cid Marcos Gonçalves Andrade

Investigation of Design Parameters of Microalgae Panel Bio-Reactors for Building Façade Applications 307
Emin Selahattin Umdu, İlker Kahraman, Nurdan Yildirim & Levent Bilir

Empirical Analysis of Energy Efficiency in South Africa 315
Janet Bruce-Brand & Marcel Kohler

Investigation of Flow Characteristics of Synthetic Jet Driven by Duty Cycle Signal 327
Yahya Erkan Akansu, Mustafa Sarıoğlu, Mehmet Seyhan & Hürrem Akbıyık

Prediction of the Influence of the Liquid Temperature Effect on Two-Phase Flow Through a Granular Medium **337**
Adel Oueslati, Adel Mecriche

Theoretical and Experimental Study of Air Humidification by Sea Water in an Air Lift Pump Packed Column Humidifier **351**
Adel Oueslati & Ahmed Hannachi

Nanomaterial-Based Biocatalysts **363**
Katja Vasić, Mateja Primožič, Željko Knez & Maja Leitgeb

Energy – Water Interactions, Industrial Context **371**
Petar Sabev Varbanov, Jiří Jaromír Klemeš, Zhi-Yong Liu & Zdravko Kravanja

Improving the Visual Comfort and Energy Performance Of Office Buildings **379**
Daniel Uribe, Waldo Bustamante, Sergio Vera & María José Yáñez

Operation of Distributed Energy Supply Systems **389**
Dušan Kragelj, Tomaž Kramberger, Bojan Rupnik, Danijela Urbancl & Darko Goričanec

Innovative Solution for Energy Efficient Urban Freight Deliveries **399**
Tomislav Letnik, Matej Mencinger & Stane Božičnik

Energy Recovery Optimization of an Ammonia-Water Power Cooling Cycle Using Exergy-Pinch Method **409**
Jouan Rashidi, Changkyoo Yoo, Pouya Ifaei & Jeong Tai Kim

Ship Power Plant Environmental Impact and Costs Rationalization **421**
Žiga Schäffer, Stojan Petelin & Ivan Bajsić

Double Stage High Temperature Heat-Pump for District Heating **439**
Igor Ivanovski, Darko Goričanec, Tina Žagar & Saša Pozeb

Linear Oscillatory Synchronous Generator Designed for a Stirling Engine **449**
Miralem Hadžiselimović, Gregor Srpčič, Iztok Brinovar, Zdravko Praunseis, Sebastijan Seme & Bojan Štumberger

Energy Optimisation of Parallel Operating Processes for the Production of Formaldehyde **463**
József Mursics, Tina Žagar & Darko Goričanec

Study of CNF Coating for Pool-Boiling and Condensation **471**
Shoukat Alim Khan, Adnan Ali, Muataz A. Hussien & Muammer Koc

The Effects of Zirconium on the Microstructure and Mechanical Properties of FeCrAl Alloys For 4r Generation Nuclear Power Plants **477**
Victor Geantă, Ionelia Voiculescu, Adrian Dan Jianu & Horia Binchiciu

10TH INTERNATIONAL CONFERENCE ON SUSTAINABLE ENERGY AND ENVIRONMENTAL PROTECTION (JUNE 27TH – 30TH, 2017, BLED, SLOVENIA), ENERGY EFFICIENCY
J. Krope, A.Ghani Olabi, D. Goričanec & S. Božičnik

Energy Simulation and Analysis of an Intermittent Ventilation System Under Two Climates

ALAN KABANSHI, ARMAN AMEEN, BIN YANG, HANS WIGÖ & MATS SANDBERG

Abstract Energy use on heating, ventilation and air conditioning (HVAC) accounts for about 50% of total energy use in buildings. Energy efficient HVAC systems that do not compromise the indoor environmental quality and at the same time meet the energy reduction directives/policies are necessary and needed. The study herein, evaluates the energy saving potential of a newly proposed ventilation system in spaces with high occupancy density, called Intermittent Air Jet Strategy (IAJS). The aim of the study was to evaluate through simulations the potential energy savings due to IAJS as compared to a mixing ventilation (MV) system in a classroom located in a 'hot and humid' climate (Singapore), and in a 'hot and dry' climate (Kuwait). The analysis is based on IDA Indoor Climate Energy simulation software. The results herein demonstrate significant reduction of cooling energy use of up 54.5% for Singapore and up to 32.2% for Kuwait with IAJS as compared to MV. Additionally, supply fan energy savings can also be realized if well implemented.

Keywords: • Intermittent air jets • Energy simulation • Energy saving • Setpoint extension • Convective cooling •

CORRESPONDENCE ADDRESS: Alan Kabanshi, Ph.D student, University of Gävle, Department of Building, Energy and Environmental Engineering, SE-801 76 Gävle, Sweden, e-mail: alan.kabanshi@hig.se. Arman Ameen, Ph.D student, University of Gävle, Department of Building, Energy and Environmental Engineering, SE-801 76 Gävle, Sweden, e-mail: arman.ameen@hig.se. Bin Yang, Ph.D., Assistant Professor, Umeå University, Department of Applied Physics and Electronics, SE-901 87 Umeå, Sweden, e-mail: bin.yang@umu.se. Hans Wigö, Ph.D. Assistant Professor, University of Gävle, Department of Building, Energy and Environmental Engineering, SE-801 76 Gävle, Sweden, e-mail: hans.wigo@hig.se. Mats Sandberg, Ph.D., Professor, University of Gävle, Department of Building, Energy and Environmental Engineering, SE-801 76 Gävle, Sweden, e-mail: mats.sandberg@hig.se.

https://doi.org/10.18690/978-961-286-050-9.1 ISBN 978-961-286-050-9

Available at: http://press.um.si.

1 Introduction

Energy concerns are a daily ubiquitous topic due to challenges of our current energy economy and its impact on climate change. The rising energy demand necessitates aggressive reforms on energy use, conservation and efficiency, especially so because of validated assertions of a causal relationship between energy demand and greenhouse gas (GHG) emissions [1, 2]. One sector with a rising energy demand is the built environment, which currently uses more than 40% of primary energy and accounts for 30 – 40% of GHG emissions [3], of which heating, ventilation and air conditioning (HVAC) takes about 50 % of the total building energy use. Common consensus in literature shows that changes on HVAC *modus operandi* can yield substantial energy savings more so on cooling requirements. Studies [4, 5] have shown that strategies that offer possibilities to extend air temperature setpoints have a high energy saving potential on building energy use.

Intermittent air jet strategy (IAJS), which is a high-momentum air distribution system, was recently proposed for use in high occupant spaces. The strategy optimises intermittent air speeds to increase convective cooling and penetration of the supply airflow into the sitting zone [6, 7]. Figure 1 illustrates the implementation possibilities either as a primary system (Fi. 1A) or as a secondary system (Fi. 1B; for spaces with existing HVAC systems or in climates where cooling is occasionally needed).

Kabanshi et al., [6] introduced and evaluated the concept of IAJS with objective measurements. Using the air jet diffuser made out of a 160 mm diameter ventilation duct fitted having a single row of specially designed circular nozzles (d_0 = 10 mm, equidistant spacing of $1.4d_0$) and placed overhead at 1.2 m and 2.3 m from the breathing height and the floor, respectively. The diffuser installation covered the sitting column of the occupied zone. He explained the operational construct and proposed 0.4 m/s and 0.8 m/s as minimum and maximum operational velocities.

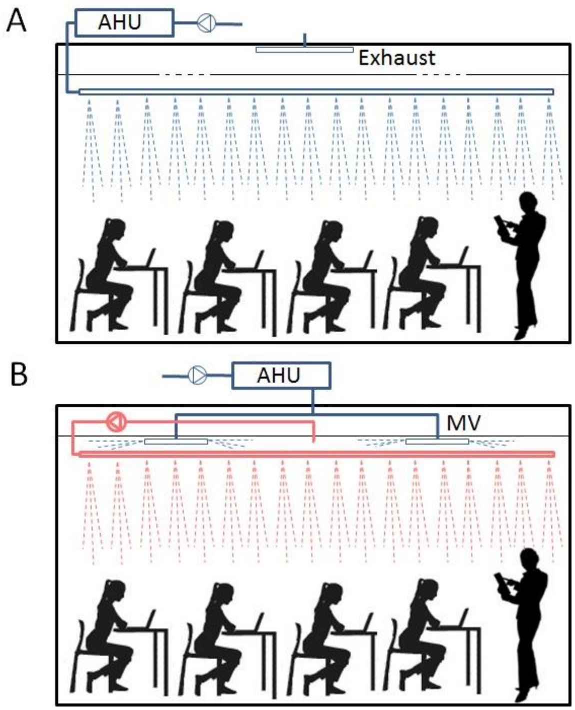

Figure 1: (A) IAJS as a primary system. (B) IAJS as a secondary system

A human response study to IAJS [7], showed that the system can offset the upper operative setpoints by 2.3 – 4.5 ºC by introducing intermittent air speeds between 0.4 and 0.8 m/s in the occupied zone. This translates to indoor operative temperature limits of 23.7 ºC to 29.1 ºC. This is critical for comfort and system energy use as the HVACs deadband or the indoor operational setpoints can be increased [4].

The predicted temperature range, gives insight on applicable climatic conditions suitable for implementation of IAJS as a primary ventilation system or as a secondary system. We can deduce that IAJS as a primary system would be most effective in indoor climate were temperatures are around/above 23.7 ºC throughout the year. As a secondary system or as a room induction unit, the strategy can work in almost all climates and it is easy to implement in buildings with existing HVAC or other air distribution systems and will only recirculate and increase room air speeds to offset increased room air temperatures.

The current study explores, by means of simulation with IDA Indoor Climate and Energy (ICE) software, the energy saving potential associated with IAJS if implemented as a primary air distribution system in "hot and humid" and in "hot and dry" climates.

2 Methods

2.1 Room and HVAC description

A single zone classroom with a lighting load of 13 W/m^2 and occupancy capacity of 30 students was simulated. The room has a floor area of 10 m x 6.4 m, and a ceiling height of 3 m. External wall is made of 280 mm medium-weight concrete (0.66 W/m·K) and the wall has 20 mm cement plaster (1.4 W/m·K) on both sides, resulting in an overall U-value of 1.8 W/(m^2·K). The room has four double pane windows (width = 1.2 m, height = 1.3 m), made of a 12 mm air gap with 4 mm glasses on both sides, and each has an overall U-value of 2.54 W/(m^2·K). The windows are on the wall facing south and have a solar heat gain coefficient of 0.37 and a light transmittance of 0.44. They are integrated with shading blinds between the panes, which activates when the incident light hitting the windows is higher than 100 W/m^2. All walls except the outer wall were considered adiabatic.

The ventilation system was set to run during weekdays between 6:00 AM and 7:00 PM. For simplicity, all cases were assumed fully occupied during this time. There was no ventilation at night and during weekends, but the model was integrated with an infiltration leakage equivalent to 0.012 m^2, amounting to a wind driven air change rate of about 0.52 ACH when the pressure difference across the between envelop was 4 Pa.

Supply air conditions were met with the air-handling unit (AHU) and the room had an internal cooling unit to keep the room temperature within the specified air temperature limits. In the simulation, we used an ideal cooling unit with a coefficient of performance (COP) of 3 and unlimited cooling capacity. No heating was done on either the supply air or room air. Thus, supply temperature was the same as outdoor temperature in conditions when the outdoor air temperature dropped below the supply temperature setpoint. Additionally, only sensible cooling was done on the supply air temperature.

2.2 Simulated climates and cases

Two climates characterised by hot and humid (Singapore), and hot and dry (Kuwait) were simulated. ASHRAE weather files were used as input data and simulations were done for 2016. Comfort conditions used for Singapore were based on values used by Schiavon et al., [8], room temperature setpoints of 22.5 °C to 24 °C under MV. For Kuwait, the maximum indoor temperature used was 25.6 °C based on neutral temperature estimated with ASHRAE *Standard* 55 [9] at clothing level of 0.51, 1.2 met and relative humidity of 30%.

Table 1 shows the simulated cases, MVref is mixing ventilation with 10 l/(s.pr) airflow-rate (Q), 16 °C supply temperature (T_s), 24 °C and 25.6 °C maximum allowed room air temperature (T_{max}) for Singapore and Kuwait, respectively. The airflow rate was based on ISO 7730 [10] for a Category I building.

Cases with IAJS are represented as shown in Table 1. For example, IAJS-0.4-16 means IAJS with room air speeds of 0.4 m/s and supply temperature at 16 ºC. Intermittency was generated by scheduling the supply fan to run with a cycle of 6 min (3 min on and 3 min off) for the occupancy period. Two airflow rates are simulated based on proposed operational velocity limits: 0.4 – 0.8 m/s. Kabanshi et al.,[6] found that the generated velocity at breathing height within the jet was proportional to the air flowrate. Fan settings of 10 l/(s.pr) resulted in air speed of 0.4 m/s, thus to generate 0.8 m/s the airflow rate extrapolates to 20 l/s. The maximum allowable indoor air temperatures under IAJS were expanded based on estimates from the overall thermal sensation (OTS) model proposed for IAJS shown below:

$$OTS = 0.31ta - 1.72V - 7.15 \tag{1}$$

Where, *V* is the air speed measured at 1.1 m from the floor and *ta* is the room air temperature. Details of the model are discussed here [7]. At 0.4 m/s, 23.7 ºC was the minimal temperature and at 0.8 m/s, 29.1ºC was the maximum temperature in compliance with acceptable thermal sensation range (-0.5 to +0.5) as stipulated in ASHRAE *Standard* 55 [9]. Thus, 23.7 – 29.1 ºC is taken as the operable indoor temperature range for IAJS. 24 ºC is used as the T_{max} in all cases with 0.4 m/s and with 0.8 m/s the temperature range is 23.7 – 29.1 ºC, simulated with different supply air temperatures.

Table 1. Simulated cases

Singapore			
Case	T_s [ºC]	T_{max} [ºC]	Q [l/s.pr]
MVref	16	24	10
IAJS-0.4-16	16	24	10
IAJS-0.8-16	16	29.1	20
IAJS-0.8-18	18	29.1	20
IAJS-0.8-20	20	29.1	20
IAJS-0.8-22	22	29.1	20
IAJS-0.8-24	24	29.1	20
Kuwait			
Case	T_s [ºC]	T_{uo} [ºC]	Q [l/s.pr]
MVref	16	25.6	10
IAJS-0.4-16	16	24	10
IAJS-0.8-16	16	29.1	20
IAJS-0.8-18	18	29.1	20
IAJS-0.8-20	20	29.1	20
IAJS-0.8-22	22	29.1	20
IAJS-0.8-24	24	29.1	20

* Velocity in m/s at breathing height.

3 Results and Discussion

The energy needed to meet the specified ventilation conditions is defined, as cited by Schiavon et al., [8] from CEN/TR 15615-2007 as, the sum of energy needed to cool the supply air (AHU Cooling) and to cool the room air (Room Cooling) in order to obtain and maintain the specified conditions for a given occupancy period. This section presents the energy simulation results and analysis of the considered cases.

3.1 Hot and humid climate (Singapore)

Figure 2 shows the annual energy use per square meter for the simulated cases based on 2016 climatic conditions for Singapore. As shown, the simulated annual energy use for the reference case was 731.7 kWh/m^2. Comparing cases with IAJS shows a reduction in the total energy use by 13.5 – 54.5%. While in most cases the AHU cooling energy use reduced, the room cooling energy use increased. Case IAJS-0.8-16, IAJS-0.8-18 and IAJS-0.8-20 show minimal requirements on room cooling as there was a reduction of

100%, 16.8% and 33.8% on room cooling compared to the supply case, respectively. This offers an option to reduce installation costs or sizing on room cooling units.

Case IAJS-0.8-24 gave the highest total energy savings of about 52.4%, resulting in an increase of 16.2% in room cooling and 65.7% reduction on AHU cooling energy need. However, *PMV* (Predicted Mean Vote) and *PPD* (Predicted Percentage of Dissatisfied) were slightly above +0.5 and 10% respectively (See Table 2). All other cases had met the requirements of -0.5 < *PMV* < +0.5 and *PPD* < 10%. Case IAJS-0.8-22 had a reduction on both room cooling (88.4%) and AHU cooling (33.8%) resulting in a total energy saving of 41.4%.

Interestingly, IAJS with 0.4 m/s (IAJS-0.4-16) and same settings as MVref, had a total energy reduction of 29%, although room cooling requirements increased twice as much but AHU cooling reduced almost by half (49.8%). However, CO_2 concentration were higher (1485.6 ppm) compared to MVref (1070.7 ppm). Kabanshi et al.,[6] found that IAJS running at 10 l/s was equivalent to a system running continuously with airflow of 8 l/(s.pr). Simulation of a continuous system with 8 l/s (not reported here) showed a drop in CO_2 concentration to 1102.8 ppm. All other cases with IAJS (0.8 m/s) had CO_2 concentration similar to the reference case.

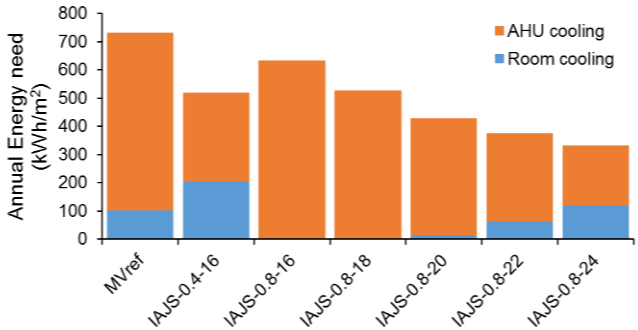

Figure 2: Annual cooling energy need

3.2 Hot and dry climate (Kuwait)

Figure 3 shows the annual energy use per square meter for Kuwait based on 2016 climatic conditions. The total annual energy need for a MVref was 319.3 kWh/m^2. Introducing IAJS with a lower room setpoint (IAJS-0.4-16) increased room cooling needs (200%) but reduced AHU cooling needs (49.8%) resulting in an overall reduction on total energy need of 21.6%. IAJS with air speed of 0.8 m/s gave a reduction in energy need from 8.4 to 32.3%. As shown, above supply temperature of 20 ºC, any increase in the supply temperature had little influence on the total energy saving but an influence on the room cooling requirements.

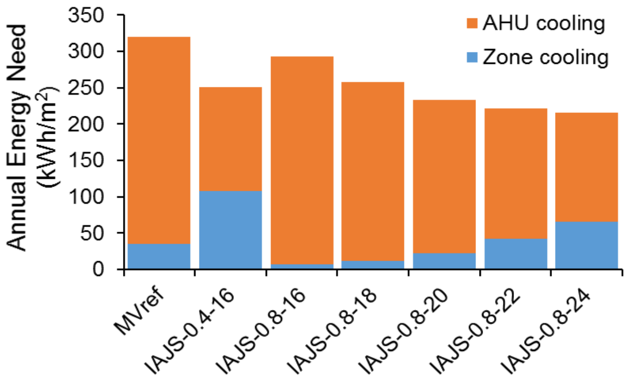

Figure 3: Annual cooling energy need

Comfort analysis showed that *PMV* ranged between -0.33 and +0.35, and *PPD* ranged between 4.22 and 8.74. In January, the average indoor operative temperature was 22.8 ^{o}C, lower than the limit of 23.1 ^{o}C proposed for IAJS. Relative humidity was between 24.6 and 43.7%. CO_2 concentration were similar to the results for Singapore.

3.3 Fan energy use

Figure 4 shows the fan annual energy need for each supply airflow rate. MVref had an annual energy need of about 27.2 kWh/m^2. IAJS with 10 l/s (corresponding to 0.4 m/s) gave a 68.1% reduction in fan energy use while IAJS with 20 l/s (corresponding to 0.8 m/s) had a 35.2%. These results marry with the hypothesis by Kabanshi et al.,[6] that IAJS as a primary system would offer energy saving on the supply fan close to 50%. However, realistically the instantaneous power demand on the supply fan is expected to increase due to an increase in system pressure and delivery of elevated air speeds in the room, thus energy savings due to intermittency operation would not be as high as the ones obtained in this study. The fan energy savings obtained in this simulation should be interpreted with caution, as it is unclear whether the simulation software accounts for the increase in room air speeds on the supply fan energy use.

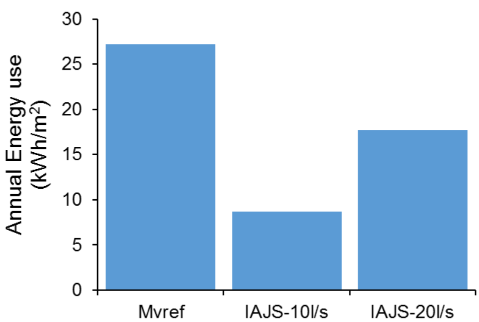

Figure 2: Fan energy use

3.4 General discussion

Under Hot and humid climate, increasing the supply temperature with IAJS has a larger effect on the energy need for AHU cooling as it reduces both sensible and latent heat in the humid air. Thus if we compare Fig. 2 and 3, we see that the reduction on the total energy need increases with increase in supply temperature for Singapore than for Kuwait (dry air) were the supply temperature has a little influence on the total energy use but has an effect on the room cooling requirements.

Schiavon et al., [8] and Yang et al., [11] reported that under personalized ventilation supply temperature has minimal influence on total energy use in hot and humid climates, this is opposite to the results obtained under IAJS herein. One explanation could be because IAJS has a wider operational room temperature range as compared to that used by Schiavon and Yang.

The wider room temperature range can also be an advantage to encourage personal adjustment. Whereas, the system air speeds can be varied automatically based on the relationship between air speed and room temperature defined by Equation 1 for a neutral thermal sensation. Occupants would have freedom to adjust their comfort outside the neutral condition settings. This will reduce on complaints of over cooled indoor spaces, which is usually the case in places like Hong Kong and Singapore [12].

4 Conclusion

The results here in give an insight on the energy saving potential of IAJS if implemented as a primary system in high occupant spaces. Based on the simulated cases and setup, the results shows that widening of the room temperature setpoints under IAJS increases the energy savings possibilities in hot and humid climate of Singapore by 13% to 54.5%, and in hot and dry climate of Kuwait by 8.4% to 32.2%. The system also offers energy saving on the supply fan amounting to 68.1% (based on the simulation results) as compared to a MV system. Overall, the study shows the potential energy benefits of implementing IAJS.

Notes

Table 2. Annual average conditions in the room

	T_o [°C]	RH [%]	PMV	PPD [%]	CO_2 [ppm]
MVref	24.76 (0.02)*	61.2 (0.4)	0.11 (0.003)	2.9 (0.1)	1066.5 (3.44)
IAJS-0.4-16	24.76 (0.02)	59.8 (0.2)	-0.06 (0.002)	2.5 (0.1)	1485.6 (8.98)
IAJS-0.8-16	27.90 (0.02)	57.2 (0.3)	0.13 (0.002)	3.3 (0.1)	1063.6 (7.57)
IAJS-0.8-18	28.74 (0.02)	57.9 (0.4)	0.26 (0.002)	5.6 (0.1)	1058.3 (5.04)
IAJS-0.8-20	29.29 (0.02)	55.3 (0.7)	0.39 (0.010)	9.2 (0.3)	1079.2 (4.64)
IAJS-0.8-22	29.45 (0.02)	56.1 (0.8)	0.45 (0.010)	11.6 (0.4)	1073.9 (4.13)
IAJS-0.8-24	29.63 (0.02)	53.9 (0.9)	0.53 (0.010)	16.8 (0.4)	1086.24 (4.88)

*mean monthly standard deviation

References

[1] L. Schipper, M. Ting, M. Khrushch, and W. Golove, "The evolution of carbon dioxide emissions from energy use in industrialized countries: an end-use analysis," *Energy Policy*, vol. 25, no. 7–9, pp. 651–672, 1997.

[2] P. Linares and X. Labandeira, "Energy efficiency: economics and policy," *J. Econ. Surv.*, vol. 24, no. 3, pp. 573–592, 2010.

[3] A. Mardiana and S. B. Riffat, "Building energy consumption and carbon dioxide emissions: threat to climate change," *J. Earth Sci. Clim. Change*, no. S3, p. 1, 2015.

[4] T. Hoyt, E. Arens, and H. Zhang, "Extending air temperature setpoints: Simulated energy savings and design considerations for new and retrofit buildings," *Build. Environ.*, vol. 88, pp. 89–96, 2015.

[5] S. Schiavon and A. K. Melikov, "Energy saving and improved comfort by increased air movement," *Energy Build.*, vol. 40, no. 10, pp. 1954–1960, 2008.

[6] A. Kabanshi, H. Wigö, and M. Sandberg, "Experimental evaluation of an intermittent air supply system - Part 1: Thermal comfort and ventilation efficiency measurements," *Build. Environ.*, vol. 95, pp. 240–250, 2016.

[7] A. Kabanshi, H. Wigö, R. Ljung, and P. Sörqvist, "Experimental evaluation of an intermittent air supply system – Part 2: Occupant perception of thermal climate," *Build. Environ.*, vol. 108, pp. 99–109, 2016.

[8] S. Schiavon, A. K. Melikov, and C. Sekhar, "Energy analysis of the personalized ventilation system in hot and humid climates," *Energy Build.*, vol. 42, no. 5, pp. 699–707, 2010.

[9] ASHRAE 55, *Thermal environmental conditions for human occupancy*. Atlanta. GA: American Society of Heating, Refrigeration and Air-Conditioning Engineers, 2013.

[10] ISO 7730, *Moderate thermal environment -Determination of the PMV and PPD indices and specification of the conditions for thermal comfort*. Geneve: International Organization for Standardization., 2005.

[11] B. Yang, C. Sekhar, and A. K. Melikov, "Ceiling mounted personalized ventilation system in hot and humid climate—An energy analysis," *Energy Build*., vol. 42, no. 12, pp. 2304–2308, 2010.

[12] S. C. Sekhar, "Thermal comfort in air-conditioned buildings in hot and humid climates – why are we not getting it right?" *Indoor Air*., vol. 26, no. 1, pp. 138–152, 2016.

10TH International Conference on Sustainable Energy and Environmental Protection (June 27TH – 30TH, 2017, Bled, Slovenia), Energy Efficiency
J. Krope, A.Ghani Olabi, D. Goričanec & S. Božičnik

Refurbishment of Multi-Family Buildings with the Application of Timber-Glass Upgrade Modules: Influence of the Building Volume Ratio on Energy Efficiency

Vesna Žegarac Leskovar, Maja Žigart, Miroslav Premrov & Maja Lešnik

Abstract Refurbishment of old existing buildings means an enormous potential for improving their energy efficiency. Besides the established renovation methods encompassing mostly measures applied to the thermal envelope the extension of existing buildings with lightweight structural upgrades has become popular especially in densely populated urban areas. While being beneficial to the reduction of transmission losses through the roof of the existing building, the above solution also results in acquisition of new floor surface.

The paper discusses the impact the timber-glass upgrade module has on energy-efficient refurbishment of existing multi-family buildings. The main variable parameter of the numerical study is the volume ratio modified through the variation in the number of storeys in the existing building and the module. The key of the study is to explore to which extent the application of the upgrade module influences the energy need of the entire building regarding their volumetric relation.

Keywords: • Energy efficiency • Building renovation • Attic extension • Building volume ratio • Timber-glass upgrade module •

Correspondence Address: Vesna Žegarac Leskovar, Ph.D., Associate Professor, University of Maribor, Faculty of Civil Eng., Transportation Eng. and Architecture, Smetanova ulica 17, 2000 Maribor, Slovenia, email: vesna.zegarac@um.si. Maja Žigart, Assistant, University of Maribor, Faculty of Civil Eng., Transportation Eng. and Architecture, Smetanova ulica 17, 2000 Maribor, Slovenia, email: maja.zigart1@um.si. Miroslav Premrov, Ph.D., Professor, University of Maribor, Faculty of Civil Eng., Transportation Eng. and Architecture, Smetanova ulica 17, 2000 Maribor, Slovenia, email: miroslav.premrov@um.si. Maja Lešnik, Assistant, University of Maribor, Faculty of Civil Eng., Transportation Eng. and Architecture, Smetanova ulica 17, 2000 Maribor, Slovenia, email: maja.lesnik6@um.si.

https://doi.org/10.18690/978-961-286-050-9.2 ISBN 978-961-286-050-9

Available at: http://press.um.si.

1 Introduction

Buildings in Europe date from different periods with specific building strategies and regulations typical of the time. A substantial proportion of the existing European housing stock is more than 50 years old. Almost 40% of residential housing stock was built prior to 1960 with a share of 50% dating from the period before 1970 [1- 3], when building regulations mandating thermal properties of building envelopes were rather loose and inadequate. The listed data referring to the age of buildings is in accordance with the situation in the field of energy use within which buildings in Europe account for approximately 40% of the final energy consumption, with the largest share being spent on heating, and are responsible for greenhouse gas emissions in an almost equal proportion [3]. Several studies [4, 5], address energy saving potential to be made with energy-efficient refurbishment. A strong argument supporting the need for complex building refurbishment is also seen in a relatively low percentage of the new build representing only 1% of the total housing stock in the period from 2005 to 2010 [6]. In practice, refurbishment is often based on partial renovations, targeting improvement of the building thermal envelope including doors and windows along with modernization of the buildings technical systems. Moreover, many research studies [7-9] examine the influence of various renovation measures to reduce the building energy demand. Studies looking for systematic procedures to be applied to energy-efficient refurbishments of buildings [10-14] are less frequent. However, they exhibit the importance of complexity in the process of energy efficient renovation. In addition to the reduction of energy demand, there is also a high requirement for new usable surfaces in urban centres, especially in large central, northern and western European cities [6]. Therefore, a further level of energy performance renovation can be seen in building extensions, as one of the possible manners to increase urban density. In this context attic extensions offer a great potential by creating additional housing space while taking advantage of the existing infrastructure [15]. In addition, to ever more emerging attic extensions in common practice the attempts to explore such solutions are also recorded within design competitions [16] and research studies [12-15, 17]. According to the research in [16], ¼ of existing buildings in urban centres are strong enough to carry additional floors made of timber structure, which represents a large potential for building refurbishment with timber upgrade modules. However, there is a lack of design guidelines for energy efficient upgrades [16], which is mostly due to the fact that they have to be adjusted to individual buildings and tend to require high planning efforts [15, 17]. Attempts to integrate timber energy efficient upgrades in the existing building refurbishment have already been made in a few studies [12-15, 17]. The research [14] conducted on two case studies in Velenje indicates positive impact of different upgrade modules on the total energy consumption of the refurbished building. The optimal lightweight timber-glass modules from the viewpoint of energy efficiency have been previously developed [18] in regard to possible geometries of existing buildings. With regard to the limited load-bearing capacity of existing buildings the selection of timber as a construction material for upgrades is especially suitable in comparison with other building materials due to its low weight, cost and energy efficiency.

The above mentioned research works present an appropriate basis for further investigation. Within the aim to develop general guidelines for energy retrofitting of buildings with the use of lightweight structural upgrades this paper discusses the effectiveness of such renovation measure according to the relation between the volume sizes of the existing building and the upgrade module. The novelty of this study goes to the analysis of the extent to which the application of the upgrade module influences the need for heating and cooling of the entire building regarding their volumetric relation.

The content of the current paper is divided into 5 sections with the research background and the objectives in Section 1. A brief interpretation of energy efficient renovation measures is presented in Section 2. Section 3 considers the numerical study analysis with the interpretation of the results in Section 4. Section 5 reveals the conclusions applicable to buildings located in the Cfb climate zone [19] having a similar ground floor geometry and orientation.

2 Energy Efficiency of Buildings and Renovation Measures

Energy-efficient building design requires a careful balance of the energy consumption, energy gain and energy storage [20]. The purpose of energy efficient renovation is to reduce energy losses, the transmission heat losses (Q_t) and ventilation heat losses (Q_v), and to increase useful energy gains, the solar heat gains (Q_s) and in some cases also the internal heat gains (Q_i), with the aim to reducing the energy consumption for heating and cooling and reach a high quality of indoor climate. The latter can be achieved through the implementation of various renovation measures (Figure 1), such as:

a) improvement of the building envelope thermal performance (non-transparent),
b) replacement of old windows/doors with new energy-efficient ones,
c) improvement of airtightness,
d) enlargement of the south-oriented glazing,
e) installation of the heat recovery ventilation system,
f) attic extension with the energy-efficient structural upgrade module.

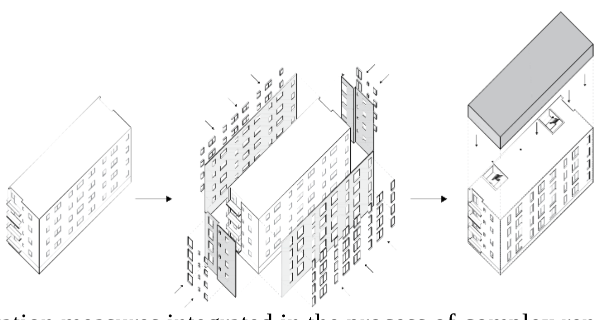

Figure 1. Renovation measures integrated in the process of complex renovation

Our study focuses on the efficiency analysis of the last measure (f). However, the highest energy savings can be achieved through a complex renovation, where the combination of above stated measures (a-f) is selected carefully, in accordance with the existing building specifics.

3 Parametric Numerical Study

3.1 The aim of the study and its basic limitations

The study is divided in two parts with the first part based on the case study of a residential building which underwent the process of renovation including different renovation measures (a-c, e). The second and also the main part of the study discusses the effectiveness of the renovation measure of attic extension (f). Since existing buildings have limited load-bearing capacity they can be mostly upgraded with lightweight structures of one or two storeys. However, the number of existing building storeys varies from case to case, therefore the aim of the study is to explore to which extent the application of the upgrade module influences the energy demand of the entire upgraded building with regard to the existing building height and to their volumetric relation. The results are based on the selected case study, whereas a comparison with the study [14] indicates a possibility of wider use.

Besides the limitation in the number of storeys of the upgrade module, some additional limitations are the following:

- within the renovation process only the energy efficiency is analysed,
- the load-bearing capacity of the existing building is assumed to be appropriate for attic extension,
- the upgrade module is constructed in the timber-frame panel system,
- the longer façade of the existing building and the upgrade module has the north-south orientation,
- the climate under consideration is the Cfb climate zone according to the Köppen-Geiger climate map [19],
- the efficiency of the heating system is not considered.

3.2 Software

The numerical study is computed with the Passive House Planning Package (PHPP) [21] which is a certified software designed for planning low-energy and passive houses. It is based on the EN ISO 13790 standard [22] as well as on other European standards.

3.3 Description of the case study building

The selected existing multi-family building (hereinafter EB) was built in 1954. Two main entrances lead to the ground floor and the next three floors enclosed with the thermal envelope. In addition, there is an unheated basement underneath. With four apartments per story there are 16 apartments in total.

Figure 2. The existing case-study building prior to renovation

The south and the north-oriented façades are $a = 35.42\ m$ long, the width of the building being $b = 11.10\ m$ and the maximum height of the building $h = 18.10\ m$. The total net floor area of the building is 1164.30 m^2. The building is constructed in the massive structural system with masonry walls and precast concrete ribbed slabs. The selected case study building no longer corresponds to the current energy-efficiency requirements. Apart from its insufficiently insulated thermal envelope, inefficient old windows without shading devices, the airtightness of the building is weak and accounts for $n_{50} = 7.0\ h^{-1}$. The building is naturally ventilated. As the first step towards the complex energy renovation the individual measures (a-c, e) are carried out on EB. Apart from improving the envelope thermal transmittance, the ventilation mode of the renovated existing building (hereinafter REB) is switched to a heat recovery system with the efficiency of $\eta = 85\%$. The airtightness is improved as well, to $n_{50} = 2.0\ h^{-1}$. The main thermal properties of the envelope elements of EB and REB are given in Table 1.

Table 1. Thermal transmittance of EB and REB envelope elements

Envelope element	U (W/m²K)	
	EB	REB
Windows: frame Windows: glass	2.50 2.20	0.78 0.50
External wall	1.45	0.164
Roof	1.83	0.154
Basement ceiling	1.59	0.163

3.4 Description of the timber-glass upgrade module

Different types of timber-glass upgrade modules were designed with the aim to verifying their influence on the energy efficiency of the refurbished existing building. They are all constructed in the timber-frame panel system, but vary in the number of stories (M_1, M_2), *U*-value of the thermal envelope (U_1, U_2) and glazing-to-wall area ratio ($AGAW_{opt}$, $AGAW_{ave}$). Floor plan dimensions of modules were adjusted to EB dimensions in order to cover the entire roof area of the existing building. The height of the single-storey module (M_1) is $hM_1 = 3.0\ m$ with that of the two-storey module (M_2) being $hM_2 = 5.91\ m$. The net floor areas of M_1 and M_2 are $AM_1 = 318.22\ m^2$ and $AM_2 = 636.44\ m^2$ respectively. As the upgrade module is applied onto the roof of the renovated existing building, it is designed without a floor slab. It is assumed that there is no heat transfer between the REB and the module. The optimal glazing-to-wall area ratio $AGAW_{opt,south} = 50{,}41\%$ was selected according to [18] whereby the meaning of "optimal" refers to the indication of the lowest energy demand for heating and cooling. In such modules the triple insulating glazing is designed only in the south façade, which does not always contribute to the living comfort. Taking into account also other design factors, such as the need for a good visible connection with the environment, day lighting quality, etc., the modules with an average glazing distribution in all main cardinal façades are additionally treated in this study. The average glazing-to-wall area ratios $AGAW_{ave,\ south} = 40\%$, $AGAW_{ave,north} = 25\%$ and $AGAW_{ave,\ east,\ west} = 10\%$ were selected. External shading devices (blinds) with the shading factor of $z = 50\%$ for summer shading are provided for solar control. With the air change rate $n_{50} = 0.6\ h^{-1}$ the airtightness of the upgrade modules is very good. The heat recovery ventilation system with the efficiency of $\eta = 85\%$ is used. Thermal characteristics of the treated upgrade modules are given in Table 2.

Table 2. Thermal transmittance of the upgrade module envelope elements U_1 and U_2

Envelope element	U_1 (W/m^2K)	U_2 (W/m^2K)
Windows: frame Windows: glass, g = 50%	0.78 0.50	0.78 0.50
External wall	0.10	0.165
Roof	0.10	0.159

Variations of modules are shown in Table 3.

Table 3. Eight different module types with regard to their main variable parameters

	M_1 single-storey		M_2 two-storey	
	AGAW opt	AGAW ave	AGAW opt	AGAW ave
U_1	$M_{1\,opt}\,U_1$	$M_{1\,ave}\,U_1$	$M_{2\,opt}\,U_1$	$M_{2\,ave}\,U_1$
U_2	$M_{1\,opt}\,U_2$	$M_{1\,ave}\,U_2$	$M_{2\,opt}\,U_2$	$M_{2\,ave}\,U_2$

3.5 Methodology

As the result of the refurbishment process (a-c, e) conducted on the case study building prior to application of the extension measure (f) a prominent reduction in energy need is evident for REB in Table 4.

Table 4. Energy need for heating (Q_h) and cooling (Q_c) of EB and REB

	EB	REB
Q_h (kWh/m^2a)	213.5	23.1
Q_c (kWh/m^2a)	1.0	0.4
$Q_h + Q_c$ (kWh/m^2a)	214.5	23.5

It can be seen that the energy need for cooling is almost negligible in EB and REB, while the reduction of energy need for heating is evidently stronger, since it accounts for *190 kWh/m²a* or *89%.*

As the next step, the parametric numerical analysis was performed in order to explore to which extent the application of the upgrade module influences the energy need of the entire building regarding their volumetric relation. For the purposes of the research the following parameters are varied:

- the volume of REB expressed with the number of storeys (from 2 to 20),
- every variation of REB is upgraded with each of the 8 module types composing the new hybrid building (REB+M).

- The results under observation are the following:
- energy need for heating and cooling (Q_h + Q_c) for different heights of REB,
- energy need for heating and cooling (Q_h + Q_c) for different volumes of REB extended with different module types (variations of REB + M),
- energy savings (%) for different volumes of REB extended with different module types (variations of REB + M),
- comparison in energy savings with [14].

3.6 Climate data

The climate data for Maribor are taken into consideration. The city belongs to the Cfb climate zone according to the Köppen–Geiger climate map [19]. The average annual temperature in Maribor is 10.7 ˚C with the lowest average temperature of -0.8 ˚C in January and highest of 20.8 ˚C in July. The average length of the heating period is 187 days. The average annual horizontal solar radiation in Maribor is 1225 kWh/m^2 with the average heating period radiation of 350 kWh/m^2 [23].

4 Results

The first interest is to explore the influence of the increasing number of storeys of REB itself on the energy need. As the next step, the additional influence of attic extension with different modules is presented in Figure 3.

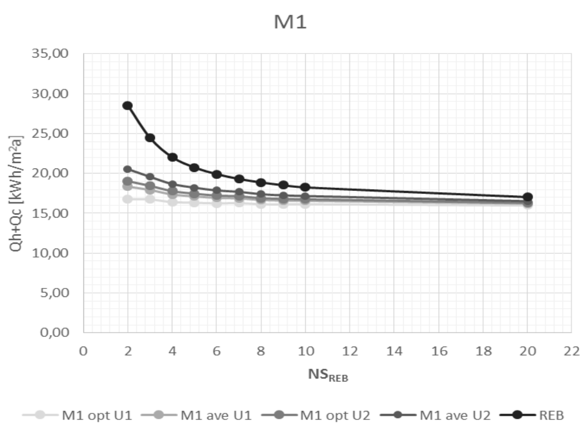

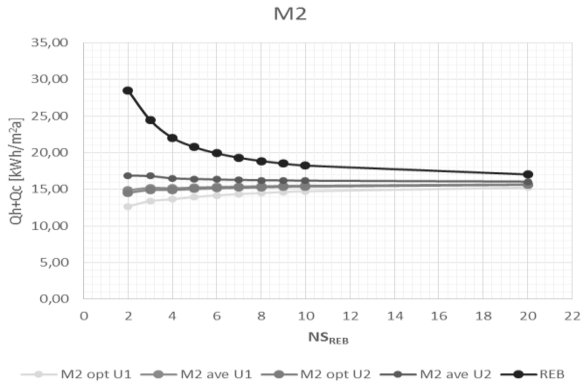

Figure 3. Energy need for heating and cooling (Q_h+Q_c) for different volumes of REB and HB upgraded with different types of modules, (M_1–above) and (M_2–below)

As seen in Figure 3, the sum of the energy need for heating and cooling ($Q_h + Q_c$) of REB, if considered per m^2 of the floor area, increases exponentially with the cutting of the number of floors. Furthermore, the analysis of the impact the upgrade module (M_1) has on the energy need of the hybrid building (REB+M_1), shows an evident reduction in the energy need for all types of upgrades if compared to the renovated building without attic extension. However, the impact of the attic extension is increasing with the decreasing number of REB storeys. Also the differences in impact of individual module types are higher if they are installed on lower REB. With ten-storey buildings and higher ones the differences in energy need between REB and REB+M become lower than *1.08 kWh/m²a*, which is almost negligible. The same applies to the impact of different M_1 module types, therefore the selection of optimal renovation variations is sensible only for the heights of the REB up to 10 storeys in the case of upgrading with single-storey modules.

The highest reduction of $Q_h + Q_c$ is seen with the module type (M_1 opt U_1) and accounts for *11.78 kWh/m²a* in the case of the extension of a two-storey REB. If the same building is extended with an average module having the same thermal properties, with windows installed in all main cardinal façades (M_1 ave U_1) the energy reduction is somewhat smaller and accounts for *10.19 kWh/m²a*. This weaker impact arises mainly as a consequence of north-oriented windows which are not exposed to direct solar radiation in the heating period but only to transmission losses. Also M_1 modules with $U_2 = 0.165$ W/m^2K have a weaker impact on account of slightly higher transmission losses through the thermal envelope.

A similar situation is evident in the case of refurbishment with two-storey modules. However, the impact is stronger owing to a larger upgrade unit in comparison to renovation with M_1. The highest reduction in energy need compared to REB only is seen in the case of extending the two-storey renovated building with (M_2 opt U_1) having a better thermal envelope and the optimal glazing size, which accounts for 15.88 kWh/m^{2}a. Similarly to refurbishment with single-storey modules, the difference in the energy need between REB and REB+M decreases with the increasing REB volume. With the 10-storey REB, the impact of modular extension with M_2 is at least two times stronger in comparison to REB+M_1, exhibiting the difference of *2.06* up to *3.52 kWh/m^{2}a*. However, modular extension of such buildings shows relatively small differences between individual types of modules which are smaller than *1.46 kWh/m^{2}a*. In this manner the selection of module variations proves to be influential only for buildings under 10 storeys.

Figure 4 shows the energy savings in the case of extension with different module types for certain analysed volume ratios. The volume ratio is expressed through the relation between the number of module's stories (NS_M) and the number of renovated building storeys (NS_{REB}).

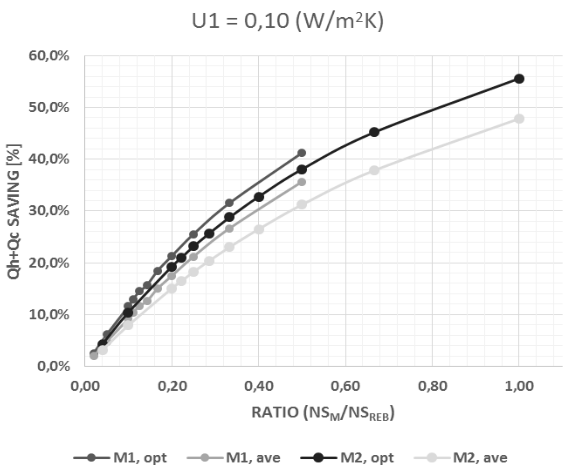

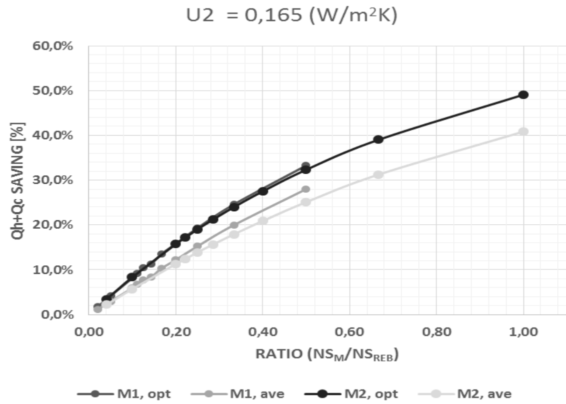

Figure 4. Energy savings (%) for REB extension with different variations of upgrade modules (U_1-above) and (U_2-below) for different volume ratios

The results show greater energy savings in the case of renovation with modules of better thermal properties (U_1). The savings increase with the increasing volume ratio, which is in fact expected. The highest energy savings are shown in the case of renovation of a two-storey REB with (M_2 opt U_1) and account up to 56% in regard to a two-storey REB without extension. It is interesting to see that the highest energy savings for volume ratios ($NS_M/NS_{REB}) = \leq 0.50$ are shown in the case of renovation with the optimal single-storey module (M_1 opt U_1), followed by the optimal two-storey module (M_2 opt U_1), the average single-storey module (M_1 ave U_1) and as the least effective, the average two-storey module (M_2 ave U_1). However, it is necessary to make a deeper interpretation of these results. If observing energy savings at a specific ratio, for example the ratio (NS_M/NS_{REB}) $= 0.33$, we can see that in the case of renovating with M_1 this means the extension of a three-storey REB and for the renovation with M_2 the extension was performed on a six-storey building. Figure 3 evidently shows that the energy need ($Qh + Qc$) in a six-storey REB is already markedly lower than that in a three-storey REB, with the difference being 4.55 kWh/m2a. Additional renovation with modular extension brings additional savings, nevertheless at the same volume ratio the impact of the modular extension does not exceed the basic difference in energy efficiency, resulting from a larger number of REB storeys. It is obvious that the results presented in Figure 4 take into account both influences, the influence of the REB energy efficiency in dependence on the number of its storeys and the impact of modular extension. However, if comparing the extension of REB of the same base height with single and two-storey modules (Figure 3), the energy need is always lower in the case of extension with two-storey modules.

Figure 5 demonstrates energy savings separately for the extension with single and two-storey modules. The results for M_1 (Figure 5-above) show the highest energy savings in the case of extension with module (M_1 opt U_1), followed by (M_1 ave U_1), (M_1 opt U_2) and (M_1 ave U_2).

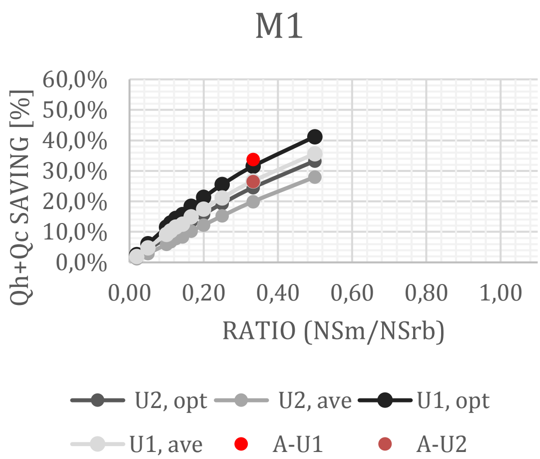

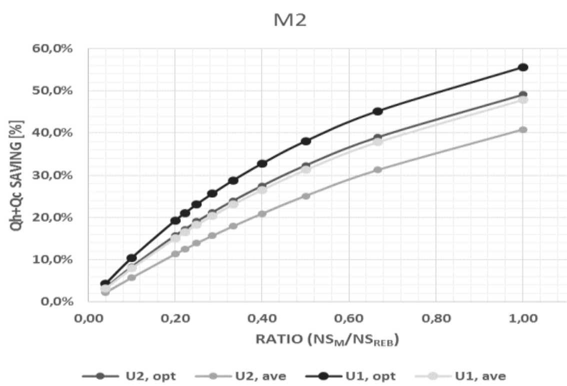

Figure 5. Energy savings (%) for REB extension with different variations of upgrade modules (M_1-above) and (M_2-below) at different volume ratios

In the case of extension with two-storey modules (Figure 5 - below) the highest savings can also be observed with the optimal module having better thermal properties (M_2 opt U_1). However, the second highest savings are shown in the case of extension with the optimal module having weaker thermal properties (M_2 opt U_2), which shows the strengthening influence of the optimal glazing size within two-storey modules. The savings are slightly lower for (M_2 ave U_1) and the lowest for (M_2 ave U_2). Additionally, an interesting comparison to the study [14] is shown in Figure 5 (above). The marked dots represent the energy savings for REB extension with single-storey modules (M_1 opt U_1) and (M_1 opt U_2) with identical volume ratio. The building under consideration in [14] has the same orientation with a slightly different aspect ratio and glazing distribution.

Even though there are minor differences in the design of both case study buildings, the current one and that from [14], the energy savings are very similar in both studies.

5 Conclusion

Aiming at reducing the final energy consumption, the refurbishment of energy inefficient buildings is treated as one of the urgent tasks of building sector. Exploring different manners of energy efficiency renovation leads towards determination of general guidelines for energy retrofitting of buildings. The current paper considers the refurbishment of an existing building integrating different measures among which the efficiency of the building extension with different types of lightweight timber-glass modules is specifically analysed. The impact of the modular extension on energy savings of the hybrid building is generally increasing with the increase of the volume ratio. The similarity of the results to [14] indicates the universality of the presented findings. However, some additional analyses have to be implemented before declaration of the widespread applicability. The results can serve to designers and decision makers as a tool for the approximate prediction of energy savings in the case of using the upgrade modules for the renovation of the existing buildings. Further analyses of such renovation for different floor plans, orientations and energy standards of buildings are planned in order to obtain sufficient information for the preparation of general guidelines.

Acknowledgements

The authors acknowledge:

- the financial support from Slovenian Research Agency (research core funding No. P2-0129), and
- the investment is co-financed by Republic of Slovenia and the European Union under the European Regional Development Fund (research core funding IQ HOME - Intelligent home of the new generation designed on smart appliances and wood).

References

[1] Eurostat, E. a. E. (2010). Eurostat yearbook 2010. Office for Official Publications of the European Communities (Luxembourg).

[2] Norris, M., Shiels, P. (2004). Regular National Report on Housing Developments in European Countries. Synthesis Report, The Housing Unit, Dublin, Ireland.

[3] Poel, B., van Cruchten, G. in Balaras, C. A. (2007). Energy performance assessment of existing dwellings. Energy and Buildings, 39(4), 393-403.

[4] Lechtenböhmer, S. and A. Schüring, The potential for large-scale savings from insulating residential buildings in the EU. Energy Efficiency, 2011, 4(2), p. 257-270.

[5] G.P. Waide, W. Smith, High-rise refurbishment the energy-efficient upgrade of multi-story residences in the European Union, in: IEA Information Paper, International Energy Agency, 2006.

[6] Economidou M., AtanasiuB., Despret C., Economidou M., Maio J., Nolte I., Rapf O. (2011). Europe's buildings under the microscope, Buildings Performance Institute Europe.

[7] Liu, Y. and W. Guo, Effects of energy conservation and emission reduction on energy efficiency retrofit for existing residence: A case from China. Energy and Buildings, 2013, 61, p. 61-72.

[8] Petrović Bećirović, S. and M. Vasić, Methodology and results of Serbian Energy-Efficiency Refurbishment Project. Energy and Buildings, 2013, 62, p. 258-267.

[9] Boyano, A., P. Hernandez, and O. Wolf, Energy demands and potential savings in European office buildings: Case studies based on EnergyPlus simulations. Energy and Buildings, 2013. 65, p. 19-28.

[10] Paiho, S., Hedman A., Abdurafikov R., Hoang H., Sepponen M., Kouhia I., Meinander M., Energy saving potentials of Moscow apartment buildings in residential districts. Energy and Buildings, 2013, 66, p. 706-713,

[11] Niemelä T., Kosonen R., Jokisalo J., Cost-effectiveness of energy performance renovation measures in Finnish brick apartment buildings, Energy and Buildings, Volume 137, 15 February 2017, Pages 60-75, ISSN 0378-7788,

[12] Konstantinou, T., in Knaack, U. (2011). Refurbishment of Residential Buildings: A Design Approach to Energy-Efficiency Upgrades. Procedia Engineering, 21, 666-675.

[13] Konstantinou, T., in Knaack, U. (2013). An approach to integrate energy efficiency upgrade into refurbishment design process, applied in two case-study buildings in Northern European climate. Energy and Buildings, 59, 301-309.

[14] Špegelj, T., Žegarac Leskovar, V., Premrov, M. (2016). Application of the timber-glass upgrade module for energy refurbishment of the existing energy-inefficient multi-family buildings. Energy and Buildings, 116, 362-375.

[15] Jaksch, S., Angelika Franke, A., Österreicher, D., Treberspurg, M. (2016). A systematic approach to sustainable urban densification using prefabricated timber-based attic extension modules. Energy Procedia, Volume 96, 638-649.

[16] The city above the city – New international design competition, Press release (2016). MetsäWood. last accessed on 16.12.16 at http://www.multivu.com/players/uk/7875651-metsa-wood-the-city-above-the-city/.

[17] Jaksch, S., Angelika Franke, D., Treberspurg, M. (2016). A timber based attic extension system for sustainable urban densification. WCTE 2016 e-book, 5598-5606. last accessed on 11.02.17 http://wcte2016.conf.tuwien.ac.at/home/

[18] Špegelj T., Premrov M., Žegarac Leskovar V., Development of the timber-glass upgrade module for the purpose of its installation on energy-inefficient buildings in the refurbishment process, Energy Efficiency (2016).

[19] Peel M.C., Finlayson B.L, McMahon T.A., Updated world map of the Köppen–Geiger climate classification, Hydrol. Earth Syst. Sci. (2007) 1633–1644.

[20] Žegarac Leskovar V., Premrov M., Energy-efficient timber-glass houses, Springer Verlag, 2013.

[21] Feist W. Passive House Planning Package, Energy balance and Passive House design tool for quality approved Passive Houses and EnerPHit retrofits, 2012.

[22] EN ISO 13790: 13790: 2008 Energy performance of buildings – Calculation of energy use for space heating and cooling (ISO 13790:2008).

[23] Meteonorm 7.0, Global Meteorological Database for Engineers, Planners and Education http://www.meteonorm.com.

10TH INTERNATIONAL CONFERENCE ON SUSTAINABLE ENERGY AND ENVIRONMENTAL PROTECTION (JUNE 27TH – 30TH, 2017, BLED, SLOVENIA), ENERGY EFFICIENCY
J. Krope, A.Ghani Olabi, D. Goričanec & S. Božičnik

Influence of Building Shape on Energy Performance of Timber-Glass Buildings Located in Warm Climatic Regions

MAJA ŽIGART, MIROSLAV PREMROV & VESNA ŽEGARAC LESKOVAR

Abstract The features of timber as a natural raw material and glass lead to the development of a new type of highly attractive structures, the so-called timber-glass buildings. In such cases an optimal proportion and appropriate orientation of the glazing surfaces usually play an important role due to exploitation of solar radiation as a source of renewable energy for heating applicable mostly only for buildings located in cold and moderate climatic regions. However, the situation for timber-glass buildings located in warm climatic regions is completely different, because energy demand for cooling presents the main contribution to annual energy demand.The optimal solutions for such cases should therefore avoid overheating, which hasn't been widely analysed in the previous scientific literature. The paper presents the results of the numerical study performed on one and two-storey box-house models of timber-glass buildings with different shapes and variable size of glazing placed separately on the south or north facade of the building. The models are analysed for locations in Madrid and Athens. The influence of the described parameters on annual energy demand is deeply analysed and can serve the architects as systematic guidelines in designing highly attractive timber-glass buildings with different shapes also in warm climate conditions.

Keywords: • Timber • Glass • Buildings • Energy efficiency • Building shape • Energy need for cooling •

CORRESPONDENCE ADDRESS: Maja Žigart, Assistant, University of Maribor, Faculty of Civil Engineering, Transportation Engineering and Architecture, Smetanova ulica 17, 2000 Maribor, Slovenia, e-mail: maja.zigart1@um.si. Miroslav Premrov, Ph.D., Professor, University of Maribor, Faculty of Civil Engineering, Transportation Engineering and Architecture, Smetanova ulica 17, 2000 Maribor, Slovenia, e-mail: miroslav.premrov@um.si. Vesna Žegarac Leskovar, Ph.D., Associate Professor, University of Maribor, Faculty of Civil Engineering, Transportation Engineering and Architecture, Smetanova ulica 17, 2000 Maribor, Slovenia, e-mail: vesna.zegarac@um.si.

https://doi.org/10.18690/978-961-286-050-9.3 ISBN 978-961-286-050-9

Available at: http://press.um.si.

1 Introduction

Climate changes of the last few decades do not only encourage researches into the origins of their onset but they also mean a warning and an urgent call for a need to remove their causes and alleviate the consequences affecting the environment. Eco-friendly solutions in residential and public building construction remains our most vital task, whose holistic problem solving requires knowledge integration. Using different building materials with quite different material properties in a way to optimally consider all possible advantages of them in a hybrid structural composition of buildings could be a relative new approach in designing of high energy-efficient buildings.

Only in recent decades has timber been rediscovered, partly due to the contemporary manufacture of prefabricated timber elements and partly owing to high environmental potential of this renewable natural building material. On the other hand, in contrast, glass definitely cannot be treated as a sustainable material and used to be treated for many years as the weakest point of the building envelope from the thermal point of view. However, dynamic evolution of the glazing in the last decades resulted in insulating glass products with highly improved physical and strength properties, suitable for application in contemporary energy-efficient buildings, not only as material responsible for solar gains and daylighting, but also as a component of structural resisting, Premrov et al. [1].

With suitable technological development and appropriate use, timber and glass are nowadays becoming essential construction materials as far as the energy efficiency is concerned. Because of a great difference in many material properties their combined use is extremely complicated, from the field of energy efficiency and structural points of view as well. The features of both building materials presented above in last years lead to the development of new type of structures, so-called timber-glass buildings, Žegarac Leskovar and Premrov [2]. In such buildings an optimal proportion and an appropriate orientation of the glazing surfaces play an important part due to exploitation of solar radiation as a source of renewable energy in a passive use of energy for heating.

There are many numerical studies analysing the influence of glazing size on energy demand for heating or/and cooling in different climate areas.

There are many studies about influence of glazing size and building geometry on energy demand for buildings located in cold climate conditions, [2]-[6]. It was pointed by all studies to a strong correlation between the final energy use for heating and the shape of the building witnessed in colder climates. It was generally suggested that a cold climate may increase the impact of the building shape on the energy need. In such cases an optimal proportion and appropriate orientation of the glazing surfaces usually play an important role due to exploitation of solar radiation as a source of renewable energy for heating applicable mostly only for buildings located in cold and moderate climatic regions.

However, the situation for timber-glass buildings located in warm climatic regions is completely different, because energy demand for cooling presents the main contribution to annual energy demand. Additionally, because of the relative low thermal capacity, there is a risk of a strong overheating in a summer period. The optimal solutions for such cases should therefore avoid overheating, which hasn't been widely analysed in the previous scientific literature. There are several studies relating the energy need for cooling in hot non-European climate conditions. Bouden [7] investigated the appropriateness of glass curtain walls for the Tunisian local climate. The influence of windows on the energy balance of apartment buildings in Amman, Jordan, was analysed in the study performed by Hassouneh et al. [8]. The impact of relative compactness (RC) on the building's annual cooling energy demand and the total annual energy demand was for example investigated by Al Anzi et al. [9], whose research involved a prototypical building with over 20 floors based in Kuwait. The results of the study indicate that the energy use decreases as the relative compactness increases. For our study there is a special interest for studies related to warm climate conditions in Europe, where additionally beside cooling also a slide energy need for heating can occur. In this way Depecker et al. [10] studied the relationship between shape and energy requirements during the winter season in two French localities with different climate conditions. They found no correlation between the energy consumption of a building and its shape in mild climate. Albatici and Passerini [11] were encouraged to research new indicators of energy performance in mild and warm climate conditions in relation to the building shape. Heating requirements of buildings with different shapes placed in the Italian territory were presented and confirms that compactness is more important in cold localities than in warm ones.

To assess to what extent building geometry may influence on the building energy efficiency in warm European regions, the current study analyses twelve differing single and two-storey models of timber-glass single-family houses with a varying building aspect ratio located in two selected European capital cities with relative warm climate conditions (Madrid and Athens). It is important to stress that the main benefit of the study comparing with all previous similar studies is in a fact that two opposite situations are separately analysed: with the optimal size of glazing placed in the south façade only and with the same size of glazing placed in the north façade only.

2 Influence of the Building Shape on Energy Demand

As it was previously briefly presented building shape can significantly influence on the energy demand of buildings, but this influence generally depends also on the given climate conditions. In this way, and to present adequate conclusions based on the obtained numerical results and theoretical correlations, it is a need first to present some basic theoretical facts about energy flows in buildings.

Building energy need can be generally considered as the sum of the energy need for heating (Q_h) and cooling (Q_c). A building is therefore analysed as a thermal system consisting of the transmission heat losses (Q_t), ventilation heat losses (Q_v), internal heat gains (Q_i) and solar heat gains (Q_s). The energy need is generally calculated in the form normed per 1 m^2 of usable floor area (A_{TFA}):

$$\Delta Q = (Q_t+Q_v) - \eta_G \cdot (Q_s+Q_i) / ATFA \qquad (1)$$

The utilization factor η_G approximately represents a part of energy gains which cannot be accumulate in a building. Based on different temperatures of the building and its surroundings we can distinguish between two opposite heat flow scenarios; the heating and the cooling period. In heating periods of the year when the average outdoor temperature is generally lower than the prescribed or chosen indoor temperature, the sum of all heat flows in the building is usually negative. Energy flows in the summer period are in the opposite directions, therefore there is a need for cooling to avoid an overheating in a building. The transmissions heat losses Q_t are calculated for every building element of the heat-exchanging envelope in the form of:

$$Q_t = A \cdot U \cdot f_T \cdot G_t / A_{TFA} \qquad (2)$$

where A is the building envelope area, U is the building envelope thermal transmittance, f_T is the reduction factor for reduced temperature difference and G_t is temperature difference time integral (heating degree hours). Respecting Eq. (2) it can be concluded that an enlarged building envelope area (A) generally increases the transmission losses and consequently has a negative impact on energy demand for heating.

The solar heat gains Q_s are calculated using:

$$Q_s = r \cdot g \cdot A_w \cdot G / A_{TFA} \qquad (3)$$

where r is the total shading reduction factor, g is the degree of solar energy transmitted through the glazing normal to the irradiated surface, A_w is the window area (rough opening) and G is the total radiation during the heating period. Respecting Eq. (3) it can be concluded that an enlarged glazing area (A_w) increases the solar gains but, on the other hand, also has a negative impact on the transmission losses which are increased because of a higher thermal transmittance of the windows comparing with the thermal transmittance of the wall elements. This is an interesting situation which mostly depends also on the given climate conditions (temperature difference and solar potential in the heating and summer period). The parameter which can significantly influence the amount of solar gains and consequently the total energy demand for heating and cooling is the glazing-to-wall area ratio ($AGAW$) described as the ratio between the total area of glazing (A_{gs}) to the total area of the wall (A_{wall}):

$$AGAW = A_{gs} / A_{wall} \qquad (4)$$

As it was already mentioned in Chapter 1 there are many, mostly numerical studies about the optimal size of glazing placed on different facades of the building in various climate conditions. In the studies Žegarac Leskovar and Premrov [2], [12] an attempt at a more systematic analysis was made, with the model of a building being performed in many variations of timber construction systems. Based on an extensive parametric analysis, a generalisation of the problem was performed concerning the optimal glazing area size ($AGAW_{opt}$) dependence on one single variable, the U_{wall} -value which becomes the only variable parameter for all contemporary prefabricated timber construction systems, independently of their type. However, the analysis was performed only for the heating period for cities with a relative strong winter conditions (Helsinki, Munich and Ljubljana).

Another important parameter often used to determine solar access of a building, assuming that the latter is of a given height and optimally oriented, is the aspect ratio *(AR)*, a ratio between the building's length and width ($AR = L/W$), Figure 1. There are many studies about the aspect ratio variation, but mostly only for the cold climate conditions and for the glazing placed on the south façade only. For example, it was presented in Chiras [13], that the ideal aspect ratio for a rectangular-shaped solar house design ranges from 1.3 to 1.5.

3 Numerical Study

3.1 Simulation model

Parametric Variation of the Model Geometry

The presented numerical research is based on a case study considering box models of single and two-storey houses built in the prefabricated timber-frame structural system with different thermal transmittance of the external wall elements ($U_1=0.102\ W/m^2K$ and $U_2=0.200\ W/m^2K$). To obtain relevant theoretical results of the three-layered glazing size influence on energy demand the glazing with $U_g=0.51\ W/m^2K$ and $U_f=0.73\ W/m^2K$ is used. The size of glazing with a value of $AGAW = 35\%$ according to Eq. (4) is separately used for the south and then also for the north façade. Three groups of rectangular models are parametrically analysed using a systematic variation of the building aspect ratio ($AR = L/W$) from 0.83 to 1.69, schematically presented in Figure 1:

- Model group A: single-storey models with a constant occupied floor area $A_{TFA} = 81\ m^2$ and a heated volume $V = 243\ m^3$.
- Model group B: single-storey models with a doubled constant occupied floor area $A_{TFA} = 162\ m^2$ and a heated volume $V = 486\ m^3$.
- Model group C: two-storey models with a doubled basic occupied floor area of each storey $A_{TFA} = 81\ m^2$ and a heated volume of each storey $V = 243\ m^3$.

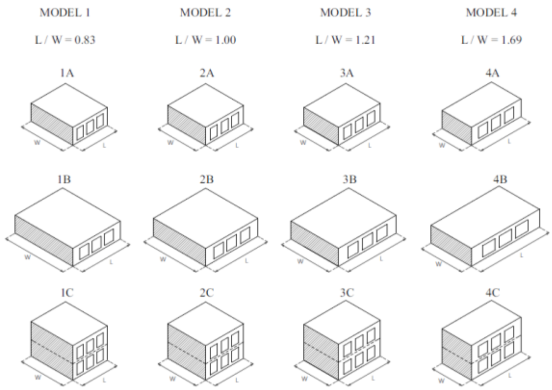

Figure 1. Schematic presentation of the analysed house models

Climate Data

The study analyses the energy performance for two different European cities with relative warm climate conditions (Athens and Madrid). Climate information from Meteonorm [14] was used for calculations, Table 1.

Table 1. Climate data for Athens and Madrid

	Athens	Madrid
Average annual temperature (°C)	18.6	16.3
Average annual temperature in the heating period (°C)	9.0	8.0
Length of the heating period (days/an.)	65.6	133.7
Total annual solar radiation G on the south vertical surface (kWh/m^2)	1100	1280
Total solar radiation G on the south vertical surface in the heating period (kWh/m^2)	151	436
Total annual solar radiation G on the north vertical surface (kWh/m^2)	444	370
Total solar radiation G on the north vertical surface in the heating period (kWh/m^2)	41	75

3.2 Results and discussion

The calculated results for energy demand for heating (Q_h), cooling (Q_c) and total annual energy demand (Q_{total}) for Athens and Madrid are graphically presented for all analysed models in Figure 2 for the both selected U-values of the envelope elements.

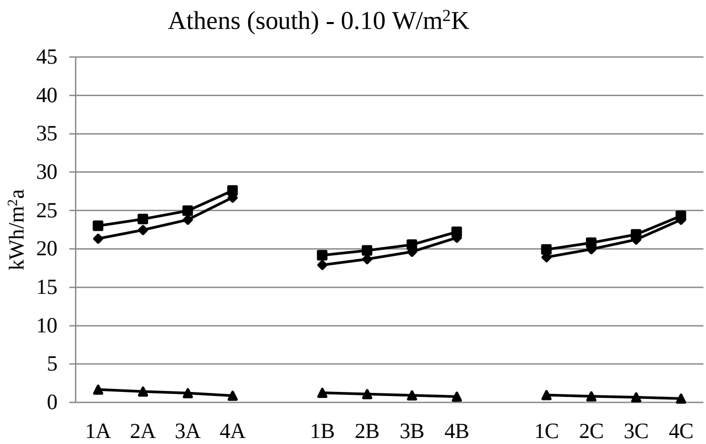

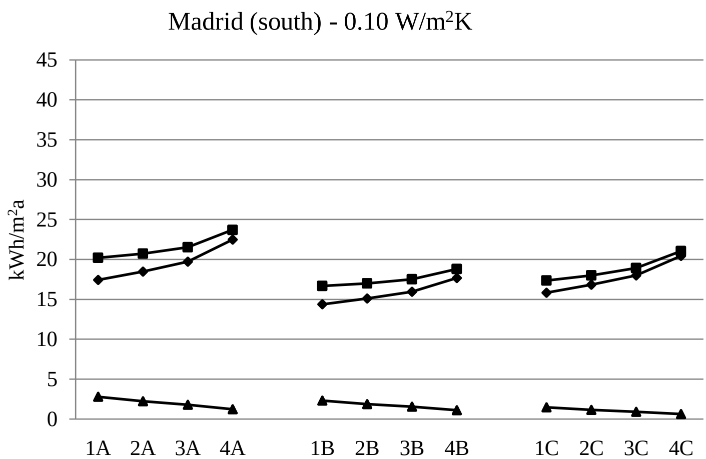

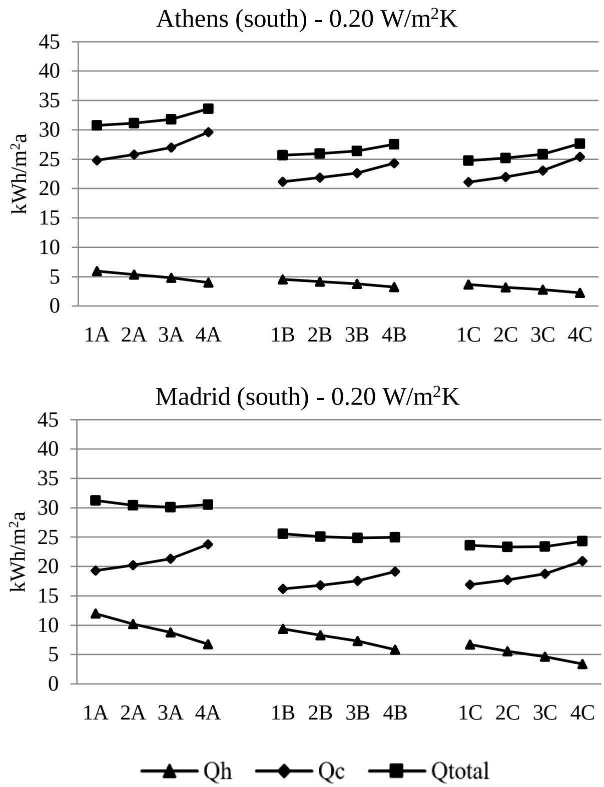

Figure 2. Results for the south orientation of glazing

It is evident from the presented results that the energy need for heating (Q_h) is estimated to be extremely low for the case of *U=0.102 W/m²K*, thus the findings relative to the total energy need (Q_{total}) depend basically on findings on cooling (Q_c). Because of the increasing size of glazing with the increasing length of the south façade (*L*) is deduced that the energy need for cooling increases in an almost exponent dependence with the increasing aspect ratio (*AR*). The functions behaviour for the analysed energy demand (Q_h, Q_c and Q_{total}) for Athens and Madrid according to the increasing aspect ratio is very similar, only the absolute values are slightly different owing to a small temperature difference between both cities. It is also of a special interest by comparing the models from the all three selected groups (A, B and C) that the results for the total annual energy demand (Q_{total}) for the models of group B are only slightly lower than by the models of group C.

The findings for the case of *U=0.20 W/m²K* are slightly different. Because of the higher U-value the transmission losses according to Eq. (2) are higher which results in an increasing energy demand for heating (Q_h). This is especially evident for Madrid with lower average temperature in a heating period, see Table 1. Because the glazing size is the same the results for cooling (Q_c) for the both locations do not especially differ from the case with $U=0.102\ W/m^2K$. Comparing the results between all analysed groups it is evident that the results for Q_{total} are very similar for group B and C, but are generally lower than by group A.

In a sense to especially analyse the problem with the overheating the case with the same glazing size to be placed only on the north façade instead on the south facade is additionally treated. The calculated parametrical results are graphically presented in Figure 3. It is of a practical interest to present only the results for the case with higher transmission losses ($U=0.20\ W/m^2K$).

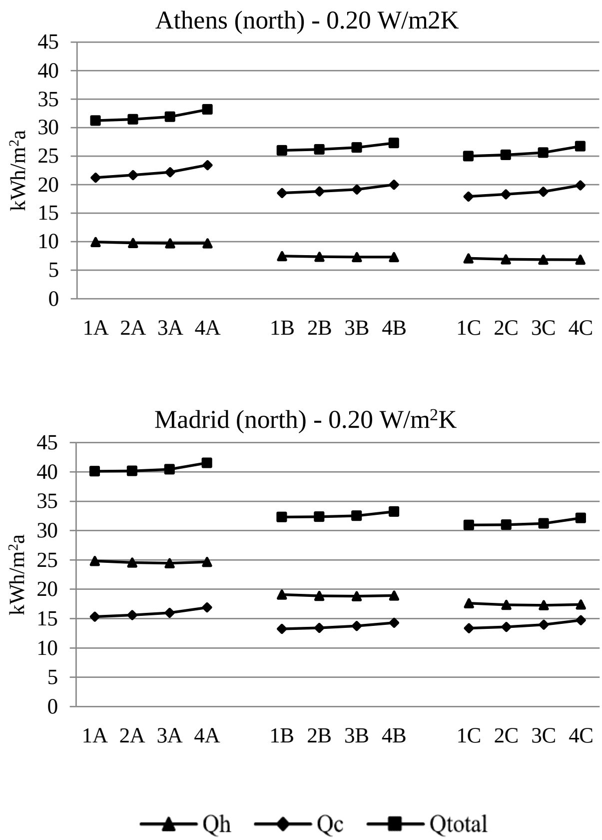

Figure 3. Results for the north orientation of glazing

Particularly comparing the results from Figures 2 and 3 for Athens it can be found out that the results for the heating demand (Q_h) are higher for the north orientation of glazing, but according to Eq. (3) and lower value of G from Table 2 the cooling demand (Q_c) is in this case lower because of lower solar gains (Q_s) in the summer period. Consequently, an interesting fact appears for Athens that the obtained results for the total annual energy demand for the north position of glazing practically do not differ from the results with the south orientation of glazing (Figure 2). However, such conclusion cannot be adopted for Madrid at all. The heating demand (Q_h) evidently increased according to the results from Figure 2 and even became higher than the demand for cooling (Q_c). Consequently, the total energy demand (Q_{total}) for Madrid is in the case of the north orientation of glazing evidently higher than for the south orientation (Figure 2).

4 Conclusions

The presented parametrical numerical results of the study can serve to designers many interesting findings which can be efficiently used by prediction of energy demand for buildings located in warm climate area. It can be generally concluded from the presented results that the total annual energy need (Q_{total}) in warm climates consist mostly of those for cooling (Q_c), which brings about a conclusion that the energy need increases with the increasing aspect ratio (*AR*). The latter does not correspond well with the findings in [13], where the rectangular shapes with aspect ratios from 1.3 to 1.5 were favourable, but for the cold climates.

It was presented in our study that the influence of the varying aspect ratio strongly depends on the climate conditions and additionally also on the thermal transmittance (U-value) of the building envelope and orientation of the glazing areas. To prevent overheating it is generally more convenient to place the glazing on the north side of the building, but in this case then transmission losses increase. Comparing the results for Athens from Figures 2 and 3 we come to interesting findings that the total energy need by the U-value of the thermal envelope of 0.20 W/m^2K is practically identical if the same size of the glazing is placed on the south (Figure 2) or on the north facade of the building (Figure 3). Therefore, in the case with similar U-values of the thermal envelope designers are free to choose similar size of glazing to be placed on south or north side of a building.

This is not a case with a decreasing average temperature in a heating period (increasing of geographical location to the north, Madrid in our case) where the negative impact of the north placed glazing increases. In this case because of lower temperature and higher U-values higher transmission losses occur and the heating demand becomes even higher than cooling. Comparing the results between all analysed groups (one and two-storey) it is evident that the results for Q_{total} are very similar between groups B (single-storey) and C (two-storey model), but are generally lower than by group A. The last fact is especially evident for the both selected cities when the glazing is placed on the north façade of the building.

Acknowledgements

The authors acknowledge the financial support from the Slovenian Research Agency (research core funding No. P2-0129).

References

[1] M. Premrov, V. Žegarac Leskovar, and K. Mihalič, "Influence of the building shape on the energy performance of timber-glass buildings in different climatic conditions". *Energy*, vol. 108, pp. 201-211, 2016.

[2] V. Žegarac Leskovar, and M. Premrov, *Energy-efficient timber-glass houses*. Springer Verlag, 2013.

[3] P. Depecker, C. Menezo, J. Virgone, and S. Lepers, "Design of building shape and energetic consumption". *Building and Environment,* vol. 36(5), pp. 627-635, 2001.

[4] H. Bülow-Hübe, *The effect of glazing type and size on annual heating and cooling demand for Swedish offices*. (Report No TABK--01/1022). Department of Construction and Architecture, Lund University, Division of Energy and Building Design, Lund, 2001.

[5] M.L. Persson, *Windows of Opportunities, The Glazed Area and its Impact on the Energy Balance of Buildings.* PhD Thesis, Uppsala Universitet, 2006.

[6] C. Ratti, N. Baker, and K. Steemers, "Energy consumption and urban texture". *Energy and Buildings*, vol. 37(7), pp. 762-776, 2005.

[7] C. Bouden, "Influence of glass curtain walls on the building thermal energy consumption under Tunisian climatic conditions: The case of administrative buildings". *Renewable Energy*, vol. 32, pp. 141-156, 2007.

[8] K. Hassouneh, A. Alshboul, and A. Al-Salaymeh, "Influence of windows on the energy balance of apartment buildings in Amman". Energy Conversion and Management 2010; 51:1583-1591.

[9] A. Al Anzi, D. Seo, and M. Krarti, "Impact of building shape on thermal performance of office buildings in Kuwait". *Energy Conversion and Management*, vol. 50(3), pp. 822-828, 2009.

[10] P. Depecker, C. Menezo, J. Virgone, and S. Lepers, "Design of building shape and energetic consumption". *Building and Environment*, vol. 36(5), pp. 627-635, 2001.

[11] R. Albatici, and F. Passerini, "Bioclimatic design of buildings considering heating requirements in Italian climatic conditions - A simplified approach". *Building and Environment*, vol. 46(8), pp. 1624-1631, 2011.

[12] V. Žegarac Leskovar, and M. Premrov, "An approach in architectural design of energy-efficient timber buildings with a focus on the optimal glazing size in the south-oriented façade". *Energy and Buildings*, vol. 43(12), pp. 3410–3418, 2011.

[13] D. Chiras, *The Solar House: Passive Heating and Cooling*. Chelsea Green Publishing, White River Junction, VT, 2002.

[14] Meteonorm Software, Meteotest, Bern.

10TH International Conference on Sustainable Energy and Environmental Protection (June 27TH – 30TH, 2017, Bled, Slovenia), Energy Efficiency
J. Krope, A.Ghani Olabi, D. Goričanec & S. Božičnik

Phase-Changing Materials for Thermal Stabilization of Buildings

Marjan Krasna & Samo Kralj

Abstract In a temperature driven thermodynamic first order (discontinuous) phase transition the latent heat is released (absorbed) on entering (exiting) the low temperature phase. This mechanism could be exploited for thermal stabilization of buildings. In the simplest case one would need a layer coating a building, containing a phase-changing material with the phase transition temperature Tc in the regime of ambient temperatures. In the paper we present theoretical analysis, suggests how one can tune Tc to a desired value. For this purpose a material exhibiting a continuous symmetry breaking phase transition is needed. The symmetry breaking phase is then characterized by an amplitude and gauge component of the relevant order parameter characterizing the transition. We demonstrate, that by imposing a distortion to the gauge component on a characteristic length scale R, one could control Tc by varying the strength of distortions. We demonstrate what geometrical and material properties are needed for an efficient phase-changing material for thermal stabilization at ambient temperatures

Keywords: • Thermal isolation • Phase changing material • Continuous symmetry breaking • First order phase transition • Latent heat •

Correspondence Address: Marjan Krašna, Ph.D., Lecturer, University of Maribor, Faculty of Natural Sciences and Mathematics, Koroška cesta 160, 2000 Maribor, Slovenia, e-mail: marjan.krasna@um.si. Samo Kralj, Ph.D., Lecturer, University of Maribor, Faculty of Natural Sciences and Mathematics, Koroška cesta 160, 2000 Maribor, Slovenia, e-mail: samo.kralj@um.si.

https://doi.org/10.18690/978-961-286-050-9.4 ISBN 978-961-286-050-9

Available at: http://press.um.si.

1 Introduction

Continuous symmetry breaking phase and structural transitions are ubiquitous in nature [1] [2]. In fact, the rich diversity of patterns observed nature is almost entirely based on them. The physics describing basic facts, i.e. qualitative behavior, is strongly universal, independent of material details. At the other hand, quantitative behavior is material dependent. Landau [3] derived a universal theory of phase transition based on symmetry properties of systems. He introduced an order parameter field to distinguish the competing phases in a phase transition event. In the paper we present key properties emerging from the universal Landau theory of phase transitions which might be implemented in future phase-changing materials used for thermal stabilization at ambient temperatures.

In a temperature driven thermodynamic [4] discontinuous phase transition the latent heat is released on entering a low temperature phase. Thus, if a system is heated below the phase transition it releases heat. In case of large enough heat release one could at least temporary stabilize temperature of the system. On the other hand by adsorbing energy symmetry broken phase can be reentered. Consequently, the first (second) described phenomenon could be exploited to prevent or reduce a temperature decrease (increase) in a system. Appropriate phase-change materials have a strong potential to be exploited in designing future phase-changing materials for thermal stabilization of buildings.

For this purpose it is of interest to be able to control phase transition temperature of such phase-changing materials. To identify key mechanism enabling this control we refer to basics of Landau-type theories of phase transitions. Any continuous symmetry breaking phase transition can be represented by an order parameter field $\boldsymbol{Q}$ [5]. It can be either a vector or tensor and it consists of two qualitatively different components. The first component is commonly referred to as the amplitude (also called hydrodynamic) field. It measures the strength of ordering in the symmetry broken phase. For given conditions it possesses a single equilibrium value. If one locally perturbs its value it relaxes to equilibrium value on order parameter correlation length, which is material and also temperature dependent. The second component is referred to as the gauge (also called symmetry breaking or non-hydrodynamic) field. The gauge component determines a symmetry breaking "choice", that was selected in the continuous symmetry phase transition. The corresponding order parameter space is strongly degenerated (i.e., there are infinite number of equivalent "choices"). Consequently, if a gauge field is locally perturbed it responds in absence of an external field on a geometrically imposed scale, which is in general not material or temperature dependent. This property could be exploited to control the phase transition temperature.

In the paper we illustrate such mechanisms to control T_c in a phase change material. In Sec. II we present our model. In Sec. III we derive key results and in the last section we summarize our findings.

2 Mesoscopic Modeling

Of our interest is to demonstrate relatively simple ways how one could control phase transition temperature in a first order phase transition. We use a Landau-type approach in terms of a relevant order parameter $\boldsymbol{Q}$ to model a temperature driven phase transition. In bulk in a symmetry broken phase (quasi) long-range order in the gauge field component is established, and the order parameter amplitude is spatially homogeneous.

For demonstration purposes we treat three qualitatively different systems from symmetry perspective to emphasize universality of the phenomenon. We consider three qualitatively different order parameters $\boldsymbol{Q} = \boldsymbol{Q}(\vec{r})$. Here $\vec{r}$ stands for the position vector, $\boldsymbol{Q}$ equals zero in the higher symmetry phase and $\boldsymbol{Q} \neq 0$ fingerprints key local ordering properties of a symmetry broken phase. In our illustrative cases, local properties of the low temperature phase are described either by (i) a vector order parameter, (ii) tensorial uniaxial order parameter or (iii) complex order parameter. We express them as [6]

$$\boldsymbol{Q}^{(i)} = \overrightarrow{Q} = s\vec{e}, \boldsymbol{Q}^{(ii)} = \underline{Q} = s(\vec{e} \otimes \vec{e} - \underline{I}/3),$$
$$\boldsymbol{Q}^{(iii)} = se^{i\phi}. \tag{1}$$

The classical examples where these order parameter are used are (i) paramagnetic-magnetic phase transition in ferromagnets, (ii) isotropic-nematic liquid crystal (LC) phase transition, (iii) normal fluid-superfluid, magnetic-supermagnetic, or nematic-smectic A LC phase transition. In the expression for $\underline{\boldsymbol{Q}}$ the quantity $\underline{I}$ is the identity tensor and $\otimes$ marks the tensorial product. Note that the first two examples describe phase transitions in orientational ordering, where in bulk symmetry broken phase orientational ordering is homogeneously aligned along a single symmetry breaking direction $\vec{e}$, $|\vec{e}|=1$. In $\boldsymbol{Q}^{(ii)}$ the orientations $\pm\vec{e}$ are physically equivalent (i.e. $\boldsymbol{Q}^{(ii)}(\vec{e}) = \boldsymbol{Q}^{(ii)}(-\vec{e})$). The 3rd order parameter determines onset of translational order. For example (to which we restrict in the following), in a smectic A phase the symmetry broken structure consists in bulk of periodic layers determined by the phase factor $\phi = \vec{r}.\vec{q}$. Here $\vec{q} = (2\pi/d)\vec{e}$ stands for the wave vector describing position of smectic layers. The layer distance is given by d and $\vec{e}$ stand for the unit normal of the layers. In all three cases s is the amplitude component of the order parameter, and $\vec{e}$ is the gauge field component.

In bulk equilibrium $s(\vec{r})$ and $\vec{e}(\vec{r})$ are spatially homogeneous. The equilibrium value of $s \equiv s_{eq}$ minimizes the condensation free energy potential f_c, which is independent of the gauge field component. The lowest order symmetry allowed order parameter expansion in f_c yielding discontinuous phase transition is given by

$$f_c(\vec{Q}) = a|\vec{Q}|^2 - b|\vec{Q}|^4 + c|\vec{Q}|^6 = as^2 - bs^4 + cs^6| \tag{2a}$$

$$f_c(\underline{Q}) = \frac{3a}{2} Tr\underline{Q}^2 - \frac{9b}{2} Tr\underline{Q}^3 + \frac{9c}{4}\left(Tr\underline{Q}^2\right)^2 = as^2 - bs^3 + cs^4 \tag{2b}$$

$$f_c(Q) = a|Q|^2 - b|Q|^4 + c|Q|^6 = as^2 - bs^4 + cs^6 \tag{2c}$$

Here $a=a_0(T - T_*)$, a_0, b, c are positive material constants, T stands for the temperature, and T_* is the supercooling temperature of the higher symmetry phase.

To enforce homogeneous ordering we need to introduce elastic free energy terms. The most essential terms in the lowest order expansions in $\boldsymbol{Q}$ they can be expressed as

$$f_e(\vec{Q}) = L|\nabla\vec{Q}|^2 \approx L|\nabla s|^2 + Ls^2|\nabla\vec{e}|^2 \tag{3a}$$

$$f_e(\underline{Q}) = L|\nabla\underline{Q}|^2 \approx L|\nabla s|^2 + Ls^2|\nabla\vec{e}|^2 \tag{3b}$$

$$f_e(Q) = L\left(|(\vec{e}\times\nabla)Q|^2 + \left|(\nabla + iq_0\vec{e})Q\right|^2\right) \approx L|\nabla s|^2 + Ls^2\left(|\vec{e}\times\nabla\phi|^2 + (q - q_0)^2\right) \tag{3c}$$

where L is a positive representative elastic constant and in Eq.(3c) the wave vector $q_0 = 2\pi/d_0$ introduces the equilibrium layer constant d_0. Note that the above equations impose homogeneous ordering in s and $\vec{e}$. In addition the Eq.(3c) imposes the equilibrium layer spacing d_0.

3 Phase Transition Temperature Shift

We next estimate phase transition temperature shifts if one imposes elastic distortions to the gauge field component of a relevant order parameter. In cases of orientational ordering we assume that the phase-change material is confined within a cell of characteristic thickness R, where we impose at different plates different orientational ordering. In case of translational order we set that the cell imposed thickness is not commensurate will the equilibrium "layer" distance $d_0 = 2\pi/q_0$ of the material. In the other two dimensions of area A we assume homogeneous orientational or translational ordering. Therefore, in these directions we do not impose conflicting boundary conditions to the gauge field.

To estimate the resulting phase behavior on varying R it is convenient to introducing appropriate scaling. We scale distances with respect to R by introducing the dimensionless position vector $\vec{x} = \vec{r}/R$, dimensionless gradient $\widetilde{\nabla}=R\nabla$, and define scaled order parameters $s/s_0 \rightarrow s$ where $s_0 = s_{eq}(T_c)$ Here T_c stands for the bulk equilibrium phase transition in absence of elastic distortions, and s_0 determines the corresponding order parameter jump at T_c. Furthermore, we introduce the dimensionless temperature $t = (T–T_*)/(T_c–T_*)$. Note that in bulk $t(T = T_c) = 1$ and $t(T = T_*) = 0$. We also introduce material dependent order parameter correlation length which we express at $T = T_c$ where it attains its maximal value: $\xi_c=\sqrt{L/a_0(T_c - T_*)}$. We set that that the elastic distortions on $\vec{e}$ (for orientational ordering) or ϕ (for translational ordering) are imposed over the geometrically imposed cell thickness R. In cases of orientational ordering typical elastic distortions are of order $|\nabla\vec{e}\,| \approx 1/R$. In cases of translational ordering we have $\nabla\phi - q_0\vec{e} = (q - q_0)\vec{e}$. Furthermore, the elastic distortions are relatively homogeneously spatially distributed and do not cause substantial melting of ordering. Thus it is sensible to assume that $|\nabla s\,| \approx 0$ and s is consequently spatially homogeneous.

In terms of these quantities and with assumption listed above we express the dimensional free energy expressions as

$\widetilde{F}^{(\alpha)} = (R^{(\alpha)}/\xi_c)^2\, \widetilde{F}_c^{(\alpha)} + \widetilde{F}_e^{(\alpha)}$, where $\alpha = \{i, ii, iii\}$, $R^{(i)} = R^{(ii)} = R$, $R^{(iii)} = d_0$. Furthermore, by performing integration along the cell thickness we obtain

$$\widetilde{F}_c^{(i)} = \widetilde{F}_c^{(iii)} = \int_0^1 \left(t\tilde{s}^2 - 2\tilde{s}^4 + \tilde{s}^6\right)dx \approx t\bar{s}^2 - 2\bar{s}^4 + \bar{s}^6,$$

$$\widetilde{F}_c^{(ii)} = \int_0^1 \left(t\tilde{s}^2 - 2\tilde{s}^3 + \tilde{s}^4\right)dx \approx t\bar{s}^2 - 2\bar{s}^3 + \bar{s}^4,$$

$$\widetilde{F}_e^{(i)} = \widetilde{F}_e^{(ii)} \approx \bar{s}^2,$$

$$\widetilde{F}_e^{(iii)} \approx \bar{s}^2 (d_0/d - 1)^2,$$

where $\bar{s}$ stands for the spatially averaged amplitude of a relevant order parameter. From these relations we express effective dimensionless spatially average condensation terms $\bar{f}_c^{(\alpha)}$ as

$$\begin{aligned}\bar{f}_c^{(i)} &= t\bar{s}^2 - 2\bar{s}^4 + \bar{s}^6 + \bar{s}^2\left(\frac{\xi_c}{R}\right)^2 \\ &= t_{eff}^{(i)}\bar{s}^2 - 2\bar{s}^4 + \bar{s}^6\end{aligned} \quad (4a)$$

$$\bar{f}_c^{(ii)} = t\bar{s}^2 - 2\bar{s}^3 + \bar{s}^4 + \bar{s}^2\left(\frac{\xi_c}{R}\right)^2 = t_{eff}^{(ii)}\bar{s}^2 - 2\bar{s}^3 + \bar{s}^4 \tag{4b}$$

$$\bar{f}_c^{(iii)} = t\bar{s}^2 - 2\bar{s}^4 + \bar{s}^6 + \left(\frac{\xi_c}{d_0}\right)^2 \bar{s}^2 (d_0/d - 1)^2 = t_{eff}^{(iii)}\bar{s}^2 - 2\bar{s}^4 + \bar{s}^6 \tag{4c}$$

We have introduced effective temperatures as $t_{eff}^{(i)} = t_{eff}^{(ii)} = t + \left(\xi_c/R\right)^2$ and $t_{eff}^{(iii)} = t + \left(\xi_c/d_0\right)^2 (d_0/d - 1)^2$. Via minimization of $\bar{f}_c^{(\alpha)}$ we obtain equilibrium values of average amplitudes:

$$\bar{s}_{eq}^{(i)} = \sqrt{\left(2 + \sqrt{4 - 3t_{eff}^{(i)}}\right)/3} \tag{5a}$$

$$\bar{s}_{eq}^{(ii)} = \left(3 + \sqrt{9 - 8t_{eff}^{(ii)}}\right)/4 \tag{5b}$$

$$\bar{s}_{eq}^{(iii)} = \sqrt{\left(2 + \sqrt{4 - 3t_{eff}^{(iii)}}\right)/3} \tag{5c}$$

where the phase transition are realized for $t_{eff}^{(\alpha)} \equiv 1$, for which $\bar{s}_{eq}^{(\alpha)} \equiv 1$. From the critical conditions $t_{eff}^{(\alpha)} \equiv 1$ we obtain the corresponding critical temperature shifts phase changing materials

$$\frac{T_c^{(i)}(R) - T_c}{T_c - T_*} = \frac{T_c^{(ii)}(R) - T_c}{T_c - T_*} = -\left(\xi_c/R\right)^2$$
$$\frac{T_c^{(iii)}(d) - T_c}{T_c - T_*} = -\left(\frac{\xi_c}{d_0}\right)^2 \left(\frac{d_0}{d} - 1\right)^2 \tag{6}$$

Here $T_c^{(\alpha)}\left(R^{(\alpha)}\right)$ mark phase transition temperatures in elastically distorted phase change materials the ordering of which is described by order parameters $Q^{(\alpha)}$.

4 Conclusions

Of our interest are phase-change materials for thermal stabilisation materials. For this purpose we consider systems exhibiting continuous symmetry breaking phase transitions. First of all, such systems should possess a large phase transition latent heat L. In terms of our modelling parameters it can be expressed as $L \approx a_0 T_c \bar{s}^2$. Therefore, a material characterised by a relatively large value of the product $a_0 T_c$ is needed. Secondly, for buildings it is advantageous to have materials with the critical temperature in the ambient temperature regime. For this purpose, one could use appropriate binary mixtures of materials and make use of the "slave-master" mechanism [7]. In this system the "slave" and "master" correspond to the component possessing higher and lower phase transition temperature. The order parameters of the component should be coupled where the coupling strength D could be controlled. By changing the strength D one controls the value of T_c of the "slave". An example represents the coupling between nematic and smectic amplitude order parameter in nCB LCs. In this case the strength of D is controlled by the length of nCB flexible chains [8]. Thus, "slave-master" mechanism could be implemented to tune T_c within a desired temperature window. However, it is difficult to readily control the strength of the coupling constant for "interactive" changes in T_c. For this purpose one could use a relatively sensitive dependence of T_c on a relevant gauge field. The latter could be relatively easily varied either by controlling boundary conditions of the cell confining the phase change material or by changing the confining cell thickness R. Furthermore, to obtain moderate changes in temperature shift it is desirable to have large ration R/ξ_c, where ξ_c is the material dependent length.

References

[1] W. H. Zurek, „Cosmological experiments in condensed matter," Nature, pp. 505-508, 1985.

[2] N. Mermin, „The topological theory of defects in ordered media," Rev. Mod. Phys., Izv. 51, št. 3, pp. 591-648, 1979.

[3] J.-C. Tolédano in P. Tolédano, The Landau Theory of Phase Transitions, Singapore; New Jersey; Hong Kong: World Scientific, 1987.

[4] K. Sanford in N. Gregory, Thermodynamics, Cambridge: Cambridge University Press, 2012.

[5] P. Palffy-Muhoray, „The diverse world of liquid crystals," Physics Today, Izv. 60, št. 9, pp. 54-60, 2007.

[6] P. M. Chaikin in T. C. Lubensky, Principles of condensed matter physics, Cambridge: Cambridge University Press, 1995.

[7] S. Kralj, Z. Bradac in V. Popa-Nita, „The influence of nanoparticles on the phase and structural ordering for nematic liquid crystals," Journal of Physics: Condensed Matter, Izv. 20, št. 24, 2008.

[8] M. Trček, Lavrič, M., G. Cordoyiannis, B. Zalar, B. Rožič, S. Kralj, V. Tzitzos, G. Nounesis in Z. Kutnjak, „Electrocaloric and elastocaloric effects in soft materials," Philosophical transactions. Series A, Mathematical, physical, and engineering sciences, Izv. 374, 2016.

10TH INTERNATIONAL CONFERENCE ON SUSTAINABLE ENERGY AND ENVIRONMENTAL PROTECTION (JUNE 27TH – 30TH, 2017, BLED, SLOVENIA), ENERGY EFFICIENCY
J. Krope, A.Ghani Olabi, D. Goričanec & S. Božičnik

Electrocaloric Effect in Nematic Liquid Crystal Phase

EVA KLEMENČIČ, MAJA TRČEK, ZDRAVKO KUTNJAK & SAMO KRALJ

Abstract The electrocaloric effect (ECE) describes the heating or cooling of an electrocaloric material triggered by switching on or off adiabatically an external electric field. It relies on the exchange between entropic reservoirs related to field-dependent material ordering and other degrees of freedom. In the paper, we demonstrate that liquid crystals (LCs) could be exploited as efficient electrocaloric material. Namely, they could display a relatively large electrocaloric effect close to the isotropic-nematic phase transition. In theoretical modelling, we model orientational LC ordering using Landau - De Gennes mesoscopic approach in terms of the nematic tensor orientational parameter. Numerical investigation reveals in which regime the strongest ECE responses are expected. Our simulation results are in the qualitative agreement with recent high precision calorimetry experimental results.

Keywords: • Electrocaloric effect • Nematic liquid crystals • External field • Entropy • Landau •

CORRESPONDENCE ADDRESS: Eva Klemenčič, Assistant, University of Maribor, Faculty of Natural Sciences and Mathematics, Koroska cesta 160, 2000 Maribor,Slovenia, e-mail: eva.klemencic@um.si. Maja Trček, Young Researcher, Jozef Stefan Institute, Jamova cesta 39, 1000 Ljubljana, Slovenia, e-mail: maja.trcek@ijs.si. Zdravko Kutnjak, Ph.D., Professor, Jozef Stefan Institute, Jamova cesta 39, 1000 Ljubljana, Slovenia, e-mail: zdravko.kutnjak@ijs.si. Samo Kralj, Ph.D., Professor, University of Maribor, Faculty of Natural Sciences and Mathematics, Koroska cesta 160, 2000 Maribor,Slovenia, e-mail: samo.kralj@um.si.

https://doi.org/10.18690/978-961-286-050-9.5 ISBN 978-961-286-050-9

Available at: http://press.um.si.

1 Introduction

Electrocaloric effect (ECE) [1,2] is related to a change in entropy due to an adiabatically applied external electric field $\vec{E}$ yielding the temperature change. ECE has a strong potential for variety of applications, in particular in the future heating and cooling devices.

ECE manifests in dielectric materials as adiabatically applied electric field changes the dielectric subsystem entropy [1,2]. Recently, several studies [3-5] investigated ECE responses in soft materials such as liquid crystals (LCs). LC phases are of constant interest for years from both applicational and fundamental perspectives due to their softness, optical anisotropy and diversity of different phases [6]. Uniaxial bulk nematic (N) phase exhibits a long range orientational order and is typically reached on lowering temperature from isotropic (I) phase via 1st order phase transition [6,7]. In nematic phase, the local orientational ordering of anisotropic LC molecules is commonly described by the nematic director field $\vec{n}$, where $\pm\vec{n}$ states are equivalent and $|\vec{n}|=1$ In bulk N tends to be homogeneously aligned along a symmetry breaking direction.

Recent experimental study [5] reveals that in vicinity of the I-N phase transition temperature T_{IN}, a relatively large ECE response could be achieved. The aim of this paper is to theoretically analyse ECE driven temperature changes in nematic LC close to T_{IN}. The structure of the paper is as follows. In the first section we introduce our mesoscopic modelling. In the second section we derive equations yielding ECE driven temperature changes. Next, numerical simulations are carried out and results are discussed. In the last section, we summarize our results.

2 Modelling

We consider minimal model to describe qualitatively EC effect in nematic LC based on a Landau-de Gennes mesoscopic approach. We describe liquid crystalline orientational uniaxial ordering using the nematic tensor order parameter [8]:

$$\mathbf{Q} = S\left(\vec{n}\otimes\vec{n}-\frac{1}{3}\mathbf{I}\right), \qquad (1)$$

where S is uniaxial order parameter that describes fluctuations around local uniaxial ordering direction represented by unit vector $\vec{n}$. Note that the states $\pm\vec{n}$ are physically equivalent. The symbol $\otimes$ marks a tensorial product and $\mathbf{I}$ is the identity tensor.

The nematic free energy density f can be expressed as a sum of the nematic condensation (f_c), elastic (f_e) and external field (f_f) contributions. These are written as:

$$
\begin{aligned}
f_c &= \frac{3a_0}{2}\left(T-T_*\right) tr\mathbf{Q}^2 - \frac{9b}{2} tr\mathbf{Q}^3 + \frac{9c}{4}\left(tr\mathbf{Q}^2\right)^2, \\
f_e &= L_0 \left|\nabla \mathbf{Q}\right|^2, \\
f_f &= -\frac{3\varepsilon_0 \Delta\varepsilon}{2} \vec{E}.\mathbf{Q}\vec{E}.
\end{aligned} \tag{2}
$$

Here a_0, b and c are positive material constants; T stands for temperature and T_* is the isotropic phase supercooling temperature. The bulk I-N first order phase transition temperature is given by $T_{IN} = T_* + b^2/(4a_0c)$. The elastic contribution penalizes departures from a spatially homogeneous orientational ordering by the positive elastic constant L_0. The field term describes the impact of an external electric field $\vec{E}$, where ε_0 and $\Delta\varepsilon$ stand for the dielectric permittivity constant and dielectric anisotropy respectively. We limit to EC effects in bulk and set that $\vec{n}$ is homogeneously aligned along a single symmetry direction. Furthermore, we assume that $\vec{E}$ is imposed along the same direction.

For analytical convenience we introduce scaled quantities. With this aim we introduce the nematic uniaxial correlation length ξ_n and the nematic external field extrapolation length ξ_e at $T \sim T_{IN}$:

$$
\xi_n = \sqrt{\frac{L_0}{a_0(T_{IN}-T_*)}}, \xi_e = \sqrt{\frac{L_0 S_0}{\varepsilon_0 \Delta\varepsilon E^2}}. \tag{3}
$$

Here S_0 is equilibrium value of the uniaxial order parameter at the phase transition in absence of an external field. We introduce the following scaled and dimensionless quantities:

$$
\tilde{S} = \frac{S}{S_0},\ t = \frac{T-T_*}{\Delta T_0}, \sigma = \left(\frac{\xi_n}{\xi_e}\right)^2, \tag{4}
$$

where $\Delta T_0 = T_{IN} - T_*$. In this scaling, the dimensionless free nematic energy density $\tilde{f} = f / \left(a_0 S_0^2 \Delta T_0\right)$ is expressed as

$$\tilde{f} = t\tilde{S}^2 - 2\tilde{S}^3 + \tilde{S}^4 - \sigma\tilde{S}. \tag{5}$$

In the absence of an external electric field for $\sigma = 0$ the I-N phase transition occurs at $t_c = 1$ where $S_c = 1$, and the supercooling (overheating) temperature takes place at $t_* = 0$ ($t_{**} = 9/8$).

For $\sigma > 0$ isotropic ordering is replaced by the paramagnetic P ordering that is a relatively weakly orientationally ordered isotropic phase. P-N phase transition temperature increases with σ until the critical value $\sigma_c = 0.5$ is reached. For $\sigma < \sigma_c$ it holds $t_c[\sigma] = 1 + \sigma$ corresponding to:

$$T_{IN}[\sigma] - T_{IN}[0] = \Delta T_0 \sigma. \tag{6}$$

Above the critical value, the P-N transition becomes supercritical.

3 Ece Response

We analyse typical ECE responses at the I-N transitions. The entropy of the system can be expressed as a sum of orientational LC ordering contribution $\Omega_{LC}[\sigma, T]$ and lattice contribution $\Omega_l[T]$:

$$\Omega[\sigma, T] = \Omega_{LC}[\sigma, T] + \Omega_l[T]. \tag{7}$$

Orientational LC ordering contribution can be directly manipulated by an external field. Our focus is a temperature change due to adiabatic switching on or off of the external field. In the adiabatic process the total change of entropy equals zero, therefore:

$$\Delta\Omega_{LC} = \Delta\Omega_l, \tag{8}$$

where $\Delta\Omega_{LC} = \Omega_{LC}\left[\sigma_2, T_2\right] - \Omega_{LC}\left[\sigma_1, T_1\right]$ and $\Delta\Omega_l = \Omega_l\left[T_2\right] - \Omega_l\left[T_1\right]$. Here subscripts "1" and "2" refer respectively to the initial state $\{\sigma_1, T_1\}$ and the final state $\{\sigma_2, T_2\}$ of the adiabatic process. The change in lattice entropy is given by:

$$\Delta\Omega_l = \int \frac{C_l\left[T\right]}{T} dT \approx C_l\left[T\right] \ln\left(T_2 / T_1\right), \tag{9}$$

where $C_l\left[T\right]$ is the lattice heat capacity per unit volume. Constant value of $C_l\left[T\right]$ is assumed within the temperature interval [T_1, T_2]. The orientational LC ordering contribution can be expressed as the partial derivative at a constant value of σ:

$$\Omega_{LC}\left[\sigma, T\right] = -\left[\frac{\partial f}{\partial T}\right]_E = -a_0 S^2. \tag{10}$$

Combining Eq.(8) and Eq.(9) we obtain a self-consistent equation for T_2:

$$T_2 = T_1 \exp\left(\frac{a_0}{C_l}\left(S^2\left[\sigma_2, T_2\right] - S^2\left[\sigma_1, T_1\right]\right)\right) \tag{11}$$

In the following examples, we consider cases where $\sigma_1 = 0$, $T_1 \equiv T > T_{IN}$ and $\sigma_2 = \sigma > 0$, $T_2 \equiv T + \Delta T > T_{IN}$. We switch on the field in the isotropic phase where $S^2\left[\sigma = 0, T_1\right] = 0$.

Assuming $\Delta T / T << 1$ it holds:

$$\Delta T / T \sim S^2\left[T + \Delta T\right] a_0 / C_l. \tag{12}$$

Using dimensionless quantities, we express Eq.(12) for the ECE response and the equilibrium equation $\partial f / \partial S = 0$ determining degree of nematic order at $T = T_2$ as:

$$\begin{aligned} &t_2 - t_1 - \gamma \tilde{S}^2 = 0, \\ &2t_2\tilde{S} - 6\tilde{S}^2 + 4\tilde{S}^3 - \sigma = 0. \end{aligned} \tag{13}$$

Here $t_1 \equiv t\left[T_1\right]$, $t_2 \equiv t\left[T_2\right]$, $\tilde{S} = \tilde{S}\left[t_2\right]$ and

$$\gamma = \frac{a_0 T_* S_0^2}{C_l \Delta T_0}. \tag{14}$$

For common LCs close to T_{IN} it holds a_0 ~10^5 J/Km^3, T_* ~300 K, ΔT_0 ~ 1 K, S_0 ~0,3, and C_l ~ $4 \cdot 10^6$ J/m^3. Therefore, γ ~ 1, $T_* / \Delta T_0 > 100$ and $t + T_* / \Delta T_0$ ~ $T_* / \Delta T_0$.

4 Results

Of our interest is an external field driven thermal change just above the I-N phase transition where one expects largest ECE response. By applying a strong enough external field, the field-induced phase transition into nematic ordering could be realized. Consequently, the change in orientational entropy would be relatively large, leading to relatively large ΔT , see Eq.(11). If the initial temperature T_1 is close above $T_{IN}[\sigma = 0]$ on applying the field, the condition $T_{IN}[\sigma] > T_1$ could be realized, see Eq.(6). In dependence of ΔT value different scenario could be experimentally realized because T_2 might fall within a bistable temperature regime.

For this purpose we first determine the bistability regime, where both N and P phase can exist for fields ranging from $\sigma = 0$ to $\sigma = 0.5 \equiv \sigma_c$. In Figure 1 we demonstrate typical temperature variation of nematic ordering in presence of an external field for cases $\sigma < \sigma_c$. The phase transition takes place at $t_c = 1 + \sigma$. On gradually increasing temperature above $t_c[\sigma]$ nematic ordering could persist in metastable state till $t_{**}[\sigma]$. Alternatively, on gradually decreasing temperature isotropic (paranematic) ordering could persist below $t_c[\sigma]$ till $t_*[\sigma]$. The bistability regime is depicted in Figure 2.

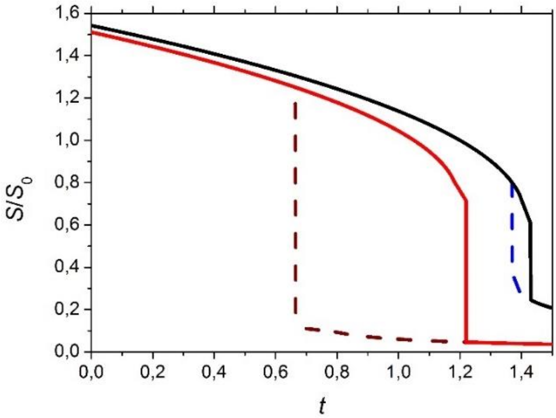

Figure 1. The order parameter variation on increasing (solid line) and decreasing (dashed line) temperature for an external field σ = 0,1 (red) and σ = 0,4 (blue). The corresponding phase transition temperatures are equal to t_c = 1.1 and t_c = 1.4, respectively.

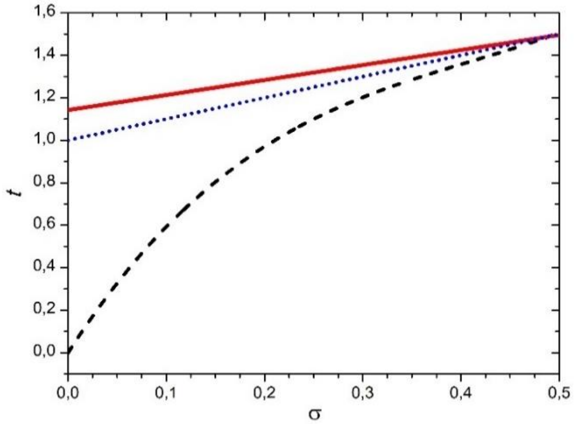

Figure 2. Supercooling (t_*: black dashed line), overheating (t_{**}: red solid line) and phase transition (t_c: blue dotted line) temperatures as a function of an external field strength σ.

We next numerically calculate the ECE response where initial temperature is just above T_{IN}. In Figures 3 we plot typical EC responses following the adiabatic switching on of an external dimensionless field σ for different initial temperatures $T_1 > T_{IN}[\sigma = 0]$. In Figure 3a we plot $S = S[\sigma, T_1]$, and in Figure 3b the accompanying $\Delta T = \Delta T[\sigma, T_1]$

dependencies. One sees that on decreasing T_1 towards T_{IN}, the dependencies monotonously exhibit increasingly steeper and larger s-shape type responses. Note that for γ = 1 these responses are subcritical.

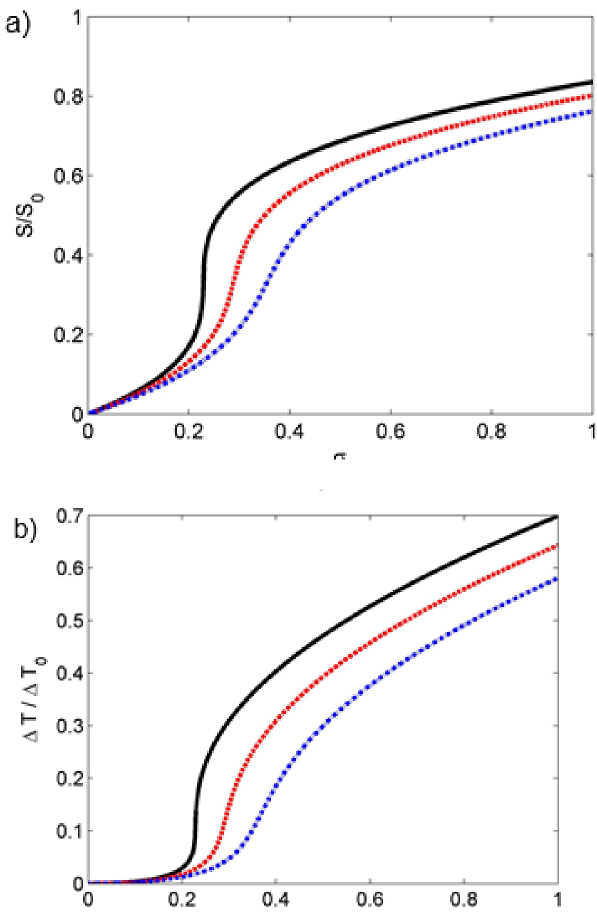

Figure 3. a) The nematic response $S(T_2 = T_1 + \Delta T)$. b) Temperature increase $\Delta T = T_2 - T_1$. Black full line: $(T_1 - T_{IN})/\Delta T_0 = 1.01$, red dashed line $(T_1 - T_{IN})/\Delta T_0 = 1.1$, blue dash-dotted line: $(T_1 - T_{IN})/\Delta T_0 = 1.2$, $\gamma = 1$, $\Delta T_0 = T_{IN} - T_*$ ~1 K.

Next, we analyze behavior on varying γ, which measures relative importance of nematic and remaining degrees of freedom entering the entropy expression. We limit to a temperature T_1 close to T_{IN} where the EC responses are relatively large. Figure 4a reveals that on decreasing γ the $S = S[\sigma]$ dependency becomes steeper and below some critical value of γ exhibits a 1st order-type phase transition. The related temperature ΔT responses are shown in Figure 4b. One sees that despite a relatively weaker contribution of the nematic contribution in Ω the responses could be larger due to the observed discontinuous response.

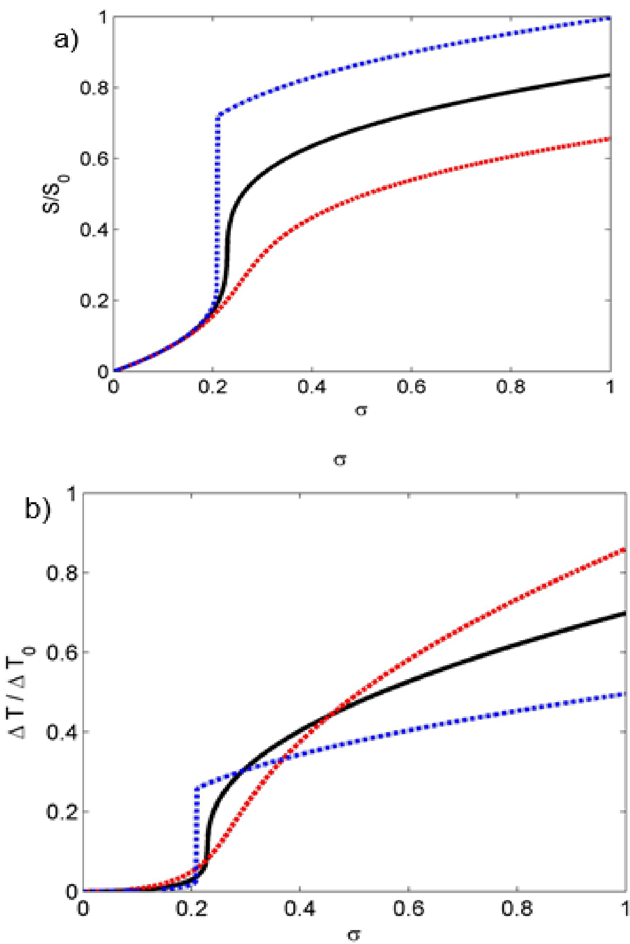

Figure 4. a) Nematic response $S(T_2)$. b) Temperature increase ΔT. Black full line: $\gamma = 1$, red dashed line $\gamma = 2$, blue dash-dotted line: $\gamma = 0.5$.

$$(T_1 - T_{IN}) / \Delta T_0 = 1.01.$$

5 Conclusions

We studied the ECE response close to the isotropic-nematic phase transition. We first derived the equation yielding the temperature change on applying adiabatically an external field. In deriving it, we assumed that the total change in entropy equals zero. By equating the entropy change in orientational degree of freedom with the entropy change in *lattice* contribution, we arrived at the equation relating the change in temperature with the change in orientational ordering. We calculated nematic ordering from the equilibrium Euler Lagrange equation in presence of an external field. Thus, we assumed that the nematic order parameter relaxation time is much shorter with respect to the characteristic thermal relaxation time. We first determined the bistability regime where both isotropic (paranematic) and nematic phase could be (meta) stable. This calculation reveals the regime where results might be in addition to the external field value also "history" dependent. Then we numerically analysed the ECE response as a function of temperature and LC material properties. The results indicate that the largest responses are expected just above the I-N phase transition that is in line with recent experimental measurements [5]. In the near future we intend to calculate the ECE response close to the direct Isotropic-Smectic A phase transition, which is for example realized in 12CB LC. We expect even stronger ECE responses because smectic ordering plays an effectively similar role as an external field. Therefore, on applying an external field, its effect is expected to be enhanced by smectic layer formation

Acknowledgements

SK acknowledges the financial support from the Slovenian Research Agency (research core funding No. P1-0099).

References

[1] T. Correia and W. Zhang, *Electrocaloric materials*, Berlin: Springer-Verlag Berlin Heidelberg, 2014.
[2] Z. Kutnjak, B. Rožič, R. Pirc, „Electrocaloric effect: Theory, Measurrements, and Applications," *Wiley Encyclopedia of electrical and electronics engineering*, pp. 1-19, March 2015.
[3] H de J Wim, *Liquid crystal elastomers: Materials and applications,* Berlin: Springer-Verlag Berlin Heidelberg, 2012.
[4] I. Küpfer, H. Finkelmann, „Nematic liquid single crystal elastomers," *Makromol. Chem. Rapid Commun,* vol. 45, pp. 717-726, Dec. 1991.
[5] M. Trček et al, „Electrocaloric and elastocaloric effects in soft materials," *Philos Trans A Math Phys Eng Sci.,* vol. 374, Aug. 2016.
[6] M. Kleman and O. D. Lavrentovich, *Soft matter Physics,* Berlin: Springer-Verlag Berlin Heidelberg, 2002.
[7] S. Tripathi, C. Rosenblatt, F. M. Aliev, „Orientational susceptibility in porous glass near a bulk nematic-isotropic phase transition", *Physical review letters,* vol.72, pp. 2725-2728, 1994.

[8] S. Kralj, A. Majumdar, "Order reconstruction patterns in nematic liquid crystal wells," *Proceedings of The Royal Society of London, Series A: Mathematical, Physical and Engineering Sciences*, vol. 470, 18 pages, 2014.

10TH INTERNATIONAL CONFERENCE ON SUSTAINABLE ENERGY AND ENVIRONMENTAL PROTECTION (JUNE 27TH – 30TH, 2017, BLED, SLOVENIA), ENERGY EFFICIENCY
J. Krope, A.Ghani Olabi, D. Goričanec & S. Božičnik

Comparative Study on the Thermal Performance and Environmental Footprint of Traditional and Contemporary Masonry Systems Used in Southern Europe

ANDREAS KYRIAKIDIS, AIMILIOS MICHAEL, ROGIROS ILLAMPAS, DIMOS C. CHARMPIS & IOANNIS IOANNOU

Abstract This paper presents a comparative computational study on the thermal performance and environmental impact of traditional and contemporary walling systems. Three types of building elements were examined: vernacular adobe load-bearing walls, and contemporary thermally insulated infill walls composed of either fired clay bricks or drywall panels. Their behaviour under thermal loads was investigated by means of heat flux analysis using 3D Finite Element (FE) models. The environmental footprint was assessed in terms of the walls' total embodied energy. According to the outcomes obtained, contemporary masonry systems have lower thermal transmittance compared to traditional constructions. However, adobe walls are capable of providing thermal comfort by efficiently controlling temperature fluctuations, mainly due to their higher thermal mass. The results also highlight the limited footprint of traditional earthen structures; this is attributed to the simple construction processes adopted and the use of local raw materials.

Keywords: • Heat flux analysis • Time lag • Embodied energy • Decrement factor • Masonry systems •

CORRESPONDENCE ADDRESS: Andreas Kyriakidis, Ph.D Student, Research Associate, University of Cyprus, Department of Architecture, 75 Kallipoleos Street, 1678, Nicosia, Cyprus, e-mail: kyriakidis.andreas@ucy.ac.cy. Aimilios Michael, Ph.D., Lecturer, University of Cyprus, Department of Architecture, 75 Kallipoleos Street, 1678, Nicosia, Cyprus, e-mail: aimilios@ucy.ac.cy. Rogiros Illampas, Ph.D., Post-Doctoral Researcher, University of Cyprus, Department of Architecture, 75 Kallipoleos Street, 1678, Nicosia, Cyprus, e-mail: rilamp01@ucy.ac.cy. Dimos C. Charmpis, Ph.D., Associate Professor, University of Cyprus, Department of Civil and Environmental Engineering, 75 Kallipoleos Street, 1678, Nicosia, Cyprus, e-mail: charmpis@ucy.ac.cy. Ioannis Ioannou, Ph.D., Associate Professor, University of Cyprus, Department of Civil and Environmental Engineering, 75 Kallipoleos Street, 1678, Nicosia, Cyprus, e-mail: ioannis@ucy.ac.cy.

https://doi.org/10.18690/978-961-286-050-9.6 ISBN 978-961-286-050-9

Available at: http://press.um.si.

1 Introduction

Masonry walls are responsible for 29-59% of the thermal losses in buildings [1]. Furthermore, masonry manufacturing and construction accounts for 13% of the total energy consumed during the building process [2-3]. This highlights the importance of assessing the thermal performance and environmental footprint of masonry systems.

Several studies have been undertaken to determine the U-value of masonry (e.g. [4]). More recently, particular emphasis has been given on examining the thermal mass of walls [5-11], as this is considered a good indicator of thermal behaviour for moderate climates (e.g. Mediterranean climate). The main parameters used to describe the influence of thermal mass are the time lag and the decrement factor [5]. Time lag refers to the time it takes for the temperature wave to propagate from the outer to the inner surface, while decrement factor refers to the decreasing ratio of its temperature amplitude [5]. According to [12], an effective environmental design strategy should include a detailed consideration of the building elements' thermal mass. In general, if a wall exhibits high time lag and low decrement factor it will limit indoor air temperature fluctuations, thus enhancing the feeling of thermal comfort.

Following a numerical study on the time lag and decrement factor of different materials, Asan [5] concluded that the thickness of the building element critically affects its thermal mass. According to Zhang et al [10] and Kontoleon et al [11], who examined the thermal inertia parameters of walls, an increase in the heat capacity of a masonry layer would increase time lag and decrease decrement factor, while an increase in the thermal conductivity of a masonry layer would have the opposite effect. The influence that the thickness and distribution of insulation layers pose on the walls' time lag and decrement factor were examined in [7], [9]. Experimental measurements [8], [12] have shown that indoor temperatures in vernacular buildings have limited fluctuation due to the high thermal mass offered by traditional load-bearing adobe walls. Fgaier et al. [8], who experimentally studied the thermophysical properties of unfired earth bricks, noted that a thermal lag of 10-12 hours can be achieved with a 30-40 cm thick wall. Asan [5] mentions time lags > 8 hours for 30 cm thick adobe walls.

Another important aspect of the overall environmental performance of masonry systems is embodied energy. This is the energy consumed by all processes associated with the production and construction of a building element (i.e. from the quarrying and processing of raw materials to the manufacture, transport, delivery, handling and assemblage of the end-products). Thormark [13] states that, in a life span of 50 years, embodied energy can account for up to 45% of the total energy need in buildings. Masonry walls, in particular, constitute one of the major energy consuming building components [14]. Significant energy savings can be achieved when using alternative construction materials and techniques. Research has shown that unfired earth blocks are environmentally friendly [15] and their use entails much lower embodied energy compared to ceramic bricks [16] and concrete blocks [17]. However, conventional masonry laying construction techniques are considered to be more energy demanding than methods involving the use of pre-fabricated panellised frame systems [18].

In light of the above, the present study aims to compare both the thermal and environmental performance of traditional and contemporary masonry systems used in Southern Europe. Heat flux analyses were carried out using finite element models of adobe and fired clay brick walls and drywall panels to assess their U-value, time lag and decrement factor. The embodied energy of the wall systems under study was also computed using relevant data from the literature

2 Methodology

2.1 Masonry systems under study

Focus was given on examining three distinctly different walling systems that are encountered in many countries of Southern Europe. These include the thermally insulated fired clay brick walls and exterior drywall panels commonly used as infills in contemporary concrete and steel structures, and the load-bearing adobe walls incorporated in many vernacular buildings.

More specifically, the following typical configurations of wall elements were studied:

(a) *MS1*: A 30 cm thick wall constructed of perforated fired clay bricks arranged in a running bond pattern with 1 cm thick cement mortar joints between them. A 5 cm thick extruded polystyrene board is fixed on the exterior surface of the masonry, while both sides of the wall are coated with 2.5 cm thick cement plaster.

(b) *MS2*: A 12 cm thick drywall panel. This consists of a metal framework (i.e. ‘C’ channels 0.1 cm thick placed vertically every 60 cm) with a 2.5 cm thick gypsum board on the interior side and a 1.25 cm thick cement board on the exterior side. The cement board is coated with a 0.75 cm layer of cement plaster. At the core of the system, 7.5 cm thick rock wool is installed.

(c) *MS3*: A 50 cm thick load-bearing masonry wall. The wall features a foundation made of natural stone building blocks. Above this, adobe bricks are set with the application of thin layers (0.5 cm) of earth mortar. Adobe masonry is coated with 2.5 cm layers of lime plaster both internally and externally.

The characteristics of the aforementioned systems’ constituent materials are shown in Table 1. The values of the physical and thermal properties were adopted from EN 1745 [19], while embodied energy data were derived from the literature [2], [15]

Table 1. Constituent material properties for contemporary and traditional masonry systems

Material	Thermal Conductivity λ (W/mK)	Density ρ (kg/m)	Specific heat C_p (J/kgK)	Embodied Energy E (MJ/kg)
MS1: Fired clay Brick with External Thermal Insulation				
Fired clay Brick Polystyrene	0.40 0.03	1000 30	1000 1450	3 88
Cement mortar	0.82	1800	1000	1.55
MS2: Lightweight Drywall System				
Gypsum Board	0.25	900	1000	3.48
Cement Board	0.36	1150	1000	6.75
Framework Steel	50	7800	450	45.68
Rock Wool	0.035	140	1030	16.8
MS3: Traditional Adobe Masonry Wall				
Stone	1.40	1900	1000	0.3
Adobe brick	0.55	1350	1000	0.033
Lime mortar	0.61	1600	1000	1.8

2.2 Thermal Performance

To evaluate the thermal performance of the various walling systems, 3D numerical models were developed in Comsol Multiphysics 5.2. Each model represents a square meter of the system considered. The models were discretized into 4-noded tetrahedral elements with an average side length of 0.02 m. Adiabatic boundary conditions were assumed at the four side edges of the simulated walls. FE analysis was performed to simulate the 3D heat transfer through the walls and the corresponding temperature distribution. To calculate each system's U-value, steady-state analyses were performed. Time-dependent transient heat analyses were conducted to estimate the time lag and decrement factor.

The thermal transmittance of each system was calculated by the following equation:

$$U = \frac{Q}{\Delta T \cdot A}, \tag{1}$$

where Q is the total heat flux at the external surface, ΔT is the temperature difference between the internal and external wall surfaces, A is the external surface of the wall. The internal and external air temperatures during the steady-state analyses were set as T_{si}= 25°C and T_{se}= 15°C.

The thermal inertia parameters, time lag (φ) and decrement factor (f), of each system were defined as [6], [13]:

$$\phi = t_{Ti,\max} - t_{Te,\max}, \tag{2}$$

$$f = \frac{T_{i,\max} - T_{i,\min}}{T_{e,\max} - T_{e,\min}} \tag{3}$$

In (2) and (3), $t_{Ti,max}$ and $t_{Te,max}$ indicate the instances of time when the temperatures at the interior and exterior surfaces of the walls reach their peak values. $T_{i,max}$, $T_{i,min}$, $T_{e,max}$ and $T_{e,min}$ correspond to the maximum and minimum temperatures generated at the walls' interior and exterior surfaces.

Numerical calculations were based on the assumption that heat transfer is governed by conduction without heat generation:

$$\nabla \cdot (\lambda \nabla \mathrm{T}) = \rho \cdot C_p \cdot \frac{\partial T}{\partial t}, \tag{4}$$

where λ is the thermal conductivity, ρ is the density and C_p is the specific heat of the material.

The boundary conditions at the exterior and interior surfaces of the walls were provided by eqs. (5) and (6), respectively:

$$-\lambda \nabla \mathrm{T} = h_e \cdot (T_{sa} - T_e), \tag{5}$$

$$-\lambda \nabla \mathrm{T} = h_i \cdot (T_i - T_{in}), \tag{6}$$

where h_e, h_i are the exterior and interior surface heat transfer coefficients due to combined convection and radiation, T_{sa} is the sol-air temperature, T_e is the temperature at the exterior surface of wall, T_i is the interior surface temperature and T_{in} is the indoor air temperature.

For the dynamic heat analyses, sinusoidal variations of the sol-air temperature were considered over a 24-hour period [5]:

$$T_{sa}(t) = \frac{T_{max} - T_{min}}{2} \cdot sin(\frac{2\pi t}{P} - \frac{\pi}{2}) + \\ + \frac{T_{max} - T_{min}}{2} + T_{min} \tag{7}$$

In equation (7), P is the period (86400s), while T_{max} and T_{min} are the maximum and minimum outdoor temperatures, respectively. The following assumptions are made in this study based on data of [20]: T_{max}= 35°C, T_{min}= 15°C, T_{in}= 25°C, h_e= 25 W/m^{2}K, h_i= 7.7 W/m^{2}K . In all cases, the walls' interior surface at the beginning of the dynamic analysis was considered to have a uniform temperature of T= 25°C.

2.3 Environmental Footprint

Embodied energy was hereby adopted as the primary environmental footprint indicator. The total embodied energies of the fired clay masonry and of the drywall systems were estimated using the 'cradle-to-gate' data given in the Inventory of Carbon and Energy (ICE) database of the University of Bath [2]. In the case of adobe masonry, the 'cradle-to-site' data reported in [15] were used, instead, since adobe bricks were traditionally manufactured on-site.

Initially, the mass of each constituent material was calculated based on the volume (V) it occupies per m^3 of wall system and its specific density (ρ):

$$M = \rho \cdot V . \tag{8}$$

The total embodied energy (e_E) of the wall system was then computed as the sum of the products between each constituent material's mass M (kg) and embodied energy E (MJ/kg):

$$e_E = \sum_{i=m}^{n} E_{,m} \cdot M_{,m} + E_{,m+1} \cdot M_{,m+1} + ... + E_{,n} \cdot M_{,n} \tag{9}$$

3 Results and Dissussion

3.1 U-Value

The results obtained from the steady-state thermal numerical analyses are presented in Figure 1. Contour diagrams of heat flux for all cases hereby considered are given in Figure 2.

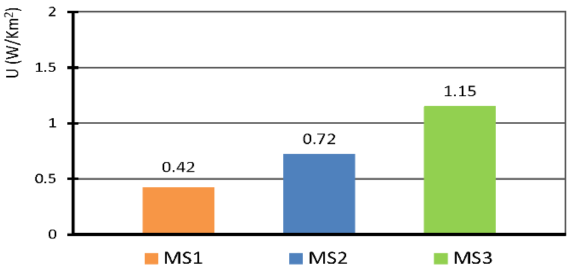

Figure 1. Computed U-values for the masonry systems under study.

The U-value of *MS1* is 0.42 W/m^{2}K and is the lowest determined. The numerical analysis predicts that higher heat fluxes will develop at the vicinity of the mortar joints (Figure 2a). However, the continuous insulation layer installed at the external surface of the wall prevents the development of thermal bridges.

The U-value obtained in the case of *MS2* is in the region of 0.7 W/m^{2}K, while the corresponding result for *MS3* exceeds 1 W/m^{2}K. The inferior thermal transmittance of *MS3* is primarily attributed to the absence of any insulation. The rather high thermal conductivity of the adobe wall's stone base also affects the overall performance of the system, since increased heat flux tends to develop at this section (Figure 2c). A similar phenomenon is observed in *MS2*, where the metal frame of the drywall panel tends to act as a thermal bridge promoting heat concentration (Figure 2b). These results are in agreement with the observations of other researchers regarding the effect of thermal bridges on the behaviour of wall elements [21].

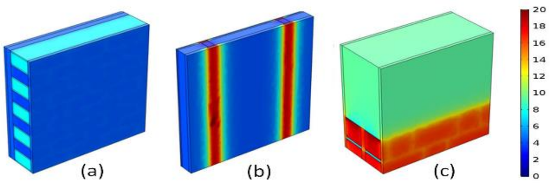

Figure 2. Heat flux through the masonry systems under study: (a) MS1; (b) MS2 and (c) MS3

3.2 Time lag and decrement factor

The time lag and decrement factor values that were computed from the time-dependent numerical analyses are presented in Figures 3 and 4. Figure 5 shows the temperature fluctuations on the exterior and interior surfaces of all simulated systems.

According to the outcomes obtained, *MS2* has the lowest time lag (3 hours). This result is in line with the data reported in [5]. The estimated time lag of *MS3* exceeds 10 hours and is the highest among the three systems under study. This value is within the range of analogous results found in [5]. The transient analysis gave a prediction of 5.6 hours for the time lag of the *MS1* masonry wall. This is slightly lower than the 6-7 hours reported in [5] and [9] for analogous construction configurations.

The importance of the thermal mass in indoor comfort conditions is further highlighted by the decrement factor results. The *MS1* and *MS3* walls have decrement factors in the region of 0.005-0.006, whereas the corresponding value for *MS2* is an order of magnitude higher: 0.07. These outcomes are in total agreement with the decrement factors obtained in similar studies [5] [8], [9].

The numerically predicted temperature fluctuation at the interior surface of the various systems verifies the superior thermal performance of masonry walls compared to drywall panels. As shown in Figure 5, *MS1* and *MS3* can retain almost constant indoor surface temperatures. Some degree of temperature fluctuation is expected to occur at the interior surface of the much thinner *MS2* drywall panel.

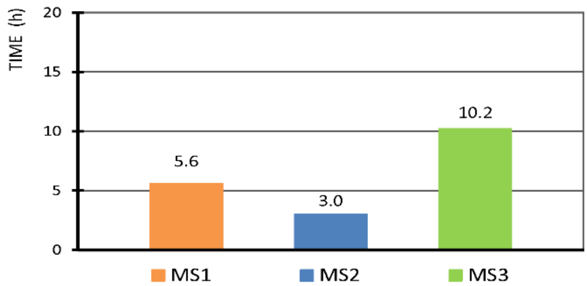

Figure 3. Estimated time lag for the masonry systems under study

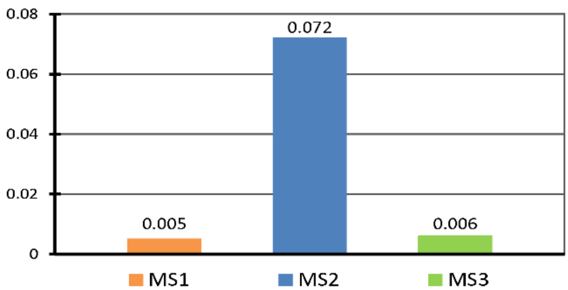

Figure 4. Estimated decrement factor for the masonry systems under study

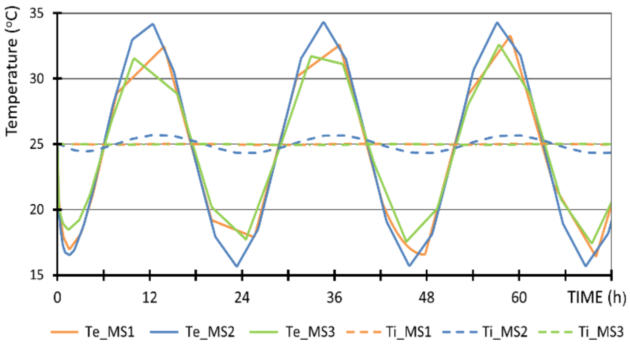

Figure 5. Simulated temperature fluctuations on the external and internal surface of the masonry systems under study

3.5 Embodied energy

The embodied energy values computed for the different masonry systems are presented in Figure 6. As expected, MS3 has the lowest environmental footprint: 229 MJ/m2. This is due to the simple manufacturing processes involved in the fabrication of adobe bricks and the relatively low energy required for the production of stone blocks. MS2 and MS3 have significantly higher environmental footprints: 489 MJ/m2 and 723 MJ/m2, respectively. This is mainly due to the use of insulation materials with rather high embodied energies. The energy intensive industrial procedures involved in the manufacturing of polystyrene and rock wool increases the total energy requirements for these systems. The firing process used for the production of the masonry units composing MS1 also negatively influences this system's environmental performance. In line with the data hereby reported, many studies emphasize the energy savings achieved when using unfired earth instead of fired clay ceramics [15], [16].

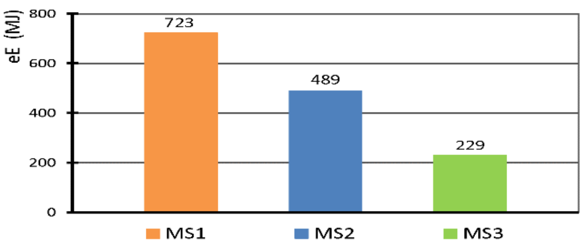

Figure 6. Estimated embodied energy for the masonry systems under study

4 Conclusions

A comparative study of the thermal performance and environmental footprint of traditional and contemporary masonry systems used in Southern Europe has been conducted.

The thermal performance of the investigated systems was evaluated in terms of U-value, time lag and decrement factor. Steady-state and transient thermal analyses were conducted to compute the aforementioned indicators. The results have shown that thermally insulated fired clay brick masonry has the lowest U-value. Despite its rather high U-value, adobe masonry can provide sufficient thermal comfort due to its considerable thermal mass. Drywall systems, on the other hand, exhibit lower time lag and higher decrement factor. The overall thermal performance of walling systems is clearly affected by the presence of thermal bridges and by the thickness of the building elements.

The total embodied energy values hereby computed verify the environmentally friendly character of earthen architecture. Contemporary fired clay brick masonry and drywall panel systems have higher embodied energies, since the industrial procedures involved in the manufacturing of their constituent materials increases energy consumption

References

[1] C. A. Balaras, K. Droutsa, A. A. Argiriou, and D. N. Asimakopoulos, "Potential for energy conservation in apartment buildings," *Energy Build.*, vol. 31, no. 2, pp. 143–154, 2000.
[2] P. G. Hammond and C. Jones, "Inventory of Carbon & Energy (ICE)," *Mech. Eng.*, vol. 161, pp. 1–49, 2006.
[3] C. I. Jones and G. P. Hammond, "Embodied energy and carbon in construction materials," *Proc. ICE - Energy*, vol. 161, no. 2, pp. 87–98, 2008.
[4] D. Bikas, and P. Chastas, "Environmental Assessment of Typical Construction Solutions in Residential Buildings in Greece," Journal of Sustainable Architecture and Civil Engineering, 6(1), pp. 18-26, 2014a.
[5] H. Asan, "Numerical computation of time lags and decrement factors for different building materials," *Build. Environ.*, vol. 41, no. 5, pp. 615–620, 2006.
[6] X. Jin, X. Zhang, Y. Cao, and G. Wang, "Thermal performance evaluation of the wall using heat flux time lag and decrement factor," *Energy Build.*, vol. 47, pp. 369–374, 2012.
[7] M. Ozel and K. Pihtili, "Optimum location and distribution of insulation layers on building walls with various orientations," *Build. Environ.*, vol. 42, no. 8, pp. 3051–3059, 2007.
[8] F. El Fgaier, Z. Lafhaj, E. Antczak, and C. Chapiseau, "Dynamic thermal performance of three types of unfired earth bricks," *Appl. Therm. Eng.*, vol. 93, pp. 377–383, 2016.
[9] S. A. Al-Sanea and M. F. Zedan, "Improving thermal performance of building walls by optimizing insulation layer distribution and thickness for same thermal mass," *Appl. Energy*, vol. 88, no. 9, pp. 3113–3124, 2011.
[10] L. Zhang, J. Zhang, F. Wang, and Y. Wang, "Effects of wall masonry layers thermophysical properties and insulation position on time lag and decrement factor," *Indoor Built Environ.*,

vol. 25, no. 2, pp. 371–377, 2016.

[11] K. J. Kontoleon, T. G. Theodosiou, and K. G. Tsikaloudaki, “The influence of concrete density and conductivity on walls’ thermal inertia parameters under a variety of masonry and insulation placements,” *Appl. Energy*, vol. 112, pp. 325–337, 2013.

[12] A. Michael, D. Demosthenous, and M. Philokyprou, “Natural Ventilation for Cooling in Mediterranean Climate: A Case Study in Vernacular Architecture of Cyprus,” *Energy Build.*, 2017.

[13] C. Thormark, “A low energy building in a life cycle—its embodied energy, energy need for operation and recycling potential,” *Build. Environ.*, vol. 37, no. 4, pp. 429–435, 2002.

[14] B. V. Venkatarama Reddy and K. S. Jagadish, “Embodied energy of common and alternative building materials and technologies,” *Energy Build.*, vol. 35, no. 2, pp. 129–137, 2003.

[15] E. Christoforou, A. Kylili, P. A. Fokaides, and I. Ioannou, “Cradle to site Life Cycle Assessment (LCA) of adobe bricks,” *J. Clean. Prod.*, vol. 112, pp. 443–452, 2016.

[16] F. Pacheco-Torgal and S. Jalali, “Earth construction: Lessons from the past for future eco-efficient construction,” *Constr. Build. Mater.*, vol. 29, pp. 512–519, 2012.

[17] C. Galán-Marín, C. Rivera-Gómez, and A. García-Martínez, “Embodied energy of conventional load-bearing walls versus natural stabilized earth blocks,” *Energy Build.*, vol. 97, pp. 146–154, 2015.

[18] J. Monahan and J. C. Powell, “An embodied carbon and energy analysis of modern methods of construction in housing: A case study using a lifecycle assessment framework,” *Energy Build.*, vol. 43, no. 1, pp. 179–188, 2011.

[19] EN 1745, 2012. Masonry and masonry products. Methods for determining thermal properties, Brussels: CEN.

[20] EN ISO 6946: 2007. Building components and building elements – Thermal resistance and thermal transmittance – Calculation method.

[21] T. G. Theodosiou and A. M. Papadopoulos, “The impact of thermal bridges on the energy demand of buildings with double brick wall constructions,” *Energy Build.*, vol. 40, no. 11, pp. 2083–2089, 2008.

10TH INTERNATIONAL CONFERENCE ON SUSTAINABLE ENERGY AND ENVIRONMENTAL PROTECTION (JUNE 27TH – 30TH, 2017, BLED, SLOVENIA), ENERGY EFFICIENCY
J. Krope, A.Ghani Olabi, D. Goričanec & S. Božičnik

Ldm Compact – a Highly Efficient Method for Developing Gas Engines for Use with Low Environmental Impact Non-Natural Gas

GERHARD PIRKER, EDUARD SCHNEßL, IGOR ŠAUPERL & ANDREAS WIMMER

Abstract Today's large gas engines have reached an advanced state of development and are being used to efficiently generate low emission energy. Besides natural gas, non-natural gases (NNG) such as waste gases from industrial processes, landfill gas and flare gas can be used to operate these engines. Using NNG reduces CO2 emissions and replaces natural gas from fossil fuel sources. The special characteristics of the individual NNG require tailor made engine solutions. Additionally, the cost of development of combustion concept design and optimization must be kept down. LDM COMPACT represents a methodology that permits highly efficient development of combustion concepts for NNG without the need for extensive testing on a multicylinder engine.

This paper introduces the general approach of LDM. The fundamentals and main innovative features of the methodology are outlined. A recent development project along with its results is provided as an example of an application.

Keywords: • Development methodology• Gas engines • Combustion concept• Non-natural gas • Blast furnace gas

---

CORRESPONDENCE ADDRESS: Gerhard Pirker, Ph.D., Area Manager – Simulation & Validation, LEC GmbH, Inffeldgasse 19, 8010 Graz, Austria, e-mail: gerhard.pirker@lec.tugraz.at. Eduard Schneßl, Ph.D., Area Manager – Engine Applications, SCE Test Center, LEC GmbH, Inffeldgasse 19, 8010 Graz, Austria, e-mail: eduard.schnessl@lec.tugraz.at. Igor Šauperl, Ph.D., Business Development Manager, LEC GmbH, Inffeldgasse 19, 8010 Graz, Austria, e-mail: igor.sauperl@lec.tugraz.at. Andreas Wimmer, Ph.D., Professor, Graz University of Technology, Institute of Internal Combustion Engines and Thermodynamics, Inffeldgasse 19, 8010 Graz, Austria, e-mail: wimmer@ivt.tugraz.at.

https://doi.org/10.18690/978-961-286-050-9.7 ISBN 978-961-286-050-9

Available at: http://press.um.si.

1 Introduction

The use of gas engines for power generation and heat that are fueled by non-natural gases (NNG) is key to exploiting resources in a more environmentally friendly manner and achieving a general reduction in CO2 emissions, cf. Figure 1. Gas engines that burn NNG are normally more difficult to operate than those that run on natural gas (NG). NNG encompasses landfill gas, flare gas, coal mine gas, sewage gas, biogas and a range of other special gases. This group of special gases includes above all waste gases from industrial processes (e.g., gases from steel production). Frequently these gases are not used at all or are used inefficiently to produce (thermal) energy. Due to their very specific characteristics, each of these gases requires a specially designed engine concept. In most cases, development of a multicylinder engine on the site where the gas is produced is not economically viable due to the frequently fluctuating boundary conditions as well as high cost of support and components. Consequently, these challenges prevent expedient use of the gas. Likewise, the development of a multicylinder engine on the test bed of the engine manufacturer is equally unfeasible from an economic perspective. In this case, the factor that drives costs is the fuel since it must be mixed together from the main components and consumption by the multicylinder engine is very high. The lower the number of engines initially expected for commercialization, the more economic concerns become aggravated. With many gases, implementation is only possible if the cost of development is limited.

Driven by these boundary conditions, a method for the economically viable design and optimization of a combustion concept for gas engines that can be applied to a wide variety of non-natural gases is key. To achieve sufficient economic viability, it is important that the method does not require testing on the multicylinder engine and that the result obtained from simulation and single cylinder engine measurements can be transferred directly to the on-site facility without any additional multicylinder engine tests.

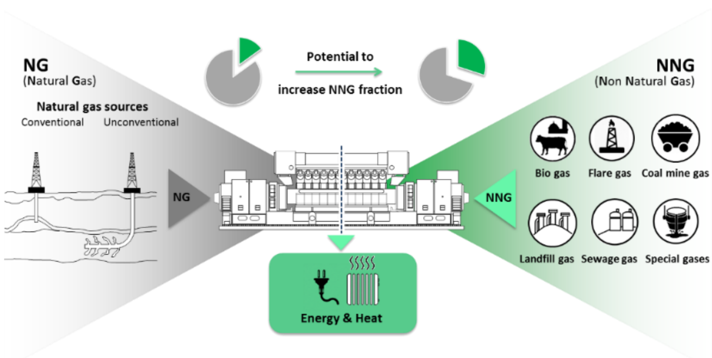

Figure 1. Low-emission energy production that maximizes the use of non-natural gases

The methodology should be feasible for use with niche applications where only a small number of engines are produced. The main goal in this area is to significantly reduce CO2 emissions and reduce the use of natural gas from fossil fuels.

2 Approach

The classic LEC Development Methodology (LDM) was elaborated in order to support efficient engine development [1][2]. It is a general methodology for developing and optimizing combustion concepts for large engines and is based on an intensive interaction between simulation and experimental investigation on single-cylinder research engines (SCE). The methodology makes use of 0D and 1D engine cycle simulation as well as 3D CFD simulation. While 3D CFD simulation is employed above all to optimize the details of relevant processes (e.g., piston geometry, charge motion), 0D/1D engine cycle simulation is applied to preoptimize significant engine parameters (e.g., compression ratio, valve timing). In addition to the basic development of combustion concepts for steady-state engine operation, the methodology comprises an integrated treatment of all combustion related processes such as durability, wear, ignition and fuel supply as well as the development of transient combustion concepts and controls.

In order to meet the requirements for NNG combustion concepts, LDM has been further enhanced: LDM COMPACT methodology can be applied to development processes that are performed without extensive testing on a multicylinder engine. These processes primarily rely on simulation tools as well as measurements on a SCE.

LDM COMPACT consists of two basic steps, cf. also Figure 2:

- Preselection and basic design of essential engine parameters based on simulation
- Experimental optimization of the concept on a single cylinder research engine.

To preselect the combustion concept, each gas is first characterized using the knock index (GPN) [3] developed at the LEC or similar criteria for knock assessment as well as reaction kinetic calculations that provide information about the expected laminar flame speed. Based on these results, the combustion concept can be preselected; the possible concepts and the basic engine parameters are stored systematically in a catalog according to gas category. 0D and 1D engine cycle calculations are then conducted to describe the operating parameters in detail. For gases with very challenging characteristics such as gases with a very high share of inert gas components – which implies extremely small lower calorific values – stable and efficient combustion requires a high degree of turbulence in the combustion chamber. Part of the development methodology, 3D CFD simulation provides responses to these and other important questions.

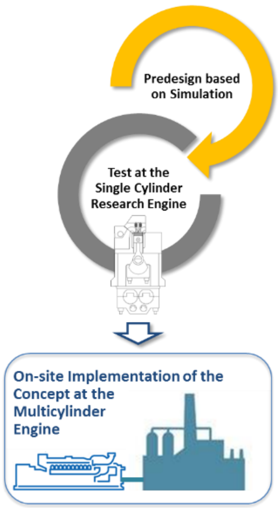

Figure 2. LDM Compact

A very efficient and flexible test bed infrastructure was set up for experimental investigations on a single cylinder research engine. Continual developments in the areas of gas mixing (up to 6 different gas components), gas supply, gas storage and safety technology enable testing of almost any gas composition on the single cylinder research engine. After the required engine components have been procured, the relevant engine operating areas are typically determined in a screening phase. To reduce test time when determining the optimal parameters, intensive use is also made of statistical design of experiments (DoE) methods. The focus of experimental investigations is on determining the efficiency and load potential of each gas while at the same time achieving the lowest possible emissions. Sensitivity observations that consider fluctuations in gas quality are also carried out. These fluctuations are critical to the design of an engine control concept and to the determination of whether higher quality gases need to be added. The results of this iterative process of just simulation and SCE measurements can finally be used to directly implement the concept into the on-site multicylinder engine, cf. Figure 2.

The main innovation of the presented methodology is the improvement of the characterization of different gases and simulation possibilities to the point that a very advanced combustion concept for each gas can be achieved in combination with experimental development on the single cylinder research engine. As a result, implementation in many NNG applications that in many cases could otherwise not be exploited finally becomes economically viable. Critical to development of the methodology are both the systematic evaluation of basic gas components with regard to their influence on knock behavior and the derivation of a catalog from which the basic combustion concept can be selected based on prior NNG developments.

3 Application Example

3.1 CO_2 reduction through the efficient use of blast furnace gas

The development methodology presented in this paper was established and applied at LEC to numerous different research projects over the course of many years in order to develop NNG combustion concepts that are almost exclusively concerned with sustainable solutions for energy production and transportation. The available database consists of several thousand measurements of different single cylinder research engines.

The following section presents an example of a sophisticated concept for sustainable power generation in large gas engines that efficiently and flexibly exploits blast furnace gas (BFG). BFG is an important but difficult to exploit byproduct of the steelmaking process. The objective was to develop a highly efficient, high power output combustion concept for a large gas engine in the 4 MW power range using BFG [4]. This concept must comply with the TA Luft emission limits, ensure sufficient combustion stability despite fluctuations in gas quality and exhibit good starting behavior. As on-site development on the multicylinder engine was not feasible due to the reasons stated in the previous section, the innovative development methodology was applied.

3.2 Selection and preoptimization of the combustion concept using simulation

In the first step, a suitable concept for the combustion of BFG was selected and preoptimized mainly by using simulation tools. The extremely unfavorable properties of BFG, which contains a great amount of inert gases and possesses a calorific value lower than 1 kWh/m_n^3, require a very specific combustion concept. Gas scavenged, mixture scavenged and unscavenged prechamber concepts as well as open chamber concepts are all possible with large gas engines. Engines of the size selected for the development of this combustion system are normally equipped with prechambers. However, 0D/1D simulation revealed that ignition could not be successfully induced due to the unfavorable mixture composition in the prechamber at ignition timing. This finding was obtained before any experiments were conducted by determining the mixture composition in the prechamber at ignition timing with a 1D simulation model. Based on the conditions in the prechamber, the simulation provides a detailed description of the mass overflow between the prechamber and main combustion chamber. Thus the main focus of combustion system development was on the open chamber concept. With this concept, a sufficient level of turbulence induced by charge motion must be achieved to obtain an appropriate flame speed. To obtain this level of turbulence in the combustion chamber during combustion, a very high swirl level was combined with an appropriate piston shape. 3D CFD simulation was extensively used during the optimization process.

Figure 3 presents selected results from this process. The locally averaged turbulent kinetic energy (TKE) was chosen to evaluate the different variants.

The chart shows the optimized variant as well as two intermediate development steps (variants A and B) in relation to the baseline variant. Based on these investigations, the most promising piston shapes in combination with the swirl level were determined and preselected for the experimental tests on the SCE.

3.3 Experimental development on the single cylinder research engine

Measurements were taken on a single cylinder research engine to verify the simulation results and to determine certain engine performance values (e.g., efficiency, emission level, combustion stability). Combustion chamber variants with increased TKE had a shortened combustion duration, which resulted in significantly faster fuel conversion with the optimized variant. After the best piston variant had been chosen and the optimal compression ratio determined, the engine operating parameters (e.g., ignition timing, mixture temperature, charge pressure) were optimized. The goal was to obtain the largest operating range possible, i.e. the range between knock limit and misfire limit, which is crucial for robust gas engine operation.

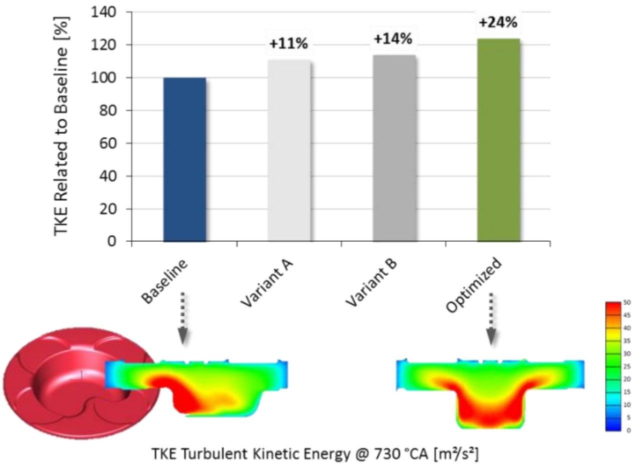

Figure 3. Predesign of the combustion concept using 3D CFD simulation

The fluctuations in the composition of BFG cause dramatic changes in the combustion behavior of the gas. If the share of hydrogen (H_2) in particular noticeably varies, it greatly influences the combustion. Thus investigations were carried out on the single cylinder research engine to evaluate the sensitivity of the engine concept to fluctuations in H_2 content. Figure 4 and Figure 5 present selected results of these investigations with the optimal variant; the misfire limit and the knock limit restrict the operation range. While Figure 4 depicts the achievable engine efficiency versus load and H_2 content, Figure 5 shows combustion stability versus the same parameters.

A special control concept adapted to BFG application was developed for the multicylinder engine in order to ensure stable engine operation with variable load and fluctuating gas quality. Through continuous optimization of both combustion and gas mixing, a maximum energy yield can be guaranteed at any time and at any operating point. The simulation based control concept relies upon on-board cylinder pressure measurement and admixing of an additional gas (e.g., coke gas).

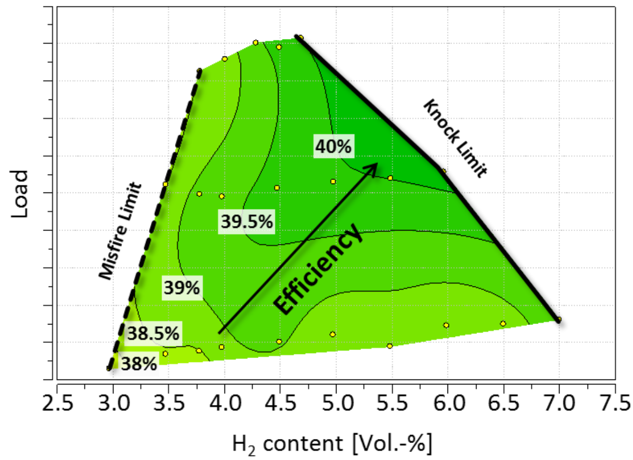

Figure 4. Operating range: Efficiency versus load and H_2 content

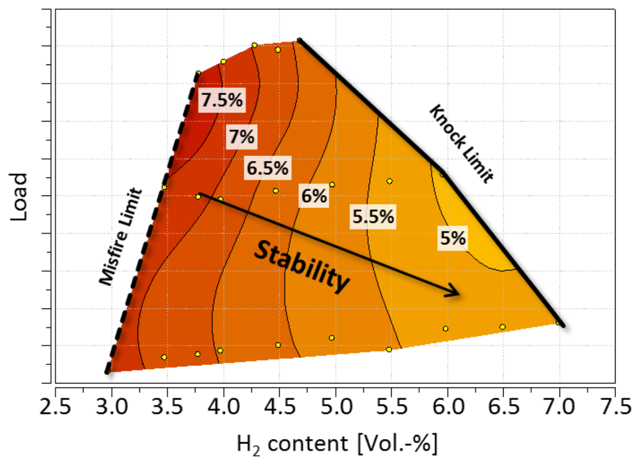

Figure 5. Operating range: Combustion stability versus load and H_2 content

4 Outlook and Potential

Economically and ecologically viable implementation of NNG applications into large gas engines have enormous potential on a global level. The losses from drilling for natural gas alone are estimated to be about 5% of global natural gas production; these losses arise to a great extent from the flaring of components unable to be directly exploited. In terms of CO_2 emissions, this translates into almost 900 million tons of CO_2 (assuming a CO_2 equivalent of 500 g/kWh) that could be saved by exploiting these gases for energy. Even if only a small fraction is saved, the potential is extremely high. As a result, it is imperative that gas engine development focuses on this area.

LDM COMPACT is the result of many years of research and several successful projects at the LEC that have developed NNG combustion concepts for large gas engines. The methodology allows direct implementation of an engine concept into the on-site multicylinder engine without prior cost-intensive tests on a multicylinder engine. The reduced development cost and time for the engine manufacturer can be passed on to the user as an investment advantage and is thus an important enabler of this technology, which aims to produce energy with a low environmental impact and few CO_2 emissions.

The application of this methodology can reduce the cost of development of implementing a specific gas into an engine by more than 90% compared to multicylinder engine development. Consequently, it is possible for gas engines characterized by flexibility and a potentially modular structure to enter into the very extensive arena of NNG applications

Acknowledgements

The authors would like to acknowledge the financial support of the "COMET - Competence Centres for Excellent Technologies Programme" of the Austrian Federal Ministry for Transport, Innovation and Technology (BMVIT), the Austrian Federal Ministry of Science, Research and Economy (BMWFW) and the Provinces of Styria, Tyrol and Vienna for the K1-Centre LEC EvoLET. The COMET Programme is managed by the Austrian Research Promotion Agency (FFG).

References

[1] Wimmer, A., Winter, H., Schnessl, E., Pirker, G., Dimitrov, D., "Combustion Concept Development for the Next Generation of GE Jenbacher Gas Engines", presented at the 7th Dessau Gas Engine Conference, Dessau, Germany, March 24-25, 2011.
[2] Wimmer, A., Pirker, G., Schnessl, E., Trapp, C., Schaumberger, H., Klinkner, M., "Assessment of Simulation Models for the Development of Combustion Concepts for the New Generation of Large Gas Engines," presented at the 10th International Symposium on Combustion Diagnostics, Baden-Baden, Germany, May 22-23, 2012
[3] Wimmer, A, Chmela, F, Kirsten, M, Pirker, G, Christiner, P, Trapp, C & Schaumberger, H 2013, LEC-GPN – a new index for assessing the knock behavior of gaseous fuels for large

engines. in Knocking in Gasoline Engines, S. 239-254, Berlin, Germany, 9-10 December 2013.

[4] Schneßl E.; Pirker G.; Wimmer A.: „Opti-mierung von Brennverfahren für Sondergasanwendungen auf Basis der Simulation und Versuch am Einzylinder-Forschungsmotor“, MTZ-Konferenz Heavy Duty-, On- und Off-Highway-Motoren, Friedrichshafen, November 2009

10TH INTERNATIONAL CONFERENCE ON SUSTAINABLE ENERGY AND ENVIRONMENTAL PROTECTION (JUNE 27TH – 30TH, 2017, BLED, SLOVENIA), ENERGY EFFICIENCY
J. Krope, A.Ghani Olabi, D. Goričanec & S. Božičnik

A Review on Analysis on Cooling Technologies of Concentrated Solar Power System

MANXUAN XIAO, LLEWELLYN TANG, XINGXING ZHANG, ISAAC YU FAT LUN & GUOZHEN LI

Abstract The application of the Concentrated Solar Power (CSP) system has attracted an ever-increasing attention with the deepening worldwide energy crisis. Operating temperature is one of the most important factors for CSP system that affects the solar photoelectric conversion efficiency. Reasonable cooling method cannot only decrease the operative temperature, balance flare inhomogeneity, also should display the characteristics of convenient installation, low power consumption and high reliability. Based on a comprehensive literature review, this work conducted a thorough compilation on different cooling techniques of CSP system. It includes the commonly used air cooling and water cooling, also illustrates the promising ground coupled cooling, impinging jet cooling, liquid immersion cooling, microchannel cooling, heat pipe cooling and Phase Change Material systems etc. Besides, the advantages and disadvantages of different cooling technologies are briefly analysed. It is expected that this paper could provide guidance for development and optimization of cooling technologies in CSP system.

Keywords: • Temperature • Efficiency • Cooling Technology • Concentrated Solar Power System • Heat transfer •

CORRESPONDENCE ADDRESS: Manxuan Xiao, Ph.D., University of Nottingham Ningbo, Department of Architecture and Built Environment, 199 Taikang East Road, 315100 Ningbo, China, email: Manxuan.Xiao@nottingham.edu.cn. Llewellyn Tang, Ph.D., Head & Associate Professor, University of Nottingham Ningbo, Department of Architecture and Built Environment, 199 Taikang East Road, 315100 Ningbo, China, email: Llewellyn.Tang@nottingham.edu.cn. Xingxing Zhang, Ph.D., Associate professor, Solar Energy Research Center (SERC), Dalarna University, Högskolegatan 2, 791 31 Falun, Sweden, email: xza@du.se. Isaac Yu Fat Lun, Ph.D., Assistant Professor, University of Nottingham Ningbo, Department of Architecture and Built Environment, 199 Taikang East Road, 315100 Ningbo, China, email: Isaac.Lun@nottingham.edu.cn. Guozhen Li, Ph.D., University of Nottingham Ningbo, Department of Architecture and Built Environment, 199 Taikang East Road, 315100 Ningbo, China, email: Jason.Li@nottingham.edu.cn.

https://doi.org/10.18690/978-961-286-050-9.8 ISBN 978-961-286-050-9

Available at: http://press.um.si.

1 Introduction

Concentrated solar power (CSP) system uses the low cost reflective mirrors or lenses to concentrate the sunlight onto photovoltaic (PV) cells. It realises higher efficiency, more output and lower cost with the use of the same PV cells. But only around 15% of the absorbed luminous energy can be converted to electricity with the rest will be converted into thermal energy [1], which rises PV cell temperature and reduces system's output performance. Research indicated that 0.2 % to 0.5 % output power increase can be achieved with 1 K temperature decrease of PV cells [2]. Moreover, the long-term working under high temperature would make PV cells rapidly age and further shorten its service life. CSP can effectively avoid PV technology's limitation of low efficiency and high cost, on the other hand it suffers performance losses with the rise of operative temperature. Advanced researches of effective cooling technologies are therefore eagerly awaited.

2 Cooling Technologies of Concentrated Solar Power System

Cooling technologies of CSP system can be divided into two types: passive cooling and active cooling, the working mediums usually are water or air. Passive cooling system has the advantages of none energy consumption, low cost and easy installation. It is mainly been applied in low concentrated PV power generation system due to its limited cooling effect. Back metal plate of high conductivity material with or without fins and heat pipe cooling system are the representative models.

Active cooling system also uses fins or channels to strengthen the convection heat transfer. The difference is the use of forced circulation system. Thus the additional consumption of electricity is unavoidable. Its characteristics of high heat dissipating capacity making it to be commonly adopted in high concentrated PV power generation system.

Table 1 compares air and water's convective heat transfer coefficient (CHTC) under natural and forced cooling situations. It is obvious that water is a better cooling medium compared to air, and the CHTC of active cooling system is much higher than that of passive cooling system.

Table 1. Convective Heat Transfer Coefficient of Air and Water

Condition		Convective Heat Transfer Coefficient ($W/m^2 \cdot K$)
Natural Convection	Air	1 ~ 10
	Water	200 ~ 1000
Forced Convection	Air	20 ~ 100
	Water	1000 ~ 15000

2.1 Air cooling

Air cooling either by forced or natural flow provides a low-cost and simple heat-dissipating way, but the poor thermo-physical characteristic of air offers a relatively low cooling efficiency [3]. The heat exchange performance of air cooling is related to air flow rate, flow length and height etc., higher heat transfer effect could be achieves by optimising these parameters. Brinkworth and Sandberg indicated that for a certain length of PV array, the best cooling performance would be achieved when the ratio of PV array length (L) to air flow's hydraulic diameter (D) is 20 (L/D=20) without consideration of the influence of other factors [4]. This helps to choose the power rating of blower to avoid unnecessary energy waste. Araki, Uozumi and Yamaguchi [5] investigated the natural convection cooling performance of single PV cell with 500 Suns, the results demonstrated a good thermal contact between batteries and aluminum plate is critical for cell temperature decrease.

A heat transfer model was developed by Amri and Mallick [6] to cool a multi-junction CSP system under 100, 150 and 200 Suns. A forced air cooling system with 1.5mm thick aluminium plate was adopted in this experiment. The results showed this cooling system can adequately cool the PV cell under medium concentration ratios with maximum 50% temperature decrease, while it is less effective for high concentration ratios and the channel width needs to narrow to micro-meter value in order to achieve the required cooling efficiency. The conjugation effect, air inlet velocity and channel width were found to have noticeable effects on PV temperature. A novel air-cooled condenser for CSP system was proposed by Moore et al. [7], which has two significant advantages over the existing state-of-the-art. Firstly, its pre-assembled modular format could reduce installation costs. Secondly, smaller speed controlled fans are integrated with the individual modules to instead the large fixed speed fans, which allows the changing of the operational point of condenser and further maximises the plant efficiency.

2.1.1 Ground coupled cooling system

The ground has been used as a heat sink for cooling for a long time, it is indeed a brand-new perspective in the realm of the cooling of PV panels. Sahaya et al. [8] designed and optimised an innovative Ground-Coupled Central Panel Cooling System (GC-CPCS) for cooling of Solar PV panels, of which air is the cooling medium. The new system was proved that it can maximise the increase in output to the energy spent in the cooling system and provide low capital cost per watt output. The schematic design is shown in Figure 1.

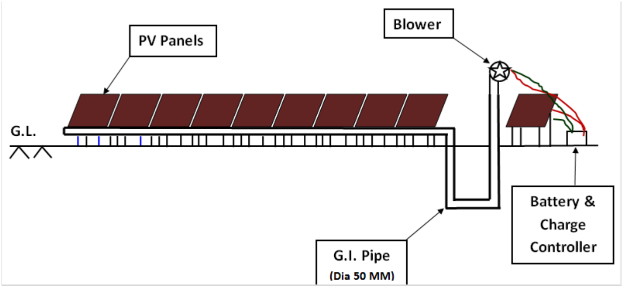

Figure 1. Schematic Design of GC-CPCS[8]

Sahaya et al. [9] then installed and actual tested the GC-CPCS system by using Smoke Flow Visualization technique. More effective cooling performance and hence better conversion efficiency were proved to be achieved by the system. It was unique to introduce the concept of Central cooling of PV panels. Also it was the first time for Ground Coupled Heat Exchanger to be used in Solar PV Panel Cooling System.

2.2 Water cooling

Water cooling technology can be divided into two types, natural and forced circulation cooling. The crucial factor of this technology is to ensure the good heat conduction and electric insulation between PV cell and surface of heat exchanger, the leakage problem of working medium should also be taken into consideration. A typical water cooling system is composed by heat exchanger, water tank and valves etc., the schematic is shown as Figure 2.

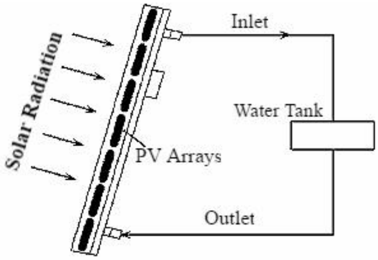

Figure 2. Schematic of Water Cooling Technique

Chaabane, Mhiri and Bournot [10] presented a 3D computational fluid dynamics model to predict the thermal and electrical performance of a water-cooled concentrated photovoltaic (CPV) system. To avoid the hot spots in the cell module, a rectangular channel was finally employed after increasing the number of water cooling pipes. The final optimum design presented a solar cell temperature of 315.15K and respectively a thermal and combined (thermal plus electrical) efficiency of 74.2% and 83.5%. The results showed the number of pipes and water flow rate significantly affect the thermal electrical efficiency.

A CPV with active water-cooling system was developed by Du, Hu and Kolhe [11]. Operating temperature, power output and efficiency were tested to investigate the PV module's performance. It is found that cooling water flow rate significantly affects the heat extraction rate which helps manage cell temperature. A Computational Fluid Dynamics simulation of high concentrated active water-cooled solar cells has been performed by Sabry [12] to investigate the effect of CHTC, water flow rate and tube internal diameter on PV temperature. Results showed that increasing CHTC significantly reduces PV temperatures operating at low flow rates and high concentration ratios with further increase in water flow rate would be of no effect.

2.2.1 Jet impingement cooling

Jet impingement cooling can realize a very low thermal resistances, generally is 105 ~106 Km^2/W [13]. Its potential of achieving high heat transfer rates makes it become an attractive cooling method. A jet impingement cooling device was designed by Royne and Dey [14] for cooling densely packed PV cells under high concentration. They developed a model to predict the pumping power of different shape devices. The studies showed that the performance improved by increasing the nozzle number per unit area. Besides, Huber and Martin models were adopted for different concentration level. PV cell temperature reduced from 60°C to 30°C at 200 Suns and from 110°C to 40°C at 500 Suns in both models.

An outdoor test of a hybrid jet impingement /micro-channel cooling device for densely packed CPV cells was conducted by Barrau et al. [15]. A dummy cell was used instead of using a real solar cell for testing. According to the results, the thermal resistance coefficient and the temperature uniformity offered by this cooling system can meet the requirements of CPV receivers. And they correlated the flow rate and concentration ratio as a function of temperature.

Hasan et al. [16] investigated the effect of nanoparticles (SiC, TiO_2 and SiO_2) with water as base fluid on the electrical and thermal performance of a photovoltaic thermal (PVT) collector equipped with jet impingement. Solar irradiances and mass flow rates were set to conduct the test. The highest electrical and thermal efficiency were achieved by the use of SiC/water nanofluid system, and 62.5% increase of the P_{max} of PVT was realized compared to the conventional PV module.

2.2.2 Liquid immersion cooling

Han et al. [17] developed and tested a CPV integrated with direct liquid-immersion cooling system. The long-term stability and performance of silicon PV cells were researched through four separate liquid immersion experiments respectively: ethyl acetate, dimethyl silicon oil, isopropyl alcohol (IPA) and De-ionized (DI) water. The cell efficiency increased 8.5-15.2% with a 1.5 mm liquid film. More power output could achieve under higher concentration ratios. But it was difficult for PV cell to maintain stable electrical performance when immersed in 9 mm liquid layer of deionized water.

Electrical characteristic investigation of a triple-junction PV cell immersed in dimethyl silicon oil of 1.0–30.0 mm thickness at 500 Suns was proposed by Xin et al. [18]. Results showed cell electrical performances reduced with the increase of silicon oil thickness. The maximum increase of output power and conversion efficiency were achieved with the solar cell immersed in silicon oil of 1.0 mm thickness, from 39.567% and 19.556 W to 40.572% and 20.083 W respectively. The cell efficiency and output power would less than those without liquid-immersion when the silicon oil thickness exceeds 6.3 mm. However, the thickness should not less than 2.5 mm according to CFD simulation for low and uniform cell temperature.

Kang et al. [19] conducted a new direct-contact phase-change liquid immersion cooling method for high concentrating photovoltaic (HCPV) system. This cooling system can modulate automatically and run self-propelled steadily without consuming extra energy. Studies showed the surface heat transfer coefficient of PV cell was up to 46.98 kW/m^{2}K when the temperature was well controlled in the range between 87.3°C and 88.5°C under the concentration ratio of 398.4. The light loss at the interface between bubble and ethanol is dominant for the decline of electrical performance that I_{sc} and P_{max} decreased 10.2% and 7.3% respectively of triple-junction PV cells.

2.3 Microchannel cooling

Research indicated that microchannel cooling technique can provide the utmost possible reduction of PV cell temperature compared to other cooling technologies [20]. A novel CPV cooling system using multi-layer manifold microchannel system was developed by Yang and Zuo [21] for improving the uniformity of surface temperature distribution. The experiments showed the CPV cell temperature reduced from 44.1°C to 20.4 °C with the flow rate of 0.00535kg/s to 0.0232kg/s and would not change beyond the flow rate of 0.0232kg/s under 28 Suns. This cooling system presented a heat transfer coefficient of 8235.84W/m^{2}K with a pressure drop less than 3 kPa. Besides, it proposed a small surface temperature difference (less than 6.3 °C) of the CPV cells.

Radwan et al. [22] developed a new microchannel heat sink with nanofluids to cool the low concentrated photovoltaic-thermal (LCPV/T) systems, in which Al_2O_3-water and SiC-water were cooling mediums. A major temperature reduction of PV cell was observed with the increase of nanoparticles' volume fraction, while SiC-water nanofluid achieved a relatively higher decline in cell temperature than Al_2O_3-water nanofluid. The studies proved that LCPV/T system can realise better performance by using nanofluids than water with the cell temperature reduced to 38°C and the electrical efficiency increased to 19%, especially at high solar concentration ratios.

Similarly, the performance of the LCPV/T system incorporated with a microchannel heat sink was investigated by a comprehensive thermal model at different operating conditions according to Radwan et al. [20]. It also has been proved that microchannel heat sink has strong abilities in solar cell temperature reduction and uniform temperature distribution.

For all values of concentration ratios, the performance of the LCPV/T system was significantly enhanced by the increase of cooling fluid Reynolds number, which was presented as higher electrical and thermal efficiency, and lower cell temperature.

2.4 Heat pipe cooling

Heat pipe has the characteristics of high heat transfer and high thermal conductivity ability make it can be a good alternative to large heat sink, especially space is limited [23]. Anderson et al. [24] proposed a copper/water heat pipe integraed with aluminum fins for cooling a CPV system by natural convection at 30 Suns, of which toulene, ammonia, pentane, methanol and water are the different working fluids. CFD software was used to decide the optimum spacings and fin sizes. Water was found as the best working medium compared to others. The heat pipe rejected the heat by natural convection with a total cell-to-ambient temperature rise of only 40°C under a cell level waste heat flux of 40 W/cm^2.

A fabrication method of a novel hybrid-structure flat plate (NHSP) heat pipe was designed and investigated by Hsin-Jung et al. [25] for a CPV system. NHSP heat pipe contained a flattened copper pipe and a sintered wick structure which was supported by a coronary-stent-like rhombic copper mesh. Experiments demonstrated that the NHSP heat pipe reduced the thermal resistance hence increased the conversion efficiency of CPV system by approximately 3.1% in a single PV cell. Khairnasov et al. [26] indicated that several methods for improving the robustness of high-temperature heat pipe wick for their application in CSP system with Stirling engine were conducted. They proposed, developed, and demonstrated a compromise wick structure which could restore performance without giving up strength. The wick testified excellent performance of the durability bench test with over nearly 13,600h at 775 °C vapour temperature.

2.5 Phase change material

Phase change material (PCM) can keep a relative stable temperature during the heat absorption process, hence attracted an ever-increasing attention in thermal management [27]. Sharma et al. [28] experimental evaluated PCM via thermal regulation to enhance performance of low-concentration Building-Integrated Concentrated Photovoltaic (BICPV) system, which has not been reported so far. This work proposed and implemented a new analytical model for the in-house controlled experiments. Results showed that PCM effectiveness varies with irradiance, an raise in relative electrical efficiency by 7.7% and an average decline in module centre temperature by 3.8 °C were observed of BICPV-PCM integrated system in comparison with naturally ventilated system at 1000Wm^{-2}.

Cui et al. [29] designed a novel concentrated photovoltaic–thermoelectric (PV–TE) system integrated with PCM to keep the system operating under an ideal working temperature. The feasibility of four types of PV–PCM–TE system was investigated: GaInP/InGaAs/Ge (III–V), single-junction GaAs, CIGS, C-Si, and PV cells. A theoretical model was presented to evaluate the efficiency. The results indicated the PV–PCM–TE system is superior to single PV cells and/or PV–TE systems in performance. But controlling thermal contact resistances is extremely necessary when the system is operating under higher optical concentrations.

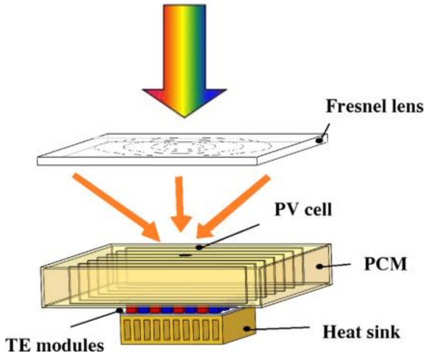

Figure 3. Schematic of PV–PCM–TE [29]

Cui et al. [30] then experimentally analysed the performance of PV–PCM–TE system. The research indicated this system can maintain the working temperature at a desired level during a day and has higher energy conversion efficiencies compared to pure PV system. It hence possesses a promising potential on the full-spectrum utilization of solar energy. The schematic is shown in Figure 3.

3 Conclusion

This part analysed the advantages and disadvantages of different cooling technologies adapted from the above literatures and Jakhar et al. [31].

Air cooling: it is low-cost and simple and the hot air is a useful resource for space heating. But this approach has low mass flow rate and low cooling efficiency.

Ground coupled cooling: it is a brand-new perspective in Solar PV panels cooling that research studies are inadequate.

Water cooling: the water possesses higher thermal conductivity, higher heat capacity and higher mass flow rate. But water cooling system requires higher maintenance cost and operation cost with the pumping power. The corrosion problem and low life cycle are also the dominate problems for water pipeline.

Jet impingement cooling: can achieve very low thermal resistance that make it can be used for HCSP system and replace heat sink. But disturbances would occur when water from one jet meets the water from neighbouring jet.

Liquid immersion cooling: it eliminates the contact thermal resistance without electricity consumption. But more complicated system design and high cost are required. It is proved that is most suitable for densely packed CPV.

Microchannel cooling: can remove a mass of heat with low power requirements in a smaller area. The low thermal resistance make it can be applied for high concentration level. But it has limited pressure drop and uneven temperature distributions.

Heat pipe: an easy integrated passive heat exchange device, which can accept heat at very high heat fluxes and transfer heat across long distance. But is has corrosion problem and high cost, usually be used for low and medium concentration level.

Phase change material: a passive heat exchange device can store a large amount of thermal energy. Its characteristics of maintenance-free, compatibility, reliability and high cooling capacity without electricity consumption, make it can be used for high heat fluxes and thermal storage applications. But it has high initial cost and some PCMs have fire safety issue and are toxic.

Reasonable cooling method should maintain low and uniform cell temperature, also needs to display high efficiency, convenient installation, low power consumption and high reliability. It is expected that this paper could provide guidance for development and optimization of cooling technologies in CSP system.

Acknowledgements

The authors would like to acknowledge their sincere appreciation for the financial support from Ningbo Enrich People Project of China (Grant No. 2016C10035) and the IDIC (International Doctoral Innovation Centre) program of the University of Nottingham (China campus).

References

1. Teo, H.G., P.S. Lee, and M.N.A. Hawlader, *An active cooling system for photovoltaic modules.* Applied Energy, 2012. **90**(1): p. 309-315.
2. He, W., et al., *Hybrid photovoltaic and thermal solar-collector designed for natural circulation of water.* Applied Energy, 2006. **83**(3): p. 199-210.
3. Tonui, J.K. and Y. Tripanagnostopoulos, *Air-cooled PV/T solar collectors with low cost performance improvements.* Solar Energy, 2007. **81**(4): p. 498-511.
4. Brinkworth, B.J. and M. Sandberg, *Design procedure for cooling ducts to minimize efficiency loss due to temperature rise in PV arrays.* Solar Energy, 2006. **80**: p. 89-103.
5. Araki, K., H. Uozumi, and M. Yamaguchi, *A simple passive cooling structure and its heat analysis for 500/spl times/ concentrator PV module*, in *Twenty-Ninth IEEE Photovoltaic Specialists Conference*. 2002: New Orleans.
6. Al-Amri, F. and T.K. Mallick, *Alleviating operating temperature of concentration solar cell by air active cooling and surface radiation.* Applied Thermal Engineering, 2013. **59**(1–2): p. 348-354.

7. Moore, J., et al., *Modelling the thermodynamic performance of a concentrated solar power plant with a novel modular air-cooled condenser.* Energy, 2014. **69**: p. 378-391.
8. Sahaya Amit , S. V.K., and T. A.C., *Design, optimisation and system integration of low cost Ground Coupled Central Panel Cooling System (GC-CPCS).* International Journal of Current Engineering and Technology, 2013. **3**(4): p. 1473-1479.
9. Sahay, A., et al., *A review of solar photovoltaic panel cooling systems with special reference to Ground coupled central panel cooling system (GC-CPCS).* Renewable and Sustainable Energy Reviews, 2015. **42**: p. 306-312.
10. Chaabane, M., H. Mhiri, and P. Bournot, *Performance Optimization of Water-Cooled Concentrated Photovoltaic System.* Heat Transfer Engineering, 2016. **37**(1): p. 76-81.
11. Du, B., E. Hu, and M. Kolhe, *Performance analysis of water cooled concentrated photovoltaic (CPV) system.* Renewable and Sustainable Energy Reviews, 2012. **16**(9): p. 6732-6736.
12. Sabry, M., *Temperature optimization of high concentrated active cooled solar cells.* NRIAG Journal of Astronomy and Geophysics, 2016. **5**(1): p. 23-29.
13. W.M., R., H. J.P., and C. Y.I., *Handbook of Heat Transfer,*. third ed. 1998, New York.
14. Royne, A. and C.J. Dey, *Design of a jet impingement cooling device for densely packed PV cells under high concentration.* Solar Energy, 2007. **81**(8): p. 1014-1024.
15. Barrau, J., et al., *Outdoor test of a hybrid jet impingement/micro-channel cooling device for densely packed concentrated photovoltaic cells.* Solar Energy, 2014. **107**: p. 113-121.
16. Hasan, H.A., et al., *Experimental investigation of jet array nanofluids impingement in photovoltaic/thermal collector.* Solar Energy, 2017. **144**: p. 321-334.
17. Han, X., Y. Wang, and L. Zhu, *The performance and long-term stability of silicon concentrator solar cells immersed in dielectric liquids.* Energy Conversion and Management, 2013. **66**: p. 189-198.
18. Xin, G., et al., *Experimental study of liquid-immersion III–V multi-junction solar cells with dimethyl silicon oil under high concentrations.* Energy Conversion and Management, 2015. **94**: p. 169-177.
19. Kang, X., et al., *Study on direct-contact phase-change liquid immersion cooling dense-array solar cells under high concentration ratios.* Energy Conversion and Management, 2016. **128**: p. 95-103.
20. Radwan, A., S. Ookawara, and M. Ahmed, *Analysis and simulation of concentrating photovoltaic systems with a microchannel heat sink.* Solar Energy, 2016. **136**: p. 35-48.
21. Yang, K. and C. Zuo, *A novel multi-layer manifold microchannel cooling system for concentrating photovoltaic cells.* Energy Conversion and Management, 2015. **89**: p. 214-221.
22. Radwan, A., M. Ahmed, and S. Ookawara, *Performance enhancement of concentrated photovoltaic systems using a microchannel heat sink with nanofluids.* Energy Conversion and Management, 2016. **119**: p. 289-303.
23. Peterson, G.P., *An Introduction to Heat Pipes: Modeling, Testing, and Applications*. 1994, Canada: John Wiley & Sons.
24. Anderson, W.G., et al. *Heat pipe cooling of concentrating photovoltaic cells*. in *2008 33rd IEEE Photovoltaic Specialists Conference*. 2008.
25. Hsin-Jung Huang, S.-C. Shen, and H.-J. Shaw, *Design and Fabrication of a Novel Hybrid-Structure Heat Pipe for a Concentrator Photovoltaic.* Energies, 2012. **5**(11): p. 4340-4349.
26. Khairnasov, S., et al., *Development of advanced high porosity wicks for the high temperature heat pipes of concentrating solar power.* Applied Thermal Engineering.
27. Kandasamy, R., X.-Q. Wang, and A.S. Mujumdar, *Application of phase change materials in thermal management of electronics.* Applied Thermal Engineering, 2007. **27**(17–18): p. 2822-2832.

28. Sharma, S., et al., *Performance enhancement of a Building-Integrated Concentrating Photovoltaic system using phase change material.* Solar Energy Materials and Solar Cells, 2016. **149**: p. 29-39.
29. Cui, T., Y. Xuan, and Q. Li, *Design of a novel concentrating photovoltaic–thermoelectric system incorporated with phase change materials.* Energy Conversion and Management, 2016. **112**: p. 49-60.
30. Cui, T., et al., *Experimental investigation on potential of a concentrated photovoltaic-thermoelectric system with phase change materials.* Energy, 2017. **122**: p. 94-102.
31. Jakhar, S., M.S. Soni, and N. Gakkhar, *Historical and recent development of concentrating photovoltaic cooling technologies.* Renewable and Sustainable Energy Reviews, 2016. **60**: p. 41-59.

10TH INTERNATIONAL CONFERENCE ON SUSTAINABLE ENERGY AND ENVIRONMENTAL PROTECTION (JUNE 27TH – 30TH, 2017, BLED, SLOVENIA), ENERGY EFFICIENCY
J. Krope, A.Ghani Olabi, D. Goričanec & S. Božičnik

On the Incidence of Occupant's Behavior in the Evaluation of Energy Efficiency in Buildings

LAMBERTO TRONCHIN & MASSIMILIANO MANFREN

Abstract The increasing commitment towards resource efficiency in buildings is progressively changing the way we design buildings. However, the adoption of these strategies in the Mediterranean area should be carefully evaluated to prevent overheating in intermediate seasons and increase of cooling loads in summer. Additionally, the impact on performance of occupants' comfort preferences and behaviour is generally neglected. The research presents an analysis of the potential gap between simulated and actual performance in a real case study building constructed following Passive House standard in Italy. The research compares the initial design hypothesis, obtained with a semi-stationary calculation tool, with a larger spectrum of data generated by means of parametric simulations, following a design of experiment approach. The approach aims to detect potentially critical assumptions already in preliminary design phase, ensuring the robustness of energy performance evaluation, given the implications in terms of techno-economic optimization and effective deployment of energy efficiency practices.

Keywords: • Parametric modelling • Behavioural modelling • Building performance simulation • Energy efficiency • Techno-economic optimization •

CORRESPONDENCE ADDRESS: Lamberto Tronchin, University of Bologna, Department of Industrial Engineering (DIN), Via Zamboni 33, 40126 Bologna, Italy, e-mail: lamberto.tronchin@unibo.it. Massimiliano Manfren, University of Southampton, Faculty of Engineering and the Environment, SO17 1BJ, Southampton, United Kingdom, email: M.Manfren@soton.ac.uk.

https://doi.org/10.18690/978-961-286-050-9.9 ISBN 978-961-286-050-9

1 Introduction

The increasing commitment towards resource efficiency in the building sector [1] is progressively changing the way we design and operate buildings. The decarbonisation of built environment is one of the most important objectives, considering the impact of buildings at the EU [2] and global scale. New efficiency paradigms (i.e. NZEBs) are emerging both for new and existing buildings [3]. Passive design strategies, exploiting solar and internal gains to balance heat losses due to transmission and ventilation (in heating mode), are becoming increasingly common. These strategies are mostly used in Northern countries where heating constitutes, in most of the cases, the predominant part of energy consumption. However, the adoption of these strategies in the Mediterranean area has to be carefully evaluated to prevent overheating in intermediate seasons and increase of cooling loads in summer.

Further, optimistic assumptions are often assumed in design phase and semi-stationary calculation methodologies are still commonly used. Additionally, the impact of occupants' comfort preferences and behaviour on performance is generally neglected. The paper aims to presents an analysis of the potential gap between simulated and actual performance in a real case study building constructed following Passive House standard in Italy.

2 Research Methodology

The research compares the initial design hypothesis, obtained with a semi-stationary calculation tool, PHPP [4], with a larger spectrum of data generated by means of a parametric simulation, following a Design Of Experiment approach (DOE). The approach aims to detect potentially critical assumptions already at the preliminary design level, ensuring the robustness of energy performance evaluation, given the implications in terms of techno-economic optimization and effective deployment of energy efficiency practices and policies. At the EU level a coherent strategy for both new and existing buildings is necessary [3], and the latter are, in absolute terms, much more relevant [5, 6] if we want to determine a considerable impact for the sector [1] as a whole. The importance of parametric and probabilistic analysis of building performance is becoming evident, both in new construction and retrofit interventions. Cost-optimality [7] of efficiency measures is among the most important elements to be considered for the effective deployment of energy efficiency practices and, consequently, the success of policies. However, the potential gap between simulated and measured performance can be very relevant [8], considering in particular the impact on performance of occupants' comfort preferences and behaviour [9, 10]. In order to overcome this issue, a methodological continuity between performance analysis practices across life cycle phases should be established, using parametric simulation (design phase) and progressively calibrating building model to real data, up to the control level (operation phase). Meta-models [11] (i.e. surrogate models, reduced-order models) can be successfully used for this purpose, e.g. in design optimization, [12] calibration [11] and control [13]. The model used in the research is a reduced-order grey-box dynamic model.

However, in order to render these application more transparent and automated, further research should be oriented towards the definition of multi-level performance metrics [14, 15] and visualization techniques.

3 Case Study Description

The case study chosen is a Passive House standard residential building constructed in the Province of Forlì-Cesena in the Emilia Romagna Region in Italy. The data from the original building design are used as baseline and compared to parametric simulation runs obtained using Design Of Experiment (DOE) methodology. Parameters in DOE simulations are varied with respect to the baseline design (employing PHPP semi-stationary calculation methodology) and simulation are performed by means of a grey-box dynamic model suitable to perform multiple runs in a reduced time frame. The grey-box model parameters have been initially calibrated to the baseline configuration in PHPP and then varied following a two-level factorial design [16]. Variations and multiple runs are meant to account for the variability of the performance of envelope components and of occupant's comfort preferences and behaviour. In real building operation these variations can determine a very relevant gap between simulated and measured performance, compromising the cost-effectiveness of the investment in energy efficiency and the credibility of energy efficiency practices.

Figure 1. External view of the case study building

The case study building is characterized by highly insulated envelope components, radiant heating and cooling system, mechanical ventilation with heat recovery, ground-source heat pump system (GSHP) and photovoltaic system, for on-site electricity production. In the parametric simulation performed heat recovery (mechanical ventilation) has not been considered because the system is designed for heat recovery in winter mode operation and, given the climate conditions of the site, the advantage would have been modest on a yearly base, if we consider the trade-off between energy recovered from the exhaust air stream and energy consumption of auxiliaries [17]; further, the aim of the work is comparing the original baseline with slightly less efficient and cheaper configurations to highlight the potential performance gap, already in the design phase.

4 Discussion of Results

As anticipated, the baseline configuration chosen for simulation is the one used in the building design phase. The envelope parameters used in the grey-box model (lumped parameters) have been calibrated to reproduce the same heating demand of the original model in PHPP. The internal gains assumed are averaged on a daily base and are very modest, considering the fact that the building, despite being very large, is actually used by only by 4 people. The data are summarized in Table 1.

Table 1. Baseline simulation data

Group	**Type**	**Unit**	**Value**
Geometry	Gross volume	m^3	1557
	Net volume	m^3	1231
	Heat loss surface area	m^2	847
	Net floor area	m^2	444
	Surface/volume ratio	1/m	0.54
Envelope	U value external walls	$W/(m^2K)$	0.18
	U value roof	$W/(m^2K)$	0.17
	U value transparent components	$W/(m^2K)$	0.83
Activities	Internal gains (lighting, appliances and occupancy)	W/m^2	1
Control and operation	Heating set-point temperature	°C	20
	Cooling set-point temperature	°C	26
	Air-change rate	vol/h	0.3
	Operation schedules	-	0.00-23.00

After that, the grey-box model has been used for yearly simulations, including all the energy demands from the building, namely heating, cooling, domestic hot water (DHW), lighting and appliances. The only energy carrier present is electricity, considering GSHP system, providing heating, cooling and domestic hot water, lighting system and appliances. Monthly electricity demand composition is represented in Figure 2 for the baseline configuration.

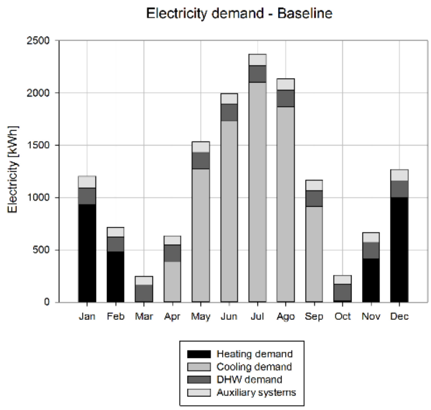

Figure 2. Electricity demand composition

The electricity meter balance with respect to demand and on-site production in reported in Figure 3, while the one presenting delivered and exported energy is reported in Figure 4.

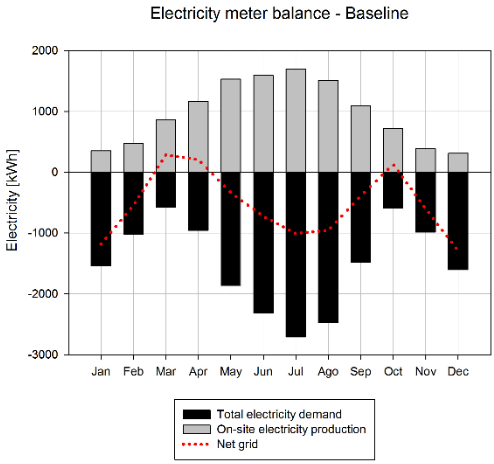

Figure 3. Electricity meter balance - on-site production and demand

The values obtained in Figure 3 highlight the fact that the photovoltaic system is able to supply a large part of the global electricity demand of the building, while the ones in Figure 4 show the interaction of the building with the grid.

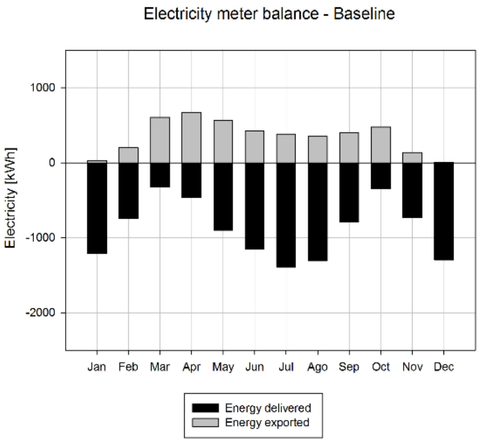

Figure 4. Electricity meter balance - delivered and exported energy

It has to be stressed the fact that this baseline configuration uses constant operating schedules, as reported in Table 1, to maintain a comparability with the original PHPP model, but more realistic schedules are considered in the parametric simulation runs. The two-level DOE strategy determines a number of simulations which depends on the amount of parameters chosen, which vary between a minimum (-1) and a maximum (+1) level. The parameters considered for DOE are described in the following table.

Table 2. Two-level Design Of Experiment simulation data

Group	**Type**	**Unit**	**Value levels**	
			-1	+1
Envelope	U value external walls	W/(m^{2}K)	0.23	0.27
	U value roof	W/(m^{2}K)	0.21	0.26
	U value transparent components	W/(m^{2}K)	1.04	1.25
Activities	Internal gains (lighting, appliances and occupancy)	W/m^2	1	1.5
Control and operation	Heating set-point temperature	°C	20	22
	Air-change rate	vol/h	0.4	0.6

In order to simulate more realistic operation conditions, coherent operating schedules have been created for heating, cooling, air-change rate (natural ventilation/infiltration) and internal gains (lighting, appliances, people).

The DOE simulation runs conducted are 3, simulating different behavioural patterns of people living in the building:

1. operation is continuous as in baseline modelling (constant operation profile);
2. operation is concentrated between 7.00 and 22.00 (variable operation profile);
3. operation is concentrated between 7.00 and 9.00 and between 17.00 and 22.00 (variable operation profile).

The results of parametric simulations are then plotted in Figures 5,6 and 7, using the same graphs as in Figures 2, 3 and 4 but reporting the configurations that determined, respectively, the minimum and maximum non-renewable primary energy demand. This performance indicator has been calculated according to the methodology proposed in the standard ISO 52000-1 [18]. As introduced before, the whole building energy demand has been taken into account, weighting delivered and imported electricity asymmetrically. The primary energy and emission factors assumed for calculation are the ones contained in Italian legislation regarding energy efficiency in buildings. However, while the delivered energy weight assumed is 1, the exported energy weight assumed here is 0.4, differently from the current building performance rating scheme adopted at the national level, which gives a 0 weight for exported energy.

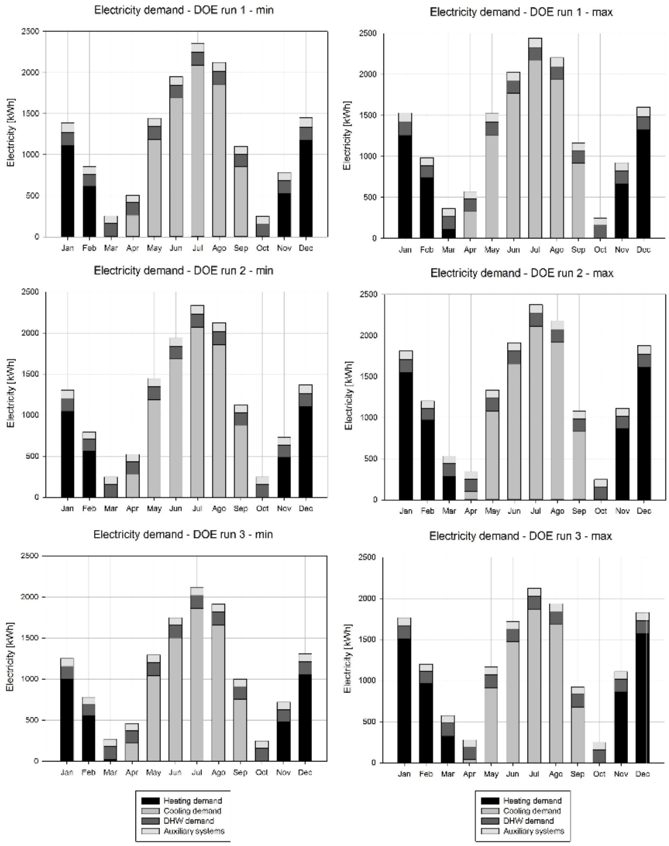

Figure 5. Electricity demand composition - DOE runs

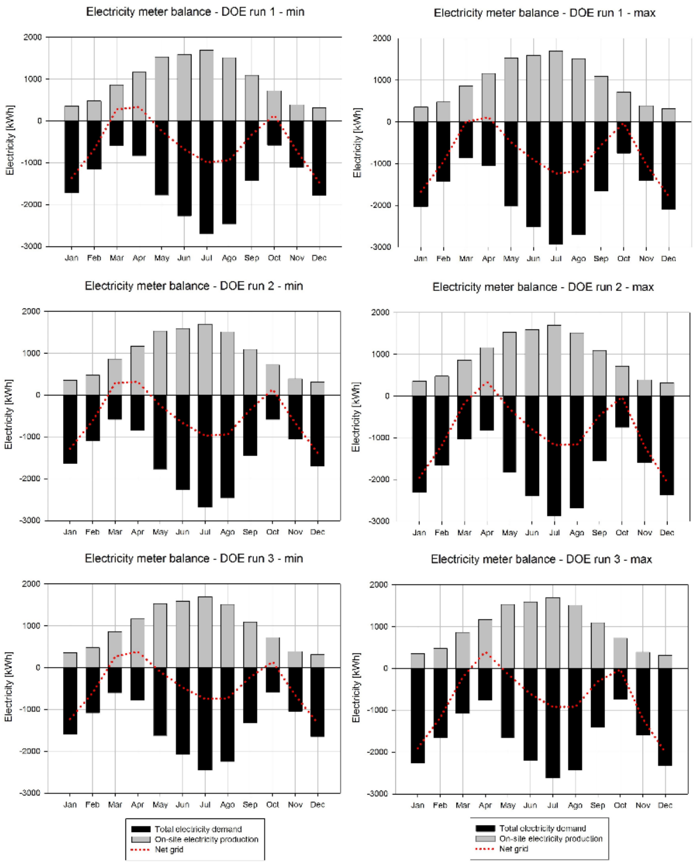

Figure 6. Electricity meter balance - on-site production and demand - DOE runs

On the one hand, the results from parametric simulations show that the electricity demand composition (Figure 5) and the relation between demand and on-site production (Figure 6) change in terms of values but not in terms of monthly patterns, having provided coherent assumptions for the selected configurations. On the other hand, results in Figure 7 show how the schedules considered affect largely the interaction between the building and the grid. This fact has profound techno-economic and environmental implications, related in particular to load-matching, prosumer (producer-consumer) business model, primary energy and CO_2 emission. Finally, the results obtained have been used to calculate key performance indicators (KPI), reported in Table 3. The sensitivity on KPI have been calculated too and expressed in terms of percentage of variation with respect to baseline configuration.

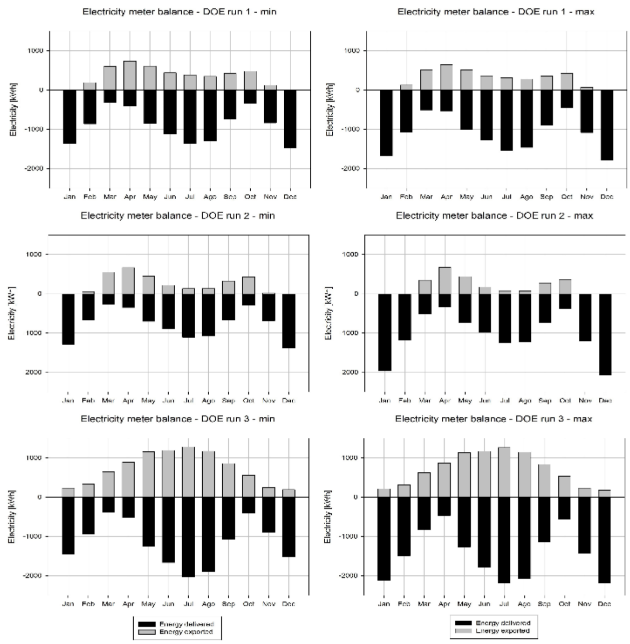

Figure 7. Electricity meter balance - delivered and exported energy - DOE runs

The values are reported in Figure 8 and indicate that the results are highly sensitive to assumptions because a relatively small variation in input data can determine a large variation in output data. Self-consumption, in particular, can largely vary depending on behavioral patterns, both in positive and negative terms, for the reason previously described with respect to Figure 7.

Table 3. Two-level Design of Experiment simulation results – KPI

Indicator	**Base**	**Run 1**		**Run 2**		**Run 3**	
		Min	Max	Min	Max	Min	Max
Heating demand (kWh/m^2)	20.4	24.8	29.6	23.0	38.1	22.3	37.8
Cooling demand (kWh/m^2)	52.3	50.1	52.9	50.2	48.5	44.4	42.0
Self-consumption (%)	63.6	62.9	69.3	74.5	79.4	25.2	27.4
Renewable Energy Ratio (%)	61.7	62.5	59.0	64.5	61.9	59.1	57.9
Primary Energy (kWh/m^2)	39.3	40.7	52.1	35.9	50.9	46.3	62.0
CO_2 Emission (kg/m^2)	8.7	9.0	11.5	7.9	11.2	10.2	13.7

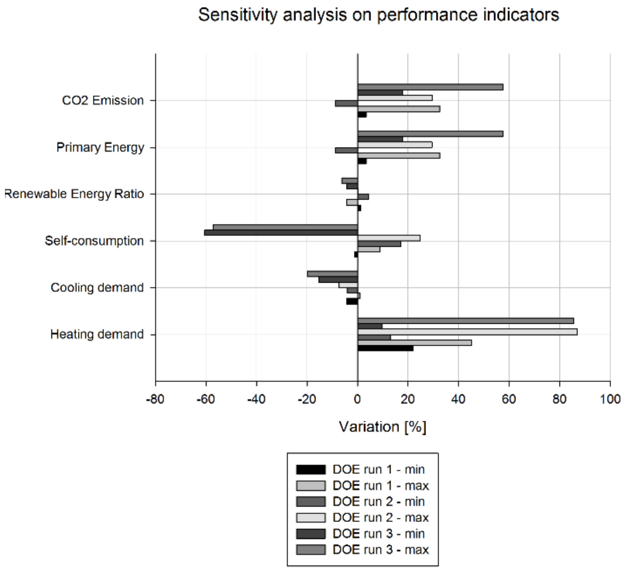

Figure 8. Sensitivity of KPI

5 Conclusion

Design optimization in buildings has often been oriented towards specific paradigms without considering properly uncertainty in design assumptions. Today we have the possibility to use parametric simulation to test robustness of design from the very beginning, assuming a more critical perspective on building performance, necessary to ensure the credibility of energy efficiency practices, especially with respect to incoming business models (e.g. prosumer) where cost-optimality is an essential requisite. Occupants' preferences and behaviour have been often neglected in design but they are essential for the success of innovative practices and policies in buildings. The patterns of delivered and exported energy, as shown for the case study, can change radically when using realistic operation profiles instead of standardized assumptions. This can determine a huge impact in economic and environmental terms. Therefore, instead of simply considering the formal correctness of modelling approaches, it is necessary to progressively introduce parametric design in practice, considering, on the one hand, more realistic operation profiles for buildings and, on the other hand, more detailed and realistic data for grid interaction (energy conversion factors, tariffs, CO2 emission etc.). In this way, design practices in the built environment could evolve coherently with energy infrastructures, in particular electric grid.

References

[1] N. Dodd, S. Donatello, E. Garbarino, and M. Gama-Caldas, "Identifying macro-objectives for the life cycle environmental performance and resource efficiency of EU buildings" JRC EU Commission, 2015.
[2] "Europe's buildings under the microscope" Buildings Performance Institute Europe (BPIE), 2011.
[3] D. D'Agostino, P. Zangheri, B. Cuniberti, D. Paci, and P. Bertoldi, "Synthesis Report on the National Plans for Nearly Zero Energy Buildings (NZEBs)" JRC EU Commission, 2016.
[4] PHPP – the energy balance and Passive House planning tool.
[5] "Energy Efficiency – the first fuel for the EU Economy, How to drive new finance for energy efficiency investments" EEFIG, 2015.
[6] Y. Saheb, K. Bodis, S. Szabo, H. Ossenbrink, and S. Panev, "Energy Renovation: The Trump Card for the New Start for Europe" JRC EU Commission, 2015.
[7] N. Aste, R. S. Adhikari, and M. Manfren, "Cost optimal analysis of heat pump technology adoption in residential reference buildings" *Renewable Energy,* vol. 60, pp. 615-624, 12/2013.
[8] P. de Wilde, "The gap between predicted and measured energy performance of buildings: A framework for investigation" *Automation in Construction,* vol. 41, pp. 40-49, 5/2014.
[9] A. C. Menezes, A. Cripps, D. Bouchlaghem, and R. Buswell, "Predicted vs. actual energy performance of non-domestic buildings: Using post-occupancy evaluation data to reduce the performance gap" *Applied Energy,* vol. 97, pp. 355-364, 9/2012.
[10] L. C. Tagliabue, M. Manfren, A. L. C. Ciribini, and E. De Angelis, "Probabilistic behavioural modeling in building performance simulation—The Brescia eLUX lab" *Energy and Buildings,* vol. 128, pp. 119-131, 9/2016.

[11] M. Manfren, N. Aste, and R. Moshksar, "Calibration and uncertainty analysis for computer models – A meta-model based approach for integrated building energy simulation" *Applied Energy,* vol. 103, pp. 627-641, 3/2013.
[12] A.-T. Nguyen, S. Reiter, and P. Rigo, "A review on simulation-based optimization methods applied to building performance analysis" *Applied Energy,* vol. 113, pp. 1043-1058, 1/2014.
[13] N. Aste, M. Manfren, and G. Marenzi, "Building Automation and Control Systems and performance optimization: A framework for analysis" *Renewable and Sustainable Energy Reviews* (in press).
[14] Z. Yang and B. Becerik-Gerber, "A model calibration framework for simultaneous multi-level building energy simulation" *Applied Energy,* vol. 149, pp. 415-431, 7/2015.
[15] L. Tronchin, M. Manfren, and L. C. Tagliabue, "Optimization of building energy performance by means of multi-scale analysis – Lessons learned from case studies" *Sustainable Cities and Society,* vol. 27, pp. 296-306, 11/2016.
[16] J. Antony, *Design of Experiments for Engineers and Scientists*: Elsevier Science, 2014.
[17] N. Aste, C. D. Pero, M. Fattore, and M. Mazzon, "Investigating on electric consumptions for residential buildings ventilation in different Italian climates" in *2015 International Conference on Clean Electrical Power (ICCEP)*, 2015, pp. 305-310.
[18] prEN ISO/DIS 52000-1:2015, Energy performance of buildings — Overarching EPB assessment – Part 1: General framework and procedures

10TH INTERNATIONAL CONFERENCE ON SUSTAINABLE ENERGY AND ENVIRONMENTAL PROTECTION (JUNE 27TH – 30TH, 2017, BLED, SLOVENIA), ENERGY EFFICIENCY
J. Krope, A.Ghani Olabi, D. Goričanec & S. Božičnik

Controlled Mechanical Ventilation: Comparison of Energy Use and Primary Applied to 20 Different Devices in a Testing Room

KRISTIAN FABBRI, CHIARA BERTOLLI & LAMBERTO TRONCHIN

Abstract Indoor air quality (IAQ) of buildings is a problem that affects both well-being of occupants and energy consumption relative to the structure. Controlled mechanical ventilation system (CMV) allow to control the air exchange rate. When using CMV systems is interesting to investigate the relationship between the useful thermal energy requirements for ventilation and the energy consumption of these systems. Is there a correlation between these two parameters?

This paper will address this question. The methodology used in this work involves the application of equations of technical regulations UNI/TS 11300 in a case study. The case study is represented by a test-room where it is assumed to be present three CMV systems (extraction, insertion, insertion and extraction) for 20 different devices available on the market.

Simulations of useful thermal energy requirements QH,ve and primary energy EP,V were performed according to the electrical power of fan W and the ventilation flow. The results show that the two values are not linearly correlated: it's not possible to associate the operating cost for CMV systems according to building requirement.The study also shows that CMV systems are especially efficient for high performance buildings, where there is not leakage that can be ascribed to windows infiltrations.

Keywords: • Energy efficiency • Indoor air quality • Controlled Mechanical • Ventilation • Natural Ventilation •

CORRESPONDENCE ADDRESS: Kristian Fabbri, Mr., Adjunct Professor, University of Bologna, School of Engineering and Architecture, Viale Europa 596, 47521 Cesena, Italy, e-mail: kristian.fabbri@unibo.it. Chiara Bertolli, Miss, University Alumnus, University of Bologna, School of Engineering and Architecture, Viale del Risorgimento 2, 40136 Bologna, Italy, e-mail: chiara.bertolli@studio.unibo.it. Lamberto Tronchin, Ph.D., Associate Professor, University of Bologna, School of Engineering and Architecture, Viale del Risorgimento 2, 40136 Bologna, Italy, e-mail: lamberto.tronchin@unibo.it.

https://doi.org/10.18690/978-961-286-050-9.10 ISBN 978-961-286-050-9

Available at: http://press.um.si.

1 Introduction

The Indoor Air Quality (IAQ) defines the air quality inside and around buildings, measuring the health and comfort of the occupants. In residential buildings, daily activities contaminate the indoor air: i.e., odors, carbon dioxide, water vapor. To ensure the healthiness of the environment and to avoid the formation of pollutants, toxic or allergens, it is necessary to dilute the concentration of the pollutants dispersed into indoor air volume through the air exchange by means of ventilation. Air exchanges could guarantee the conditions of comfort, hygiene and healthiness. Moreover, the ventilation of rooms constitutes a legislative and regulatory requirement, which concerns two aspects: (a) the healthiness of the environment or rather the removal of pollutants through ventilation, (b) the energy consumption due to the natural and mechanical ventilation, because of the entry of air masses at different temperatures and, for the Controlled Mechanical Ventilation (CMV), the energy costs required to operate the fan.

The National and International institutions, which deal with health and hygiene in indoor environments, consider CMV riskier compared to natural ventilation for the concentration of pollutants, as reported in guidelines of World Health Organization (WHO). [1]

On the other side, all people involved with national and international standards, as well as professionals working in the field of energy design in buildings, consider mandatory the CMV to reduce useful thermal energy exchanges due to air renewal, for natural ventilation and air leakage This opinion is stronger in those involved with Low Energy Buildings - LEB or Nearly Zero Energy Buildings - NZEB or Passive House.

The study of Wei [2] reported in a useful review the parameters adopted by the different green buildings certification systems (31 certifications worldwide were reviewed), and several regulations or standards (ASHRAE 62.1 [3], EN 15251 [4], EN 13779 [5], AS 1668-2 [6], etc.) regarding energy certification and IAQ that should be obtained, by means of: (a) the control of sources, or rather the removal of pollutants through the choice of building materials, finishings and furnitures; (b) the use of CMV and airtightness; (c) or experimental measurement of IAQ and the pollutants concentration.

Therefore, two approaches are possible: (1) to prefer Indoor Air Quality and environmental healthiness, and use air-leakage for ventilation, and (2) to prefer air tightness buildings provided with CMV, which ensure a high value of energy efficiency. The second approach is considered better.

Nevertheless, an appropriate level of Indoor Air Quality can also be achieved by means of a proper CMV system. Obviously, the presence of a CMV system involves energy costs, which could be avoided if natural ventilation is used. The CMV systems allows a continuous and controlled ventilation, which could not be obtained with natural ventilation. For example, during summer season, in case of natural ventilation opening the windows let the heat to come inside the building. Moreover, considering the nearly static nature of air in summer season, it is hardly feasible to obtain a fair air circulation.

2 Literature Review

2.1 Scientific literature

The scientific literature about IAQ and/or ventilation is very wide and there are different case studies concerning the use of CMV. For example, the paper of Y. Chen et al. [7] reports a study on ventilation systems with individual control of airflow rate in a hot and humid climate. The results show that when the ventilation air temperature is kept at 20 °C, the energy consumption at an ambient temperature of 23 °C is 10.8% higher than that at 26 °C. The study concludes that increasing the ambient temperature might be a solution to reduce the energy consumptions.

The research of Fehr M. et al. [8] reports the development of markets in Sweden and Germany (which are considered similar each other) of CMV systems with heat recovery. The types and the benefits for environment are described in detail. This study evidences that the new building code for the year 2000 contains requirements for the realisation of insulated buildings, where the energy requested for heating the ventilation air, reaches the 60% of the annual building energy requirement. The approach airtightness and the use of CMV is highly used and appreciated in Central and Northern Europe, as well as in Passive-house standards.

Tronchin L. et al. [9] have presented a study about the comparison among three different models for calculation of the Energy Performance of Buildings (EPB), in order to quantify their gap with real consumptions. The study has been conducting considering a single-family house in Italy and focused on the differences between numerical codes and the consumption in connection to flexible architectural solutions, which are widely used especially in rural areas in the Mediterranean countries.

Simonson C. [10] proposes in his paper the analysis of an eco-friendly single-family building situated in Helsinki, Finland, built in wood and well insulated and thoroughly measured and analyzed, relative to its energy consumption and rate ventilation. The results of the measurements and simulations show that the energy consumption is low and the outdoor ventilation rate based on the CO2 concentration is satisfying. The study proves that the primary energy and thermal energy consumptions are lower than other buildings built with traditional methods.

IAQ research particularly focus in case studies related to school buildings, since these users (children, kids) are more sensitive to respiratory problems due to the IAQ. Some relevant researches were carried out by Gao J. et al. [11], Stabile L. et al. [12] and Fabbri K. [13].

Among the research applied to residential buildings and IAQ, Fabbri K. et al. [14] reports the results obtained from the monitoring of IEQ (Indoor Environmental Quality) of a low energy building (Energy Class A+ and 25 kWh/m2y). The results show that the buildings with low energy performances not always guarantee a better level of IEQ, especially during summer season.

Fabbri K. et al. [15] have presented a study by performing a simulation energy retrofit of an Italian case study: a building made in various times, having different thermo-physical parameters. For each temporary period, four actions of energy retrofit have been applied, together with an evaluation software of the energy performances.

2.2 Standard literature

This research focuses on the study of relation between ventilation, useful to guarantee the proper value of IAQ, and the related energy costs. However, different studies on IAQ have indicated different value of ventilation, depending of the characteristics of the building under analysis (Sick Building Syndrome, etc.).

The presence of pollutants derived from the combustion products falls within the scope of the study of the IAQ. For example, the concentration of CO (carbon monoxide), produced by the incomplete combustion in the case of boilers with natural gas or LPN, biomass generators, or with open fireplaces in environment such as chimneys and stoves that produce dust. About that, the WHO has prepared a specific guideline [16]. In Europe, particularly in Italy, the annual maintenance operations of the heat generations allow considering these risks excluded. Moreover, if CMV systems are installed in high performance buildings, it is preferable to choose heat pumps.

The standard EN 12792 [17] defines the requirements of mechanical ventilation. It provides the terms and the explanations concerning ventilation in rooms; with regard to the requirements of useful thermal energy. The standard EN ISO 13790 [18] contains the calculation method to evaluate the dispersions for ventilation. Finally, EN 15251 [19] defines the parameters necessary to evaluate the Indoor Environmental Quality (IEQ) and proposes the values of air exchange for residence and tertiary sector.

In Italy, the European standards for the calculation of energy needs of buildings, which are defined by the CEN (European Committee for Standardization), have been implementing in the standards UNI/TS 11300 (series), in actualization of the transposition of Directive 2010/91/CE (EPBD) [20] and by Directive 2010/31/UE (EPBD II Recast) [21].

The calculation of thermal energy needs for ventilation is described in the UNI/TS 11300-1 standard [22]. This document contains a calculation method to evaluate the ventilation dispersions, whereas the UNI/TS 11300-2 standard [23] provides methods for the calculation of primary energy needs for ventilation and for winter heating in the presence of aeraulic systems.

3 Goals

The aim of this work consists of analyzing the relationship between useful thermal energy for ventilation and primary energy needs required for operating CMV systems.

This analysis is necessary because in the case of natural ventilation all the costs are equal zero, whereas in the case of CMV the primary energy needed to operate the plant and the related operating costs, should be added.

The research is carried out by the comparison between the energy needs for heating and cooling for ventilation Qve, and primary energy needs for ventilation $E_{P,V}$, applied to a specific case study and to a series of commercial products available on the market.

To compare different products, the calculations focus on a hypothetical case study, defined as a room having representative dimensions of a common bedroom and/or living room for residential buildings.

As far as the choice of the individual devices it is concerned, it was decided to adopt the values of ventilation rates provided by the following manufacturers: ALDES, IRSAP, FRANCE AIR, ELICENT, VORTICE.

The UNI/TS 11300 standards contain the formulas that link the useful thermal energy with the primary energy needs. As far as the thermal exchanges for transmission is concerned, both the solar contributions and the use of renewable energy have been considered identical in all simulations. Therefore, the results refer only to energy exchanges regarding ventilation, and have been plotted into graphs and histograms.

This preliminary study involves a first set of analyses, which includes:

- the definition of useful thermal energy and primary energy needs;
- the choice of CMV devices;
- the definition of management costs;

Once the algorithm and the case studies are defined, this work continues with the definition of a test room, for which the requirements for each device have been calculated. The comparison and discussion of the results are the last part of this work.

3.1 Calculation of Thermal Requirements

The technical standard UNI/TS 11300-1 provides data and methods for the evaluation of energy needs for heating and cooling. The exchanges of thermal energy are calculated, for each building's thermal area and for each month or part of a month, through the following equations:

- in the case of heating:

$$Q_{H,ve} = H_{ve,adj} \cdot (\theta_{int,set,H} - \theta_e) \cdot t \qquad (1)$$

- in the case of cooling:

$$Q_{C,ve} = H_{ve,adj} \cdot (\theta_{int,set,C} - \theta_e) \cdot t \qquad (2)$$

where $H_{ve,adj}$ is the global heat transfer coefficient for ventilation of the area considered, expressed in W/K; $\theta_{int,set,H}$ is the indoor temperature of regulation for heating of the area considered, expressed in °C and assumed equal to 26 °C; $\theta_{int,set,C}$ is the indoor temperature of regulation for cooling of the area considered; expressed in °C and assumed equal to 20°C; θ_e is the mean external temperature of month considered or of part of month, expressed in °*C* and t is the duration of month considered or of part of a month, expressed in Ms.

The global heat transfer coefficient for ventilation $H_{ve,adj}$ is obtained from the equation:

$$H_{ve,adj} = \rho_a \cdot c_a \cdot \{\Sigma_k \, b_{ve,k} \cdot q_{ve,k,mn}\} \ \text{(kWh)} \qquad (3)$$

where $\rho_a \times c_a$ is the air volumetric heat capacity, equal to 1200 J/(m^3 × K), $b_{ve,k}$ is the correction factor of temperature for the air flow and $q_{ve,k,mn}$ is the flow mediated on time of air flow, expressed in m^3/s.

In buildings where only mechanical ventilation is available, $q_{ve,k,mn}$ is calculated from the equation:

$$q_{ve,k,mn} = (\bar{q}'_{ve,x}) \cdot (1-\beta_k) + (q_{ve,f} \cdot b_{ve} \cdot FC_{ve} + \bar{q}_{ve,x}) \cdot \beta_k \qquad (\text{m}^3/\text{s}) \qquad (4)$$

where $\bar{q}'_{ve,x}$ is the additional main air flow due to the effects of wind, in the period of non-operation of mechanical ventilation, β_k is the temporal interval fraction calculation with functioning mechanical ventilation for the air flow, $q_{ve,f}$ is the nominal flow rate of mechanical ventilation, $b_{ve,k}$ is the correction factor for the effectively available temperature in the air flux, FC_{ve} is the efficiency factor of the system adjustment of mechanical ventilation and $\bar{q}_{ve,x}$ is the additional daily average air flow with functioning mechanical ventilation due to thermic and transverse natural ventilation.

The technical standard UNI/TS 11300-2 provides the method of calculation for the determination of primary energy needs for ventilation. The primary energy needs for mechanical ventilation is calculated considering the electricity requirements for the air movement.

The primary energy needs for mechanical ventilation $E_{P,V}$, expressed in kWh, it is determined through the equation:

$$E_{P,V} = f_{p,el} \cdot \Sigma\, E_{ve,el} \qquad (5)$$

where $f_{p,el}$ is the electrical energy conversion factor in primary energy and $E_{ve,el}$ is the electrical energy need of the fans, expressed in kWh. The electrical energy needs of the fans $E_{ve,el}$ it is determined through the equation:

$$E_{ve,el} = W_{ve,el} \cdot FC_{ve} \cdot t \qquad (6)$$

where $W_{ve,el}$ is the electric power of the incoming fan, expressed in W, FC_{ve} is the loaded factor of mechanical ventilation and t is the time interval of calculation, expressed in h.

4 The Case Study

Since the CMV systems here analyzed are applied in environments having less than 150 m^3 net volume and composed of one, two or three rooms of the same sizes, the test room (case study) consists of a room having dimensions of $l_1 = 4.0$ m, $l_2 = 5.0$ m, $h_{int} = 2.7$ m (net internal height), and therefore having volume equal to 54 m^3; the dimensions correspond to those of ordinary living rooms, bedrooms and similar. The calculation and comparison between useful thermal energy needs (Q_{ve}) for ventilation and primary energy needs for ventilation is related to the test room.

In the following, 20 CMV systems have been chosen and considered during the evaluations. They differed for mechanical characteristics (diameter, electrical power, volumetric flowrate). The Figure 1 shows, for each CMV device, according to the typology (emission; insertion; emission / insertion) the value of useful thermal energy needs for ventilation ($Q_{H,ve}$), expressed in kWh/y. The values are similar for the first two types of CMV. On the other hand, the third typology, which corresponds to a device with a balanced insertion and extraction systems with double conduit, presents slightly higher values.

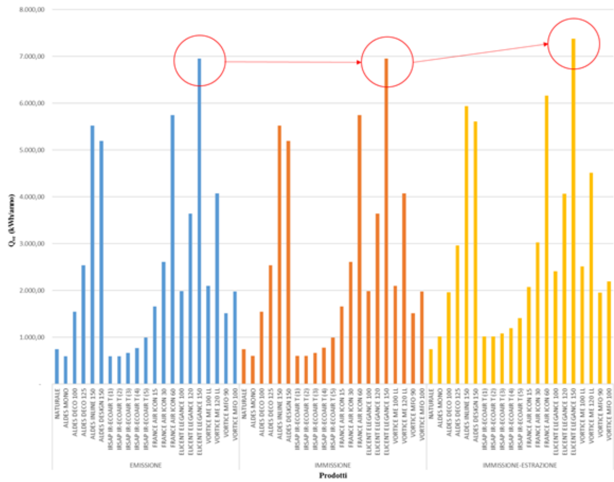

Figure 1. $Q_{H,ve}$ values for the 3 types of CMV

After that, the grey-box model has been used for yearly simulations, including all the energy demands from the building, namely heating, cooling, domestic hot water (DHW), lighting and appliances. All the demands are satisfied by means of electricity, considering the GSHP system, providing heating, cooling and domestic hot water, the lighting system and the appliances.

The simulation carried out compares the relationship between useful thermal energy needs ($Q_{H,ve}$), which depends on the geometrical characteristics of the environment (volume) and the nominal flow rate of controlled mechanical ventilation, with primary energy needs ($E_{P,V}$) which depends on the electric power of the insertion or extraction fan, that normally is provided by the manufacturer in an included table of technical data. The interest of the research is to check whether there is a linear relationship, i.e. if effectively the more the thermal energy needs increases, the more the primary energy needs increases.

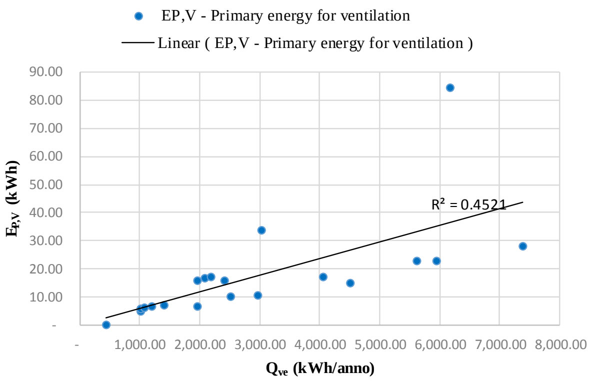

Figure 2. $Q_{H,ve}$ and $E_{P,V}$ (emission) for CMV

The Figure 2 shows the relationship between the useful thermal energy needs ($Q_{H,ve}$) on axis x, and primary energy needs ($E_{P,V}$) on axis y. The diagram shows that between the two parameters there is a linear correlation: however, in some circumstances the values deviate from the trend line represented. For all three types of CMV systems, it is evident that only the France Air model Icon 60 shows an abnormal situation. The graph shows that the useful thermal energy needs ($Q_{H,ve}$) and primary energy ($E_{P,V}$) are not strongly related each other, according to the formulas reported in UNI/TS and to the characteristics of the products CMV.

5 Conclusion

This preliminary work shows that it is interesting and useful for the design of ventilation systems in buildings, to investigate the relationship between the useful thermal energy needs for ventilation (QH,ve) and the primary energy needs for ventilation (EP, V).

It was found that there is not a strong linear correlation between the useful thermal energy needs and management costs. Therefore, it is not possible to adopt simplified design criterion: it is necessary to provide standardized solutions or examples of CMV systems applied to individual houses.

It would be useful to have the numerical values of flow and power of CMV standardized, without relying to the manufacturers. In this way it would be possible to obtain a real evaluation of the situation, referring the data to the market products. Finally, it would be useful to have a proper database available to all the professionals who are dealing with CMV.

References

[1] World Health Organization (2009), Natural ventilation for infection control in health-care settings, WHO guidelines

[2] Wei W, Ramlho O, Mandin C (2015) Indoor air quality requirements in green building certifications, Building and Environment, 92, pp.10-19

[3] ASHRAE (2016), Standard 62, Ventilation for Acceptable Indoor Air Quality

[4] EN 15251, Indoor environmental input parameters for design and assessment of energy performance of buildings addressing indoor air quality, thermal environment, lighting and acoustics

[5] EN 13779, Ventilation for non-residential buildings - Performance requirements for ventilation and room-conditioning systems

[6] Australian Standard 1668 part-2, The use of ventilation and air conditioning in buildings, Part 2: Ventilation design for indoor air contaminant control (excluding requirements for the health aspects of tobacco smoke exposure

[7] Chen Y., Raphael B., Sekhar S.C. (2016), Experimental and simulated energy performance of a personalized ventilation system with individual airflow control in a hot and humid climate, Energy and Environment, 96, 283-292

[8] Fehrm M., Reiners W., Ungemach M. (2002), Exhaust air heat recovery in buildings, International Journal of Refrigeration, 25, 439-449

[9] Tronchin L, Fabbri K. (2008), Energy performance building evaluation in Mediterranean countries: Comparison between software simulations and operating rating simulation, Energy and Buildings,40, Issue 7, 1176-1187

[10] Simonson C. (2005), Energy consumption and ventilation performance of a naturally ventilated ecological house in a cold climate, Energy and Buildings, 37, 23–35

[11] Gao J., Wargocki P., Wang Y. (2014), Ventilation system type, classroom environmental quality and pupil's perceptions and symptoms, Building and Environment, 75, 46-57

[12] Stabile L., Dell'Isola M., Frattolillo A., Massimo A., Russi A. (2016), Effect of natural ventilation and manual airing on indoor air quality in naturally ventilated Italian classrooms, Building and Environment, 98, 180-189

[13] Fabbri K. (2013), Thermal comfort evaluation in kindergarten: PMV and PPD measurement through datalogger and questionnaire, Building and Environment, 68, 202-214

[14] Fabbri K., Tronchin L. (2015), Indoor Environmental Quality in Low Energy Buildings, Energy Procedia, 78, 2778-2783

[15] Fabbri K., Tronchin L., Tarabusi V. (2014), Energy Retrofit and Economic Evaluation Priorities Applied at an Italian Case Study, Energy Procedia, 45, 379-384

[16] World Health Organization (2014), Household fuel combustion, Indoor air quality guidelines

[17] EN 12792 (2003) Ventilation for buildings - Symbols, terminology and graphical symbols

[18] EN ISO 13790 (2008) Energy performance of buildings - Calculation of energy use for space heating and cooling

[19] EN 15251 (2007) Indoor environmental input parameters for design and assessment of energy performance of buildings addressing indoor air quality, thermal environment, lighting and acoustics

[20] Directive 2002/91/EC of the European Parliament and of the Council of 16 December 2002 on the energy performance of buildings

[21] Directive 2010/31/UE of the European Parliament and of the Council of 19 May 2010 on the energy performance of buildings (recast)

[22] UNI/TS 11300 Energy performance of buildings. Part 1: Evaluation of energy need for space heating and cooling

[23] UNI/TS 11300 Energy performance of buildings Part 2: Evaluation of primary energy need and of system efficiencies for space heating, domestic hot water production, ventilation and lighting for non-residential buildings

10TH INTERNATIONAL CONFERENCE ON SUSTAINABLE ENERGY AND ENVIRONMENTAL PROTECTION (JUNE 27TH – 30TH, 2017, BLED, SLOVENIA), ENERGY EFFICIENCY
J. Krope, A.Ghani Olabi, D. Goričanec & S. Božičnik

Investigation of Performance and Emissions in a SI Engine Fuelled by Gasoline - Acetylene Mixtures

MEHMET İLHAN İLHAK, SELAHADDIN ORHAN AKANSU, NAFIZ KAHRAMAN & SEBAHATTIN ÜNALAN

Abstract In this study, an experimental study on the performance and exhaust emissions of a spark-ignition engine fuelled with gasoline – acetylene mixtures (150 g/h and 1200 g/h) were performed at 1500 engine speed and different loads. Experiments have been carried out a four-stroke cycle, four-cylinder, spark-ignition engine with a bore of 80.6 mm, a stroke of 88 mm and a compression ratio of 10:1 and at stoichiometric conditions. While load have been increased, CO and HC emission values have been decreased but NOx increased. Exhaust gas temperature remained almost the same, when compared with baseline gasoline operation.

Keywords: • Acetylene • Gasoline • SI engine • Performance • Emissions •

CORRESPONDENCE ADDRESS: Mehmet İlhan İlhak, Ph.D., Assistant, Erciyes University Engineering Faculty, Kayseri. Turkey, e-mail: ilhanilhak@gmail.com. Selahaddin Orhan Akansu, Ph.D., Professor, Erciyes University Engineering Faculty, Kayseri. Turkey, e-mail: akansu@erciyes.edu.tr. Nafiz Kahraman, Ph.D., Professor Erciyes University Engineering Faculty, Kayseri. Turkey, e-mail: nafiz@erciyes.edu.tr. Sebahattin Ünalan, Ph.D., Professor Erciyes University Engineering Faculty, Kayseri. Turkey, e-mail: s-unalan@erciyes.edu.tr.

https://doi.org/10.18690/978-961-286-050-9.11 ISBN 978-961-286-050-9

Available at: http://press.um.si.

1 Introduction

As a power source in the transportation system that works with gasoline and diesel internal combustion engines are widely used and this is especially causes air pollution in major cities [1]. Gasoline and diesel with crude oil derivatives have superior properties as a fuel. But reserves are limited and emit a high rate of emission of pollutants into the environment when used in internal combustion engines. This situation has led researchers to search alternative fuel with renewable, higher reserves and lower emissions. Gaseous fuels have great potential in this area due to lower exhaust emissions and plenty of presence. Acetylene gas (C_2H_2) is one of the gas fuels used in internal combustion engines which has excellent combustion properties. In the early the year 1900s, engines operating with acetylene gas was made. But all over the world the expansion of gasoline and diesel, studies have been stored in this area and studies have been left on the use of acetylene gas in internal combustion engines. Environmental concerns, increasing global warming and laws to force the reduced emission limits caused by vehicles has increased the search for alternative fuels and studies on the use of acetylene gas in otto and dieselengines were started again in recent years.

Lakshaman and Nagarajan [2-4] conducted experiments on a single cylinder, four-stroke, air cooled, rated output of 4.4 kW at 1500 engine speed, direct injection diesel engine using acetylene and diesel in dual fuel mode. Tests were carried out under variable load conditions with diesel as the pilot fuel and acetylene inducted as secondary fuel at different flow rates. They stated that NO_x, HC, CO and CO_2 emissions were decreased with slight increase smoke emission. GA. Karim [5] conducted experiments using hydrogen, methane, acetylene, propane, ethylene and butane in diesel engine. He stated that the maximum gas flow rate is limited due to the start of knock and also reported that primary fuel quality, injection timing, and intake temperature are important variables affecting the performance of engine which run in dual fuel mode.

S. Brusca et al. [6] studied on the possibility to run a spark ignition engine on acetylene and alcohol. This engine was single cylinder, four stroke and modified with electronic injection control system and two standard injectors. They observed that engine performance decreased about 25% with acetylene and alcohol in comparison gasoline. Acetylene and alcohol brake specific fuel consumption is lower than gasoline in almost all engine speed. They stated that exhaust emissions CO, HC and NO_x decreased using acetylene and alcohol fuel in comparison gasoline. E. Vural and S. Ozer [7] used acetylene gas in a spark ignition engine with gasoline. The experiments were conducted between 1600 and 3200 rpm increasing by 400 rpm. They observed that exhaust emissions CO, CO_2, HC and NO_x decreased in dual fuel mode at all engine speed.

Acetylene is a colourless gas with garlic smell produced from hydrolysis of calcium carbide produced from heating lime at 2760-3870 ^{0}C in the presence of coke [8]. It was discovered in the year 1836 in England by E. Davy. Acetylene has a very wide flammability limits, higher flame speed, faster energy release, lower ignition energy, lower quenching distance and high calorific value in comparison other gases. Acetylene is not a suitable fuel for SI engines as the octane number of it is reported as 50 [9]. However, the self-ignition temperature of acetylene is higher than that of gasoline and therefore it can be used with gasoline in small quantities to improve combustion. The properties of acetylene and gasoline are given in Table 1

.

Table 1.The Properties of Fuels

Properties	Acetylene	Gasoline
Formula	C_2H_2	C_8 - C_{18}
Density, kg/m3(At 1 atm, 20 °C)	1.092	720-775
Auto ignition (°C)	305	257
Stoichiometeric air fuel ratio	13.2	14.7
Flammability Limits (Volume %)	2.5 - 81	1.4-7.6
Flammability Limits (equivalence ratio)	0.3–9.6	----
Lower Calorific Value (kJ/kg)	48225	44000
Ignition energy (MJ)	0.019	0.24
Adiabatic flame temperature(K)	2500	2270
Flame speed(m/s)	1.5	0.4

2 Experimental Setup

The experimental setup is shown in Figure 1. The SI engine designed to develop 75 kW at 5500 rpm with 10:1 compression ratio. Features of the engine are given in Table 2. Speed and torque values were measured by eddy-current dynamometer. Gasoline and acetylene gas have been measured by Krohne liquid mass flowmeter and Alicat M100 gas flowmeter respectively. PCB 111A22 piezoelectric pressure transducer and Bosch BEA 060 gas analyzer equipment have been used to measure cylinder pressure values and exhaust gas constituents (CO, CO2, HC and NO_x).

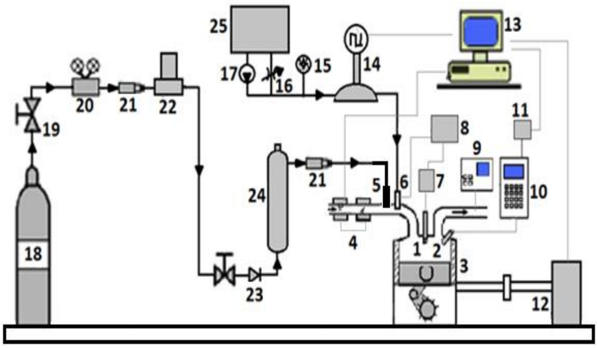

1-Spark plug 2-Pressure transducer 3-Engine 4-Air flow meter and Throttle valve position center 5- Gas injector 6-Fuel injector 7-Ignition module 8-Engine control unit 9-Exhaust gas analyzer 10-Charge amplifier 11-Data logger 12-Dynamometer 13-Computer 14-Liquid flow meter 15-Pressure gauge 16-Throttle valve 17-Fuel pump 18- Acetylene cylinder 19-Valve 20-Gas regulator 21-Flash back arrestor 22-Mass flow meter 23- Check valve 24- Wet type Flash back arrestor 25-Fuel tank

Fig. 1- Experimental setup

Gasoline was pumped to fuel injectors at 3 bar using fuel pump. Acetylene was introduced into the intake ports through four electronic gas injectors after from the cylinder stored at 22 bar pressure through gas regulator where the pressure was reduced to 10 psi. The safety devices such as check valve, flash back arrestor were used to quench the backfire from the engine. The gasoline and gas injectors were controlled by electronic card and computer, so gasoline and acetylene flows were arranged.

Table 2. Engine specifications

Engine	Ford MVH418
Silindir sayısı	4 in line
Stroke volume	1796 cm^3
Bore / Stroke	80,6 x 88 mm
Compression ration	10:1
Max. BMEP	10,7 bar
Max. Power	75 kW / 5500 rpm
Max. Tork	150 Nm / 4000 rpm
Idle / Max. Speed	800 / 6000 rpm

All experiments were conducted at 1500 rpm and stoichiometric ratio under different loads. Firstly, the experiment engine was run with gasoline and the tests were carried out for the gasoline. Then acetylene gas supplied into intake manifold. Acetylene flow rate was calculated on a mass basis using the following formula

$$m_{Acetylene} = \frac{m_{air}}{100} \quad \text{(for \%1 Acetylene)} \tag{1}$$

The beginning time of gasoline and gas injection were controlled by ECU of the test engine. İnjectors opening duration were varied by using electronic card and a computer.

3 Experimental Results

In this experiment, the performance parameters such as peak pressure, brake thermal efficiency and emission parameters such as carbon monoxide, hydrocarbon, nitrogen of oxides were compared with gasoline operation for various acetylene flow rates at 1500 rpm and different loads in a SI engine.

3.1 Peak pressure

The variation of cylinder pressure with crank angle for various acetylene gas flow rates have been illustrated Figure 2. The peak pressure was 19 bar in baseline gasoline operation at %50 load and 1500 rpm. Peak pressure is 21 bar at %1, 24 bar at %1.5 and 28 bar at %2 acetylene injection. The occurrence of peak pressure was 27° crank angle after top dead center in baseline gasoline operation. The occurrence of peak pressure was earlier than gasoline operation by 7°, 8° and 11° crank angle at %1, %1.5 and %2 acetylene induction respectively.

3.2 Brake thermal efficiency

The variation of brake thermal efficiency with brake power for various acetylene gas flow rates have been illustrated Figure 3. As seen this figure, the brake thermal efficiency is increasing at all load while acetylene is induced as supplementary fuel at 1% and 1.5% flow rates. However, the BTE is increasing at low load while acetylene is induced at 2% flow rate, marginally decreasing at full load. In generally, the increasing of acetylene amount, the brake thermal efficiency values have been decreasing. The brake thermal efficiency for gasoline is found to be 31.1% at full load. The efficiency at full load is found to be 32.3% at 1%, 31.6% at 1.5% and 29.8% at 2% gas flow rate respectively. Brake thermal efficiency for acetylene inducted 1% is higher than other flow rates at all load.

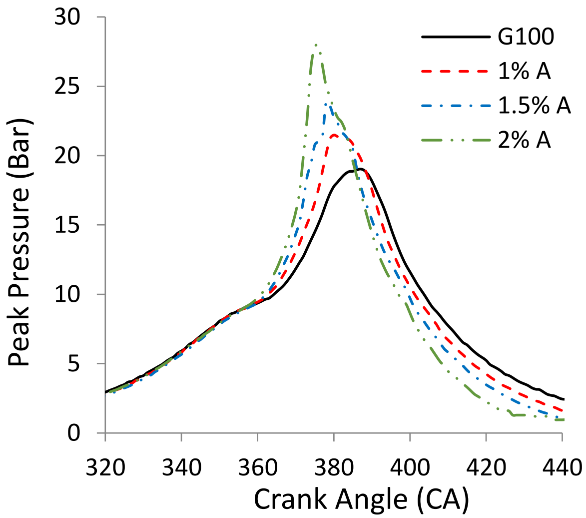

Fig. 2. Variation of cylinder pressure with crank angle

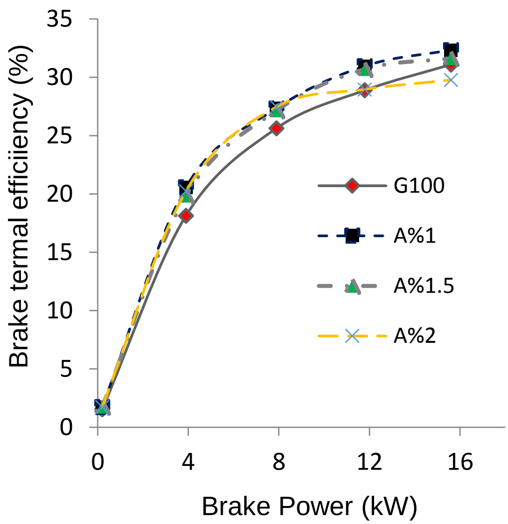

Fig. 3. Variation of brake thermal efficiency with brake power

3.3 Exhaust gas temperature

The exhaust gas temperature at all loads with brake power for various acetylene gas flow rates is shown in Figure 4. Exhaust gas temperature for gasoline is found to be 230 ^{0}C at 0% load while minimum exhaust gas temperature is found to be 195 ^{0}C at 1% acetylene gas flow rate at the same load.

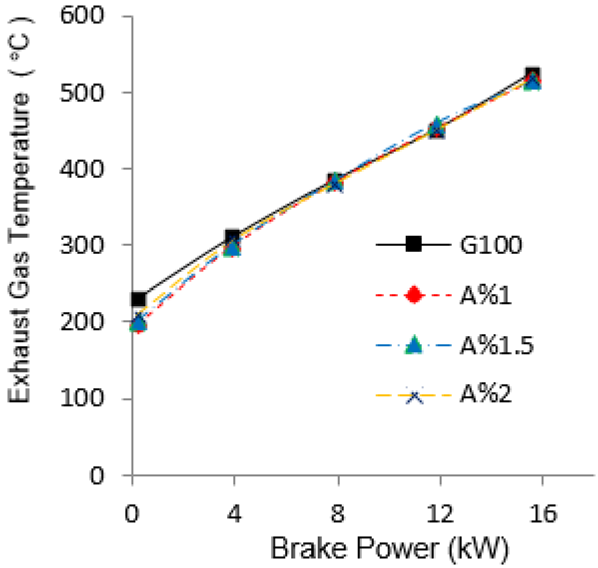

Figure 4. Variety of exhaust gas temperature with brake power

4 Emission Parameters

4.1 Carbon monoxide emissions (CO)

As seen in Figure 5 the variation of carbon monoxide emissions versus engine load were lower at all load when compared to the base line gasoline operation. The value of CO for gasoline is found to be 0.6% at full load. The value of CO at full load is found to be 0.3% at 1%, 0.33% at 1.5% and 0.66% at 2% acetylene gas flow rate respectively. Due to the complete burning of fuel and also acetylene gas has lower C/H ratio than gasoline, the CO emissions are lower when compared to the baseline gasoline operation.

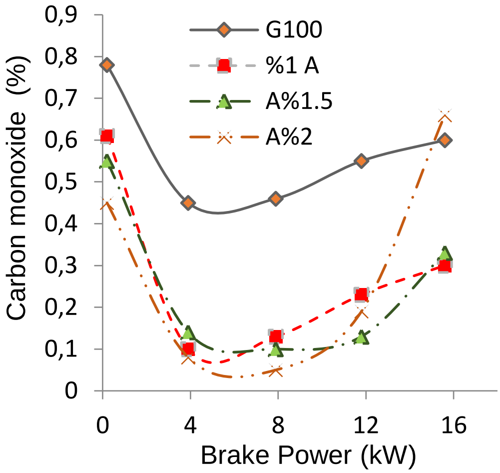

Fig. 5. Variety of carbon monoxide with brake power

4.2 Hydrocarbon emissions (HC)

The variation of HC emissions with brake power for various acetylene gas flow rate have been illustrated Figure 6. As seen figure 6, for all acetylene gas flow rate the HC emission values are always lower when compared to the baseline gasoline at all loads. The value of HC for gasoline is found to be 129 ppm at full load. The HC emission is found to be 83 ppm at 1%, 77 ppm at 1.5% and 68 ppm at 2% of gas flow rate respectively at full load. Maybe the reduction in HC emission in the case of acetylene fuel is due to the higher burning velocity of acetylene.

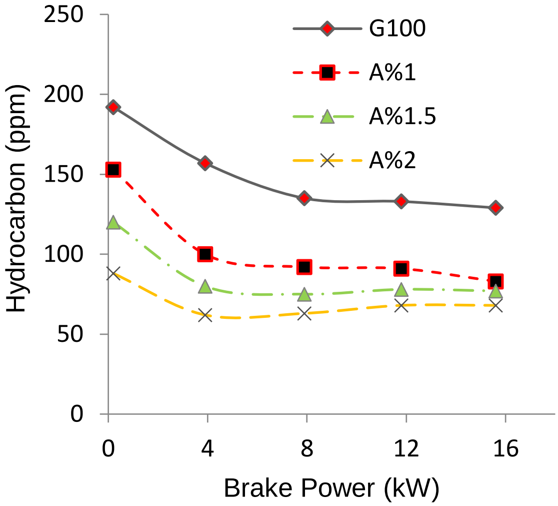

Figure 6. Variety of hydrocarbon with brake power

4.3 Oxides Of Nitrojen (NO_x)

The variation of NO_x emissions with brake power for various acetylene gas flow rate have been illustrated Figure 7. As seen figure 7, for all acetylene gas flow rate the NO_x emission values are always higher when compared to the baseline gasoline at all loads. Maximum value of NO_x for gasoline is found to be 2580 ppm at full load. The NO_x emission is found to be 3735 ppm at 1%, 3932 ppm at 1.5% and 4010 ppm at 2% of gas flow rate respectively at full load. According to zeldovich mechanism model, the formation of NO*x* is attributed to the reaction temperature, reaction duration, and the availability of oxygen [10]. Increase in NOx was attributed to the high temperature level because of faster energy release.

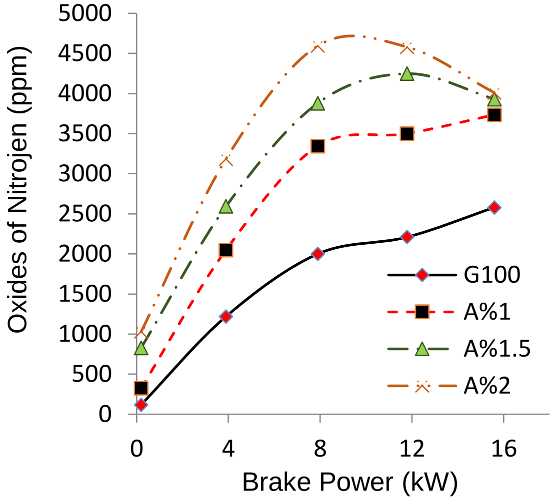

Figure 7. Variety of oxides of nitrogen with brake power

5 Conclusions

This study investigated emissions and performance of an SI engine using acetylene gas at 1500 rpm engine speed and different engine loads. It is possible to operate a SI engine using acetylene as a supplementary fuel without any undesirable combustion phenomenon.

Experimental results of this study can be summarized as follows:

- The peak pressure values were higher when compared to the baseline gasoline at all loads. The occurrence of peak pressure was earlier than gasoline operation by 7°, 8° and 11° crank angle at %1, %1.5 and %2 acetylene induction respectively.
- Brake thermal efficiency generally increase at all load while acetylene is induced as supplementary fuel at 1% and 1.5% flow rates.
- CO emissions were lower at all load when compared to the baseline gasoline operation.
- HC emission values were always lower when compared to the baseline gasoline at all loads.

NO_x emission values were always higher when compared to the baseline gasoline at all loads. Increase in NOx was attributed to the high temperature level because of faster energy release

Acknowledgements

The authors would like to acknowledge Erciyes University for the Scientific Research Projects Unit of Erciyes University, Turkey, for the financial support under the grant number FDK-2016-6302

References

[1] Karana S. 2003. The Effects of Cold Intake Temperatures on the Combustion of Gaseous Fuels in a Dual Fuel Engine, Ms Thesis, University of Calgary, Canada
[2] T. Lakshmanan, G. Nagarajan. Experimental investigation on dual fuel operation of acetylene in a DI diesel engine. Fuel Processing Techno-logy 91 (2010) 496–503
[3] T. Lakshmanan, G. Nagarajan.Experimental investigation of timed manifold injection of acetylene in direct injection diesel engine in dual fuel mode. Energy 35 (2010) 3172–3178
[4] T. Lakshmanan, G. Nagarajan. Experimental investigation of port injection of acetylene in DI diesel engine in dual fuel mode. Fuel 90 (2011) 2571–2577
[5] Karim GA. Ignition of a premixed fuel and air charge by pilot fuel spray injection with reference to dual-fuel combustion. SAE Paper No 680768.
[6] S. Bruscaa, R. Lanzafameb, A. Marino Cugno Garranob, M. Messinab. On the possibility to run an internal combustion engine on acetylene and alcohol. Energy Procedia 45, (2014) 889 – 898
[7] E. VURAL, S. ÖZER, Buji Ateşlemeli Motorlarda Yakıta Asetilen Gazı İlavesinin Egzoz Emisyonlarına Etkisinin Deneysel Analizi, BEÜ Fen Bilimleri 3(1), 24-34, 2014
[8] Mesleki Eğitim ve Öğretim Sisteminin Güçlendirilmesi Projesi (MEGEB) Temel Oksi Asetilen Kaynağı Ankara - 2007
[9] Hilden DL, Stebar RF. Evaluation of acetylene as a spark ignition engine fuel. Int J Energy Res 1979;3:59–71 [January–March].
[10] Ganesan V. Internal combustion engine. New Delhi: Tata McGraw - Hill Publishing Company Limited; 2007.

10TH INTERNATIONAL CONFERENCE ON SUSTAINABLE ENERGY AND ENVIRONMENTAL PROTECTION (JUNE 27TH – 30TH, 2017, BLED, SLOVENIA), ENERGY EFFICIENCY
J. Krope, A.Ghani Olabi, D. Goričanec & S. Božičnik

Investigation of Performance and Emissions of an SI Engine Powered with Oxygenated Fuel Blends

HÜSEYIN ENES FIL, PAOLO SEMENTA, SELAHADDIN ORHAN AKANSU, MICHELA COSTA & NAFIZ KAHRAMAN

Abstract Oxygen enrichment is one of the attractive combustion technologies to control pollution and improve combustion efficiency in SI engines. An experimental test was conducted on a two cylinders SI engine to investigate the effect of oxygen enrichment on pollutant emissions and engine performance. Increasing the oxygen concentration of the intake air from 0 to 25% by volume was considered within an experimental campaign conducted on a turbo-charged direct injection SI engine under conditions of 2000 rpm and 100% load. The results revealed that there is considerable improvement in power output and thermal efficiency of the engine with increased oxygen concentration and injection pressure. However, there is a considerable increase in nitrogen oxide emissions due to increased combustion temperature and extra oxygen available which needs to be addressed.

Keywords: • Oxygen enrichment • SI • Engine • Combustion • Emissions •

CORRESPONDENCE ADDRESS: Hüseyin Enes Fil, Erciyes University, Faculty of Engineering, Department of Mechanical Engineering, Köşk Mahallesi, Talas Yolu,38030 Melikgazi/Kayseri, Turkey, e-mail: h.enesfil@erciyes.edu.tr. Paolo Sementa, Istituto of Motori CNR, 1 Piazza Barsanti Eugenio E Matteucci Carlo, Naples, NA 80125, Italy,e-mail: p.sementa@im.cnr.it. Selahaddin Orhan Akansu, Erciyes University, Faculty of Engineering, Department of Mechanical Engineering, Köşk Mahallesi, Talas Yolu,38030 Melikgazi/Kayseri, Turkey, e-mail: akansu@erciyes.edu.tr. Michela Costa, Istituto of Motori CNR, 1 Piazza Barsanti Eugenio E Matteucci Carlo, Naples, NA 80125, Italy, e-mail: m.costa@im.cnr.it. Nafiz Kahraman, Erciyes University, Faculty of Engineering, Department of Mechanical Engineering, Köşk Mahallesi, Talas Yolu,38030 Melikgazi/Kayseri, Turkey, e-mail:nafiz@erciyes.edu.tr.

https://doi.org/10.18690/978-961-286-050-9.12 ISBN 978-961-286-050-9

Available at: http://press.um.si

1 Introduction

World's energy requirement is still supplied with fossil fuels like gasoline [1]. Petroleum based fuels are extinct depending on increasing amount of energy requirement so that increasing prices of fossil fuels, stringent emission regulations and environmental pollution force researchers to investigate new, clean, renewable and alternative fuels [2,3].

Emissions from engines are huge and contribute really in global warming. These engines, as it's known, have eight locations which produce air pollutants, such as: Crankcase, brake system, oil system and the main source is the exhaust system. Exhaust can produce many kinds of pollutants like: CO, CO2, NOx, SOx, HC and Particulate Matters (PM). The relative amounts depend on engine design and operating conditions but they are of order: NOx, 500-1000 ppm, CO: 200 g Kg-1 of fuel, HC: 3000 ppm. Pollutant emissions can be substantially reduced by carefully controlling the characteristics of engine operation, particularly combustion. [4], [5]. A number of parameters affecting engine performance can influence the amount of emissions:

- The air-fuel ratio
- Rate of air-fuel mixing (oxygen content)
- Flame temperature
- Combustion lag
- Residence time

These, in turn, can be strongly influenced by the following:

- The fuel delivery system (including carbureted versus injected and sophistication of injection/carburetion technology)
- The size and shape of the cylinders and pistons
- The nature of the exhaust gas path (direct versus re-circulated).[6],[7].

In addition, high compression ratios in the cylinders can increase fuel efficiency, decreasing directly the amount of CO2 emissions and, indirectly, HC and CO emissions.

Historically, air-fuel combustion has been the conventional technology used in nearly all industrial heating processes. In this technology when a fuel is burned, oxygen in the combustion air chemically combines with the hydrogen and carbon in the fuel to form water and carbon dioxide, releasing heat in the process. Air is made up of 21% oxygen, 78% nitrogen and 1% other gases by volume. During this combustion, the chemically inert nitrogen in the air dilutes the reactive oxygen and carries away some of the energy in the hot combustion exhaust gas.

Recent developments in oxy-fuel combustion systems have made it more amendable for a variety of applications. In the past, the benefits of using oxygen could not always offset added costs. New oxygen generation technologies, such as pressure and vacuum swing adsorption, have substantially reduced the cost of separating O2 from air. This has increased the number of applications in which using oxygen to enhance performance is cost-justified. Another important development is the increased emphasis on the environment. In many cases, OCS can substantially reduce pollutant emissions. This has also increased the number of cost-effective applications.

Oxy-fuel combustion has witnessed a tremendous innovation in the last decade. The growing demand of energy-efficient systems used in various industries has catalyzed the research going on in this sector [8].

Oxygen enhanced combustion has become one of the most attractive combustion technologies in the last decade. Significance of oxygen enhanced combustion is increasing due to strict environmental regulations and awareness on pollution. Thus the purpose of this study is to investigate the effects of oxygen enriched combustion on a single cylinder, direct injection SI engine with different levels of oxygen concentrations [9].

2 Experimental

2.1 Materials and Methods

2.1.1 Engine specifications

Studies are carried out on a 0.25 litter, 1 cylinder and 4 stroke SI engine. Test engine properties are given in details in Table 1. The original engine ECU is protected and no significant modification is made on the engine.

2.2 Experimental system

Experimental studies were carried out at Istituto Motori (Italy). In the experimental studies, motor power, torque and speed value measurements were performed by connecting the test motor AVL DynoPerform electric dynamometer. In addition, cylinder internal pressure values AVL GH14DK pressure sensor was used for combustion analysis. The obtained pressure signals were transferred to a computerized AVL brand combustion analyzer and the results were obtained. For the measurement of exhaust emissions, AVL brand 'M.O.V.E. GAS PEMS Portable Exhaust Gas Analyzer Gas emission device is used.

In experimental studies, the internal combustion engine was operated at full speed in stoichiometric and poor mixture ratios at different rates and oxygen enrichment ratios. Oxygen enrichment is provided to the intake manifold of the oxygen line from an oxygen tube. The amount of oxygen was measured by a flow meter located on this line. The oxygen enrichment rate was determined by the oxygen concentration calculations in equation 2.1 in the combustion equation.

$$C_8H_{18} + 12.5\ O_2 \rightarrow 8\ CO_2 + 9\ H_2O \qquad (2.1)$$

Experiments were carried out with different air excess coefficient ratios at 2000 rpm with 5% and 10% oxygen enrichment in the air. Figure.1 a and b show the schematic and experimental test system, respectively.

Table 1. Engine Specifications

Definition	Unit	Value
Number of cylinders	-	1
Cubic capacity	L	0.250
Bore	mm	72
Stroke	mm	60
Open/Close Valf Timing	degree	IVO=6 ATDC, IVC=50 ABDC, EVO=41 BBDC, EVC=1 ATDC
Maximum intake pressure	bar	1
Compression Ratio	-	10.5
Maximum Power	kW	16 at 8000 rpm
Maximum Brake Torque	Nm	20 at 5500 rpm

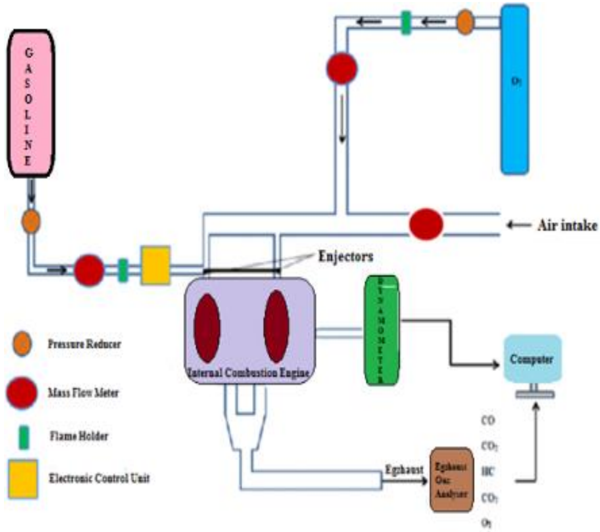

a. Schematic Setup

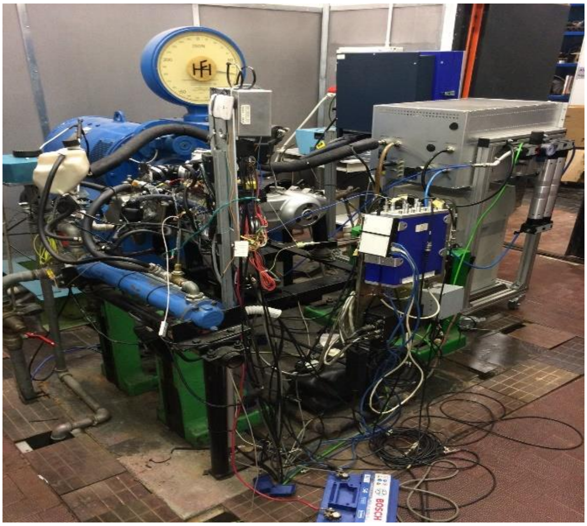

b. Experimental Test System

Fig 1. Experimental System

3 Results and Discussions

3.1 Cylinder pressure and heat release

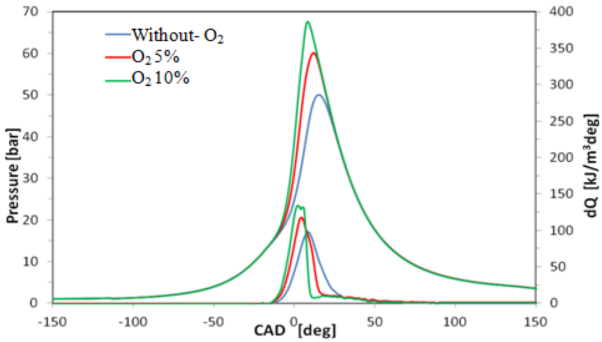

Fig 2. Pressure-CAD/Heat Release Rate-CAD diagram for different oxygen concentrations at 2000 rpm (Stoichiometric condition)

The comparison of the cylinder pressure and heat propagation as a result of experiments with oxygen free combustion and enrichment ratio of 5% and 10% oxygen shows at Figure 2. Experimental results show that as the oxygen enrichment ratio increases, the intracellular pressure value increases, and as we have seen in the experimental results, an increase of approximately 10 bar is observed with every 5% oxygen enrichment rate. Heat release rate gives us information on how and when the burn occurred. When we look at the heat release rate, as the oxygen enrichment ratio increases, the heat dissipation occurs earlier and therefore the heat dissipation rate increases. It is observed that the maximum heat dissipation increases with increasing oxygen enrichment ratio. In addition, as the oxygen enrichment ratio increases as a result of experimental studies, a heat release rate curve with two peaks has been obtained. As a result, enrichment with oxygen achieves both higher and earlier maximum heat dissipation. As the percentage of oxygen increases, the rate of reaction combustion increases. This increased the maximum pressure values by ensuring that the pressure build-up inside the cylinder was achieved at an early stage.

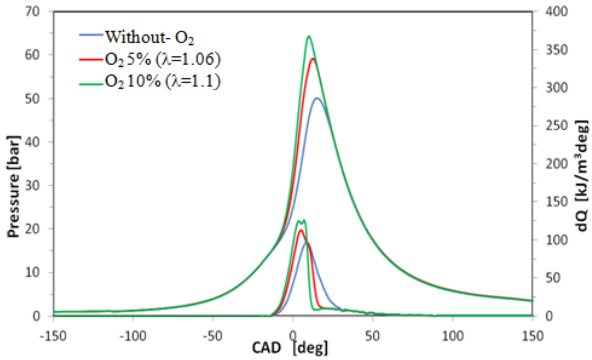

Fig 3. Pressure-CAD/Heat Release Rate-CAD diagram for different oxygen concentrations at 2000 rpm (Lean condition)

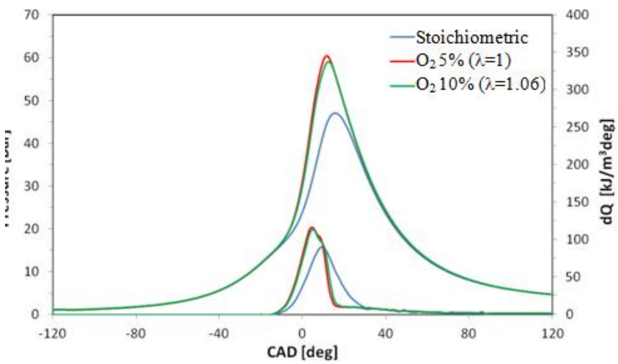

Fig 4. Pressure,Heat Release Rate-CAD diagram for stoichiometric, 5% O_2 at λ=1 and 5% O_2 at λ=1.06 at 2000 rpm

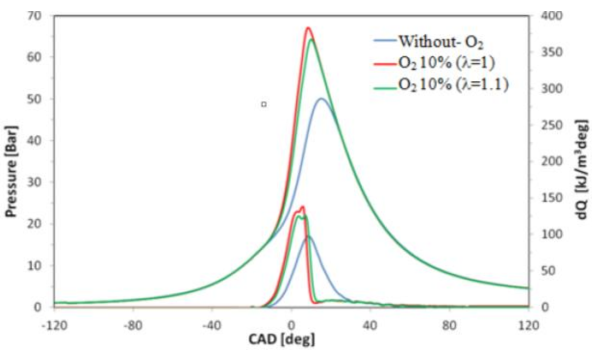

Fig 5. Pressure-CAD/Heat Release Rate-CAD diagram for stoichiometric and same oxygen concentrations (%10), different λ values at 2000 rpm

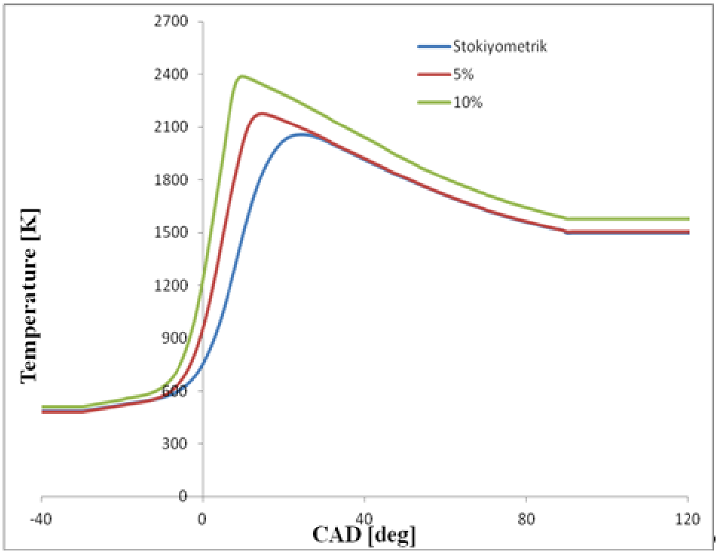

Figure 6. Temperature values versus the crank angle for different oxygen concentrations at stoichometric conditions.

3.2 Emissions

Experiments carried out with 100% load, the engine speed was taken as 2000 rpm and the CO, CO2, HC and NO emissions were investigated for 1 and 1.1 values of the lambda(λ). Emissions of CO, CO2, HC, and NOx are given in terms of the oxygen enrichment ratio for the lambda(λ) 1 and 1.1 values.

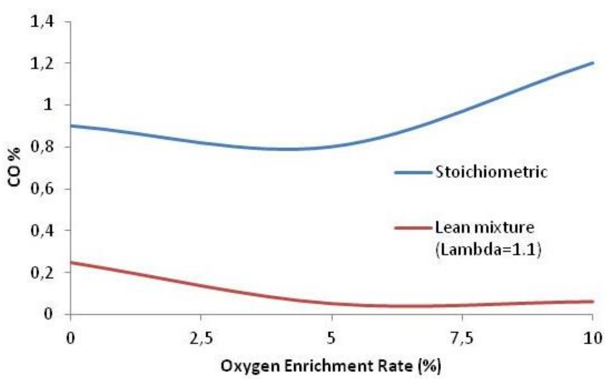

Figure 7. Oxygen Enrichment Rate-CO Emission

Figure 7 shows the change in CO emissions depending on the % oxygen enrichment ratio. When lambda(λ) is equal 1, CO emission values appear to decrease directly with increasing oxygen enrichment rate. In addition the % CO values for the 1.1 value of the lambda(λ) are reduced from 0.78 to 0.18 at %5 enrichment ratio. In the case of %10 enrichment ratio, it seems to decrease from 0.6 to 0.08. It has been observed that CO emissions are reduced when lambda and % oxygen enrichment ratio increase.

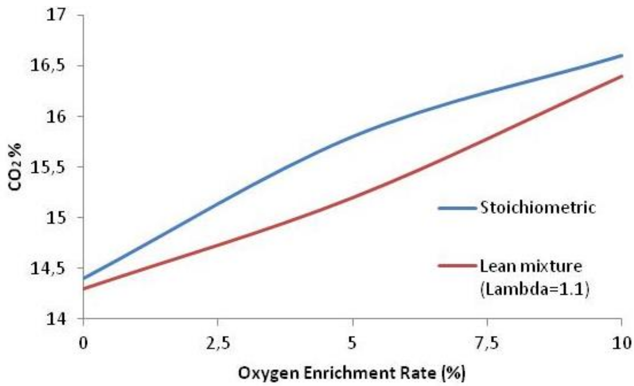

Figure 8. Oxygen Enrichment Rate-CO_2 Emission

Figure 8 shows the change in CO_2 emissions depending on the % oxygen enrichment ratio. Increasing the amount of % oxygen enrichment ratio leads to improvement of the combustion, which increases the CO_2 values. It has been observed that the amount of CO_2 decreases with the increase of the lambda because of more oxygen and nitrogen concentration.

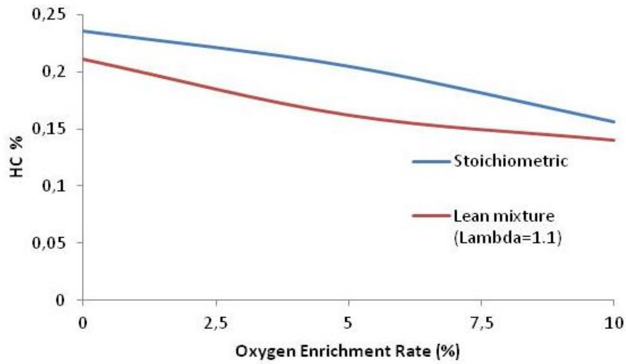

Figure 9. Oxygen Enrichment Rate-HC Emission

Figure 9 represents that when oxygen enrichment rate increases, there is not significant effect on HC emission under the lean mixture and stoichiometric conditions. However, HC emissions decrease once λ value reached from 1 to 1.1.

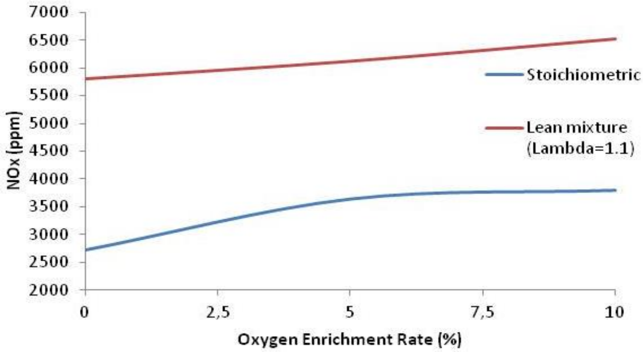

Figure 10. Oxygen Enrichment Rate-NO_X Emission

Figure 10 shows that the maximum temperature is raised with increasing content of oxygen. Therefore, NO_x emission is growth up because the maximum in-cylinder temperature is higher. The maximum NO_x emission was measured under the condition of λ value 1,1 and 10% oxygen enrichment rate.

3.3 Brake thermal efficiency

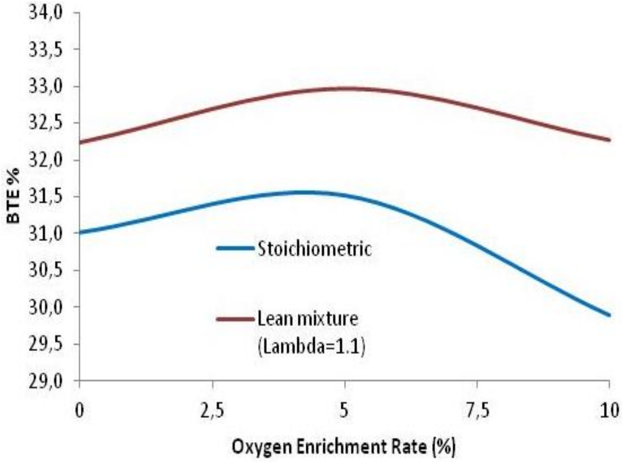

Figure 11. Brake thermal efficiency values versus the oxygen Enrichment Rate

4 Conclusions

The effects of oxygen enrichment with 0%, 5% and 10% (in volume) on an SI engine have been investigated. The main results are summarized as follows:

- In-Cylinder temperature differences were raised while oxygen enrichment rate was being increased. On the other hand, it was decreased with rising λ value at the same oxygen enrichment rate.
- In this study, the highest temperature was 2385,7 K once oxygen enrichment rate was 10% and λ value was 1. However, the lowest in-cylinder temperature was 2071,1 K without oxygen enrichment under stoichiometric condition.
- In-Cylinder pressure values were raised while oxygen enrichment rate was being increased. But it was decreased with rising λ value at the same oxygen enrichment rate. The highest in-cylinder pressure was 67.49 bar with %10 oxygen enrichment rate under stoichiometric condition.
- The highest NOx emission was 7687 ppm by the time oxygen enrichment rate was %10 and λ value was 1.17. NOx emission increased under the low oxygen enrichment rates.
- The lowest CO emission was 0.05 by the time oxygen enrichment rate was %10 and λ value was 1.17.
- The highest CO2 emission was 16.6 once oxygen enrichment rate was %10 under stoichiometric condition, the lowest CO2 emission was 14 without oxygen enrichment under stoichiometric condition.
- The highest HC emission was 0.236 without oxygen enrichment under stoichiometric condition., the lowest CO2 emission was 0.140 when oxygen enrichment rate was %10 and λ was 1.1.

Consequently, the characteristics of the application of oxygen addition to the intake air have been investigated with different oxygen enrichment rate.

References

[1] Kahraman E, Ozcanlı SC, Ozerdem B. An experimental study on performance and emission characteristics of a hydrogen fuelled spark ignition engine. Int J Hydrogen Energy 2007;32:2066e72.
[2] Yousufuddin S, Masood M. Effect of ignition timing and compression ratio on the performance of a hydrogen ethanol fuelled engine. Int J Hydrogen Energy 2009;34:6945e50.
[3] Ma F, Wang M, Jiang L, Chen R, Deng J, Naeve N, et al. Performance and emission characteristics of a turbocharged CNG engine fueled by hydrogen-enriched compressed natural gas with high hydrogen ratio. Int J Hydrogen Energy 2010;35:6438e47.
[4] API-agency, 2007. API-Reports USA. Direct web link: www.acde.ca.gov. pp:1-10.
[5] Beg, N., 1999. Scrappage programs. Annex to Thailand: Motorcycle Fleet Upgrade: Reducing Local and Global Emissions in Bangkok. Direct Web link: www.esmap.org/filez/pub/Thailand and reducing emissions Bangkok.pdf

[6] Bose, R., 1998. Automotive energy use and emissions control: A simulation model to analyze transport strategies for Indian metropolises. Energy. Policy Journal, 26: 1001-1016:1-20. DOI: 10.1016/S0301- 215(98)00045-7.

[7] Eskeland, G. and Jimenez E., 1991. Choosing policy instruments for pollution control: A review. Direct web link: http://econqa.worldbank.org/external/default/main?pagePK=64165259&theSitePK=469372& piPK=64165421&menuPK=64166093&entityID=00000926 5_3961001045114.

[8] http://www.wipo.int/export/sites/www/patentscope/en/programs/patent_landscapes/documents/lexinnova_oxy_fuel_combustion_systems.pdf

[9] Baskar P, Senthilkumar A. Effects of oxygen enriched combustion on pollution and performance characteristics of a diesel engine. Int J Engineering Science and Technology 2015..

10TH INTERNATIONAL CONFERENCE ON SUSTAINABLE ENERGY AND ENVIRONMENTAL PROTECTION (JUNE 27TH – 30TH, 2017, BLED, SLOVENIA), ENERGY EFFICIENCY
J. Krope, A.Ghani Olabi, D. Goričanec & S. Božičnik

Numerical and Experimental Investigations on Improving the Efficiency of Clean-in-Place Procedures in Closed Processing Systems: A Review

GUOZHEN LI, LLEWELLYN TANG, XINGXING ZHANG, JING HAO, MANXUAN XIAO & JIE DONG

Abstract This paper reviews the recent numerical and experimental investigations on improving the efficiency of Clean-In-Place procedures thus saving operation energy. The paper covers the fouling of equipment surfaces, the concept of CIP and its operation practices, the physical factors controlling the efficiency of CIP procedures with a special attention being paid to the hydrodynamic force of the cleaning fluids. The studies show that CIP efficiency dependents on many factors, such as the type of soil to be removed, the cleaning time, the temperature of cleaning agent, and the favourable hydrodynamic force of the moving liquid. Among the hydrodynamic factors, the wall shear stress and its fluctuation rate reported to be the dominating factor for cleaning straight circular pipes. Whilst for cleaning of more complex geometries and areas difficult to clean, the controlling factor may also include the flow pattern, flow exchange, flow turbulence, and the property of the recirculation zone.

Keywords: • Clean-in-place • Efficienc • Wall shear stress • CFD • Swirl flow

CORRESPONDENCE ADDRESS: Guozhen Li, Ph.D., The University of Nottingham Ningbo China, Faculty of Science and Engineering, Ningbo China, e-mail: Jason. Li@nottingham.edu.cn. Llewellyn Tang, Ph.D., Associate Professor, The University of Nottingham Ningbo China, Faculty of Science and Engineering, Ningbo China, e-mail: Llewellyn.Tang@nottingham.edu.cn. Xingxing Zhang, Ph.D., Associate Professor, Solar Energy Research Center (SERC), Dalarna University, Falun, Sweden, e-mail: xza@du.se. Jing Hao, Ph.D., The University of Nottingham Ningbo China, Faculty of Science and Engineering, Ningbo China, e-mail: Jane. Hao@nottingham.edu.cn. Manxuan Xiao, Ph.D., The University of Nottingham Ningbo China, Faculty of Science and Engineering, Ningbo China, e-mail: Manxuan.Xiao@nottingham.edu.cn. Jie Dong, Ph.D., The University of Nottingham Ningbo China, Faculty of Science and Engineering, Ningbo China, e-mail: Jie.Dong@nottingham.edu.cn.

https://doi.org/10.18690/978-961-286-050-9.13 ISBN 978-961-286-050-9

1 Introduction

In many industries, e.g. food and beverage industries, production lines are often cleaned daily to maintain both high heat transfer rates and low pressure drops in heat treatment units and more importantly, to ensure the appropriate level of microbial quality and thus the safety of the products [1, 2]. In many cases, the only practical way to clean closed processing systems is by using Clean-In-Place (CIP) procedures [3]. Researchers have shown that in some areas some bacteria may remain on equipment surfaces after standard CIP procedures [1, 4]. Traditional methods of improving CIP efficiency include increasing the overall cleaning fluid velocity, the concentration and temperature of the cleaning chemical and longer running time. For a company these methods increase costs and downtime, reduce production efficiency, and for the environment it is an additional load due to the extra chemical consumption. Due to the fact that CIP cleaning is typically performed at constant flow rates throughout the system, and the cleaning time is decided based on the criteria that the area most difficult to clean must be cleaned at the end of the process. One of the concerns related to improvement of cleaning efficiency is finding a way to locally increase the hydrodynamic force of fluid acting at the fluid/equipment interfaces without increasing the overall cleaning fluid velocity. To facilitate a better understand of the factors controlling the cleaning process and to identify methods which potentially improve the CIP procedures without consuming more energy, this paper reviews the relevant knowledges concerning the improvement of CIP procedures in closed processing systems which include: the fouling problems of the equipment surface, the CIP process, the factors influencing the CIP efficiency and the numerical and experimental studies on improving CIP by enhancing hydrodynamic effects of cleaning fluid.

2 Cleaning of Closed Processing Pipe System

2.1 Fouling of pipe surface

Fouling problems of the pipe surface in closed processing systems are common in many industries. For instance, in oil transportation industry, wax deposition on the inner walls of crude oil pipelines presents a costly problem in the production and transportation of oil. The timely removal of deposited wax is required to address the reduction in flow rate that it causes, as well as to avoid the eventual loss of a pipeline in the event that it is completely clogged [5].

Rapid and effective cleaning of closed processing pipe systems is especially important in food industries. Protein in milk processing systems [6], yeast, bacteria and beer stone on the inside of beer tubing systems [7] can decrease the heat transfer rate, increase the pressure in heat treatment unit, and more over affect the quality and flavour of the product.

Another common problem in closed processing pipe system is the formation of biofilms, as biofilms grow wherever there is water [8]. Biofilms are a collection of microorganisms surrounded by the slime they secrete, attached to the pipe surface [9]. More than 99% of all bacteria live in biofilm communities but some can be beneficial. For instance, sewage treatment plants rely on biofilms to remove contaminants from water. However, biofilms can also cause problems by corroding pipes, clogging water filters, causing rejection of medical implants, and harbouring bacteria that contaminate food in processing systems. This in turn can create a hazard to food quality and human health [9]. Efficient cleaning of fouling in processing systems is vital in food industries.

2.2 Clean in place

CIP is a method of cleaning the interior surfaces of pipes, vessels, process equipment and associated fittings, without disassembling them [3]. CIP is usually performed through the circulation of formulated detergents. This typically involves a warm water rinse, washing with alkaline and/or acidic solution, and a clear rinse with warm water to flush out residual cleaning agents [10]. Efficient CIP processes will result not only in reduced downtime and costs for cleaning but also reduced environmental impact (in the disposal of spent chemicals) [11]. Industries that rely heavily on CIP are those requiring frequent internal cleaning of their processes to meet the high levels of hygiene. These include: dairy, beverage, brewing, processed foods, pharmaceutical, and cosmetics industries. The benefit to industries by using CIP is that the cleaning is faster, less labour intensive, more repeatable and reproducible, and poses less chemical exposure risks to people.

2.3 Cleaning efficiency

Cleaning is a complex operation with its efficiency depending on many factors, e.g. the soil to be removed, cleaning time, temperature of the cleaning agent and the hydrodynamic force of the moving liquid [2, 12].

Lelièvre et al. [13] reported that soil removal is obviously affected by cleaning conditions such as the nature of cleaning agent, its concentration, its temperature, its contact time with surfaces, and lastly, the favourable effect of hydrodynamics. These factors mentioned are also reported in the studies of Changani et al. [6] and Sharma et al. [14].

According to PathogenCombat [15], a large European research project looking at safe food production, cleaning efficiency depends on four energy factors as presented using Sinners Circle (Figure 1). The factors are the mechanical energy (or hydrodynamic effect) to physically remove soil; the chemical action from detergents to dissolve soil in order to facilitate removal; the thermal energy - the cleaning temperature; and the cleaning time.

An efficient combination of those factors varies depending on the type of soil and the severity of the fouling. The idea is that a restriction in one factor may be compensated by increasing the effect of one or more of others.

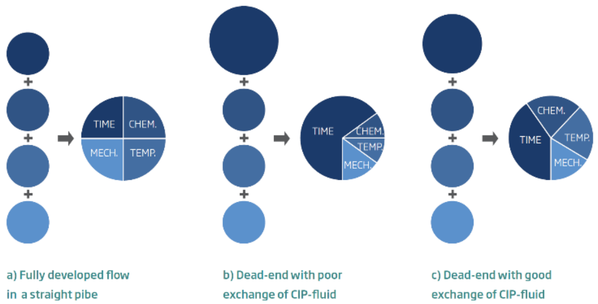

Figure 1. Sinner circles for three different cleaning situations [15]

Research established that the time taken to clean is a function of temperature, flow dynamics, and the cleaning chemical concentration. Other factors affect cleaning include the finish on the closed processing equipment surface, the geometry of the equipment, and the overall process design [6].

Cleaning Agent

Detergent and its operating temperature play an important role in CIP procedure. Leliévre et al. [13] investigated the respective contribution of both cleaning agent (sodium hydroxide 0.5%) and mechanical action of the fluid flow on the cleaning efficiency. They concluded that the sodium hydroxide and the wall shear stress have a combined action on the spore removal. The cleaning agent induced a decrease in the adhesion strength of B. cereus spores, ensuring their removal when a wall shear stress is applied since the hydrodynamic forces become greater than the adhesion force [16, 17].

Visser [18] stated the removal of colloid particles is controlled by the wall shear stress, but the presence of a cleaning detergent ensures a decrease in the adhesion force and, consequently, improves the removal of these particles. Sharma et al. [14] also found that high concentration of sodium hydroxide was found to induce a decrease in the adhesion force of colloids to surface. According to Hall [19], mechanical action and cleaning agent were fully linked to ensure a complete removal of a biofilm of Pseudomonas fragi.

Graβhoff [20] considered that cleaning of protein with NaOH-based solutions involved three stages, namely deposit swelling, uniform erosion and a final decay phase. The process is complex and the interaction of NaOH with the protein matrix is concentration dependent [11, 20, 21]. It was found that the rate of cleaning in the breakdown stage is more sensitive to wall shear stress than other stages, while the uniform stage is more sensitive to the temperature.

Adhesion Strength of Soil

According to Sharma et al. [14], the adhesion strength of soil to pipe surface varies according to the material of soil, the contact area, particle diameter etc. Sharma et al. studied the effect of particle material on the release of particles from a glass surface. They suggested that particles with a smaller Young's modulus are more difficult to removal. They also found that adhesive force increases with the particle diameter for both polystyrene and glass particles. However the adhesive force for polystyrene is significantly more than that of glass for all particle diameters. In addition, the adhesion strength of soil to pipe surface is also affected by the flow condition under which it is formed. PathogenCombat [15] found that biofilm resistance to flow during cleaning depends on the flow conditions during the build-up process. Figure 2 shows the difference between biofilm grown in three different conditions: static conditions, laminar flow and turbulent flow. The difference between the biofilm appearances is the direct result of different action of flow on bacterial growth. Dreesen [9] also stated that how the biofilm layer reaches certain equilibrium thickness depends on the flow condition and nutrient level.

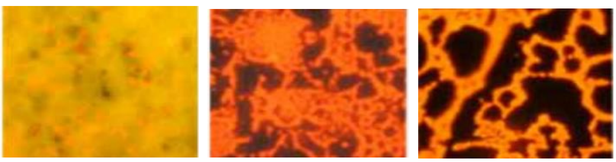

Static Laminar Turbulent

Figure 2. Microscope pictures of biofilm grown under three conditions [15]

Other factors influence the adhesion strength of soil to pipe surface may include surface roughness of the equipment, and deposition time, which is the length of time for particles to settle at the equipment surface. [14].

3 Numerical and Experimental Studys on Hydrodynamic Effects of Cleaning Fluid on Cip Efficiency

This section reviews numerical and experimental investigations on the hydrodynamic aspect of the CIP procedures. In general, it was suggested that methods which give rise to the increase of wall shear stress, its fluctuation rate, and flow turbulence would enhance the CIP efficiency whilst the existence of recirculation zones would hinder the CIP efficiency.

3.1 Wall shear stress

Published work stated that cleaning efficiency depends, besides other criteria, on the hydrodynamic effect. The flow of detergent is an important factor in the cleaning of closed processing equipment. The cleaning liquid generates local tangential force acting on the soil on the surface and acts as a carrier for the chemicals and heat [22]. The shear force of the cleaning fluid at fluid/equipment interfaces are of importance in the cleaning mechanism. The removal kinetics is functions of fluid detergent velocity and of the wall shear stress [23-26]. In addition, the wall shear stress was proposed as a more local removal control parameter than the velocity [27, 28].

Experimental studies have been performed in laminar regime and most of the studies conclude that the wall shear stress is the controlling factor for the rate and amount of microbial adhesion and removal [19, 29-31].

Lelièvre et al. [13] investigated the removal of Bacillus cereus spores on 304L stainless steel pipes. Their numerical and experimental study confirmed that the flow condition applied during soiling procedures has a significant effect on removal rate constant. In addition, the effective removal rate constant is significantly influenced by the wall shear stress applied during cleaning.

3.2 Fluctuation rate of WSS

Lélievre et al. [1] performed local wall shears stress analysis and cleanability experiments on different pieces of equipment made of stainless steel that represent production lines. In their study, the influence of the mean wall shear stress on bacterial removal was confirmed. The influence of loop arrangement was shown, particularly with the upstream effect of the gradual expansion pipe. Moreover, this work demonstrated the effect of the fluctuation rate on bacterial removal. It indicated that some low wall shear stress zones could be considered as cleanable because in these areas a high level of turbulence was observed, therefore, a high fluctuation rate. They therefore suggested that to predict cleaning, it is necessary to take into account not only the mean local wall shear stress, but also its fluctuation rate [1]. The presence of large wall shear stress fluctuation is because of flow pattern and hence, the geometry [2].

Fluctuation rate of the wall shear stress was also studied by other researchers. Paulsson and Bergman’s work [16, 32] showed that the mean wall shear stress has an influence on the removal of clay deposit but no influence of the fluctuation rate of the wall shear stress was demonstrated. Bénézech et al. [33] compared experimental removal results (Bacillus spores in complex medium) with local measurements of wall shear stress made by Focke et al. [34] in a corrugated plate heat exchanger. They concluded that the relevant parameter for cleaning efficiency was the fluctuation rate of wall shear stress.

Jensen et al. [2] numerically investigated the test set-up of Leliévre et al. [1] in terms of wall shear stress and its fluctuation using steady-state computational fluid dynamics (CFD) simulation adopting STAR-CD. A good correlation has been demonstrated between CFD predictions and measured values of wall shear stress in discrete points by Leliévre et al. [1]. The author suggested that a combination of the mean wall shear stress and the fluctuating part of the wall shear stress can be used for evaluating cleaning properties.

3.3 Recirculation zones

Friis and Jensen [3] investigated the design of closed process equipment with respect to cleanability. The study of hydrodynamic cleanability of closed processing equipment was discussed based on modelling the flow pass through a valve house, an up-stand and various expansions in tubes as shown in Figure 3. The CFD simulations were validated using the standardized cleaning test proposed by the European Hygienic Engineering and Design Group.

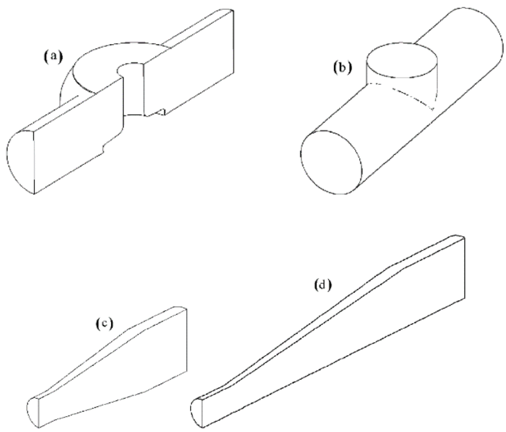

Figure 3. Geometries used for showing the influence of flow patterns on the cleanability of equipment [3]

Their study showed that the wall shear stress was one of but not the sole parameter involved in the cleaning process of closed process equipment. The nature of the fluid flow was also an important factor determining the cleaning efficiencies. It was found that the fluid exchange downstream of the up-stand was three times slower than in the main stream, which was caused by a recirculation zone in this area. Recirculation zones are known to be a problem. In the up-stand and tube expansion where the fluid exchanges in a steady recirculation is much slower than that in the main stream. The EHEDG test [35] showed that tubes with recirculation were more difficult to clean. Friis and Jensen concluded that the though wall shear stress plays a major role in cleaning of closed process systems, another significant factor is the nature of recirculation zone presented. Steady recirculation zones such as the one found in the up-stand and concentric expansion can reduce cleaning efficiency.

3.4 Flow turbulence

PathogenCombat [15] stated that to improve cleaning efficiency, it is beneficial to promote turbulent flow or to introduce flow disturbance. These flow phenomena are advantageous during both production and cleaning. Turbulent flow is achieved at high flow rate (i.e. Reynolds number above 10,000). The alternative solution is to induce flow disturbances which locally may introduce flow patterns similar to turbulence and this way reduce residual contamination downstream.

Disturbances can be induced by geometry e.g. contractions, expansions or asymmetrical features as seen in a curvature or bend. PathogenCombat summarized methods to improve Cleaning-In-Place efficiency as following: ①local enhancement of turbulence intensity and wall shear stress of flow; ②introduction of high mean wall shear stress; ③applying pulsating turbulent flow as a mean to break static flow patterns.

4 Conclusions

This paper attempted to review the problems of the fouling and cleaning of processing equipment with a special attention paid to the numerical and experimental findings on factors contributing to the improvement of CIP procedures toward a more sustainable and environment friendly way. Apparently the CIP efficiency dependents on many factors, such as the type of soil to be removed, the cleaning time, the temperature of the cleaning agent and the favourable hydrodynamic force of the moving liquid. Among the hydrodynamic factors, the wall shear stress, which is a measure of the mechanical action of fluid flow on a process surface, is considered the dominating factor for cleaning. The effective removal rate is significantly influenced by the wall shear stress applied during cleaning. In addition, the fluctuation rate of the wall shear stress was also reported to be important in the CIP efficiency. Therefore, to predict cleaning, it is necessary to take into account not only the mean local wall shear stress, but also its fluctuation rate. The literature also indicate that, for straight circular pipes, the mean wall shear stress and its fluctuation are the dominating factors controlling cleaning. Whilst for cleaning of more complex geometries and areas difficult to clean, the influencing factor may also include the flow pattern, flow exchange, flow turbulence, and the property of the recirculation zone.

References

[1] C. Leliévre, P. Legentilhommeb, Cécile Gaucherb, J. Legrandb, C. Faillea, and T. Bénézecha, "Cleaning in place: effect of local wall shear stress variation on bacterial removal from stainless steel equipment," *Chemical Engineering Science,* vol. 57, pp. 1287-1297, 2002.

[2] B. B. B. Jensen, A. Friis, T. Bénézech, P. Legentilhomme, and C. Lelièvre, "Local Wall Shear Stress Variations Predicted by Computational Fluid Dynamics for Hygienic Design," *Food and Bioproducts Processing,* vol. 83, pp. 53-60, 2005.

[3] A. Friis and B. B. B. Jensen, "Prediction of Hygiene in Food Processing Equipment Using Flow Modelling," *Food and Bioproducts Processing,* vol. 80, pp. 281-285, 2002.

[4] K. T. Elevers, A. C. Peters, and C. J. Griffith, "Development of biofilms and control of biofilm in the food industry " in *Biofims: The good, the bad, the ugly (pp. 139-145)*, J. Wimpenny, P. Gilbert, J. Walker, M. Brading, and R. Bayston, Eds., ed UK: Bioline, 1999, pp. 139-145.

[5] A. Aiyejina, D. P. Chakrabarti, A. Pilgrim, and M. K. S. Sastry, "Wax formation in oil pipelines: A critical review," *International Journal of Multiphase Flow,* vol. 37, pp. 671-694, 2011.

[6] S. D. Changani, M. T. Belmar-Beiny, and P. J. Fryer, "Engineering and chemical factors associated with fouling and cleaning in milk processing," *Experimental Thermal and Fluid Science,* vol. 14, pp. 392-406, 1997.

[7] M. MATIC. Importance of Beer Line Cleaning [Online]. Available: http://www.micromatic.com/draft-keg-beer-edu/importance-beer-line-cleaning-aid-72.html

[8] I. SpiroFlo. spiroflo and biofilms [Online]. Available: http://www.spiroflo.com/media/spiroflo_and_biofilms_brochure.pdf

[9] P. Dreesen. Biofilm:The Key to Understanding and Controlling Bacterial Growth in Automated Animal Drinking Water Systems [Online]. Available: http://www.edstrom.com/file.aspx?DocumentId=21

[10] S. R. S. Dev, A. Demirci, R. E. Graves, and V. M. Puri, "Optimization and modeling of an electrolyzed oxidizing water based Clean-In-Place technique for farm milking systems using a pilot-scale milking system," *Journal of Food Engineering,* vol. 135, pp. 1-10, 2014.

[11] C. R. Gillham, P. J. Fryer, A. P. M. Hasting, and D. I. Wilson, "Cleaning-in-Place of Whey Protein Fouling Deposits," *Food and Bioproducts Processing,* vol. 77, pp. 127-136, 1999.

[12] H. L. M. Lelieveld, M. A. Mostert, J. Holah, and B. White, *Hygiene in Food Processing* vol. 1st edn. Cambridge, UK: Woodhead Publishing, 2003.

[13] C. Lelièvre, G. Antonini, C. Faille, and T. Bénézech, "Cleaning-in-Place Modelling of Cleaning Kinetics of Pipes Soiled by Bacillus Spores Assuming a Process Combining Removal and Deposition," *Food and Bioproducts Processing,* vol. 80, pp. 305-311, 2002a.

[14] M. M. Sharma, H. Chamoun, D. S. H. S. R. Sarma, and R. S. Schechter, "Factors Controlling the Hydrodynamic Detachment of Particles from Surfaces," *Journal of Colloid and Interface Science,* vol. 149, pp. 121-134, 1991.

[15] PathogenCombat. Factors affecting fouling and cleanability of closed food contact surface [Online]. Available: http://www.pathogencombat.com/Publications/~/media/Adtomic/Unique%20Achievemen

ts/Leaflets/Factors%20affecting%20fouling%20and%20cleanability%20of%20closed%20food%20contact%20surface.ashx

[16] B. O. Bergman and C. Trägårdh, "An approach to study and model the hydrodynamic cleaning effect," *Journal of Food Process Engineering,* vol. 13, pp. 135-154, 1990.

[17] S. G. YIANTSIOS and A. J. KARABELAS, "Detachment of Spherical Microparticles Adhering on Flat Surfaces by Hydrodynamic Forces," *JOURNAL OF COLLOID AND INTERFACE SCIENCE,* vol. 176, pp. 74-85, 1995.

[18] J. Visser, "PARTICLE ADHESION AND REMOVAL: A REVIEW," *Particle Science and Technology,* vol. 13, pp. 169-196, 1995.

[19] J. E. Hall, "Computational fluid dynamics: A tool for hygienic design," in *Fouling and cleaning in food processing*. vol. 98, D. I. Wilson, P. J. Fryer, and A. P. M. Hasting, Eds., ed Cambridge: Jesus College, 1998, pp. 144-151.

[20] A. Graβhoff, "Cleaning of heat treatment equipment," in *Fouling and Cleaning of Heat Treatment Equipment*, I. D. Federation, Ed., ed Brussels: International Dairy Federation, 1997, pp. 32-44.

[21] M. R. Bird and P. J. Fryer, "An experimental study of the cleaning of surfaces fouled by whey proteins," *Trans IChemE, Food Bioprod Proc,* vol. 69C, pp. 13-21, 1991.

[22] B. B. B. Jensen, M. Stenby, and D. F. Nielsen, "Improving the cleaning effect by changing average velocity," *Trends in Food Science & Technology,* vol. 18, pp. S58-S63, 2007.

[23] T. Gallot-Lavallée, M. M. Lalande, and G. Corrieu, "Cleaning kinetics modeling of holding tubes fouled during milk pasteurization," *Journal of Food Process Engineering,* vol. 7, pp. 123-142, 1984.

[24] A. Graβhoff, "Hygienic design:The basis for computer controlled automation," *Food and Bioproducts Processing, Transactions of The Institution of Chemical Engineers Part C,* vol. 70, pp. 69-77, 1992.

[25] J. Visser, "Measurement of the force of adhesion between submicron carbon-black particles and a cellulose film in aqueous solution," *Journal of Colloid interface Science,* vol. 34(1), pp. 26-31, 1970.

[26] M. M. Sharma, Chamoun, H., & Sita Rama Sarma, D. S. H., "Factors controlling the hydrodynamic detachment of particles from surfaces," *Journal of Colloid interface Science,* vol. 28(3), pp. 121-134, 1991.

[27] C. Paz, E. Suárez, M. Concheiro, and J. Porteiro, "Experimental study of soot particle fouling on ribbed plates: Applicability of the critical local wall shear stress criterion," *Experimental Thermal and Fluid Science,* vol. 44, pp. 364-373, 2013.

[28] C. Paz, E. Suárez, A. Eirís, and J. Porteiro, "Experimental evaluation of the critical local wall shear stress around cylindrical probes fouled by diesel exhaust gases," *Experimental Thermal and Fluid Science,* vol. 38, pp. 85-93, 2012.

[29] J. E. Duddridge, C. A. Kent, and J. F. Laws, "Effect of surface shear stress on the attachment of Pseudomonas fluorescence to stainless steel under defined flow conditions," *Biotechnol Bioengng,* vol. 24, pp. 153-164, 1982.

[30] M. S. Powell and N. K. H. Slater, "Removal rates of bacterial cells from glass surfaces by fluid shear," *Biotechnol Bioengng,* vol. 24, pp. 2527-2537, 1982.

[31] H. W. Fowler and A. J. McKay, "The measurement of microbial adhesion," in *Microbial Adhesion to Surfaces*, R. C. W. Berkeley, J. M. Lynch, J. Melling, P. R. Rutter, and B. Vincent, Eds., ed Chichester: Ellis Horwood Limited, 1980, pp. 143–161

[32] B. O. Paulsson and C. Trägårdh, "Removal of soil particles in wall boundary layer flows-The hydrodynamic effect," in *Fouling and cleaning in food processing*, prien, 1989.

[33] T. Bénézech, C. Faille, and S. Lécrigny-Nolf, Eds., *Removal of Bacillus spores from closed equipment surfaces under cleaning-in-place conditions* (Fouling and cleaning in food processing '98. Cambridge: Jesus College, 1998, p.^pp. Pages.

[34] W. Focke, J. Zachariades, and I. Olivier, "The effect of corrugation inclination angle on the thermodynamic performance of plate heat exchangers," *International Journal of Heat and Mass Transfer,* vol. 28, pp. 1469-1479, 1985.

[35] P. S. Richardson, R. M. George, and R. D. Thorn, "Application of computational fluid dynamics simulation to the modelling of cleanability of food processing equipment," in *Food & Drink 2000 Processing Solutions for Innovative Products,* ed Rugby, UK: Institution of Chemical Engineers, 2000, pp. 64-66.

Comparative Evaluation Model for Smart Envelope Systems

MARKO JAUŠOVEC & METKA SITAR

Abstract In smart architecture design processes, the stakeholders have to take one of the key decisions on optimal external envelope system that will reduce energy consumption, eliminate wastage and, particularly, optimize the life cycle costs. The paper presents a specific extended evaluation model that was developed to evaluate and compare different construction systems of envelopes in the early design phase in order to the optimize the balance between the benefits expected of the architectural building design project and the resources consumed for its implementation. The comparative evaluation model is based on the life cycle cost assessment for a 50-years lifetime in relation to the initial construction costs, demonstrating that this calculation does not only depend on the energy related costs. This model was developed by using BIM use purposes in combination with the Value for Money evaluation method, while the case study was limited to a small one-family house.

Keywords: • Smart • Envelope • Evaluation • Energy • Cost •

CORRESPONDENCE ADDRESS: Marko Jaušovec, Ph.D., Assistant, University of Maribor, Faculty of Civil Engineering, Transportation Engineering and Architecture, Smetanova ulica 17, 2000 Maribor, Slovenia, e-mail: marko.jausovec@um.si. Metka Sitar, Ph.D., Professor, University of Maribor, Faculty of Civil Engineering, Transportation Engineering and Architecture, Smetanova ulica 17, 2000 Maribor, Slovenia, e-mail: metka.sitar@um.si.

https://doi.org/10.18690/978-961-286-050-9.14 ISBN 978-961-286-050-9

Available at: http://press.um.si.

1 Introduction

The residential sector in Slovenia accounts for approximately 25% of total primal energy consumption. In Slovenia, single-family houses represent 75% of residential sector floor area and 55% of the entire building sector area [1]. The efforts to raise energy efficiency of buildings require an appropriate design approach to support sustainable housing design for current and future generations.

One question that remains is about what kind of technologies will emerge from the multitude of different solutions for energy efficient buildings.

However, technical solutions, which are certainly vital, represent only one of the many aspects that define the paradigm of sustainable architecture. Technology is therefore not the principle impulse in architectural design [2]. For the stakeholders (the owner, the architect, the contractor, the user, among others), the main aspect most commonly are the initial construction costs, often set at the minimum value that does not necessarily improve the lifetime performance of a building [3]. Moreover, it is estimated that the initial costs represent less than 30% of the total Life Cycle Cost (LCC) as significant for the total cost perspective and the value of investment [4]. Therefore, it is important in an early design phase to inform the stakeholders on the relationship between different design solutions and the resulting final value of a building. This approach is not only limited to specific types of projects [5], but is also usable in the building construction industry [6]. In correspondence to that, the presented extended evaluation model is based on the case study method implemented to compare the envelopes of different prefabricated lightweight systems for a single-family house. Stakeholders should define them in the early design phase for adopting the most appropriate envelope system.

2 Preliminary Study

2.1 Methods applied

In scientific literature, the studies on the LCC assessment used for economic evaluation of buildings and building industry products are very scattered. When assessing different technological systems, the majority of research uses the case study method. Finally, we estimated the Value for Money (VfM) evaluation method that includes the building function and the LCC as the most appropriate one. However, no study combines case study method with the LCC in a comprehensive way. For example, the studies by Lee et al. [7], Hasan et al. [8], Leckner and Zmeureanu [9], and Matic [10] et al. used partly either the LCC or the operational costs. According to Li et.al., two highest risk allocations in private sector are the Construction time delay with 97,6%, and the Higher Maintenance costs with 97,5% [11]. Therefore, by using the VfM method, this study focuses on the assessment of prefabricated construction envelope systems, characterized by controlled construction time, while the LCC main parameter assesses the maintenance costs.

2.2 Value for money

Recently, smart management with available resources and the optimization of the value of a building or a building system seem to be more important than ever. While traditional economic real estate evaluations are focused on the asset's market value, the investors mostly evaluate the investment's opportunity based on the relationship between the investment costs and the final value of a building or building system. A building offers better value for money, when the derived benefits significantly exceed the lifetime cost. However, these benefits derive from the functions a building performs rather than from the building itself. This means that to improve the VfM the project team should clearly define the needs of the client in order to eliminate unnecessary expenditure, and obtain optimum balance between cost, time and the quality of a building [12].

$$\text{Value} \quad \propto \quad \frac{\text{Benefits Delivered}}{\text{Resources Used}}$$

Figure 1. The value ratio [13]

According to Dallas, the term value generally characterizes the balance between how well the building satisfies the owner's expectations and the sacrifices, in terms of resources used he must make in order to get it. The ratio between benefits delivered and resources used is referred to as the Value Ratio [13].

3 Comparative Evaluation Model Development

3.1 Comparative evaluation process

The process of developing the comparative evaluation model and the software applied for the case study evaluation was determined according to the BIM use purposes. According to Kreider [14], a BIM Use can be defined as "…a method of applying Building Information Modelling during a facility's lifecycle to achieve one or more specific objectives." Further, two types of software were used; for gathering and generating information the BIM software Archicad and for the case study analyses the integrated LCC analysis software Legep. To simplify the workflow, the evaluation of different envelope systems was limited to a small single-family house BIM model with simple functionality. Based on the total cost per year calculations, the resources used for the building construction were analysed. In this way, the operational costs were included in the LCC assessment.

BIM Generation [14]

The first step is based on the BIM Generation for which two primary BIM Use purposes are used. To Gather, the geometric and attribute data are captured for representing the current or wanted status concerning the building and building elements. To Generate, all information needed is identified in Archicad virtual building constructed with the attributes of building materials. Building elements are a combination of different materials in composites, such as walls, slabs, roof, etc.

BIM Evaluation [14]

The second step represents the BIM Evaluation to Analyze the BIM and to Communicate the results between Archicad and Legep. It includes the analyses of construction and operational costs, called Forecast. To be able to Forecast, a construction costs database or manual input of the data is needed. To Communicate means that the quantity information of each element with all parameters is exported out of Archicad and imported into Legep to carry out the LCC analysis for obtaining final results for VfM evaluation based on the quantity take-off list of each element from the virtual building model.

VfM Evaluation

The final step represents the extended VfM that first Analyzes the LCC and VfM, and then Realizes the results as recommended for the future stakeholders' decision on the appropriate envelope system in the early design phase. The LCC assessment includes the calculation, evaluation and forecast of the LCC including supply and disposal, maintenance, service and repair, and cleaning costs.

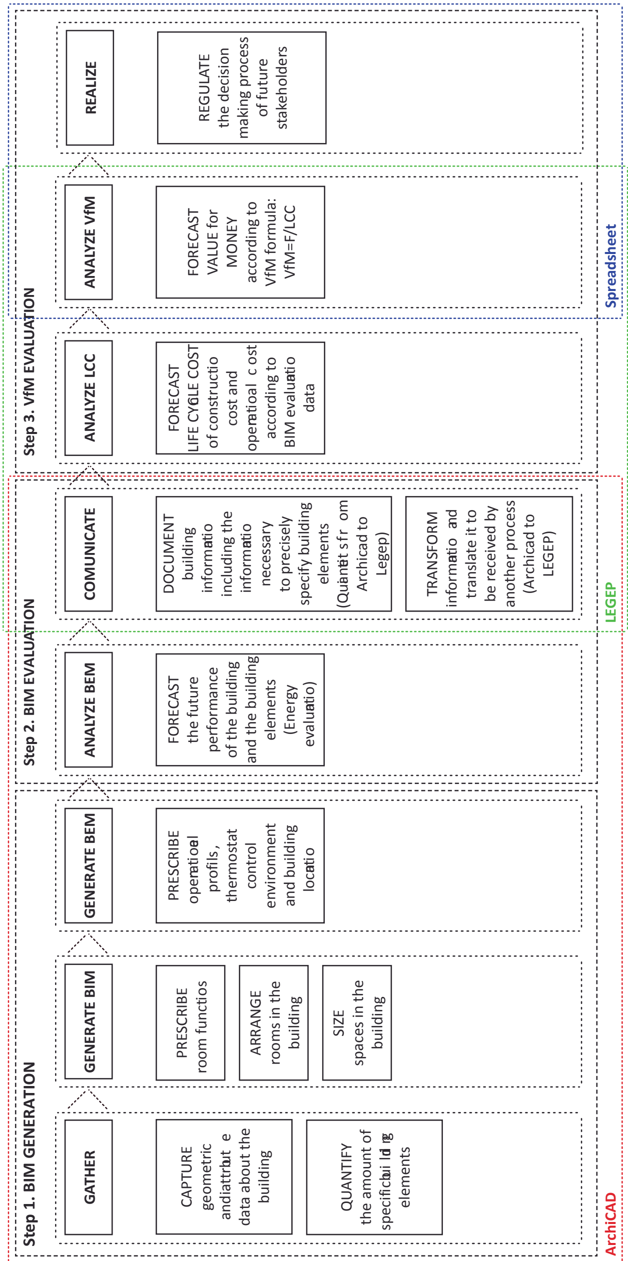

Figure 2. Extended Value for Money evaluation model with BIM use purposes

3.2 Case-study method

Reference building

The reference building presents a two-story single-family house for a couple with two children with ground floor, upper floor and the flat roof construction. The fix internal horizontal dimensions are 7.2 m x 7.2 m. The total heated floor area of the building is 98,77 m^2 and the total heated volume is 249,90 m^3. The shape factor (Fi=A/V) of the building is 0.78 m^{-1}.

Construction

The external envelope types of the building are performed in different lightweight construction systems. The impacts of different thermal capacities were taken into the consideration, as follows. External envelopes of walls and of the roof construction are considered as changing parameters. The foundation slab (U=0,15 W/m^2K), the first floor slab and internal walls are considered as fixed parameters for all the cases.

Windows

External windows are considered as fixed parameters in their size and energy specifications for all cases. The overall window U-value for energy calculation is 0,87 W/m^2K. The windows are shaded with external shading devices of louvers.

Location, orientation and climate data

The reference building is located in the surroundings of Maribor at the geographical location of 46° 34' 53" N latitude and 15° 38' 22" E longitude at the altitude of 297m, and is oriented to the south with the open glazed facade.

Building operation profiles

In case of single-family house, the operation profile is estimated as residential, separated in workdays from Monday to Friday and the weekends. The maximum temperature is 26°C and the minimum 20°C during the day and 18°C during the night.

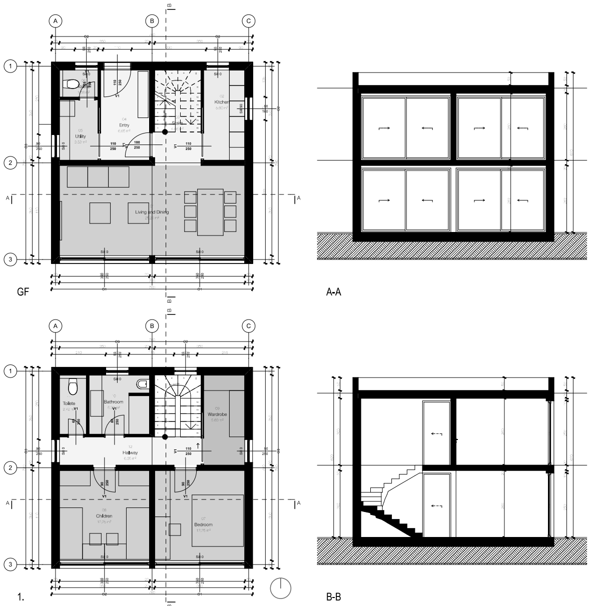

Figure 2. Case study model floor-plans

3.3 Case studies of external envelopes

The case studies were determined on the basis of four different types of external envelopes in light-weight construction systems analysed for a reference building. The first case is the Slovenian prefabricated houses type Lumar Primus, the other three cases are prototype envelope systems presented for the Solar Decathlon Competition Europe 2012.

Lumar Primus

The Lumar Primus construction system presents a timber panel system incorporating the external wall with the U-value of 0,119 W/m2K, and the flat roof construction with the U-value of 0.11 W/m2K. All the other parameters are considered as fix values.

Canopea

The Canopea is a high performance thermal envelope system. The primary envelope is made of prefabricated steel frames filled with cellulose thermal insulation combined with innovative vacuum insulation panels in the interior and Kerto-Q LVL panels in exterior. The external walls have a very good U_{wall} value of 0,08 W/m^{2}K. The flat roof has the U-value of 0.07 W/m^{2}K.

Ecolar

This high-tech external envelope system consists of a special opaque facade element that combine the impacts of passive and active solar energy gains. The primary structure of prefabricated elements is a timber frame system. The final weather protective layer is laminated glazing that creates the dynamic U-value with a measured value of less than 0,01 W/m^{2}K during the heating season. The walls have the dynamic U_{wall} value with the average of 0,10 W/m^{2}K. The flat roof construction has the U_{roof}-value of 0.13 W/m^{2}K

Med in Italy

The external envelope system is based on the innovative low-tech solution of light-weight alloy pipes that are transported on the site and filled with humid sand to gain the inertial mass. The reduction of the structure's total weight is up to 30% less. The walls have the U_{wall} value of 0,14 and the roof has the U_{roof}-value of 0.14 W/m^{2}K.

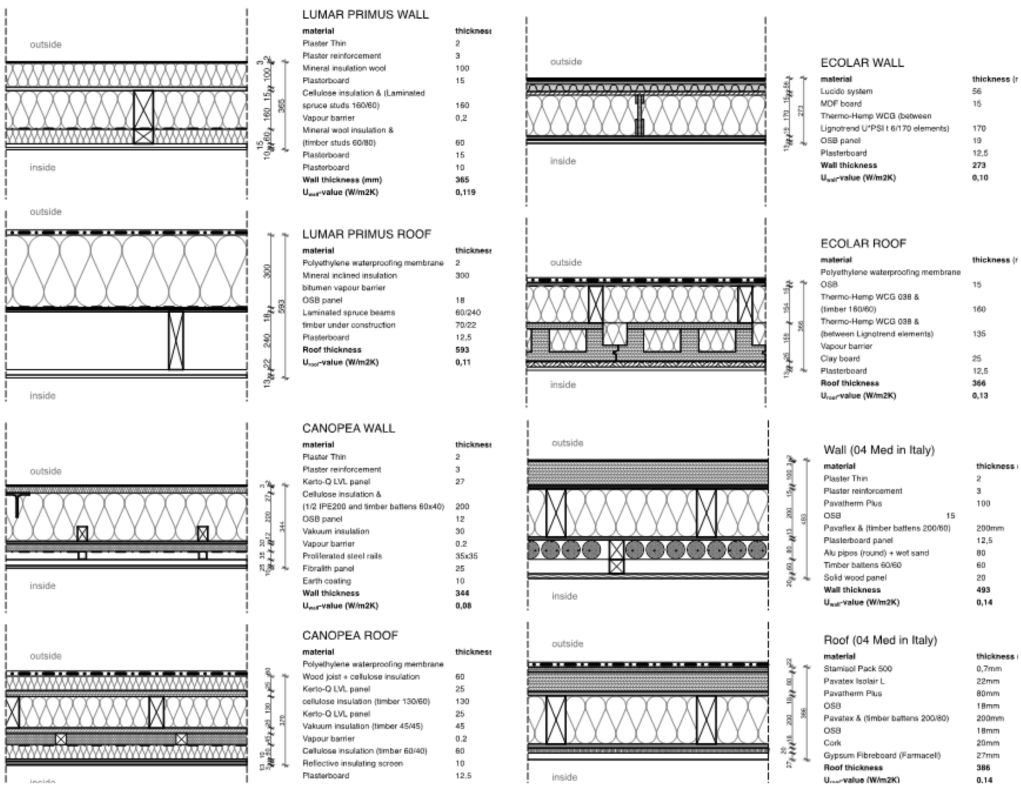

Figure 3. Case studies external envelopes

4 Results

In order to determine the VfM, the case studies of four different envelope systems referring to a single-family house are evaluated and compared. The construction costs data are evaluated according to the Cat. 300 and 400, DIN Standard [15].

Table 1. Comparison of Construction Costs

Case studies	Construction cost net in EUR (300 and 400)	Diff. (%)	Building cost gross in EUR
Lumar P.	108.764,67	±00,0	136.911,53
Canopea	119.459,53	+08,9	148.624,67
Ecolar	144.487,68	+24,7	176.028,59
MED	116.728,76	+06,8	145.633,02

As presented in Table 1, the differences in construction arise from the alteration among material- labor- and toll processing costs. The lowest construction costs are in case of Lumar Primus and the highest in case of Ecolar, due to the high-tech wall envelope and material for the façade. Other two envelope systems are of very good U-values because of the low-tech based insulation, with exception of expensive vacuum insulation panels in case of Canopea. Table 2 shows the LCC, including operational costs that vary because of the differences between the construction and operational costs calculated for the 50 years' lifetime of the building. The lowest LCC are in case of Lumar Primus, the highest in case of Ecolar. The supply and disposal costs are the highest in case of Lumar Primus and the lowest in case of Canopea. As expected, the MED value is lower than the other cases due to its smart aluminum pipes filled with wet sand for heat capacity purposes. The highest operational costs in case of Ecolar are the result of high-tech external wall envelope that does indeed reduce supply and disposal costs by app. 1% but requires 20,4% higher maintenance and service costs compared with Lumar Primus.

Table 2. Comparison of Supply and Disposal costs, Operational costs, LCC and VfM

Case Study	Supply and Disposal in EUR	Diff. in Supply and Disposal in (%)	Operational cost (NaWoh) in EUR	Diff. in Operational Costs in %	LCC (including Construction cost) in EUR	Diff. in LCC in %	Value for Money in %
Lumar Pr.	16.718,39	±00,00	83.060,28	±00,00	191.824,95	±00,00	100
Canopea	16.214,44	-03,11	84.901,59	+02,17	204.361,12	+06,13	94
Ecolar	16.634,80	-00,50	104.322,31	+20,40	248.809,99	+22,90	77
MED	16.674,43	-00,26	89.466,42	+07,16	206.195,18	+06,97	93

Value for Money evaluation

The function of the reference building is set as residential, and is identical for all case studies. The evaluation is based on the LCC present value calculated for 50 years' lifetime. As a reference, the value of Lumar Primus with the highest VfM value is set, followed by Canopea and MED. The lowest VfM value is calculated in case of Ecolar.

5 Conclusion

The use of extended VfM comparative evaluation model presents some interesting results. When observing construction costs it is important to highlight that all the evaluated cases have a very good U-values between 0,07 and 0,14 W/m^{2}K. They are far below the legislation minimum. However, the initial construction costs (KGR 300 and 400) differentiate in net value up to 25%. There are certain specifics identified, as follows. In case of high-tech prototype like envelope systems, a high increase of initial construction costs is partly repaid by lower supply and disposal. Considering only the construction costs, the case of Canopea with best U-value indeed indicates the highest initial construction costs. The case of Ecolar with high tech dynamic U-value that was expected to reach good results performs only 0,5% lower costs compared to the reference case, but produces 22% higher initial construction costs. On one hand, the high-tech envelope systems reduce the energy supply costs, on the other hand, due to very high maintenance and service costs produce additional operational costs up to 20%. Moreover, supply and disposal merely represent 16 to 20% of total LCC net present value.

We conclude that regardless on higher initial construction costs often perceived as an investment in expected lower future operational costs seem reasonable, the net present value of the building results show another reality. Namely, lower supply and disposal costs do not compensate higher replacement and maintenance costs in 50 years' lifetime. In Slovenian case, in which 77% of housing is privately owned, lower initial construction costs and less operational costs mean a better net present value and therefore a better solution in the owners' perspective. Although often reported of high-tech external envelopes with substantial benefits in energy supply the results offer a new look at the feasibility of this type of envelope systems.

The presented comparative evaluation model can be recommended as smart operational tool to be introduced in the early design phase. It focuses not only on the cost reduction but also on the improvement of the comprehensive value of the building in its lifetime. To implement the model in daily practice, the basic data on the main characteristics of the layers of external envelope systems is needed. The future research on smart housing development shall be focused more on the quality on the comprehensive architectural design

References

[1] M. Šijanec Zavrl, H. Gjerkeš and M. Tomšič, Integration of Nearly Zero Energy Buildings in Sustainable Networks – a Challenge for Sustainable Building Stock, World engineering forum 2012, 2012, p. 163.

[2] G. Staib, A. Dörrhöffe and M. Rosenthal, Components and Systems, Modular Construction – Design, Structure, New Technologies, Munich: Birkhäuser, 2008, p. 10.

[3] J. Schade, Life cycle cost calculation models for buildings, vol. 18, Luleå: Luleå tekniska universitet, 2007, p. 321–329.

[4] S. M. Far, A. I. Pastrana and C. M. Duarte, Building Information Electronic Modelling (BIM) Process as an Instrumental Tool for Real Estate Integrated Economic Evaluations, Istanbul: 22nd European Real Estate Society Conference, Proceedings Istanbul 2015, 2015.

[5] F. Rangelova and M. Traykova, Project management in construction, Sofia: University of architecture, civil engineering and geodesy, 2014, pp. 429-434.

[6] A. E. Oke, D. O. Aghimien and S. O. Olatunji, Implementation of value management as an economic sustainability tool for building construction in Nigeria, Akure: Department of Quantity Surveying, Federal University of Technology, 2015, p. 55.

[7] S. Lee, K. Sunkuk and Y. Na, Comparative analysis of energy related performance and construction cost of the external walls in high-rise residential buildings, vol. 99, Elsevier B.V., 2015, pp. 67-74.

[8] A. Hasan, M. Vuolle and K. Siren, Minimisation of life cycle cost of a detached house using combined simulation and optimisation, vol. 43, Elsevier, 2008, pp. 2022-2034.

[9] M. Leckner and R. Zmeureanu, Life cycle cost and energy analysis of a Net Zero Energy House with solar combisystem, vol. 88, Elsevier, 2011, pp. 232-241.

[10] D. Matic, Economically feasible energy refurbishment of prefabricated building in Belgrade, Serbia, vol. 98, Elsevier, 2015, pp. 74-81.

[11] B. Li, A. Akintoye and C. Hardcastle, VFM and Risk Allocation Models in Construction PPP Projects, vol. 12, „Public Private Partnership, CIB TG 72ARCOM Doctoral Workshop 12 , 2011, pp. 16-21.

[12] Building.co.uk, "Building.co.uk," Building.co.uk, 2000. [Online]. Available: http://www.building.co.uk/cost-model-value-for-money/1348.article. [Accessed 18 11 2015].

[13] M. F. Dallas, Value and Risk Management: A Guide to Best Practice, Oxford: Blackwell Publishing, 2006, p. 14.

[14] R. G. Kreider and J. I. Messner, The Uses of BIM: Classifying and Selecting BIM Uses, Version 0.9, PA: The Pennsylvania State University, 2013, pp. 10-11.

[15] *Kosten im Bauwesen - Teil 1: Hochbau,* Beuth Verlag, 2008.

10TH INTERNATIONAL CONFERENCE ON SUSTAINABLE ENERGY AND ENVIRONMENTAL PROTECTION (JUNE 27TH – 30TH, 2017, BLED, SLOVENIA), ENERGY EFFICIENCY
J. Krope, A.Ghani Olabi, D. Goričanec & S. Božičnik

Practical Approach for Energy Consumption Optimisation in Educational and Research Buildings - Case Study Cluster Computers and Data Room

BORIS SUCIC, SANDI CIMERMAN, MARKO PECKAJ & FOUAD AL-MANSOUR

Abstract Experience from many modern educational and research facilities has shown that energy consumption of cluster computers and data rooms represents very significant share in the overall consumption. The research work described in this paper presents a practical approach for energy consumption optimisation in educational and research buildings with the special emphasis on cluster computers and data rooms. In the addressed case study, preliminary evaluation of the energy performance of the data room revealed the following weak points: poor airflow management, overcooling, blending air (hot and cold), unused servers and no energy management system for data centre. In the absence of a proper energy management system on building level, it was not unusual that the certain machines in the data room were running even when it was not necessary. Initial testing results are indicating that on the annual level 82.3 MWh of electricity can be saved which results in simple payback period of 2.2 years.

Keywords: • Electricity consumption optimisation • Cluster computers • Data room • Performance indicators • Energy management •

CORRESPONDENCE ADDRESS: Boris Sucic, Jozef Stefan Institute, Jamova cesta 39, 1000 Ljubljana, Slovenia, e-mail: boris.sucic@ijs.si. Sandi Cimerman, Jozef Stefan Institute, Jamova cesta 39, 1000 Ljubljana, Slovenia, e-mail: sandi.cimerman@ijs.si, Marko Peckaj, Jozef Stefan Institute, Jamova cesta 39, 1000 Ljubljana, Slovenia, e-mail: marko.peckaj@ijs.si. Fouad Al-Mansour, Ph.D., Jozef Stefan Institute, Jamova cesta 39, 1000 Ljubljana, Slovenia, e-mail: fouad.al-mansour@ijs.si.

https://doi.org/10.18690/978-961-286-050-9.15 ISBN 978-961-286-050-9

Available at: http://press.um.si.

1 Introduction

A systematic approach to energy consumption optimisation in buildings requires proper understanding of interactions among the main factors influencing energy performance, namely technical systems and end-users preferences. According to [1], electricity accounts for 30% of current energy consumption in the buildings sector, but due to strong growth it is expected to rise to more than 40% in 2040. Even though that many countries have developed comprehensive national energy efficiency action plans where the majority of contemporary energy efficiency related policies and instruments are oriented to technical systems (building envelope, heating systems, electrical appliances), the soft organisational potentials for energy efficiency improvements is unfortunately still very underestimated both at the national and at the local level [2,3].

In 2008, the European Code of Conduct for Data Centres has been launched as a voluntary market transformation programme addressing primarily data centre owners and operators, and secondly the supply chain [4]. According to [5], electricity consumed in data centres, including enterprise servers, IT and communication equipment, cooling equipment and power equipment, is expected to contribute substantially to the electricity consumed in the European Union (EU) commercial sector in the near future. Additionally, even though that Eco-design Directive (Directive 2009/125/EC) introduces common minimum efficiency requirements just the selection of energy efficient equipment is not guaranteeing that the data centre will be efficient. Systematic overview of available energy-saving technologies and opportunities for renewable energy integration for data centres is presented in [6,7].

When it goes for small server rooms it has been noticed that inefficiencies mainly resulted from organizational rather than technical issues [8]. According to [9], the fear experienced by datacentre administrators presents an ongoing problem due to the low percentage of machines that they are willing to switch off in order to achieve durable energy savings. It is clear that upgrading the data centre cooling facilities is a continuous process and in this sense monitoring of energy use and environmental conditions is imperative in order to assess overall data centre energy efficiency and thermal management effectiveness [10,11]. As it is reported in [12,13], reducing the power consumption of the cooling systems is considered as a high priority in the data centres operation and significant energy savings can be achieved. According to [14], the use of liquid cooling technology allows the infrastructure first to reduce its energy consumption due to the possibility to cool down the liquid by free cooling, and second to use the waste heat of the IT equipment in other applications such as space heating [14]. The results of a case study presented in [15], indicate that potential energy savings of up to 75% are achievable when utilising heat pipe based free cooling systems. Economic evaluation of seven different cooling strategies presented in [16], are indicating that energy cost constituted the largest share of the total costs regardless the type of selected cooling strategy. Hartmann and Farkas [17] have recently proposed a power loss model, capable of supporting the optimal selection of different subsystems and consequently leading to decreased power losses in the distribution and power conversion infrastructure of the data centre. Additionally, Oró et al. [18] have developed dynamic energy model based on a component-by-component approach in order to study different energy efficiency strategies and to evaluate its effects on the operational conditions, energy consumption and carbon footprint of the data centre. According to [19], it is worth to invest time and resources to develop the computational fluid dynamics (CFD) model to analyse and design thermal air flows in data centres.

Due to characteristics of data centre load profile there are several opportunities how to exploit it in the various demand response initiatives [20]. Additionally, data centres can play different roles in future development of Smart Grids and providing support for numerous necessary auxiliary services [21,22].

The research work described in this paper was inspired by the recommendations proposed by Fernández-Montes et al. [6] and Lajevardi et al. [11], where the future research should focus on solutions capable to overcome the fear of data centre administrator and make him aware of the energy performance in real-time. Additionally, this paper evaluates the effectiveness of the widely used performance indicators like power usage effectiveness or data centre infrastructure efficiency in the process of performance monitoring and verification of energy efficiency improvements. One of the basic assumptions of the presented research work is that the monitored energy consumption, enriched with information about its context, can be the basis for the identification of energy profiles and future optimisation of operational practice.

2 Methodology

The methodology of the proposed practical approach evolved from the traditional management structure, plan-do-check-act (PCDA) model which has been upgraded in the integrated performance monitoring system for promotion of energy awareness in buildings like it is presented in [23]. The core element of the model is called energy cost centre (ECC). The concept of energy consumption monitoring and targeting based on network of ECCs has been introduced by Morvay and Gvozdenac [24] and it starts with the integration of energy within the activity flow charts, Figure 1.

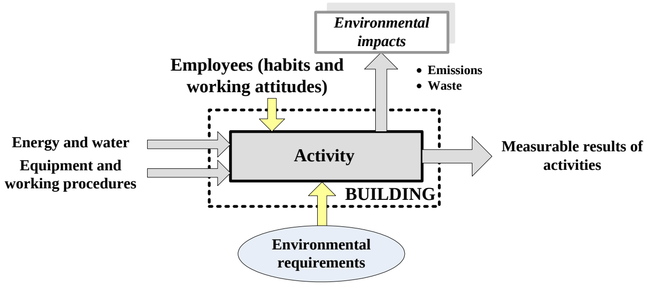

Figure 1. Concept of energy cost centre based modelling [24]

According to [24], an ECC can be any department, section or machine that uses a significant amount of energy or creates significant environmental impacts. In each ECC loads are called energy cost units (ECU) and classified into controllable and uncontrollable loads. Waste energy from one ECU, for example waste heat, can be input for another ECU or ECC. After setting up the network of ECCs with associated ECUs it is necessary to define the system of relevant and case specific performance indicators (PI). Outputs of the performance evaluation are the baseline for progress evaluation, directions and targets for performance improvement. The first step in analysing the possibilities to improve data centre energy efficiency is to evaluate the historical development of the electricity consumption in combination with activities or the useful work produced by installed IT equipment. In case of cluster computers an effective PI can be defined as a ratio of average cluster load (C_{load}) to total energy consumption (E_{total}) and is called cluster energy productivity (CEP).

$$CEP = \frac{C_{load}}{E_{total}} \tag{1}$$

Power usage effectiveness (PUE) has been developed by the Green Grid Association and is the most widely adopted metric used by the data centre industry [25]. The PUE is the ratio of total energy consumption to run the data centre facility to IT equipment energy consumption (E_{IT}) and is given by the following equation:

$$PUE = \frac{E_{total}}{E_{IT}} \tag{2}$$

Total energy consumption to run the data centre facility beside energy consumption of IT equipment includes consumption of all other necessary systems like cooling, lighting and others. In terms of energy efficiency lower values of PUE are better. However, according to literature review once a low PUE is achieved, power supply efficiency and IT load have the greatest impact on its value [11,26]. The reverse metric of PUE is called data centre infrastructure efficiency (DCIE) and it measures the IT equipment energy consumption divided by the total energy consumption of data centre facility [25]. DCIE is expressed as a percentage and it is given by the following equation:

$$DCIE = \frac{E_{IT}}{E_{total}} = \frac{1}{PUE} \tag{3}$$

The next step in the process of improving data centre energy efficiency is the assessment of current operational procedures and evaluation of energy management practices through energy audit. Vital outputs of energy audit are the baseline for the performance monitoring and set of measures how energy efficiency can be improved. The activities within the energy audit are not limited on analysis of technical systems but they also include the evaluation of the role and impacts of the human factor in the overall energy performance of data centre.

3 Results and Disscussion

Described practical approach has been tested at data room located within the complex of buildings for educational and research purposes in Slovenia. The objective of this case study was to examine how the energy performance of equipment installed in the data room at the selected location can be optimised. Slovenian location has provided a real testing environment with the full support of management and maintenance staff and open access to all requested data for the validation of proposed practical approach for energy efficiency optimisation.

Configuration of addressed data room is given in Figure 2. The data room operates continuously 24h/7 days a week. Average power consumption of IT load is 38 kW and average PUE before implementation of corrective actions was 1.44.

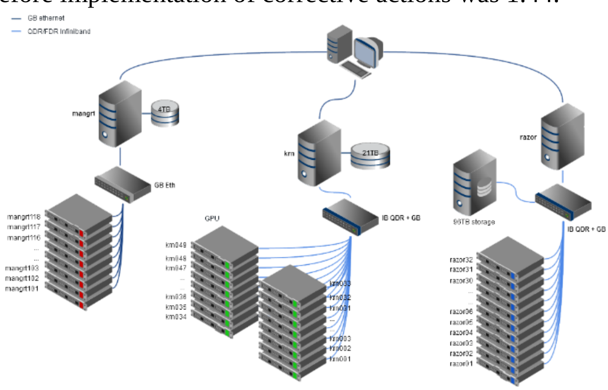

Figure 2. Configuration of addressed data room

Preliminary evaluation of the energy performance of the addressed data room revealed the following weak points:

- poor airflow management,
- overcooling,
- blending air (hot and cold),
- unused servers and
- no energy management system for data centre.

In the absence of a proper energy management system on the building level, it was not unusual that the certain equipment in the data room was running even when it was not necessary. During the energy performance evaluation the addressed data room was treated as a single ECC containing all together 6 different ECUs. Data about average aggregated load on addressed cluster computers was obtained from the control and monitoring system, Figure 3. Once again it has been confirmed that in many modern buildings different monitoring and control systems are used, but majority of them are not directly connected with the energy consumption optimisation.

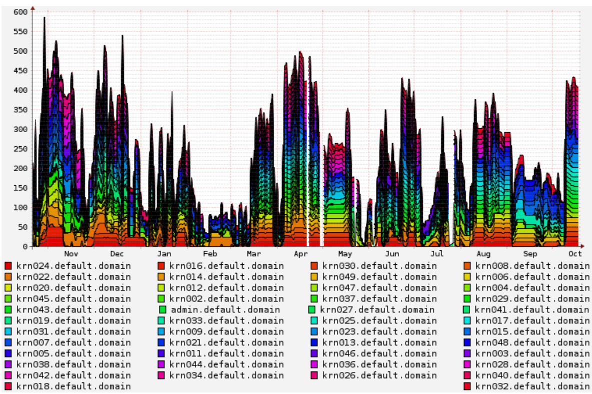

Figure 3. Aggregated load on one of addressed cluster computers

Additionally, comprehensive set of measurements during testing various cooling strategies has been done, Figure 4.

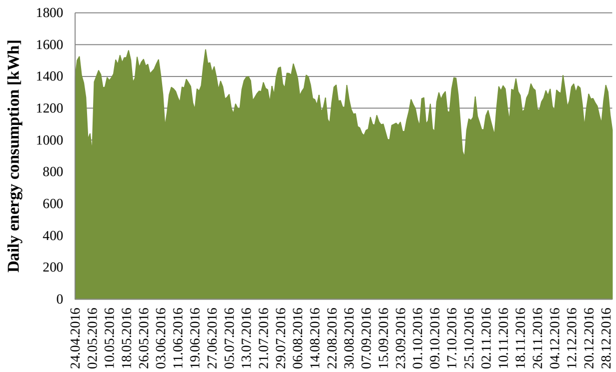

Figure 4. Results of comprehensive set of measurements during testing various cooling strategies

Inspired by the recommendation from [19] and before actual implementation, identified energy efficiency measures related with cooling system were re-examined by using the CFD model of the data centre configuration, Figure 5.

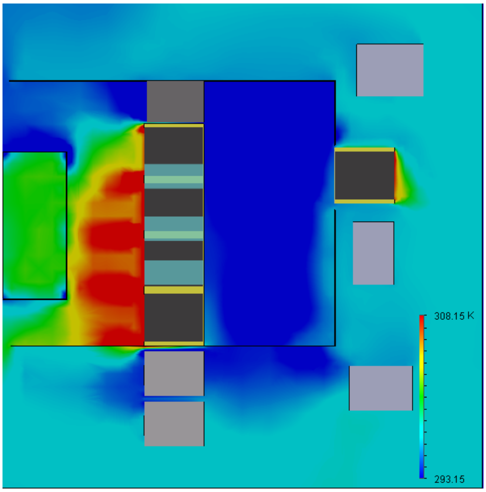

Figure 5. Results of CFD simulation of thermal air flows in the addressed data room

After implementation of selected corrective actions the issues related with blending air (hot and cold) were resolved and appropriate airflow volume to ICT equipment was ensured. Additionally, energy management system for data room including measuring, alarming, monitoring and targeting is implemented and consequently unused servers are turned off. After implementation of above mentioned corrective actions PUE reduced to 1.37.

Summary of main energy, environmental and economy achievements related with the improvement of energy performance of addressed data room is given in Table 1.

Table 1. Feasibility of implemented energy efficiency actions

Potential reduction in electricity consumption (MWh/year)	82,3
Indirect (electricity induced) CO_2 emission reduction (t CO_2 / year)	42,2
Cost reduction (€ / year)	6.200
Payback period (static) (year)	2,2
Net present value (€) (economic lifetime 5 years and discount rate 10%)	9.900
Internal Rate of Return (%)	36
Potential reduction in electricity consumption (MWh/year)	82,3

Future activities related with the energy performance improvements of the addressed data room will include the additional waste heat utilisation for space heating and sanitary hot water preparation, replacement of existing UPS units with new ones with higher energy efficiency and additional work with users.

4 Conclusion

Presented research work confirmed that achievement of measurable energy performance improvements require significant amount of time, efforts and experience and must be supported with the promotion of energy awareness. Performance monitoring is a process of learning through people's performance evaluation. During the practical implementation two main barriers have been resolved, fear of change (the process is so complicated) and focus on the primary function. Honest relationship and cooperation between energy efficiency experts and IT manager were the two most important factors for reaching energy savings.

However, it is important to emphasise the need for continuous upgrade of the proposed approach with novel research inputs especially having in mind the recommendations presented by Whitehead et al. [27] where future research challenges are related with the development of decision support tools for design engineers and data centre operators to quickly evaluate the life cycle impact of the decisions they make during the design and life time of a data centre facility.

References

[1] International Energy Agency, *World Energy Outlook 2016*, OECD/ IEA, 2016.

[2] V. Bukarica, and S. Robić, "Implementing energy efficiency policy in Croatia: Stakeholder interactions for closing the gap", *Energy Policy*, vol. 61, pp. 414-422, Oct. 2013.

[3] A. Podgornik, B. Sucic, and B. Blazic, "Effects of customized consumption feedback on energy efficient behaviour in low-income households", *Journal of Cleaner Production*, vol. 130, pp. 25-34, Sept. 2016.

[4] Joint Research Centre, "EU Code of Conduct on Data Centre Energy Efficiency - Participant Guidelines and Registration Form - Version 3.0.0", Ispra, 2016.

[5] P. Bertoldi, "A Market Transformation Programme for Improving Energy Efficiency in Data Centres", presented at the ACEEE Summer Study on Energy Efficiency in Buildings, Pacific Grove, 2014, pp. 9/14-9/26.

[6] E. Oró, V. Depoorter, A. Garcia, and J. Salom, "Energy efficiency and renewable energy integration in data centres. Strategies and modelling review", *Renewable and Sustainable Energy Reviews*, vol. 42, pp. 429-445, Feb. 2015.

[7] H. Rong, H. Zhang, S. Xiao, C. Li, and C. Hu, "Optimizing energy consumption for data centers", *Renewable and Sustainable Energy Reviews*, vol. 58, pp. 674-691, May 2016.

[8] I. H. Y. Cheung, S. Greenberg, R. Mahdavi, R. Brown, and W. Tschudi, "Energy Efficiency in Small Server Rooms: Field Surveys and Findings", presented at the ACEEE Summer Study on Energy Efficiency in Buildings, Pacific Grove, 2014, pp. 9/50-9/61.

[9] A. Fernández-Montes, D. Fernández-Cerero, L. González-Abril, J. A. Álvarez-García, and J. A. Ortega, "Energy wasting at internet data centers due to fear", *Pattern Recognition Letters*, vol. 67 (1), pp. 59-65, Dec. 2015.

[10] C. A. Balaras, J. Lelekis, E. G. Dascalaki, and D. Atsidaftis, "High Performance Data Centers and Energy Efficiency Potential in Greece", *Procedia Environmental Sciences*, vol. 38, pp. 107-114, 2017.

[11] B. Lajevardi, K. R. Haapala, and J. F. Junker, "Real-time monitoring and evaluation of energy efficiency and thermal management of data centers", *Journal of Manufacturing Systems*, vol. 37 (2), pp. 511-516, Oct. 2015.

[12] J. Cho, and Y. Kim, "Improving energy efficiency of dedicated cooling system and its contribution towards meeting an energy-optimized data center", *Applied Energy*, vol. 165, pp. 967-982, Mar. 2016.

[13] A. Habibi Khalaj, T. Scherer, S. K. Halgamuge, "Energy, environmental and economical saving potential of data centers with various economizers across Australia", *Applied Energy*, vol. 183, pp. 1528-1549, Dec. 2016.

[14] A. Carbó, E. Oró, J. Salom, M. Canuto, M. Macías, and J. Guitart, "Experimental and numerical analysis for potential heat reuse in liquid cooled data centres", *Energy Conversion and Management*, vol. 112, pp. 135-145, Mar. 2016.

[15] H. Jouhara, and R. Meskimmon, "Heat pipe based thermal management systems for energy-efficient data centres", *Energy*, vol. 77, pp. 265-270, Dec. 2014.

[16] K. Cho, H. Chang, Y. Jung, and Y. Yoon, "Economic analysis of data center cooling strategies", *Sustainable Cities and Society*, vol. 31, pp. 234-243, May, 2017.

[17] B. Hartmann, and C. Farkas, "Energy efficient data centre infrastructure - Development of a power loss model", *Energy and Buildings*, vol. 127, pp. 692-699, Sept. 2016.

[18] E. Oró, M. Codina, and J. Salom, "Energy model optimization for thermal energy storage system integration in data centres", *Journal of Energy Storage*, vol. 8, pp. 129-141, Nov. 2016.

[19] R. Basmadjian, L. Müller, and H. De Meer, "Data centres' power profile selecting policies for Demand Response: Insights of Green Supply Demand Agreement", *Ad Hoc Networks*, vol. 25 (B), pp. 581-594, Feb. 2015.

[20] M. Mäsker, L. Nagel, A. Brinkmann, F. Lotfifar, and M. Johnson, "Smart Grid-aware scheduling in data centres", *Computer Communications*, vol. 96, pp. 73-85, Dec. 2016.

[21] D. Arnone, A. Barberi, D. La Cascia, E. Riva Sanseverino, and G. Zizzo, "Green Data Centres integration in smart grids: New frontiers for ancillary service provision", *Electric Power Systems Research*, vol. 148, pp. 59-73, July 2017.

[22] B. Sučić, A. S. Anđelković, and Ž. Tomšić, "The concept of an integrated performance monitoring system for promotion of energy awareness in buildings", *Energy and Buildings*, vol. 98, pp. 82-91, July 2015.

[23] Z. K. Morvay, and D. D. Gvozdenac, *Applied Industrial Energy and Environmental Management*, John Wiley & Sons, 2008.

[24] B. Whitehead, D. Andrews, A. Shah, and G. Maidment, "Assessing the environmental impact of data centres part 1: Background, energy use and metrics", *Electric Power Systems Research*, vol. 82, pp. 151-159, Dec. 2014.

[25] G. A. Brady, N. Kapur, J. L. Summers, H. M. Thompson, "A case study and critical assessment in calculating power usage effectiveness for a data centre", *Energy Conversion and Management*, vol. 76, pp. 155-161 Dec. 2013.

[26] A. Almoli, A. Thompson, N. Kapur, J. Summers, H. Thompson, and G. Hannah, "Computational fluid dynamic investigation of liquid rack cooling in data centres", *Applied Energy*, vol. 89 (1), pp. 150-155, Jan. 2012.

[27] B. Whitehead, D. Andrews, A. Shah, and G. Maidment, "Assessing the environmental impact of data centres part 2: Building environmental assessment methods and life cycle assessment", *Building and Environment*, vol. 93 (2), pp. 395-405, Nov. 2015.

10TH INTERNATIONAL CONFERENCE ON SUSTAINABLE ENERGY AND ENVIRONMENTAL PROTECTION (JUNE 27TH – 30TH, 2017, BLED, SLOVENIA), ENERGY EFFICIENCY
J. Krope, A.Ghani Olabi, D. Goričanec & S. Božičnik

Energy Efficiency of Camelina and Crambe Biomass Production Under Different Cultivation Conditions

MARIUSZ JERZY STOLARSKI & MICHAŁ KRZYŻANIAK

Abstract Camelina and crambe are oil crops which are attractive feedstock for bioproducts and bio-energy industry due to their valuable properties. The objective of a two-year study was to determine the input and the energy efficiency of biomass production of camelina and crambe under different, large scale production conditions. Production variants were analysed: (i) traditional tillage and reduced tillage systems; (ii) with or without foliarly-applied herbicide.

Energy inputs were higher in traditional tillage compared to the reduced tillage system. The yield energy value varied widely depending on the year and variant of crop production. The highest yield energy value was obtained for crambe cultivation in the reduced tillage system and when no foliar herbicide was used (73 GJ ha-1). In this production variant, the best energy efficiency ratio (4.9) was obtained as well. The value of this ratio for camelina was contained in a wide range from 2.6 up to 4.7.

Keywords: • Oil crops • Camelina sativa • Crambe abyssinica • Energy input • Energy balance • Energy intensity Energy efficiency ratio •

CORRESPONDENCE ADDRESS: Mariusz Jerzy Stolarski, Ph.D., Full Professor, University of Warmia and Mazury in Olsztyn, Faculty of Environmental Management and Agriculture, Department of Plant Breeding and Seed Production, Centre for Bioeconomy and Renewable Energies, Plac Łódzki 3/420, 10-724 Olsztyn, Poland, e-mail: mariusz.stolarski@uwm.edu.pl. Michał Krzyżaniak, Ph.D., Assistant Professor, University of Warmia and Mazury in Olsztyn, Faculty of Environmental Management and Agriculture, Department of Plant Breeding and Seed Production, Centre for Bioeconomy and Renewable Energies, Plac Łódzki 3/421, 10-724 Olsztyn, Poland, e-mail: michal.krzyzaniak@uwm.edu.pl.

https://doi.org/10.18690/978-961-286-050-9.16 ISBN 978-961-286-050-9

1 Introduction

The main oleaginous plant cultivated in Europe is rapeseed, which can be used for both the food and the energy industry. Frequently, this species intended either for consumption or energy, is cultivated with the application of the same method. However, in the production of a feedstock intended for energy production, biomass production energy efficiency is an important factor. Moreover, the energy efficiency ratio of biomass is influenced mainly by the crop species and production regime. The production technology determines the demand for energy (energy input) and the amount of energy accumulated in biomass (energy output) [1, 2, 3].

Camelina (*Camelina sativa* L. Crantz) and Crambe (*Crambe abyssinica* Hochst ex R.E. Fries) may be an alternative to rapeseed, especially on lower quality soils. Camelina and crambe are oil crops which due to their valuable properties such as short growing season, resistance to drought and frost, low means of production input requirements (fertilisers, plant protection products), high oil content and their valuable composition are becoming attractive feedstock for the bio-energy industry. These species have recently been the focus of many research centres and companies interested in using oils for bioproducts and biofuels. Accordingly, an important issue justifying the use of camelina and crambe as a source of biomaterials is to evaluate the energy efficiency of their production. Therefore, the objective of this two-year study conducted in north-eastern Poland was to determine the input and the energy efficiency of biomass production (seeds and straw) of camelina and crambe under different, large scale production conditions.

2 Materials and Methods

2.1 Field experiments

The study involved field experiments performed in 2015-2016, in north-eastern Poland on fields owned by the University of Warmia and Mazury in Olsztyn. The soil was prepared according to good agricultural practice. Seeds of crambe (Galactica variety) and camelina (Midas variety) were sown with a drill; 13 kg ha^{-1} and 6 kg ha^{-1}, respectively. The 2015 experiment was established near Samławki over an area of 1.5 ha (0.5 ha crambe + 1 ha camelina). It involved traditional tillage system without foliarly-applied herbicide. The experiment of 2016 was organised in two locations of Łężany (A) and Kocibórz (B). The Łężany (A) experiment extended over the area of 1 ha (0.5 ha crambe + 0.5 ha camelina) and involved traditional tillage system without foliarly-applied herbicide. The crambe plantation on this field was badly infected by diamondback moth (*Plutella xylostellai*) and, apart from the insecticide spraying (Avaunt (indoksakarb) at the dose of 0.170 dm^3 ha^{-1}), it was impossible to protect the plants. For this reason, no crambe seed or straw technological yield was obtained from the Łężany field. On the other hand, in Kocibórz (B) reduced tillage systems, with or without foliarly- applied herbicide, were used over the total area of 2 ha (1 ha crambe + 1 ha camelina). In this study, the following production variants were analysed: (i) traditional tillage and reduced tillage systems; (ii) with or without foliarly-applied herbicide. In order to evaluate the possibility of chemical protection of crambe and camelina against weed spread, Gala 334 SL a post-germination herbicide (chlopyralid and pikloram) was applied at the dose of 0.35 dm^3 ha^{-1}. On each experimental field and in each year, nitrogen fertilizer was applied as ammonium nitrate at a dose of 100 kg ha^{-1} N.

2.2 Input-output and energy efficiency analyses

Energy input-output and energy efficiency analyses were conducted with the application of the methodology presented in previous studies [1, 4]. The energy inputs included several energy sources: direct energy carriers (diesel fuel), exploitation of fixed assets (tractors, machines, equipment), consumption of materials (mineral fertilisers, agrochemicals, seeds) and human labour.

The total energy input for crambe and camelina biomass production was calculated based on the unit consumption of materials and the energy intensity of their production. The energy conversion coefficients for diesel fuel (43.1 MJ kg^{-1}), nitrogen fertilizers (48.99 MJ kg^{-1} N) and pesticides (268.4 MJ kg^{-1} of active substance) were based on the indexes presented in literature [5]. The energy input for the use of tractors (125 MJ kg^{-1}), machines (110 MJ kg^{-1}) and human labour (60 MJ $hour^{-1}$) in the production process was calculated with the coefficients provided in the literature and data provided in materials published by manufacturers of tractors and machines [6, 7].

Energy gain was the difference between the crambe or camelina biomass yield energy value and the total input for its production. The energy efficiency ratio of biomass (seeds + straw) production was the ratio of the yield energy value (energy output) to energy input for its production. Energy intensity was the energy consumption per 1 Mg of seeds, straw and oil. It was the ratio of total energy input to the yield of each component.

3 Results

The yielding of crambe and camelina varied to a large extent and depended on a species, cultivation technology and the experimental year (Fig. 1). The highest camelina and crambe seed yield was obtained in 2016 following the application of reduced tillage systems without foliarly-applied herbicide. The lowest yield was recorded for the same field after foliarly-applied herbicide.

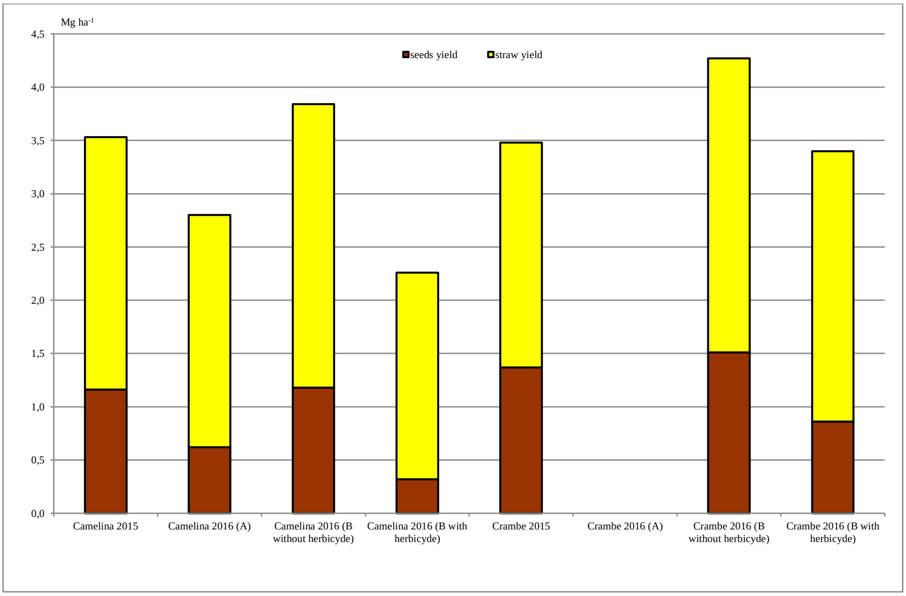

Fig. 1. Yield of seeds and straw camelina and crambe depending on the production technology and year of study.

Energy inputs, depending on the variety and cultivation technology ranged from 14.57 to 15.15 GJ ha^{-1}. Energy inputs were higher in traditional tillage (in the 2-4% range) compared to the reduced tillage system. Also, the use of foliar herbicide had higher energy input (in range 1-2%) compared to when herbicide was not used. Yield energy value varied widely, depending on the year and variant of crops production. The highest yield energy value (seeds + straw) was obtained for crambe cultivation in the reduced tillage system and when no foliar herbicide was used (73 GJ ha^{-1}) (Fig. 2). In this production variant, the best energy efficiency ratio (4.9) was obtained as well (Fig. 3). The value of this ratio for camelina ranged widely from 2.6 up to 4.7. The energy intensity for straw, seeds and oil ranged between 5.4-7.6; 9.8-46.1 and 30.5-124.3 GJ Mg^{-1}, respectively (Fig. 4).

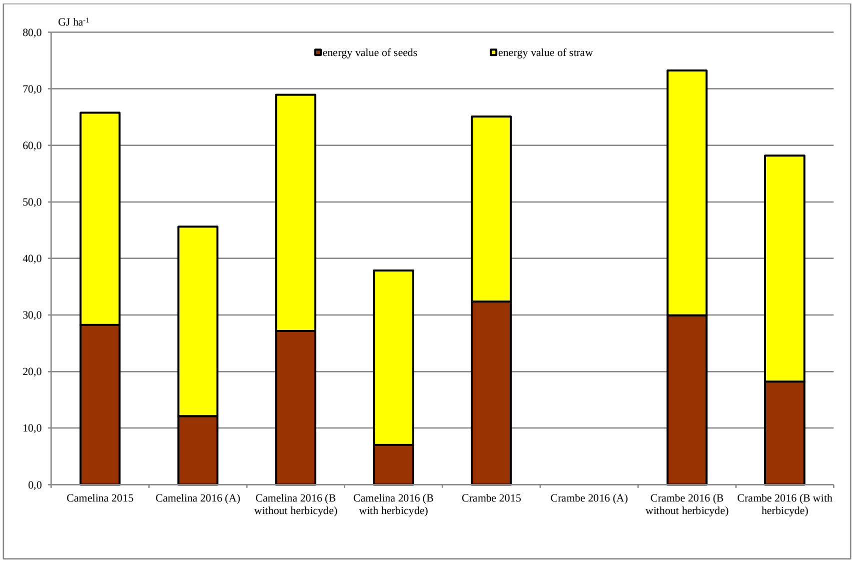

Fig. 2. Camelina and crambe energy value of seeds and straw yield depending on the production technology and year of study.

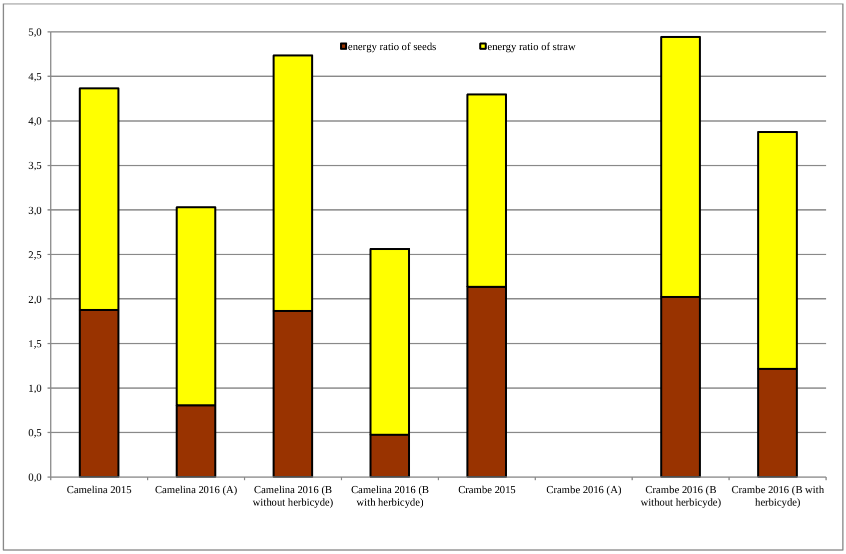

Fig. 3. Camelina and crambe energy efficiency ratio of seeds and straw depending on the production technology and year of study.

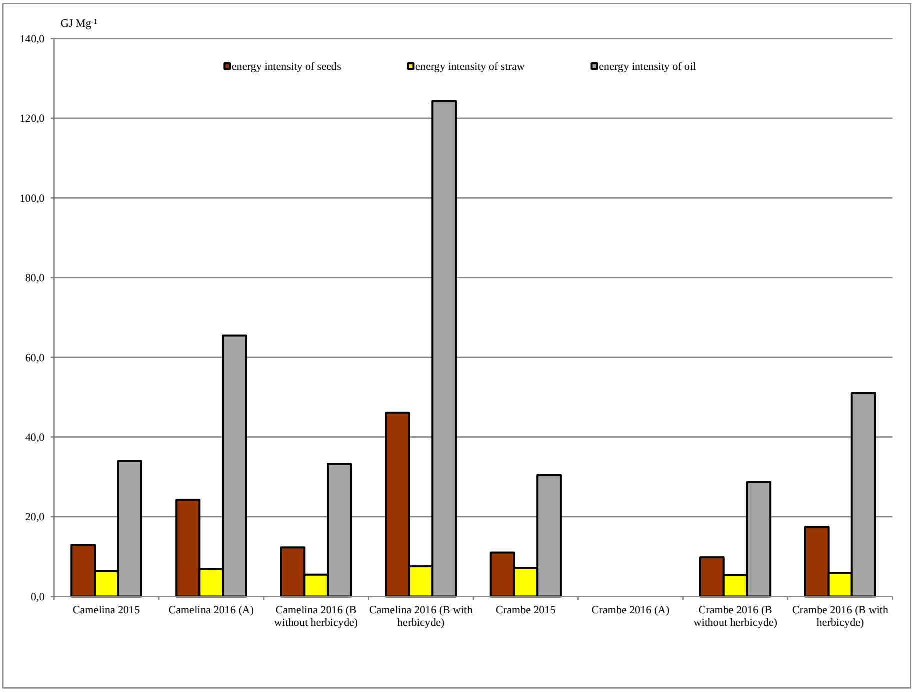

Fig. 4. Camelina and crambe energy intensity for seeds, straw and oil production depending on the production technology and year of study

Acknowledgements

This work was funded by European Union Horizon 2020 research and innovation programme under grant agreement No 635405 (project COSMOS).

References

[1] K.J. Jankowski, W.S. Budzyński and Ł. Kijewski. An analysis of energy efficiency in the production of oilseed crops of the family Brassicaceae in Poland, Energy, vol. 81, pp. 674–681, Mar. 2015.

[2] W.S. Budzyński, K.J. Jankowski and M. Jarocki. An analysis of the energy efficiency of winter rapeseed biomass under different farming technologies. A case study of a large-scale farm in Poland, Energy, vol. 90, pp. 1272–1279, Oct. 2015.

[3] F. Alluvione, B. Moretti, D. Sacco and C. Grignani. EUE (energy use efficiency) of cropping systems for a sustainable agriculture, Energy, vol. 36, pp. 4468–4481, July. 2011.

[4] M.J. Stolarski, M. Krzyżaniak, J. Tworkowski, S. Szczukowski and D. Niksa. Analysis of the energy efficiency of short rotation woody crops biomass as affected by different methods of soil enrichment, Energy, vol. 113, pp. 748–761, Oct. 2016.

[5] J. Neeft, Gagnepain, B. Bacovsky, D. Lauranson, R. Georgakopoulos, K. Fehrenback, H. et al. Harmonized calculations of biofuel greenhouse gas emissions in Europe, Netherlands, BioGrace standard values – version 4 – Public.xls, www.BioGrace.net. 2011.
[6] A. Szeptycki and Z. Wójcicki. Technical development and energy inputs in agriculture till 2020. Warsaw, IBMER, 2003 (in Polish).
[7] Institute of Technology and Life Sciences. Catalogue of agricultural machines. Warsaw (cd–rom), 2016 (in Polish).

10TH INTERNATIONAL CONFERENCE ON SUSTAINABLE ENERGY AND ENVIRONMENTAL PROTECTION (JUNE 27TH – 30TH, 2017, BLED, SLOVENIA), ENERGY EFFICIENCY
J. Krope, A.Ghani Olabi, D. Goričanec & S. Božičnik

Climate Change and Thermal Comfort in Educational Buildings of Southern Europe: the Case of Cyprus

CHRYSO. HERACLEOUS & AIMILIOS. MICHAEL

Abstract It has become evident that Southern Europe will experience more adverse climate change effects compared to other European regions. The existing educational building stock, which mostly relies on natural ventilation during the cooling period, is expected to have a significant impact on users' thermal comfort, well-being and productivity. The study presented herein aims to investigate the vulnerability of educational buildings in Cyprus in view of future climatic conditions, by means of a dynamic simulation software, presenting a methodology for the assessment of thermal comfort and energy performance. More specifically, the European Standard EN 15251 is employed to assess the thermal comfort in naturally ventilated buildings using the adaptive comfort approach. Moreover, this paper looks at the overheating criteria from CIBSE TM 52 and tests them on a typical archetype. The research indicates that educational buildings in southern Europe are unable to meet the thermal comfort criteria of the future, creating a major impact on the environmental, economic and social interaction of people and buildings. The evaluation of the resilience of existing educational buildings is useful in understanding the necessity of energy retrofitting measures in view of future climate conditions, contributing to energy efficiency policies and decision-making regarding retrofit interventions.

Keywords: • Adaptive comfort • Overheating • Climate change • Educational buildings • Cyprus •

CORRESPONDENCE ADDRESS: Chryso Heracleous, Dipl.Arch.Eng., M.Sc., Ph.D. Candidate, University of Cyprus, Department of Architecture, P.O. Box 20537, 1678, Nicosia Cyprus, email: echryso@ucy.ac.cy. Aimilios Michael, Ph.D., Lecturer, University of Cyprus, Department of Architecture, P.O. Box 20537, 1678, Nicosia Cyprus, email: aimilios@ucy.ac.cy.

https://doi.org/10.18690/978-961-286-050-9.17 ISBN 978-961-286-050-9

Available at: http://press.um.si.

1 Introduction

The awareness about climate change and the urgent need to decrease carbon emissions in buildings, in combination with concerns about occupants' comfort due to the rise of temperature, are increasing. Harmful health impacts resulting from climate change are related to increasing heat stress, extreme weather conditions, poor air quality, water and vector borne diseases. It has become evident that Southern Europe will experience more adverse climate change effects compared to other European regions [1, 2]. In modern societies, people spend over 90% of their time indoors. With the exception of their home, students spend more time in educational buildings than in any other place, highlighting the importance of providing comfortable indoor thermal conditions in these buildings. The positive impact of thermal comfort in students' performance, the promotion of healthier conditions and energy saving have been thoroughly studied over the years [3]. In cases where comfortable indoor conditions are not met, air-conditioning systems are used to provide thermally comfortable spaces which in turn, lead to increased energy consumption.

The existing educational building stock, which mostly relies on natural ventilation during the cooling period, is expected to have a significant impact on the users' thermal comfort, well-being and productivity as it is expected to cope with conditions for which it was not initially designed. The study presented herein aims to investigate the vulnerability of educational buildings in Cyprus in view of future climatic conditions by means of a dynamic simulation software, presenting a methodology for the assessment of thermal comfort and overheating risks. The evaluation of the resilience of educational buildings is useful in understanding the necessity of energy retrofitting measures in view of future climate conditions, contributing to energy efficiency policies and decision-making regarding retrofit interventions.

2 Methodology

The school building is the first contact of a person with a public building. It is, at the same time, a highly demanding space as far as comfort levels are concerned. The majority of educational buildings in Cyprus consists of typical typologies and construction characteristics. For the needs of this particular research, 114 educational buildings of secondary education all over Cyprus were investigated. 102 educational buildings of the sample under study, i.e. 90.5%, fall in the category of typical school buildings. These buildings were designed and erected by the Technical Services of the Cyprus Ministry of Education and Culture and are characterized by uniformity in terms of typology, morphology and construction. The architectural designs of school buildings show significant similarities, extensive standardization of building components and construction methods [4].

As overheating is becoming a key problem in building design, the present study aims to investigate how educational buildings will perform in view of rising temperatures in the future and examine the implications on both energy performance and people's health. For the assessment of the thermal comfort vulnerability of schools in Cyprus, dynamic thermal simulations were undertaken using the Integrated Environmental Solutions-Virtual Environment (IES-VE). The European Standard EN 15251 [5] is used to assess the thermal comfort in naturally ventilated buildings using the adaptive comfort approach. Moreover, this paper looks at the overheating criteria from CIBSE TM 52 [6] and tests them on a typical archetype.

2.1 Description of the case study

For the evaluation of the thermal performance of educational buildings in future climatic scenarios in Cyprus, a typical secondary school in the coastal region (Larnaca), i.e. Vergina Secondary school, is selected as a representative case study due to its typical characteristics in terms of the typology, construction, as well as integration of environmental design principles.

Classrooms mainly consist of two construction moduli, resulting to slightly rectangular plans with dimensions of approximately 7.00 × 8.00 × 3.20 m (W × L × H). The linear disposition of classrooms in typical educational buildings allows for openings along the two long sides of the space. In typical educational buildings, linear building volumes appear in all four orientations. In the majority of classrooms, the facade with extensive glazed surface is oriented towards the internal courtyard, while the facade with clerestories faces the external environment. Access to the classrooms is achieved through a linear, semi-open corridor 2.00 m wide (Fig. 1 and 2).

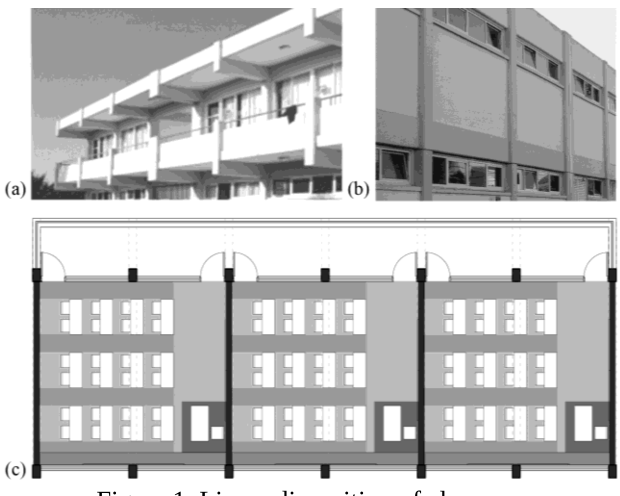

Figure 1. Linear disposition of classrooms

Typical educational buildings in Cyprus are not described by climatic consistency as they do not exhibit a conscious incorporation of key environmental design principles [7-10], particularly in terms of proper insolation, shading [9,11] or natural lighting [12].

Four typical classrooms of general education, one in each orientation, were selected for in depth analysis. Openings along the two long sides of the space (i.e. extensive windows towards the interior side and clerestories towards the exterior) provide solar gains and daylighting into the classroom. The openings to floor ratio is 35%. It should be noted that openings are not directly shaded by building or plant elements. The direct connection of classrooms with semi-open corridors is achieved through an external overhang of 2.00m to all windows, allowing the regulation of solar radiation and of natural lighting. The clerestories in the other long side of the classroom have no external shading control. It is noted that all openings of the typical classroom (both windows and clerestories) have internal black-out curtains that allow shading control by users. Internal blinds are needed when solar radiation incident on the window is above 120 W/m2 (Table 1). Airtightness requirements were set at 10m3/hr/m2 (i.e. 4ac/h) at 50Pa [13]. The existing educational building stock relies on natural ventilation during the cooling period. Night cooling is not adopted for safety reasons. The classroom has an occupancy profile of 20 students on weekdays from 07:30 to 13:35 with 3 small breaks. A summary of occupancy, as well as window and blinds operation during the year, is presented in Table 1, while construction details are summarized in Table 2.

Table 1. Window / Blinds operation and occupancy

Schedule and Occupancy		**Window/Blinds**		
		Interim	**Summer**	**Winter**
07.30-09.00	1	0/0	1/idn>120	0/0
25 min break	0	1/0	1/0	1/0
09.25-10.55	1	1/idn>120	1/idn>120	0/idn>120
15 min break	0	1/0	1/0	1/0
11.10- 12.40	1	1/idn>120	1/idn>120	0/idn>120
10 min break	0	1/0	1/0	1/0
12.50-13.35	1	0/idn>120	0/idn>120	0/idn>120
0: occupancy off, 1: occupancy on; idn>120: direct normal irradiance > 120W/m^2				

Table 2. Construction characteristics and material of a typical school

Building Elements	**Construction Detail**	**U-Value (W/m^2K)**	**Effective Thermal Capacity (KJ/m^2K)**
External Wall	200mm single layer of brick and three layers of plaster (20-25mm)	1.389	120
Internal Wall	100mm single layer of brick and three layers of plaster (20-25mm)	1.235	120
Roof	Concrete slab and asphalt layer of 5mm	3.239	240
Ground Floor	Concrete slab and tiles	1.6	232
Window	6mm single glazed and aluminum frame	6	g-value 0.82

2.2 Dynamic simulation

For the assessment of the thermal comfort vulnerability of schools in Cyprus, dynamic thermal simulations were undertaken using Integrated Environmental Solutions-Virtual Environment (IES-VE). IES-VE uses the Energy Plus engine which is widely acknowledged as a credible and valid tool to evaluate free-running indoor environments, in dynamic regimes, using hourly and sub-hourly simulations [14, 15]. For the evaluation of thermal comfort, the dynamic simulation was first run under the current climatic conditions and then under the climate change projections in all orientations of classrooms.

2.3 Future climatic scenarios

A key objective of this study was to develop a methodology that would allow the estimation of the climate change impact on the thermal comfort of educational buildings in Cyprus. The 2050s and 2090s were selected as the future time periods for which climate data was required through climatic scenarios. The impact of weather changes increases in the second half of the century, compared to the first half, according to the IPCC [2]. The PRECIS (Providing Regional Climates for Impacts Studies) climate model developed by the Hadley Centre was used. The emission scenario SRES A12 [2] was employed for the customized runs. In brief, the A1B scenario represents rapid economic growth with a balanced technological development, meaning that no particular energy source is heavily relied on but rather, similar improvement rates apply to all energy supply and end-use technologies (fossil fuel and renewable alike). The specific scenario was chosen because it rests between the 'business as usual' and the 'united sustainable planet' extremes.

2.4 Thermal comfort criteria

The basic approach to the development of the European Standard, on which TM52 (overheating) is based, is described by Nicol and Humphreys [16]. Using the data from the free-running buildings alone, one arrives at the following relation between the indoor comfort temperature calculated from the data and the running mean of the outdoor temperature:

$$Tc = 0.33Trm + 18.8(°C) \tag{1}$$

where, *Tc* is the predicted comfort temperature when the running mean of the outdoor temperature is *Trm*.

In this standard, there is an implication that building 'A' is better than building 'B' or 'C'. CIBSE recommends that new buildings, major refurbishments and adaptation strategies should conform to Category II in BS EN 15251 [5], which sets a maximum acceptable temperature of 3 °C above comfort temperature levels (from equation 1) for buildings in free-running mode. For such buildings, the maximum acceptable temperature (Tmax) is calculated from the running mean of the outdoor temperature (Trm) using the formula:

$$T\max = 0.33Trm + 21.8(°C) \tag{2}$$

where, *Tmax* is the maximum acceptable temperature (upper threshold).

Figure 2 shows the upper and lower thresholds calculated using equation (1). The graph highlights the significant range of operative temperatures falling within the acceptable range of comfort depending on the exterior conditions (Fig.2).

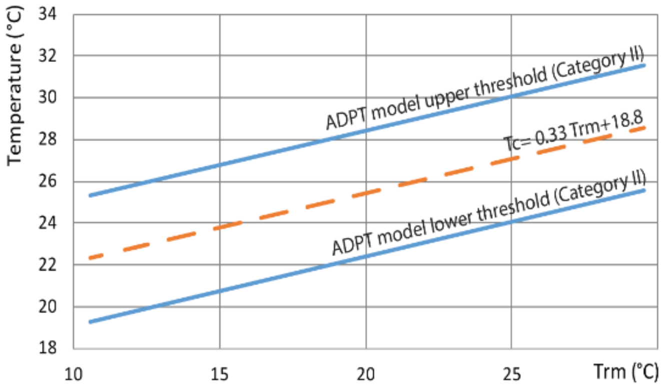

Figure 2. Design values for adaptive models of comfort as a function of outdoor temperature running mean. (Source: [5])

In order to implement the EN15251, the resulting Tc hourly values from simulations are compared to the operative temperatures produced by Eq. (1). If the simulated temperature is higher than the one produced by the model, the area is taken to be in a discomfort zone for that whole hour. The following three criteria, taken together, provide a robust, yet balanced, assessment of overheating risks of buildings in Europe [6].

Criterion 1: Hours of exceedance (H_e)

The first criterion sets a limit for the number of occupied hours that the operative temperature can exceed Tmax during a typical non-heating season (1 May- 30 September). This number shall not exceed 3 per cent of occupied hours.

Criterion 2: Daily weighted exceedance (W_e)

The second criterion deals with the severity of overheating within any one day, which is given in terms of temperature rise and duration and sets a daily acceptability limit.
To allow for the severity of overheating the weighted exceedance (We) shall be less than, or equal to, 6 in any one day where:

$$We = \Sigma(he\ x\ wf)\ We = (heo\ x\ 0) + (he1\ x\ 1) + (he2\ x\ 2) + (he3\ x\ 3) \qquad (3)$$

Where the weighting factor $w_f = 0$ if $\Delta T \leq 0$, otherwise $w_f = \Delta T$, and h_{ey} is the number of hours when $w_f = y$.

Criterion 3: Upper limit temperature (T_{upp})

To set an absolute maximum value for the indoor operative temperature, the value of ΔT shall not exceed 4 K.

$$Tupp = T\max + 4 \tag{4}$$

3 Results

Simulation can predict the likelihood of overheating in typical classrooms of educational buildings. Table 3 presents the results for the three criteria in the middle class of the ground floor for different orientations for the current typical meteorological year, for 2050, and 2090. Criterion 2 presents the weighted exceedance (in brackets) and criterion 3 shows the exceedance in hours (in brackets).

For the present TMY, the south and north oriented classroom, i.e. the classroom with the largest windows facing south and north respectively and the clerestories facing the opposite side, passed the criteria 1 and 3. Specifically, the numbers of hours in the non-typical heating season that operative temperature exceeded Tmax is exactly 3% of the occupied time while indoor temperature never exceeded 4K compared to Tmax. However, east and west oriented classrooms failed to pass criterion 1 by 1%; while they passed criterion 3. The classroom in all orientations did not meet criterion 2. Looking at the future climatic scenarios of 2050 and 2090, there is a clear tendency for severe overheating. Classrooms in all four orientations failed all the criteria and were unable to cope with overheating predictions solely relying on the current passive cooling strategies. In 2050, more than half of the occupied period is predicted to suffer from overheating, while in 2090, more than 70% of the time. Moreover, a large amount of hours exceeded the limit of maximum absolute value of 4K which indicates that adaptive actions will be insufficient to restore personal comfort and the vast majority of occupants will complain about excessive heat. North oriented classrooms show the lowest tendency for overheating due to lower solar gains.

Increased discomfort hours make the need for cooling predominant in order to achieve acceptable comfort conditions.

Table 3. TM52 criteria for different classroom orientations in line with climatic predictions

	TMY		2050		2090	
South						
C1	Pass	3%	Fail	66%	Fail	68%
C2	Fail	33	Fail	608	Fail	476
C3	Pass	-	Fail	51	Fail	191
North						
C1	Pass	3%	Fail	57%	Fail	70%
C2	Fail	38	Fail	635	Fail	476
C3	Pass	-	Fail	41	Fail	207
East						
C1	Fail	4%	Fail	66%	Fail	75%
C2	Fail	51	Fail	743	Fail	382
C3	Pass	-	Fail	51	Fail	253
West						
C1	Fail	4%	Fail	66%	Fail	73%
C2	Fail	40	Fail	724	Fail	384
C3	Pass	-	Fail	53	Fail	255

4 Future Implementation

This study highlights the problem of temperature rise as a result of climate change and the impact on educational buildings in Cyprus. This impact is expected to be further aggravated for typical classrooms in the top floors of buildings and in city centres as a result of the urban heat island effect. Future research should consider these factors in analysing the effect of climate change. The densification of cities, in correlation with the increase in living standards, will intensify the overheating scenario. Furthermore, ventilation and occupant behaviour are significant factors affecting the thermal performance of the building and thus require further investigation. Alternative strategies to deal with overheating in buildings need to be promoted; i.e., strategies that do not fully rely on active systems that are often dependent on energy derived from fossil fuels.

The EN 15251 and CIBSE TM52 criteria form a valid approach to predict the vulnerability of buildings to climate change and possibly to suggest ways by which they can be adapted to assess the long term sustainability of new and existing educational buildings.

5 Conclusion

The climate is changing and there are clear indications that temperatures will rise. The existing educational building stock, which mostly relies on natural ventilation during the cooling period, is expected to have significant impact on users' thermal comfort, well-being and productivity. The classrooms in all orientations will require active systems to cope with overheating. Regulations and guidelines need to effectively address this scenario and promote solutions to minimise its cooling loads. The development of the methodological tool for the evaluation of the resilience of existing educational buildings can be of interest to city planners and retrofit decision making agents, as well as emergency response planners.

Acknowledgements

The authors would like to thank the Cyprus Institute and especially Dr. Panos Hajinicolaou for their assistance in regional climate modelling, essential for the successful execution of this study.

References

[1] T. Zachariadis, "Climate Change in Cyprus: Impacts and Adaptation Policies", *Cyprus Economic Policy Review*, Vol. 6, No. 1, pp.21-37, 2012.

[2] IPCC Fifth Assesment Synthesis Report. Climate Change 2014 Synthesis Report. 2014. http://www.ipcc.ch/report/ar5/ accessed 5 Dec 2016.

[3] Z. S. Zomorodian, M. Tahsildoost, M. Hafezi, "Thermal comfort in educational buildings: A review article", *Renewable and Sustainable Energy Reviews*, vol. 59, pp. 895-906, 2016.

[4] A. Michael and C. Heracleous, "Assesment of natural lighting performance and visual comfort of educational architecture in Southern Europe: The case of typical educational school premises in Cyprus", *Energy and Buildings,* vol, 138, pp. 1-15, 2017.

[5] CEN, Indoor environmental input parameters for design and assessment of energy performance of buildings addressing indoor air quality, thermal environment, lighting and acoustics, EN 15251:2007, 2007.

[6] CIBSE, The limits of thermal comfort: avoiding overheating in European buildings. CIBSE Technical Memorandum No. 52. London, Charted Institution of Building Services Engineers, 2013.

[7]. M. Philokyprou, A. Michael, Evaluation of the Environmental Features of Vernacular Architecture. A Case Study in Cyprus. International Journal of Heritage in the Digital Era 2012, 1, pp. 349-354. DOI: http://dx.doi.org/10.1260/2047-4970.1.0.349

[8] M. Philokyprou, A. Michael, St. Thravalou, Assessment of the Bioclimatic Elements of Vernacular Architecture. The Historic Centre of Nicosia, Cyprus, Argenziano, P. et al (eds.), Le Vies dei Mercanti XI Forume Internationalle di Studi, Aversa | Capri, Italy, La scuola di Pitagora editrice, Napoli, 2013, ISBN 978-88-6542-290-8, pp. 666-675.

[9] M. Philokyprou, A. Michael, St. Thravalou, I. Ioannou, Evaluation of Sustainable Design Elements in the Historic Centre of Nicosia, Cyprus. Correia, M., Carlos, G., Rocha, S. (eds.), Vernacular Heritage and Earthern Architecture, Taylor & Francis, London, 2013, ISBN: 978-1-138-00083-4, pp. 631-636.

[10] M. Philokyprou, A. Savvides, A. Michael, E. Malaktou, Examination and assessment of the environmental characteristics of vernacular rural settlements. Three case studies in Cyprus, Correia, M., Carlos, G. & Sousa, S. (Eds.). Vernacular Heritage and Earthen Architecture: Contribution to Sustainable Development. London (UK), Taylor & Francis Group, 2014, ISBN: 978-1-138-00083-4, pp. 613-618.

[11] A. Savvides, A. Michael, E. Malaktou, M. Philokyprou, Examination and assessment of insolation conditions of streetscapes of traditional settlements in the Eastern Mediterranean area, Habitat International 53 2016, pp. 442-452, http://dx.doi.org/10.1016/j.habitatint.2015.12.002

[12] A. Michael, C. Heracleous, S. Thravalou, M. Philokyprou, Lighting performance of urban vernacular architecture in the East-Mediterranean area: Field study and simulation analysis, Indoor and Built Environment 12/2015 DOI:10.1177/1420326X15621613.

[13] Infotrend Innovations/ BRE for the Ministry of Commerce, Industry and Tourism, Methodology for Assessing the Energy Performance of Buildings. 2009 http://www.mcit.gov.cy/mcit/mcit.nsf/. accessed 5 Dec 2016.

[14] S. Attia, L. Beltrán, A. De Herde, J. Hensen, “Architect Friendly”: a comparison of ten different building performance simulation tools, in: Proceeding of Eleventh International IBPSA Conference (online), Glasgow, Scotland, July 27–30, 2009, pp. 204–211, Available from: http://www.modelbenders.com/ (accessed 2 November 2016).

[15] D.B. Crawley, J.W. Hand, M. Kummert, B. T. Griffith, "Contrasting the capabilities of building energy performance simulation programs", Building and Environment, pp. 661-673, 2008.

[16] J.F. Nicol and M.A. Humphreys. "Derivation of the equation for comfort in free-running buildings in CEN Standard EN15251". *Building and Environment*, Vol 45 (1), pp. 11-17, 2010.

10TH INTERNATIONAL CONFERENCE ON SUSTAINABLE ENERGY AND ENVIRONMENTAL PROTECTION (JUNE 27TH – 30TH, 2017, BLED, SLOVENIA), ENERGY EFFICIENCY
J. Krope, A.Ghani Olabi, D. Goričanec & S. Božičnik

An Experimental Study on Heat Transfer of CO_2 at Supercritical Conditions

GREGOR KRAVANJA, GAŠPER ZAJC, ŽELJKO KNEZ, MOJCA ŠKERGET & MAŠA HRNČIČ KNEZ

Abstract This study covers a comprehensive investigation on heat transfer characteristics of CO_2 in the vicinity of the critical point. A double pipe heat exchanger set-up to study effects of different operating parameters on heat transfer performance over a wide range of temperatures (298.15 K to 363.15 K) and pressures (5 MPa to 30 MPa) has been developed. Heat flux of supercritical CO_2 was measured in the inner pipe in counter-current with water in the outer pipe. Obtained results were compared and assessed with known theoretical correlations and literature data.

Keywords: • heat exchanger • heat transfer coefficients • critical point • supercritical CO2 • water •

CORRESPONDENCE ADDRESS: Gregor Kravanja, Young Researcher, Assistant, University of Maribor, Faculty of Chemistry and Chemical Engineering, Smetanova ulica 17, 2000 Maribor, Slovenia, e-mail: gregor.kravanja@um.si. Gašper Zajc, Student, University of Maribor, Faculty of Chemistry and Chemical Engineering, Smetanova ulica 17, 2000 Maribor, Slovenia, e-mail: gasper.zajc@student.um.si. Željko Knez, Ph.D., Full Professor, University of Maribor, Faculty of Chemistry and Chemical Engineering, Smetanova ulica 17, 2000 Maribor, Slovenia, e-mail: zeljko.knez@um.si. Mojca Škerget, Ph.D., Full Professor, University of Maribor, Faculty of Chemistry and Chemical Engineering, Smetanova ulica 17, 2000 Maribor, Slovenia, e-mail: mojca.skerget@um.si. Maša Knez Hrnčič, Ph.D., Assistant Professor, University of Maribor, Faculty of Chemistry and Chemical Engineering, Smetanova ulica 17, 2000 Maribor, Slovenia, e-mail: masa.knez@um.si.

https://doi.org/10.18690/978-961-286-050-9.18 ISBN 978-961-286-050-9

Available at: http://press.um.si.

1 Introduction

Study of a heat transfer at supercritical conditions is necessary to design and optimize trans-critical CO_2 power cycles in refrigeration systems, air conditions, and heat pumps as well as in other technological applications of supercritical fluids, mainly extraction, particle formation and reaction processes. Every of those applications in its flowsheet involves high-pressure heat exchanger that plays an important role to transfer heat from one loop to the other one. In supercritical extraction plants, the purpose of heat exchangers can be to pre-heat the supercritical fluids before being fed to the high-pressure vessel, or cool down supercritical fluids before compression or separation of the solubilized solutes. In power cycles, among thermal-hydraulic performance, the heat exchanger has a significant effect on total efficiency, compactness, and operating cost of the system.

When pressure and temperature of fluids used in heat exchangers approach near its critical point, their thermo-physical properties vary complexly. Consequently, the heat transfer coefficient (HTC) in that region has much higher values than at subcritical pressures. CO_2 is beside supercritical water, which has a relatively high critical point (T_c=374.14 °C, P_c=22.12 MPa), the most studied fluid at high pressures [2]. On the contrary, it has an easily accessible, relatively low critical point (T_c=31.05 °C, P_c=7.38 MPa) which means that operating cost are reduced. In recent years, supercritical CO_2 has been intensely studied as a refrigerant [3]. It has many environmental advantages like zero Ozone depletion potential (ODE), low global warm poetical (GWP), and non-toxicity comparing to halo-hydrocarbon freons.

Heat transfer at high pressure has been widely reported in the literature between the water and CO_2 systems. Ma et al. [4] studied heat transfer performance of supercritical CO_2 in double pipe heat exchanger using a supercritical CO_2-water loop. They concluded that total and supercritical CO_2-side heat transfer coefficients with temperature behave similarly to specific heat and contribution of buoyancy force to the heat transfer performance is large at small mass flux. Duffey et al. [5] presented literature survey, where stated three heat transfer modes at supercritical pressures: normal heat transfer deteriorated, heat transfer with lower values of the heat transfer coefficient (HTC) and improved heat transfer with higher values of the HTC compared to those of normal heat transfer. Song et al. [6] established that heat transfer had similar characteristic irrespective of heat transfer improvement or deterioration if the ratio of tube length to tube diameter and the ratio of heat flux to mass flux were kept constant. Liu et al. [7] performed a numerical study of heat transfer characteristic for supercritical CO_2 in a heated helically coiled pipe. They showed that a circumferential heat transfer distribution in the helically coiled tube is influenced by both, the buoyancy force and the centrifugal force. Effect of flow direction was investigated among other authors, Li et al. [8] and Bruch et al. [9]. While Li et al. found that the heat transfer coefficients were better at downward flow than that at upward flow, Bruch et al. came to opposite conclusion in the pseudo-critical region. Lia and Zhao [10] investigated heat transfer in the upward and horizontal flow. They observed the heat transfer in both horizontal and upward flow was enhanced, while the heat transfer in downward flow was impaired significantly near the pseudo-critical region.

Despite numerous investigation of heat transfer to supercritical CO_2 and water stated above, there are still variations among them and unknowns that need to be clarified. It is hard to say that heat transfer deterioration is caused by only one factor.

In the present paper, a double pipe heat exchanger set-up to study effects of different operating parameters on heat transfer performance over a wide range of temperatures (298.15 K to 363.15 K) and pressures (6 MPa to 30 MPa) have been developed. A brief evaluation of the effect of mass flux, heat flux, pressure and temperature on heat transfer coefficients is provided.

2 Experimental Setup

Heat transfer coefficients (HTC) have been determined using a new optimized experimental setup which enables measurements at high pressures (Figure 1). The experimental setup is comprised of two separated closed loops, i.e., supercritical CO_2 loop and water loop. In the supercritical (high-pressure) fluid loop, gas released from the tank (CO_2 at 5 MPa) was cooled to fully liquefy and was then compressed to desired pressures with a high-pressure liquid pump (NWA PM-101) that can operate at the maximum pressure of 60 MPa. To minimalize pressure impulsion as an outcome of the high-pressure pump, gas was pumped in 1 L buffer vessel and then preheated with (LAUDA E-300) heating system to the desired working temperature. Digital differential pressure transmitter (WIKA-CHP 6200) was installed to measure the dense gas pressure at the inlet and outlet section of the heat exchanger. The accuracy of the transmitter is ±0.01 MPa. The inlet and outlet temperature of booth setup loops were controlled by the heaters, and the K-type thermocouples with an accuracy of ±0.15 K. The supercritical fluids flow rate was measured using a mass flow meter (RHEONIK RHM 03) equipped with flow indicator (RHEONIK RHE 02) that is suitable for all flow applications with high accuracy of measurements up to 90 MPa and 623 K. In the water loop, the flow rate of water was measured with needle valve rotameter (LZT-1002-M). Water was circulated with a help of a heater with a centrifugal pump (both LAUDA E200).

Heat exchange was measured in a double-pipe tube design with countercurrent flow (Figure 2). Previously heated supercritical fluid flows horizontally through the inner tube made of stainless steel 304-L with an outer diameter 9.65 mm and a wall thickness of 2.07 mm, and liquid water flows counter-currently in the annulus tube made of PVC with an outer diameter 20.00 mm and a wall thickness of 0.8 mm. To reduce heat losses from the heat exchanger and other pipes in the cycle-based system, thermal insulation ARMAFLEX with 20 mm of thickness was used. After the heat exchanger, a micro-expansion valve and cooling vessel were placed to reduced pressure and temperature in order to establish conditions that the dense gas could be fully recycled. The reduced pressure was measured by an electronic pressure gauge (WIKA, Germany) with an uncertainty of 0.01 MPa.

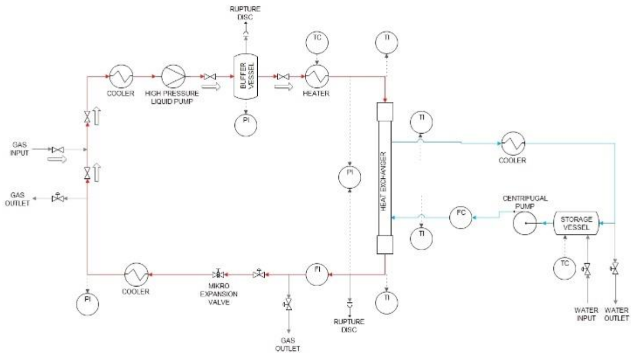

Figure 1: The experimental setup consists of two separated closed loops, i.e., supercritical fluid (CO_2 or ethane) loop and water loop.

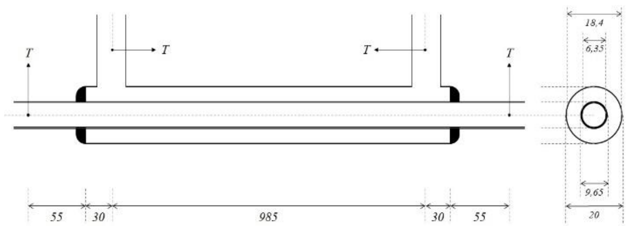

Figure 2: High pressure double pipe heat exchanger.

2.1 Experimental evaluation

The total heat transfer coefficient U_{tot} based on the supercritical fluid-side heat transfer area is calculated by:

$$U_{tot} = \frac{Q_a}{A_{SCF}\,\Delta T}, \tag{1}$$

where, Q_a is average heat transfer rate, A_{SCF} is the heat transfer area of supercritical fluid side, and ΔT is the logarithmic mean temperature difference in the counter current flow between the hot and cold sides. The average heat transfer rate is calculated by:

$$Q_a = \frac{(Q_{SCF} + Q_{water})}{2} \tag{2}$$

$$Q_{water} = \dot{m}(H_{water,out} - H_{water,in}) \tag{3}$$

$$Q_{SFC} = \dot{m}(H_{SCF,in} - H_{SCF,out}) \tag{4}$$

Where, Q_{water} is the heat transfer rate on the water side, and Q_{SCF} is the heat transfer rate on the supercritical fluid (CO_2 or ethane) side, $H_{water,\,in}$, and $H_{water\,,out}$ are the enthalpy of water at the inlet and outlet, while $H_{SCF,in}$ and $H_{SCF,out}$ are the enthalpy of supercritical fluid at the inlet and outlet. The thermal physical properties of pure supercritical CO_2 and ethane in wide range of pressure and temperature have been obtained from the NIST database, respectively. According to the thermal resistance network in the double pipe heat exchanger, the total heat transfer coefficient U_{SCF} can also be calculated by:

$$\frac{1}{U_{tot}} = \frac{1}{\alpha_{SCF}} + \frac{A_{CO2} \ln\left(\frac{D_{outer}}{D_{inner}}\right)}{2\pi\lambda L} + \frac{A_{SCF}}{\alpha_{water} A_{water}} \tag{5}$$

Therefore, heat transfer coefficients α_{SCF} on supercritical fluid side is calculated by:

$$\alpha_{SCF} = 1 / \left(\frac{1}{U_{tot}} - \frac{A_{SCF} \ln\left(\frac{D_{outer}}{D_{inner}}\right)}{2\Pi\lambda L} - \frac{A_{SCF}}{\alpha_{water} A_{water}} \right) \tag{6}$$

where, D_{outer} is the outer diameter of the inner tube, D_{inner} is the inner diameter of inner tube, and λ is the thermal conductivity of 304-L stainless steel. Heat transfer coefficient (α_{water}) in the annular space of water side is obtain by taking into account the equivalent diameter and Nusselt number for the annular cross-section:

$$D_e = \frac{4\left(\frac{\pi}{4}\left(D_{outer}^2 - D_{inner}^2\right)\right)L}{\pi\left(D_{outer} + D_{inner}\right)L} = D_{outer} - D_{inner} \tag{7}$$

$$Nu = \frac{\alpha_{water} L}{\lambda} \tag{8}$$

$$Nu_{D_e} = 0,02 \, \mathrm{Re}_{D_e}^{4/5} \, \mathrm{Pr}^{1/3} \left(\frac{D_{inner}}{D_{outer}}\right)^{0,53} \tag{9}$$

Where, Prandtl and Reynolds number are calculated by:

$$\mathrm{Pr} = \frac{c_p \eta}{\lambda} \tag{10}$$

$$\mathrm{Re} = \frac{\rho v D_e}{\eta} \tag{11}$$

3 Results and Discussion

Heat transfer coefficients (HTC) of supercritical CO_2 and ethane in a water loop have been measured over a wide range of temperatures (298.15 K to 363.15 K) and pressures (6 MPa to 30 MPa). During the entire process, there was one phase region throughout the inner high-pressure tube. Measurements were performed at pressures above the pseudo critical pressure and around the pseudo critical temperature. In the displayed figures, the variations of the bulk temperature T_b present average values of the output and input temperature of supercritical fluids.

3.1 Effect of pressure and temperature

Total and supercritical-side HTC have the highest peaks near the pseudo-critical point of investigated fluids. (Figure 3). This is caused by a stronger change of thermo-physical properties, especially the larger increase in specific heat at pressures closer to the critical pressure [7]. The highest peak value of total HTC occurs at the location where the temperature is slightly higher than the pseudo-critical point. A possible explanation could be that the temperature of supercritical fluid near the wall in inner tube is lower than in the bulk and the average temperature of supercritical fluid in cross-section is not reduced to the pseudo-critical temperature, but shows near the wall values closely to the critical temperature [4]. The experimental data were obtained from five isobars: 7.5, 8.0, 10, 20 and 30 MPa. As shown in Figure 4, total HTC of supercritical CO_2 decreases with the increasing pressure. The supercritical CO_2-side HTC peaks reach much higher values compared to total HTC under the same conditions (Figures 3, 4).

3.2 Effect of mass flux

Supercritical-side mass flux was kept constant (near maximum operating conditions of the high-pressure pump) 0.08 kg/min for supercritical CO_2 and 0.05 kg/min for supercritical ethane. Effect of supercritical-side mass flux is significantly smaller then effect of water-side flux rate on HTC [4]. The influence of water rate flux on the total heat transfer coefficients was investigated for pressures near and above the pseudo critical point. As shown in the Figure 5, the total HTC increases for more than 25 % when increasing the flux rate of water-side from 1 L/min up to 2 L/min.

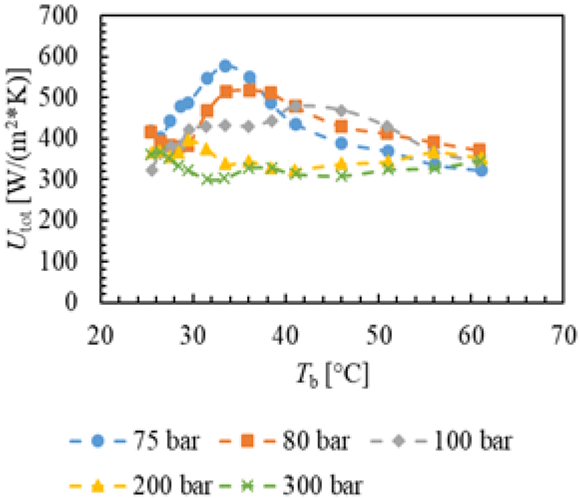

Figure 3: Effect of supercritical CO_2-side pressure on total heat transfer coefficients (U_{tot}) at average temperature (T_b) of heating fluid and at constant water flux of 1 L/min.

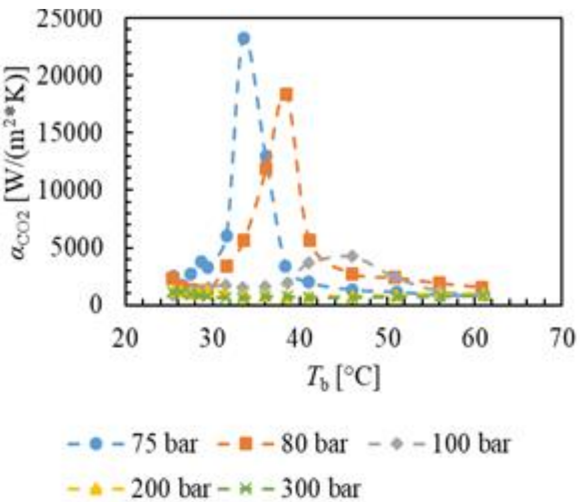

Figure 4: Effect of supercritical CO2-side pressure on supercritical CO2-side heat transfer coefficient at constant water flux of 1 L/min

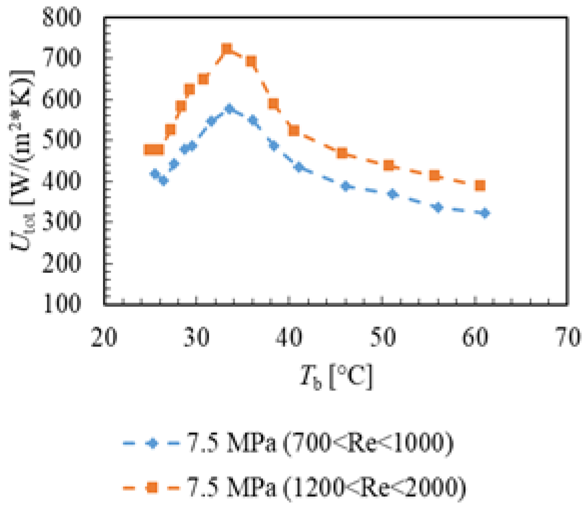

Figure 5: Effect of water-side mass flux on the total heat transfer coefficient (Utot)

4 Conclusion

Heat transfer coefficients (HTC) have been determined using a new optimized experimental setup comprised of two separated closed loops, i.e., supercritical fluid (CO_2 or ethane) loop and water loop. Measurements were performed at pressures above the pseudo critical pressure and around the pseudo critical temperature. The main conclusions are summarized as follows:

a) Total and supercritical-side HTC have highest peaks near the pseudo-critical point of investigated fluid. Total HTC of supercritical CO2 decreases with the increasing pressure. The supercritical CO2-side HTC peaks reaches much higher values compared to total HTC under the same conditions
b) The influence of water rate flux on the total and supercritical-side HTC is inconsiderable. The total HTC increases for more than 25 % when increasing the flux rate of water-side from 1 L/min (700<Rewater<1000) up to 2 L/min (1200<Rewater<2000).

Future research will focus on azeotropic mixtures. Ethane is one of a few gases that forms azeotropic mixture over a wide range of temperature and pressure that has a minimum boiling point that could have improved cooling properties in heat pumps compared to pure CO_2

Acknowledgements

The authors would like to acknowledge the Slovenian Research Agency (ARRS) for financing this research within the frame of Programme P2-0046 (Separation Processes and Production Design)

References

[1] D. Huang, Z. Wu, B. Sunden and W. Li, A brief review on convection heat transfer of fluids at supercritical pressures in tubes and the recent progress, *Applied Energy*, vol.162, pp. 494–505, 2016.

[2] M. K. Hrnčič, G. Kravanja and Ž. Knez, Hydrothermal treatment of biomass for energy and chemicals, *Energy*, vol. 116 part 2, pp. 1312–1322, 2016.

[3] J. Oignet, H. M. Hoang, V. Osswald, A. Delahaye, L. Fournaison and P. Haberschill, Experimental study of convective heat transfer coefficients of CO_2 hydrate slurries in a secondary refrigeration loop, *Applied Thermal Engineering*, vol. 118, pp. 630–637, 2017.

[4] T. Ma, W. Chu, X. Xu, Y. Chen and Q. Wang, An experimental study on heat transfer between supercritical carbon dioxide and water near the pseudo-critical temperature in a double pipe heat exchanger, *International Journal of Heat and Mass Transfer*, vol. 93, pp. 379–387, 2016.

[5] R. B. Duffey and I. L. Pioro, Experimental heat transfer of supercritical carbon dioxide flowing inside channels (survey), *Nuclear Engineering and Design*, vol. 235(8), pp. 913–924, 2005.

[6] J. H. Song, H. Y. Kim, H. Kim and Y. Y. Bae, Heat transfer characteristics of a supercritical fluid flow in a vertical pipe, *The Journal of Supercritical Fluids*, vol. 44(2), pp. 164–171, 2008.

[7] X. Liu, X. Xu, C. Liu, J. Ye, H. Li and W. Bai, Numerical study of the effect of buoyancy force and centrifugal force on heat transfer characteristics of supercritical CO_2 in helically coiled tube at various inclination angles, *Applied Thermal Engineering*, vol. 116, pp. 500–515, 2017.

[8] Z. H. Li, P. X. Jiang, C. R. Zhao and Y. Zhang, Experimental investigation of convection heat transfer of CO_2 at supercritical pressures in a vertical circular tube, *Experimental Thermal and Fluid Science*, vol. 34(8), pp. 1162–1171, 2010.

[9] A. Bruch, A. Bontemps and S. Colasson, Experimental investigation of heat transfer of supercritical carbon dioxide flowing in a cooled vertical tube, *International Journal of Heat and Mass Transfer*, vol. 52(11-12), pp. 2589–2598, 2009.

[10] S. M. Liao and T. S. Zhao, An experimental investigation of convection heat transfer to supercritical carbon dioxide in miniature tubes, *International Journal of Heat and Mass Transfer*, vol. 45(25), pp. 5025–5034, 2002.

[11] F. Lastari, V. Pareek, M. Trebble, M. O. Tade, D. Chinn and N. C. Tsai, Extractive distillation for CO_2-ethane azeotrope separation, *Chemical Engineering and Processing: Process Intensification*, vol. 52, pp. 155–161, 2012.

[12] B. S. Petukhov, A. F. Polyakof, V. A. Kuleshov and Y. L. Sheckter, Turbulent flow and heat transfer in horizontal tubes with substantial influence of thermos-gravitational forces, 5th International Heat Transfer Conference, Tokyo, 1974.

10TH INTERNATIONAL CONFERENCE ON SUSTAINABLE ENERGY AND ENVIRONMENTAL PROTECTION (JUNE 27TH – 30TH, 2017, BLED, SLOVENIA), ENERGY EFFICIENCY
J. Krope, A.Ghani Olabi, D. Goričanec & S. Božičnik

Critical Review of Micro-Nano Scale Surface Modification for Phase Change Heat Transfer

SHOUKAT ALIM KHAN, ADNAN ALI, MUATAZ A. HUSSIEN & MUAMMER KOC

Abstract Recently developed micro-nano scale coating techniques, for modification of surface geometry and chemistry, has been playing an important role in the enhancement of boiling and condensation phase change heat transfer. Boiling and condensation are important heat transfer processes with a wide range of applications i.e. steam power plants, thermal desalination, domestic heating and cooling, refrigeration and air-conditioning, electronic cooling, cooling of turbo-machinery, waste heat recovery and many more. Due to its enormous field of applications, any slight improvement in this area leads to significant economic, environmental and energy efficiency outcomes. Both condensation and boiling are surface phenomena and have common variables i.e. surface area, thermal conductivity, wettability, porosity, roughness etc. Compared to subtractive methods surface coating is more versatile in material selection, geometry; simple, quick, robust in implementation; and quite functional to apply for already installed systems. A critical review of present status of these coatings methods along with their future challenges, enhancement potentials, comparison, limitations and possibilities of industrial applications are discussed in this paper.

Keywords: • Phase change • Heat transfer • Pool boiling • Condensation • Coating •

CORRESPONDENCE ADDRESS: Shoukat Alim Khan, Ph.D. Candidate, Sustainable Development Division, Hamad Bin Khalifa University (HBKU), Qatar Foundation, Education City, Doha, Qatar, e-mail: shokhan@hbku.edu.qa. Adnan Ali, Ph.D., Post-Doc, QEERI, Hamad Bin Khalifa University (HBKU), Qatar Foundation, Education City, Doha, Qatar, e-mail: adali@hbku.edu.qa, Muataz A. Hussien, Ph.D., Associate Professor and Senior Scientist, QEERI, Hamad Bin Khalifa University (HBKU), Qatar Foundation, Education City, Doha, Qatar, e-mail: mhussien@qf.org.qa. Muammer Koc, Ph.D., Professor, Hamad Bin Khalifa University (HBKU), Qatar Foundation, Education City, Doha, Qatar, e-mail: mkoc@hbku.edu.qa.

https://doi.org/10.18690/978-961-286-050-9.19 ISBN 978-961-286-050-9

Available at: http://press.um.si.

1 Introduction

Heat transfer is involved in every energy utilization, conversion, and recovery application. Phase change heat transfer is mainly used in processes where high thermal energy is needed to be transferred in compact space. Boiling and condensation are an important phase change heat transfer due to its vast range of applications i.e. thermal power plants, electronic cooling, food processing, desalination, waste heat recovery, cooling of turbo machinery, domestic cooling and heating.

In almost all industrial applications, boiling and condensation phenomena are highly sensitive to surface properties like roughness, porosity, wettability and nucleation sites. Recent developments in the field of micro-nano scale manufacturing and surface functionalization have expanded the boundaries for heat transfer enhancement through surface treatment. Compared to other modification methods, surface coating is quick, robust and versatile in material selection. This paper presents a critical review of present status of coating techniques for boiling and condensation along with their enhancement abilities, limitations, future challenges and possible applications on industrial scale.

2 Boiling

2.1 Enhancement of boiling heat transfer: Overview

High latent heat of vaporization makes boiling an efficient energy transfer process [1]. The mechanism of heat transfer through boiling process can be best understood form boiling curve introduced by Nukiyama et al. [2], see Figure 1. This section overviews the physics involved in boiling heat transfer, using boiling heat transfer curve. Nucleate boiling heat transfer (NBHT) to Film boiling (FB) transition, Heat transfer coefficient (HTC) and Critical heat flux (CHF) are key factors of this phenomena.

Nucleate boiling heat transfer (NBHT) to film boiling (FB)

NBHT can be best understood by renowned boiling curve, Figure 1. This curve is initially proposed by researchers like Nukiyama, Jacob, Drew and Muller [3]–[5]. In this figure, q''_s represents heat flux, T_{sat} is saturation temperature, T_s surface temperature and h is heat transfer coefficient. Boiling process starts when T_{sat} overcomes T_s . During NBHT boiling more mature vapour bubbles nucleate on surface and they quickly leave. These bubbles are replaced by new bubbles just after their departure and the process continues. This process causes advanced mixing of fluid in region near to the surface and thus caused in enhancement in h and q''_s [6]. Further increase of heat flow results in an increase in nucleation density of bubbles. At point when rate of generation of bubbles overcome its rate of departure, the bubbles start to merge together and form blanket of vapours on the surface. At this stage, the boiling phenomena is called Film boiling, as shown in Figure 5. The efficiency of the boiling process decreases drastically during film boiling because of low thermal conductivity of vapour. Delaying film boiling and improvement in nucleate boiling regime are two desiring goals in enhancement of boiling heat transfer process

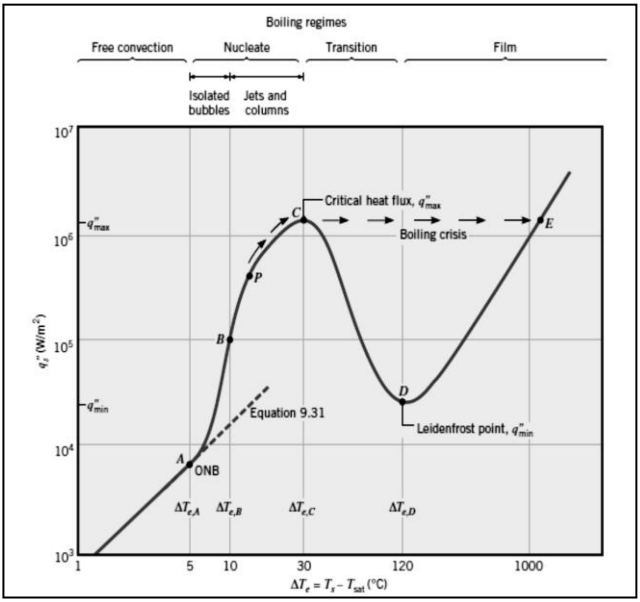

Figure 4. Boiling heat transfer curve [6].

Critical heat flux (CHF) and heat transfer coefficient (HTC/ h)

CHF represents a performance parameter for boiling heat transfer and it is the maximum limit of NBHT. For design, safety and efficiency of boiling process, it is important to know its exact value of CHF. The goal of every NBHT design process is to work close to the CHF point and at the same time caution needs to be taken because any little increase in the surface temperature could lead to the a failure of the process [6]. On the other hand, HTC is the best representation of thermal efficiency of process and is the slope of NBHT curve.

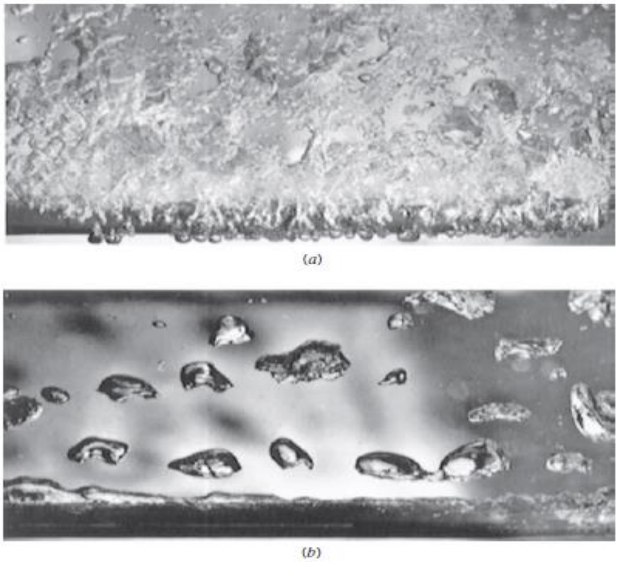

Figure 5: Two different conditions for same substrate: (a) Nucleate boiling. (b) Film boiling, [6].

2.2 Surface coatings for boiling heat transfer enhancement

Nature of Surface, working temperature and pressure, and fluid properties such as viscosity, thermal conductivity, heat capacity, are the main parameters for NBHT [6]. For most of the application it is hard to change working fluid so surface remains as main variable to optimize to enhance overall process. Jakob [7] reported for the first time the effectiveness of surface roughness in NBHT process. The theory stems from the observations of many researchers that cavities on the surface originate the bubbles and entrap them inside. This theory was experimentally verified by many researchers [8]–[10]. Surface coating for boiling can be classified into the following categories.

Metal nanoparticles coating

Coating of nano-particles on substrate started with the study of nano-fluid application for boiling. Properties such as high thermal conductivity and enhancement in NBHT with very low concentration, make the use of nano-fluid interesting for boiling heat transfer [11], [12]. However, the study of Vassallo et al. [13] changed the direction of the research by reporting the deposition of nano-particles on the substrate as main source of heat transfer enhancement in pool boiling. Kim et al. [14] confirmed this observation recently by modifying the surface with alumina, silica and zirconia nanofluids. During bubbles' evaporation, nano particles settle down on the surface and form porous layer [14]. These coated nano-particles then act as nucleation points for bubbles generation and also extend overall surface area [15], [16].

Wettability: Hydrophobic and hydrophilic coatings

Hydrophilic surface helps in delaying dry out by drawing liquid while hydrophobic surfaces act as nucleation sites [1], [17]. A combination of hydrophobic and hydrophilic coating patterns has a significant effect on the overall heat transfer enhancement [1]. Different patterns of both coatings have been studied in literature and reported high values for HTC and CHF as 100 KW/m2K 100W/cm2 respectively [18]. Techniques for changing the wettability of the surface are either by altering the surface topology or chemistry.

Micro-porous coatings

Microporous surfaces help in increasing the nucleation sites, the overall surface area and the capillary effect [19]. These in turn result in lowering the super heat and increasing the CHF. Modulated surface results in decreasing the resistance of liquid and vapour flow during NBHT. A complete separation of these two phases, during NBHT, could result in an optimum enhancement [19]. Researchers have used different methods in the preparation of modulated porous surfaces. Some of these methods are: hot powder compaction [19], direct coating of copper foam [20], sintering [21], [22].

CNT and graphene coatings

Due to significantly higher thermal conductivity and lower wettability, CNT and Graphene coating have a positive effect on the overall enhancement of boiling heat transfer. Different studies have confirmed the positive role of both multi-wall and single-wall CNT. For CNT coating on metal substrate, CNT acts as nucleation sites of bubbles' generation while the metal substrate, due to its hydrophilic nature, acts as a source of liquid. The study of CNT coating density and length have shown that a higher value of these parameters always resulted in a better performance.

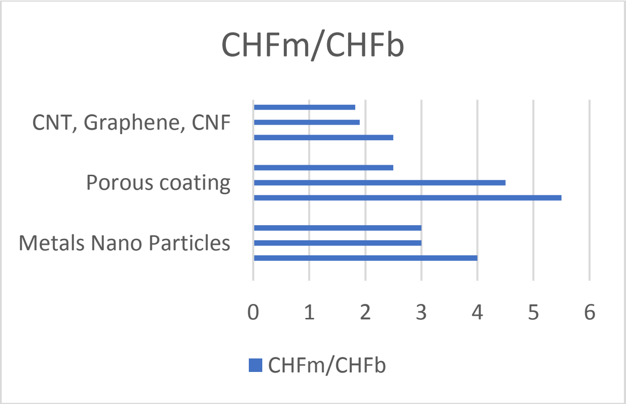

Figure 6. Comparative study of different NBHT enhancement studies. m represents coated or modified surface while b represents bare or uncoated surface. References (from Top row to bottom): [23], [24], [25], [26], [27], [28], [29], [30], [13].

3 Condensation

3.1 Condensation heat transfer enhancement: Overview

Direct contact condensation is the most common type of condensation, which occurs in almost all industrial applications due to its lower energy barrier [31]. During this process, vapour is brought into a direct contact with a cold substrate. This process results in the formation of liquid drops on the surface called Dropwise condensation (DWC). If the rate of the formation of drops on the surface overcomes their rate of departure, this results in the formation of a thin liquid film on the substrate surface called film-wise condensation (FWC), as shown in Figure 7. DWC is most efficient and desiring condensation condition which makes sure direct contact of vapour and cold substrate [32]. Surface tension, roughness and energy of the surface plays an important role in final form of condensation. Direct condensation is surface phenomena and can be easily optimized with surface modification.

3.2 Surface coating for condensation:

This paper focuses on surface modification by coating to achieve DWC. Below are type of coating techniques reported in literature for enhancing DWC.

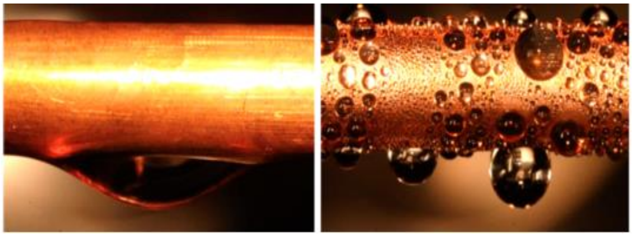

Figure 7. For same substrate: Film-wise condensation (left) before coating and Dropwise condensation (right) after graphene coating [33].

Coating with noble metals and rare earth oxides:

Nobel metals have low surface energy, hence high contact angle i.e. Au: 55-85^0, Rh: 65-82^0, Ag 68-89^0, and Pd: 74^0 [34], and are highly resistant to oxidation and corrosion. These metals have high ability to absorb hydrocarbons and impurities which make them favourable for DWC [35]. Metals like Gold [36] and silver [37] have been extensively studied by researcher for condensation and reported enhanced results.

Similarly to Nobel metals, rare earth oxide also shows significant results in the improvement of condensation phenomena due to their hydrophobic nature [38]–[40]. The electronic configuration $5s^2p^6$ of outer shell of these metals decrease their interaction with water molecules. Rare earth oxides are used for super hydrophobic surfaces and reported significant performance for DWC [41].

Ion implantation

DWC phenomena for ion implanted technology modified surfaces were first reported by Zhang et al. [42] and Zhao et al. [43] on Copper substrate using HE, Ar, N and H. These layers are durable and have negligible resistance due to their negligible thickness. These surfaces were reported better in performance than compared to Silver, Teflon and Gold coated surfaces [43].

Polymer coatings

The cost and performance of polymer coating makes it favourable coating for condensation as compared to other available coating techniques [44]. However, the durability of these coatings is ensured up-to now only for high thickness which results in high thermal resistance. Researchers suggested different methods to increase their durability i.e. binding material in between of substrate and coated polymer layer [45], surface processing. Techniques like Chemical vapour deposition (CVD) [46], initiated chemical vapour deposition (iCVD) and Plasma enhanced chemical vapour deposition (PECVD) [47] have been used in literature for polymer coating.

Self-Assembled Micro/nano Silver (SAM)

SAM have negligible thermal resistance and ensure thin coating up-to individual molecular level [48]. They are mostly consisting of polymer with functional group attached to one side. One side of polymer are hydrophobic in nature and helps in condensation while other ensure adhesion with surface [49].

Lubricant Infused Surfaces (LIS)

LIS are hydrophobic in nature surfaces coated with lubricant [45]. These surfaces are good in formation of drops and also its mobility [50]. Durability and limited application are main problems of these coating.

Graphene, CNT, CNF and DLS coating for condensation enhancement

Graphene, CNT and CNF coatings are favourable DWC due to their high thermal conductivity and hydrophobic nature. Preston et al. [33] studied single layer thin graphene coating on 99.99% pure copper, see Figure 7, and reported 4 times enhancement in HTC through DWC. Also, the durability was observed up-to two weeks. Like Graphene, CNT [51] and CNF [52] and DLS [53] coating has also been reported by researcher for high DWC performance.

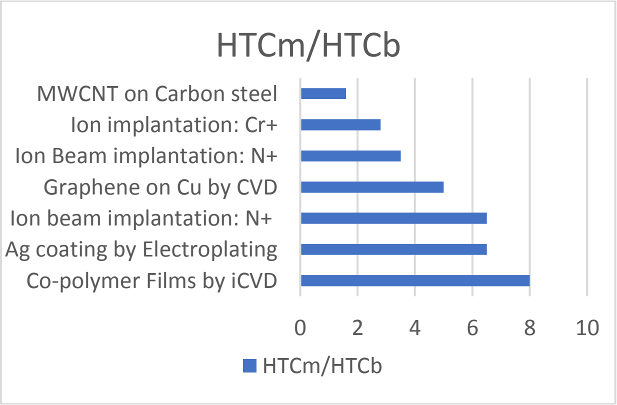

Figure 8. Comparative study of condensation enhancement studies. m represents coated or modified surface while b represents bare or uncoated surface. References (from top row to bottom): [54], [55], [56], [33], [57], [37], [58]

References

[1] A. R. Betz, J. Xu, H. Qiu, and D. Attinger, "Do surfaces with mixed hydrophilic and hydrophobic areas enhance pool boiling?," *Appl. Phys. Lett.*, vol. 97, no. 14, pp. 14–16, 2010.

[2] S. Nukiyama, "The maximum and minimum values of the heat Q transmitted from metal to boiling water under atmospheric pressure," *Int. J. Heat Mass Transf.*, vol. 9, no. 12, pp. 1419–1433, Dec. 1966.

[3] S. Nukiyama, "The maximum and minimum values of the heat Q transmitted from metal to boiling water under atmospheric pressure," *Int. J. Heat Mass Transf.*, vol. 9, no. 12, pp. 1419–1433, 1966.

[4] and W. L. Jakob, M., "Der Wärmeübergang beim Verdampfen von Flüssigkeiten an senkrechten und waagerechten Flächen.," *Phys. Z*, vol. 36.8, pp. 267–280, 1935.

[5] C. M. T.B. Drew, "Boiling," *Trans. AAIChE 33*, p. 449, 1937.

[6] A. S. Bergman, T. L., Incropera, F. P., DeWitt, D. P., & Lavine, *Fundamentals of heat and mass transfer*. 2011.

[7] M. Jakob, "Heat transfer in evaporation and condensation," *Mech. Eng. (Am. Soc. Mech. Eng.)*, pp. 643–660., 1936.

[8] J. W. WESTWATER, "BOILING HEAT TRANSFER," *Am. Sci.*, vol. 47, pp. 427–446.

[9] J. W. Clark, H.B. ; Strenge, P.S. ; Westwater, "Active sites for nucleate boiling," *Chem. Eng. Progr.*, vol. 55, 1960.

[10] S. G. Bankoff, "EBULLITION FROM SOLID SURFACES IN THE ABSENCE OF A PRE-EXISTING GASEOUS PHASE," *Trans. Am. Soc. Mech. Eng*, vol. 79, no. 1957–05–01, 1957.

[11] et al. Eastman, Jeffrey A., "Anomalously increased effective thermal conductivities of ethylene glycol-based nanofluids containing copper nanoparticles.," *Appl. Phys.*, vol. letters 78, pp. 718–720., 2001.

[12] S. U. S. Choi, Z. G. Zhang, W. Yu, F. E. Lockwood, and E. A. Grulke, "Anomalous thermal conductivity enhancement in nanotube suspensions," *Appl. Phys. Lett.*, vol. 79, no. 14, p. 2252, 2001.

[13] P. Vassallo, R. Kumar, and S. D'Amico, "Pool boiling heat transfer experiments in silica–water nano-fluids," *Int. J. Heat Mass Transf.*, vol. 47, no. 2, pp. 407–411, Jan. 2004.

[14] H. Kim, "Enhancement of critical heat flux in nucleate boiling of nanofluids: a state-of-art review," *Nanoscale Res. Lett.*, 2011.

[15] C. M. Patil and S. G. Kandlikar, "Pool boiling enhancement through microporous coatings selectively electrodeposited on fin tops of open microchannels," *Int. J. Heat Mass Transf.*, vol. 79, pp. 816–828, Dec. 2014.

[16] A. Jaikumar and S. G. Kandlikar, "Enhanced pool boiling heat transfer mechanisms for selectively sintered open microchannels," *Int. J. Heat Mass Transf.*, vol. 88, pp. 652–661, Sep. 2015.

[17] A. R. Betz, J. R. Jenkins, C.-J. Kim, and D. Attinger, "Significant boiling enhancement with surfaces combining superhydrophilic and superhydrophobic patterns," in *2011 IEEE 24th International Conference on Micro Electro Mechanical Systems*, 2011, pp. 1193–1196.

[18] A. R. Betz, J. Jenkins, C. J. Kim, and D. Attinger, "Boiling heat transfer on superhydrophilic, superhydrophobic, and superbiphilic surfaces," *Int. J. Heat Mass Transf.*, vol. 57, no. 2, pp. 733–741, 2013.

[19] S. G. Liter and M. Kaviany, "Pool-boiling CHF enhancement by modulated porous-layer coating: theory and experiment," *Int. J. Heat Mass Transf.*, vol. 44, no. 22, pp. 4287–4311, Nov. 2001.

[20] Y. Yang, X. Ji, and J. Xu, "Pool boiling heat transfer on copper foam covers with water as working fluid," *Int. J. Therm. Sci.*, vol. 49, no. 7, pp. 1227–1237, 2010.

[21] D. Deng, J. Feng, Q. Huang, Y. Tang, and Y. Lian, "Pool boiling heat transfer of porous structures with reentrant cavities," *Int. J. Heat Mass Transf.*, vol. 99, pp. 556–568, 2016.

[22] D. Deng, W. Wan, J. Feng, Q. Huang, Y. Qin, and Y. Xie, "Comparative experimental

study on pool boiling performance of porous coating and solid structures with reentrant channels," *Appl. Therm. Eng.*, vol. 107, pp. 420–430, 2016.
[23] A. Jaikumar, K. S. V. Santhanam, S. G. Kandlikar, I. B. P. Raya, and P. Raghupathi, "Electrochemical Deposition of Copper on Graphene with High Heat Transfer Coefficient," *ECS Trans.*, vol. 66, no. 30, pp. 55–64, Aug. 2015.
[24] H. Seo, J. H. Chu, S.-Y. Kwon, and I. C. Bang, "Pool boiling CHF of reduced graphene oxide, graphene, and SiC-coated surfaces under highly wettable FC-72," *Int. J. Heat Mass Transf.*, vol. 82, pp. 490–502, Mar. 2015.
[25] S. O. Ujereh, I. Mudawar, P. B. Amama, T. S. Fisher, and W. Qu, "Enhanced Pool Boiling Using Carbon Nanotube Arrays on a Silicon Surface," in *Heat Transfer, Part A*, 2005, vol. 2005, pp. 691–696.
[26] Z. G. Qu, Z. G. Xu, C. Y. Zhao, and W. Q. Tao, "Experimental study of pool boiling heat transfer on horizontal metallic foam surface with crossing and single-directional V-shaped groove in saturated water," *Int. J. Multiph. Flow*, vol. 41, pp. 44–55, 2012.
[27] T. J. Hendricks, S. Krishnan, C. Choi, C. H. Chang, and B. Paul, "Enhancement of pool-boiling heat transfer using nanostructured surfaces on aluminum and copper," *Int. J. Heat Mass Transf.*, vol. 53, no. 15–16, pp. 3357–3365, 2010.
[28] S. Jun, J. Kim, S. M. You, and H. Y. Kim, "Effect of heater orientation on pool boiling heat transfer from sintered copper microporous coating in saturated water," *Int. J. Heat Mass Transf.*, vol. 103, pp. 277–284, Dec. 2016.
[29] S. B. White, A. J. Shih, and K. P. Pipe, "Boiling surface enhancement by electrophoretic deposition of particles from a nanofluid," *Int. J. Heat Mass Transf.*, vol. 54, no. 19–20, pp. 4370–4375, Sep. 2011.
[30] S. M. You, J. H. Kim, and K. H. Kim, "Effect of nanoparticles on critical heat flux of water in pool boiling heat transfer," *Appl. Phys. Lett.*, vol. 83, no. 16, p. 3374, 2003.
[31] D. Kashchiev, *Nucleation: basic theory with applications*. Butterworth Heinemann: Boston, 2000.
[32] D. Attinger, C. Frankiewicz, A. R. Betz, T. M. Schutzius, R. Ganguly, A. Das, C. Kim, and C. M. Megaridis, "Surface Engineering for Phase Change Heat Transfer : A Review," vol. 1, no. September, pp. 1–85, 2014.
[33] D. J. Preston, D. L. Mafra, N. Miljkovic, J. Kong, and E. N. Wang, "Scalable Graphene Coatings for Enhanced Condensation Heat Transfer," *Nano Lett.*, vol. 15, no. 5, pp. 2902–2909, May 2015.
[34] R. A. Erb, "Wettability of Metals under Continuous Condensing Conditions," *J. Phys. Chem.*, vol. 69, no. 4, pp. 1306–1309, Apr. 1965.
[35] R. Erb and E. Thelen, "PROMOTING PERMANENT DROPWISE CONDENSATION," *Ind. Eng. Chem.*, vol. 57, no. 10, pp. 49–52, Oct. 1965.
[36] D. W. Woodruff and J. W. Westwater, "Steam Condensation on Various Gold Surfaces," *J. Heat Transfer*, vol. 103, no. 4, p. 685, 1981.
[37] G. A. O'neill and J. W. Westwater, "Dropwise condensation of steam on electroplated silver surfaces," *Int. J. Heat Mass Transf.*, vol. 27, no. 9, pp. 1539–1549, 1984.
[38] G. Azimi, H.-M. Kwon, and K. K. Varanasi, "Superhydrophobic surfaces by laser ablation of rare-earth oxide ceramics," *MRS Commun.*, pp. 1–5, Sep. 2014.
[39] S. Zenkin, Š. Kos, and J. Musil, "Hydrophobicity of Thin Films of Compounds of Low-Electronegativity Metals," *J. Am. Ceram. Soc.*, vol. 97, no. 9, pp. 2713–2717, Sep. 2014.
[40] G. Azimi, R. Dhiman, H.-M. Kwon, A. T. Paxson, and K. K. Varanasi, "Hydrophobicity of rare-earth oxide ceramics," *Nat. Mater.*, vol. 12, no. 4, pp. 315–320, Jan. 2013.
[41] G. Azimi, R. Dhiman, H.-M. Kwon, A. T. Paxson, and K. K. Varanasi, "Hydrophobicity of rare-earth oxide ceramics," *Nat. Mater.*, vol. 12, no. 4, pp. 315–320, Jan. 2013.
[42] and L. J. Dongchang, Zhang, Lin Zaiqi, "'New surface materials for dropwise

condensation.,'" in *Proceedings of the 8th International Heat Transfer Conference*, 1986.
[43] Q. Zhao, D. Zhang, and J. Lin, "Surface material with dropwise condensation made by ion implantation technology," *Int. J. Heat Mass Transf.*, vol. 34, no. 11, pp. 2833–2835, 1991.
[44] K. M. Holden, A. S. Wanniarachchi, P. J. Marto, D. H. Boone, and J. W. Rose, "The Use of Organic Coatings to Promote Dropwise Condensation of Steam," *J. Heat Transfer*, vol. 109, no. 3, p. 768, 1987.
[45] R. Enright, N. Miljkovic, J. L. Alvarado, K. Kim, and J. W. Rose, "Dropwise Condensation on Micro- and Nanostructured Surfaces," *Nanoscale Microscale Thermophys. Eng.*, vol. 18, no. 3, pp. 223–250, 2014.
[46] M. Gupta, V. Kapur, N. M. Pinkerton, and K. K. Gleason, "Initiated Chemical Vapor Deposition (iCVD) of Conformal Polymeric Nanocoatings for the Surface Modification of High-Aspect-Ratio Pores," *Chem. Mater.*, vol. 20, no. 4, pp. 1646–1651, Feb. 2008.
[47] R. Xiao, N. Miljkovic, R. Enright, and E. N. Wang, "Immersion condensation on oil-infused heterogeneous surfaces for enhanced heat transfer.," *Sci. Rep.*, vol. 3, p. 1988, 2013.
[48] I. Orkan Uçar and H. Y. Erbil, "Droplet condensation on polymer surfaces: A review," *Turkish J. Chem.*, vol. 37, no. 4, pp. 643–674, 2013.
[49] R. W. Bonner III, "Dropwise condensation life testing of self assembled monolayers," *Proc. 14th Int. Heat Transf. Conf.*, pp. 1–6, 2010.
[50] S. Anand, A. T. Paxson, R. Dhiman, J. D. Smith, and K. K. Varanasi, "Enhanced Condensation on Lubricant- Impregnated Nanotextured Surfaces," *ACS Nano*, vol. 6, no. 11, pp. 10122–10129, 2012.
[51] C. H. Chen, Q. Cai, C. Tsai, C. L. Chen, G. Xiong, Y. Yu, and Z. Ren, "Dropwise condensation on superhydrophobic surfaces with two-tier roughness," *Appl. Phys. Lett.*, vol. 90, no. 17, pp. 1–4, 2007.
[52] T. J. Ko, E. K. Her, B. Shin, H. Y. Kim, K. R. Lee, B. K. Hong, S. H. Kim, K. H. Oh, and M. W. Moon, "Water condensation behavior on the surface of a network of superhydrophobic carbon fibers with high-aspect-ratio nanostructures," *Carbon N. Y.*, vol. 50, no. 14, pp. 5085–5092, 2012.
[53] A. Leipertz and A. P. Froba, "Improvement of condensation heat transfer by surface modifications," *Heat Transf. Eng.*, vol. 29, no. 4, pp. 343–356, 2008.
[54] M.-S. Kim, K. A. L. Ada, O. K. Kwon, and C. W. Park, "A comparison of condensation heat transfer performance of MWCNT/Fe composite coatings on steel substrate," *J. Mech. Sci. Technol.*, vol. 28, no. 4, pp. 1589–1596, 2014.
[55] Q. Zhao and B. M. Burnside, "Dropwise condensation of steam on ion implanted condenser surfaces," *Heat Recover. Syst. CHP*, vol. 14, no. 5, pp. 525–534, Sep. 1994.
[56] A. B. Kananeh, M. H. Rausch, A. P. Fröba, and A. Leipertz, "Experimental Study of Dropwise Condensation on Plasma-Ion-implanted Stainless Steel Tubes," *Int. J. Heat Mass Transfer*. pp. 5018–5026, 2006.
[57] M. H. Rausch, A. Leipertz, and A. P. Fröba, "Dropwise condensation of steam on ion implanted titanium surfaces," *Int. J. Heat Mass Transf.*, vol. 53, no. 1–3, pp. 423–430, 2010.
[58] A. T. Paxson, J. L. Yagüe, K. K. Gleason, and K. K. Varanasi, "Stable Dropwise Condensation for Enhancing Heat Transfer via the Initiated Chemical Vapor Deposition (iCVD) of Grafted Polymer Films," *Adv. Mater.*, vol. 26, no. 3, pp. 418–423, Jan. 2014.

10TH INTERNATIONAL CONFERENCE ON SUSTAINABLE ENERGY AND ENVIRONMENTAL PROTECTION (JUNE 27TH – 30TH, 2017, BLED, SLOVENIA), ENERGY EFFICIENCY
J. Krope, A.Ghani Olabi, D. Goričanec & S. Božičnik

Stochastic Model for Prediction of Photovoltaic Production Uncertainty Based on Measured Data

MARINKO BARUKČIĆ, MIRALEM HADŽISELIMOVIĆ & SEBASTIJAN SEME

Abstract This paper deals with the description of a photovoltaic (PV) production prediction by the probability distribution function. Based on experimental on-site measured data of PV production, it is observed that there are different PV power production levels for the same solar irradiation and PV panel temperature. These PV power dispersions (for same irradiance and panel temperature) can be caused by different factors, including non-ideal working of maximal power point tracking (MPPT) devices, device efficiencies, different spectral response of PV panel and PV cell used for the solar irradiance measurement, different temperatures over the PV panel, and others Due to the stochastic character of these occurrences, they can be very difficult take into account in the deterministic mathematical models usually used for PV power prediction. A probabilistic method for PV power production is proposed based on randomly generated PV production using the probability density function with respect to the solar irradiation.

Keywords: • Curve fitting • Photovoltaic power production • Probability density function • Irradiance ranges • Uncertainty •

CORRESPONDENCE ADDRESS: Marinko Barukčić, Ph.D., Assistant Professor, J. J. Strossmayer University of Osijek, Faculty of Electrical Engineering, Computer Science and Information Technology Osijek, Kneza Trpimira 2B, 31000 Osijek, Croatia, e-mail: marinko.barukcic@etfos.hr. Miralem Hadžiselimović, Ph.D., Associate Professor, University of Maribor, Faculty of Energy Technology, Hočevarjev trg 1, 8270 Krško, Slovenia, e-mail: miralem.h@um.si. Sebastijan Seme, Ph.D., Associate Professor, University of Maribor, Faculty of Energy Technology, Hočevarjev trg 1, 8270 Krško, Slovenia, e-mail: sebastijan.seme@um.si.

https://doi.org/10.18690/978-961-286-050-9.20 ISBN 978-961-286-050-9

Available at: http://press.um.si.

1 Introduction

The prediction of photovoltaic production is of interest to research in renewable energy sources. Due to the stochastic character of the energy source (solar irradiance), the probabilistic approach is often employed. In [1], the PV production is predicted based on the solar irradiance estimated by using the probability density function of the clearness index, which is modelled based on the Bayesian approach here. Bayesian approach to prediction PV energy production is also used in [2]. The time series method for PV power forecasting depends on the day of the year and the time of day is presented in [3]. In [4] the authors use an Artificial Neural Network (ANN) with ambient and panel temperatures and irradiance as input data to obtain PV power as output from ANN. ANN is also used in [5], [6], [7], [8] and [9] for PV power estimation. In [10], a combination of different time series and ANN models tuned by using a Genetic Algorithm (GA) is used for PV power prediction. Genetic Programming (GP) to evolve the fuzzy inference system for PV power production is presented in [11]. The historical data processed with a data mining technique are used in [12] to estimate PV power production. In [13] and [14], support vector machines (SVM) using numerically forecast weather data is used for PV energy and power prediction. Randomly generated PV power with respect to time of the day is presented in [15]. This literature was also one of the motivations for the authors to conduct research presented here.

As is known, irradiance and panel temperature have the main impact on PV power. During the analysis of the measured data of the PV plant, the authors noticed that there are cases in which different PV power levels was measured even though values of irradiance and PV panel temperature were the same. The causes of this occurrence can be due to the non-ideal work of MPPT, different spectral response of PV panel and PV cell used for the solar irradiance measurement, different temperatures over the PV panel, different air masses, and other factors. Because of the stochastic character of these causes, they bring uncertainty when PV production is estimated. This was the motivation for this research. The hypothesis is that this uncertainty can be quantified by using the probability density function. The probability density function parameters are determined based on historical measured PV plant data at a micro-location in Slovenia. The PV power production model only consider irradiance is proposed here because the irradiance has main impact to PV power. The proposed method has can use existing software tools to avoid too much code writing during the method implementation. The rest of the article is organized as follows: the overview of the proposed model is given in Section 2, simulation results are presented in Section 3, and in the last section the conclusion is given.

2 Modelling Uncertainty of PV Power Production Based on Measurement Data

A main idea of the method is that uncertainty in PV power production can be modelled by generating random numbers according to normal distribution depending only on irradiance. Here, the question is how to estimate mean and standard deviation of the probability density function of the normal distribution. The amount of PV power data at specific irradiation is not always large enough for each irradiation values to be statistically significant. This is the case even though 15-minute PV power data are considered on a monthly level. Two different procedures are proposed here to overcome this. Both procedures use the measured data grouped according to irradiance ranges as shown in Figure 1. The procedures consider distribution mean and deviation irradiance dependence. These dependences are modelled with analytical polynomial functions. The coefficients (parameters) in these functions are determined by using a curve-fitting technique. In both procedures, the mean is defined in the same way but the distribution deviations are not. The distribution mean dependent on irradiance is defined as polynomial functions; the best fit all measured PV power data (N_m data of P_m) over measured irradiance (N_m data of G_m) range (red line in Figure 1) as:

$$P_{mean}\left(G, G_{m,1:Nm}, P_{m,1:Nm}\right) = \sum_{h=0}^{H} a_h \cdot G^h \tag{1}$$

The next step in both of the procedures is calculating the average value of the irradiance for each irradiance range ($G_{avr,i}$ in Figure 1). The irradiance range average value is defined as the arithmetic mean of the irradiance range bounds:

$$G_{avr,i} = \frac{G_{min,i} + G_{max,i}}{2};\ i \in \left(1 \cdots N_r\right) \tag{2}$$

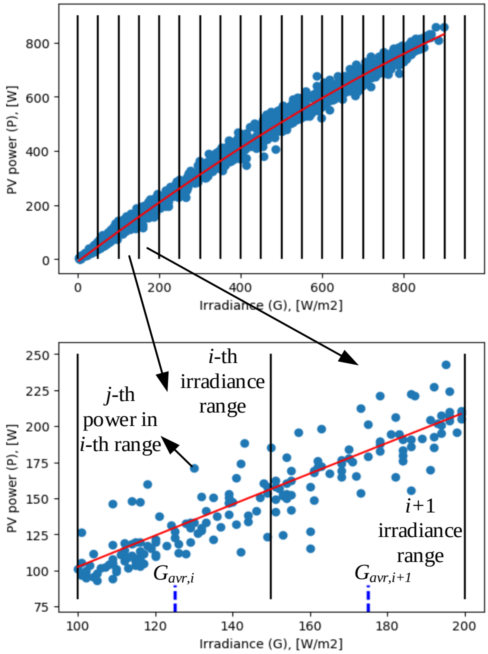

Figure 1. Grouping measured data in irradiance ranges

In the first procedure (PROC 1), the standard deviations of the measured PV power samples for each irradiance range are calculated according to:

$$\sigma_i = \sqrt{\frac{1}{N_i - 1} \cdot \sum_{j=1}^{N_i} \left(Pm_{i,j} - \bar{P}m_i \right)^2} \tag{3}$$

where, $Pm_{i,j}$ is measured the j-th PV power within the i-th irradiance range, $\bar{P}m_i$ is average values (mean) of the measured PV powers of the i-th irradiance range and N_i is number of measured PV powers in i-th irradiance range.

Based on deviations calculated according to equation (3) and irradiance range means according to equation (2) using a curve-fitting tool, the polynomial function is determined:

$$\sigma_1 \left(G, G_{avr,1:N_r}, \sigma_{1:N_r} \right) = \sum_{k=0}^{K} b_k \cdot G^k \tag{4}$$

The last step in the proposed procedure is randomly generating PV powers (for any irradiance) by using the normal distribution with probability density function has the mean according to equation (1) and deviation according to equation (4):

$$P(G) \sim N\left(P_{mean}(G), \sigma_1(G)\right) \quad (5)$$

Equation (5) models the PV power dependent on irradiance, considering uncertainty. In the second procedure (PROC 2), the standard deviation of the distribution is determined differently than in PROC 1 while all other steps are the same (Figure 2). In PROC 2, the distribution deviation is defined by means of the range dispersion factor. The dispersion factor of the irradiance range is defined here as:

$$df_i = \sqrt{\frac{1}{N_i} \cdot \sum_{j=1}^{N_i} \left(Pm_{i,j} - P_{mean}\left(G_{i,j}\right)\right)^2} \quad (6)$$

P_{mean} in equation (6) is calculated according to equation (1). The distribution deviation dependent on the irradiance in PROC 2 is defined as the polynomial function, which fits the range dispersion factors (equation (6)) with respect to the irradiance range averages (equation (2)):

$$\sigma_2\left(G, G_{avr,1:N_r}, df_{1:N_r}\right) = \sum_{m=0}^{M} c_m \cdot G^m \quad (7)$$

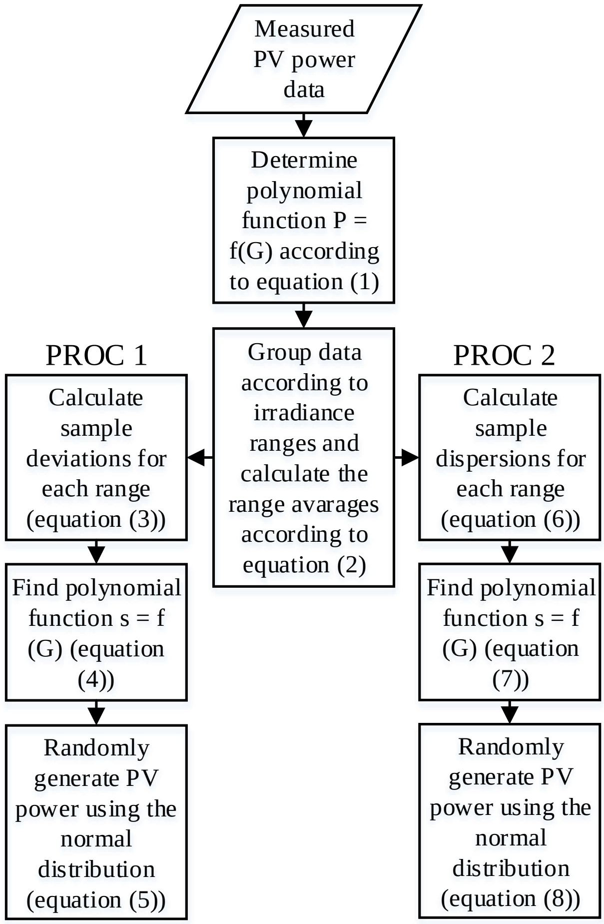

Figure 2. The proposed procedures for generating PV power output involving uncertainty

The model of PV power dependent on irradiance considering uncertainty in PROC 2 is now defined as:

$$P(G) \sim N\left(P_{mean}(G), \sigma_2(G)\right) \tag{8}$$

The overview of the procedures for generating PV power dependent of irradiance considering uncertainty proposed above is given in the form of the flowchart in Figure 2.

3 Case Study Simulation Results

Because the source and intensity of the uncertainties can depend on a specific PV system (devices used) and weather conditions at a micro-location, the proposed method is applied to a case study of the specific PV system. The system used in the case study is installed at the town of Krško (45.95915° N, 15.49167° E), Slovenia at the micro-location of the Krško-Sevnica School centre. The rated power of the PV system is 1.05 kW_p. The PV panels used in the system is a Solar World SW175 monocrystalline panel. The irradiance and panel temperature are measured with a Sunny SensorBox. The irradiance sensor is placed at the same angle as the PV panels. The mathematical implementation of the proposed method on the computer is performed in the Python programming environment using scipy [16] and numpy [17] packages. The numpy functions "*numpy.polyfit*" is used to find coefficients in polynomial functions in equations (1), (4) and (7). The measured data are collected during the year 2013. For the measured data, the polynomials of the model distribution mean and deviations are:

$$\begin{aligned} P_{mean}(G) &= -1.217\text{e-}12 \cdot G^5 + 3.728\text{e-}09 \cdot G^4 \\ &- 4.145\text{e-}06 \cdot G^3 + 0.001757 \cdot G^2 \\ &+ 0.7501 \cdot G - 10.5 \end{aligned} \tag{9}$$

according to PROC 1:

$$\begin{aligned} \sigma_1(G) &= 1.728\text{e-}15 \cdot G^6 - 4.099\text{e-}12 \cdot G^5 \\ &+ 3.476\text{e-}09 \cdot G^4 - 1.274\text{e-}06 \cdot G^3 \\ &+ 0.0001155 \cdot G^2 + 0.07986 \cdot G + 2.429 \end{aligned} \tag{10}$$

according to PROC 2:

$$\begin{aligned} \sigma_2(G) &= 3.349\text{e-}15 \cdot G^6 - 9.232\text{e-}12 \cdot G^5 \\ &+ 9.846\text{e-}09 \cdot G^4 - 5.164\text{e-}06 \cdot G^3 \\ &+ 0.001313 \cdot G^2 - 0.08845 \cdot G + 10.22 \end{aligned} \tag{11}$$

After the distribution mean and deviation dependent on irradiance are determined, the PV power can be generated using the proposed model according to equations (5) and (8) taking into account equations (9) – (11). The measured yearly data and the irradiance dependent distribution mean are shown in Figure 3. The results of the simulation are given in Figures 4-16.

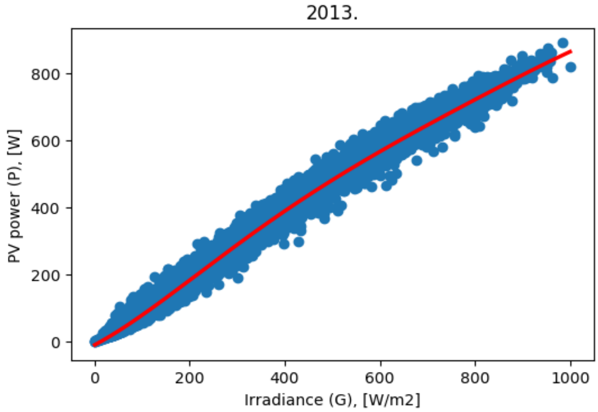

Figure 3. Measured PV power in 15-minute intervals during 2013 and fitted distribution mean (red line, equation (9))

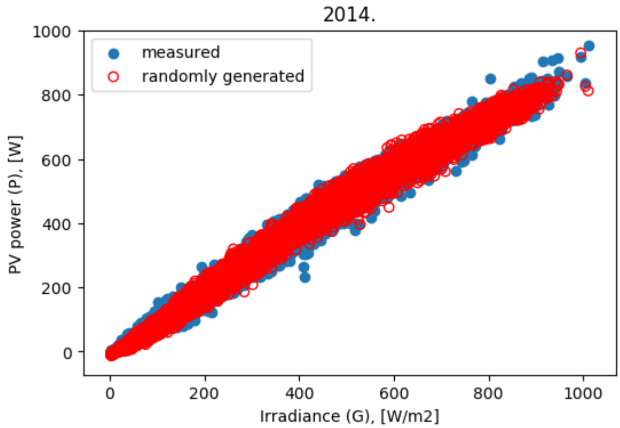

Figure 4. Measured and generated PV power during 2014 – PROC 1

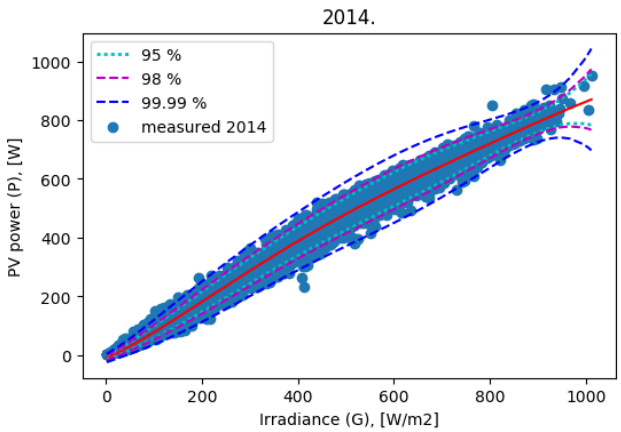

Figure 5. Measured PV power and percentiles for 2014 – PROC 1

Figures 4 and 8 show PV power on a yearly basis (for 2014) generated by using proposed model tuned with measured data during the previous year (2013). As can be seen, both proposed procedures (PROC 1 and PROC 2) give similar results. In Figure 6, the generated PV power data for the month of the winter season are given and in Figure 10 for the month of the summer season. Figures 12 and 14 show the PV power data generated by using the proposed method for the examples of the sunny day and of the cloudy, day respectively.

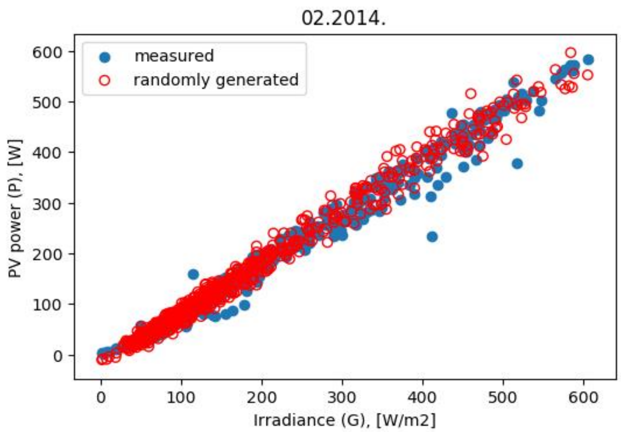

Figure 6. Measured and generated PV power during February 2014 – PROC 1

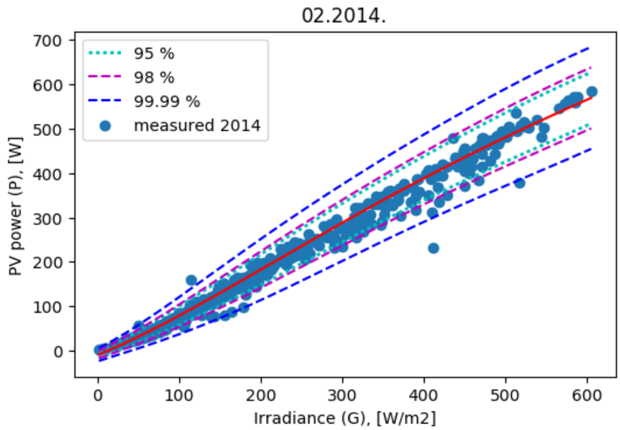

Figure 7. Measured PV power and percentiles for February 2014 – PROC 1

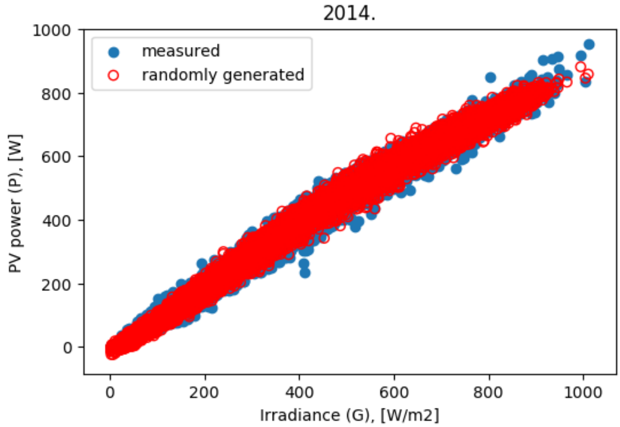

Figure 8. Measured and generated PV power during 2014 – PROC 2

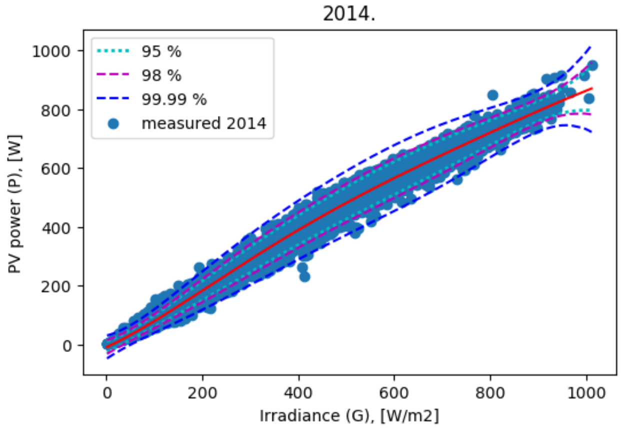

Figure 9. Measured PV power and percentiles for 2014 – PROC 2

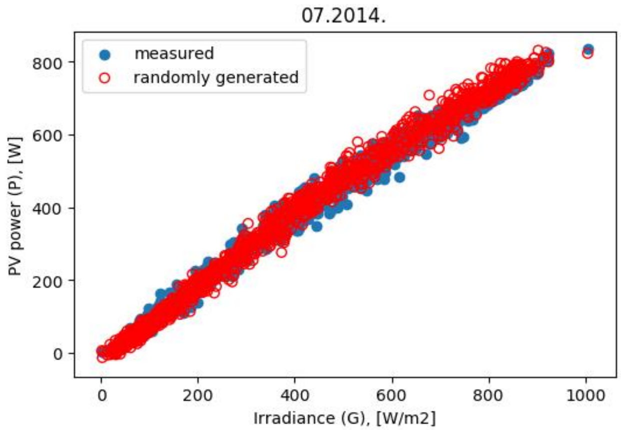

Figure 10. Measured and generated PV power during July 2014 – PROC 2

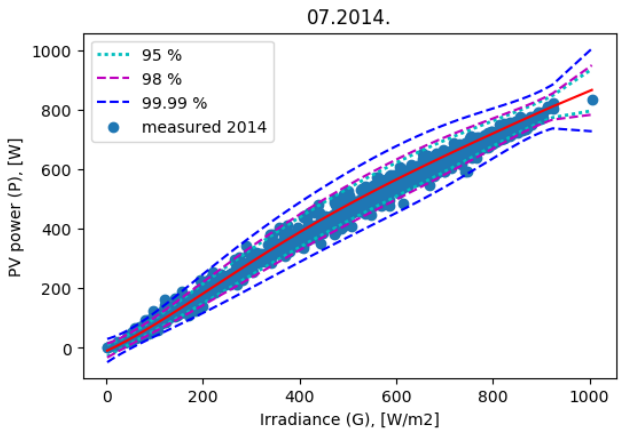

Figure 11. Measured PV power and percentiles for July 2014 – PROC 2

In addition, the percentiles of the distribution density function obtained according to the proposed procedures on yearly (Figures 5 and 9), monthly (Figures 7 and 11), and daily (13 and 15) levels are given.

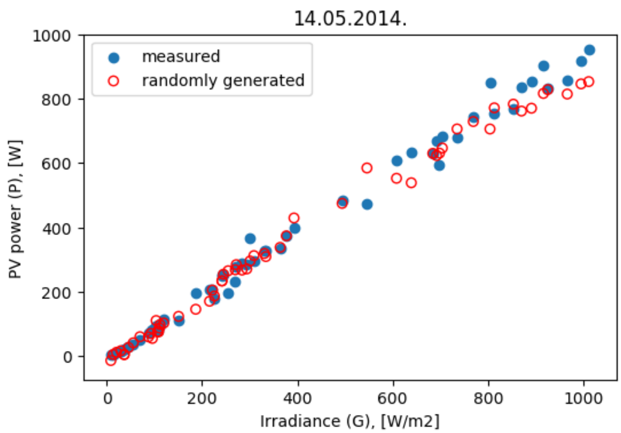

Figure 12. Measured and generated PV power on 14.05.2014. – PROC 2

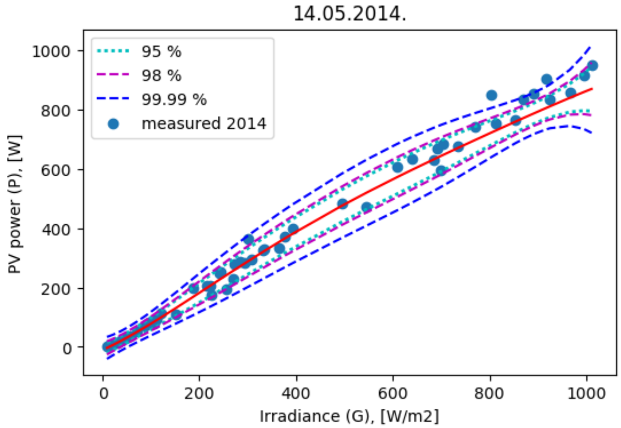

Figure 13. Measured PV power and percentiles on 14.05.2014. – PROC 2

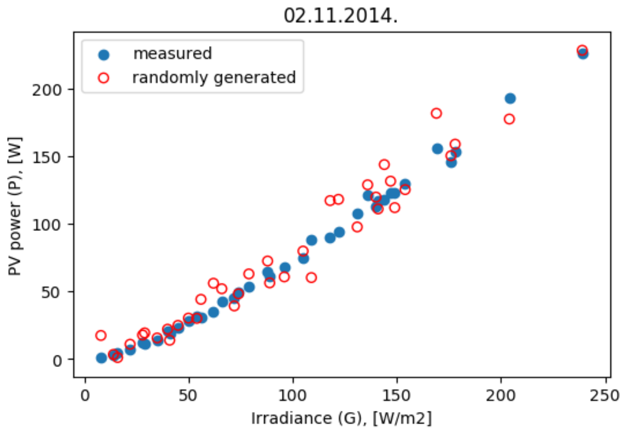

Figure 14. Measured and generated PV power on 02.11.2014. – PROC 2

It is very interesting to note that the PV energy determined based on the randomly generated PV power is very close to the measured energy on yearly, monthly and daily basis as can be seen in Table 1.

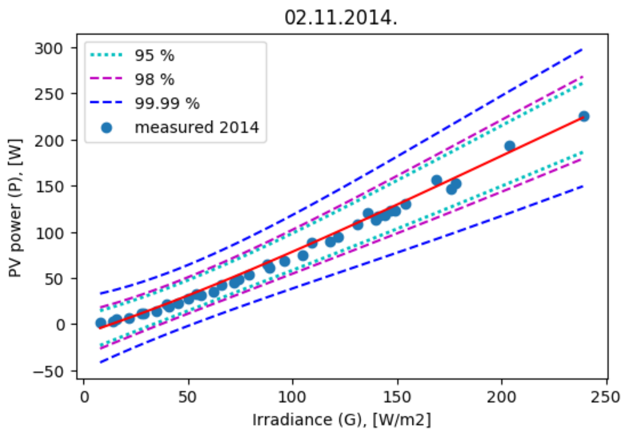

Figure 15. Measured PV power and percentiles on 02.11.2014. – PROC 2

4 Conclusion

This paper presents the procedure for quantification of the PV power production that has a stochastic character. The randomly generated number using the probability density function of the normal distribution is used for the purpose. Two procedures for determining the parameters (mean and standard deviations) of the normal probability density function are proposed. As can be seen from the simulation results of the case study, the proposed stochastic model is capable of emulating PV system power production with respect to solar irradiance. The drawback of the proposed method is the need for a large number of previously measured data at a PV system micro-location. The proposed stochastic model can be used to predict the PV system production for a given irradiance profile. Further research will be about using different timespans of the previously measured data (database for determining the model parameters) and different probability distributions.

Table 1. Comparison of measured PV energy and the energy estimated by means of PV power generated by using the proposed model

Period	W_{meas} [kWh]	W_{est} [kWh]	Diff [%]
14.05.2014.	5.264	5.095	-3.21
02.11.2014.	0.7	0.738	5.43
01.2014.	3.887	4.033	3.75
02.2014.	25.286	26.092	3.19
03.2014.	77.276	75.739	-1.99
04.2014.	91.856	90.606	-1.36
05.2014.	131.062	129.551	-1.15
06.2014.	138.353	140.218	1.35
07.2014.	124.161	126.713	2.06
08.2014.	89.182	91.674	2.78
09.2014.	49.310	50.848	3.12
10.2014.	33.969	35.225	3.70
11.2014.	17.746	18.648	5.08
12.2014.	14.984	14.407	-3.86
2014.	797.072	803.351	0.788

References

[1] A. Bracale, P. Caramia, G. Carpinelli, A. R. Di Fazio, and G. Ferruzzi, "A Bayesian method for Short-Term probabilistic forecasting of photovoltaic generation in smart grid operation and control," *Energies*, vol. 6, no. 2, pp. 733–747, 2013.

[2] P. Chakraborty, M. Marwah, M. Arlitt, and N. Ramakrishnan, "Fine-grained photovoltaic output prediction using a Bayesian ensemble," *Proc. Natl. Conf. Artif. Intell.*, vol. 1, pp. 274–280, 2012.

[3] P. Bacher, H. Madsen, and H. A. Nielsen, "Online short-term solar power forecasting," *Sol. Energy*, vol. 83, no. 10, pp. 1772–1783, 2009.

[4] M. G. De Giorgi, P. M. Congedo, M. Malvoni, and M. Tarantino, "Short-Term Power Forecasting By Statistical Methods for Photovoltaic Plants in South Italy," *4th Imeko TC19 Symp. Environ. Instrum. Meas. Prot. Environ. Clim. Chang. Pollut. Control*, pp. 171–175, 2013.

[5] M. Ding, L. Wang, and R. Bi, "An ANN-based approach for forecasting the power output of photovoltaic system," *Procedia Environ. Sci.*, vol. 11, no. PART C, pp. 1308–1315, 2011.

[6] E. Izgi, A. Öztopal, B. Yerli, M. K. Kaymak, and A. D. Şahin, "Short-mid-term solar power prediction by using artificial neural networks," *Sol. Energy*, vol. 86, no. 2, pp. 725–733, 2012.

[7] D. Riley and J. Johnson, "Photovoltaic prognostics and heath management using learning algorithms," *Conf. Rec. IEEE Photovolt. Spec. Conf.*, no. June, pp. 1535–1539, 2012.

[8] S. . Sulaiman, T. . A. Rahman, and I. Musirin, "Partial Evolutionary ANN for Output Prediction of a Grid-Connected Photovoltaic System," *Int. J. Comput. Electr. Eng.*, vol. 1, no. 1, pp. 40–45, 2009.

[9] M. Saberian, Aminmohammad and Hizam, H and Radzi, MAM and Ab Kadir, MZA and Mirzaei, "Modelling and Prediction of Photovoltaic Power Output Using Artificial Neural

Networks,” *Int. J. Photoenergy*, vol. 2014, 2014.

[10] R. Yuan-Kang, Wu; Chao-Rong, Chen; Hasimah Abdul, “A Novel Hybrid Model for Short-Term Forecasting in PV Power Generation,” *Int. J. Photoenergy*, vol. 2014, 2014.

[11] P. Kromer, L. Prokop, V. Snasel, S. Misak, J. Platos, and A. Abraham, “Evolutionary prediction of photovoltaic power plant energy production,” *Proc. fourteenth Int. Conf. Genet. Evol. Comput. Conf. companion - GECCO Companion ’12*, p. 35, 2012.

[12] C. Monteiro, T. Santos, L. A. Fernandez-Jimenez, I. J. Ramirez-Rosado, and M. S. Terreros-Olarte, “Short-term power forecasting model for photovoltaic plants based on historical similarity,” *Energies*, vol. 6, no. 5, pp. 2624–2643, 2013.

[13] J. G. da Silva Fonseca, T. Oozeki, T. Takashima, G. Koshimizu, Y. Uchida, and K. Ogimoto, “Use of support vector regression and numerically predicted cloudiness to forecast power output of a photovoltaic power plant in Kitakyushu, Japan,” *Prog. Photovoltaics Res. Appl.*, vol. 20, no. 7, pp. 874–882, Nov. 2012.

[14] J. Shi, W. J. Lee, Y. Liu, Y. Yang, and P. Wang, “Forecasting power output of photovoltaic systems based on weather classification and support vector machines,” *IEEE Trans. Ind. Appl.*, vol. 48, no. 3, pp. 1064–1069, 2012.

[15] Y. Su, L.-C. Chan, L. Shu, and K.-L. Tsui, “Real-time prediction models for output power and efficiency of grid-connected solar photovoltaic systems,” *Appl. Energy*, vol. 93, pp. 319–326, 2012.

[16] “SciPy.org — SciPy.org.” [Online]. Available: https://www.scipy.org/. [Accessed: 17-Mar-2017].

[17] “NumPy — NumPy.” [Online]. Available: http://www.numpy.org/. [Accessed: 17-Mar-2017].

[18] A. G. Olabi and J. Smith, *Title of the book*. London: John-Wiley, 2003.

[19] A. G. Olabi, S. Tedesco, and M. Montingelli, “Title of the conference paper,” 2015, pp. 90–96.

[20] P. Trop, D. Goricanec, and A. G. Olabi, “Title of journal paper,” *Energy*, vol. 108, pp. 155–161, Aug. 2016.

10TH INTERNATIONAL CONFERENCE ON SUSTAINABLE ENERGY AND ENVIRONMENTAL PROTECTION (JUNE 27TH –30TH, 2017, BLED, SLOVENIA), ENERGY EFFICIENCY
J. Krope, A.Ghani Olabi, D. Goričanec & S. Božičnik

Shaping the Envelope of Buildings by Looking at Both Architectural Layout and Technical Performance in Order to Maximize the Energy Efficiency of the Whole Ensemble

EUGEN MANDRIC, MUGUREL-FLORIN TĂLPIGĂ & FLORIN IORDACHE

Abstract The paper presents an analysis of different energy performance levels for buildings where the result was a direct consequence of its envelope compliance in terms of architecture and technical characteristics. The methodology employed to calculate the energy consumption rests upon the degree day concept of assessing a building's demand for heating energy during the winter period and cooling energy during the summer period, while introducing the notion of equilibrium external temperature. Annual energy consumption was computed for scenarios comprised of different approaches for the envelope, where the ratios between the transparent and opaque external elements, solar transmission coefficients and different glazing thermal transmittance values vary. The results are presented graphically in order to gain a synthetic image upon the spectrum of the envelope characteristics that lead to near zero energy performance for buildings.

Keywords: • Building envelope • Glazed buildings • nZEB • Solar radiation • Degree day •

CORRESPONDENCE ADDRESS: Eugen Mandric, Mechanical Engineer, PhD. candidate, Technical University of Civil Engineering of Bucharest, Faculty of Building Services, 116-122 Dorobanti ave., 6th bl., A ent., 22nd ap. no., Bucharest, Romania, e-mail: e_mandric@yahoo.com. Mugurel-Florin Tălpigă, Electronic Engineer, Ph.D. candidate, Technical University of Civil Engineering of Bucharest, Faculty of Building Services, 2/III Pipera ave., NG1, Bucharest, Romania, e-mail: talpiga.mugurel@gmail.com. Florin Iordache, Ph.D., Professor, Technical University of Civil Engineering of Bucharest, Faculty of Building Services, 66 Pache Protopopescu blv., Bucharest, Romania, e-mail: fliord@yahoo.com.

https://doi.org/10.18690/978-961-286-050-9.21 ISBN 978-961-286-050-9

Available at: http://press.um.si.

1 Introduction

The Directive 2010/31/EU of the European Parliament [1] set up a clear schedule for all Member States, to ensure that by the end of December 31, 2020, all the new buildings will be nearly zero-energy buildings (nZEB). As the European Union consists of Member States that are an inhomogeneous aggregate of countries from a meteorological and an energy sector performance point of view, each country must define its own technical and legal framework that defines the notion of nZEB.

Throughout the last 25 years, great achievements have been made in the building construction sector, starting with one of the first passive houses built in 1994 in Germany, the Heliotrope house [4], which is estimated to generate four times more energy than it consumes in one year.

Along all this time the focus of building energy efficient houses has gradually shifted from innovation and clever design to standardization and clear established performance criteria. The main target now is to design and put up energy efficient buildings as a standard way for the construction industry.

The pressure now rests on the shoulders of all participant members of the industry, the design teams, government institutions, the construction companies, the product manufacturers, etc.

One of the most important steps in all this process is represented by the early architectural concept design stages, when the building defines its shape and characteristics. In most of the cases this is the stage where many of the performance criteria are set up. Going back and changing this values usually generates time delays and budget losses.

Because of these reasons, a good starting point can ensure the success in meeting all the performance criteria in terms of energy efficiency when designing and constructing buildings, leaving aside the trial and error approach.

The study's aim was to search for patterns, technical characteristics and correlations between these characteristics, so that by complying the architecture of the building's envelopes with all of these findings, achieving nZEB efficiency will be enabled from an early design stage.

In order to achieve this, the research focused on two main approaches, one being the realization of a computer program based on an established methodology of assessing the annual energy demand of a building and the other being the possibility to set up a complex set of modifiable values for a theoretical generic building that would be placed in different geographic areas with clearly defined meteorological profiles in order to analyse the way it responds to different external thermal stresses.

2 The Generic Building

The object of analysis is represented by a theoretical building, for which a set of predefined characteristics were chosen. For the study's purpose, the building was created in such a way that the compactness factor, understood as the ratio between the surface of the thermal envelope and the volume of the building, to be in the range of 0.15 and 0.25, this way the thermal and solar stresses acting upon the building through the envelope won't dissipate in a very big volume, making the analysis of the effects hard to identify. Thus, a building was created where all the points inside are in the vicinity of the façade, at a maximum distance of 8.5 m. The choice for the shape was based on the rectangular footprint, with a ratio between the width and the length of approximately 1:3, this way, a fully exposed façade to the sun was obtained, ensuring clarity in the output data. In the picture below there is a graphical representation of the building geometry that was used as a model for the study, in two versions, where the glazing ratio is the differentiating factor. For the model, a ground floor plus four levels, each having 3.5 m in height, were considered.

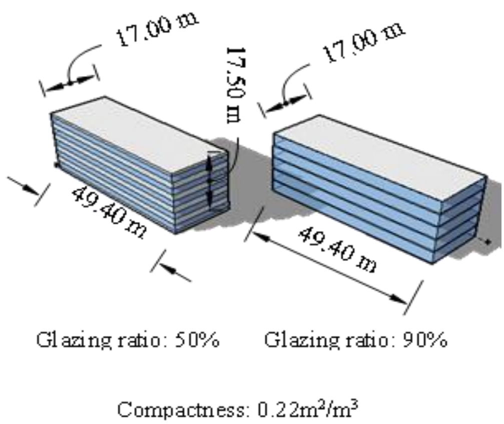

Figure 9. The generic building with different glazing ratio

In the present paper we will refer to this conceptual building model as the "generic building". The main standard values considered for the generic building are as follows:

i. Thermal resistances for the envelope's elements:

a. Walls, R_{wall}: 1.80 m²K/W;
b. Glazing, R_{window}: 0.80 m²K/W;
c. Glazing's solar factor g: 0.4;
d. Window's frame: 0.77 m²K/W;
e. Roof: 5.00 m²K/W;

ii. Building's characteristics:

a. Windows ratio with the vertical surface of each level: 50%;
b. Window's frames ratio out of the total windows area: 15%;
c. Internal temperature during winter time, t_{i0}: 20 ºC;
d. Internal temperature during summer time, t_{i0}: 24 ºC;
e. Outside air infiltration rate, n_a: 0.6 h^{-1};
f. Orientation: the length is perpendicular to the North-South axis.

The energy sources considered for connecting the building services heating and cooling plants, are the natural gas from the local supplier and electricity from the local grid. Gas boilers will be connected to the gas distribution for heat production and air cooled frigorific machines (chillers) using mechanical compression of Freon vapours for the cooling energy production. Inside all spaces 4-pipe fan coil units were considered for maintaining the indoor air temperatures during the winter and summer time. In order to simulate a real case scenario, efficiencies were considered for the distribution system, fan coil units control and energy production, as follows:

iii. Building services efficiencies:

a. Fan coil units control efficiency: 98%;
b. Distribution form the plants to the fan coil units efficiency: 95%;
c. Boiler efficiency: 92%;
d. Chiller ESEER: 3.6

3 Methods

3.1 Thermal connection factor

The algorithm used to evaluate the annual energy demand for heating and cooling the generic building's internal spaces is based on the concept of complex thermal connection between the outside meteorological conditions and the indoor microclimate [2]:

$$\dot{Q}_{nec} = H \cdot (t_{i0} - t_e) \quad (1)$$

The above equation describes the way the heating or cooling demand, $\dot{Q}_{nec}$, is calculated using the complex thermal connection coefficient H. This coefficient denotes the heating flux that is exchanged between the external thermal potential, rated at the t_e temperature and the indoor thermal potential fixed by the design criteria at t_{i0} temperature.

The thermal connection coefficient H comprises two components, one related to the thermal envelope of the building and one related to the outside air infiltration [2]:

$$H = H_T + H_V = \frac{S_T}{R_m} + 0.34 \cdot n_a \cdot V \quad (2)$$

The H_T coefficient is linked to the heat transmission through the thermal boundary of the building, namely the envelope, described by its total area S_T and its average thermal resistance R_m. The H_V coefficient is associated with the outside air infiltration rate n_a considering the building's volume V. This coefficient bares a unit conversion factor, which is 0.34 $\left[\frac{W \cdot h}{m^3 \cdot K}\right]$, that also comprises the values of the air's density and specific mass heat.

Combining the equations (1) and (2) the building's heat demand mathematical relation will be of the form [2]:

$$\dot{Q}_{nec} = \left(\frac{S_T/_V}{R_m} + 0.34 \cdot n_a\right) \cdot V \cdot (t_{i0} - t_e) \quad (3)$$

3.2 Degree days

To generate prompt results when the input data is changed, the methodology of evaluating the building's annual energy demand rests upon the degree-days concept [2], [3]:

$$Q_{a\_nec} = H \cdot \left[\int_{\tau_{hi}}^{\tau_{hf}} \left(t_{i0} - t_e(\tau)\right) d\tau + \int_{\tau_{ci}}^{\tau_{cf}} \left(t_{i0} - t_e(\tau)\right) d\tau\right] \quad (4)$$

Where (τ_{hi}, τ_{hf}) and (τ_{ci}, τ_{cf}) represent the time periods when the building is heated and respectively cooled. Integrating the temperature variations, the degree-days values for the heating period $N_{HDD}[°\mathrm{C} \cdot day]$ and the degree-days for the cooling period $N_{CDD}[°\mathrm{C} \cdot day]$ are determined. Thus, using the meteorological records for the location where the generic building is placed, the annual energy demand is calculated with the formula [2], [3]:

$$Q_{a\_nec} = 0.024 \cdot H \cdot (N_{HDD} + N_{CDD}) \ \left[\frac{kWh}{year}\right] \quad (5)$$

where, 0.024 represents a conversion factor from $Wday$ to kWh.

3.3 Equilibrium external temperature

In order to encompass the effects of the solar energy and the indoor heat generated by human presence, electrical equipment and lighting systems, the equations (4) and (5) were modified by introducing the variable t_{ee} denoted as the equilibrium external temperature [2]:

$$t_{ee} = t_{i0} - \frac{\dot{Q}_{gain}}{H} \tag{6}$$

Where $\dot{Q}_{gain}$ sums the total indoor heat dissipation and the external solar gains.

Plotting the temperatures variations, the degree-days value represents the area between the t_{ee} segments and the monthly outdoor average temperatures segments, denoted t_{ema}, as depicted in figure (2):

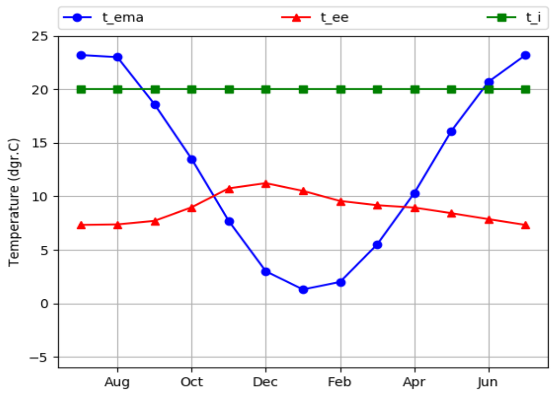

Figure 10. Heating period

4 Results

The methodology described in the previous chapter was translated into a calculation algorithm that was used to write a computer program that evaluates the annual energy demand of the generic building described in the second chapter. The code, named *AVO*, was written, debugged and validated by the research authors using the Python language. All the graphs were generated by *AVO*, using the *matplotlib* library.

4.1 Meteorological data

A database was created to hold meteorological information for several places in Romania that have different temperature profiles and different availability of solar energy throughout the year. The average temperatures and total solar radiation for these places are depicted in table (1).

Table 2. Yearly average temperatures and total solar radiation for different cities

City	Yearly average temperature	Total radiation on horizontal plane
	[°C]	[W/m²/year]
Bucharest	*10.7*	*1684.9*
Constanța	*12.1*	*1783.8*
Iași	*10*	*1606.4*
Târgu Mureș	*9.2*	*1644.0*
Târgu Secuiesc	*7.2*	*1631.8*

4.2 Energy demand variation with the geographical position

Using the standard input data as described in chapter 2, the generic building was placed in each of the five cities, keeping the same orientation (the building's length perpendicular on the N-S axis), for annual energy demand calculations at the connection points. The results of the total annual energy demand and the heating and cooling demand ratios are depicted in table (2).

Table 3. Annual energy demand comparison

City	Annual energy demand 50% glazing	Heating/Cooling ratios
	[kWh/m²/year]	[-]
Bucharest	*53.3*	*71% / 29%*
Constanța	*42.2*	*59% / 41%*
Iași	*58.8*	*77% / 23%*
Târgu Mureș	*59.1*	*80% / 20%*
Târgu Secuiesc	*66.0*	*87% / 13%*

4.3 Energy demand variation with the glazing ratio and the thermal characteristics of the envelope

Fixing the building's geographical position to Bucharest and considering the thermal resistances of the opaque and glazed elements belonging to the envelope's vertical part, together with the glazing's solar factor, set to the values in table (3), the annual energy demands were computed considering the variation of two elements.

Table 4. Envelope's properties

Thermal resistance of external walls R_{wall}	Thermal resistance of external windows R_{window}	Glazing solar factor g
[m²K/W]	*[m²K/W]*	*[-]*
2.00	1.00	0.4

Three scenarios were investigated for which the first element that varies is an architectural one, namely the glazing ratio (denoted GR), whose values range from 10% up to 90%. For each scenario, a high resolution variation surface was plotted using small computation steps for the change in values of the two elements considered.

In the first scenario, the thermal resistance of the walls (R_{wall}) ranges between the values 0.50 and 3.00 m²K/W generating the variation surface shown in figure (3).

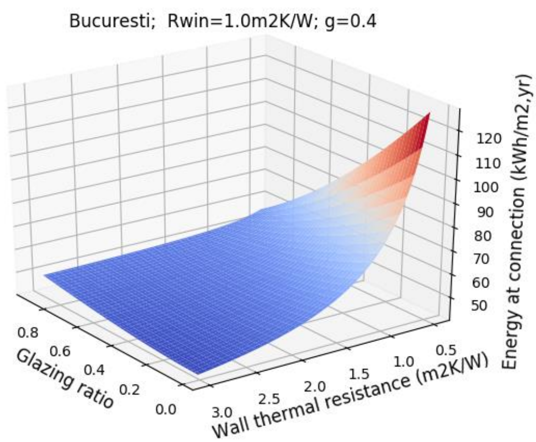

Figure 11. Variation surface / GR and Rwall

In the second scenario, the thermal resistance of the windows (R_{win}) ranges between the values 0.50 and 2.00 m²K/W generating the variation surface shown in figure (4).

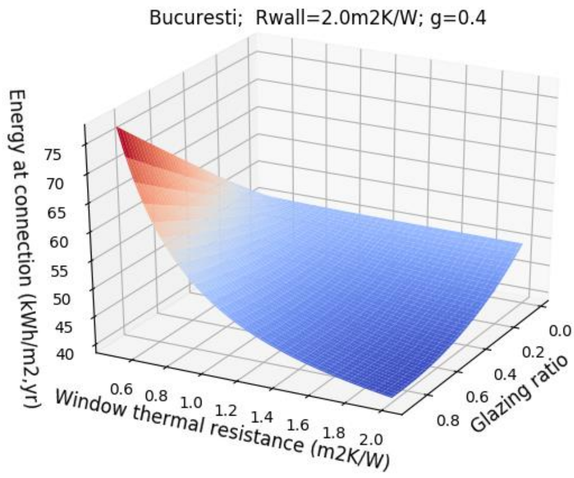

Figure 12. Variation surface / GR and Rwin

In the third scenario, the solar factor of the glazing (g) ranges between the values 0.25 and 0.40 generating the variation surface shown in figure (5).

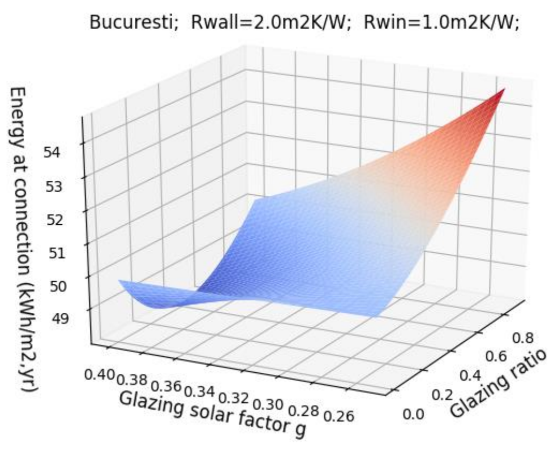

Figure 13. Variation surface / GR and g

5 Discussions

From the early stages of the research, the resulting values for the energy demand by performing computations on the generic building placed in different geographical places, as shown in table (2), reveals the necessity to adapt the building's performance criteria according to the meteorological profile of the construction location. The building's annual energy demand, if the location is Târgu Secuiesc, is 56% more than the annual energy demand of the same building placed in Constanța. Breaking down the annual energy consumption into heating and cooling demands, shows that more in-depth analysis of the envelope's individual components characteristics is required in order to understand how the building responds to the exterior thermal stresses. As shown in table (2) the generic building placed in Constanța should have an envelope that complies with a meteorological profile that is more demanding during the summer time, opposed to the design choices to be taken in order to make the envelope comply with a meteorological profile of city Târgu Secuiesc city that is more demanding during the winter time.

Analysing the way the annual energy demand varies with the glazing ratio and solar factor, as shown in figure (5), it results that choosing a glazing with a higher solar factor it affects in a positive way the heating and cooling consumption profiles for a building placed in a geographical area where the thermal stress is much greater during winter time.

Table 5: Târgu Secuiesc / g=0.4

Heating demand	Cooling demand	Heating period duration	Cooling period duration
[kWh/m²/yr]	[kWh/m²/yr]	[h]	[h]
49.8	*9.4*	*4155*	*3992*

Târgu Secuiesc / g=0.25

Heating demand	Cooling demand	Heating period duration	Cooling period duration
[kWh/m²/yr]	[kWh/m²/yr]	[h]	[h]
59.3	*6.2*	*4637*	*3460*

As shown in table (4), reducing the solar factor from 0.4 to 0.25 will result in a 19% increase in heating demand. There is also a consequence for the cooling demand, which decreases, but taking into consideration that the required cooling energy throughout the year is considerably lower compared to the heating energy, overall, choosing a glazing with a solar factor of 0.25 will result in an increase of the annual energy demand with 10.6% compared to choosing a glazing with a solar factor of 0.4. The effects can also be seen by analysing the heating period that increases with 482 h when taking the value of the solar factor from 0.4 to 0.25, which add up to 20 days.

The variation surface in figure (3) shows large curvature values corresponding to areas where the wall's thermal resistance ranges between 0.5 and 1.00 m²K/W. This range corresponds to walls that are poorly insulated relative to the performance criteria needed for buildings to meet the nZEB requirements. This range can be assimilated to the past construction standards according to which a lot of the existing buildings were built. The curvature becomes larger as the glazing ratio decreases, meaning there is less solar energy to penetrate the building and the average thermal resistance of the envelope becomes less efficient.

Looking at both figures (3) and (4) a pattern emerges, pointing to the fact that there are sets of values that once applied to the generic building as input data, will lead to a resulting annual energy demand that has a very small variation in between the range of the glazing ratio, as shown in figure (6).

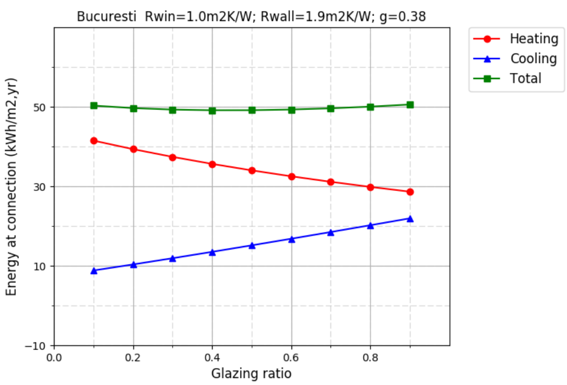

Figure 14. Constant annual energy demand

During winter time, as the glazing ratio increases, more solar energy enters the windows, compensating some of the energy lost through the envelope. During summer time the effect is opposite, meaning the energy coming from the sun that increases with the glazing ratio adds up to the heat that is already building up inside, counteracting the decrease in heating energy needed during the winter time, thus keeping the overall annual energy demand constant.

6 Conclusions

After computing many annual energy demand values corresponding to different scenarios a set of patterns emerged throughout each simulation. One of the first conclusions is linked to the meteorological profile of the geographical position. Depending on the ratio of the heating period compared to the ratio of the cooling period should the spectrophotometric characteristics of the glazing to be chose. In case the outside thermal stress is higher during the winter time, windows with solar factors bigger than 0.35 should be considered, in order to allow the solar energy to compensate the heat losses. But if the outside thermal energy stress is more demanding for the building during the summer time, windows with solar factors lower than 0.35 should be taken into consideration, the challenge being to prevent the outside heat as much as possible from getting inside the building.

Contrary to the general tendency to endow the buildings with glazing elements that have low to very low solar factors, most of our results show that this will only decrease the cooling power of the HVAC systems, but the overall annual energy demand will only increase compared to using glazing elements with higher solar factors.

We suggest that future researches be done to investigate how a generic building responds to outside thermal stresses if it is placed in very different locations from a meteorological point of view. What would be an optimum spectrophotometric value for the glazing if the location is in south of Europe or if it is in north of Europe?

Another solid pattern shows that for each scenario we investigated there was a set of input values that led to small variations in the annual energy demand with the variation of the glazing ratio. This means that conforming the characteristic of the envelope with the right set of values, the architectural teams have the freedom not to freeze the glazing ratio during the early stages of designing the building without having to consider what would be the consequences on the targeted annual energy demand.

Future researches should investigate how do the CO_2 emissions vary with the glazing ratio considering different types of energy sources, like natural gas, electricity from the grid and others

References

[1] *Directive Of The European Parliament And Of The Council On The Energy Performance Of The Buildings*, 2010/31/Eu, 2010.
[2] *Romanian Ministry Of Transport, Construction And Tourism. Methodology Of Calculation Of The Energy Performance Of Buildings*, Mc 001, 2006.
[3] *Romanian Standards Association. Heating Systems. Annual Number Of Degree-Days*, Sr 4839, 2014.
[4] C. Ionescu, T. Barca, G. E. Vlad, H. Necula And A. Badea, "The Historical Evolution Of Energy Efficient Buildings", *Renewable And Sustainable Energy Reviews*, Vol. 49, Pp. 243-253, Sept. 2015

10TH INTERNATIONAL CONFERENCE ON SUSTAINABLE ENERGY AND ENVIRONMENTAL PROTECTION (JUNE 27TH – 30TH, 2017, BLED, SLOVENIA), ENERGY EFFICIENCY
J. Krope, A.Ghani Olabi, D. Goričanec & S. Božičnik

Performance Evaluation of a Mobile Air Conditioning Unit: An Exergetic Approach

HUSEYIN GUNHAN OZCAN, HUSEYIN GUNERHAN & ARIF HEPBASLI

Abstract Mobile air conditioning systems play a key role in terms of refrigerant emission to the atmosphere with their one-third amount due to systems faults, service processes and accidents. In this study, a public bus (having a capacity of 99 passengers and a volume of 70 m3) and its mobile air conditioning unit (utilizing R134a as a refrigerant) are considered. The low-exergy (the so-called lowex) analysis method, which has been mostly applied to buildings, will be utilized to assess the performance of the public bus along with its air conditioning unit (the air-conditioned bus) for the first time to the best of the authors' knowledge. The air-conditioned bus is evaluated from the energy production to the bus envelope stage by stage through the low-exergy method while inefficiencies at each stage and the overall energy/ exergy efficiencies of the air-conditioned bus are determined under climatic conditions of Izmir in Turkey. Total exergy efficiency values of the whole system (exergy demand room/total exergy input) are obtained to be 4.4% and 2.9% for the heating and cooling modes, respectively.

Keywords: • Mobile air conditioning • Exergy • Lowex • Performance assessment • Heating and cooling •

CORRESPONDENCE ADDRESS: Huseyin Gunhan Ozcan, Ph.D student, Assistant, Yasar University, Faculty of Engineering, Üniversite Caddesi No:37-39, 35100 İzmir, Turkey, e-mail: huseyin.ozcan@yasar.edu.tr. Huseyin Gunerhan, Associate Professor., Ege University, Faculty of Mechanical Engineering, Ege Üniversitesi Kampüsü, 35100 İzmir, Turkey, e-mail: huseyin.gunerhan@ege.edu.tr. Arif Hepbasli, Professor, Yasar University, Faculty of Engineering, Üniversite Caddesi No:37-39, 35100 İzmir, Turkey, e-mail: arif.hepbasli@yasar.edu.tr.

https://doi.org/10.18690/978-961-286-050-9.22 ISBN 978-961-286-050-9

Available at: http://press.um.si.

1 Introduction

Over the last decades energy saving potential became a crucial concept in terms of energy efficiency and sustainability. Buildings account for more than one third of the global primary energy demand. For this reason, studies have mostly focused on this area. Applications associated with building envelope and environment appears to be active and passive systems. While passive systems benefit from immediate environment potential (sun, wind, ventilate, etc.), active systems consume various energy sources such as electricity and fossil fuels usually with a high valued. In this regard, lowex systems have become very popular due to their low valued energy utilization in heating and cooling applications (practically processes occur at a temperature close to room temperature), which provides low cost, wide distribution and environment friendly solutions. Also when they are compared with the traditional ones, they offer flexible fuel choice and more energy efficient. But initial investment might be slightly higher.

Hepbasli [1] performed a comprehensive review study on low exergy technologies and applications for sustainable buildings and societies. Strengths and weaknesses of these technologies compared to conventional ones were discussed. Also, historical background, impact area and calculation method of a lowex

guidebook used on these technologies was introduced. Schmidt [2] emphasised on importance of energy management potential (from generation, distribution, consumption within the environment) beside energy saving applications and low quality energy source utilization simultaneously lowering the heating/cooling demand. Exergy analysis methodologies, exergy efficient community supply systems, exergy efficient building technology and knowledge transfer, dissemination were introduced as sub tasks of the lowex method. Meggers et al. [3] investigated low exergy building systems implementation in prototypes, pilots and simulations which maintain low temperature lifts led to increase coefficient of performance. They also presented that low temperature-lift heat pumps were thermodynamically feasible and produced the first prototype.

In this study, differently from buildings, the performance of a public bus along with its air conditioning unit was assessed from the lowex point of view.

2 System Description

In this study, a public bus along its HVAC system is regarded as lowex system, as shown in Figure 1, is travelled in the city of Izmir, Turkey, in a Mediterranean climate. For steady state instantaneous exergy load calculation, indoor comfort temperatures are taken to be 20 °C and 26 °C based on EN 14750-1 standard for category A vehicles [4], corresponding to 0 °C and 35°C outside air temperatures for heating and cooling options, respectively.

Figure 1. Lowex System

Main data of the lowex system are given in Table1. Additionally, construction materials and their dimensions are galvanized sheet with 0.001 m, polystyrene foam with 0.04 m and plywood with 0.004 m, respectively. Besides these values, outdoor and indoor convection heat transfer effects are regarded in transmission heat loss calculations.

Table 1. Main Data Used

Parameters	**Value**	**Unit**
Length/height/ width of the bus	12/2.3/2.5	m
Exterior wall area lateral/rear-front/floor	15.2/5.75/30	m^2
Window wall area lateral/rear/front	16/1.5/4.5	m^2
Door/roof area	24/30	m^2
Fresh air rate per passenger	15	m^3
Heat exchanger efficiency	0.8	-
Solar radiation	1324	W/m^2
Number of standing/siting occupants	66/31	-
Lightening power	5	W/m^2

3 Analysis

Energy and exergy analyses of the considered system are carried out through an Excel tool, which has been developed within the framework of International Energy Agency (IEA) formed within the Energy Conservation in Buildings and Community Systems Programme (ECBCSP) Annex 37. The tool and the calculation approach follow the method developed by Schmidt. The main equations of energy and exergy analyses are given below [5]. Fresh air effect, which is mandatory for mobile air conditioning systems, is added to the ventilation heat losses.

3.1 Energy analysis

Heat losses

$$\dot{Q}_T = \sum (U_i . A_i . F_{xi}).(T_i - T_o), \tag{1}$$

$$\dot{Q}_V = (c_p . \rho . V . n_d . (1 - \eta_V)).(T_i - T_o), \tag{2}$$

Heat gains

$$\dot{Q}_S = \sum (I_{s,j} . (1 - F_f) . A_{w,j} . g_j . F_{sh} . F_{no}), \tag{3}$$

$$\dot{Q}_o = \dot{Q}''_o . no_o, \tag{4}$$

$$\dot{Q}_e = \dot{Q}''_e . A_N, \tag{5}$$

Other uses

$$P_l = p_l . A_N = \dot{Q}_l, \tag{6}$$

$$P_V = p_V . V . n_d, \tag{7}$$

Heat demand

$$\dot{Q}_h = (\dot{Q}_T + \dot{Q}_V) - (\dot{Q}_S + \dot{Q}_o + \dot{Q}_e + \dot{Q}_l), \tag{8}$$

$$\dot{Q}''_h = \dot{Q}_h / A_N, \tag{9}$$

3.2 Exergy analysis

Envelope

$$F_{q,air} = 1 - \frac{T_o}{T_i}, \tag{10}$$

$$\dot{E}x_{air} = F_{q,air} . \dot{Q}_h \,, \tag{11}$$

Indoor air

$$T_{heat} = \frac{T_{in} - T_{ret}}{\ln\left(\dfrac{T_{in} - T_i}{T_{ret} - T_i}\right)} \cdot \tfrac{1}{2} + T_i \,, \tag{12}$$

$$F_{q,heat} = 1 - \frac{T_{ref}\,[K]}{T'_{heat}\,[K]} \,, \tag{13}$$

$$\dot{E}x_{heat} = F_{q,heat} \cdot \dot{Q}_h \,, \tag{14}$$

Heating system

$$\dot{Q}_{loss,HS} = \dot{Q}_h . \left(\frac{1}{\eta_{HS}} - 1 \right), \tag{15}$$

$$P_{aux,HS} = p_{aux,HS} . \dot{Q}_h \,, \tag{16}$$

$$\Delta\dot{E}x_{HS} = \frac{\left(\dot{Q}_h + \dot{Q}_{loss,HS}\right)}{\left(T_{in} - T_{ret}\right)} \left\{ \left(T_{in} - T_{ret}\right) - T_{ref} . \ln\left(\frac{T_{in}}{T_{ret}}\right) \right\} \,, \tag{17}$$

Distribution

$$\dot{Q}_{loss,dis} = (\dot{Q}_h + \dot{Q}_{loss,HS}) . \left(\frac{1}{\eta_{dis}} - 1 \right), \tag{18}$$

$$P_{aux,dis} = p_{aux,dis} . (\dot{Q}_h + \dot{Q}_{loss.HS}) \,, \tag{19}$$

$$\Delta\dot{E}x_{dis} = \frac{\dot{Q}_{loss,dis}}{\Delta T_{dis}} \left\{ T_{dis} - T_{ref} . \ln\left(\frac{T_{dis}}{T_{dis} - \Delta T_{dis}} \right) \right\} \,, \tag{20}$$

Generation

$$\dot{Q}_{HP} = (\dot{Q}_h + \dot{Q}_{loss,HS} + \dot{Q}_{loss,dis}).(1 - F_S).\frac{1}{\eta_{HP}}, \tag{21}$$

$$P_{aux,HP} = p_{aux,HP}.(\dot{Q}_h + \dot{Q}_{loss,HS} + \dot{Q}_{loss,dis}), \tag{22}$$

$$\dot{E}x_{HP} = \dot{Q}_{HP}.F_{q,S}, \tag{23}$$

$$P_W = \frac{V_W.\rho.C_p.\Delta T_{DHW}.no_o}{\eta_{DHW}}, \tag{24}$$

$$\dot{E}x_{plant} = \left(P_l + P_V\right).F_{q,el}, \tag{25}$$

3.3 Energy transformation

$$\begin{aligned}\dot{E}_{p,tot} &= \dot{Q}_{HP}.F_P + (P_l + P_V + P_{aux,HP} + P_{aux,dis} + P_{aux,HS}).F_{p,el} \\ &+ P_W.F_{DHW}\end{aligned}, \tag{26}$$

$$\dot{E}_R = \dot{Q}_{HP}.F_R + \dot{E}_{env}, \tag{27}$$

$$\begin{aligned}\dot{E}x_{tot} &= \dot{Q}_{HP}.F_p.F_{q,s} + (P_l + P_V + P_{aux,HP} + P_{aux,dis} + P_{aux,HS}).F_{p,el} \\ &+ \dot{E}_R.F_{q,R} + P_W.F_{DHW}.F_{q,S,DHW}\end{aligned}, \tag{28}$$

3.4 Energy and exergy inputs

$$\dot{E}''_{tot,pa} = \frac{\dot{E}_{tot}}{A_N}, \tag{29}$$

$$\dot{E}''_{tot,pv} = \frac{\dot{E}_{tot}}{V_N}, \tag{30}$$

$$\dot{E}x''_{tot,pa} = \frac{\dot{E}x_{tot}}{A_N}, \tag{31}$$

$$\dot{E}x''_{tot,pv} = \frac{\dot{E}x_{tot}}{V_N}, \tag{32}$$

3.5 Energy and exergy efficiencies

$$\eta_{sys} = \frac{\dot{E}_{building}}{\dot{E}_{tot}}, \tag{33}$$

$$\psi_{sys} = \frac{\dot{E}x_{building}}{\dot{E}x_{tot}}, \tag{34}$$

3.6 Exergy destruction and flexibility

$$\dot{E}x_{dest} = (1-\psi_{sys})\dot{E}x_{tot}, \tag{35}$$

$$F_{flex} = \frac{\dot{E}x_{HS}}{\dot{E}x_{tot}}, \tag{36}$$

3.7 Exergy efficiency and sustainable index

$$\psi = 1 - \frac{1}{SI}, \tag{37}$$

$$SI = \frac{1}{1-\psi}, \tag{38}$$

While applying calculations (1) – (38), assumptions made for heating and cooling modes are listed in Table 2.

Table 2. Assumptions made

Parameter	**Unit**	**Symbol**	**Value**
Air exchange rate	ach/h	n_d	0.6
Heat exchanger efficiency	-	η_V	0.8
Specific heat of indoor air	kJ/kgK	C_p	1.005
Density of indoor air	kg/m^3	ρ	1.2
Window frame fraction	-	F_f	0.8
Total transmittance	-	g_j	0.58
Solar radiation: SE to SW, NW to NE	W/m^2	$I_{s,j}$	20 50
Emitted heat per occupant	W/person	$\dot{Q}''_o$	130
Specific internal gains of equipment	W/m^2	$\dot{Q}''_e$	0.04
Specific lighting power	W/m^2	p_l	5
Specific ventilation power	W/m^2	p_V	32.142
Temperature drop	K		<5
Heat loss/efficiency	-	η_{dis}	0.86
Auxiliary energy	W/kW$_{heat}$	$p_{aux,dis}$	2.24
Solar fraction	-	F_S	0
Radiator inlet temperature	°C	T_{in}	35
Radiator return temperature	°C	T_{ret}	25
Auxiliary energy	W/kW$_{heat}$	$p_{aux,HS}$	0.01
Max. heat emission	W/m^2	$p_{heat,\max}$	34
Heat loss/efficiency	-	η_{HS}	0.95
Efficiency	-	η_{CB}	-
Primary energy factor source	-	F_P	-
Quality factor of source	-	$F_{q,S}$	-
Max. supply temperature in cooling / heating	°C	$T_{CB,max}$	11/35
Auxiliary energy	W/kW$_{heat}$	$p_{aux,Gen}$	10
Auxiliary energy constant	W	$P_{aux,gen,const}$	-
Primary energy electricity factor	-	$F_{P,el}$	3

3 Results and Discussion

In this study, energetic, exergetic and sustainability performances of a public bus with a volume of 70 m^3 and a floor area of 30 m^2 are evaluated. Calculations given by Equations

(1) – (38) are made under the climatic conditions of Izmir in Turkey. Using the assumptions made given in Table 2, total heating and cooling demands are calculated as 12,685.40 W and 28,681.25 W, respectively. Heat loss rates based on Equations (1) - (7) for the heating mode are 3,680.12 W for transmission and 10,203.28 W for ventilation, fresh air and infiltration. There are no occupants and solar heat gain assumption is made for getting maximum heat demand of the system. But internal heat gains from equipment utilization, lightning and ventilation power are calculated to be 1.048 W, 150 W and 1,349.96 W, respectively.

Heat gain rates calculated from Equations (1) - (7) for the cooling mode are determined to be 656.05 W for transmission and 10,195.28 for ventilation, fresh air and infiltration regarding latent heat loss affect. This effect led to find almost the same amount with the value occurs in the heating mode although the temperature difference is 9 °C (almost half of the heating mode 20°C). Heat gain rates are 12,870 W for occupants, 1,048 W for appliances, 150 W for lightening and 1,349.96 W for ventilation power, respectively.

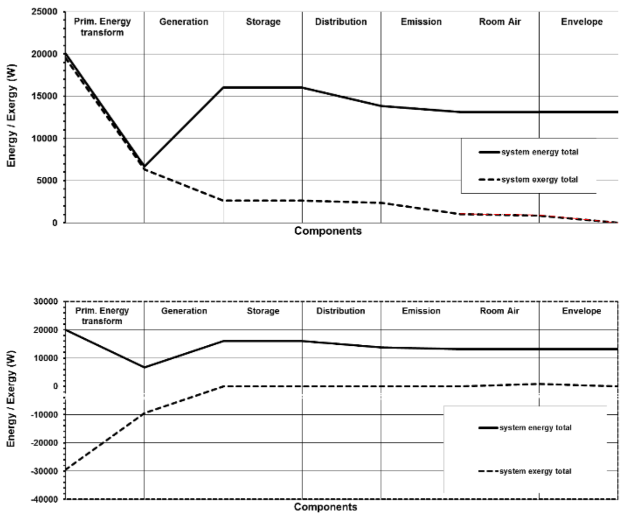

Figure 2. Exergy and energy flows through components for heating and cooling modes

After calculations of total heating and cooling demands, both energy and exergy flows and losses of the system in a heating or cooling mode in terms primary energy transformation, generation, storage, emission, indoor air and envelope amounts are determined and can be seen in Figure 2 where one can say that the system has to supply 19,536.22 W and 29,495.55 W primary energy rates for heating and cooling modes, respectively. The highest heat loss occurs after primary energy transformation with 13,375.74 W both in the heating and cooling modes. For the heating mode, exergy losses are followed by 3,785.85 W (generation), 261.48 W(distrubition), 1.366,77 W(emission), 187.04 W(inside air) and 895.81 W (envelope) respectively as can be seen from Figure 3 given below.

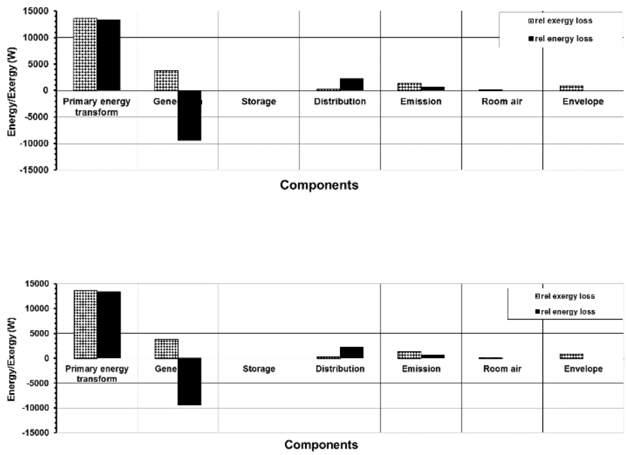

Figure 3. Exergy losses/consumption by components for heating and cooling modes

4 Conclusions

In this study, energy and exergy analyses for sustainability are handled and applied to the cooling and heating options of a mobile HVAC system for a public bus in Izmir.
The main concluding remarks can be listed as follows:

- Specific energy input rates (primary and renewable energy + internal and solar gains) of the system are 1,045.17 W/m^2 and 447.93 W/m^3 in the heating mode, 1,223.47 W/m^2 and 524.34 W/m^3 in the cooling mode, respectively.
- Total exergy efficiency values of the entire system (exergy demand room/total exergy input) are obtained to be 4.4% and 2.9% for the heating and cooling modes, respectively.

Exergy flexibility factor (exergy demand emission/total exergy input) is determined to be 0.121 for the heating mode

Acknowledgements

The authors would like to thank the SAFKAR Inc. for sharing some basic data on the mobile HVAC system studied

Nomenclature

A	area (m^2)
c_p	specific heat at constant pressure (kJ/kg.K)
$\dot{E}$	energy rate (W)
$\dot{E}x$	exergy rate (W)
f	approximation factor (-)
F	factor (-)
g	total transmittance (-)
I	radiation intensity (W/m^2)
l	length (m)
N	percentage of equipment resistance
n_d	air exchange rate (1/h)
no	number (-)
P	power (W)
p	specific power, pressure (W/m^2, N/m^2)
$\dot{Q}$	heat transfer rate (kW)
R	pressure drop of the pipe (Pa/m)
R_R	renewability ratio (-)
SI	sustainability index (-)
T	temperature (K)
U	thermal transmittance (W/m^{2}K)
$\dot{V}$	volumetric flow rate (m^3/s)
V	volume (m^3)

Greek letters

η	energy efficiency (-)
ψ	exergy efficiency (-)
ρ	density (kg/m^3)
Δ	difference

Subscripts

air	indoor air
aux	auxiliary energy requirement
circ	circulation
dest	destruction
dis	distribution system
dt	design temperature
En	energetic
Ex	exergetic
e	equipment
el	electricity

env	environment
ex	external
f	window frame, parameter
flex	flexibility
HP	heat production system
HPP	heat production system position
HS	heating system
h	heat
heat	heater
i	indoor, counting variable
in	input, inlet
ins	insulation
j	counting variable
l	lighting
loss	thermal losses
max	maximum
N	netto
no	effect of non-orthogonal radiation
o	outdoor, occupants
p	primary energy
pa	per area
plant	plant
pv	per volume
q	quality
R	renewable energy
ref	reference
ret	return
S	solar
s	source
sh	shading effects
sys	system
T	transmission
td	temperature drop
tot	total
usf	useful
V	ventilation
w	window, water
x	part x

Superscripts

over dot rate

Abbreviations

COP	coefficient of performance
DHW	domestic hot water
ECBCS	energy conservation in buildings and community systems programme
IEA	international energy agency
LowEx	low exergy

References

[1] A. Hepbasli, "Low exergy modelling and performance analysis of greenhouses coupled to closed earth-to-air heat exchangers (EAHEs)," Energy Build., vol. 64, pp. 224–230, 2013.labi and J. Smith, *Title of the book*. London: John-Wiley, 2003.

[2] D. Schmidt, "Low exergy systems for high-performance buildings and communities," *Energy Build.*, vol. 41, no. 3, pp. 331–336, 2009.

[3] F. Meggers, V. Ritter, P. Goffin, M. Baetschmann, and H. Leibundgut, "Low exergy building systems implementation," *Energy*, vol. 41, no. 1, pp. 48–55, 2012.

[4] EN 14750-1, Railway applications - Air conditioning for urban and suburban rolling stock, Part1: Comfort parameters, 2006.

[5] A. Hepbasli and N. Yildirim, "Exergetic and Sustainability Evaluation of a Building Heating System in Izmir, Turkey," vol. 8, no. 9, pp. 1003–1011, 2014.

10TH INTERNATIONAL CONFERENCE ON SUSTAINABLE ENERGY AND ENVIRONMENTAL PROTECTION (JUNE 27TH – 30TH, 2017, BLED, SLOVENIA), ENERGY EFFICIENCY
J. Krope, A.Ghani Olabi, D. Goričanec & S. Božičnik

Cycle of Power and Steam Generation in Sugar-Energy Industries

MAYKON CESAR SPOLTI FERREIRA, JOAO MARCOS RONCARCI MARI, MARCUS VINICIUS RONCARI MARI, W. A. S. CONCEIÇÃO & CID MARCOS GONCALVES ANDRADE

Abstract Ethanol is an ecologically alternative fuel in relation to gasoline and diesel, in many situations, the production of ethanol or sugar are at market mercy. This work has approached the theme of application of cycle of power and steam generation in sugar-energy industries, trying to clarify the doubt: "Is there a standardization, with regard of flow diagram, at the cycles of power and steam generation in sugar-energy industries?". Therefore, it was accomplished a bibliographic review, introducing the historical of sugar-energy sector, introducing too about the process of sugar and ethanol production and finally, treated the way that the sugar-energy industries run at the perspective of final product and the cycle of power and steam. At the end of bibliographic review, it has demonstrated that the cycle of power and steam differ between the industries by their final product and the needs of each sugar-energy industry.

Keywords: • Sugar-energy • Ethanol • Industry • Generating • Flow diagram •

CORRESPONDENCE ADDRESS: Maykon Cesar Spolti Ferreira, Master's degree students, Mechanical Engineering Department, Technology Center, State University of Maringá, Paraná, Brazil; email: spolti.maykon@gmail.com. Joao Marcos Roncarci Mari, Master's degree students, Mechanical Engineering Department, Technology Center, State University of Maringá, Paraná, Brazil; email: spolti.maykon@gmail.com. Marcus Vinicius Roncari Mari, Master's degree students, Mechanical Engineering Department, Technology Center, State University of Maringá, Paraná, Brazil; email: spolti.maykon@gmail.com. W. A. S. Conceição, Professor, Mechanical Engineering Department, Technology Center, State University of Maringá, Paraná, Brazil; email: wasconceicao@gmail.com. Cid Marcos Goncalves Andrade, Professor, Chemical Engineering Department, Technology Center, State University of Maringá, Paraná, Brazil; email: cmgandrade@uem.br.

https://doi.org/10.18690/978-961-286-050-9.23 ISBN 978-961-286-050-9

Available at: http://press.um.si.

1 Introduction

The sugar-energy sector are companies, private limited companies or public limited companies, which process biomass to the purpose of obtaining sugar, ethanol and electricity energy. According to [1], the production of ethanol can be obtained using diverse raw materials, such as sugar cane, corn, potatoes, wheat, among others.

The history of sugar-energy sector varies from country to country. Ethanol production in the US from 1980 to 2000 was very low, rising dramatically after 2005 with the first standards on renewable fuels, as explains [2]. Just like in Colombia, which, according to [3], it is beginning, in recent years, to increase the production of ethanol.

Some factors are responsible for the behavior presented by the history of the sugar-energy industries, among them, according [2], [4], requirements for fuels that are less aggressive to environment and, as explains [2], [4]–[7], the sugar and ethanol international market.

Brazil is at the vanguard of world sugar and ethanol producers, as assert [3], with around 45 % of the world's ethanol production and containing in its territory , more than 400 plants in operation, as noted in [3], [8].

The production of sugar in Brazil is an activity that dates back to the beginning of the 16th century. The mosaic crisis of 1920 provided an increase in the technology of the sector, in which new species of sugar cane were developed. Due to the market, the production of ethanol had as purpose to absorb the excess of the production of sugar.

The Brazilian production of ethanol suffered a significant increase between the years 1921 and 1970 due to the policy of ethanol, which aimed at the use of ethanol in mixture with imported gasoline, as explains [9].

In 1970, according to [10], due to the oil crisis, the Brazilian government created the Proálcool program, which aimed to stimulate the production of ethanol with the purpose of replacing petroleum products, which resulted in the increase of sugarcane industries in Brazilian territory up to the present day.

Due to the greater requirements on the environment, the demand for ethanol in the world tends to grow, resulting in greater foreign investments in Brazil and in other sugar and ethanol producing countries, as assert [5], [7]. Knowing this, it is necessary to clarify a doubt, which is not so common: "on the production of sugar and ethanol, is there a standardization in the flow chart of the sugarcane plants?". Thus, the objective of this work is to seek to answer this question through a bibliographical review.

2 Methodology

The methodology of this work will be, through a bibliographical review, comment on the process of obtaining sugar and fuel alcohol and after, it will be comment on the mode of operation of the plants with regard to steam flow chart.

3 Process of Sugar and Ethanol Obtainment

Approximately 60% of sugar production marketed in the world comes from sugar cane, the other 40%, from beet, as assert [11].

The method of obtaining sugar for the two raw materials differ only at the beginning of the process, as seen in [11]–[15].

As commented by [12], the name of the stages may vary from industry to industry, but the sequence of obtaining sugar and ethanol remains the same.

3.1 Process of sugar obtainment

Initially, as assert [12], the sugar cane is crushed in the hoppers, as can be seen on Figure 1, with the intention of extracting the raw juice (cane juice), which is rich in sucrose. At the same stage, the bagasse is mix with water in order to extract more sucrose. From the stage of hoppers then, obtaining the bagasse and the raw juice.

The initial process for the beet consists of a cleaning with water for the removal of any impurity, so the beet is slice into long, thin pieces, called cossetes. The extraction of the sucrose then occurs by diffusion, submerging the cossetes in water at 70-73 ° C, obtaining raw juice, as asserts [11], [13], [15].

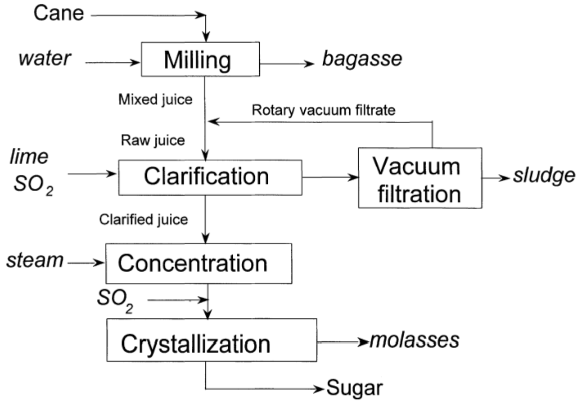

Figure 1. Process of obtainment of sugar by sugar cane. [16]

In sequence, for both of raw materials, as comment [12], [14], the raw juice is transferred to an alkalization tank and is called the clarification stage. At this stage, raw juice, as assert [11], is heated to 80-90 ° C and is clarified by two distinct steps, as discussed in [13], first is added calcium oxide (CaO) and subsequent carbonation. This stage aims to precipitate the non-sugars from the raw juice for subsequent extraction. The precipitated material is remove by filtration while the refined juice goes to the next stage.

The refined juice, is then, heated to the boiling point and transferred to the evaporation tanks in order to evaporate the water present in the refined juice, as assert [14]. The evaporation stage, according to [12], Consists of about three steps. In the first step, there is the refined juice flow through the evaporator, evaporating about 80% water, with the resulting product being the syrup. The other two steps aims to further, reduce the concentration of water. At the end of this stage, the product is molasses.

The molasses then is transfer to the stage of crystallization, which is form by two stages. First the molasses passes through the crystallizer, where the rest of water is evaporated, as assert [14], and in sequence is transferred to the centrifugation, where the crystallized sugar is separated from the molasses. Of this process, has the sugar and molasses as the final product.

3.2 Process of ethanol obtainment

As stated [1], [17]–[21] comment on the possibility of obtaining ethanol for a range of raw materials. According to [17], there are three ways of obtaining ethanol, by lignocellulose materials (agricultural residues, biomass, etc.), starch-based materials (cereals, corn, etc.) and sugar-based materials, such as sugar cane, beet, etc. Products (biogas, CO2, etc.), as can be seen in Figure 2.

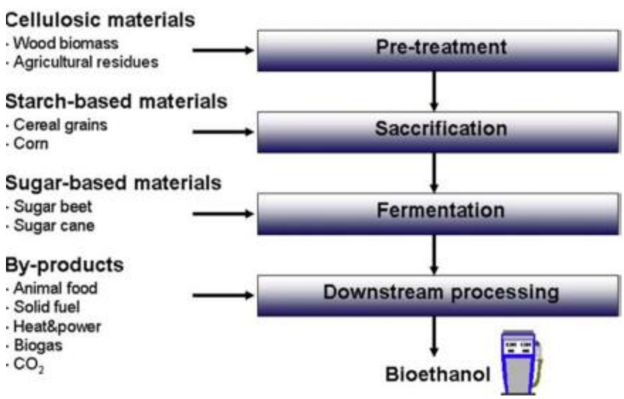

Figure 2. Process of ethanol production by range raw materials. [17].

The process of obtaining ethanol varies among raw materials. As explains [18], the conversion of lignocellulose material to ethanol has four steps. The first stage, called pretreatment, has the purpose of disorganizing the crystalline structure of the biomass, removing components that may prevent or hinder the next process.

Then, as assert [18], occurs the hydrolysis, whose purpose is to transform the sugars, present in the crystalline structure of the biomass, into pentose and hexose. This step can occur by chemical or enzymatic hydrolysis, depending of company-to-company.

The third stage called fermentation; it is at this stage that the pentose and hexose are transform into ethanol, using microorganisms, which can be bacteria, fungi or yeasts. The product resulting from the fermentation called beer and contains between 7 and 10% of ethanol.

Finally, two variants of the distillation may occur, depending on the final product that the industry needs. As assert [18], the beer is then distilled by steam, producing hydrated ethanol. Depending on the needs of the company, it can distilled a second time the hydrated ethanol, producing anhydrous ethanol.

It can be seen of Figure 2, that for sugar-based materials, as explains [19], [20], after the extraction of the raw juice, it undergoes fermentation and distillation. For starch-based materials, as asserts [17], [21], this it undergoes hydrolysis to obtain pentose and hexose and then goes on to fermentation and distillation. Thus, for lignocellulose materials, there are four stages until ethanol is obtain, for starch-based materials, three stages and finally two-stage for sugar-based materials.

4 Steam Cycle

In sugar-energy industries, the use of steam has the purpose of transferring energy, in which energy stored in the form of water vapor supplies the energetic demand of the company. According with [22], some industries use steam, not only for energy transfer, but for electricity generation. For this, the steam is superheat above the saturation temperature in order to undergo expansion in the turbine, generating electricity. The steam, after undergoing expansion, leaves the turbine, at different temperatures and pressures, and is distributed by the company's processes, as asserts [23], [24].

The use of steam, as an energy carrier, is not only about for reducing energy prices, but also, about the benefits that this process brings to the company, such as operability, flexibility and better transient operations, as commented by [22]. [24]–[28] comment that steam production can be divide into three parts, high-pressure steam, medium pressure steam and low-pressure steam. The high-pressure steam has a configuration of the order of 60 bar, the medium pressure steam, 22 bar and the low-pressure steam of the order of 6 bar. According with [23], in sugar energy industries, the choice of sugar and ethanol production influences the company's steam generation, since the need of steam for sugar and ethanol processes is different.
For the process of obtaining sugar, the initial stage is the one that most needs steam, since, the medium pressure steam is intended to be used in the hoppers, as asserts [23]–[26],

while in stages requiring diffusion, low-pressure steam is used, as commented by [25]. Clarification is another stage that uses steam, but in this case, the steam used has low pressure, as assert [25]. [29], [30] comment that the evaporation process uses low-pressure steam, this is done in order to heat and maintain the temperature of the refined juice in the evaporators. Finally, the crystallization stage uses low pressure steam, as commented by [23], [30].

In the process of obtaining ethanol, the distillery and hoppers are the stages that most require steam, as asserts [24], [30], the hoppers require medium pressure steam and the distillery, steam at low-pressure, as commented by [23].

As studied by [23], the industry has produced steam at 100 bar and 530 ° C, for [24], the industry has produced steam at 27,6 bar and 530°C, [25] approaches an industry that produces steam at 21 bar and 300°C, for [26], the industry has produced steam at 80 bar and 480°C and finally, for [30], 22 bar and 300°C.

On average, the medium pressure steam, that is used in all plants was in the range of 20 to 22 bar, while the low pressure steam was in the range of 6 to 2 bar, with steam at 6 bar being used in the distillery, as assert [23], and the steam between 2 and 2.5 bar, used to supply the remaining energy demand, as commented by [23], [25], [26], [29], [30].

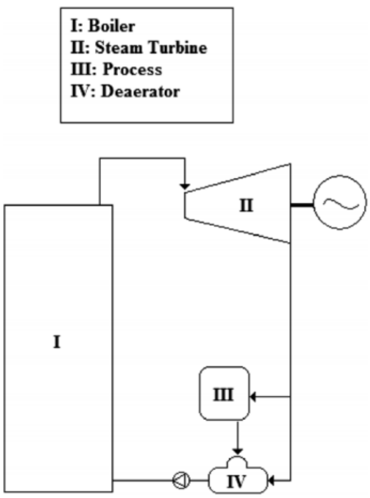

Figure 3. Steam cycle flow chart.[30]

The Figure 3 represents the simplified flow chart of the plant studied by [30], in which, the steam leaves the boiler (I) at 22 bar and 300 ° C, is expanded in the turbine (II), generating electrical energy and then, part of the exhaust vapor is directed to the process (III) and the remainder to the Deaerator (IV).

The process of steam integration, studied by [23], [25], [26], [28], reduce the steam demand in the plant due to the reuse of the vapors generated in the process. However, these integrations alter the steam flow diagram in the plants. According with [25], [26], The vapor produced in the evaporator, by the evaporation of the water present in the refined juice, can be used on steam integration.

Already [25], [30] comment on industries that use high-pressure steam for generation of electric power, with this, the same company can have several configurations of steam cycles, depending on its purpose. Some variations of the flowchart described by Figure 3 are described by [30], one of them can be seen in the Figure 4, in which the high pressure steam leave the boiler, enters the two-stage turbine, in the first stage, the steam is directed to the process and the deaerator, while the exhaust steam (last stage) is directed to the condenser.

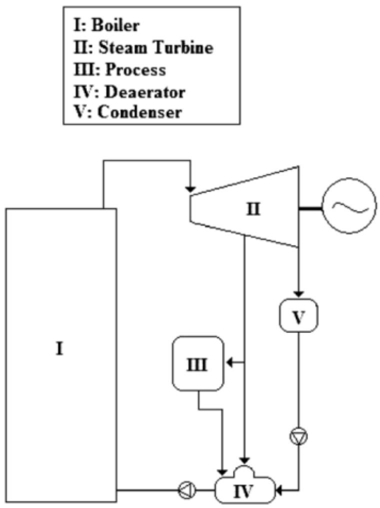

Figure 4. High-pressure steam cycle flow chart.[30]

The Figure 3 and Figure 4 represents only the global change of flow chart between a sugar-producing industry, or sugar and ethanol industry to a sugar-energy industry. Within process (III), the steam may have a different flowchart from industry-to-industry, according to the raw material used and the final product desired, as be seen in [23]–[30].

It can be observed that there is a heterogeneity in the sugar-energy sector, from centennial mills with production of sugar or sugar and ethanol, to new mills, using the latest technologies, as commented by [5]. Therefore, due to this heterogeneity, for the sugar-energy industries, there is no standardization of the steam cycle, that is, each company has its own steam cycle that differs from others in the sector

5 Conclusion

The sugar-energy industry go back to past centuries, and have evolved considerably over the years.

Its main producer of sugar and ethanol is Brazil. Sugar and ethanol can be obtain from a number of sources of raw material, changing only the complexity of the stages, where complexity varies from one type of raw material to another.

Due to the heterogeneity of the industry, caused by different objectives (generation of energy, final product, technology) from company-to-company, there is no standardization in the steam cycle, resulting in a difficulty to establish studies of energy and exergy that aims to improve the efficiency of the sector generally

Acknowledgements

This work has been realized with support of Coordenação de Aperfeiçoamento de Pessoal de Nível Superior (CAPES) – Brazil

References

[1] J. F. Reyes-Aroca and C. A. Vidaurre-*Parra, "Technical and Economical* Analysis of a Combined Biogas-Ethanol-Biodiesel Plant in Central Chile," *Agrociencia*, vol. 47, no. 6, pp. 621–632, 2013.

[2] B. A. Mccarl and A. Texas, "Impacts of U.S. Production-Dependent Ethanol Policy on Agricultural Markets," 2016.

[3] B. M. Julca-brice and M. F. Neves, "Caracterización de sistemas agroindustriales : un estudio comparativo de los sectores sucroenergéticos de brasil y colombia Bryan Manuel Julca-Briceño y Marcos Fava Neves," vol. 36, no. May, pp. 356–364, 2011.

[4] J. E. R. Morales and F. R. López, "Regulación, política agro-energética y la evolución del mercado de carburantes renovables en Brasil," *Derecho PUCP Rev. la Fac. Derecho*, no. 75, pp. 355–384, 2015.

[5] C. N. Pereira, "Análise exploratória da eficiência produtiva das usinas de cana-de-açúcar na região centro-sul do Brasil com o método análise envoltória de dados (DEA) - índice de Malmquist," p. 140, 2012.

[6] P. L. Cruz, "Análisis del Sector Azucarero y Etanol," *Cuad. Adm.*, vol. 43, pp. 99–112, 2010.

[7] S. S. O. Caso, D. A. Empresa, and E. T. H. Bioenergia, "Estratégias de novos empreendimentos internacionais no setor sucro-alcooleiro: o caso da empresa eth bioenergia," *Strategies*, pp. 66–92, 2009.

[8] D. A. Salla, F. D. P. B. Furlaneto, C. Cabello, and R. A. D. Kanthack, "Avaliação energética da produção de etanol utilizando como matéria-prima a cana-de-açúcar," *Ciência Rural*, vol. 39, pp. 2516–2520, 2009.

[9] F. B. Dunham, J. V. Bomtempo, and D. L. Fleck, "A Estruturação do Sistema de Produção e Inovação Sucroalcooleiro como Base para o Proalcool," *Rev. Bras. Inovação*, vol. 10, no. 1, pp. 35–72, 2011.

[10] BiodieselBR, "ProÁlcool: História da indústria sucroalcooleira," 2006. [Online]. Available: https://www.biodieselbr.com/proalcool/pro-alcool/programa-etanol.htm. [Accessed: 30-Mar-2017].

[11] S. Gul and M. Harasek, "Energy saving in sugar manufacturing through the integration of environmental friendly new membrane processes for thin juice pre-concentration," *Appl. Therm. Eng.*, vol. 43, pp. 128–133, 2012.

[12] G. Montoya, J. Londoño, P. Cortés, and O. Izquierdo, "Quantitation of trans-Aconitic Acid in Different Stages of the Sugar-Manufacturing Process," *J. Agric. Food Chem.*, vol. 62, no. 33, pp. 6–10, 2014.

[13] J. Klein, J. Altenbuchner, and R. Mattes, "Nucleic acid and protein elimination during the sugar manufacturing process of conventional and transgenic sugar beets," *J. Biotechnol.*, vol. 60, no. 3, pp. 145–153, 1998.

[14] S. Chantasiriwan, "Distribution of juice heater surface for optimum performance of evaporation process in raw sugar manufacturing," *J. Food Eng.*, vol. 195, pp. 21–30, 2017.

[15] S. Lissane Elhaq, F. Giri, and H. Unbehauen, "Modelling, identification and control of sugar evaporation - theoretical design and experimental evaluation," *Control Eng. Pract.*, vol. 7, no. 8, pp. 931–942, 1999.

[16] A. M. Ghosh, M. Balakrishnan, M. Dua, and J. J. Bhagat, "Ultrafiltration of sugarcane juice with spiral wound modules: On-site pilot trials," *J. Memb. Sci.*, vol. 174, no. 2, pp. 205–216, 2000.

[17] F. Lipnizki, "Membrane process opportunities and challenges in the bioethanol industry," *Desalination*, vol. 250, no. 3, pp. 1067–1069, 2010.

[18] M. A. Kamzon, S. Abderafi, and T. Bounahmidi, "Promising bioethanol processes for developing a biorefinery in the Moroccan sugar industry," *Int. J. Hydrogen Energy*, vol. 41, no. 45, pp. 20880–20896, 2016.

[19] N. A. Brown *et al.*, "Transcriptional profiling of Brazilian Saccharomyces cerevisiae strains selected for semi-continuous fermentation of sugarcane must," *FEMS Yeast Res.*, vol. 13, no. 3, pp. 277–290, 2013.

[20] S. Sánchez-Segado, L. J. Lozano, A. P. de los Ríos, F. J. Hernández-Fernández, C. Godínez, and D. Juan, "Process design and economic analysis of a hypothetical bioethanol production plant using carob pod as feedstock," *Bioresour. Technol.*, vol. 104, pp. 324–328, 2012.

[21] B. Amigun, D. Petrie, and J. Görgens, "Economic risk assessment of advanced process technologies for bioethanol production in South Africa: Monte Carlo analysis," *Renew. Energy*, vol. 36, no. 11, pp. 3178–3186, 2011.

[22] F. Maréchal and B. Kalitventzeff, "Targeting the optimal integration of steam networks: Mathematical tools and methodology," *Comput. Chem. Eng.*, vol. 23, no. SUPPL. 1, pp. 5133–5136, 1999.

[23] E. a. Pina, R. Palacios-Bereche, M. F. Chavez-Rodriguez, A. V. Ensinas, M. Modesto, and S. a. Nebra, "Reduction of process steam demand and water-usage through heat integration in sugar and ethanol production from sugarcane – Evaluation of different plant configurations," *Energy*, 2015.

[24] M. Ali Mandegari, S. Farzad, and J. F. Görgens, "Economic and environmental assessment of cellulosic ethanol production scenarios annexed to a typical sugar mill," *Bioresour. Technol.*, vol. 224, pp. 314–326, 2016.

[25] L. F. Pellegrini and S. de Oliveira Junior, "Combined production of sugar, ethanol and electricity: Thermoeconomic and environmental analysis and optimization," *Energy*, vol. 36, no. 6, pp. 3704–3715, 2011.

[26] M. Modesto, R. J. Zemp, and S. A. Nebra, "Ethanol Production from Sugar Cane: Assessing the Possibilities of Improving Energy Efficiency through Exergetic Cost Analysis," *Heat*

Transf. Eng., vol. 30, no. 4, pp. 272–281, 2009.

[27] T. Taner and M. Sivrioglu, "Energy-exergy analysis and optimisation of a model sugar factory in Turkey," *Energy*, vol. 93, pp. 641–654, 2015.

[28] V. Lundberg, E. Axelsson, M. Mahmoudkhani, and T. Berntsson, "Process integration of near-neutral hemicellulose extraction in a Scandinavian kraft pulp mill - Consequences for the steam and Na/S balances," *Appl. Therm. Eng.*, vol. 43, pp. 42–50, 2012.

[29] Y. Casas, J. Dewulf, L. E. Arteaga-Pérez, M. Morales, H. Van Langenhove, and E. Rosa, "Integration of Solid Oxide Fuel Cell in a sugar-ethanol factory: Analysis of the efficiency and the environmental profile of the products," *J. Clean. Prod.*, vol. 19, no. 13, pp. 1395–1404, 2011.

[30] A. V. Ensinas, S. A. Nebra, M. A. Lozano, and L. M. Serra, "Analysis of process steam demand reduction and electricity generation in sugar and ethanol production from sugarcane," *Energy Convers. Manag.*, vol. 48, no. 11, pp. 2978–2987, 2007.

Informatics Solution for Energy Efficiency Improvement and Consumption Management

SIMONA VASILICA OPREA, ADELA BÂRA & ADRIANA REVEIU

Abstract Although, in 2012 European Union has promoted the energy efficiency in order to ensure a 20% reduction of energy consumption by 2020, gradually, its targets related to energy efficiency increase and extend to new time horizons. Therefore, in 2016, a new proposal for 2030 of energy efficiency target of 30% has been agreed. However, during the last previous years, although the electricity consumption by households decreased in the EU-28, the largest expansion was recorded in Romania.

Energy consumption management for residential activities is an important measure for energy efficiency improvement. In this paper, we proposed an informatics solution as prototype that helps electricity consumers to identify those energy intensive appliances. The informatics solution includes three modules regarding electricity consumption optimization, profiles and forecast. By this solution, the appliances can be scheduled in order to minimize the peak consumption and reduce the stress on the grid.

Keywords: • Energy efficiency • Consumption management • Informatics solution • Optimization • Profiles and forecast consumption •

CORRESPONDENCE ADDRESS: Simona Vasilica Oprea, Ph.D., Assistant, University of Economic Studies, Faculty of Cybernetics, Statistics and Informatics, 6 Romana Square, Bucharest, Romania, e-mail: simona.oprea@csie.ase.ro. Adela Bâra, Ph.D., Professor, University of Economic Studies, Faculty of Cybernetics, Statistics and Informatics, 6 Romana Square, Bucharest, Romania, e-mail: bara.adela@ie.ase.ro. Adriana Reveiu, Ph.D., Associate Professor, University of Economic Studies, Faculty of Cybernetics, Statistics and Informatics, 6 Romana Square, Bucharest, Romania, e-mail: reveiua@ase.ro.

https://doi.org/10.18690/978-961-286-050-9.24 ISBN 978-961-286-050-9

Available at: http://press.um.si.

1 Introduction

Energy efficiency targets to reduce greenhouse gas emissions, improve energy security, enhance competitiveness and sustainable development of entire society.

The European Union has committed itself in 2007 to energy and climate change objectives for 2020. It comprises a 20 % reduction of energy consumption by the year 2020 compared to baseline projections, higher share of renewable energy of 20 % and reduction of emissions by 20 % [1]. In 2012, the EU adopted Directive 2012/27/EU on energy efficiency that establishes a common framework of measures for the promotion of energy efficiency within the EU in order to ensure a 20 % reduction of energy consumption by the year 2020. Gradually, the EU targets related to energy efficiency increase and extend to new time horizons. Therefore, in October 2014, EU countries agreed on a new energy efficiency target of at least 27 % or greater by 2030. In November 2016, a new proposal for 2030 of binding energy efficiency target of 30 % for the European Union came up.

According to Eurostat, during the last ten years, although the households' electricity consumption decreased by 1.3% in the EU-28, among the EU members with higher electricity consumption, the largest expansions were recorded in Romania (48.1%), Lithuania (27.1%), Spain (21.8%), etc. [2].

Therefore, starting from the fact that our informatics solution attempts to handle the electricity consumption, in this article, we have described the main components of the electricity consumption management, proposed prototype architecture, presented informatics technologies and a few implemented functionalities for electricity consumers.

2 Related Works

Energy consumption management for residential, industrial and retailers' activities brings significant benefits to consumers, prosumers, suppliers and grid operators. In terms of electricity consumption optimization, we showed in [3], [4] that planning of appliances operation brings savings to consumers and decrease the hourly demand peak.

Also, in [3] the optimum capacity of a storage device (SD) that significantly contributes to peak shaving of electricity consumption for residential consumers is calculated. It is based on the solution of two optimization problems: payment minimization and consumption peak minimization. In order to minimize their electricity payment (bills), the consumers shift to lower tariff rates that are usually at night even though the photovoltaic panel does not generate. In case no SD is used, time-of-use tariff will lead to new peaks that would increase the electricity payment due to necessary investments in order to manage the new peaks. In case we consider the SD, it is noticed that its capacity does not depend on the operation of the PV, but rather programmable appliances. Based on the results of [3], the best approach is to use SD to effectively contribute to the peak minimization and PV to obtain some savings.

In [5], [6], authors developed methods for load profile calculation using self-organizing maps and applied classification or clustering in order to calculate accurate dynamic load profiles that could be used for electricity consumption forecasts, market settlements and optimization of consumption. In [6] based on the obtained results, the self-organizing maps are suitable for calculation of dynamic load profiles. Comparative analysis between [5] and [6] has shown that the best method for load profiles with specific patterns is clustering, while for well-delimited profiles, SOM is the most suitable method.

European Project Optimus aims to create a framework for assessing the local characteristics via the instrument OPTIMUS-SCEAF (Smart City Energy Assessment Framework) in the cities, develop a decision support system (DSS) to optimize energy use, implement it in three pilot European cities (Savona - Italy, San Cugat – Spain and Zaanstac - Netherlands) and make necessary training for expanding implementation of DSS [7].

Development of DSS for optimizing energy use by Optimus DSS has been initiated due to increased energy consumption in cities. They consume about two-thirds of the total consumption, are the largest sources of greenhouse gases and may affect about 70% of the total environmental footprint [8].

Optimus DSS is designed with the following modules: predictive module of consumption and production for renewable energy sources, statistics analysis module, consumers' profiles module and consumption of electricity and heat optimization module.

In [9] the authors built IntelligEnSia solution (Intelligent Home for Energy Sustainability) that is focused on the prediction analytic using Web and Android technologies. For prediction of the energy consumption, the authors applied three regression models. Their models predict the energy consumption based on the independent variable related to a particular day and dependent variables: current, voltage and power. The proposed models can support the decision making process in obtaining the energy consumption management.

In [10], the authors evaluated the impact of implementation of Energy Management System. It is based on energy consumption and contributes towards sustainable development. The article performs an experimental design, using Multiple Linear Regression to obtain a model that predicts energy consumption

3 Electricity Consumption Management Components

Base on emerging technologies such as smart metering systems, appliances, sensors, and communications, the advanced consumption management has been significantly enabled.

In our opinion, the electricity consumption management mainly implies the interaction among several components shown in figure 1, such as: smart metering system, programmable/non-programmable appliances, sensors, electricity consumption management instances (ECMI), control centre (CC) managed by electricity supplier and accessed by grid operator, authorities and/or regulators.

The informatics prototype may assist decisions regarding consumption management and is developed as an online accessible solution with three types of users: *electricity supplier* has access to all consumption data and interacts via messages with consumers; *consumer* has access to its consumption data by means of ECMI and *grid operator*, *authority* and/or *regulator* have access to consumption data for monitoring, analysing and reporting purposes.

Each consumer has access to his own ECMI via web interface that is developed in *Oracle Application Development Framework (ADF)*.

Consumption data is considered in the three prototype modules that are built up based on methods and specific algorithms: electricity consumption optimization module, profile module and forecast module

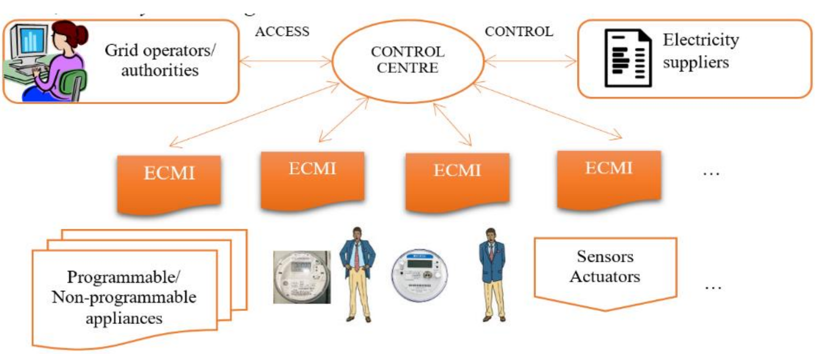

Figure 1. Electricity consumption management components

Through the interface, the consumer's consumption preferences and characteristics of electric appliances are added. Also the interfaces display information about the optimized consumption, tariff rates, payments, etc. Electric appliances and smart meters are connected through a sensors network designed to control electrical devices, storage resources (car batteries, UPS and other devices for energy storage), sources of generation and operation state (on/off, operation step). In figure 2, we described the main components of the control centre and ECMI. Also, through the interface, the consumer visualizes the hourly consumption, degree of network load, and various information from the supplier: electricity quality; tariff, trends, etc.

Based on customer input regarding appliances and his preferences, the optimization module available through CC optimizes the hourly consumption, providing the schedule of electric appliances

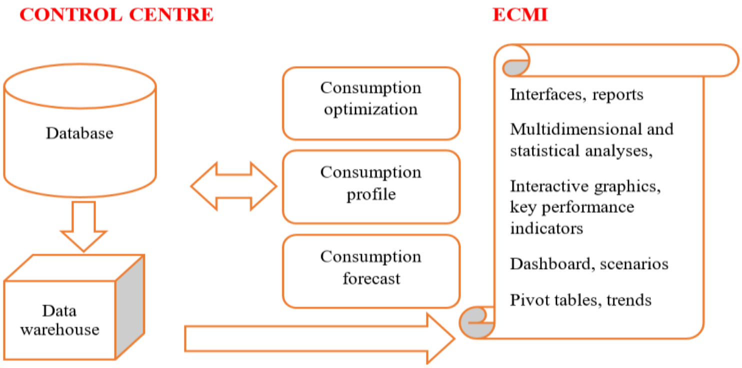

Figure 2. Control centre and ECMI main components

Optimizing individual consumption of each consumer is performed at the control centre level, the operation of the electric appliances is stored in the database and subsequently in the data warehouse. Consumption optimization process considers also the non-programmable appliances, such as: refrigerator, lighting etc., but it is achieved mainly through programmable appliances, such as washing machine, bread oven etc.

After consumption optimization, CC sends to each ECMI the planning (scheduling) consumption for a certain period of time, usually 24 hours. Compared with the present situation, when hourly consumption is unknown, based on detailed data collected from consumers, the supplier and network operator are able to analyse consumption and provide forecasts at the CC, which have a positive impact on grid operation planning and actions on electricity wholesale market. Also, based on the consumption data recorded at regular intervals of time (15 minutes), the consumption profiles can be obtained at different time intervals as well as consumption forecast with high accuracy

4 Prototype Architecture

For consumption management purposes, we developed an informatics prototype that allows advanced analyses for suppliers that include data visualization elements via dashboards, predictive analyses, *what if* scenarios, planning and reporting tools that are developed with *business intelligence* (BI) technologies.

Also, the prototype includes functionalities for consumers such as real-time consumption and tariff scheme visualization, alerts and consumption thresholds, comparisons between their consumption and similar consumption while preserving the data confidentiality, consumption estimations and predictions. In figure 3, the prototype architecture based on data, models and interfaces levels is shown. The proposed architecture is flexible to new technology tendencies related to appliances, sensors, smart meters, Internet of Things (IoT) etc

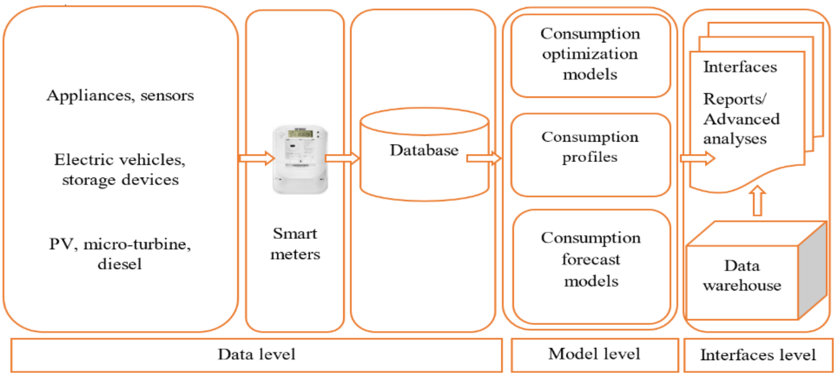

Figura 3. Informatics prototype architecture

5 Business Intelligence Interfaces' Prototype

In order to implement our informatics prototype that is mainly designed to serve the needs of consumers and electricity suppliers/grid operators, we used the following technologies: Oracle JDeveloper 12c with ADF; Oracle Database 11g R2; Oracle Business Intelligence Suite; Matlab R2015a; SAS Enterprise Guide.

After the optimization, the consumer can see the results as in Figure 4 in the form of optimum appliances operation schedule for the next 24 hours. Also, the consumer can see the information about electricity consumption by category of consumption during a selected period. In Figure 4, the consumer can view hourly optimal schedule operation of electric appliances for a given place of consumption

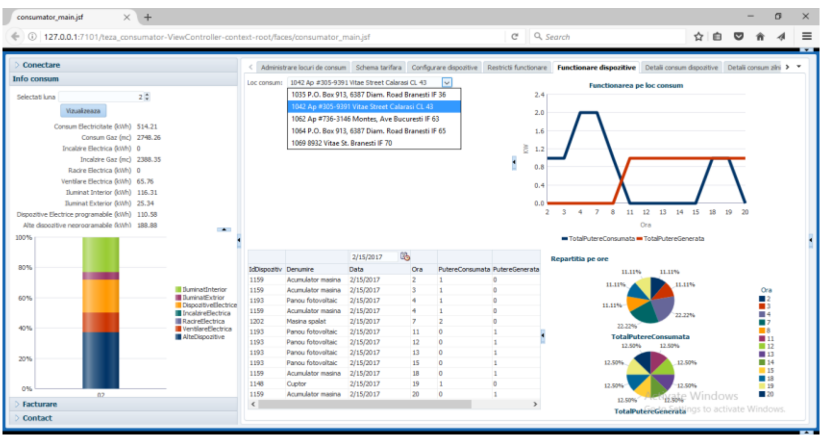

Figure 4. Appliances operation programming

In tables, the hourly consumption/generation data for each appliance is depicted. In Figure 5, the supplier views for each existing profile the number of consumers that belongs to that profile and their average consumption

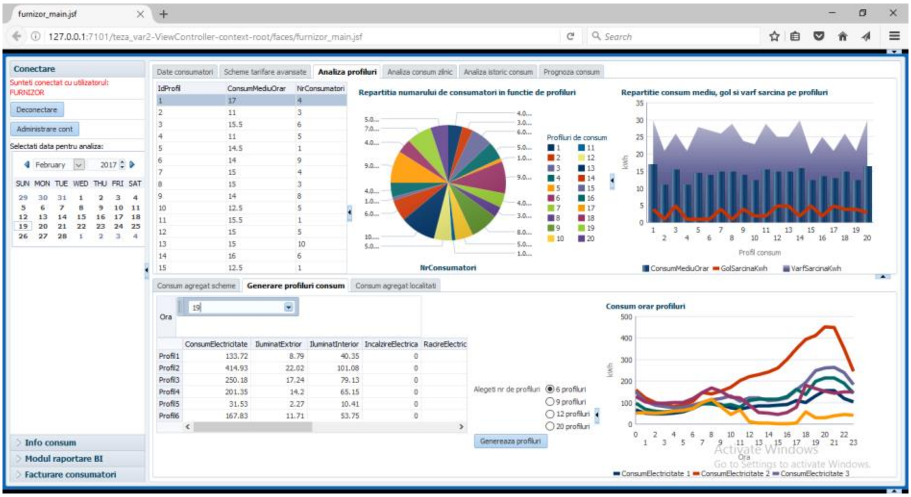

Figura 5. Consumption profiles management

Also, the supplier views the number of consumers for each profile and distribution on profiles of the average, peak and low consumption for a selected date. The supplier can reconfigure the existing profiles and this information helps the supplier to make decisions on tariff scheme implementation.

6 Conclusion

In this paper we presented an informatics solution for consumption management that assist both consumers and supplier in finding the best decisions regarding consumption optimization, identification of intensive appliances and profiles. Also, the solution leads to peak consumption and payment minimization, improves the consumption forecast accuracy and increase the awareness regarding the consumption management.

The solution is developed based on business intelligence technologies that offers friendly interfaces, both consumer and supplier being able to visualize data through interactive controls such as pivot tables, charts, maps, scenarios and gauges

Acknowledgements

This paper presents some results of the research project: Sistem inteligent pentru predicția, analiza și monitorizarea indicatorilor de performanță a proceselor tehnologice și de afaceri în domeniul energiilor regenerabile (SIPAMER),research project, PNII – Parteneriate în domeniile prioritare, PCCA 2013, code 0996, no. 49/2014 funded by NASR

References

[1] http://ec.europa.eu/eurostat/statistics-explained/index.php/

[2] http://ec.europa.eu/eurostat/statistics explained/index.php/Electricity_production,_consumption_and_market_overview

[3] S.V Oprea, A. Bara, M.E. Cebeci and O.B. Tör, *Promoting peak shaving while minimizing electricity consumption payment for residential consumers by using storage devices*, TURKISH JOURNAL OF ELECTRICAL ENGINEERING & COMPUTER SCIENCES, Turk J Elec Eng & Comp Sci, E-ISSN: 1303-6203, ISSN: 1300-0632, Available online: 31.03.2017, DOI: 10.3906/elk-1606-152

[4] SV. Oprea, *Informatics solutions for electricity consumption optimization*, 16th IEEE International Symposium on Computational Intelligence and Informatics – CINTI 2015,ISBN 978-1-4673-8520-6, IEEE Xplore,Budapesta Universitatea Obuda, http://conf.uni-obuda.hu/cinti2015/

[5] S.V. Oprea and A. Bâra, *Electricity load profile calculation using self-organizing maps*, 20th International Conference on System Theory, Control and Computing (ICSTCC), (Joint conference SINTES 20, SACCS 16, SIMSIS 20), 13-15 oct 2016, Sinaia, Romania, ISBN 978-1-5090-2720-0, IEEE Catalog Number CFP1636P-ART, ISBN 978-1-5090-2719-4, IEEE Catalog Number CFP1636P-DVD, pp. 860-865

[6] SV. Oprea, A. Bâra and I. Lungu, *Methods for electricity load profile calculation within deregulated markets*,19th InternationalConference on System Theory, Control and Computing Joint Conference SINTES 19, SACCS 15, SIMSIS 19,ISBN 978-1-4799-8481-7, IEEE Xplore, pag. 848 – 853, DOI: 10.1109,October 14 - 16, 2015 Cheile Gradistei - Fundata Resort, Romania, http://www.aie.ugal.ro/icstcc2015

[7] http://www.optimus-smartcity.eu/

[8] S. Zoellner, *Optimising Energy Use in Cities through Smart Decision Support Systems*, EU Sustainable Energy Week 2015 (EUSEW 2015), Workshop: Energy Management for Sustainable Action Plans, June 18, 2015, Brussels, Belgium

[9] A. Kewo, R. Munir and A. K. Lapu, *IntelligEnSia based Electricity Consumption Prediction Analytics using Regression Method*, The 5th International Conference on Electrical Engineering and Informatics 2015 August 10-11, 2015, Bali, Indonesia

[10] P. Golding, O. Hylton and V. Tennant, *The Impact of a ZigBee Enabled Energy Management System on Electricity Consumption Research-in-Progress*, Energy Management System using ZigBee, Proceedings of the Nineteenth Americas Conference on Information Systems, Chicago, Illinois, August 15-17, 2013

10TH INTERNATIONAL CONFERENCE ON SUSTAINABLE ENERGY AND ENVIRONMENTAL PROTECTION (JUNE 27TH – 30TH, 2017, BLED, SLOVENIA), ENERGY EFFICIENCY
J. Krope, A.Ghani Olabi, D. Goričanec & S. Božičnik

Changes on Building Energy Consumption Using Future High Spatial Resolution Climate Data

ROBERTO SAN JOSÉ, JUAN L. PÉREZ, LIBIA PÉREZ & ROSA MARIA GONZALEZ BARRAS

Abstract The future global climate will impact on building energy demand. We have modelled the HVAC energy consumption of prototype and real buildings under present and future climatic conditions with the EnergyPlus model. We have produced detailed meteorological information with 50 meters of spatial resolution through dynamical downscaling process combining regional, urban and computational fluid dynamics models which include the effects of the buildings on urban wind patterns. The city of Madrid has been chosen for our experiment. The impacts on energy demand are calculated for year 2100 versus 2011 based on two IPCC climate scenarios, 4.5 (stabilization of emissions) and 8.5 (not reduction of emissions). The results show that climate change will have a large effect in the building energy demand, with increments in cooling demand for 8.5 and the annual heating gas demand for buildings will increase for 4.5.

Keywords: • Energy • Climate • Impact • Downscaling • Urban •

CORRESPONDENCE ADDRESS: Roberto San José, Ph D., Professor, Environmental Software and Modelling Group, Computer Science School, Technical University of Madrid (UPM), Madrid, Spain, e-mail: roberto@fi.upm.es. Juan L. Pérez, Ph D., Professor, Environmental Software and Modelling Group, Computer Science School, Technical University of Madrid (UPM), Madrid, Spain, e-mail: jlperez@fi.upm.es. Libia Pérez, Ph D., Professor, Environmental Software and Modelling Group, Computer Science School, Technical University of Madrid (UPM), Madrid, Spain, e-mail: lperez@fi.upm.es. Maria Gonzalez Barras, Ph D., Professor, 2Department of Physics and Meteorology, Faculty of Physics, Complutense University of Madrid (UCM), Ciudad Universitaria, 28040 Madrid, Spain, e-mail: rgbarras@gmail.com.

https://doi.org/10.18690/978-961-286-050-9.25 ISBN 978-961-286-050-9

Available at: http://press.um.si.

1 Introduction

Heating, ventilation and air conditioning (HVAC) related energy consumption has been rising in recent years throughout Europe, in particular in Southern Europe. The buildings designed according to the climatic condition of recent years may become increasingly costly to operate and maintain in the present and future [1].The energy demand for space heating and cooling is sensitive to climate variables, e.g. air temperature radiation and wind seep and so on. Space heating and cooling and the associated energy demand is affected by climate change [2].

Cities are areas where the local response to global climate change is most pronounced [3], recent studies have suggested that global climate change will have a significant impact on local weather [4]. Building energy consumption is vulnerable to climate change due to the direct relationship between outside climate and space cooling/heating. The urban microclimate is determined by different factors: local wind speed and direction, temperature, humidity and solar radiation. To assess how climate change will affect buildings energy demand, it is necessary to develop new sets of future climate data to use as inputs to the building energy demand model using climate change projections with very high spatial resolution. The impact of climate change on heating and cooling energy use in different locations will vary because of their different climates, [5]. A detailed analysis of heating and cooling energy use in the future is needed to better understand the impact of climate change on building energy consumption.

Energy demand sensitivities to climate change should be performed at urban scale because global or regional climate is not enough to have geographically distinct impacts [6]. In previous studies for the USA [7] and [8], the UK [9] and, Greece [10], climate change was found to have significant implications for energy consumption in buildings. These studies are regional based and only focus on a few types of buildings, thus could not predict the general. Studies of impacts on future energy demands have high uncertainty arising from uncertainties in methods of projecting future climate conditions [11].

The atmospheric flow and the special microclimate of cities are influenced by the characteristics of the urban surface [12]. Global climate models (GCMs) have a spatial resolution of approximately one degree, so we need to use higher resolution horizontal numerical models to obtain accurate data on the urban microclimate, taking into account all its special characteristics [13].Therefore, it must be carried out at a fine scale, as this study where climate is calculated at 50 meters of spatial resolution, taking into account the shape of buildings, modelled as 3D structures, their effects on the ventilation.

2 Dynamical Downscaling

To calculate the energy consumption of a building every hour of the year, you need data of several climatic variables: dry bulb temperature, wet bulb temperature, global solar radiation, wind speed, wind direction, humidity and pressure. You need to generate 8760 values of these variables each year. The meteorological data is used not only to know the hourly response of a building to the climate, but also to dimension the systems of air conditioning of the building. We are following the next methodology to get the best possible urban meteorological information.

The outputs from the global model (CCSM) are used as boundary and initial conditions (BSC and ICs) for the regional scale run (Europe). A nesting approach is used from regional (25 km) to urban level (1 km) with the WRF/Chem model (in the urban level the urban canopy model is activated). The produced 3D fields of meteorological variables are used as BCs and ICs for the street scale runs over the selected urban areas. At this scale the Computational Fluid Dynamics (CFD) model called the MICROSYS is applied with 50 meters of resolution. The urban climate model UCM (urban canopy model) was used inside of the WRF/Chem model for investigating the impact of the climate projections on the local urban climate and air pollution for urban scale level. This resolution allows that every building block has its own meteorological datasets. The meteorological data are calculated as the spatial average of the 50 meters grid cells which are around of the building block. The description of the dynamical downscaling method was published already, for detailed information; refer to publication [14].

The impacts of climate change on energy consumption of buildings for two Representative Concentration Runs (RCPs) [15] have been studied, RCP 4.5 and RCP 8.5. These climate scenarios are currently being used in simulations of global climate models for the IPCC's fifth assessment report (AR5). The scenario 8.5 [16] is due to a small effort to reduce emissions and represents a failure to curb warming by 2100. It is characterized by increasing greenhouse gas emissions over time RCP 4.5 is a stabilization scenario in which total radiative forcing stabilizes around 2050 using a range of technologies and strategies to reduce greenhouse gas emissions. This can be considered as a weak climate mitigation scenario [17]. The selection of these two possible scenarios is due to the fact that we wanted to show the extreme changes that can occur under these two scenarios that would correspond to the worst case scenario (8.5) and the best possible realistic scenario (4.5).

3 Energy Demand Impacts

The impacts were quantified by calculating the differences between energy demands for future minus present for each climate scenario. Energy demand of buildings is modelled by EnergyPlus (Department of Energy of USA). It is well-known and accepted tool in community building energy analysis worldwide and the model is highly validated. Taking into account the local climate of each building, EnergyPlus calculated hourly HVAC energy demand of the building to satisfy occupant thermal comfort over a period of one year. EnergyPlus is based on complex calculations of gain and loss of heat, including different physical processes such as transient heat conduction through the building envelope elements. Also it realizes the transfer of heat and mass impacting the sensible and latent heat loads due to ventilation and infiltration. The prototypes are based on ASHRAE 90.1 Prototype Building Modeling Specifications [18]. It is assumed that the buildings don´t change for the future simulations to isolate effects of the global climate on the energy demand of the buildings.

4 Results

Relative (%) spatial differences (50m of spatial resolution) of annual mean temperature changes between (the future) 2100 and 2011 (present) for RCP 4.5 and RCP 8.5 in a Madrid area of 2 km by 2km are showed in Figure 1 and Figure 2 respectively. The temperature has been calculated using the dynamical downscaling approach which was explained in the past sections. In Figures 3, largest increases in building energy consumption are found in the summer where the outdoor temperature could be increase up to 22% in July and the energy demand up to 40 %.

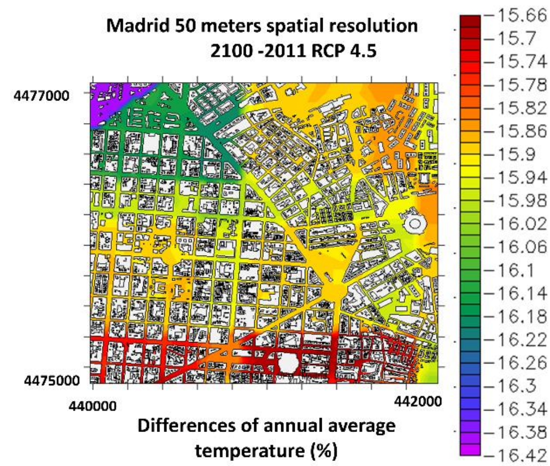

Figure 1. Madrid differences (%) between 2100 and 2011 spatial distribution (50 meters of resolution) of one-year average mean air temperature with RCP 4.5.

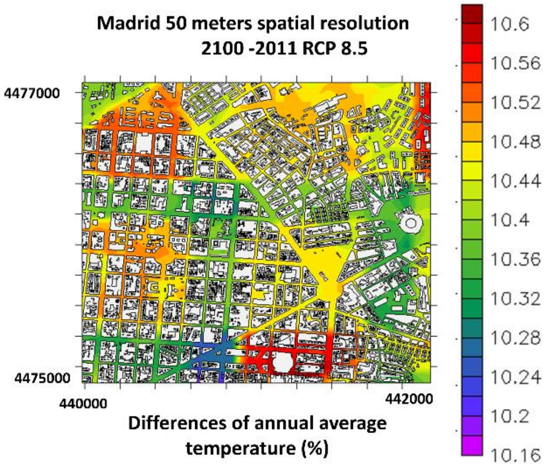

Figure 2. Madrid differences (%) between 2100 and 2011 spatial distribution (50 meters of resolution) of one-year average mean air temperature with RCP 8.5.

Figure 1 shows than with the scenario 4.5 we can observe a decrease in temperature for the year 2100 up to 16% compared to 2011. In Figugre 2, the climate scenario 8.5 results in an increase of the temperature for the year 2100 up to 10.9% compared to 2011 in this area of Madrid where the energy consumption of 15 prototype building will be analyzed in the next section. It is interesting to observe, that between two very close points can be differences up to 0.5%., so the location of the buildings is very important from a meteorological and energy points of view.

The table 1 compares the impact of climate change on HVAC annual total energy demand for fifteen types of prototype buildings by the 2100 respect to 2011 under the two possible climate scenarios.

Table 1. Change in annual HVAC energy demand for 15 different types of buildings, RCP 4.5 and RCP 8.5

2100 - 2011	Δ Total Energy (%)	
	RCP 4.5	RCP 8.5
Apartment	25,45	0,008
Hospital	11,81	-4,71
Large Hotel	31,67	-7,7
Small Hotel	9,87	4,93
Large Office	21,94	-4,2
Medium Office	20,73	5,33
Small Office	9,75	3.05
Outpatient Healthcare	4,08	3,7
Fast Food	30,86	-0,7
Sit Down Restaurant	26,42	1,21
Standalone Retail	17,89	2,25
Stripmall	25,71	2,23
Primary School	9,41	6,63
Secondary School	25,03	-1,64
Non-refrigerated warehouse	16,23	4

In case of the RCP 4.5 climate scenario, the increments of the energy demand is clear and important for all type of buildings, it is mainly because they will need more gas for heating the building as consequence of an outdoor temperature redaction. For the RCP 8.5 decreases are observed in big buildings (hospital, large hotels, large office and secondary schools) because they will need less gas for heating thank you to warmer temperatures, but the rest of type of building will spend more electrical energy for refrigerating process.

Figure 3 describes monthly average total HVAC energy demand variations (%) of a primary school. Fig. 3 corresponds with climate scenario RCP 8.5. Primary school is the type of building which will suffer the major increment of the energy demand (6.63 %).

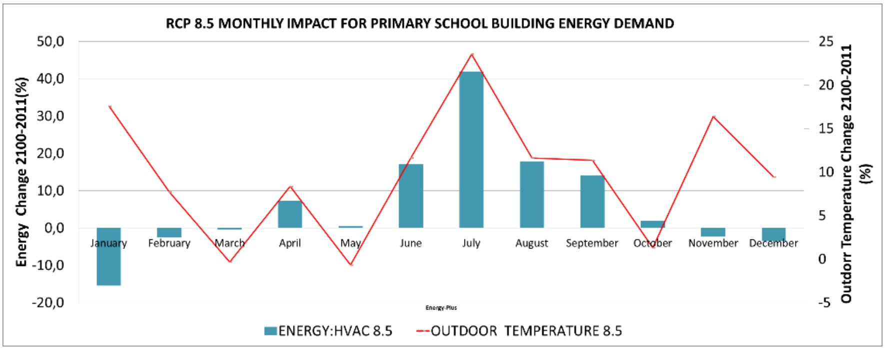

Figure 3. Change 2100-2011 (%) in monthly energy demand (gas and electricity) and outdoor temperature for a prototype primer school building of Madrid with RCP 8.5 climate scenario

Now, full years heating and cooling hourly demands are calculated for each of the 3 "real" buildings found in an area of 1km by 1km of Madrid, they are an office, apartment and hotel. They are modelled, starting from a prototype where the major characteristics have been adapted for each specific simulated building

Because it is intended to be the most realistic possible. Table 2 shows for each building, the change (%) on the annual total energy demand, annual electricity demand by the HVAC and heating gas demand of the three types of building.

Table 1. Variations on energy demand for 2100 versus 2011 of 3 types of buildings

2100-2011 (%)	Total-Energy		Electricity-HVAC		Gas-Heating	
Building/Scenario	RCP 4.5	RCP 8.5	RCP 4.5	RCP 8.5	RCP 4.5	RCP 8.5
Ofice	23,49	-0,46	-7,7	10,36	63,47	-15,49
Apartment	23,42	-2,09	-7,14	8,18	54,88	-13,52
Hotel	24,77	0,93	-12,11	19,23	58,35	-16,55

Gas demand shows a significant increase in the RCP 4.5 climate scenario, the increase of heating (54-65%) dominates over the decrease of cooling (8-20%). Total energy demand increase between 23.42% and 24.77% by air temperature decrements. The increase in heating energy demand is much more dramatic than the decrease in cooling energy demand, when responding to the climate scenario. The RCP 8.5 may benefit from global warming in terms of the reduction in the energy demand. It is interesting to notice that increased future local temperatures translate in lower energy consumption for heating.

5 Conclusions

The objectives of this research have been achieved. The impacts of climate change on the energy consumption of different types of buildings in Madrid have been shown. For this, it was necessary to generate climatic data of very high spatial and temporal resolution that have been reduced dynamically from a global scale of 1 to a street scale where a CFD model has been applied for a spatial resolution of 50 meters. In this study, the climate projections were based on two climatic scenarios of the IPCC: RCP 8.5 and RCP 4.5. Heating and cooling energy consumption of fifteen prototypes buildings and three real buildings during 2011 and 2100 in Madrid were simulated by using EnergyPlus model. We have showed the results for assessing energy demand responses to climate change. Results indicate that building energy demand in Madrid is very sensitive to the climate. The most serious impacts occur with the RCP 4.5 climate scenario for year 2100.

The scenario RCP 4.5 for 2100 project to increases energy demand by around 23-24%, relative to the energy demand in 2011 for the three simulated buildings. Although part of the assessment is carried out for specific building prototypes, it demonstrates that both increase in heating energy and decrease in cooling energy over the RCP 8.5 can be significant due to climate change and the opposite results could be obtained with the RCP 8.5 with increments of electricity for cooling. The RCP 8.5 will produce climate conditions that are more favorable from a building energy demand point of view because it is characterized by temperature increments, so only increments for cooling are needed. The results through changes modelled in climate indicate that climate change (RCP 8.5) will not cause an increment of the energy consumption but if it is combatted (RCP 4.5) may increase energy consumption by 2100. In general, decreasing heating energy compensates the increased cooling energy.

The established methodology is of interest for its results and that can be applied to other buildings in other cities. These types of impacts assessments help to identify solutions that will both enhance the resilience of buildings to future climate changes. The large variations found in the relationship between climate change and building energy consumption highlight the importance of assessing climate change impacts at local scales

Acknowledgements

The UPM authors acknowledge the computer resources and technical assistance provided by the Centro de Supercomputación y Visualización de Madrid (CeSViMa). The UPM authors thankfully acknowledge the computer resources, technical expertise and assistance provided by the Red Española de Supercomputación).

References

[1] G. H. Radhi, "Evaluating the potential impact of global warming on the UAE residential buildings - A contribution to reduce the CO2 emissions," Building and Environment, 2009, vol. 44, pp. 2451-2462.

[2] D. J. Arent et al. (2014) Key economic sectors and services. In: Field CB et al. (eds). Climate Change 2014: Impacts, Adaptation, and Vulnerability. Part A: Global and Sectoral Aspects. Contribution of Working Group II to the Fifth Assessment Report of the Intergovernmental Panel of Climate Change. Cambridge University Press: Cambridge, UK and New York.

[3] Oleson, K. W., A. Monaghan, O. Wilhelmi , M. Barlage , N. Brunsell , J. Feddema , L. Hu , and D. F. Steinhoff. Interactions between urbanization, heat stress, and climate change. Climatic Change 2010; 129, 525-541, doi:10.1007/ s10584-013-0936-8.

[4] Mickley, L. J., Jacob, D. J., Field, B. D., and Rind, D. Effects of future climate change on regional air pollution episodes in the United States, Geophys. Res. Let. 2004; 31, L24103.

[5] D. J. Sailor, "Relating residential and commercial sector electricity loads to climate: Evaluating state level sensitivities and vulnerabilities," Energy, vol. 26, pp. 645-657, 2001.

[6] M. Ruth and A. D. Amato, "Regional Energy Demand Responses to Climate Change: Methodology and Applications to the Commonwealth of Massachusetts," Climatic Change, 2005, vol. 70, no. 1, pp. 175-201.

[7] D. H. Rosenthal, H. K. Gruenspecht, and E. A. Moran, "Effects of global warming on energy use for space heating and cooling in the United States," Energy J, vol. 16, pp. 77–96, 1995.

[8] D. B. Belzer, J. M. Scott, and R. D. Sands, "Climate change impacts on U.S. commercial building energy consumption: An analysis using sample survey data," Energy Sources, vol. 18, pp. 177–201, 1996.

[9] S. E. C. Pretlove and T. Oreszczyn, "Climate change: Impact on the environmental design of buildings," in Proc CIBSE A Build Serv Eng Res Technol, 1998, vol. 19, pp. 55–58

[10] C. Cartalis, A. Synodinou, M. Proedrou, A. Tsangrassoulis, and M. Santamouris, "Modifications in energy demand in urban areas as a result of climate changes: An assessment for the southeast Mediterranean region," Energy Conversion Manage, vol. 42, pp. 1656–1674, 2001.

[11] D. H. W. Li, L. Yang, and J. C. Lam, "Impact of climate change on energy use in the built environment in different climate zones – A review," Energy, vol. 42, pp. 103-112, 2012.

[12] M. Piringer, E. Petz, I. Groehn, and G. Schauberger, "A sensitivity study of separation distances calculated with the Austrian Odour Dispersion Model (AODM)," Atmospheric Environment, vol. 41, pp. 725-1735, 2007.

[13] J. H. Christensen and O. B. Christensen, "A summary of the PRUDENCE model projections of changes in European climate by the end of this century," Climatic Change, vol. 81, pp. 7–30, 2007.

[14] R. José, J. Pérez, L. Pérez, R. González , J. Pecci, A. Garzón, and M. Palacios, "Impacts on the Urban Air Quality and Health of Global Climate Scenarios Using Different Dynamical Downscaling Approaches," Journal of Geoscience and Environment Protection, vol. 4, pp. 168-174, 2016.

[15] Vuuren, D.P., Edmonds, J., Kainuma, M., Riahi, K., Thomson, A., Hibbard, K., Hurtt, G.C., Kram, T., Krey, V., Lamarque, J.F., Masui, T., Meinshausen, M., Nakicenovic, N., Smith, S.J., Rose, S.K.The representative concentration pathways: an overview. Climatic Change 109, 2011, 5-31.

[16] Riahi, S. Rose, P. Runci, R. Stouffer, D. van Vuuren, J. Weyant, T. Wilbanks, J. P. van Ypersele, and M.a Zurek, "Towards new scenarios for analysis of emissions, climate change, impacts, and response strategies," Intergovernmental Panel on Climate Change, 2008, Geneva, pp. 132.

[17] Smith, R. J. Stouffer, A. M. Thomson, J. P. Weyant1, and T. J. Wilbanks, "The next generation of scenarios for climate change research and assessment," Nature, vol. 463, pp. 747-756, 2010.

[18] PNNL. Enhancements to ASHRAE Standard 90.1 Prototype Building Models. Pacific Northwest National Laboratory, Richland, Washington 2014; Available at https://www.energycodes.gov/development/commercial/90.1_models.

10TH INTERNATIONAL CONFERENCE ON SUSTAINABLE ENERGY AND ENVIRONMENTAL PROTECTION (JUNE 27TH – 30TH, 2017, BLED, SLOVENIA), ENERGY EFFICIENCY
J. Krope, A.Ghani Olabi, D. Goričanec & S. Božičnik

Development of an Energy Simulation-Occupant Behavior Coupling Model to Reduce Building Energy Consumption

TAEHOON HONG, CHAN-JOONG KIM, JIMIN KIM, MYEONGHWI LEE & JAEMIN JEONG

Abstract Reducing energy consumption is the major issue that building managers are facing all over the world. It is not easy, however, to reduce energy consumption by controlling occupant behavior in a real building. To solve this problem, this study aims to develop an energy simulation-occupant behavior (ESOB) coupling model that can simulate the current state of the target facility with less time and effort. The model is developed using the energy simulation program and optimization algorithm. This study was conducted in five steps: (i) selection of target facility information; (ii) simulation of base energy model with physical building characteristics; (iii) Development of ESOB coupling model; (iv) simulation modelling with the occupant behavior; (v) calculation of error rate of ESOB coupling model. The error rate was reduced below 20%, consistent with the ASHRAE guideline 14. Proposed model improved calibration between actual building and simulation model with less time and effort.

Keywords: • Occupant behavior • Building energy simulation • Genetic algorithm • Coupling model • Calibration •

CORRESPONDENCE ADDRESS: Taehoon Hong, Ph.D., Professor, Yonsei University, Department of Architect and Architectural Engineering, Seoul, 03722, Republic of Korea, e-mail: hong7@yonsei.ac.kr. Chan-joong Kim, Ph.D. student, Yonsei University, Department of Architect and Architectural Engineering, Seoul, 03722, Republic of Korea, e-mail: kimcj5712@hotmail.com. Jimin Kim, Ph.D. and Postdoctoral Fellow, Yonsei University, Department of Architect and Architectural Engineering, Seoul, 03722, Republic of Korea, e-mail: cookie6249@yonsei.ac.kr. Myeonghwi Lee, graduate research assistant, Yonsei University, Department of Architect and Architectural Engineering, Seoul, 03722, Republic of Korea, e-mail: ddkddk35@yonsei.ac.kr. Jaemin Jeong, graduate research assistant, Yonsei University, Department of Architect and Architectural Engineering, Seoul, 03722, Republic of Korea, e-mail: ss96011@naver.com.

https://doi.org/10.18690/978-961-286-050-9.26 ISBN 978-961-286-050-9

Available at: http://press.um.si.

1 Introduction

Climate change, one of the most complex and challenging issues, has now become a problem facing everyone involved in the construction industry [1]. With population growth and economic growth in developing countries, total energy demand in 2035 is expected to increase by 48.3% over 2010. Energy consumption accounts for the largest portion of the building sector [2, 3].

In this regard, Building Energy Simulation (BES) plays an important role in predicting energy conservation in buildings after estimating energy usage and applying remodelling strategies [3].

BES builds a schedule based on the occupants' behavior after modelling based on physical building characteristics of the building. They also play an important role in analysing energy savings through remodelling strategies [4-6]. BES has several advantages: (i) when the experiment is not possible, the use of the BES can help to obtain results; (ii) the results can be analysed through the BES prior to apply a variety of energy conservation measures (ECMs); (iii) the BES requires a little more time for analysis; (iv) the base model continues to be developed through the BES; (iv) even things difficult to consider in the experiment, things such as the weather, can be taken into account in the BES; (v) buildings and residents are not disturbed by the BES; (vi) parts that are difficult to measure in the experiment can be identified through the BES; and (viii) immediate results can be obtained through the BES.

However, the energy consumption result through the BES model differs from the actual building result [7,8]. Therefore, the reliability of the BES model depends on how similar the simulated results are to the actual usage of the target facility. ASHRAE 14, International Performance Measurement and Verification Protocol (IPMVP) and Federal Energy Management Program (FEMP) set the benchmark for determining the similarity (i.e., error rate) between the BES model and the target facility [9].

Previous studies utilized several methodologies to minimize the error rate between the BES model and the target facility: (i) manual and iterative calibration is performed until the criteria are met based on trial-and-error through the user's experience and proper input parameters [7, 9, 10]; (ii) graphical and statistical methods present statistical display and graphical representations with respect to the results of the calibration procedures [4-6, 8, 11-15]; and (iii) automated calibration methods present specific tests and measurements through the analytical procedures based on the calibration [3, 16, 17].

Each of the previous studies has the following limitations: (i) manual and iterative calibration requires a lot of time and effort because it meets error rate criteria through the manual and repeat performance of the BES model; (ii) graphical and statistical methods are designed to calculate the BES model to minimize the error rate by selecting key impact variables through statistical analysis, such as sensitivity analysis, which can minimize the error rate through key impact variables. However, the repetitive simulating the BES model consumes a lot of time and effort; (iii) automated calibration methods use automated optimization algorithms to perform repetitive tasks, which requires less time and effort than manual and repetitive tasks. However, accuracy may be reduced by the choice of the objective function set by the designer.

In order to solve the above-mentioned limitations, this study aims to develop an energy simulation-occupant behavior (ESOB) coupling model that simulates the current state of the target facility with less time and effort. This model was developed using energy simulation programs and optimization algorithms. The study was conducted in five steps: (i) selection of target facility information; (ii) simulation of the basic energy model with physical building characteristics; (iii) development of an ESOB coupling model; (Iv) simulation modeling using resident behavior; (V) Calculation of error rate of ESOB coupling model.

2 Material and Methods

2.1 Selection of target facility information and simulation of the basic energy model with physical building characteristics

For the application of ESOB coupling model, basic information gathering and energy modelling for standard buildings were conducted. In order to solve the problem of standardization of design plan of various buildings, energy modelling was carried out and was simulated based on the standard housing design proposed in 'Guidelines for Construction Standards and Performance Evaluation of Eco-Friendly Housing Buildings' [18]. As a tool for energy modelling, we used Design Builder based on Energy Plus, a building energy simulation developed by the US Department of Energy. In order to accurately apply the local climate in Korea, we have set up climate data as Seoul. The basic conditions of energy simulation for target facility are summarized in Table 1.

Table 6. Basic Condition of Target Facility

Class	Detailed information		
Region	Seoul, South Korea		
Building area	3 stories, 4,265m² (2,723m²)		
Roof area	1,466m²		
Conditioning system	packaged EHP (electric heat pump)		
Thermal characteristics of wall	Thickness (mm)	Conductivity (W/m·K)	U-value (W/m^2·K)
External wall	180	0.62	3.44
External wall insulation	34	0.06	1.76
Internal wall	150	1.35	9.00
Internal wall insulation	125	0.04	0.32
Characteristics of electrical system	Air-conditioned zone	Non-air-conditioned zone	
Lighting load density	23w/m^2	6w/m^2	
Equipment load density	16w/m^2		
Ventilation air flow rate	36m^3/h·Person	36m^3/h·Person	
Setting temperature	18 ºC (Winter)	26 ºC (Summer)	
Period (month)	1~4, 10~12	5~9	

The study considered external wall insulation (EWI) thickness and conductivity, internal wall insulation (IWI) thickness and conductivity. insulation is Korea's insulation criterion [19].

2.2 Development of an ESOB coupling model

An ESOB coupling model was developed to minimize the error rate between the energy use of BES model and those of the actual building. This step involves the process of using the genetic algorithm to derive the optimal solution of various optimal parameters related to building energy (i.e., HVAC and lighting). Furthermore, it aims at minimizing the error rate of energy consumption of real buildings and simulation models in a short time. The algorithm pseudo-code for developing the automatic correction technique is as Figure 1.

```
t ← 0
Initialize the Population[P(t)]
Evaluate the Population[P(t)]
While Minimized (CV(RMSE) and NMBE)
    P'(t) ← Variation[P(t)]
    Evaluate the Population[P'(t)]
    Calculate the CV(RMSE) and NMBE
    Next Generation Population
    t ← t + 1
endwhile
```

Figure 15. Automatic Calibration Pseudo Code

Based on the standard model generated by the automatic calibration technique, the energy savings according to occupants' behavior are predicted. Using the user interface, the user can set various occupants' behavior ranges, and the system automatically changes within the parameter range to create various occupants' behavior. This study used Python-based Django server web framework for high productivity and stable web page implementation. Django consists of components that help user quickly and easily develop website, and can also help user maintain or improve website (refer to Figure 2).

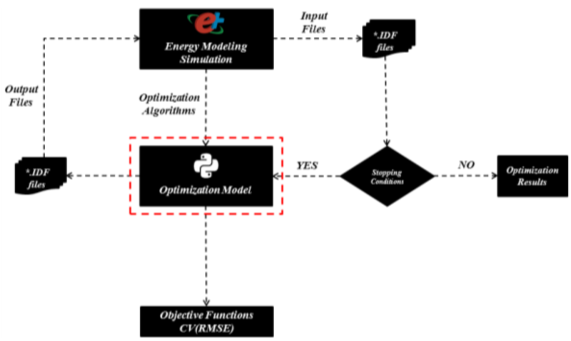

Figure 16. Flow chart of the ESOB coupling model

2.3 Simulation modelling with the occupant behavior and calculation of error rate of ESOB coupling model

The selection of the occupants' behavior is important to improve the accuracy of calibration. For calibration in previous studies, indoor temperatures and the lighting were considered as occupants' behavior [3-9, 14-15]. Table 2 shows detail information on occupants' behavior.

Table 7. Information on occupants' behaviour

Component	Sub component	Range	Step
Indoor temperature	Cooling set point (°C)	26.0 ~ 28.0	0.1
	Heating set point (°C)	18.0 ~ 20.0	0.1
Lighting 1	efficiency	0 ~ 1	0.01
Lighting 2	efficiency	0 ~ 1	0.01
Lighting 3	efficiency	0 ~ 1	0.01
Lighting 4	efficiency	0 ~ 1	0.01
Lighting 5	efficiency	0 ~ 1	0.01
Lighting 6	efficiency	0 ~ 1	0.01
Lighting 7	efficiency	0 ~ 1	0.01
Lighting 8	efficiency	0 ~ 1	0.01
Lighting 9	efficiency	0 ~ 1	0.01
Lighting 10	efficiency	0 ~ 1	0.01
Lighting 11	efficiency	0 ~ 1	0.01
Lighting 12	efficiency	0 ~ 1	0.01
Lighting 13	efficiency	0 ~ 1	0.01

Occupant can control the indoor temperature and lighting, therefore, indoor temperature and lighting efficiency was selected as occupants' behavior [5,9, 13-15]. In this study, the error rate was selected as the objective function. If the results that meet the termination criteria are obtained, the optimization is automatically terminated. As shown in Figure 2, a flowchart for approaching the minimum error rate was presented through the optimization using ESOB coupling model.

3 Results and Discussion

As shown in Table 3, the values of occupants' behavior were presented as a result of the optimization.

Table 8. Occupants' behavior after optimization

Component	Sub component	Value
Indoor temperature	Cooling set point (°C)	26.1
	Heating set point (°C)	19.9
Lighting 1	Efficiency	0.72
Lighting 2	Efficiency	0.78
Lighting 3	efficiency	0.74
Lighting 4	efficiency	0.77
Lighting 5	efficiency	0.13
Lighting 6	efficiency	0.51
Lighting 7	efficiency	0.58
Lighting 8	efficiency	0.76
Lighting 9	efficiency	0.74
Lighting 10	efficiency	0.59
Lighting 11	efficiency	0.66
Lighting 12	efficiency	0.94
Lighting 13	efficiency	0.12

After optimization, the cooling set point was 26.1°C. This indicates that cooling during the summer period continues to be maintained. The heating temperature was also 19.9°C, confirming that heating continues to be operated during the winter period. With regards to the lighting efficiency, lighting efficiency of more than 0.7 was applied to lighting 1,2,3,4,8,9, and 12, and therefore energy consumption was found to be higher compared to other lightings. Meanwhile, the lighting efficiency was relatively low in lighting 5,6,7,10,11, and 13, suggesting that energy consumption was low.

The ESOB coupling model results show that the error rate is reduced by more than 5% compared to the basic energy model.

4 Conclusion

This study aimed to develop an ESOB coupling model that can simulate the current state of the target facility with less time and effort. The model is developed using the energy simulation program and optimization algorithm. The ESOB coupling model results show that the error rate is reduced by more than 5% compared to the basic energy model.

The results of this study allow user to simulate a BES model similar to a real building with less time and effort. Based on the results of the ESOB coupling model, a guideline for occupants' behavior can be presented. In addition, with the basic BES model, various energy saving techniques can be applied to calculate the effect more easily.

Acknowledgements

This work was supported by the National Research Foundation of Korea (NRF) grant funded by the Korea government (MSIP; Ministry of Science, ICT & Future Planning) (No. NRF-2015R1A2A1A05001657 and NRF- 2016R1A6A3A11932132).

References

[1] U.S. Climate Action report 2014; U.S. department of state, USA, 2014, pp. 1-2.
[2] The 2nd energy master plan, Ministry of Trade, Industry and Energy, Korea, 2014, pp. 10-12.
[3] T. Hong, C. Kim, J. Jeong, J. Kim, C. Koo, K. Jeong, M. Lee, "Framework for approaching the minimum CV(RMSE) using energy simulation and optimization tool," presented at Applied Energy Symposium and Summit 2015 Low Carbon Cities and Urban Energy Systems (CUE 2015), Fuzhou, Nov 2015.
[4] J. Cipriano, G. Mor, D. Chemisana, D. Pérez, G. Gamboa, X. Cipriano, "Evaluation of a multi-stage guided search approach for the calibration of building energy simulation models," *Energy and Buildings*, vol. 87, pp. 370-385, 2015.
[5] J. Sun, T.A. Reddy, "Calibration of building energy simulation programs using the analytic optimization approach (RP-1051)," *HVAC&R RESEARCH*, vol. 12(1), pp. 177-196, Jan. 2006.
[6] F.S. Westphal and R. Lamberts, "Building simulation calibration using sensitivity analysis," presented at Ninth International IBPSA Conference, Montreal, Aug. 2005, pp. 1331-1338.
[7] P. Raftery, M. Keane, A. Costa, "Calibrating whole building energy models: Detailed case study using hourly measured data," *Energy and Buildings*, vol. 43(12), pp. 3666-3679, 2011.
[8] G. Mustafaraj, D. Marini, A. Costa, M. Keane, "Model calibration for building energy efficiency simulation," *Applied Energy*, vol. 130, pp. 72-85, 2014.
[9] Y. Pan, Z. Huang, G. Wu, "Calibrated building energy simulation and its application in a high-rise commercial building in Shanghai," *Energy and Buildings*, vol. 39(6), pp. 651-657, 2007.
[10] P. Raftery, M. Keane, J. O'Donnell, "Calibrating whole building energy models: an evidence-based methodology," *Energy and Buildings*, vol. 43(9), pp. 2356-2364, 2011.
[11] F. Lei and P. Hu, "A baseline model for office building energy consumption in hot summer and cold winter region," presented at 2009 International Conference on Management and Service Science (MASS 2009), Wuhan, Sep. 2009, pp. 1-4.
[12] R. Priyadarsini, W. Xuchao, L.S. Eang, "A study on energy performance of hotel buildings in Singapore," *Energy and Buildings*, vol. 41(12), pp. 1319-1324, 2009.
[13] M. Royapoor and T. Roskilly, "Building model calibration using energy and environmental data," *Energy and Buildings*, vol. 94, pp. 109-120, 2015.
[14] K.H. Kim, J.S. Haberl, "Development of methodology for calibrated simulation in single-family residential buildings using three-parameter change-point regression model," *Energy and Buildings*, vol. 99, pp. 140-152, 2015.

[15] Y. Heo, R. Choudhary, G.A. Augenbroe, "Calibration of building energy models for retrofit analysis under uncertainty," *Energy and Buildings*, vol. 47, pp. 550-560, 2012.
[16] S.C. Chu, H.L. Yang, "One-time ray-tracing method for the optimization of illumination system," presented at International Conference on Optics in Precision Engineering and Nanotechnology, Singapore, Jun. 2013, pp. 87692M-87692M.
[17] J.R. New, J. Sanyal, M. Bhandari, S. Shrestha, "Autotune e+ building energy models," presented at the 5th National SimBuild of IBPSA-USA, Madison, Aug. 2012, pp.1-3.
[18] Korea Meteorological Administration. Available online: http://www.kma.go.kr/ (accessed on 2 April 2017).
[19] Korea Ministry of Government Legislation. Available online: https://www.law.go.kr (accessed on 2 April 2017).

10TH INTERNATIONAL CONFERENCE ON SUSTAINABLE ENERGY AND ENVIRONMENTAL PROTECTION (JUNE 27TH – 30TH, 2017, BLED, SLOVENIA), ENERGY EFFICIENCY
J. Krope, A.Ghani Olabi, D. Goričanec & S. Božičnik

Exergetic Analysis of Cogeneration Processes: Study of Case

MARCUS VINICIUS RONCARI MARI, JOÃO MARCOS RONCARI MARI, MAYKON CESAR SPOLTI FERREIRA, ETIENE NATANIEL PEDRO DUNDÃO, DANILO TOLEDO RIBEIRO DA SILVA, ANDERSON RODRIGO VISCONCINI, EUGÊNIA LEANDRO ALMEIDA, FERNANDO CASTRO VIEIRA FILHO & CID MARCOS GONÇALVES ANDRADE

Abstract Currently in the industrial sector one of biggest concerns is about energetic costs. Some frequent studies have been developing in order to reduce energetic losses and at the same time to develop more efficient systems. Exergetic analysis is an important tool, because when is compared with energetic analysis shows more representative results. Therefore, this work had as objective to perform an exergetic analysis in a process plant, where there is a cogeneration process, which operates in a Rankine cycle. And also to perform an exergetic analysis in this same plant, but now, using all available thermal source coming from the same fuel used in the cogeneration process, to generate electric power, thus supplying the heat demand by electric resistance. Both situations have simulated in EES software (Engineering Equation Solver). After the results obtained, it was possible to verify which case showed more satisfactory results.

Keywords: • Cogeneration • Exergetic analysis • Exergetic efficiency • Rankine cycle • Exergy •

CORRESPONDENCE ADDRESS: Marcus Vinicius Roncari Mari, Master's Degree Student, State University of Maringá, Department of Mechanical Engineering, Av. Colombo, 5790 - Vila Esperanca, Maringá - PR, 87020-900, Brazil, email: vinicius_roncari@hotmail.com. João Marcos Roncari Mari, Degree Student, State University of Maringá, Department of Mechanical Engineering, Av. Colombo, 5790 - Vila Esperanca, Maringá - PR, 87020-900, Brazil, email: joao_roncari@hotmail.com. Maykon Cesar Spolti Ferreira, Master's Degree Student, State University of Maringá, Department of Mechanical Engineering, Av. Colombo, 5790 - Vila Esperanca, Maringá - PR, 87020-900, Brazil, email: spolti.maykon@gmail.com. Etiene Nataniel Pedro Dundão, Master's Degree Student, State University of Maringá, Department of Mechanical Engineering, Av. Colombo, 5790 - Vila Esperanca, Maringá - PR, 87020-900, Brazil, email: etiene100nataniel@hotmail.com. Danilo Toledo Ribeiro da Silva, Master's Degree Student, State University of Maringá, Department of Mechanical Engineering, Av. Colombo, 5790 - Vila Esperanca, Maringá - PR, 87020-900, Brazil, email: danilotoledoo@gmail.com. Anderson Rodrigo Visconcini, Master's Degree Student, State University of Maringá, Department of Mechanical Engineering, Av. Colombo, 5790 - Vila Esperanca, Maringá - PR, 87020-900, Brazil, email: avisconcini@hotmail.com. Eugênia Leandro Almeida, Master's Degree Student, State University of Maringá, Department of Chemical Engineering, Av. Colombo, 5790 - Vila Esperanca, Maringá - PR, 87020-900, Brazil; email: eugenia-almeida@hotmail.com. Fernando Castro Vieira Filho, Doctor's Degree Student, State University of Maringá, Department of Production Engineering; Av. Colombo, 5790 - Vila Esperanca, Maringá - PR, 87020-900, Brazil, email: epfernando@gmail.com. Cid Marcos Gonçalves Andrade, Professor, State University of Maringá, Department of Chemical Engineering; Av. Colombo, 5790 - Vila Esperanca, Maringá - PR, 87020-900, Brazil, email: cid@deq.uem.br.

https://doi.org/10.18690/978-961-286-050-9.27 ISBN 978-961-286-050-9

Available at: http://press.um.si.

1 Introduction

One of the main concerns in the industrial sector nowadays is related to energetic costs, whereas they are straightly related to the operational costs and consequently with financial and environmental costs as well [1]. In this way, there are some studies aiming to develop ways to reduce energetic losses and to improve systems efficiency. Recently it has been increasing the interest in applying exergetic analysis in the industrial sector [2]. Exergetic analysis aims to identify within a system, places where losses and exergy destruction occurs, in order to classify them about their importance, which allows operational improvements and to optimize the process. Thus, there is a direct relation between exergy and economic value [3, 4, 5]. The first law of thermodynamics states that energy can be transformed, but never destroyed, so energy is always conserved [6]. Therefore, when a situation involves real processes the first law of thermodynamics becomes inadequate. On the other hand, exergy is not conserved and can be destroyed by means of irreversibilities. It is closely related to the foundations of the second law of thermodynamics [7]. Exergy can be defined as the maximum possible work that can be performed by a global system, which is formed by a system and a reference state, also called as environment. Thus, exergy is a measure of the deviation between system state and environment [5, 8]. A cogeneration plant can supply the energy requirements of industries, making the plant energy-independent, besides a possible supplier of electric power in the grid [9]. The National Electric Energy Agency of Brazil, at the Normative Resolution 235 (2006) defines cogeneration such as the process of transforming thermal energy of a fuel into more than one form of useful energy [10]. The most common form of energy is mechanical energy, which is used to generate electrical energy and / or to move equipments present in the process, whereas the thermal energy is used to meet the heat demand in the process, such as for example, at heat transfers, evaporators, etc. The main industrial technologies used in the cogeneration process involve cycles that operate with gas turbines, as Brayton cycle and steam turbines, as Rankine cycle, it can also be operated in a combined cycle, as Brayton-Rankine [11]. By the context presented, the work aims to do an exergetic analysis in a process plant that there is a cogeneration process, in order to evaluate the exergetic viability of plant.

2 Study of Case

The case study aimed to perform an exergetic analysis in a process plant, taking into account two situations. The first situation is to evaluate, exergetically, a cogeneration process, in which the energy from biomass is converted into electric and thermal energy. The second situation is based on converting all the energy, derived from the same biomass used in the first situation, into electric energy, using electrical resistance to supply the thermal energy demand in the plant, replacing the equipment that works by steam for others that works by electricity. This proposal arises because the electrical system presents some advantages, such as lower maintenance cost, ease of monitoring and controlling the temperature in a process, being able to be turned off when needed and to have a "leaner". After performing the exergetic analyzes in both cases and calculating their respective efficiencies, it was compared which system presented greater exergetic efficiency. Figure 17, Figure 18 and Table 9 represent the system.

Table 9. State data for Figure 18

State	Temperature (°C)	Pressure (bar)	Mass flow (kg/h)
1	510	86	-
2	37	0,06	290.000
3	Saturated Liquid	0,06	-
4	41	86	-
C1	21	1	-
C2	40	1	-
T11	21	1	-
T12	60	1	-

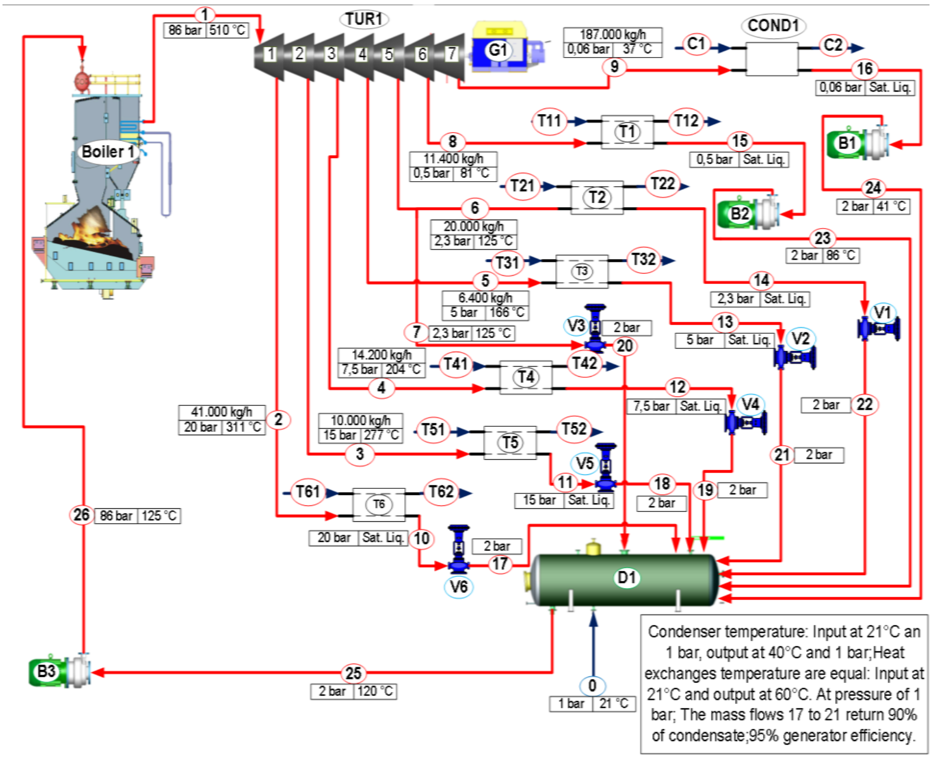

Figure 17. Process flow diagram of cogeneration system

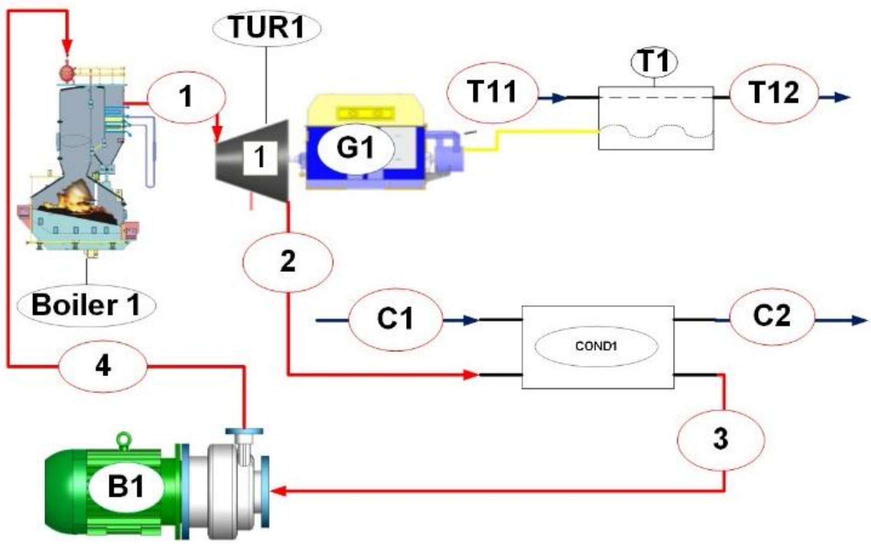

Figure 18. Process flow diagram of electrical system

3 Equation

In order to do a thermodynamic assessment of each system, it was utilized the software Engineering Equation Solver (EES). Some basic equations such as mass balance, energy balance and specific exergy were used to development of study. These equations are shown below:

$$\frac{dm}{dt} = \sum_e \dot{m}_e - \sum_s \dot{m}_s \qquad (1)$$

$$\frac{dE_{VC}}{dt} = \dot{Q} - \dot{W} + \sum_e \left[\dot{m}_e \left(h_e + \frac{V_e{}^2}{2} + gz_e\right)\right] - \sum_s \left[\dot{m}_s \left(h_s + \frac{V_s{}^2}{2} + gz_s\right)\right] \qquad (2)$$

$$e_x = h - h_0 - T_0(s - s_0) + \frac{V^2}{2} + gz \qquad (3)$$

Where $\dot{m}$, $\dot{Q}$, $\dot{W}$, h, V, g, z, T and s represent, respectively, mass flow, heat, work, enthalpy, velocity, gravity and entropy. While the subscripts e, s and 0, refer to input, output and dead state, respectively [5]. In order to calculate the exergetic efficiency of the whole system, it was realized an exergy balance, for a control volume, which it was excluded the boiler, because of both studied cases this component is the same. Thus, the Equation 4 shows the exergetic efficiency of system [5].

$$\varepsilon_x = \frac{\sum[\dot{m}_f(e_{x_s} - e_{x_e})] + \dot{W}_l}{\dot{m}_q(e_{x_e} - e_{x_s})} \qquad (4)$$

Where $\dot{m}_f$ and $\dot{m}_q$ represent the cold and hot mass flows, respectively, e_{x_s} and e_{x_e} the specific exergy of output and input, respectively and $\dot{W}_l$ the liquid work of system [5].

4 Results and Discussion

The parameters were used for the simulation are available in the Figure 17, Figure 18 and Table 9. Except for the vapour quality values at the turbine output of the electrical system, which were varied for the quality bands of 1.0, 0.95 , 0.90, 0.85 and 0.80.

Figure 19 shows the results of the exergetic efficiency, as a function of the number of stages in the turbines, and the vapour quality at the exit. In Figure 20 we have the useful work that must be converted into electricity.

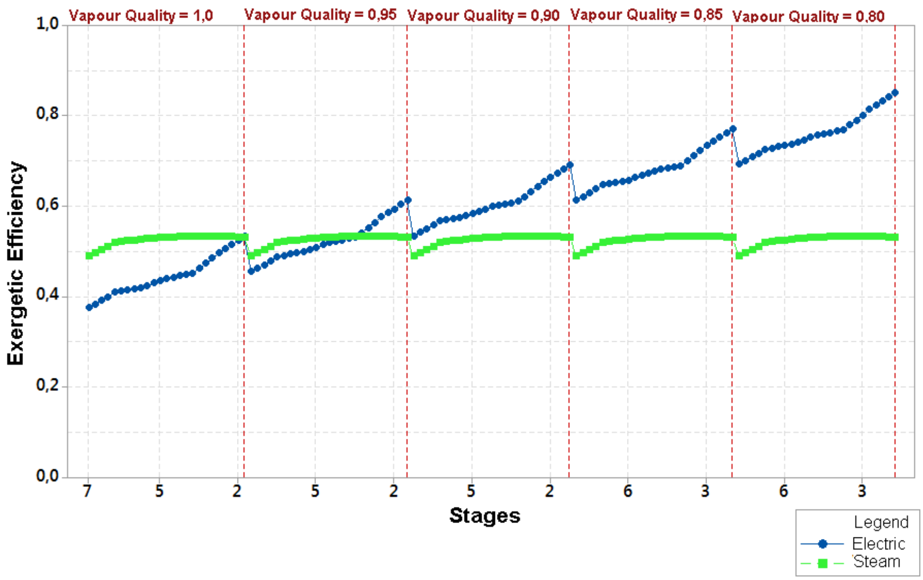

Figure 19. Exergetic Efficiency according to the number of stages.

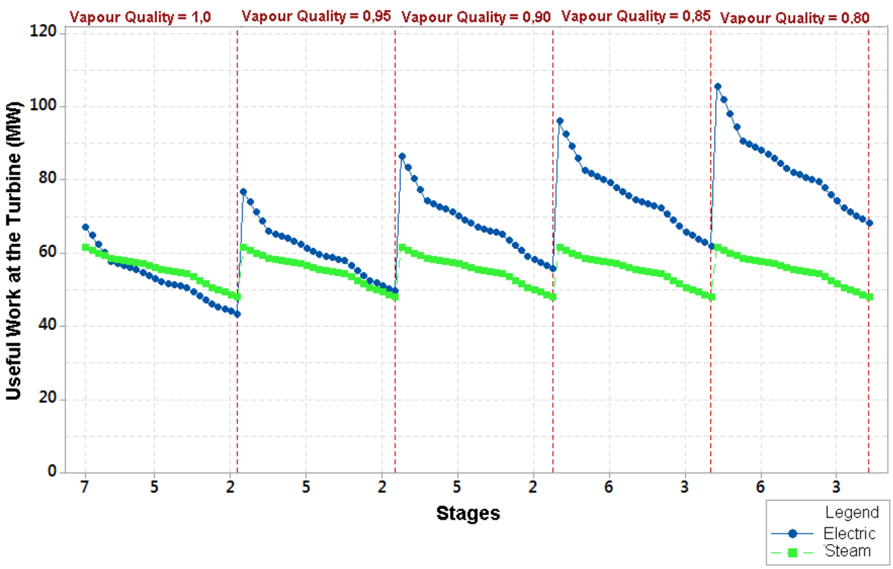

Figure 20. Useful work available at the turbine

Comparing the work in the turbine, in relation to the stages and the quality, in Figure 19, it is possible to see that the work obtained by the electric system is superior to the work of the steam system, for the vapour quality inferior to 0.95. However, in the vapour quality of 1, the work behavior in the electrical system starts higher than that of the steam system, but, as the stages fall, the work of the electrical system becomes smaller than that of the system at steam. This occurs because the steam system has a flow chart inherent to its operation process, which in the electrical system, there is not. In that, even with the total mass flow cut, for the processes, there would still be a required mass flow rate in state 7. Analyzing Figure 19 and Figure 20, with respect to large differences in exergetic efficiencies, this occurs due to the increase of the work generated by the turbine, since it takes advantage of the latent heat of the steam, besides the sensible heat.

5 Conclusion

It could be seen in Figure 19 that the exergetic efficiency of the electrical system becomes better than the steam system by reducing the vapour quality at the output of turbine, this occurs because in the electrical system the sensitive and latent energy of the steam are better used. In the steam system, the sensitive energy is converted into electrical energy at turbine and the total latent energy of the steam is converted into thermal energy in the heat exchangers, for the case studied. In the electrical system, the energy of the steam is just utilized in the turbine, thus when the vapour quality at the output of turbine is 1, only sensible energy is converted into electric energy. However, when the vapour quality at the turbine output is less than 1, both the sensitive energy and the latent energy of the steam are converted into electrical energy. The exergy efficiency of the electrical system overcomes the steam system, because the total efficiency of the electrical system (turbine, generator, transmission, electric heat exchanger) is greater than the efficiency of the heat exchanger in the steam system. This analysis is preliminary, with ideal hypotheses. Future works could be developed in order to evaluate the exergetic efficiency of real systems. Other option could be an economic analysis to give support at assessment.

Acknowledgements

This work has been realized with support of Coordenação de Aperfeiçoamento de Pessoal de Nível Superior (CAPES) - Brazil.

References

[1] E. A. Abdelaziz, R. Saidur, and S. Mekhilef, "A review on energy saving strategies in industrial sector," *Renew. Sustain. Energy Rev*., vol. 15. pp. 150–168, 2011.

[2] G. BoroumandJazi, B. Rismanchi, and R. Saidur, "A review on exergy analysis of industrial sector," *Renew. Sustain. Energy Rev*., vol. 27. pp. 198–203, 2013.

[3] M. Gong, and G. Wall, "Exergy Analysis of the Supply of Energy and Material Resources in the Swedish Society," *Energy*., vol. 9. pp. 1-16, 2016.

[4] S. C. Silva, F. E. da Costa, and A. O. S. Costa, "Fundamental concepts of thermodynamics property and examples of aplications for analysis in real process," *Enciclopédia Biosfera*., vol. 8. pp. 2025 -2037, 2012.

[5] M. J. Moran and H. N. Shapiro, *Fundamentals of Engineering Thermodynamics*. Rio de Janeiro: LTC, 2009.

[6] J. M. Smith, H. C. V. Ness, and M. M. Abbott, *Introduction to Chemical Engineering Thermodynamics*. Rio de Janeiro: LTC, 2007.

[7] M. A. Rosen, "Evaluation of energy-utilization efficiency in Canada using energy and exergy analyses," *Energy*, vol. 17. pp. 339–350, 1992.

[8] H. Sciubba, and G. Wall, "A brief Commented History of Exergy," *International Journal of Thermodynamics*., vol. 10. pp. 1-26, 2007.

[9] M. C. Barbeli, "Energy cogeneration and their point of view the importance of Technical, Economic and Enrironmental," *Empreendedorismo, Gestão e Negócios*., vol. 4. pp. 238-246, 2015.

[10] ANEEL Agência Nacional de Energia Elétrica. Available: http://www2.aneel.gov.br. Accessed: 1 Fev. 2017.

[11] P. Meherwan, *Handbook for Cogeneration and Combined Cycle Power Plants.* Michigan : ASME Press, 2002.

10TH INTERNATIONAL CONFERENCE ON SUSTAINABLE ENERGY AND ENVIRONMENTAL PROTECTION (JUNE 27TH – 30TH, 2017, BLED, SLOVENIA), ENERGY EFFICIENCY
J. Krope, A.Ghani Olabi, D. Goričanec & S. Božičnik

Investigation of Design Parameters of Microalgae Panel Bio-Reactors for Building Façade Applications

EMIN SELAHATTIN UMDU, İLKER KAHRAMAN, NURDAN YILDIRIM & LEVENT BILIR

Abstract Application of microalgae has multiple functions such as CO2 fixation, biomass production, and waste water treatment. Microalgae cultivation systems, especially closed photo bioreactors can be implemented as components in buildings. Bio-reactors on a building's façade has the added benefit of acting as an effective insulation system. This can significantly decrease the energy demand for microalgae culture compared to solar standalone units and building energy demand. Furthermore, microalgae can give a dynamic appearance with a liquid façade that also works as an adaptive sunshade. Yet there are only a handful of examples in application and even less information on how these systems affect building energy behaviour. In this study, the thermal transmittance (U value) of different bio-reactors was determined. Experimental design methods were used for parametric study and analysis of observed data was performed. Heat transfer behaviour of the manufactured panel reactors at different operational conditions, which satisfies both thermal comfort in building and microalgae growth conditions, was evaluated.

Keywords: • Building Façade • Energy Efficiency in Buildings • Thermal Transmittance • Microalgae • Bio-Reactors •

CORRESPONDENCE ADDRESS: Emin Selahattin Umdu, Unda Engineering Industry and Trade Inc., Depark Technopark, İnciraltı Mahallesi, Mithatpasa Cad. No:56 D:20, 35340 Balçova/İzmir, Turkey, e-mail: selahattinumdu@gmail.com. İlker Kahraman, Yaşar University, Architecture & Environmental Design Department, No:37-39, Ağaçlı Yol, Bornova, İzmir, Turkey, e-mail: ilker.kahraman@yasar.edu.tr. Nurdan Yildirim, Yaşar University, Energy Systems Engineering Department, No:37-39, Ağaçlı Yol, Bornova, İzmir, Turkey, e-mail: nurdan.yildirim@yasar.edu.tr, Levent Bilir, Yaşar University, Energy Systems Engineering Department, No:37-39, Ağaçlı Yol, Bornova, İzmir, Turkey, e-mail: levent.bilir@yasar.edu.tr.

https://doi.org/10.18690/978-961-286-050-9.28 ISBN 978-961-286-050-9

Available at: http://press.um.si.

1 Introduction

Nearly zero-energy buildings contain systems and renewable energy harvesters which help to fulfil current minimum energy performance requirements. Yet they cannot actively capture CO_2. Algae-culture offers one of the most productive ways to make a sustainable energy source. Application of microalgae has multiple functions such as CO_2 fixation, biomass production, O_2 generation and waste water treatment. Microalgae cultivation systems, especially closed photo bioreactors can be implemented as components in buildings. Application of bio-reactors on a building façade has the added benefit of acting as an effective insulation system, keeping out the heat of the summer and the chill of the winter. This could significantly decrease the energy demand for microalgae culture, compared to solar standalone units, [1] and the energy demand of the building [2]. Furthermore, microalgae can give a dynamic appearance with a liquid façade that also works as an adaptive sunshade [3]. With increasing biomass concentration during the cultivation process, the appearance of the building will change in colour and transparency.

Although microalgae integrated systems, especially in buildings, has been a hot topic in recent years, there are only a handful of examples in application and even less information on how these systems affect building energy behaviour. Other studies on microalgae mostly focused on single application approach targeting either CO_2 utilization through biomass production or biofuel production. And this approach resulted in negative net energy for produced fuel [4].

Microalgae panel bio-reactors for building façade system addresses three mechanisms; increasing thermal resistivity of building facade, creating a constant temperature shell around the building and increasing thermal mass. In this study, the thermal transmittance (U value) of different bio-reactors was determined. Possible applications for use as a building element was investigated. Experimental design methods were used for parametric study and analysis of observed data was performed. Heat transfer behaviour of the manufactured panel reactors at different operational conditions, which satisfies both thermal comfort in building and microalgae growth conditions, were evaluated.

2 Design and manufacture of panel reactors

The evaluated bioreactors were investigated as a façade element at 5-30 cm thickness with various wall thickness. To be able to see the insulation effect, the bioreactors were considered with and without air layer at the exterior surface. A view of the panel reactors is given in Figure 1. The reactor panels were produced from transparent acrylic, polymethylmethacrylate (PMMA) sheets. One side of the panel reactor is isolated with air inside and the other side is used for as photo-bioreactor.


Figure 1. View of an evaluated photo bio-reactor

Experimental design methods were implied in order to determine the effect of design parameters on the desired outcomes. For this purpose, the system and/or process were identified using the least sources by statistical methods. In this way, the sufficient information about the system can be achieved with the minimum number of experiments and mathematical models can be set up to achieve optimum results.

Box-Behnken design, which is one of the most referenced experimental design method in this field, was used in this study. The number of the experiments was determined as 13 by Box-Behnken methods with the results of 3-factors experimental design. In total, 13 different panels were used in experiments. The information about experimental design is presented in Table 1.

Table 1. Dimensions of 4 different panel reactors tested

Panel Reactor Name	dx1 (cm)	dx2 (cm)	dx3 (cm)
PR 1	5	0	1.5
PR 2	30	0	1.5
PR 3	5	5	1.5
PR 4	30	5	1.5
PR 5	5	2.5	0.6
PR 6	30	2.5	0.6
PR 7	5	2.5	2
PR 8	30	2.5	2
PR 9	17.5	2.5	0.6
PR 10	17.5	5	0.6
PR 11	17.5	2.5	2
PR 12	17.5	5	2
PR 13	17.5	2.5	1.5

3 Experimental setup

In order to simulate the building façade application and to determine the required heat transmission coefficient and energy requirement behaviour of the system, an experimental setup was designed. The view of the experimental setup is presented in Figure 2. One surface was heated by circulation of hot water in aluminium heat exchanger plate contacted to entire wide side of the panel bioreactor, where the other opposing side was cooled by circulation of cold water in another aluminium heat exchanger plate contacted.

CO_2 needed for microalgae growth is supplied by air feed line from 0.55 kW blower equipped with pipelineair rotameter and directly feed to the bottom of the panel reactor with a straight supply line in the middle of the reactor. 25 L/min air supplied to the reactors during heat transfer experiments.

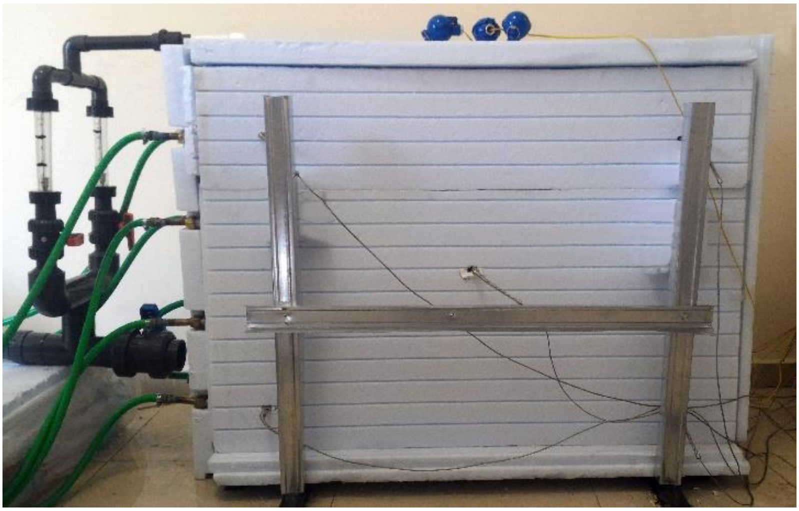

Figure 2. View of the heat transfer experimental setup

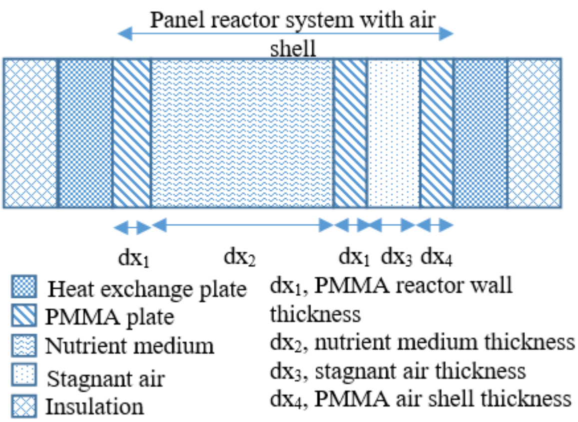

Figure 3. Cross section of the experimental system

The two sides of the manufactured panels were held at different temperatures by two large surfaces connected on the opposite sides of the panels. One side was heated at a desired temperature while the other side was cooled at a desired temperature by circulating hot and cold water inside the channels of the large surfaces. The cross section of the experimental setup is presented in Figure 3. The hot and cold water at constant temperatures were supplied by the refrigerator and heating units. The environment and panel temperatures were recorded regularly and consistently. In order to measure the surface temperature of the panels, five thermocouples were employed as shown in Figure 4. The surface area of a panel is 0.885 m^2.

Nanno chloropsis occulata used in preliminary studies and F2 medium was used as the growth medium [5]. Optical density was used to monitor the algae growth [6].

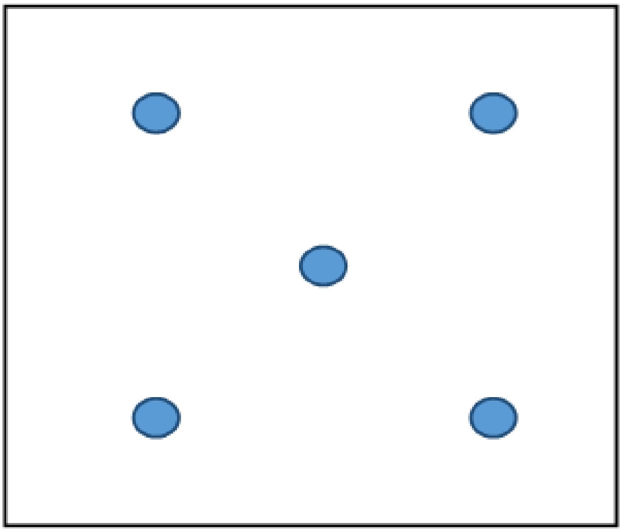

Figure 4. Locations of thermocouples on the surface of a panel

Briefly, the temperatures at 16 points of the experimental setup were monitored and recorded by data loggers. The locations of the temperature measurement are given below:

- 5 points of the outer surface of the panel for both sides (4 at the corners, 1 at the centre)
- Water temperature in the panel at 3 points, middle of each wall and middle of the panel reactor
- Environment (outdoor) temperature of the experimental setup

When the system reaches steady state, the overall heat transfer coefficient (U) can be calculated using the measured temperatures and the heat transfer rate through the panel.

4 Calculation of overall heat transfer coefficient for a panel

Microalgae uses light and some inorganic salts to grow and as they grow. They decrease light transmittance due to increased biomass. Heat transfer of a façade system is a phenomenon that covers all aspects of heat transfer; conduction, convection and radiation. To simplify this, an experimental system was designed in such a way that there is no air between panel reactor and heat exchange plates, and entire system is well insulated. Thus there is no convection between panel reactor and heat exchange plates and radiation terms are negligible. Overall heat transfer coefficient for entire system including; PMMA walls, microalga growth medium and air shell, was calculated by the Equation 1 given as follows;

$$U = \frac{Q}{A\,\Delta T} \tag{1}$$

5 Results and discussion

Overall heat transfer coefficient (U) value was calculated by using temperature and energy consumption data acquired during steady state operational conditions and selected heat transfer coefficients from experimental results are given in Table 2. During the experiments one side of the reactors were considered at indoor comfort temperature condition, 24 °C, while outside temperature of 32 °C, which is average outdoor temperature in İzmir, was employed. Panel reactors without stagnant air shell has the highest U value, 85.24 W/m^{2}K as expected, even if reactor plate thickness is quite high. Addition of an air shell with internal width of 5 cm at outside facing surface decrease U value down to 4.54 W/m^{2}K. Increasing reactor growth volume by increasing thickness only results in increase of U value from 18.57 to 26.09 W/m^{2}K for 0.6 cm PMMA plate thickness reactors with 2.5 cm air shell.

Table 2: Overall heat transfer coefficients for selected panel reactors

Panel Reactor Name	dx1 (cm)	dx2 (cm)	dx3 (cm)	U (W/m^{2}K)
PR 1	1.5	5	0	85.28
PR 3	1.5	5	5	4.54
PR 5	0.6	5	2.5	18.57
PR 9	0.6	17.5	2.5	26.09

Preliminary microalgae growth studies showed also that low and high temperature ranges has similar low growth results and light transmittance behaviour. These limiting temperatures results in low culture concentration thus system transmits more light to the building. Light transmission changes as a function of growth and light transmittance is dropped down to %10 for 10 cm thickness of growth medium in 12 days at optimum conditions.

6 Conclusion

Possible applications of flat plate photo bioreactors for use as a building element was investigated. The results showed that although reactors itself has quite high overall heat transfer coefficient, panel reactors coupled with air shells decreased overall heat transfer coefficients significantly. Furthermore, even low thicknesses of microalgae growth medium has potential to prevent solar radiation to reach building surface and absorb radiative heat from outdoors to be directed off the building.

Acknowledgements

The authors would like to express their gratitude to Yaşar University and Nilüfer, Bursa Municipality for the financial support of the project Yaşar-BAP039, from which the results of the present study were derived.

References

[1] J. Pruvost, B. Le Gouic, O. Lepine, J. Legrand, F. Le Borgne, "Microalgae culture in building-integrated photobioreactors: Biomass production modelling and energetic analysis", *Chemical Engineering Journal*, vol. 284, pp. 850–861, 2016

[2] J. Entwistle, "Algae powered architecture", *Ingenia*, Issue 64, 2015.

[3] G. Proksch, "Growing sustainability - Integrating Algae, Cultivation into the Built Environment", *EAR*,vol. 33, 2013.

[4] L. Gouveia, *Microalgae as a Feedstock for Biofuels*, Heidelberg Dordrecht London New York: Springer, ISSN 2191-5385, 2011.

[5] Guillard, R.R.L., "Culture of phytoplankton for feeding marine invertebrates", In Smith W.L. and Chanley M.H (Eds.) Culture of Marine Invertebrate Animals. Plenum Press, New York, USA, 26-60, 1975

[6] Chen, Meng, et al. Effect of nutrients on growth and lipid accumulation in the green algae Dunaliellatertiolecta. Bioresource Technology, 2011, 102.2: 1649-1655.

10TH INTERNATIONAL CONFERENCE ON SUSTAINABLE ENERGY AND ENVIRONMENTAL PROTECTION (JUNE 27TH –30TH, 2017, BLED, SLOVENIA), ENERGY EFFICIENCY
J. Krope, A.Ghani Olabi, D. Goričanec & S. Božičnik

Empirical Analysis of Energy Efficiency in South Africa

JANET BRUCE-BRAND & MARCEL KOHLER

Abstract Improvements in energy efficiency are a cost-effective way to reduce energy consumption and CO2 emissions internationally. The study focuses on determinants of energy efficiency in South Africa to understand the drivers of changes in energy use. The model employed estimates both a long and a related short run equation for determining energy efficiency using time series analysis. In the long run, the use of energy is dependent on capital stock, output and investment in the economy. The R2 is high, at 0.92. The short run relates changes in energy use specifically to the capital/output ratio. A rise in the capital/output ratio is found to reduce energy use, whilst a fall in the ratio increases it. The research suggests the relationship between energy and capital has to change if South Africa is to become energy efficient. Energy policy should therefore focus on monitoring the energy/capital ratio to promote energy efficiency.

Keywords: • energy • efficiency • decomposition • economy • South Africa •

CORRESPONDENCE ADDRESS: Janet Bruce-Brand, M.Com., Research Assistant, University of KwaZulu-Natal, School of Accounting, Economics and Finance, University Road, Westville, 4000 Durban, South Africa, e-mail: brucebrandj@ukzn.ac.za. Marcel Kohler, M.Com., Senior Researcher and Academic Leader for Economics, University of KwaZulu-Natal, School of Accounting, Economics and Finance, University Road, Westville, 4000 Durban, South Africa, e-mail: kohler@ukzn.ac.za.

https://doi.org/10.18690/978-961-286-050-9.29 ISBN 978-961-286-050-9

Available at: http://press.um.si.

1 Introduction

Improvements in energy efficiency are accepted internationally as one of the most cost-effective means in addressing crosscutting issues such as energy security, climate change, competitive-ness, and the promotion of technology transfers to assist countries in reducing their energy intensity. By international standards the economy of South African is extremely energy intensive with just a few countries having higher intensities. South Africa's primary energy use per unit of GDP is amongst the highest in the world standing at 0.13 tonnes of oil equivalent (toe) per thousand 2005 US dollars of GDP calculated using purchasing power parities in 2010. This compares with values for 2010 of 0.22 and 0.16 for Russia and China and averages of 0.09 and 0.15 respectively for OECD and non-OECD countries. According to reference [1] what is a source of concern is the relatively small reduction in South Africa's energy use per unit of GDP of 29% for the period 1990 to 2010 in comparison to a 38% decline for non-OECD countries on average and a reduction of 34% for Russia and 67% for China over this period. 3

The proposed study contributes to the energy efficiency literature by undertaking an econometric analysis of energy efficiency in South Africa. The regression estimation employs

an energy use index constructed for the country from a decomposition of the economy's use of energy. In this manner, the research isolates and highlights the drivers of economy-wide changes in South Africa's energy use over the period 1971 to 2012.

2 Background

Energy efficiency according to reference [2] and [3] involves a reduction in the energy input of a given service or level of economic activity. The resulting reduction in energy consumption whilst usually associated with technological changes can also come about as a result of better management or improved economic conditions in the sector under investigation. Energy efficiency is measured as the change recorded in energy intensity in order to account for its quantitative nature. A common definition of energy intensity formalised in a study by reference [4] measures this intensity in terms of energy consumption per national production unit such as the J (joule) per US$ of GDP. The study here follows this approach. Improving the energy efficiency of production processes is generally regarded as a low cost and effective way of curbing energy demand in an economy.

2.1 South African Energy Efficiency

Figure 1 shows the aggregate energy intensity of South Africa from 1971 to 2012. The trend seems to be decreasing through the years. This should not be interpreted as a reduction in the energy consumption over the studied period. Both economic output and energy consumption increased through the years but the increase in energy consumption was lower than the increase in GDP so the overall ratio decreased. In other words, the value of energy intensity shows how many units of energy (in this case TJ) are consumed for the production of 1 unit of economic output (in this case ZAR millions). Given this explanation, the total economy decreased its energy demand to produce R1 million from 1.335 TJ in 1971 to 0.727 TJ in 2012. In other words, the required energy to produce R1 million decreased by 62.95% from 1971 to 2012, with an average year-on-year decrease of 1.49%.

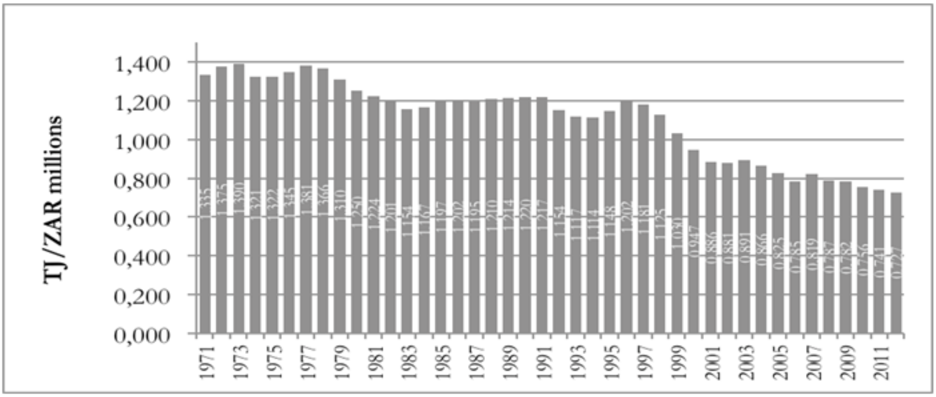

Figure 1. Aggregate SA Energy Intensity

Importantly, from the perspective of this study, there is a need to put the energy usage of each economic sector in perspective by comparing the energy intensities of the various sub-sectors.

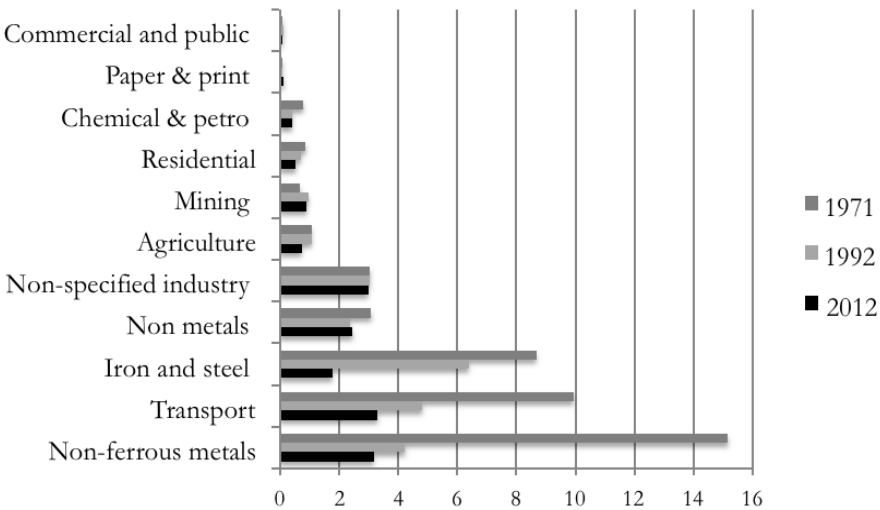

Figure 2. Energy Intensity per SA Sector

Figure 2 shows the energy intensity per sector, defined as energy usage in TJ divided by value added in R millions for the years 1971 and 2012. In 1971, the most energy intensive sectors of the South African economy were ‘non-ferrous metals’, ‘transport’, ‘iron and steel’, ‘non-metallic minerals’ and ‘non-specified industry’. The picture has not changed drastically in 2012 with the exception of the non-ferrous metals and transport sectors which have seen substantial reductions in their energy intensity over the analysis period. These sectors continue however to be the most energy intensive for 2012, as well, with ‘agriculture’ and ‘mining’ also taking places in the top intensive sectors alongside iron and steel, non-metallic minerals and non-specified industry.

3 Methodology

To highlight changes in energy use intensity, the study adopts an index decomposition analysis approach as in reference [5]. Decomposition methodology is an extensively employed tool, particularly in resource and materials related modelling and research over the last two decades.

3.1 Decomposition analysis

The study adopts the fisher ideal index approach to perform a decomposition analysis. The main advantage of this method is that it does not involve any residual terms, which would make it difficult to interpret the relative importance of structural and intensity (technical) effects. Specifically, reference [6] emphasises that perfect decomposition methods are preferred in the case of two-factor decomposition owing to their theoretical foundation and adaptability, as well as the ease with which their results can be interpreted. In this study, changes in South Africa's energy use *(e_t)* are decomposed into structural and intensity components. Following the decomposition literature, the research problem is set in terms of total energy use *(E)* and total production *(Y)*, as well as sub-indices for economic sector *(i)* and years *(t)*. Thus, the aggregate energy use intensity *(e)* can be written as:

$$e_t = \frac{e_t}{Y_t} = \sum_i^n \frac{e_{it}}{y_{it}} \frac{Y_{it}}{Y_t} = \sum_i^n e_{it} s_{it} \tag{1}$$

Equation 1 indicates that a change in energy use may be due to changes in energy intensity (e_{it}) and structural composition (s_{it}). One of the main practical advantages of this approach is that, by construction, the energy uses in the different sectors need to form a partition (i.e., they must not overlap), but the measures of economic activities do not need to satisfy this condition. In fact, they do not even need to be expressed in the same units. This facilitates the identification of good indicators to account for the structural composition (s_{it}). Following the theory on index numbers, dividing Equation (1) by the aggregate energy intensity for a base year *(e_0)* allows a perfect decomposition of the aggregate energy use intensity index into intensity (F^{int}) and structural (F^{str}) indices with no residual. The result, the fisher ideal index, is a geometric mean of the Laspeyres and Paasche price indices. Reference [7] showed that this index satisfied perfect decomposition of an expenditure index into a price and quantity component. In the context of this study, the Fischer Ideal index provides a perfect decomposition of South Africa's aggregate energy use intensity index.

$$e_t/e_0 \equiv I_t = F_t^{\mathrm{str}} F_t^{\mathrm{int}} \qquad (2)$$

By taking the logarithm of equation (2), it is possible to observe the additive contribution of the structural effect (F_t^{str}) and the intensity effect (F_t^{int}) to the total variation in energy use per output unit (I_t). This decomposition suggests a way to attribute changes in energy consumption arising from improvements in energy use intensity. Energy savings ($\mathbf{\Delta}Et$) due to changes in energy intensity are then defined as:

$$\mathbf{\Delta}E_t = E_t - \hat{E}_t \qquad (3)$$

where E_t is actual energy use and $\hat{E}_t$ is the energy use that would have occurred had energy use remained at its 1971 level. The study attributes the change in energy use between intensity and economic structure as follows:

$$\mathbf{\Delta}E_t = \mathbf{\Delta}E_t[\ln(F_t^{str})/\ln(I_t)] + \mathbf{\Delta}E_t[\ln(F_t^{int})/\ln(I_t)]\ Ft \quad \equiv \mathbf{\Delta}E_t^{str} + \mathbf{\Delta}E_t^{int} \qquad (4)$$

3.2 Data

The data employed in the analysis are obtained from two specific sources. Economic sub-sector and total energy consumption data is sourced from various issues of the International Energy Agency (IEA) reference [2]. In the IEA Energy Balances, the economy consists of five sectors (industrial, commercial, agricultural, residential and transport) disaggregated in 22 sub-sectors. The identified total energy consumption includes consumption of the following fuel types: coal, crude oil, petroleum, gas, nuclear, hydro, geothermal, solar, renewables, waste and electricity. The real economic output information for the economy and per sectoral contribution is obtained from reference [8] the Quantec Easy databases. The data on investment (real gross fixed capital formation, excluding residential, 2005 prices) and capital stock (real productive capital stock, total excluding residential, 2005 prices) have been taken from the South African reserve bank historical data archives.

4 Empirical results

The first results are for the Fisher decomposition of South Africa's energy intensity computed by partitioning the country's aggregate energy use into industrial, transportation, commercial, agricultural and residential sub-sectors by assigning appropriate economic activity measures to each of these energy sectors. Thereafter the result of the regression analysis that seeks to determine the main drivers of changes in South Africa's energy indexes is presented.

4.1 SA Energy Intensity Trends

Figure 3 depicts the results for the South Africa energy indexes with the year 1971 serving as the base year in the analysis. Aggregate energy intensity in 2012 is calculated to be 53 percent of its intensity level in 1971. The activity index was 101 percent basically back at the same level it was in 1971 while the efficiency index was 52 percent of its 1971 level. In other words, had the composition of economic activity not changed between 1971 and 2012, energy intensity would have been 52 percent of its 1971 level. The forty eight percent improvement in South Africa's energy intensity was due to improvements in energy efficiency. Similarly, had energy efficiency been fixed at its 1971 levels for all sectors, changes in economic activity would have led to a 1 percent increase in energy intensity.

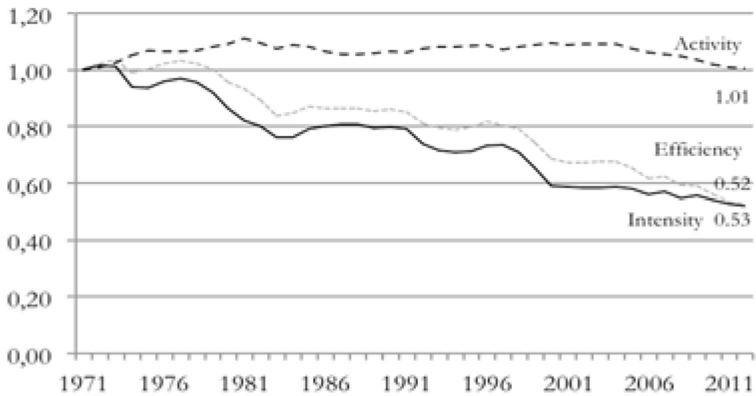

Figure 3. South African Energy Indexes

Using Equation (4), the study allocates the change in energy use (relative to the amount that would have been consumed had energy intensity remained at its 1971 level) between efficiency and economic activity. Based on this approach, nearly all of the 53 quads of energy reduction arising from improvements in energy intensity can be attributed to improvements in energy efficiency. In contrast to this changes in the composition of economic activity have adversely impacted on the country's energy intensity.

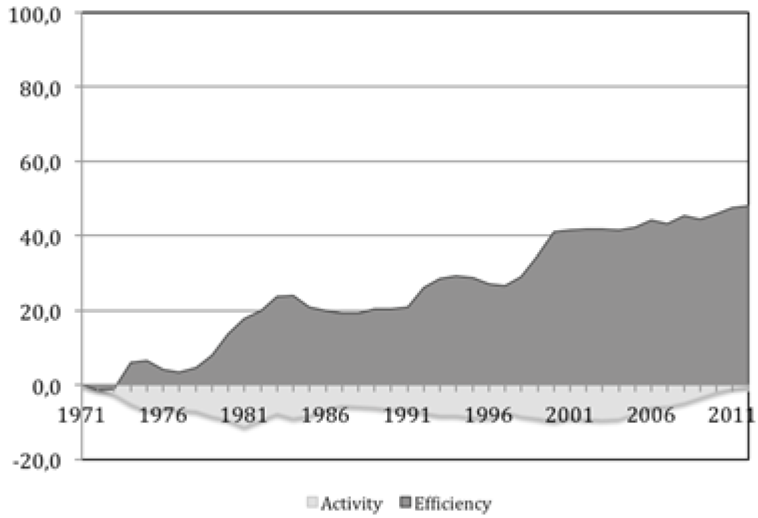

Figure 4. Energy Savings Relative to 1971

Figure 4 shows the contributions of improve-ments in energy efficiency and compositional changes on energy savings between 1971 and 2012. Through out the period under investigation changes in energy consumption can be attributed almost entirely to improvements in efficiency. The effects of the changing mix of South African economic activity has had an adverse impact on the country's energy savings by contributing to increases in energy intensity almost throughout but this adverse impacts disappears by 2012. It is important to highlight that the decomposition is conditional on the particular choice of energy sectors identified in the analysis and used in the partitioning of the data.

4.1 Drivers of south africa's energy use

The decomposition results highlight the significance of technological improvements in driving changes in South Africa's energy use intensity. The intensity (or technical) effect is the dominant factor that contributes to downward pressure on the country's energy consumption. This is because the intensity effect works in either of two ways (or a combination thereof), namely, (1) technical progress can motivate users of energy to substitute other production inputs for energy resources and/or (2) it could encourage them to decrease their energy usage through the recycling of energy use. Policy makers should, therefore, implement appropriate policies to promote technical progress and the re-use of energy resources. Although reductions in energy use intensity embodied in new capital may well account for a proportion of the intensity (technical) effect, one would still expect this effect to be relatively small and constant over time, and not a driver of the large short-run fluctuations in the intensity effect.

Turning the study focus on the intensity effect, the decomposition analysis seems to show that energy intensity rises during periods of low economic growth and falls in periods of high economic growth. It would seem from casual observation that this effect is due to higher levels of investment in periods of high economic growth. With the new capital stock being less energy-intensive than that which it replaces, there has been a corresponding marked improvement in energy use intensity in the economy. Such an explanation does not however appear to make intuitive sense. This is because the proportion of the total capital stock replaced in any year, even in a year when economic growth is high, is relatively low. Furthermore, it is not clear why energy use intensity would rise even in periods when investment is low. For even in years when investment in South Africa has been low, the level of investment has been more than enough to offset depreciation, thereby lifting the country's capital stock.

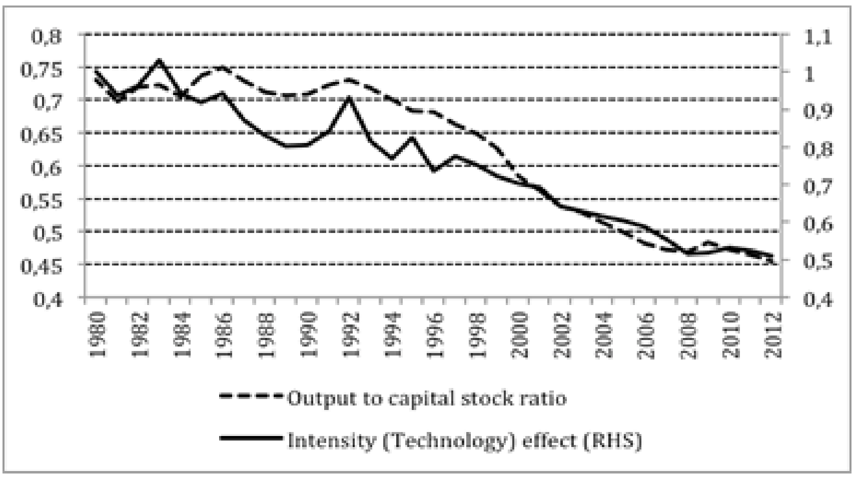

Figure 5. Capacity Utilisation

On closer examination it appears that variations in South Africa's energy use intensity are more likely to be due to changes in capacity utilisation (see figure 5). A relatively high proportion of energy use in economic activities is fixed, with energy being used for cooling, heating, cleaning purposes etc. The remainder reflects changes in production levels, and represents the variable proportion of total energy costs. It is changes in these variable costs that reflect short-run changes in the aggregate level of economic activity. Because of the fixed component, total energy use will not fluctuate as much as output. The study derives capacity utilisation for the economy by taking the ratio of capital stock/output. Figure 5 indicates that capacity utilisation and the intensity effect track each other fairly closely. Remember that the intensity (technical) effect index represents the movement in the residual component of the energy/output ratio after adjustment for industrial structure. Hence, the intensity (technical) effect index is a good indicator of the intensity of energy use. Note that a rise in the capital/output ratio indicates a fall in capacity utilisation, and vice versa. Hence, Figure 5 reveals that the energy/output ratio falls as capacity utilisation rises, and rises as capacity utilisation falls. This trend is consistent with the notion of having separate fixed and variable costs associated with energy usage.

What remains to be explained is why the energy/output ratio would actually rise during periods when net investment is positive. To interrogate this, the study runs a number of regressions, to verify the magnitude of the various relationships. Regressing the intensity effect on the capital/output ratio generates a R^2 of 0.74. Regressing the intensity effect on investment produces an R^2 of only 0.07. The R^2 of both series together against the intensity effect is 0.82. To check that this is not a result of multi-collinearity between investment and the capital/output ratio, the one is regressed against the other; at 0.004, the R^2 does not suggest a significant relationship between these two series. The regression analysis therefore indicates that the intensity effect, or energy use per unit of output, is affected by both capacity utilisation and investment, with the equation being:

$$ln(IE)=5.05+1.10ln(KS/Y)-0.24ln(GFKF) \qquad (5)$$

where:

IE is the intensity (technical) effect index
KS/Y is the real productive capital stock/output ratio
GFKF is the real gross fixed capital stock (investment).

Given that the coefficients of the equation are in logs, we can interpret these as elasticities. Hence a 1 percent rise in the capital/output ratio can be expected to result in a 1.1 percent increase in the energy/output ratio, while a 1 percent rise in GFKF will result in a 0.24 percent fall in the energy/output ratio. Hence both factors are at work. A rise in capacity utilisation will lower the intensity of energy use, as will a fall in investment. The analysis therefore suggests that when investment levels in South Africa are lower than in the previous year, the contribution from investment causes a rise in the energy/output ratio. This development still appears to be counter-intuitive. As mentioned earlier, even in years when investment falls in South Africa, the level of investment is still substantial. It therefore does not seem to follow that an easing in the level of investment will necessarily result in a rise in the energy/output ratio. On closer inspection investment is found to be highly correlated with output, with an R^2 of 0.85. Hence, investment may have entered into Equation (5) because of its correlation with output, which is the denominator of the dependent variable in this equation, namely: the energy/output ratio.

Suppose that the output level is not used as the denominator of energy use (the dependent variable) in Equation (5) but instead the regression analysis simply represents the variables of interest in the study in levels. That is, the analysis represents energy use as a function of the capital stock and the investment level, as in equation (6).

$$E = f(KS_{t-1}, GFKF) \qquad (6)$$

This representation of energy use makes intuitive sense, especially if the economy's capital stock is lagged by one year. That is, energy use is then dependent on last year’s capital stock and this year’s increment to the capital stock (investment). This suggests that the capital stock level generally determines energy use. But do the data back this up?

A closer inspection of the data sheds light on the changes in the energy/output ratio, which in the mid 1980s and early 1990s was due to falls in output. The analysis suggests, energy use generally reflects the level of capital stock supporting the view that the fixed component of energy use is high. Specifically, energy use in economic activity is related to the machinery, equipment and infrastructure of the economy, rather simply the level of output produced. The study next adopts a co-integration approach, estimating a long run model of energy use based on the economy's capital stock, output, and capacity utilisation. The best-fit relationship (with a R^2 of 0.92) is for South Africa's energy use expressed as a function of the economy's stock of capital. An interesting feature of the long run relationship is the coefficient on the capital stock, which at 0.963, is less than 1. This implies that a 1 per cent rise in the capital stock will be accompanied by a 0.96 per cent rise in energy use. It points to the country's capital stock becoming less energy-intensive although the rate of change is slow.

5 Conclusions

The study draws a number of conclusions from the decomposition and regression analysis that help inform energy policy within South Africa. Firstly, the decomposition analysis suggests that the improvements in South Africa's energy intensity are almost entirely driven through the efficiency rather than the activity channel. The regression analysis indicates that in the long run, energy use in the South African economy is related to the capital stock. It also suggests that the capital stock is becoming more energy-efficient over time, but that this change is gradual.

The relationship between energy and the economy's capital stock has to change, if South Africa is to become more energy efficient. The study indicates this is far better than monitoring the country's energy/output ratio, and drawing strong conclusions from the later, as this is fraught with difficulties. The study supports the use of a combination of approaches in the management of South Africa's energy resources including information-based tools such as labelling and the education of producers and consumers. Together a mixture of energy management tools will incentivise innovation and the adoption of new processes and technologies. This will reduce the intensity of energy use across all sectors of the economy and assist policy makers to decouple energy use and its impact on South Africa's economic growth.

Acknowledgements

The authors acknowledge the financial support of Economic Research Southern Africa.

References

[1] Organisation for Economic Cooperation and Development, *Economic Surveys: South Africa*. Paris: OECD, 2013.

[2] International Energy Agency, *Energy balances for non-OECD countries*. Paris: OECD, various years.

[3] World Energy Council, *Energy efficiency policies around the world: review and evaluation*. New York: WEC, 2008.

[4] J.W. Sun and B.W. Ang, "Some properties of an exact energy decomposition model", *Energy*, vol. 25(12), pp. 1177-1188, 2000.

[5] R. Hoekstra and J.C. Van den Bergh, "Comparing structural decomposition analysis and index", *Energy Economics*, vol. 25, pp. 39-64, 2003.

[6] B.W. Ang and F.Q. Zangh, "A survey of index decomposition analysis in energy and environmental studies", *Energy*, vol. 25(12), pp. 1149-1176, 2000.

[7] I. Fisher, "The Best Form of Index Number", *Quarterly Publications of the American Statistical Association*, vol. 17(133), pp. 533-537, 1921.

[8] Quantec, *Easy Database*. Pretoria: Quantec, various years.

10TH INTERNATIONAL CONFERENCE ON SUSTAINABLE ENERGY AND ENVIRONMENTAL PROTECTION (JUNE 27TH – 30TH, 2017, BLED, SLOVENIA), ENERGY EFFICIENCY
J. Krope, A.Ghani Olabi, D. Goričanec & S. Božičnik

Investigation of Flow Characteristics of Synthetic Jet Driven by Duty Cycle Signal

YAHYA ERKAN AKANSU, MUSTAFA SARIOĞLU, MEHMET SEYHAN & HÜRREM AKBIYIK

Abstract An experimental study is carried out to investigate flow characteristics of synthetic jet driven by a duty cycle signal in quiescent air. A loudspeaker is used as an actuator in order to generate synthetic jet. This actuator is driven with different frequencies between 5 and 50 Hz and the duty cycle, changing from 10% and 50% with the increment of 10%, is applied at f = 20 Hz. Single and tandem signals up to five periods are obtained by arranging duty cycle frequency. Three different flow mode is obtained that are blowing-suction (the first mode), core jet velocity (second mode) and losing momentum at core region (third mode). For the duty cycle case, the number of peak is always one more than driving frequency.

Keywords: • Synthetic jet • hot-wire anenometer • duty cycle signal• quiescent air. • velocity •

CORRESPONDENCE ADDRESS: Yahya Erkan Akansu, Ph.D, Associate Professor, Ömer Halisdemir University, Faculty of Engineering and Mechanical Engineering, Niğde, Turkey, e-mail: akansu@ohu.edu.tr. Mustafa Sarıoğlu, Ph.D., Assistant Professor, Karadeniz Technical University, Faculty of Engineering and Mechanical Engineering, Trabzon, Turkey, e-mail: sarioglu@ktu.edu.tr. Mehmet Seyhan, MSc., Research Assistant, Karadeniz Technical University, Faculty of Engineering and Mechanical Engineering, Trabzon, Turkey, e-mail: mehmetseyhan@ktu.edu.tr. Hürrem Akbıyık, MSc., Research Assistant, Çukurova University, Faculty of Engineering and Mechanical Engineering, Adana, Turkey, e-mail: hakbiyik@cu.edu.tr.

https://doi.org/10.18690/978-961-286-050-9.30 ISBN 978-961-286-050-9

Available at: http://press.um.si.

1 Introduction

Synthetic jet actuator is one of the most known active flow control methods. Synthetic jet (SJ) or Zero Net Mass Flux (ZNMF) can be produced with the help of a piezoelectric diaphragm [1]–[3], a piston cylinder mechanism [4], [5] and a loudspeaker [6], [7]. It works by ingesting ambient air and expelling air inside cavity through an orifice consecutively. SJ actuators have some advantages such as no external air supply and no plumbing as compared to continuous jet [8], [9]. They have wide usage areas including heat transfer enhancement [9]–[11], flow control [12]–[14] and fuel cell performance enhancement [15], [16].

Qayoum et al. [17] showed that how synthetic jet characteristic changes with variation in the voltage and frequency. They reported that the amplitude modulation seriously affects the basic synthetic jet characteristics and also increased both the magnitude of rms velocity fluctuations and the jet flow direction. Crispo et al. [18] compared the flow area by producing synthetic jet with chevron and conventional model nozzle exits. In the models, the electric power, Reynolds number and Strouhal number are set the same values. This indicated that the flow field clearly depends on the output geometry of the nozzles. Feero et al. [8] experimented with cylindrical, conical and contraction models in order to show the space change on synthetic jet performance. They noted that the radial velocity profiles are the same in all three models, but differ in magnitude. Tesar and Kordik [19] defined the vortex lengths which are proportional to the diameter of the nozzle with the Tollmien hypothesis. They reported that the vortices are small and slow while the Stokes number increases. Travnicek et al. [20] described four different flow field regimes by flow visualization in their experimental study. These regimes are creeping flow without SJ formation, SJ formation and propagation without vortex rollup, SJ with vortex rollup, and vortex structure breakdown-instability-transition to turbulence. Their results indicated that the synthetic jet regimes differed in low, medium and high Stokes numbers.

The purpose of this study is to investigate the effect of duty cycle changing between 10% and 50%.

2 Experimental setup

The experiments were performed to investigate influence of driving signal over loudspeaker synthetic jet actuator by measuring the instantaneous velocity via hot-wire anemometer. As shown in Figure 1, experimental setup consists of a synthetic jet actuator, a hot-wire probe, a two axis traverse mechanism, a computer, a function generator, an oscilloscope, a traverse controller, a constant temperature anemometer (CTA), an amplifier, a power supply, a current probe, and BNC data acquisition.

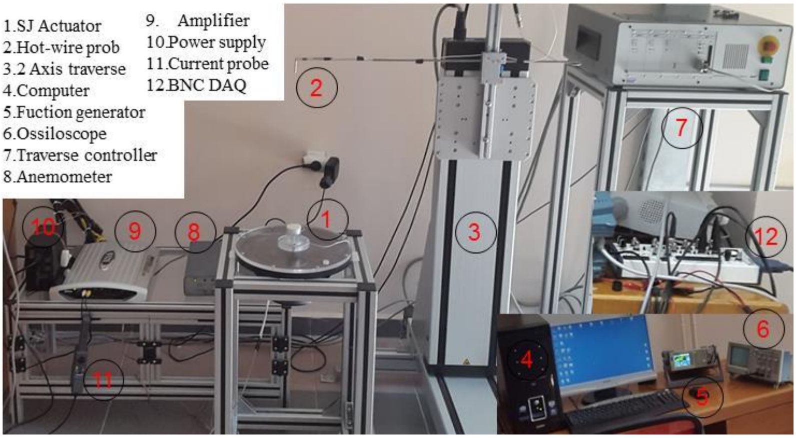

Figure 1. SJ actuator experimental setup

Loudspeaker driven synthetic jet actuator composes of the loudspeaker, the plexiglass sheet creating a cavity volume, plexiglass pipe and cap having diameter (d) of 20 mm. The velocity measurement was carried out via 6 channels DANTEC Multichannel CTA from 55P11 single wire probe. Desired signal modulations such as duty cycle (DC) and shifting phase angle are generate by using AA TECH brand AWG-1010 function waveform generator. Generated signal is amplified with BOSS brand 1000 W amplifier in order to operate the Jameson brand JW-36 model 1000 W subwoofer loudspeaker. Driving signal monitored with oscilloscope. Data collections of instantaneous velocity and current signal are carried out with NI PCI-6220 data acquisition card. Tektronix A622 AC/DC current probe used to obtain driving signal.

Experiments were carried out for the driving frequencies of 5, 10, 20 and 50 Hz in order to obtain synthetic jet characteristic of the SJ actuator. Furthermore, the actuator is driven with a burst signal having 500 ms period at the duty cycle changing from 10% and 50% with the increment of 10%. Experimental uncertainty of the velocity measurements calculating by the uncertainty analysis method suggested by Coleman and Steele [21] is 4.7%.

3 Results

Figure 2 shows the average velocity distributions in the radial direction of the blowing frequency at y / D = 1, 2 and 5. Here, it is seen that the velocity distributions are uniform in the radial direction $-0.5 \leq r/D \leq +0.5$, which corresponds to low driving voltage in the region very close to the nozzle exit (y/D = 1). Moreover, it gradually turns into a parabolic form with increasing frequency. It can be seen that the velocity of the jet on the radial direction at y/D = 1, 2 and 5 preserve the level of velocity over the jet axis despite the expansion in the radial direction.

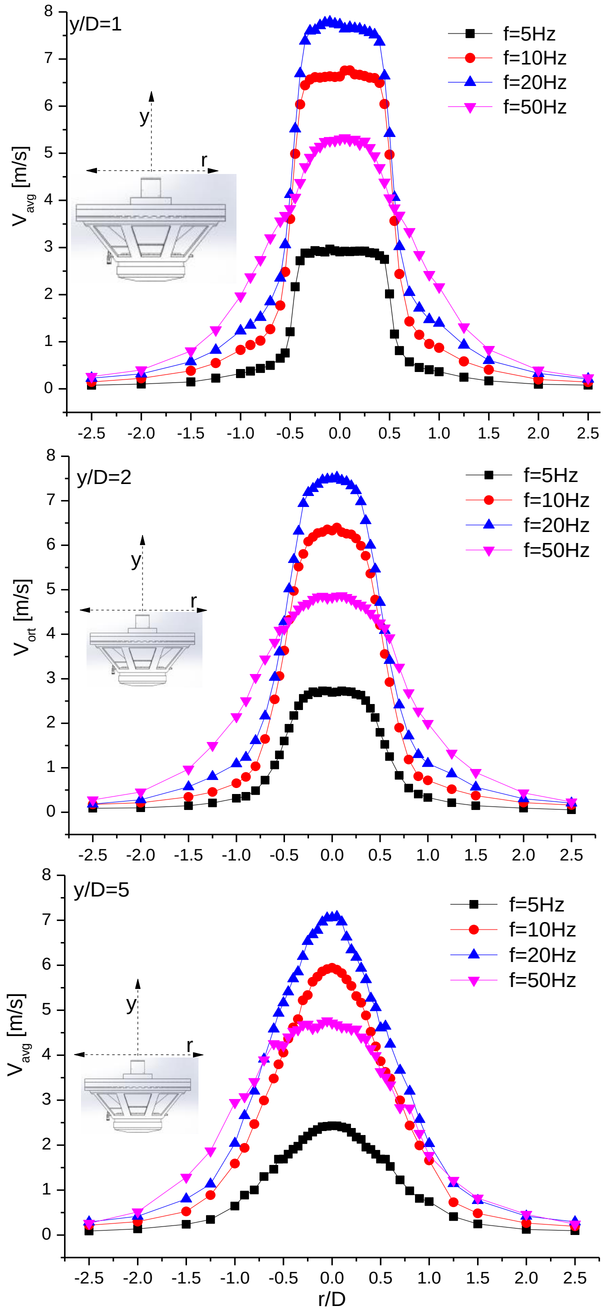

Figure 2. Averaged velocity distribution for continuous driving signal with different frequency at y/D=1, 2 and 5

Figure 3 shows the current-time variation obtained from the current probe of the actuator signal for 5 different states between 10% and 50% of the duty cycle value. At 10% duty cycle, sinusoidal signal is obtained as single period. In the case of DC = 50%, 5 consecutive periods are formed.

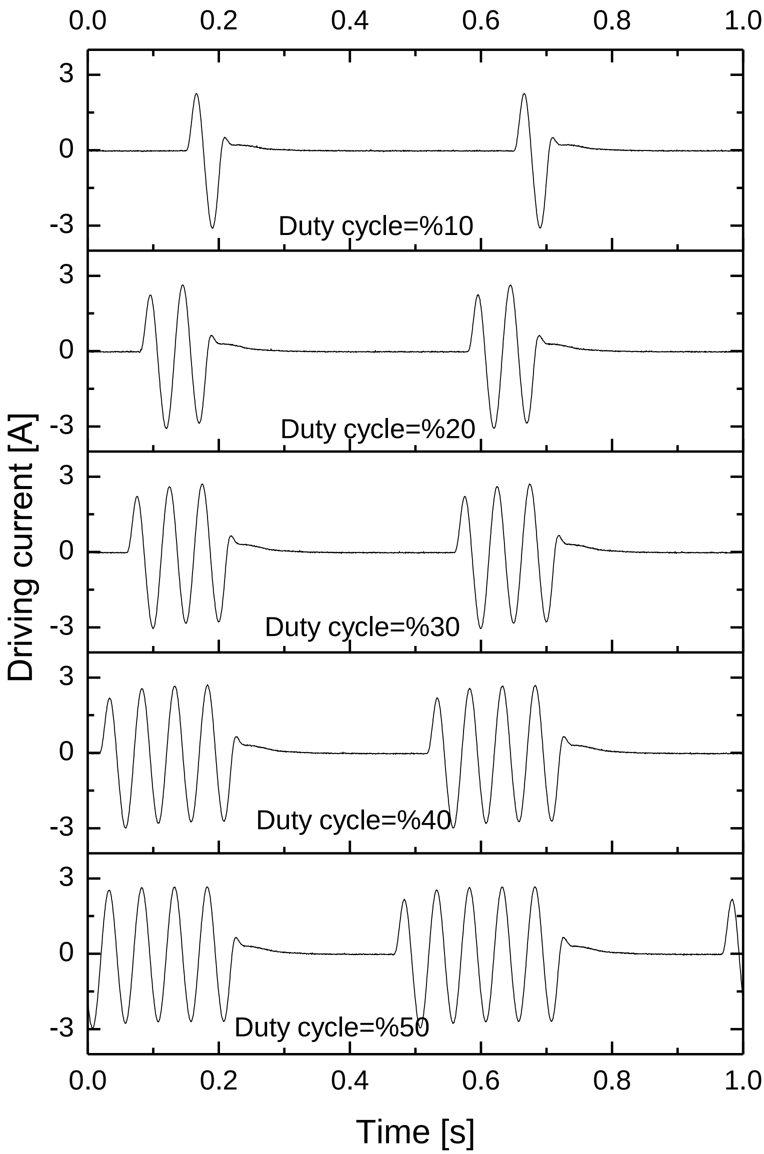

Figure 3. Current signal - time history for different duty cycle values

The instantaneous velocity distributions for these signals are given in Fig. 4 and 5 for y/D = 0 and 5 probe positions, respectively. In Fig. 4, red line and black line indicate blowing and suction of the actuator, respectively. In the velocity measurements taken from y/D = 0 position, instantaneous velocity changes in both the blowing and the suction cases as the probe stay at just outside of the nozzle. At DC = 10%, the first peak here indicates the blowing jet (red line) which is occurred with flowing signal from the zero level to the positive amplitude, the second peak indicates instantaneous velocity which is flowing from positive signal amplitude to the negative signal amplitude in the suction mode, and the third peak indicates the jet formed during the change from negative to zero amplitude of the signal. The velocity in suction mode intrinsically has negative value according to the axis of the nozzle but the hot wire anemometer independent from measurement axis measures the velocity perpendicular to the direction of the wire, therefore the measured velocity is shown in the plot as the positive value.

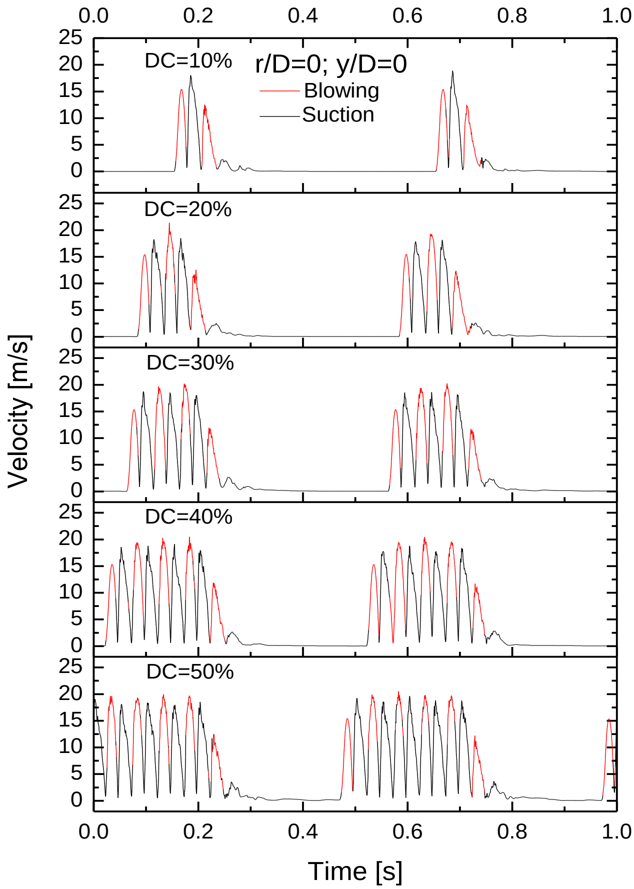

Figure 4. Instantaneous velocity distribution for DC = 10%, 20%, 30%, 40% and 50% at y/D = 0

When examined the velocity distribution at y/D = 5, only the first and third velocity peaks are visible because the suction mode is not effective at this position. The number of velocity peaks of jets is formed due to the phase angle of the sinusoidal signal starting from zero. In other words, when the number of signals generated based on the duty cycle mode is 1-5, the number of peaks in the velocity distribution is 2-6. The first and last velocity peaks were lower than interval velocity peaks due to the half-amplitude signal. It is seen that the maximum velocity values of the jet are up to 20 m/s.

Figure 6 shows the comparisons of the continues sinusoidal signal (f_{cs}=20 Hz) and the duty cycle signal in terms of the average velocity distribution along the synthetic jet axis. The flow structure here consists of three modes. It can be seen that the average velocities decrease rapidly up to y/D=1 denoted as Mode-1. In this first mode, the measured velocity includes both suction and blowing velocity.

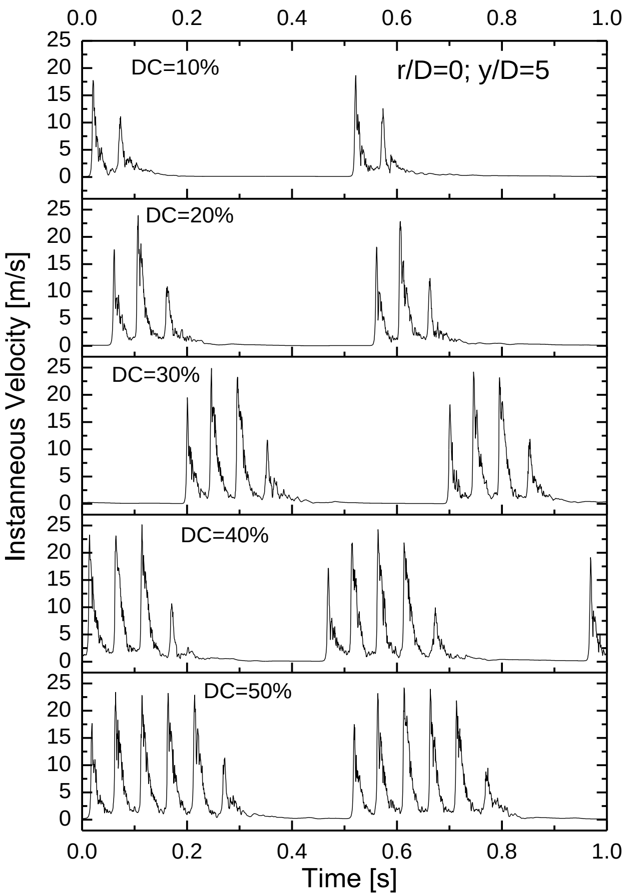

Figure 5. Instantaneous velocity distribution for DC = 10%, 20%, 30%, 40% and 50% at y/D = 5

Since the hot-wire probe is far enough away from the nozzle (up to about 1D), the average velocity of the jets only include the blowing of the actuator that is called as second mode. The average velocities stay at about the same level because the velocity in the jet axis within the core region does not change in the range of y / D = 1-3.5. After this distance, it is indicated that the averaged velocity of jet at radial direction is gradually decreased at the centre axis between y/D= 3.5 and y/D=10. At these ranges, flow mode is called as third mode. When the duty cycle is increased from DC = 10% to DC= 50%, the averaged velocity distribution along jet axis is gradually augmented due to increasing the number of cycle. In the range of y/D= 1 and y/D=3.5, the averaged velocities for DC=50% and f_{cs}=20 Hz are 4.1 m/s and 7.5 m/s, respectively. Even though the number of cycle within one second is decreased at rate of 50%, decrease in the maximum velocity is obtained as 45.3% as compared to continuous sinusoidal signal.

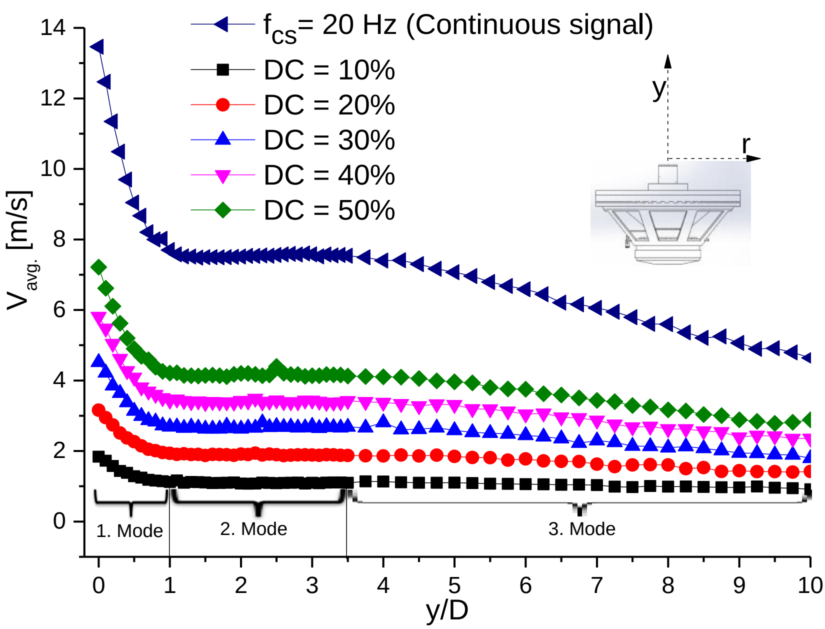

Figure 6. Instantaneous velocity distribution for DC = 10%, 20%, 30%, 40% and 50% and continuous sinusoidal signal at f = 20 Hz.

4 Conclusıon

Effect of duty cycle changing from 10% and 50% over the performance of the synthetic jet actuator is experimentally investigated. Three flow regime for the synthetic jet based on y/D is identified. The first mode include blowing and suction of jet up to y/D= 1, the second mode involve core jet velocity between y/D= 1 and y/D= 3.5 and third mode indicated the losing momentum up to y/D =10. For the duty cycle case, the number of peak is always one more than driving frequency.

Acknowledgements

The authors would like to acknowledge the financial support of this work by the Scientific and Technological Research Council of Turkey (TUBITAK) under the Contract Number of 215M920.

References

[1] C. Lee, G. Hong, Q. P. Ha, and S. G. Mallinson, “A piezoelectrically actuated micro synthetic jet for active flow control,” *Sensors Actuators, A Phys.*, vol. 108, no. 1–3, pp. 168–174, 2003.

[2] a. Seifert, S. Eliahu, D. Greenblatt, and I. Wygnanski, “Use of piezoelectric actuators for airfoil separation control,” *AIAA J.*, vol. 36, no. 8, pp. 1535–1537, 1998.

[3] S. and Dahalan, M.N., Mansor and A. Ali, “Cavity Effect of Synthetic Jet Actuators Based on Piezoelectric Diaphragm,” *Appl. Mech. Mater.*, vol. 225, no. September 2015, pp. 85–90, 2012.

[4] T. M. Crittenden and A. Glezer, “A high-speed, compressible synthetic jet,” *Phys. Fluids*, vol. 18, no. 1, pp. 1–18, 2006.

[5] J. M. Shuster and D. R. Smith, “Experimental study of the formation and scaling of a round synthetic jet,” *Phys. Fluids*, vol. 19, no. 4, 2007.

[6] P. Gil and P. Strzelczyk, “Performance and efficiency of loudspeaker driven synthetic jet actuator,” *Exp. Therm. Fluid Sci.*, vol. 76, pp. 163–174, 2016.

[7] A. McGuinn, R. Farrelly, T. Persoons, and D. B. Murray, “Flow regime characterisation of an impinging axisymmetric synthetic jet,” *Exp. Therm. Fluid Sci.*, vol. 47, pp. 241–251, 2013.

[8] M. a. Feero, P. Lavoie, and P. E. Sullivan, “Influence of cavity shape on synthetic jet performance,” *Sensors Actuators A Phys.*, vol. 223, pp. 1–10, 2015.

[9] L. D. Mangate and M. B. Chaudhari, “Heat transfer and acoustic study of impinging synthetic jet using diamond and oval shape orifice,” *Int. J. Therm. Sci.*, vol. 89, pp. 100–109, 2015.

[10] D. I. Rylatt and T. S. O’Donovan, “Time and frequency domain investigation of the heat transfer to a synthetic air jet,” *J. Phys. Conf. Ser.*, vol. 395, no. 1, p. 12046, 2012.

[11] X. M. Tan, J. Z. Zhang, S. Yong, and G. N. Xie, “An experimental investigation on comparison of synthetic and continuous jets impingement heat transfer,” *Int. J. Heat Mass Transf.*, vol. 90, pp. 227–238, 2015.

[12] M. Amitay, D. R. Smith, V. Kibens, D. E. Parekh, and A. Glezer, “Aerodynamic flow control over an unconventional airfoil using synthetic jet actuators,” *AIAA J.*, vol. 39, no. 3, pp. 361–370, 2001.

[13] D. C. Mccormick, “Boundary Layer Separation Control with Directed Synthetic Jets,” *AIAA-Paper*, pp. 2000–519, 2000.

[14] S. H. Kim and C. Kim, “Separation control on NACA23012 using synthetic jet,” *Aerosp. Sci. Technol.*, vol. 13, no. 4–5, pp. 172–182, 2009.

[15] J. Choi, E. Lee, J. Jang, Y. H. Seo, and B. Kim, "Development of synthetic jet air blower for air-breathing PEM fuel cell," *Development*, vol. 475, pp. 13138, 2009.

[16] Y. H. Seo, H. J. Kim, W. K. Jang, and B. H. Kim, “Development of active breathing micro PEM fuel cell,” *Int. J. Precis. Eng. Manuf. Technol.*, vol. 1, no. 2, pp. 101–106, 2014.

[17] A. Qayoum, V. Gupta, P. K. Panigrahi, and K. Muralidhar, “Influence of amplitude and frequency modulation on flow created by a synthetic jet actuator,” *Sensors Actuators, A Phys.*, vol. 162, no. 1, pp. 36–50, 2010.
[18] C. M. Crispo, C. S. Greco, F. Avallone, and G. Cardone, “On the flow organization of a chevron synthetic jet,” *Exp. Therm. Fluid Sci.*, vol. 82, pp. 136–146, 2017.
[19] V. Tesař and J. Kordík, “Quasi-similarity model of synthetic jets,” *Sensors Actuators, A Phys.*, vol. 149, no. 2, pp. 255–265, 2009.
[20] Z. Trávníček, Z. Broučková, J. Kordík, and T. Vít, “Visualization of synthetic jet formation in air,” *J. Vis.*, vol. 18, no. 4, pp. 595–609, 2015.
[21] H. W. Coleman and W. G. Steele, *Experimentation, validation, and uncertainty analysis for engineers*. John Wiley & Sons, 2009.

10TH INTERNATIONAL CONFERENCE ON SUSTAINABLE ENERGY AND ENVIRONMENTAL PROTECTION (JUNE 27TH – 30TH, 2017, BLED, SLOVENIA), ENERGY EFFICIENCY
J. Krope, A.Ghani Olabi, D. Goričanec & S. Božičnik

Prediction of the Influence of the Liquid Temperature Effect on Two-Phase Flow Through a Granular Medium

ADEL OUESLATI & ADEL MECRICHE

Abstract A new setup, consisting of a glass column packed with calibrated solid particles, has been designed, achieved and tested. It operates on the principle of an air lift pump. It was designed for the best contact between air and water. The fluid circulation in a granular medium is achieved by an air-lift pump. A unidimensional model, based on that of literature, has been developed. The effect of liquid temperature, on the hydrodynamic, has been considered in this model. The developed model is used to predict gas holdup, pressure drop, and liquid and gas flow rates at any liquid temperature. The results, obtained with the model, are found to agree with experimental data.

Keywords: • Airlift pump • Granular medium • Two-phase flow • Liquid temperature effect • one dimension model •

CORRESPONDENCE ADDRESS: Adel Oueslati, Higher technological studies institute of zaghouan, Mogren, 1140, Tunisia. adel.oueslati@laposte.net. Adel Mecriche, Faculty of Sciences of Tunis, Al Manar university, 1001, Tunisia. Adel.mecriche@fst.rnu.tn.

https://doi.org/10.18690/978-961-286-050-9.31 ISBN 978-961-286-050-9

Available at: http://press.um.si.

1 Introduction

Two-phase flow through a porous media is an important topic of research. It has several applications in chemical, nuclear, oil, and other industries. In these applications, the high surface area of heat and mass transfer, between phases, is looked. But, the heat and mass transfer depend, mainly, on the hydrodynamic in the granular medium [1, 3]. So, the literature exam shows that several models describing the hydrodynamic are developed. Maldonado et al. [1] showed the effect of packing particles on the hydrodynamic. The tests are achieved in small values of velocities of phases. Turpin & Huntington [5] studied the influence of operating conditions on the pressure drop. In their study, a new model was developed and validated. For the same goal, a new model was developed by Yang et al. [4]. The model is more accurate than that of Turpin et. al [5]. In another hand, Tung & Dhir developed a new model [2]. In each flow regime and the transition between regimes was described by specific equations. The uncertainty of this model is almost 15%. A new research project of upward flow of two-phases in a granular medium where liquid circulation is achieved by an air-lift pump was developed by Oueslati et al. [6-15]. In this project the effect of several variables on the hydrodynamic was studied. The originality of this works consists in the combination between airlift pump and a two-phase flow in a granular medium. The most previous models are validated in restricted operating conditions and the uncertainty is relatively high. Although the mistakes in the development of equations, the model of Tung and Dhir [3] provides the best accuracy and large operating conditions applications. So, the objective of this paper is to develop a new model based on that of Tung and Dhir. Therefore, in the new model the variables of an airlift pump and the liquid temperature will be considered.

2 Experimental setup

The setup is shown in fig.1. The riser is a glass tube with 2m in length and 72 mm inner dimeter. It is filled with glass Rashig rings. The down comer is a glass of 72 mm inner dimeter. The upper end of the riser is connected to a collecting tank (6) where the air escapes to atmosphere. The air coming from the compressor enters the riser through the jacket holes and moves with it, in the upward direction, the liquid. The water, pumped, passes from tank (6) to the water feeding tank. Its flow rate is measured by a calibrated float flow meter. The water is, already, heated by the heater (12). The level of the liquid in the tank (8) is controlled by an automatic regulator (10).

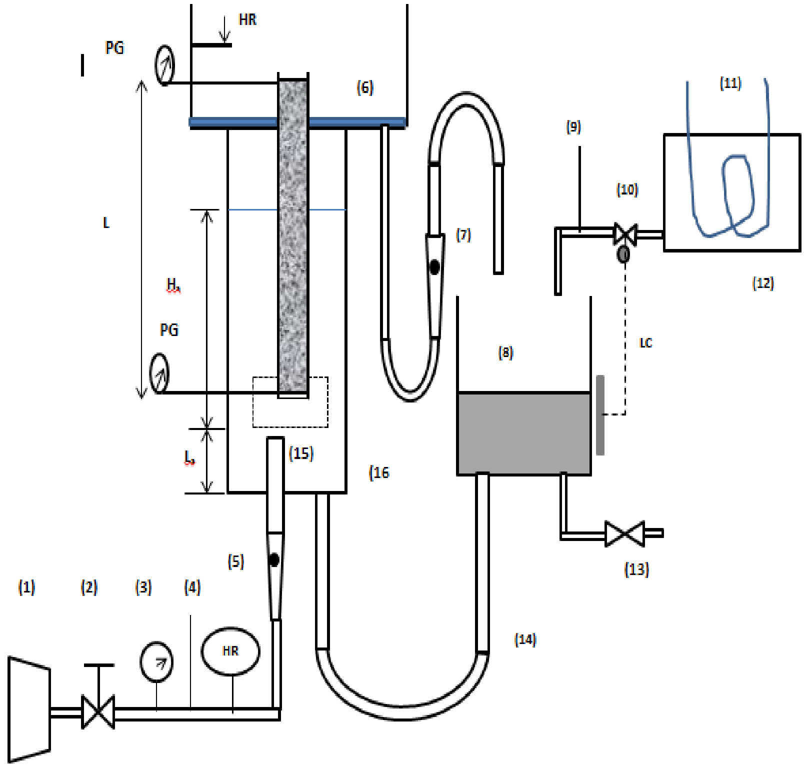

Figure-1: Experimental setup

1. compressor, 2. Valve, 3.pressure gauge, 4. Thermometer, 5. Air flow meter, 6. Collecting tank, 7. Water flow meter, 8. Water feeding tank, 9.thermometer, 10. Level control, 11.heater 12. Heating tank, 13. Valve, 14. Down comer, 15. Air-jacket, 16.holding tank, HR. Relative humidity sensor, LC. Level control. PG. Pressure Gauge.

The pressure, the temperature and the flow rate of inlet air are measured by calibrated instruments. The relative humidity of air is measured at the foot and at the head of the riser by calibrated hygrometers. The humidity ratio is calculated from measured values of RH using equation detailed in [15].

The air injector consists of 63 small holes of 2 mm dimeter uniformly distributed around the pipe perimeter in nine rows and seven columns to unsure uniform feed of the air into the pipe. Various liquid temperatures for each submergence ratio were investigated in the present study. The range of liquid temperature was obtained in increments of 5°C. For each liquid temperature and submergence ratio, the air flow rate was varied and the corresponding flow rate of water and humidity of air were measured. A procedure of specified and planed measurements was followed for each run.

Table 1: Physical characteristics of the packing particles

Type of packing particles	Glass rings
Density (kg/m3)	2.187
Average diameter: d_p (m)	0.008
Average length: l_p (m)	0.008
Fixed bed porosity: ϵ	77.3
Form factor: φ	0.681

3 Modeling

The model is based on the forces balances on fluid phases and the correlations established by [2] in the case of sphere glass as a packing. In the present work, we will use the same equations of [2] after modification. So, the Forces balance on the gas phase is given by the following equation:

$$-\frac{dP}{dz}\varepsilon_G\varepsilon = \rho_G g\varepsilon_G\varepsilon + F_{pG} + F_i \quad (1)$$

Forces balance on the liquid phase is:

$$-\frac{dP}{dz}(1-\varepsilon_G)\varepsilon = \rho_L g(1-\varepsilon_G)\varepsilon + F_{pL} - F_i \quad (2)$$

We define the dimensionless quantities:

$$P^* = \frac{-\frac{dP}{dz}}{g(\rho_L-\rho_G)} \quad (3)$$

$$F^* = \frac{F}{g\varepsilon(\rho_L-\rho_G)} \quad (4)$$

$$\rho^* = \frac{\rho_G}{\rho_L} \quad (5)$$

Therefore, the forces balances on gas and liquid phases can be written, with dimensionless quantities, as follows:

$$P^*\varepsilon_G = \frac{\rho^*\varepsilon_G}{(1-\rho^*)} + F_{PG}^* + F_i^* \quad (6)$$

$$P^*(1-\varepsilon_G) = \frac{(1-\varepsilon_G)}{(1-\rho^*)} + F_{PL}^* - F_i^* \quad (7)$$

These equations (6 & 7) contain five variables. So, for solving these equations we need three equations. In the following section, F_{PG}^*, F_{PL}^* and F_i^* are given by three models.

$$F_{pG}^{*} = a^{*}\frac{\mu_G\, U_G}{k_G} + b^{*}\frac{\rho_G\, U_G^2}{\eta_G} \quad (8)$$

Where the expressions of a^{*}, b^{*}, k_G and η_G are calculated by the model defined in [2].

The dimensionless drag force due to the flow of the liquid is given by the following relation:

$$F_{PL}^{*} = a^{*}\frac{\mu_L\, U_L}{k_L} + b^{*}\frac{\rho_L\, U_L U_L}{\eta_L} \quad (9)$$

The permeabilities relative to the liquid phase and the dimensionless interfacial force, F_i^{*}, are calculated by the model described in [2].

The elimination of the pressure gradient between equations (6) and (7) yields:

$$\varepsilon_G F_{PL}^{*} - (1 - \varepsilon_G) F_{PG}^{*} - F_i^{*} = 0 \quad (10)$$

The pressure gradient can be calculated using either equation (6) or equation (4) or by adding the two equations to obtain:

$$\mathrm{P}^{*} = \frac{(1 - \varepsilon_G + \rho^{*}\varepsilon_G)}{(1-\rho^{*})} + \mathrm{F}_{PL}^{*} + \mathrm{F}_{PL}^{*} \quad (11)$$

The volumetric flow rate of gas can be written as:

$$Q_G = \frac{m_{as}}{\rho_G}(1 + X) \quad (12)$$

Where:

$$\rho_G = \rho_0 * \frac{T_0}{T} * \frac{P}{P_a} * \frac{\delta*(1+X)}{\delta+X} \quad (13)$$

The average absolute humidity is given by:

$$X = \frac{X_{in} - X_{out}}{Ln(\frac{X_{in}}{X_{out}})} \quad (14)$$

The water liquid density is calculated by the following equation [15]:

$$\rho_L = -0.0038T^2 - 0.0505T + 1002.6 \quad (15)$$

The dynamic viscosity of water liquid is given by the following equation [15]:

$$\mu_L = 10^{-5}(0{,}0046 * T + 1.7176) \quad (16)$$

The dynamic viscosity of the gas is given by the formula [15]:

$$\mu_g = \frac{9.81*10^5}{\dfrac{HR.P_{vs}}{\mu_v} + \dfrac{P_t - HR.P_{vs}}{\mu_a}} \tag{17}$$

P_{VS} is given by the DUPRE formula [15].

$$P_{Vs} = \exp[46.87 - \frac{6435}{T+273.15} - 3.868 * Ln(T_a + 273.15)] \tag{18}$$

The viscosity of the water vapor, μv, is given by the following formula [15]:

$$\mu_v = \frac{3.01472.10^{-6}}{1+\frac{673}{T+273.15}} \sqrt{\frac{T+273.15}{273.15}} \tag{19}$$

The viscosity of the air is given by the correlation [15]:

$$\mu_a = 10^{-5}(0.0046 * T + 1.7176) \tag{20}$$

The modified model is obtained by considering air humidification. Therefore, the liquid temperature is considered as an operating variable. Using this modified model, a computer program was developed in order to investigate the air-lift pump performance.

4 Results and discussions

Fig. 2 shows the variation of gas holdup (ε_G) in the packed column humidifier with superficial gas velocity (U_G). The figure shows that ε_G increases linearly with the increase of superficial gas velocity up to certain value. After this value, the effect of superficial gas velocity on the gas holdup is weak. So, the variation of gas holdup, with the variation of gas velocity, is slowly. This fact is observed for three different values of submergence ratio (Sr).

The figure shows also the effect of temperature on gas holdup. Indeed, if temperature increases then the gas holdup also increases. This is explained by water evaporation which represents an additional source of gas (vapor).

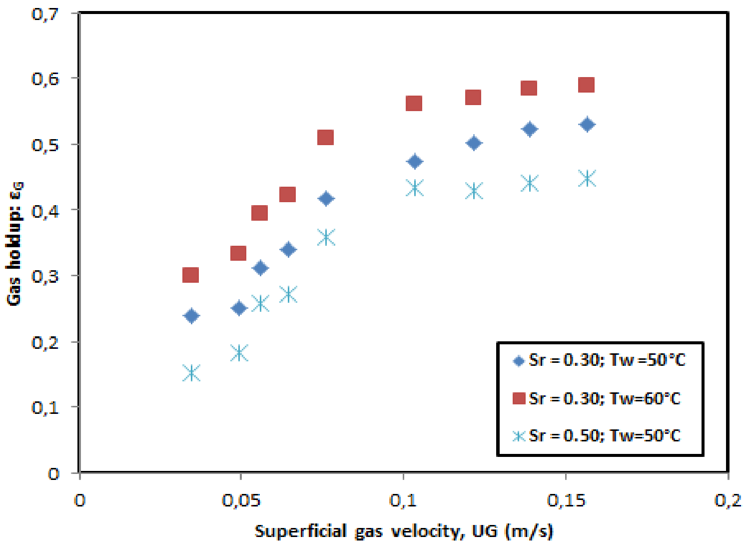

Figure-2: Effect of liquid temperature on the gas holdup.

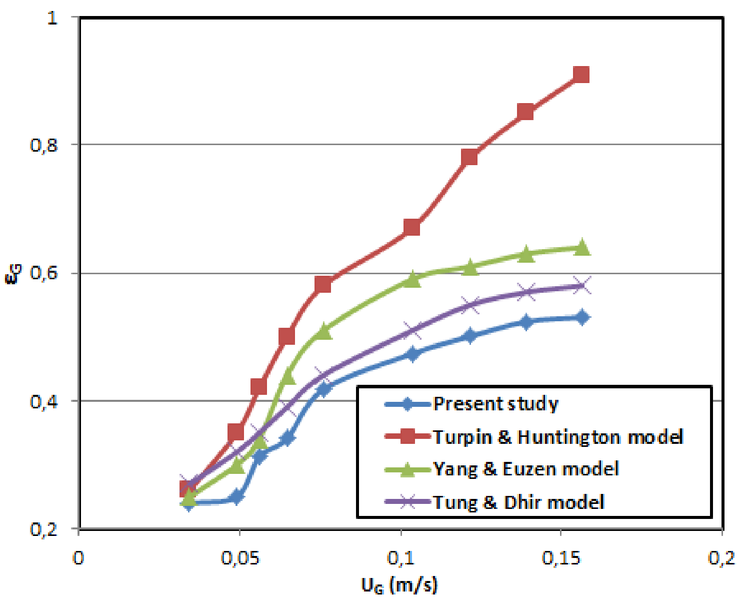

Figure-3: Comparison of predicted gas holdup with experimental data. Sr = 0.30; Tw = 50°C.

In addition, the submergence ratio increase has a negative effect on the gas holdup which is explained by the increase of liquid flow rate. Therefore, liquid holdup increase and gas holdup decreased.

Figs. 3-4 show the variation of gas holdup (ε_G) in the packed column humidifier with superficial gas velocity (U_G). The figure shows the results of the present study and three theoretical curves obtained by Turpin & Huntington, Yang & Euzen and Tung & Dhir model. We observed that the model of Tung and Dhir is the nearest model to the present study results.

This is explained by the accuracy of Tung and Dhir model. In general case, the difference between experimental results and that calculated by Tung ad Dhir model is don't exceed 15%.

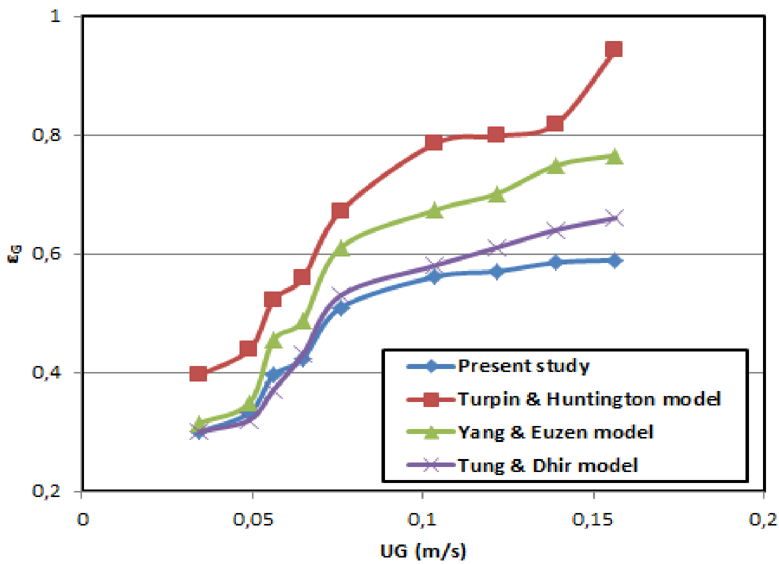

Figure-4: Comparison of predicted gas holdup with experimental data. Sr = 0.30; Tw = 60°C.

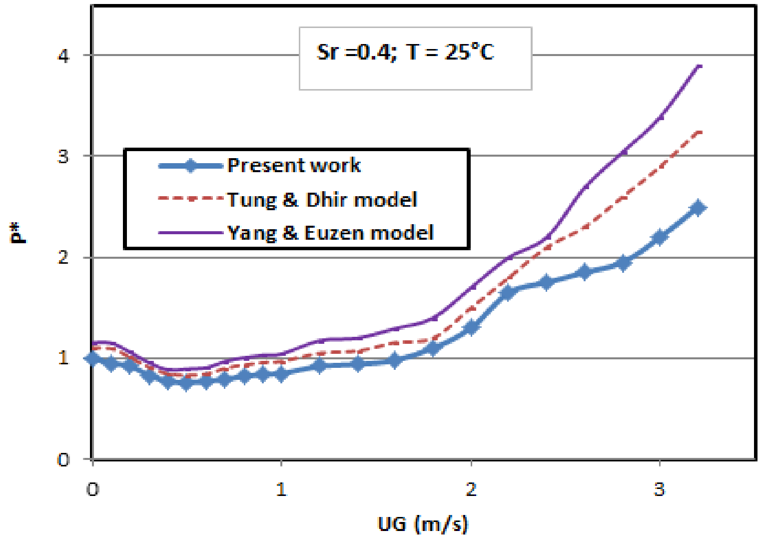

Figure-5: Comparison of predicted pressure gradient with experimental data.

This is explained by the existence of specific equations for each flow regime. So, this fact makes the model of Tung and Dhir, after modification, as the powerful tool of hydrodynamic prediction. The theoretical gas holdup calculated by the models of Turpin & Huntington and Yang & Euzen is greater than the experimental values. At high gas velocity, the difference between the experimental and theoretical results is more than 30%. This is explained by the non-accuracy of Turpin & Huntington model and Yang & Euzen model.

Figs. 5-6 show the variation of pressure drop (P*) in the packed column humidifier with superficial gas velocity (U_G). The experimental results and theoretical values calculated by Yang & Euzen and Tung & Dhir models. As, expected, the pressure drop increases with the increase of gas velocity and temperature. In addition, the Tung & Dhir model, after modification, is the nearest model to our experimental study.

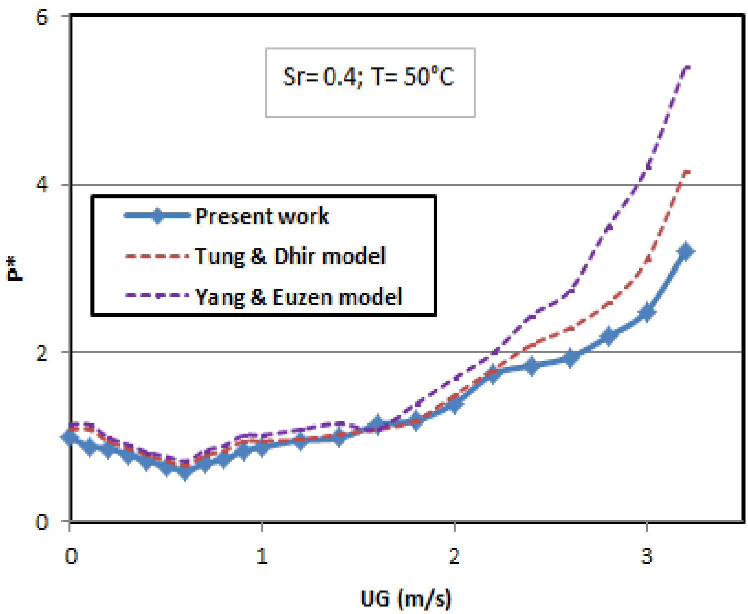

Figure-6: comparison of predicted pressure drop with experimental data.

Therefore the prediction of pressure drop of gas and liquid in upward flow in a granular medium is easy even at high temperature. But, at high values of superficial gas velocity the difference between theoretical results given in [2] and experimental results is about 18%.

The basic definition of gas holdup:

$$\varepsilon_G = \frac{Q_G}{Q_G + Q_L} = \frac{U_G}{U_G + U_L} \tag{21}$$

So,

$$U_G = \frac{\varepsilon_G}{1-\varepsilon_G} \mathrm{U_L} \tag{22}$$

Or,

$$U_G = \frac{m_G}{A * \rho_G} = \frac{m_{as}}{A * \rho_G} * (1 + X) \tag{23}$$

$$U_L = \frac{m_L}{A * \rho_L} \tag{24}$$

Therefore,

$$\frac{m_{as}}{\rho_G} * (1 + X) = \frac{\varepsilon_G}{1-\varepsilon_G}\frac{\mathrm{m_L}}{\mathrm{\rho_L}} \tag{25}$$

Tung and Dhir model gives the following values of gas holdup which correspond to regime flow change:

If $\varepsilon_G = 0.524$; The flow regime changes from bubbly to slug.

If $\varepsilon_G = 0.6$; The flow regime changes from slug to annular.

If $\varepsilon_G = 0.74$; The regime flow is annular.

The last equation (25) can be solved by giving the temperature (T), the vapor content in air X (kg v / kg a), gas holdup and dry air mass flow rate. The results of calculations are plotted in fig.7. This fig. shows the influences of gas mass flowrate, the flow regime and temperature on the mass liquid flow rate. In addition, the flow regime change varies with temperature.

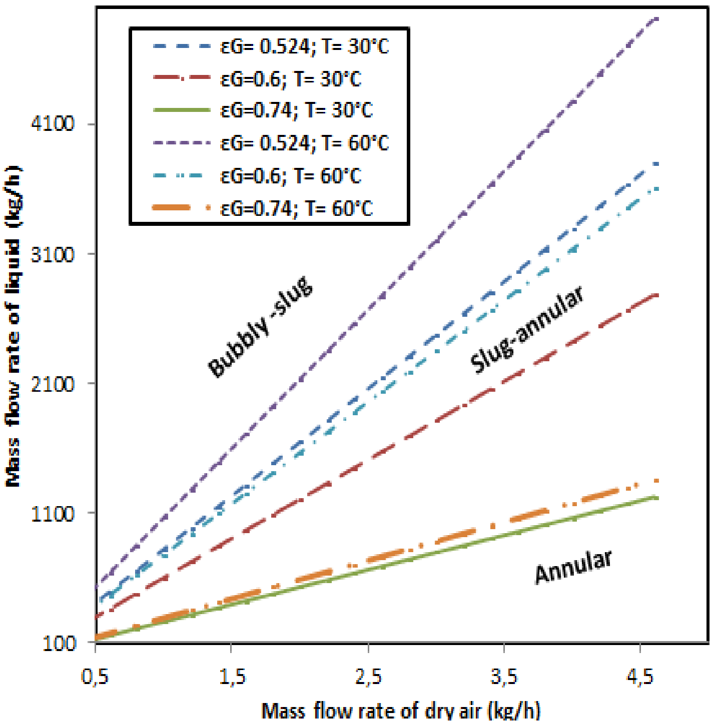

Figure-7: Theoretical Flow card regimes with saturated air.

So, the increase of liquid temperature makes the flow regime change more before that made by the increase of dry air flow rate. This fact is explained by the additional vapor comes from liquid phase to air. Indeed, the gas holdup will be increased by the water vapor and the flow regime change will occur.

5 Conclusion

The developed model is a first approach able to highlight the local mechanism of the effect of liquid temperature on the fluids flow in an airlift packed column. The gas holdup and the pressure drop can be predicted using the developed model. The flow pattern was also drawn easily with this model. The effect of liquid temperature and air humidification on the hydrodynamic can be predicted by the new model. Additional work is necessary to obtain accurate quantitative prediction of bubbles sizes, gas and liquid drag forces, and slip velocity, etc.

References

[1] G.G.Maldonado. Effet des caractéristiques physiques des matériaux sur l'hydrodynamique et le transfert de matière des lits fixes fonctionnant a co-courant ascendant de gaz et de liquide. Thèse de l'Institut des sciences appliquées de Toulouse, 2005.

[2] V. X. Tung et V. K. Dhir, A hydrodynamic model for two-phase flow through porous media, Int. J. Muhiphase Flow Vol. 14, No. I, pp. 47-65, 1988.

[3] Therning, P., Rasmuson, A. Liquid dispersion and gas holdup in packed bubble columns at atmospheric pressure. Chemical Engineering Journal, 2001, 81, pp. 69 – 81.

[4] Yang, X. L., Euzen, J. P., Wild, G. Etude de la perte de pression dans les réacteurs à lit fixe avec écoulement à cocourant ascendant de gaz et de liquide. Entropie, 1990a, No. 159, pp. 35 – 44.

[5] Turpin, J. L., Huntington, R. L. Prediction of pressure drop for two-phase, two-component concurrent flow in packed beds. AIChE Journal, 1967, Vol. 13, No. 6, pp. 1196 – 1202.

[6] Oueslati A., Hannachi A., Emaaoui M. hydrodynamic study of an adjustable height packed column operating on the principle of an air-lift pump. IJMET Vol.4, Is.2, March - April (2013), pp. 461-478.

[7] Oueslati A., Hannachi A., Elmaaoui M. Effect of air humidification on the pumping efficiency of water in a packed column humidifier, Energy Procedia 74 (2015) 1381 – 1393.

[8] Oueslati A., Hannachi A., Elmaaoui M. An experimental study on the air-lift packed column with adjustable height and many air injection points. IJARET, Vol. 4, Is. 1, Jan.-Feb. (2013), pp. 42-49.

[9] Oueslati A., Hannachi A., Elmaaoui M. Experimental Analysis of Air Humidification by Brackish Water in an Adjustable Height Packed Column Humidifier Operating on the Principle of an Air Lift pump, Int. J. of Ch. Eng. Vol.30, Is.1, 1103-1110.

[10] Oueslati A., Hannachi A., Elmaaoui M. Hydrodynamic study of an adjustable height packed column operating on the principle of an airlift pump, IJMET, Vol. 4, Is. 2, Mar.-Apr. (2013), pp. 461-478.

[11] Oueslati A., Hannachi A., Elmaaoui M. Simulation of air lift packed column, IEEE Xplore. 2013.

[12] Oueslati A., Hannachi A., ElmaaouiM. Theoretical analysis of the performance of airlift pumps used for pumping water in a closed loop, Cefd'2013, March 18-20, 2013, Sfax, Tunisia.

[13] Oueslati A., Hannachi A., Elmaaoui M. New pilot for air humidification-Dehumidification, Part I: Design basis, Icest'2017.

[14] Oueslati A., Hannachi A., Elmaaoui M. New pilot for air humidification-dehumidification, Part II: Some aspects of a new airlift packed column humidifier and dehumidifier, Icest'2017.

[15] Oueslati A. A new device for liquid pumping. Patentend in 2016. Innorpi-Tunisia.

[16] Oueslati A. conception, réalisation, expérimentation et modélisation d'un nouveau système de contact entre l'eau et l'air dans un milieu granulaire. Thèse de doctorat en génie chimique-procédés. 23 septembre ENI Gabes-Tunisie.

10TH INTERNATIONAL CONFERENCE ON SUSTAINABLE ENERGY AND ENVIRONMENTAL PROTECTION (JUNE 27TH – 30TH, 2017, BLED, SLOVENIA), ENERGY EFFICIENCY
J. Krope, A.Ghani Olabi, D. Goričanec & S. Božičnik

Theoretical and Experimental Study of Air Humidification by Sea Water in an Air Lift Pump Packed Column Humidifier

ADEL OUESLATI & AHMED HANNACHI

Abstract An experimental investigation of humidification process by air passing through sea water in air lift packed column is presented. This experimental work studied the influence of the operating conditions such as the water temperature, the submerged ratio on the vapor content difference and humidification efficiency.

The experimental results show that, the vapor content difference and the humidification efficiency of the system are strongly affected by the inlet water temperature to the evaporator chamber, submersion ratio and packing dimensions. The obtained maximum vapor content difference of the air was more than 500 gr w/kg a, at 85 °C which is high compared to that in literature.

Keywords: • Air humidification • sea water • packed column • air-lift pump • Sea Water •

CORRESPONDENCE ADDRESS: Adel Oueslati, Higher technological studies institute of zaghouan, Mogren, 1140, Tunisia. adel.oueslati@laposte.net. Ahmed Hannachi, University of Gabes, National School of Engineers of Gabes, Av. Omar Ibn-Elkhattab 6029, Gabes, Tunisia; email: ahmed.hannachi@enig.rnu.tn.

https://doi.org/10.18690/978-961-286-050-9.32 ISBN 978-961-286-050-9

1 Introduction

Air humidification is an operation that has many industrial applications and in desalination of water. It can be carried out, even at low temperature and under atmospheric pressure. A review of the literature shows that the use of packed columns [1-16] is more cost-effective than the technique of spraying water in hot air.

The countercurrent flow of water and air in a granular medium is the most effective configuration in the humidification of air. The choice of this configuration is aimed at maintaining the fixed packing particles. Therefore, bed properties such as porosity, height remain fixed during the experimental runs. Air humidification operations do not take into account the physicochemical properties of packing such as wettability, construction material, etc.

Fadi Al Naimat et al. [2] used a packed column to humidify the air. He attempted to establish a relationship between the results obtained and the position of the packing particles in the column.

In this article, we will study the diameter effect of glass rings used as packing particles on the humidification of the air by direct contact with seawater. The fluids are flowing upward in a packed column operating on the principle of an airlift pump. This co-current flow favors the dispersion of the material and a large exchange surface is offered [7]. Note that the glass rings favor the transfer of heat and material between the fluids thanks to the increase of the gas retention [16].

2 Theory

The submersion ratio, Sr, is calculated by the following equation:

$$S_r = H_s/L \qquad (1)$$

Where: H_S and L are the initial height of liquid in the riser before injecting air and the packed height column respectively (Fig.1).

The pressure of vapor, Ps, at saturation conditions is given by Dupre [**7**] which is valid between -50°C and 200°C.

$$P_s(T)=ex[46.784-(6435/\,(T+273.15))-3.868*\,ln\,(T+273.15)] \qquad (2)$$

Where: T is the Temperature in (°C), Ps(T) is the pressure of vapor at saturation conditions in (mmHg). The relative humidity, HR, is calculated by the following ratio:

$$HR = Pv\,(T)\,/\,P(T) \qquad (3)$$

P(T): is the vapor pressure at the temperature T. His value can be calculated by the equation (4):

$$P(T) = HR * P_S(T) \tag{4}$$

The mass of water vapor per kg dry air, X, at a temperature T and a total pressure P is given by the following expression:

$$X = 0.622\ Pv\ (T)\ /\ (P - Pv\ (T)) \tag{5}$$

The vapor content difference is defined as:

$$\Delta X = X_{out} - X_{in} \tag{6}$$

Where X in, X out are the inlet outlet humidity of the evaporator chamber. The humidification efficiency of the evaporator chamber is given by

$$\eta_{hu} = 100 \times \Delta X\ /\ (X_{out\,(Sat)} - X_{in}) \tag{7}$$

Where: $X_{(out)\,sat}$ is the outlet humidity of saturated air. Its value is calculated by equation (5) at saturated air conditions.

3 Experimental setup and procedure

The setup is shown in fig.1. The riser is a glass tube with 2m in length and 72 mm inner dimeter. It is filled with glass rings. The down comer is a glass of 72 mm inner dimeter. The upper end of the riser is connected to a collecting tank (6) where the air escapes to atmosphere. The air coming from the compressor enters the riser through the jacket holes and moves with it, in the upward direction, the liquid. The water, pumped, passes from tank (6) to the water feeding tank. Its flow rate is measured by a calibrated float flow meter. The water is, already, heated by an electrical heater (12).

The level of the liquid in the tank (8) is controlled by an automatic regulator (10). The pressure, the temperature and the flow rate of inlet air are measured by calibrated instruments. The relative humidity of air is measured at the foot and at the head of the riser by calibrated hygrometers. The humidity ratio is calculated from measured values of RH using equation detailed in [7].

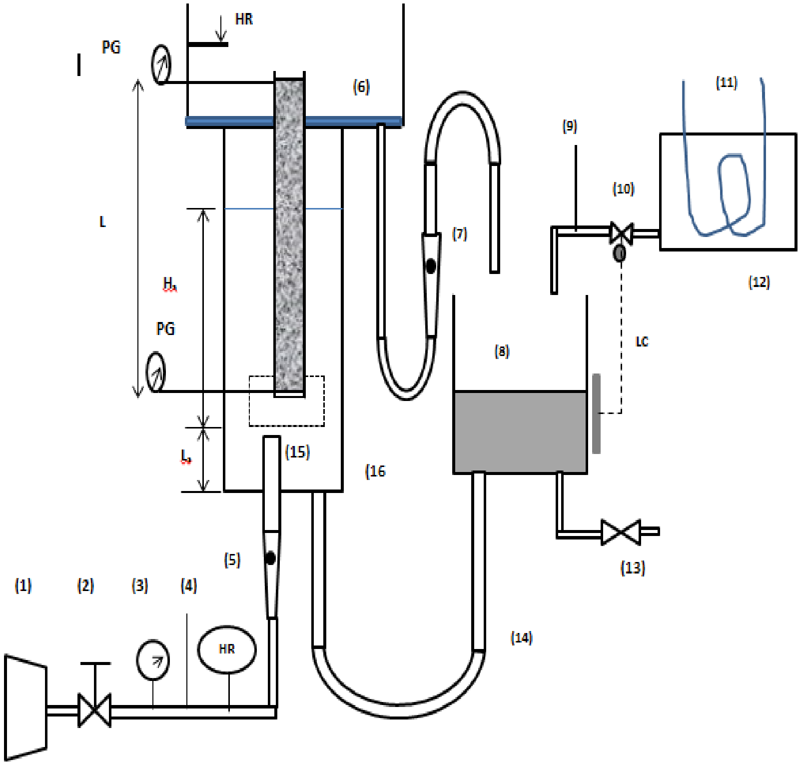

Figure-1: Experimental setup

1. compressor, 2. Valve, 3.pressure gauge, 4. Thermometer, 5. Air flow meter, 6. Collecting tank, 7. Water flow meter, 8. Water feeding tank, 9.thermometer, 10. Level control, 11.heater 12. Heating tank, 13. Valve, 14. Down comer, 15. Air-jacket, 16.holding tank, HR. Relative humidity sensor, LC. Level control, PG. Pressure Gauge.

Various liquid temperatures for each submergence ratio were investigated in the present study. The range of liquid temperature was obtained in increments of 5°C. For each liquid temperature and submergence ratio, the air flow rate was varied and the corresponding flow rate of water and humidity of air were measured.

The experimental runs are carried out considering the following procedure:

(1) The temperatures of the water and air are measured before supplying the electrical power to ensure a uniform temperature of the system.

(2) The temperature of the water is adjusted to the desired temperatures automatically through the digital reading and controller microcomputer thermometer that it operated the electrical heater.

(3) The supply air velocity is adjusted to the desired velocity through the compressor valve.

(4) The temperatures, inlet and outlet Relative Humidity (RH) of air, water and air flow rate are recorded every 15 min until the steady state condition is achieved.This condition was satisfied when there was no change on the temperatures, relative humidity, air and water flow rates reading with time.

For the relative humidity (RH) measurement , a thermo-hygrometer S.P.S.I. (B) type, which gives the measured values of temperature in the range of (-40°C ; 140°C) and RH in the range of (0; 100%). The uncertainty of the measurement instrument is about 5% according the supplier. The humidity at the inlet and outlet of the evaporator chamber is calculated by software. The inlet and outlet temperatures of air and water are measured by Thermocouple k type, with accuracy of±1, connected to a digital reading microcomputer.

The initial height of water in the riser, Z s, is measured by using graduate lever with accuracy of ±1 mm.

4 Results And Discussion

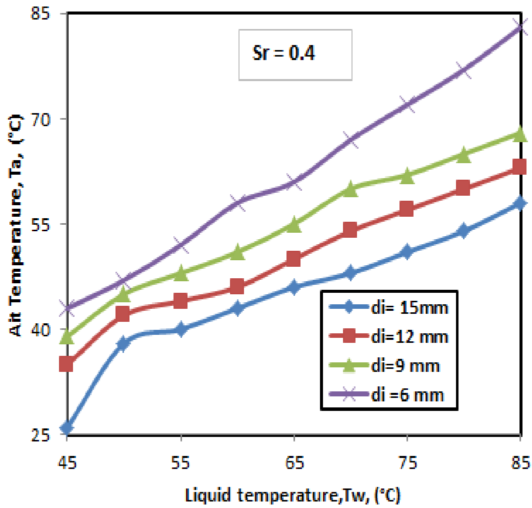

Figure-2: Air temperature after humidification.

Fig. 2 shows the variation of air temperature (T_a) in the packed column humidifier with liquid temperature (T_w). The figure shows that T_a increases with the increase of liquid temperature. This fact is observed for different diameters of solid packing particles (di).

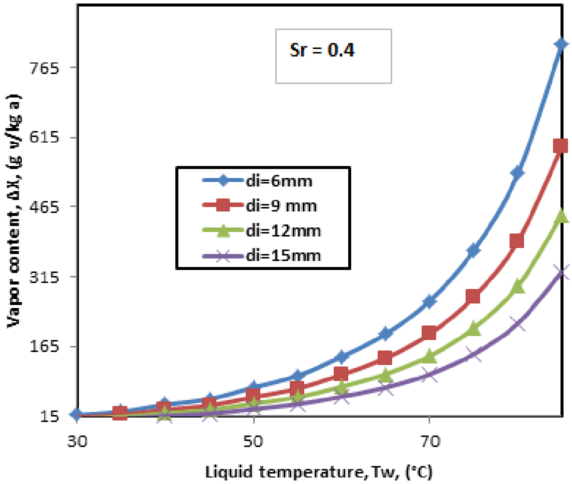

Figure-3: Vapor content in air after humidification; mas=5kg/h.

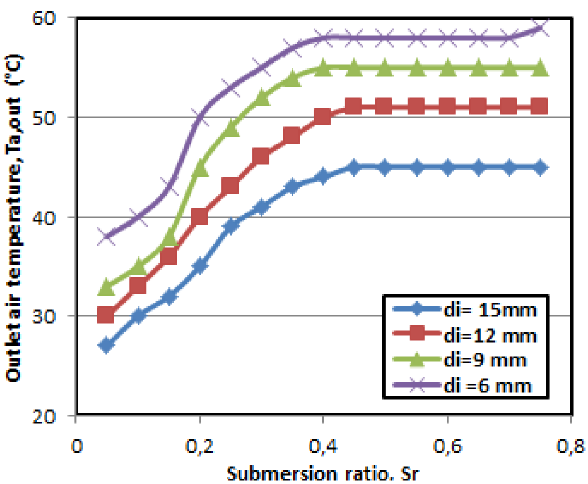

Figure-4: air temperature after humidification; Tw= 60°C, mas = 4.5 kg/h.

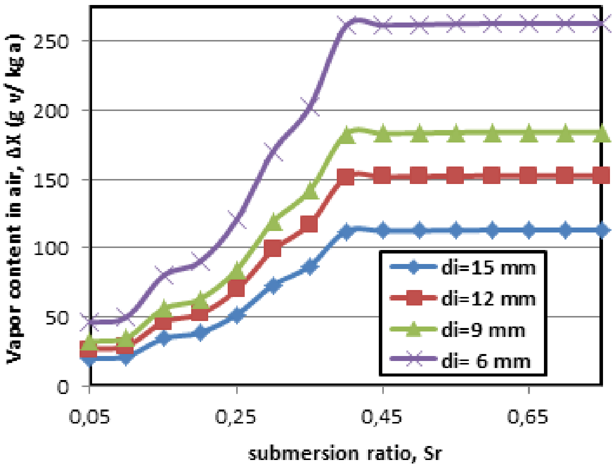

Figure-5: Vapor content in air after humidification; ΔX= F(Sr), mas= 5kg/h, Tw=70°C, Ta,in = 18°C.

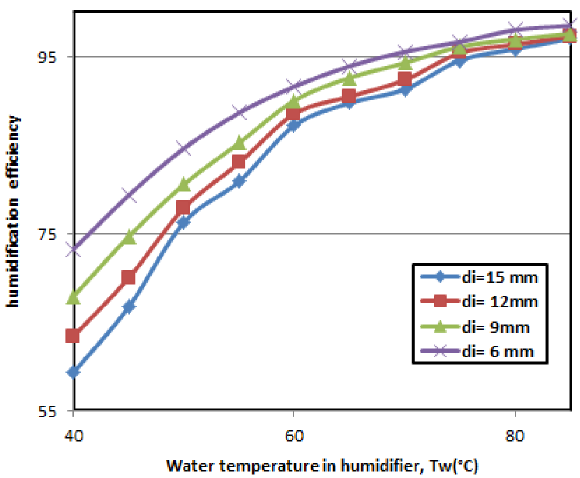

Figure-6: Humidification efficiency;

Sr =0.45; mas = 5kg/h; Ta,in = 18°C

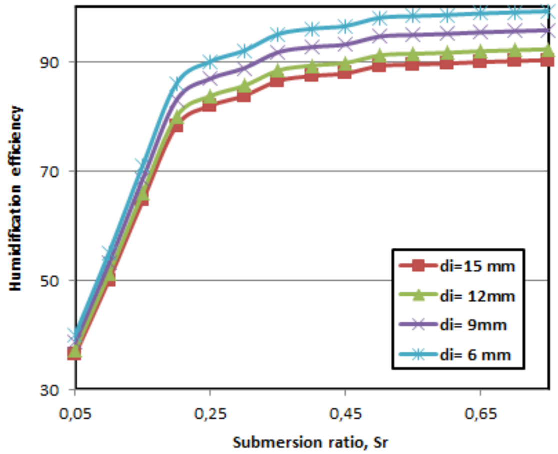

Figure-7: Effect of submersion ration on humidification efficiency; Tw=75°C; mas = 5kg/h; Ta,in = 18°C.

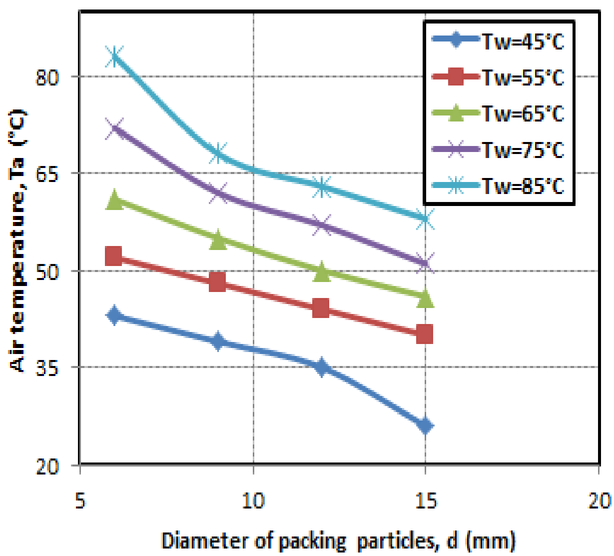

Fig-8: Effect king of diameter of packing on the outlet air temperature

The figure shows also the effect of packing diameter on air temperature. Indeed, if the diameter of packing is small then the temperature of air will be greater. This fact is confirmed by fig.8. This is explained by the small porosity of the packed column which makes difficulties against the fluid mixture flow. So, the contact area between air and water will be greater. Consequently, the heat transfer will be greater also.

Fig. 3 shows the variation of vapor content in air (ΔX) after humidification with the variation of liquid temperature (T_w). The figure shows that ΔX increases with the increase of liquid temperature. This fact is observed for different diameters of solid packing particles (di).

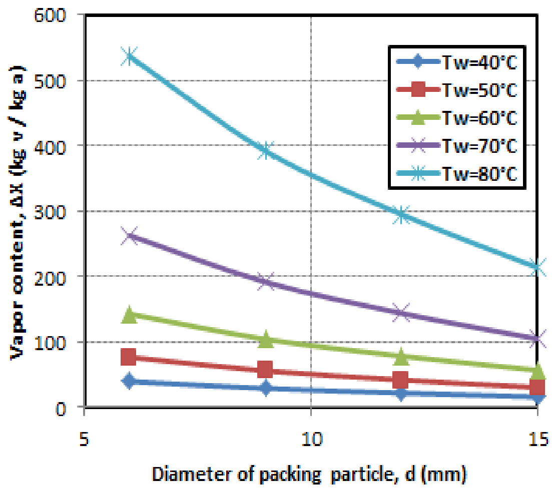

Figure-9: Effect of dimeter of packing on the vapor content in air

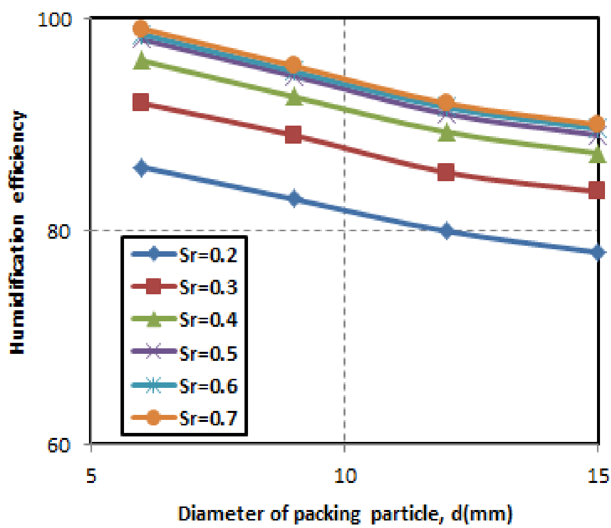

Figure-10: Effect of diameter of packing on humidification efficiency (Tw = 75°C)

The figure shows also the effect of packing diameter on vapor content. Indeed, if the diameter of packing is small then the vapor content will be greater. This fact is confirmed by fig. 9. This is explained by the small porosity of the packed column which makes difficulties against the fluid mixture flow. So, the air will be more heated and its ability for vapor transport will be greater. Consequently, the mass transfer will be greater also.

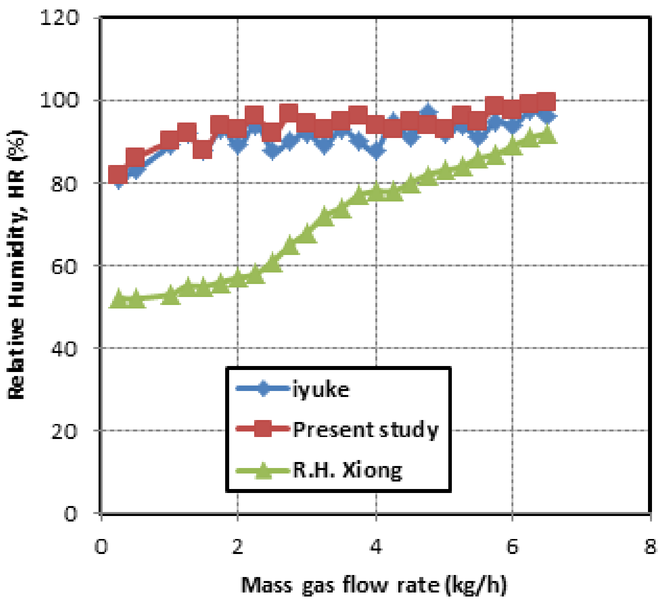

Figure-11: Effect of gas flow rate on the relative humidity; Tw = 75°C; Sr = 0.5.

Fig. 4 shows the variation of air temperature (T_a) in the packed column humidifier with submersion ratio (Sr). The figure shows that T_a increases with the increase of submersion ratio up certain value. After this value, the effect of submersion ratio on air temperature is weak. This fact is observed for different diameters of solid packing particles (di). This is explained by the increase of liquid flow rate with submersion ratio which has no effect on the heat transfer after certain value. So, after certain value the contact area between air and water will be almost constant because the increase of liquid flow rate hasn't effect on the path of fluid.

Fig. 5 shows the variation of vapour content (ΔX) after humidification with the variation of submersion ratio (Sr). The figure shows that ΔX increases with the increase of submersion ratio up certain value. After this value, the effect of submersion ratio on vapor content can be neglected. This fact is observed for different diameters of solid packing particles (di). The figure shows also the effect of packing diameter on vapor content. Indeed, if the diameter of packing is small then the vapor content will be greater. So, as expected the high liquid flow rate, can be obtained at high value of submersion ratio, but it haven't effect on the heat and mass transfer between air and water. The same conclusion is valuable for the variation of humidification efficiency with the variation of submersion ratio shown in fig. 7.

Fig. 6 shows the variation of humidification efficiency with the variation of liquid temperature. As expected, the humidification efficiency will greater at high and small diameter of solid particle packings. This is explained by the favourable conditions of heat and mass transfer between air and water. This fact is confirmed by fig. 10. The variation of efficiency with the variation of packing diameter follows a logarithmic curve with negative slop.

Fig. 11 shows a comparison of the variation of relative humidity (HR), after humidification, with the variation of gas flow rate (ma) obtained in this study with that obtained by several authors. The figure shows the weak effect of gas flow rate on the relative humidity (HR). The results obtained in this study are agreed with that of Iyuke [18] from the low values of gas flow rate. At gas flow rate more than 6 kg/hr, the relative humidity values are the same obtained in this work and obtained by other authors.

5 Conclusions

A new setup of two-phase upward flow in a granular medium was achieved and tested with solid rings as packings in different operating conditions. In this study, the following points were concluded:

The vapor content difference increases with the increase of water temperature.

The submersion ratio has an effect on the vapor content up certain value. After this value, the effect is weak. So, the liquid temperature and medium value of submersion ratio are the favorable conditions of high humidification efficiency.

The small diameters of solid particle packings have greater effect on the characteristics of air and on the humidification efficiency than the great diameters. Additional work is necessary to obtain accurate quantitative prediction the effect of quality of raw water and the characteristics of packings on the humidification rate and the efficiency of the packed column.

References

[1] G. Al-Enezi , H. Ettouney , N. Fawzy. Low temperature humidification dehumidification desalination process. Energy Conversion and Management 47 (2006) 470– 484.
[2] F. Alnaimat, J. F. Klausner , R. Mei.Transient analysis of direct contact evaporation and condensation within packed beds. International Journal of Heat and Mass Transfer 54 (2011) 3381–3393.
[3] E.H. Amer , H. Kotb, G.H. Mostafa, A.R. El-Ghalban. Theoretical and experimental investigation of humidification–dehumidification desalination unit. Desalination 249 (2009) 949–959.

[4] Oueslati A., Hannachi A., Elmaaoui M. Simulation of air humidification by direct contact with water. (Cratt-2012), Rades- Tunisia, 30-31 Octobre 2012.

[5] Oueslati A., Hannachi A., Elmaaoui M. "Hydrodynamic study of an adjustable height packed column operating on the principle of an airlift pump",(ijmet), Volume 4, Issue 2, pp. 461-478, ISSN Print: 0976 –6340), issn Online: 0976 – 6359.

[6] Oueslati A., Hannachi A., Elmaaoui M., "An Experimental Study on the Airlift Packed Column with Adjustable Height and Many Air Injection Points", (ijaret), Volume 4, Issue 1, 2013, pp. 42 - 49, Issn Print: 0976-6480, issn Online: 0976-6499.

[7] Oueslati A, Hannachi A, Elmaaoui M. "Experimental Analysis of Air Humidification by Brackish Water in an adjustable Height Packed Column Humidifier Operating on the Principle of an Air Lift pump", IJCE. Vol.30, Issue.1 1103-1110. ©Recent Science Publications Archives| May 2013|$25.00 | 27702522 |.

[8] Oueslati A., Hannachi A. Elmaaoui M. Effect of air humidification on the pumping efficiency of water in a packed column humidifier, Energy Procedia 74 (2015) 1380 –1393.

[9] Oueslati A, Hannachi A, Elmaaoui M. Simulation of air lift packed column, IEEE Xplore. 2013.

[10] Oueslati A, Hannachi A, Elmaaoui M. Theoretical analysis of the performance of air-lift pumps used for pumping water in a closed loop, Int. Symp. Comput. & Exp. Investig. on Fluid Dynamics cefd'2013, March 18-20, 2013,Sfax, Tunisia.

[11] Oueslati A., Hannachi A., 2017, New pilot for air humidification-Dehumidification, Part I: Design basis, icest'2017.

[12] Oueslati A, Hannachi A, 2017, New pilot for air humidification-Dehumidification, Part II: Some aspects of a new airlift packed column humidifier and dehumidifier, icest'2017.

[13] Oueslati Adel. New system for liquid pumping. innorpi N°258/2014. Patented in 2016.

[14] Oueslati Adel, Condenser-separator of water vapor contained in moist air. Innorpi 258/2014, patented 2016.

[15] Oueslati Adel, Recycling apparatus and solvent separation, patented in 2015.Innorpi 23761.

[16] Oueslati Adel. Conception, Realization, experimental study and modeling of air humidification-dehumidification installation by direct contact with water in granular medium. Doctoral thesis in chem. Eng. Publicly supported on September 23, 2014. ENI Gabes.

[17] R.H. Xiong, S.C. Wang, L.X. Xie, Z. ang, P.L. Li. Experimental investigation of a baffled shell and tube desalination column using the humid. Dehumid. process. desalination 180 (2005) 253-261.

[18] S.E.Iyuke, A. B. Mohamad, W. R.W. Daud. Estimation of humidification load from humidifier column by convective heat transfer in water–air–vapor system. Che.Eng.Sc. 56 (2001) 4949–4956.

10TH INTERNATIONAL CONFERENCE ON SUSTAINABLE ENERGY AND ENVIRONMENTAL PROTECTION (JUNE 27TH – 30TH, 2017, BLED, SLOVENIA), ENERGY EFFICIENCY
J. Krope, A.Ghani Olabi, D. Goričanec & S. Božičnik

Nanomaterial-Based Biocatalysts

KATJA VASIĆ, MATEJA PRIMOŽIČ, ŽELJKO KNEZ & MAJA LEITGEB

Abstract With concern for sustainable energy and environment protection, new material technologies are constantly expanding during the last few decades. Nanostructured materials offer unprecedented opportunity for sustainable energy production. Use of immobilized enzymes as bionanocatalysts presents an appropriate tool for energy costs reduction, since such processes can be performed at low temperatures with the reduction of side product formation.

Keywords: • nanostructured materials • bionanocatalysts • cross-linked enzyme aggregates • magnetic nanoparticles • energy costs •

CORRESPONDENCE ADDRESS: Katja Vasić, Ph.D. student, University of Maribor, Faculty of Chemistry and Chemical Engineering, Smetanova ulica 17, 2000 Maribor, Slovenia, e-mail: katja.vasic@um.si. Mateja Primožič, Ph.D., Assistant Professor, University of Maribor, Faculty of Chemistry and Chemical Engineering, Smetanova ulica 17, 2000 Maribor, Slovenia, e-mail: mateja.primozic@um.si. Željko Knez, Ph.D., Full Professor, University of Maribor, Faculty of Chemistry and Chemical Engineering, Smetanova ulica 17, 2000 Maribor, Slovenia, e-mail: zeljko.knez@um.si. Maja Leitgeb, Ph.D., Full Professor, University of Maribor, Faculty of Chemistry and Chemical Engineering, Smetanova ulica 17, 2000 Maribor, Slovenia, e-mail: maja.leitgeb@um.si.

https://doi.org/10.18690/978-961-286-050-9.33 ISBN 978-961-286-050-9

Available at: http://press.um.si.

1 Introduction

In recent years, nanomaterials are being developed fast and explosively and attracting a huge amount of attention. Nanomaterials and their manufacturing technologies have been seamlessly integrated into many applications. Clean energy and environmental applications often demand the development of novel nanomaterials that can provide shortest reaction pathways (reaction kinetics). Understanding the physicochemical, structural, microstructural, and surface properties of nanomaterials is vital for achieving the required efficiency, and sustainability in various technological applications.

Applications being developed for nanoparticles include deliver chemotherapy drugs directly to cancer tumors [1], resetting the immune system to prevent autoimmune diseases, delivering drugs to damaged regions of arteries to fight cardiovascular disease, create photocatalysts that produce hydrogen from water, reduce the cost of producing fuel cells and solar cells, clean up oil spills, water pollution and air pollution.

Nanoparticle applications in medicine include also use of polymer coated iron oxide nanoparticles to break up clusters of bacteria, possibly allowing more effective treatment of chronic bacterial infections [2]. The surface change of protein filled nanoparticles has been shown to affect the ability of the nanoparticle to stimulate immune responses [3]. In the near future, these nanoparticles may be used in inhalable vaccines. Some techniques are only imagined, while others are at various stages of testing, or actually being used today.

Modern immobilization methods allow enzyme immobilization with or without a carrier in the form of micro- or nano-particles. Their applications can be found in various fields, such as biomedicine, biosensors or bioreactors for different industries or environmental protection.

Cross-linked enzyme aggregates (CLEAs) are immobilized enzymes where no carrier is used.

The enzymes in the CLEAs are covalently bound to each other by a cross-linker in order to improve the stability of the enzyme against pH, temperature, solvents etc. Leakage is extremely low. By using different surface treatments, the polarity of the CLEAs can be easily tuned to the reaction, which could improve the efficacy of the enzyme in the reaction. Due to their stability and the nature of the immobilization, CLEAs can be also recycled many times [4].

CLEAs have found their role in biosensors and are very suitable for the use in bioreactors due to the very high enzyme activity and stability in this form which as a consequence enables lower energy demand in such a process.

Since magnetic nanoparticles (MNPs) have unique features (e.g. reaction to a magnetic force …), the development of a variety of applications such as drug targeting, enzyme immobilization and bioseparation has been possible. Comparing to larger sized particles, the main advantage of MNPs is in their high surface-to-volume ratio, which contributes to a higher surface energy and to excellent magnetic properties. The optimization of size of MNPs, distribution, agglomeration, coating, and shapes along with their unique magnetic properties prompted the application of MNPs in diverse fields. They have been shown to serve as recyclable supports in heterogeneous catalysis allowing easy separation of the catalyst from reaction mixture with an induced magnetic field [5]. A similar process has been shown to be effective for the removal of contaminants from water using functionalized MNPs [6].

1.1 *β*-galactosidase

β-galactosidase, mostly known as lactase, hydrolyzes lactose into glucose and galactose [7]. This process of catalysis occurs in digestion process in living organisms. The enzyme can be obtained from a variety of sources like microorganisms, plants, and animals. It can be obtained from fruits, such as apples, peaches and almonds. However, the most often sources of *β*-galactosidase are fungi and yeasts [8-9]. One of many industrial applications of *β*-galactosidase is the catalysis of a chemical reaction that converts lactose to monosaccharides. This process produces lactose-free foods for lactose intolerant individuals that are having difficulties digesting lactose containing foods. Immobilization of such enzyme has many beneficial advantages in production of lactose-free products. Due to reusability of immobilized enzyme, the production costs could be reduced [10].

2 Experimental and results

Enzyme *β*-galactosidase was immobilized via three different immobilization techniques, including preparation of: cross-linked enzymes aggregates (CLEA), magnetic cross-linked enzyme aggregates (mCLEA) and immobilization onto aminosilane magnetic nanoparticles (AS-MNPs).

2.1 Carrier-free immobilization

2.1.1 CLEA of *β*-galactosidase

Enzyme *β*-galactosidase was mixed with addition of bovine serum albumin (BSA), used for stabilization, and with pentaethylenehexamine (PEHA, 0.02 M) in a 2:1:1 ratio. So prepared enzyme solution was precipitated into cross-linked enzyme aggregates, using ethanol, acetone and 1-propanol as precipitating reagents. As a cross-linker, glutaraldehyde (GA) was added. The solution was stirred for 3 hours. Later on, sodium cyanoborohydrid ($NaBH_3CN$, 0.1 M) was added to the reaction. The solution was centrifuged and residual activity was measured. With all three precipitating reagents we managed to obtain high residual activities: 98.06 % in ethanol, 99.53 % in acetone and 99.61 % in 1-propanol.

2.2 Immobilization with carrier

2.2.1 Carrier preparation and characterization: AS-MNPs

Fe_2O_3 nanoparticles were coated with polymerizing silica (SiO_2) and later on, silanization reaction by amino silane coupling agent followed to provide highly functionalized aminosilane magnetic nanoparticles (AS-MNPs), prepared for surface treatment. Preparation of such nanoparticles is described in our previous work [11]. The morphology and particle size of AS-MNPs were characterized with scanning electron microscopy (SEM) and transmission electron microscopy (TEM) and reveal nanoparticles with the average size of about 26 nm (Figure 1 and Figure 2).

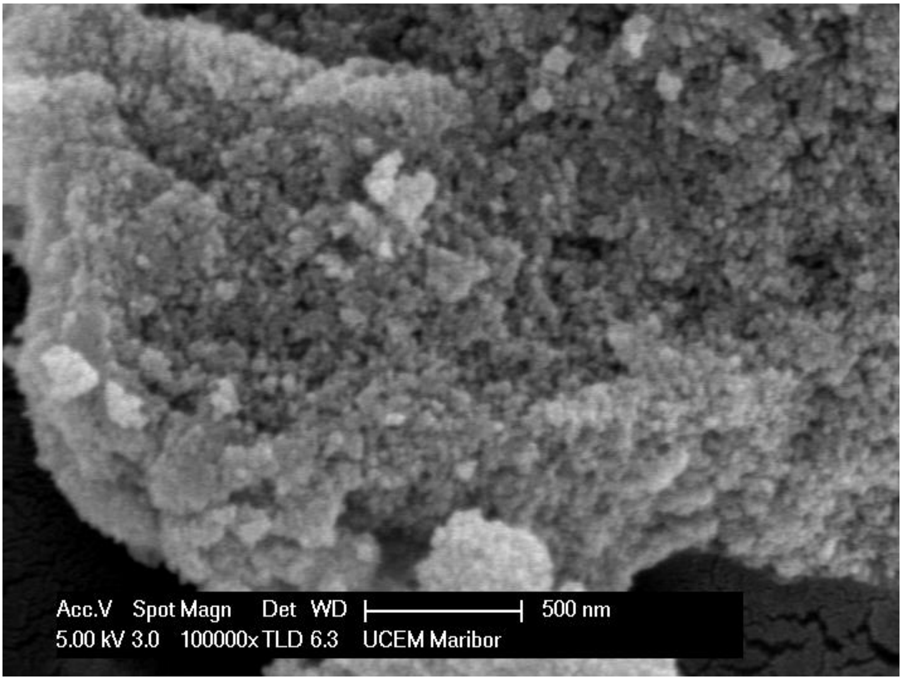

Figure 1. SEM image of aminosilane magnetic nanoparticles (AS-MNPs)

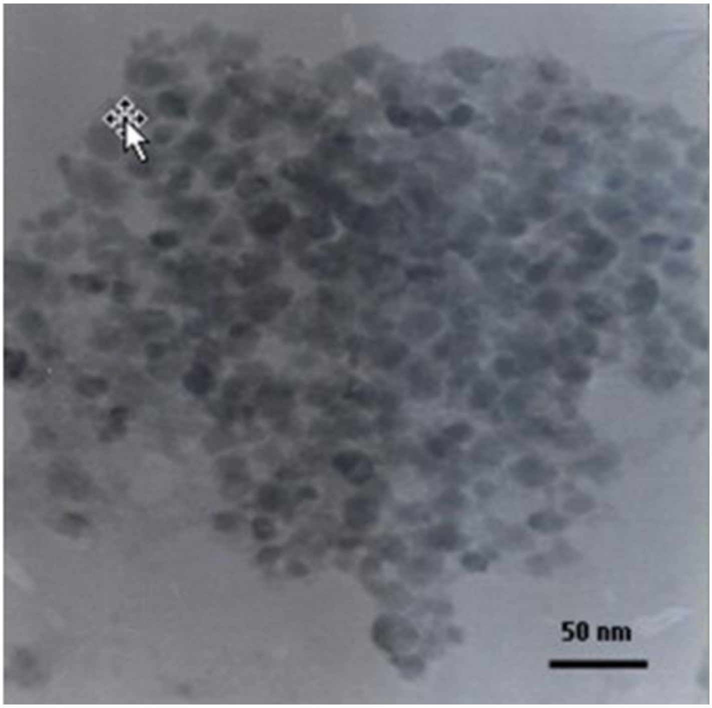

Figure 2. TEM image of aminosilane magnetic nanoparticles (AS-MNPs)

2.2.2 mCLEA of *β*-galactosidase

mCLEA was prepared with the addition of 5 mg of aminosilane magnetic nanoparticles (AS-MNPs) to the enzyme solution. AS-MNPs were mixed with β-galactosidase, BSA and PEHA (0.1 M) in a 2:1:1 ratio. So prepared enzyme solution was precipitated into 4 precipitating reagents: ethanol, acetone, 1-propanol and 2-propanol. As a cross-linker, GA was added and the mixture was stirred for 3 hours. Later on, sodium cyanoborohydrid ($NaBH_3CN$, 0.1 M) was added to the reaction. The solution was centrifuged and residual activity was measured. Very high residual activities of mCLEA in all 4 precipitating reagents were obtained: 132.10 % in ethanol, 130.64 % in acetone, 123.90 % in 1-propanol and 133.63 % in 2-propanol.

2.2.3 Immobilization of *β*-galactosidase onto AS-MNPs

Firstly, 5 mg of AS-MNPs were activated. GA and PEHA were both added to the AS-MNPs separately and in combination of both. The mixture was stirred for 2 hours. Afterwards, the suspension was rinsed with acetate buffer and separated with a magnet. To such activated AS-MNPs, enzyme β-galactosidase with acetate buffer was added in a 1:9 ratio. The mixture was stirred for 24 hours. With the addition of 2.5 % (v/v) GA, the hyperactivation of 138 % was obtained. With the addition of PEHA (20 % (v/v), 0.1 M) the highest residual activity of 154 % was obtained. When investigating the combination of both cross-linkers GA and PEHA, the hyperactivation of 125 % was obtained with 2 % (v/v) GA and 30 % (v/v) PEHA. The results with residual activities, achieved by the three different immobilization techniques are presented in Table 1.

Table 1. Residual activities of enzyme β-galactosidase immobilized with three different immobilization techniques

Immobilization method	Residual activity (%)
CLEA	
ethanol	98.06
acetone	99.53
1-propanol	99.61
mCLEA	
ethanol	132.10
acetone	130.64
1-propanol	123.90
2-propanol	133.63
Immobilization onto AS-MNPs	
2.5 % (v/v) GA	138.00
20 % (v/v) PEHA	154.00
2 % (v/v) GA + 30 % (v/v) PEHA	125.00

3 Conclusion

Enzyme *β*-galactosidase was immobilized using three different immobilization methods. For carrier-free immobilization, CLEA was investigated. For immobilization with carrier, mCLEA and immobilization onto AS-MNPs was investigated. SEM and TEM images of AS-MNPs show desirable nanoparticle sizes, which measure around 26 nm. With all three immobilization methods, we achieved high residual activities, resulting in hyperactivation of the enzyme. All methods show promising results and can be considered as immobilization techniques for high efficiency and high residual activity of the enzyme.

Acknowledgements

The authors acknowledge the financial support from the Slovenian Research Agency (research core funding No. P2-0046 - "Separation Processes and Product Design").

References

[1] E. Pérez-Herrero and A. Fernández-Medarde, "Advanced targeted therapies in cancer: Drug nanocarriers, the future of chemotherapy," *European Journal of Pharmaceutics and Biopharmaceutics*, vol. 93, pp. 52–79, Jun. 2015.

[2] K.P. Miller, L. Wang, B.C. Benicewicz and A.W. Decho, "Inorganic nanoparticles engineered to attack bacteria," *The Royal Society of Chemistry*, vol. 44, pp. 7787–7807, Jan. 2015.

[3] J. Noble, A. Zimmerman and C.A. Fromen, "Potent Immune Stimulation from Nanoparticle Carriers Relies on the Interplay of Adjuvant Surface Density and Adjuvant Mass distribution," *ACS biomaterials science & Engineering*, vol. 3, pp. 560–567, Apr. 2017.

[4] R.A. Sheldon, "Cross-Linked Enzyme Aggregates as Industrial Biocatalysts," *Organic Process Research & Development*, vol. 15, pp. 213–223, Feb. 2011.

[5] M.B. Gawande, Y. Monga, R. Zboril and R.K. Sharma, "Silica-decorated magnetic nanocomposites for catalytic applications," *Coordination Chemistry Reviews*, vol. 288, pp. 118–143, Apr. 2015.

[6] M. Kumari, C.U. Pittman Jr. and D. Mohan, "Heavy metals [chromium (VI) and lead (II)] removal from water using mesoporous magnetite (Fe_3O_4) nanospheres," *Journal of Colloid and Interface Science*, vol. 442, pp. 120–132, Mar. 2015.

[7] Z. Grosová, M. Rosenberg, M. Rebroš, M. Šipocz, B. Sedláčková, "Entrapment of β-galactosidase in polyvinylalcohol hydrogel," *Biotechnol. Lett.* vol. 30, 763–767, Apr. 2008.

[8] A.R. Prazeres, F. Carvalho and J. Rivas, "Cheese whey management: A review," J. *Environ. Manage.*, vol. 110, 48–68, Jun. 2012.

[9] L.M. Huerta, C. Vera, C. Guerrero, L. Wilson, A. Illanes, "Synthesis of galacto-oligosaccharides at very high lactose concentrations with immobilized *β*-galactosidases from *Aspergillus oryzae*," *Process Biochem.*, vol. 46, 245–252, Jan. 2011.

[10] P. Torres, F. Batista-Viera, "Improved biocatalysts based on Bacillus circulans *β*-galactosidase immobilized onto epoxy-activated acrylic supports: Applications in whey processing," *J. Mol. Catal. B Enzym.* vol. 83, 57–64, Jun. 2012.

[11] F. Šulek, M. Drofenik, M. Habulin, Ž. Knez, "Surface functionalization of silica-coated magnetic nanoparticles for covalent attachment of cholesterol oxidase," *J. Magn. Magn. Mater.*, vol. 322, 179–185, Jan. 2010.

10TH INTERNATIONAL CONFERENCE ON SUSTAINABLE ENERGY AND ENVIRONMENTAL PROTECTION (JUNE 27TH – 30TH, 2017, BLED, SLOVENIA), ENERGY EFFICIENCY
J. Krope, A.Ghani Olabi, D. Goričanec & S. Božičnik

Energy – Water Interactions, Industrial Context

PETAR SABEV VARBANOV, JIŘÍ JAROMÍR KLEMEŠ, ZHI-YONG LIU & ZDRAVKO KRAVANJA

Abstract Responding to the increasing challenges in using natural resources for water and energy supply more efficiently, this contribution reviews the trends in the global flows of energy and water, identifies the inherent limitations and pays attention to the concept of virtual water, virtual greenhouse gas emissions and the link between them. The implications for industry and of some notable recent research efforts are also reviewed. They cover footprint minimisation methodologies including simultaneous energy and water minimisation. Several directions of future research and development are suggested.

Keywords: • energy–water nexus • resource efficiency • virtual water • virtual greenhouse gas emissions • Industrial Context •

CORRESPONDENCE ADDRESS: Petar Sabev Varbanov, PhD, Senior researcher, Brno University of Technology - VUT Brno, Sustainable Process Integration Laboratory – SPIL, NETME Centre, Faculty of Mechanical Engineering, Brno, Technická 2896/2, 616 69 Brno, Czech Republic, e-mail: varbanov@fme.vutbr.cz. Jiří Jaromír Klemeš, Ph.D., Full Professor, Brno University of Technology - VUT Brno, DSc, Head of Sustainable Process Integration Laboratory – SPIL, NETME Centre, Faculty of Mechanical Engineering, Technická 2896/2, 616 69 Brno, Czech Republic, e-mail: klemes@fme.vutbr.cz. Zhi-Yong Liu, PhD, Full Professor, Hebei University of Technology, School of Marine Science and Engineering, Tianjin 300130, China, e-mail: liuzhiyong@hebut.edu.cn. Zdravko Kravanja, Ph.D., Full Professor, University of Maribor, Faculty of Chemistry and Chemical Engineering, Smetanova ulica 17, 2000 Maribor, Slovenia, e-mail: zdravko.kravanja@um.si.

https://doi.org/10.18690/978-961-286-050-9.34 ISBN 978-961-286-050-9

Available at: http://press.um.si.

1 Introduction

Industrial and residential estates consume large amounts of energy and water, releasing gaseous emissions and other effluents. They can be evaluated and optimised using environmental footprints – e.g. Greenhouse Gas (GHG), nitrogen and water footprints [1]. Dimensionality reduction by Čuček et al. [2] has been one of the key innovations, aimed at improving the modelling efficiency. The rising energy and water demands increase the cost of delivery and contribute to the depletion and potential scarcity of resources. The energy-water nexus is pervasive. It is present at all society levels –from the residential and industrial activities, up to supply chains, regions and global trade flows.

There have been studies on the energy-water nexus on the case of the Chinese economy – e.g. [3], as well as concerning water management with multiple contaminants [4]. Simultaneous energy and water minimisation in the industry via heat recovery and water reuse networks are reviewed in [5], more recently followed up for non-isothermal water network synthesis [6].

To provide the decision makers with useful guidance, the concepts, interactions and their mechanisms should be well understood and their modelling should be enabled in the tools. Following this, the current paper reviews the recent trends in water and energy supply and the related recent research results. Suggestions are provided for the further research, paying attention to the concepts of virtual water and virtual Greenhouse Gas Emissions (GHGE).

2 Industry energy / water use

The connection of water with energy supply and use has been apparent for all industrial sectors [7]. Energy generation and use impose significant water demands. Water delivery, use and treatment carry significant energy demands. Figure 1 [8] illustrates these flows for an industrial site. However, also the production of biofuels results in a considerable water footprint. Chiu et al. [9] indicated that in producing bio-ethanol, water demand just for irrigation is up to 2,140 (L water)/(L bio-ethanol).

It is important to understand the mechanism behind the energy–water nexus. It is caused by system links. Industrial utility systems are a good example of how these flows intertwine. The nexus works in both directions, amplifying the effect of the applied measures. Process flowsheets allow tracing the relevant links. Using them it is possible to identify options for combined minimisation of energy and water use.

The most powerful frameworks in industrial optimisation studies have been Process Integration (PI) and Mathematical Programming (MP) [10]. MP provides computational rigorousness and model scale up. PI is the family of methodologies allowing the combination of various process parts and establishing links for the simultaneous reduction of the resource intake and emissions to the environment. One of the advanced

Process Integration concepts has been the combined Energy and Water Integration – see [5] for an exhaustive overview.

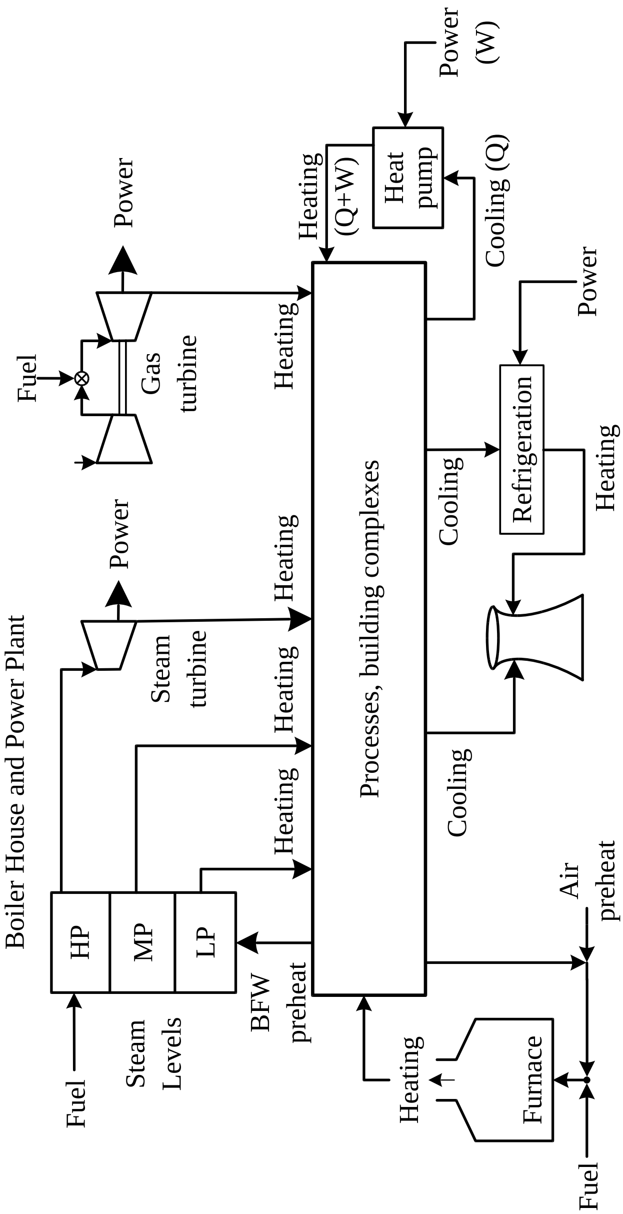

Figure 1. Hot-and-cold-utilities [15], linking energy and water flows on a site

At the site level, the key innovation has been Total Site Integration [11]. Since inception, there have been many developments. One issue is to handle the variability of the user demands and the source supplies for energy. Varbanov and Klemeš [12] introduced the Total Site Heat Cascade as a tool for visualisation of the heat flows and Time Slices, denoting heat storage use by heat transfers between Time Slices. Zhang et al. [13] studied how to sustain high energy efficiency in existing processes with advanced Process Integration Technology. An important extension has been Power Integration [14].

Nemet et al. [15], developed a framework for the optimal derivation of the time slices from supply and demand forecasts. The selection of ΔT_{min} for Total Site targeting has been investigated by Varbanov et al. [16]. They suggested that the values should be provided individually for each process, for obtaining more realistic targets.

Wan Alwi et al. [17] developed a graphical approach named "Superimposed mass and energy curves" for simultaneous water and heat reduction. That can be used for efficient visualisation of the system effects, making it a powerful decision support tool. Following up, Wan Alwi and Manan [18] described an advanced Water Pinch Methodology accounting for water loss and gain in the water networks.

Ahmetović and Kravanja [19] published a superstructure-based non-convex MINLP model for combined heat-exchange and process water networks, accounting for direct and indirect heat exchange, and incorporating streams splitting/mixing. It has been further extended for process-to-process stream integration [20].

Beal et al. [21] modelled the combined design of algal biofuel production and wastewater treatment, which separately are net energy sinks with a serious water footprint, reporting that the plants' combination is a net energy source.

3 Inter-site, regional and global water flows

At higher levels of resource flows, exchanges between sites, regional and international trade supplying resources and products, embodies resources and certain footprint values. A recent study [22] analysed the virtual CO_2 emissions and virtual water flow trends in international trade from a consumption perspective. Figure 2 illustrates the global picture in terms of GHGE.

The analysis indicates that: (1) Producers and consumers are located in different parts of the world, significantly differing in virtual GHG (Greenhouse gases) emissions. (2) The US and the EU have high absolute net CO_2 imports. (3) China and other fast-developing countries as India and Brazil, are net exporters increasingly carrying the load of virtual GHG and virtual water triggered by the consumption elsewhere. (4) By importing products with lower carbon emission intensity and less virtual water than in the domestic industry, international trade can reduce global environmental pressure.

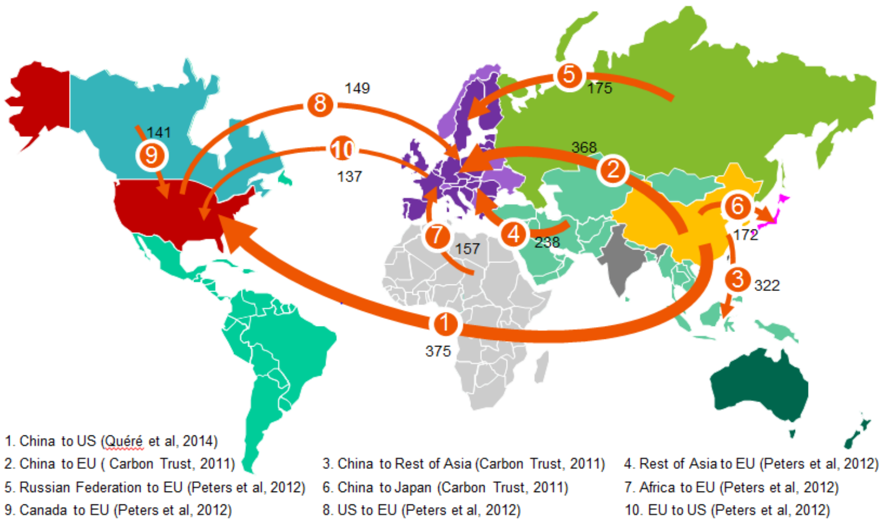

Figure 2. Inter-regional flows of embodied CO_2 emissions in 2004 (Mt CO_2) [22]

4 Conclusions

An important conclusion is that the energy-water nexus works in both directions. In the same way as energy use and water use amplify each other, energy and water savings should amplify each other. This has been exploited by the methodologies for combined energy and water minimisation. The application has been mainly within for single processes and only concerning heating or cooling. This observation points to two important new research directions. One is to extend the scope of integration for combined energy and water minimisation from process to site level and supply chains. Considering the GHGE and Virtual Water flows jointly, leading to combined GHG and Water footprinting would allow to directly exploit the energy-water nexus for sustainability improvement. Another follow up can be to add power (electricity) into the considerations alongside with water and heat.

From the global perspective, key research and development directions are necessary. At the site level, in addition to optimisation for resource efficiency and waste streams utilisation; a step change can be made by developing conceptually and procedurally the site interfaces with other sites and regional actors. This will allow regional and site-level optimisation of the exchange of resources and products.

Building upon that, development of concepts is important, for establishing links among sites, municipalities and regions complementing each other for resource utilisation and material reuse. At the regional and global levels, one of the goals should be minimising the overhead emissions from resource and product transportation.

Acknowledgements

The project "Sustainable Process Integration Laboratory – SPIL", project No. CZ.02.1.01/0.0/0.0/15_003/0000456 funded by EU "CZ Operational Programme Research, Development and Education", Priority 1: Strengthening capacity for quality research, and the collaboration SPIL agreements with Hebei University of Technology and University of Maribor have been acknowledged.

References

[1] L. De Benedetto, and J. J. Klemeš, "The Environmental Performance Strategy Map: an integrated LCA approach to support the strategic decision-making process", *Journal of Cleaner Production*, vol. 17, pp. 900-906, 2009.

[2] L. Čuček, J. J. Klemeš, and Z. Kravanja, "Objective dimensionality reduction method within multi-objective optimisation considering total footprints", *Journal of Cleaner Production*, vol. 71, pp. 75-86, 2013.

[3] A. Gu, F. Teng, and Z. Lv, "Exploring the nexus between water saving and energy conservation: Insights from industry sector during the 12th Five-Year Plan period in China", *Renewable and Sustainable Energy Reviews*, vol. 59, pp. 28-38, 2016.

[4] Z.Y. Liu, Y. Yang, L.Z. Wan, X. Wang, and K.A. Hou, "Heuristic Design Procedure for Water-Using Networks with Multiple Contaminants", *AIChE J.*, vol. 55, pp. 374–382, 2009.

[5] L.E. Savulescu, and A. Alva-Argaez, "Process Integration Concepts for Combined Energy and Water Integration". DOI: 10.1533/9780857097255.4.461, In: Klemeš J.J. (Editor), *Handbook of Process Integration (PI): Minimisation of energy and water use, waste and emissions*. Woodhead Publishing/Elsevier, Cambridge, UK, ISBN 9780857095930, 2013.

[6] E. Ahmetović, N. Ibrić, Z. Kravanja, and I. E. Grossmann, "Water and energy integration: A comprehensive literature review of non-isothermal water network synthesis", *Computers & Chemical Engineering*, vol. 82, pp. 144-171, 2015.

[7] J. J. Klemeš, "Industrial Water Recycle/Reuse", *Current Opinion in Chemical Engineering*, vol. 1, no. 3, pp. 238-245, 2012.

[8] J.J. Klemeš, F. Friedler, I. Bulatov, and P.S. Varbanov, *Sustainability in the Process Industry – Integration and Optimization*, New York, USA: McGraw-Hill, 2010.

[9] Y. Chiu, B. Walseth, and S. Suh, "Water embodied in bioethanol in the United States", *Environ Sci Technol*, vol. 43, pp. 2688–2692, 2009.

[10] J. J. Klemeš, and Z. Kravanja, "Forty Years of Heat Integration: Pinch Analysis (PA) and Mathematical Programming (MP)", *Curr. Opinion Chem. Eng.*, vol. 2, no. 4, pp. 461-474, 2013.

[11] J. Klemeš, V.R. Dhole, K. Raissi, S.J. Perry, and L. Puigjaner. "Targeting and design methodology for reduction of fuel, power and CO_2 on Total Sites", *Appl. Therm. Eng.*, vol. 7, pp. 993–1003, 1997.

[12] P.S. Varbanov, and J.J. Klemeš, "Integration and management of renewables into Total Sites with variable supply and demand". *Computers and Chemical Engineering*, vol. 35, no. 9, pp. 1815-1826, 2011.

[13] N. Zhang, R. Smith, I. Bulatov, and J. J. Klemeš, "Sustaining High Energy Efficiency in Existing Processes with Advanced Process Integration Technology", *Applied Energy*, vol. 101, pp. 26-33, 2013.

[14] S.R. Wan Alwi, O. S. Tin, N. E. M. Rozali, Z. A. Manan, and J. J. Klemeš, "New graphical tools for process changes via load shifting for hybrid power systems based on Power Pinch

Analysis", *Clean Technologies and Environmental Policy*, vol. 15, no. 3, pp. 459-472, 2013.

[15] A. Nemet, J. J. Klemeš, P. S. Varbanov, and Z. Kravanja, "Methodology for maximising the use of renewables with variable availability". *Energy,* vol. 44, no. 1, pp. 29-37, 2012.

[16] P.S. Varbanov, Z. Fodor, and J. J. Klemeš, "Total Site targeting with process specific minimum temperature difference (ΔT_{min})". *Energy*, vol. 44, no. 1, pp. 20-28, 2012.

[17] S.R. Wan Alwi, A. Ismail, Z. A. Manan, and Z. B. Handani, "A new graphical approach for simultaneous mass and energy minimisation", *Appl. Therm. Eng.*, vol. 31, pp. 1021–1030, 2011.

[18] A. R. Wan Alwi, and Z. A. Manan, Water "Pinch analysis for Water management and minimisation: An introduction", In: J. Klemeš (ed) *Process Integration Handbook*, Cambridge, UK: Woodhead Publishing, ISBN-13: 978 0 85709 593 0, doi: 10.1533/ 9780857097255.3.353, 2013.

[19] E. Ahmetović, and Z. Kravanja, "Simultaneous synthesis of process water and heat exchanger networks", *Energy*, vol. 57, pp. 236-250, 2013.

[20] E. Ahmetović, and Z. Kravanja, "Simultaneous optimization of heat-integrated water networks involving process-to-process streams for heat integration", *Appl. Therm. Eng.*, vol. 62, no. 1, pp. 302-317, 2014.

[21] C.M. Beal, A.S. Stillwell, C.W. King, S.M. Cohen, H. Berberoglu, R.P. Bhattarai, R.L. Connelly, M.E. Webber, and R.E. Hebner, "Energy Return on Investment for Algal Biofuel Production Coupled with Wastewater Treatment", *Water Environment Research*, vol. 84, no. 9, pp. 962-710, 2012.

[22] X. Liu, J. J. Klemeš, P. S. Varbanov, L. Čuček, and Y. Qian, "Virtual carbon and water flows embodied in international trade: a review on consumption-based analysis". *Journal of Cleaner Production*, vol. 146, pp. 20-28, 2017.

10TH INTERNATIONAL CONFERENCE ON SUSTAINABLE ENERGY AND ENVIRONMENTAL PROTECTION (JUNE 27TH – 30TH, 2017, BLED, SLOVENIA), ENERGY EFFICIENCY
J. Krope, A.Ghani Olabi, D. Goričanec & S. Božičnik

Improving the Visual Comfort and Energy Performance Of Office Buildings

DANIEL URIBE, WALDO BUSTAMANTE, SERGIO VERA & MARÍA JOSÉ YÁÑEZ

Abstract An increasing amount of literature has been published recently on the optimization of building energy consumption and improvement of indoor daylight. Diverse alternatives for improving building energy performance that consider different variables have been studied. The main objective of this paper is to determine the most influential variables on building energy performance and indoor visual comfort. A statistical analysis between variables and performance metrics for a case study has been performed. Through an extensive literature review, the most important variables have been determined. These variables are thermal insulation, the position of insulation, window-to-wall ratio, glazed façade orientation, type of glazing and the use of shading devices. A case study of office spaces located in three Chilean cities with different climates is presented. The metrics evaluated are energy consumption, spatial daylight autonomy and annual sunlight exposure. The results show the relationship between each variable with metrics for each location.

Keywords: • visual comfort • total energy consumption • statistical analysis • office buildings • building variables •

CORRESPONDENCE ADDRESS: Daniel Uribe, M.Sc., Researcher, Pontificia Universidad Católica de Chile, Center for Sustainable Urban Development (CEDEUS), Department of Construction Engineering and Management, School of Engineering, Av. Vicuña Mackenna 4860, 7820436 RM, Chile, e-mail: dnuribe@uc.cl. Waldo Bustamante, Ph.D., Professor, Pontificia Universidad Católica de Chile, Center for Sustainable Urban Development (CEDEUS), School of Architecture, El Comendador 1916, 7530091 RM, Chile, wbustamante@uc.cl, Sergio Vera, Ph.D., Associate Professor, Pontificia Universidad Católica de Chile, Center for Sustainable Urban Development (CEDEUS), Department of Construction Engineering and Management, School of Engineering, Av. Vicuña Mackenna 4860, 7820436 RM, Chile, svera@ing.puc.cl. María José Yáñez, Student, Pontificia Universidad Católica de Chile, Department of Construction Engineering and Management, School of Engineering, Av. Vicuña Mackenna 4860, 7820436 RM, Chile, e-mail: mjyanez1@uc.cl.

https://doi.org/10.18690/978-961-286-050-9.35 ISBN 978-961-286-050-9

Available at: http://press.um.si.

1 Introduction

In recent years, an increasing amount of literature on the optimization of energy efficiency [1] and improvement of indoor daylight [2] has been published. Diverse alternatives that consider different building variables have been studied to improve building performance.

Lechner [3] proposed three levels of approach for sustainable building. The first level addresses basic design strategies such as orientation, thermal insulation and the use of shading devices. If these are insufficient in meeting the indoor comfort requirements, which may occur, for example, in hot climates, a second level will be necessary when using hybrid passive systems based on natural energy, evaporative cooling and day/night ventilation. In already passively optimized building design, the final level, mechanical equipment, can be incorporated into the building as necessary. Conversely, Herzog et al. [4] consider the first approach to be the application of strategies such as thermal insulation, solar protection or solar heating, infiltration control and the use of supplementary strategies such as artificial lighting and air conditioning, if these are necessary.

Passive strategies to improve energy and lighting efficiency in office buildings include insulation material, insulation position, interior surface reflectance, building materials' thermo-physical properties, ceiling height, type of glazing and the use of shading devices. In the following paragraphs, the strategies most studied in the literature over the last 20 years are analyzed.

Pino et al. [5] show that the glazed area of the building envelope greatly influences the energy demand of office buildings. Büllow-Hube [6] concludes that indoor glare problems can be caused by excessive natural light incoming through the glazed envelope of workplaces. Dubois et al. [7] and Poirazis et al. [8] show that a window-to-wall ratio (WWR) between 30% and 40% is reasonable. Values smaller than this provide a substantial lighting energy savings and can reduce the risk of overheating, glare and the abuse of sun protection (associated with the reduction of natural light). Tzempelikos & Athienitis [9] conclude that a 30% WWR is sufficient to guaranteed the availability of natural light in the work area during 76% of the work time. In addition, they concluded that increasing the window size does not produce a significant increase in the natural light in a southeast Canadian office.

Reinhart [10] found that changing glass with high transmittance (75%) to glass with low transmittance (35%) reduces energy consumption by 20%. Gratia and De Herde [11] showed that in high-glazed office buildings, it is very important to choose an efficient type of glass.

Pino et al. [5] conclude that in Chile, cooling demands are usually higher than heating demands in office buildings, which highlights the importance of studying window size and their orientation.

Smeds and Wall [12] conclude that outside the warm season, direct sun due to the low angle of solar altitude can cause overheating. Therefore, the use of sun protection is highly recommended. Carletti et al. [13] evaluated different solar protections and showed that they generally produce a decrease in annual solar gains; in addition, they proved that both exterior and interior shading devices significantly improve visual comfort and the quality of natural light. Dubois et al. [7] concluded that several types of shading devices are necessary to prevent overheating, control the interior lights and prevent glare from windows.

Through this extensive literature review, the most important variables have been determined; these are insulation level, position of insulation, WWR, glazed façade orientation, type of glass and shading devices.

The main objective of this study is to perform a parametric study using an integrated lighting and energy simulation tool, considering the primary variables that influence the lighting and energy performance of office buildings according to the results of the literature review. In particular, the effect of these variables is studied by using a statistical analysis of three Chilean cities that have different climates.

2 Methodology

This study involves determining the design variables that have the greatest influence on the energy and lighting performance of a single office. This process is performed through a parametric analysis of all combinations of these variables. Because the performance metrics are the total energy consumption and visual comfort, an integrated daylighting and energy simulation tool called *mkSchedule* is used for lighting and energy simulations [14]. This tool efficiently integrates EnergyPlus and Radiance to facilitate the combined thermal and lighting analysis of buildings using complex fenestration systems and controlled luminaires. Next, a statistical analysis is performed using JMP software to qualitatively determine the most influential variables. The following sections provide details of the simulation process, a description of the office space, and a description of the parametric analysis variables.

2.1 Building

The space to be studied corresponds to an office of 4.0 m x 6.5 m x 2.8 m, as shown in Figure 1.

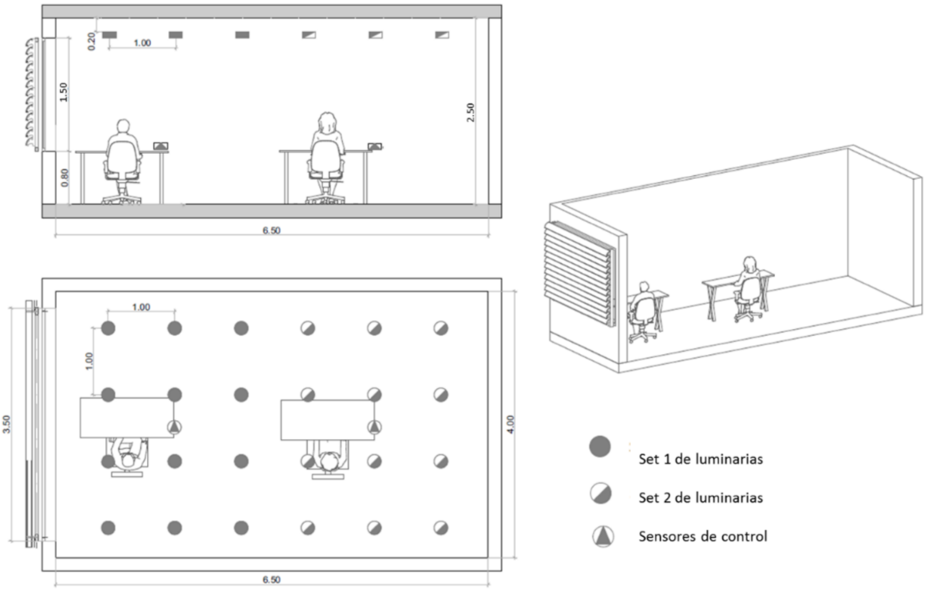

Figure 1. Office space model with louvers: (a) Isometric view; (b) Side view; (c) Plan view.

The walls, ceiling and floor are adiabatic. Only the glazed façade is exposed to the outside. The surface reflectance of the floor, ceiling, and wall are 20%, 70% and 50%, respectively. The HVAC system consists of an electric heat pump with COP 3.0 with heating and cooling thermostat set points of 20°C and 24°C, respectively. The internal heat gains of people and electric equipment are 6.7 W/m^2 and 15 W/m^2 [15], respectively. The office space includes two sets of dimmed luminaires, which are controlled to achieve 500 lux at the workplane. The internal heat gain due to the lights is 13.85 W/m^2. The schedules for people, lights, equipment and HVAC are set from 08:00 to 18:00 hrs.

2.2 Variables

Table 1 shows the variables studied and their values, ranges and steps.

Table 1. Design variables.

Variable	Minimum	Maximum	Step	Total
Orientation	0	360	45	8
City	-	-	-	3
WWR	30%	100%	5%	15
U-value window	-	-	-	15
SHGC window	-	-	-	
Exterior shading device	-	-	-	
R_T of wall insulation	0	1.5	0.1	16
Inside/outside insulation	-	-	-	2

The studied orientations correspond to north, northeast, east, southeast, south, southwest, west and northwest. The cities studied are Antofagasta (S 23.43°, W 70.45°), Santiago (S 33.38°, W 70.78°) and Punta Arenas (S 53.00°, W 70.97°), characteristic climates of the north, central and southern zones of Chile, respectively. According to the Köppen-Geiger classification, Antofagasta is a BWn, desert climate with low-latitude; Santiago is a Csb, dry summer Mediterranean climate; and Punta Arenas is a Cfc, subpolar oceanic climate. The thermal resistance range of the insulation covers all possible cases for each thermal zone, according to the current thermal regulation envelopes. For windows and shading devices, 15 combinations are evaluated; including three glasses (single clear, double clear with air and double Low-e with air) and four exterior shading devices (venetian blinds set to 0° and 45°, generic woven shades and perforated screen panels - circular).

2.3 Performance Metrics and Simulation

A total of 5400 lighting simulations and 12800 energy simulations were performed.
The performance of the building was evaluated in terms of the following parameters:
Total energy consumption (kWh/year), which represents the sum of lighting, heating and cooling energy consumption.

$sDA_{300/50\%}$ is defined as the percentage of an analysis area that meets 300 lux for 50% of the operating hours per year. An $sDA_{300/50\%}$ above 50% has been considered as the acceptable daylight level according to IES.

$ASE_{2000/400h}$ is defined as the percentage of an analysis area that exceeds 2000 lux more than 400 hours per year. An $ASE_{2000/400h}$ lower than 20% has been considered acceptable to reduce visual discomfort.

The lighting and energy simulations were performed in *mkSchedule*, a time-efficient tool that was recently developed. This tool performs integrated thermal and lighting simulations for fixed and movable CFSs using the three-phase method developed by McNeil [16]. *mkSchedule* uses Radiance for the lighting domain and EnergyPlus for the thermal domain. Using a simple case study, [14] demonstrated that *mkSchedule* integrates Groundhog (a SketchUp plug-in), Radiance and EnergyPlus, producing results within a short period of time and allowing flexibility to incorporate different design alternatives. An hourly annual schedule with the CFS position and the power fraction of the luminaires is generated for each city. This schedule is used as an input to the lighting and energy simulations, which use Radiance and EnergyPlus, respectively.

3 Results and analysis

In this section, the results of variation between the design variables with respect to the performance parameters of lighting and energy are presented.

Figure 2 shows the variation of design variables with respect to the lighting performance parameters $sDA_{300/50\%}$ and $ASE_{2000/400h}$.

The results show there is a high variation in the cases of the shading device and WWR variables. For the shading devices, high variation is expected since they are completely different systems in their transmission of light and heat via fenestration. In the case of WWR, the high variation agrees with the literature, which identifies it as the most important variable and suggests that an increase in the glazing ratio can produce visual comfort issues. The other design variables such as orientation of the façade and type of glass do not present great variation with respect to the visual comfort. Finally, Santiago has the highest glare risk probability.

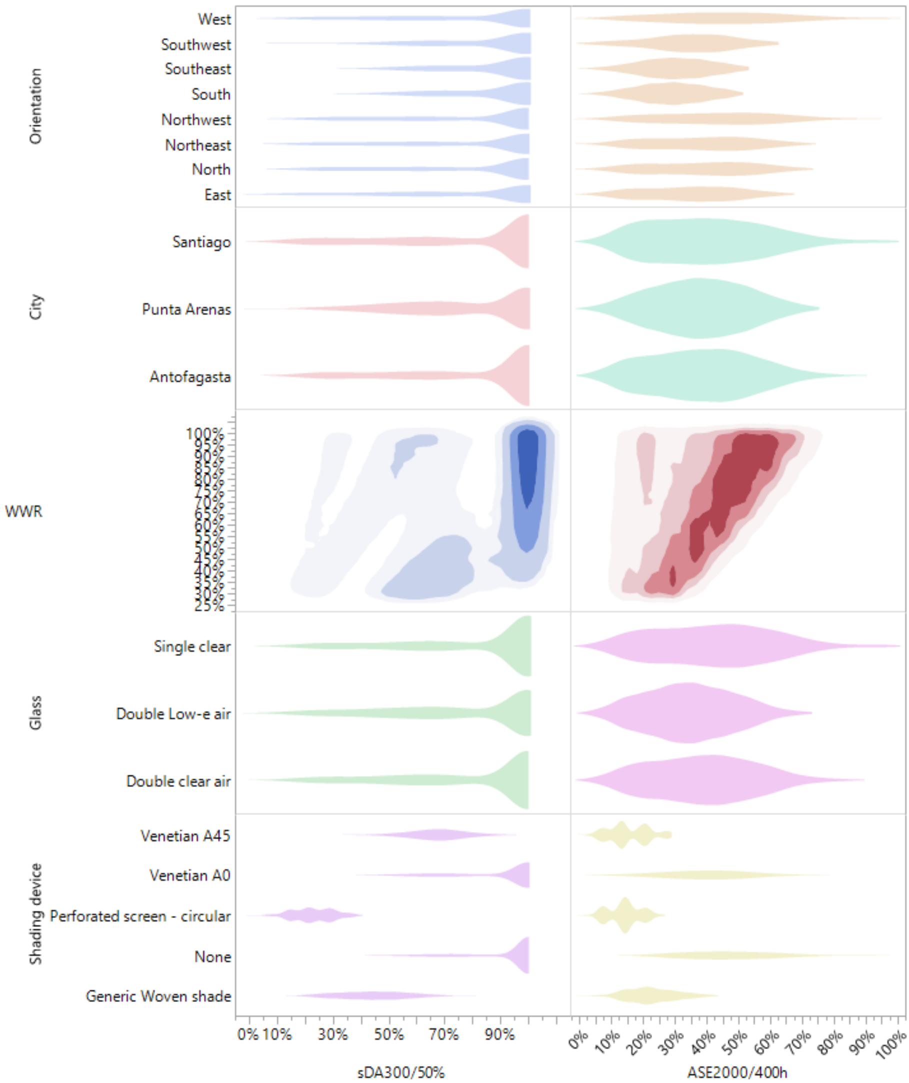

Figure 2. Density graphics for lighting results.

Figure 3 shows a density graphic that compares each design variable with respect to lighting, heating, cooling and total energy consumption.

The results show that the design variables that have a significant variation with respect to the total energy consumption are the position of the insulation, thermal resistance, shading devices and WWR. Orientation has a smaller variation. Finally, the variables that least influence the design are the city, orientation and type of glass. It should be noted that the WWR and thermal resistance of the wall tend toward a line in the area with the highest density of points.

Therefore, the most important variables are WWR, shading device, thermal resistance of the walls and position of the insulation of the wall. The orientation and city are less important than are the variables previously named. Finally, the type of glass does not greatly affect the performance of the building.

4 Conclusions

The main objective of this paper is to determine the most influential variables in building design pertaining to visual comfort and energy performance, and then perform a statistical analysis between variables and performance metrics for three Chilean cities. The total energy consumption and the visual comfort metrics $sDA_{300/50\%}$ and $ASE_{2000/400h}$ are obtained by means of energy and lighting simulations.

For the cases of the three Chilean cities, the most important design variables for building performance are WWR, thermal resistance, shading devices and position of wall insulation. City and orientation were less important and the type of glass was not significant.

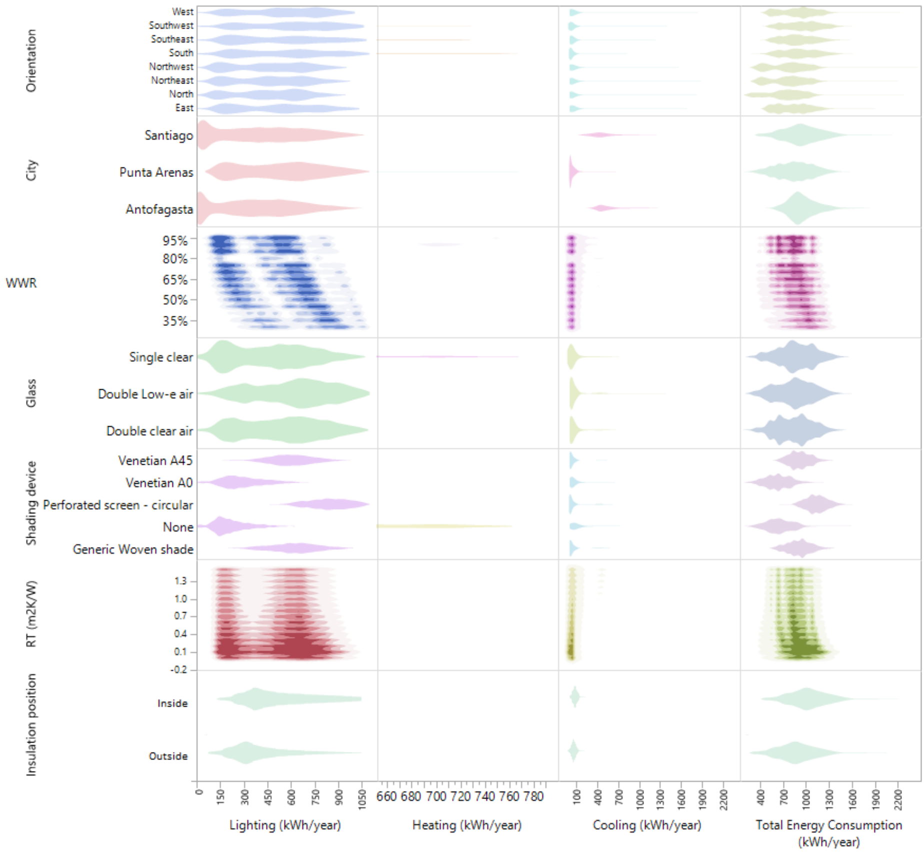

Figure 3. Density graphics for energy results.

An analysis with fit curves for the different climates and façade orientations is needed to numerically determine the relationships between the independent and dependent variables.

The results and conclusions presented in this paper are specific for the shading devices and locations studied. Further studies are recommended to evaluate other strategies, shading systems and locations.

Acknowledgements

This work was funded by the National Commission for Scientific and Technological Research (CONICYT) under research grant FONDECYT 1141240. The authors also gratefully acknowledge the research support provided by CEDEUS under the research grant CONICYT/FONDAP 15110020.

References

[1] A. Prieto, U. Knaack, T. Klein, and T. Auer, "25 Years of cooling research in office buildings: Review for the integration of cooling strategies into the building façade (1990–2014)," *Renewable and Sustainable Energy Reviews,* vol. 71, pp. 89-102, 2017.

[2] A. Kirimtat, B. K. Koyunbaba, I. Chatzikonstantinou, and S. Sariyildiz, "Review of simulation modeling for shading devices in buildings," *Renewable and Sustainable Energy Reviews,* vol. 53, pp. 23-49, 2016.

[3] N. Lechner, Wiley, Ed. *Heating, Cooling, Lighting: Sustainable Design Methods for Architects*, 4th ed. 2014.

[4] T. Herzog, R. Krippner, and W. Lang, B. B.-P. f. Architecture, Ed. *Façade construction manual*. 2004.

[5] A. Pino, W. Bustamante, R. Escobar, and F. E. Pino, "Thermal and lighting behavior of office buildings in Santiago of Chile," *Energy and Buildings,* vol. 47, pp. 441-449, 2012.

[6] H. Büllow-Hube, "The effect of glazing type and size on annual heating and cooling demand for Swedish offices," in *Renewable Energy Technologies in Cold Climates '98*, Montreal, Canada, 1998.

[7] M.-C. Dubois and Å. Blomsterberg, "Energy saving potential and strategies for electric lighting in future North European, low energy office buildings: A literature review," *Energy and Buildings,* vol. 43, no. 10, pp. 2572-2582, 2011.

[8] H. Poirazis, Å. Blomsterberg, and M. Wall, "Energy simulations for glazed office buildings in Sweden," *Energy and Buildings,* vol. 40, no. 7, pp. 1161-1170, 2008.

[9] A. Tzempelikos and A. K. Athienitis, "The impact of shading design and control on building cooling and lighting demand," *Solar Energy,* vol. 81, no. 3, pp. 369-382, 2007.

[10] C. F. Reinhart, "Effects of interior design on the daylight availability in open plan offices," in *ACEEE Summer study on energy efficient buildings*, Pacific Grove, CA (USA), 2002, pp. 1-12.

[11] E. Gratia and A. De Herde, "Design of low energy office buildings," *Energy and Buildings,* vol. 35, no. 5, pp. 473-491, 2003.

[12] J. Smeds and M. Wall, "Enhanced energy conservation in houses through high performance design," *Energy and Buildings,* vol. 39, no. 3, pp. 273-278, 2007.

[13] C. Carletti, F. Sciurpi, and L. Pierangioli, "The Energy Upgrading of Existing Buildings: Window and Shading Device Typologies for Energy Efficiency Refurbishment," *Sustainability,* vol. 6, no. 8, 2014.

[14] S. Vera, W. Bustamante, G. Molina, and D. Uribe, "A flexible and time-efficient schedule-based communication tool for integrated lighting and thermal simulations of spaces with controlled artificial lighting and complex fenestration systems," *Journal of Building Performance Simulation,* vol. 9, no. 4, pp. 382-396, 2016.

[15] *CIBSE Guide A: Environmental Design*, 2006.

[16] A. McNeil, "The Three-Phase Method for Simulating Complex Fenestration with Radiance," ed, 2013.

10TH INTERNATIONAL CONFERENCE ON SUSTAINABLE ENERGY AND ENVIRONMENTAL PROTECTION (JUNE 27TH – 30TH, 2017, BLED, SLOVENIA), ENERGY EFFICIENCY
J. Krope, A.Ghani Olabi, D. Goričanec & S. Božičnik

Operation of Distributed Energy Supply Systems

DUŠAN KRAGELJ, TOMAŽ KRAMBERGER, BOJAN RUPNIK, DANIJELA URBANCL & DARKO GORIČANEC

Abstract The paper presents a distributed energy supply system (DESS) which comprises a set of energy suppliers and consumers, heat and cooling storage facilities and power transmission lines in a region. Production and consumption of electrical power and heat, power transmissions, the district heating pipelines, cooling systems and storage of heat are taken into account in the DESS model. Nowadays, the distributed energy production has an increasingly important role in the energy market. Evaluation of the energy production cost is based on the daily operation for every season of the year. Optimal design and operation of the distributed energy supply system can be characterized by reduction of energy consumption, increase of energy efficiency and decrease of generation of pollutants and has a huge economical potential.

Keywords: • Distributed energy supply systems • Energy efficiency • Heat pump • Cogeneration • Trigeneration •

CORRESPONDENCE ADDRESS: Dušan Kragelj, M.Sc, Manager, Public Institution General Hospital Celje, Oblakova ulica 5, 3000 Celje, Slovenia, e-mail: dusan.kragelj@sb-celje.si. Tomaž Kramberger, Ph.D., Associate Professor, University of Maribor, University of Maribor, Faculty of Logistics, Mariborska cesta 7, 3000 Celje, Slovenia, e-mail: tomaz.kramberger@um.si. Bojan Rupnik, PhD, Assistant, , University of Maribor, Faculty of Logistics, Mariborska cesta 7, 3000 Celje, Slovenia, e-mail: bojan.rupnik@um.si. Danijela Urbancl, Ph.D., Assistant, University of Maribor, Faculty of Chemistry and Chemical Engineering, Smetanova ulica 17, 2000 Maribor, Slovenia, e-mail: danijela.urbancl@um.si. Darko Goričanec, Ph.D., Associate Professor, University of Maribor, Faculty of Chemistry and Chemical Engineering, Smetanova ulica 17, 2000 Maribor, Slovenia, e-mail: darko.goricanec@um.si.

https://doi.org/10.18690/978-961-286-050-9.36 ISBN 978-961-286-050-9

Available at: http://press.um.si.

1 Introduction

The paper presents an operational strategy distributed energy supply systems (DESS), daily and seasonal, of an energy system made up of a cogeneration plant equipped with compression and/or absorption heat pumps, gas fired boiler to meet the energy demands of a specific consumers. Distributed energy supply systems (DESS) are complex systems with typically excellent economies of scale and distributed units enabling more efficient operation [1]. Operation of DESS must be accounted for, i.e., economy of scale of equipment investments, limited capacities of standardized equipment, part-load performance and minimum operation loads of the equipment as well as multiple redundant units [2]. The existing DESS system poses non-trivial problems that need to be considered on two levels:

- Design level: Technical specification (capacity, operating limits, etc.).
- Operation level: Unit commitment (heat output, mass flows, temperatures, pressures, etc.).

Cogeneration systems and heat pumps are the most advanced technologies for energy savings, providing the most rational means of energy management. Integrating these two technologies into a trigeneration plant increases both plant complexity and initial investment costs, on the other hand, it greatly augments the advantages offered by each individual technology, providing a more usable system which can meet the variable and complex energy needs of a consumer.

The existing DESS configuration based on the hourly electrical, thermal and cooling load diagrams of a consumer will be upgrade with high temperature heat pumps to use renewable energy sources for economic returns maximization over a calendar year and calculates the savings.

2 The plant configuration Description

The advantages of cogeneration systems are especially evident in applications where electrical and thermal energy is required simultaneously and at a constant ratio.

The energy demands of consumers are characterized by the simultaneous request for both heating and electricity, the ratio is not always optimal, due different seasonal energy demands and changing during the single day.

For this reason it is very difficult to achieve an optimal operation of the existing DESS configuration, however a trigeneration system may offer an efficient means to meet such variable energy demands.

Very good energetic and economic results can be obtained from a trigeneration system which integrates a cogeneration plant with compression and absorption heat pumps, which are directly fed by the surplus electric and thermal energies produced by the cogeneration engine during the winter and summer months, respectively [3].

The use of compression and absorption heat pumps can guarantee a more constant supply of energy, shifting energy demand from electrical to thermal and vice versa and thus bypassing seasonal variations in energy loads.

Absorption heat pumps are important heat consuming equipment in the summer, which exploits the otherwise dissipated heat surplus generated by the CHP and compensating the reduction in heat demand in this season.

The DESS configuration on the fig. 1 is proposed to meet the energy demands of the consumer under consideration.

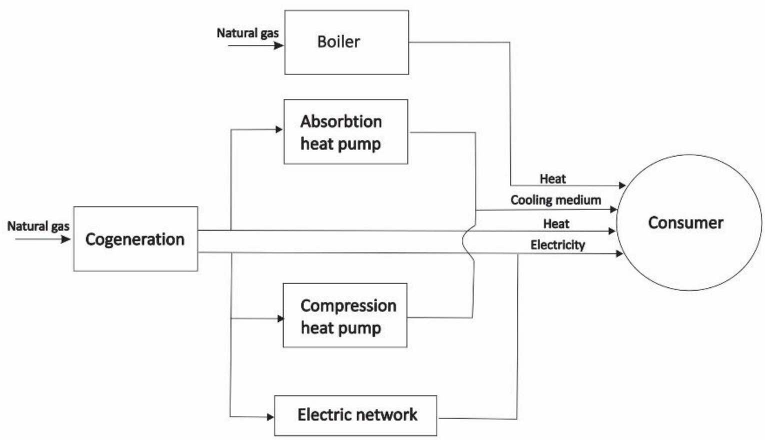

Figure 1. DESS configuration

Due different seasonal energy demands and changing during the single day the energy storage is a viable approach to balance demand and supply where a heat or cold carrier is used in the form of water. A setup includes one or more producers with a stratification tanks to shift loads in time and multiple consumers [4].

The heat distribution network of the DESS is composed of a high temperature hot water circuit to the users of the heating system as well as that needed for sanitary use and a low temperature water circuit, which supplies cold water to the refrigeration systems.

3 Energy demands of the consumer

The consumer of this study have central energy plant where provides electricity, hot and cold water for satisfying the needs of the technological services, hot water in winter, is used to run the heating system and sanitary use and the cold water for air-conditioning systems.

Figs. 2, 3, 4 and 5 illustrate the typical hourly electric, thermal, and cooling load diagrams: a single non-working holiday and working day in the winter months and the summer months.

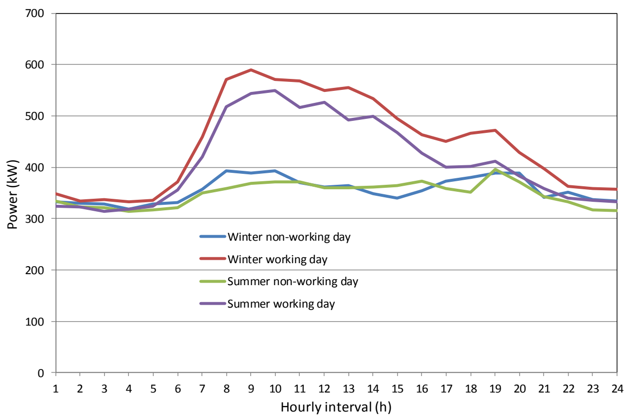

Figure 2. Typical hourly electric load

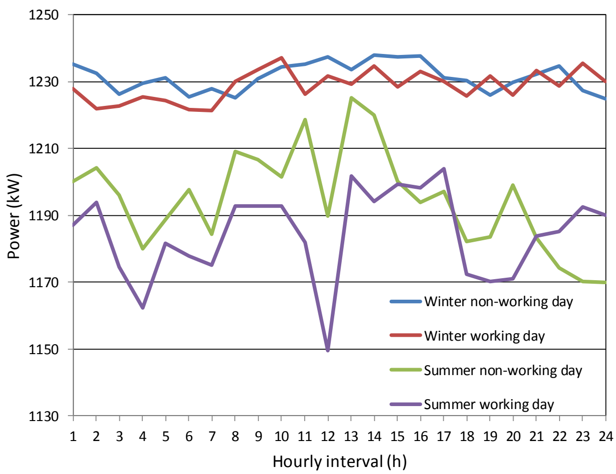

Figure 3. Typical hourly CHP thermal load

Figs. 6 and 7 illustrate the electrical and thermal energy production and consumption profile of the entire consumer complex throughout the year, which is calculated from the monthly bills.

CHP consist from internal combustion gas engines with thermal recovery from exhaust gases at high temperatures and from the engine and lubrication cooling system with temperatures ranging from 60ºC to 90ºC.

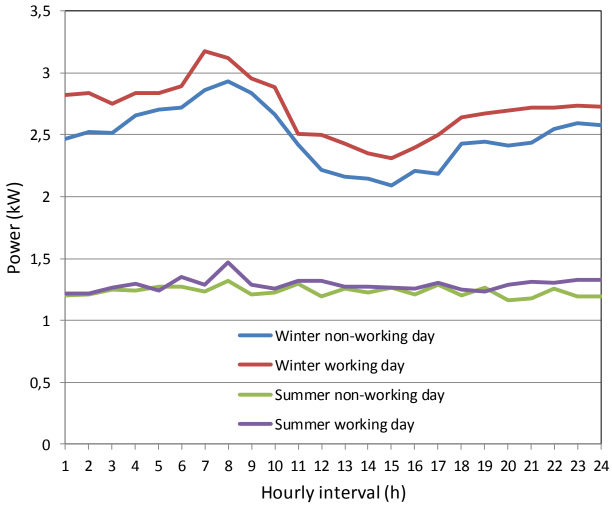

Figure 4. Typical hourly total thermal load

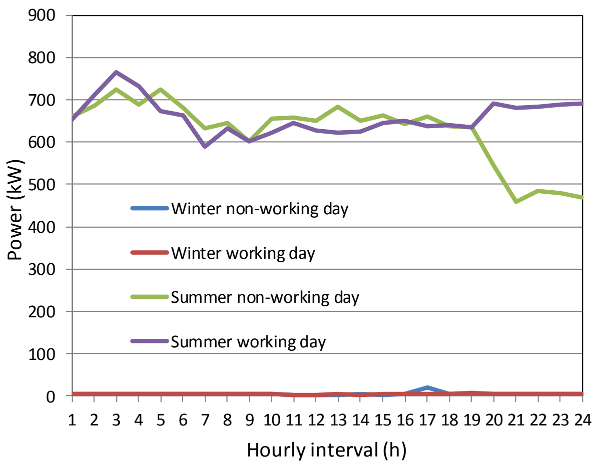

Figure 5. Typical hourly absorber thermal load

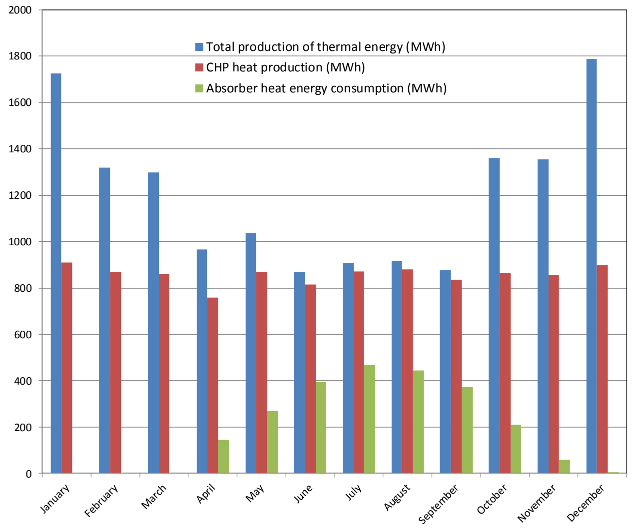

Figure 6. Production and consumption of heat by months

The absorption heat pumps used a surplus thermal energy demands for cooling needs in the summer and the electric compression heat pumps are used only to cover the missing cooling needs. The heat distribution network of the consumer is composed of a high temperature circuit, which distributes hot water to various heat users, and a low temperature circuit, which distributes cold water for the refrigeration needs.

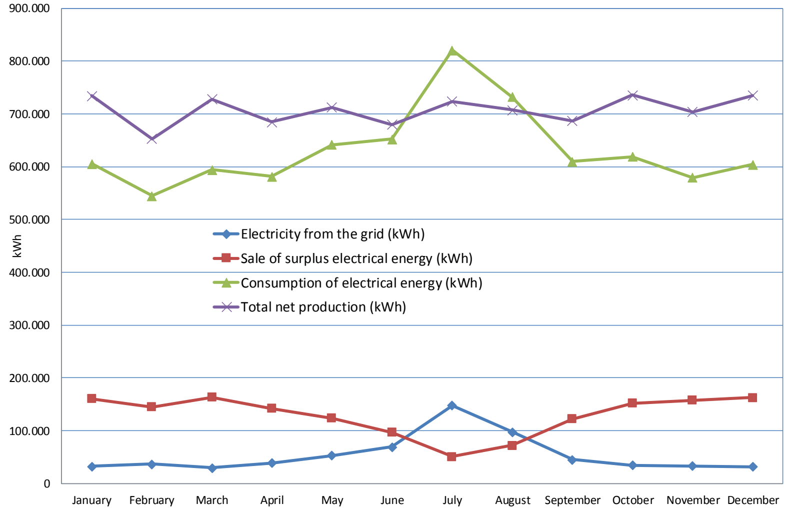

Figure 7. Production and consumption of electricity by months

The performance coefficients of the single energy appliances of the existing DESS configuration (Fig. 1) are presented in Table 1, with values referring to the standard values of common commercially available equipment.

Table 1. The performance characteristics of common commercially available equipment.

	Efficiency
Characteristics CHP	
- electrical efficiency at rated power	39.7%
- the heat efficiency at (70/90°C)	46.6%
- total efficiency at rated power	86.3%
Boiler	
- natural gas fired steam boilers	90%
Absorption heat pump	
- efficiency of cooling at (6/12ºC)	COP 0.72
Compression heat pump	
- efficiency of cooling at (6/12ºC)	COP 4.0

4 Upgrading existing DESS

In order to reduce the consumption of natural gas is proposed to upgrade the existing DESS by high-temperature heat pump. Low-temperature heat sources of high temperature heat pumps can be air, groundwater or downhole heat exchanger [5].

The high temperature heat pump would be used for heating the water of the return flow of the district heating system to the maximum permitted inlet temperature of the CHP. The proposed upgrading of the DESS configuration to meet the energy demands of the consumer is presented on the fig. 8.

Integration of the high temperature heat pump in the high temperature heating system has to further consider the differences between input and output temperature. The higher the difference, the lower is the efficiency of the system [6], [7].

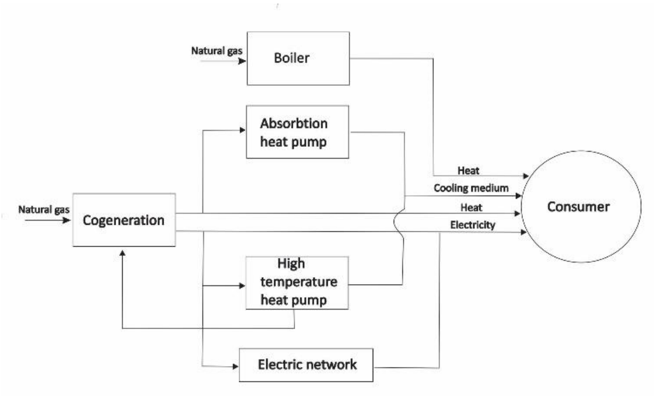

Figure 8. Proposed to upgrade the DESS configuration

For this reason, during the winter period with high-temperature heat pump heats the fluid of the return flow of high temperature heating system, but at the summer period, are at the same time produces the cold water for cooling, and the heat for the sanitary water heating.

5 Conclusion

The Renewable Energy Directive (2009/28/EC) establishes an overall policy the EU to fulfil at least 20 % of its total energy needs with renewables by 2020. The revised Renewable Energy Directive anticipates the EU as a global leader in renewable energy and ensures that the target of at least 27 % renewables in the final energy consumption in the EU by 2030 is met.

Proposed upgrading of the DESS configuration provides for ensuring the energy needs of the consumer, the use of renewable energy sources.

The surplus electricity produced by the CHP, which are now transmitted into the electricity grid would be used to drive the compressor high-temperature heat pumps. The price of electricity transmitted into the power grid is 30 €/MWh. At the estimated COP 3 of the high temperature heat pumps, the price of the heat generated will be 10 €/MWh and is more than three times less than the price of the heat produced by a gas-fired boiler, which is 34 €/MWh.

References

[1] F. Bouffard, D.S. Kirschen, "Centralised and distributed electricity systems," *Energy*, vol. 36, pp. 4504-4508, 2008.

[2] P.Velaso-Garcia, P.S. Varbanov, H. Arellano-Garcia, G. Wozny, "Utility systems operation: Optimisation-based decision making", *Applied Thermal Engineering*, vol. 31, pp. 3196-3205, 2011.

[3] P. Arcuri, G. Florio, P. Fragiacomo, "A mixed integer programming model for optimal design of trigeneration in a hospital complex", *Energy*, vol. 32, pp. 1430-1447, 2007.

[4] T.W. Scholten, C. De Persis, P. Tesi, "Modelling and Control of Heat Networks with Storage: the Single-Producer Multiple-Consumer Case", European Control Conference (ECC), 2015, pp. 2242-2247

[5] B. Kulčar, D. Goričanec, J. Krope, "Economy of exploiting heat from low-temperature geothermal sources using a heat pump", *Energy and buildings*, vol. 4, pp. 323-329, 2008.

[6] IEA (International Energy Agency), 2011, Technology Roadmap www.iea.org/publications/freepublications/publication/buildings_roadmap.pdf accessed 07.05.2017.

[7] T. Ommen, W. B. Markussen, B. Elmegaard, "Heat pumps in combined heat and power systems", *Energy*, vol. 76, pp. 989-1000, 2014.

10TH INTERNATIONAL CONFERENCE ON SUSTAINABLE ENERGY AND ENVIRONMENTAL PROTECTION (JUNE 27TH – 30TH, 2017, BLED, SLOVENIA), ENERGY EFFICIENCY
J. Krope, A.Ghani Olabi, D. Goričanec & S. Božičnik

Innovative Solution for Energy Efficient Urban Freight Deliveries

TOMISLAV LETNIK, MATEJ MENCINGER & STANE BOŽIČNIK

Abstract An innovative solution for energy efficient urban freight deliveries has been developed. The solution aims to solve simultaneously two problems: the vehicle routing problem and the problem of optimal number and location of transhipment points in urban areas. Optimisation is based on fuzzy clustering procedure where each customer has a certain degree of membership to different transhipment points. Routing algorithm uses this information for the purpose of assignment of deliveries in case the most optimal transhipment point is occupied. Optimisation procedure has been tested on a case study and have demonstrated a significant CO2 emissions and energy savings.

Keywords: • transport • urban freight • CO2 emissions • energy efficiency • fuzzy clustering •

CORRESPONDENCE ADDRESS: Tomislav Letnik, Senior lecturer, University of Maribor, Faculty of Civil Engineering, Transportation Engineering and Architecture, Smetanova 17, 2000 Maribor, Slovenia, e-mail: tomislav.letnik@um.si. Matej Mencinger, Ph.D., Associate Professor, University of Maribor, Faculty of Civil Engineering, Transportation Engineering and Architecture, Smetanova 17, 2000 Maribor, Slovenia, e-mail: matej.mencinger@um.si. Stane Božičnik, Ph.D., Associate Professor, University of Maribor, Faculty of Civil Engineering, Transportation Engineering and Architecture, Smetanova 17, 2000 Maribor, Slovenia, e-mail: stane.bozicnik@um.si.

https://doi.org/10.18690/978-961-286-050-9.37 ISBN 978-961-286-050-9

Available at: http://press.um.si.

1 Introduction

Nowadays, transport sector in the EU consumes already 21% of primary energy and produces 24% of total CO2 emissions. Road transport is the largest consumer and emitter among all transport modes, it consumes 83% share of transport energy and produce 93% of CO2 emissions [1].

The bigest share of energy consumption and production of transport emissions is realted to cities. Passenger cars are responsible for more than half of the total transport energy consumption and CO2 emissions [2] in European cities, whereby freight vehicles contribute to about 19% of energy use and 21% of CO2 emissions [3]. With increasing urban population and economic activities in cities, efficiency of urban freight will become increasingly important to influence improvement in energy savings and decrease negative effects of transport in total.

Efficiency of urban freight is nowadays confronted with challenging task of on demand and just-in-time deliveries which results in high fragmentation of urban freight demand and supply [4]–[6]. As a consequence, cities are facing an increasing number of poorly utilised urban freight transport trips which severely decrease efficiency and increase energy consumption and pollution [7], [8].

Recent empirical studies on urban freight transport show an average freight vehicle load factor of only 30-40% [9], [10] and more than 20% of vehicles drive empty [11]. Last mile is considered also as the most inefficient part of the supply chain. Although it takes only a small part of the total travelled distance, it represents a 28% of the total transportation costs [12].

Cities are trying to solve before mentioned problems with testing and implementing different policy measures, in particular restricting freight vehicles access to city centres, creating Low Emission Zones (LEZs), introducing off-peak hour deliveries, implementing Urban Consolidation Centres (UCCs), and many others. Despite these efforts, urban freight problems still exist.

Introducing innovative urban delivery solution is quite expensive and long-lasting task. For this sake, many models and modelling principles have been introduced. We can classify them into [13]: network models (evaluating impacts of policies for reducing greenhouse gas emissions from road freight vehicles); fleet models (predicting aggregate emissions from the overall fleet); routing models (developing routes that minimise the travelling distance); life cycle analysis models (estimating energy consumption and emissions of freight vehicles over their life) and other models (fuel consumption, CO2 emissions, etc.). The most recent significant advances in modelling urban freight are associated with the use of alternative transport modes, such as: electric trucks, vans, bikes, rail etc. [14]–[16]. When searching for the most efficient and sustainable approach Cherrett et al. [17] suggest modelling the option of Urban Consolidation Centres (UCCs) or loading bays (transhipment points located within urban areas) in combination with optimal vehicle routing.

Following these suggestions, the way to an innovative system for energy efficient urban last mile delivery is proposed. The system makes use of loading bays and a methodology to optimize the system performances. This methodology involves: advanced fuzzy based clustering of receivers, dynamic assignment of loading bays and optimal vehicle routing.

2 The proposed freight delivery system and the model

The proposed freight delivery system is based on using loading bays. In this article, loading bays are considered as physical places within the urban areas where delivery vehicle can stop (or park) to perform freight loading, unloading and last mile distribution operations, without disrupting traffic flows [18].

Last mile deliveries takes place in the first phase by freight vehicles (trucks or vans) from outside the urban areas, or from UCCs to loading bays. Freight vehicles are then in the second phase parked at loading bays, and drivers, or other operators, unload the goods from vehicles and deliver them to receivers: on foot, by trolleys, or by freight bikes, according to the distance from loading bay to receivers and to the dimension of consignments.

In the first phase of the model, the geographical clustering of customers is performed to determine cluster centres for predefined number of clusters (N_{LB}). In the second phase, approximation methods are implemented to define feasible and acceptable loading bays for particular clusters based on maximum acceptable distance, d_{max}, from the selected selected loading bay to the customer. In third step, the final selection of loading bay is performed based on optimal routing.

The complete scheme of the model is presented in Figure 1.

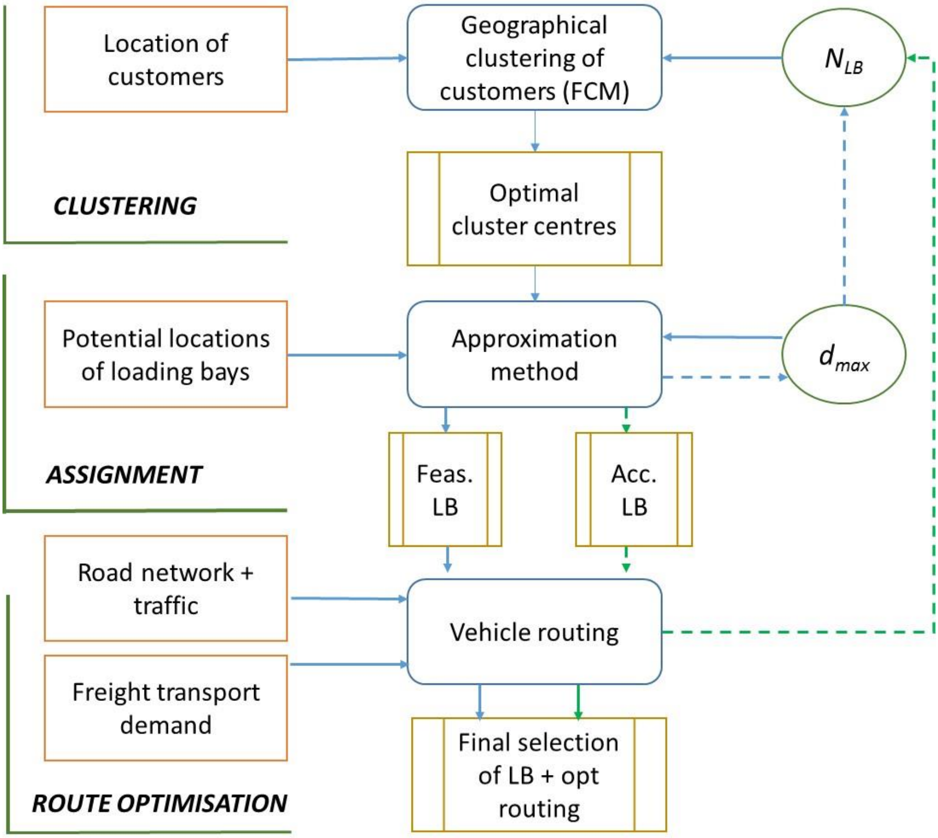

Figure 1. The complete scheme of the model

In the model, urban last mile delivery problem is therefore divided into two sub-problems: the delivery of goods from outside the city to the loading bay; and the delivery of goods from the loading bay to the receiver. The two sub-problems are resolved in a reversed order.

2.1 The first sub-problem: clustering and deffuzification

In the first sub-problem, i.e. the delivery of goods from the loading bay to the receiver, the best loading bay is determined with a fuzzy clustering algorithm (FCM). A constraint of the problem is the maximum acceptable distance, d_{max}, from a selected loading bay to a receiver. Location of customers (geographical coordinates) and a predefined number of loading bays (N_{LB}) are two main elements needed for defining the optimal location of cluster centres.

The clustering algorithm chosen in the model is the fuzzy k-means clustering [19]. In the fuzzy k-means clustering, each receiver has a certain degree of membership to each cluster (u_{ij} is the degree of membership of the receiver i to the cluster j), rather than belonging to only one cluster [20]. The degree of membership u_{ij} of the receiver i to the cluster j is inversely proportional to the distance of the receiver i from the centre of cluster j (eq. (3) in the sequel).

The fuzzy clustering aims at minimising the following cost function:

$$f = \sum_{i=1}^{N} \sum_{j=1}^{n_c} u_{ij}^{m} \left\| x_i - c_j \right\|^2 \tag{1}$$

Where:

- x_i = address of the receiver of the delivery i (it is a point in the plane with given latitude and longitude)
- c_j = centre of cluster j (it is a point in the plane with given latitude and longitude)
- u_{ij} = degree of membership of receiver i to cluster j
- m = parameter of fuzziness (after several trials we took it equal to 2)
- N = number of receivers,
- n_c = number of clusters.

We need to determine the u_{ij} and c_j values that minimise the cost function f. To solve this problem, an iterative procedure has been adopted [21].

The initial values for the degrees of membership u_{ij} (0) of the receiver i to the cluster j (i.e. the initialisation step) have been determined assuming the positions of the cluster centres uniformly distributed in the area.

At the generic k^{th} iteration, the positions $c_j^{(k)}$ of cluster centres and the degrees of membership $u_{ij}^{(k)}$ are updated according to eq. (2) and (3) [22]:

$$c_j^{(k)} = \frac{\sum_{i=1}^{N} u_{ij}^{(k-1)m} \cdot x_i}{\sum_{i=1}^{N} u_{ij}^{(k-1)m}} \tag{2}$$

$$u_{ij}^{(k)} = \frac{1}{\sum_{b=1}^{n_c} \left(\frac{\left\| x_i - c_j^{(k)} \right\|}{\left\| x_i - c_b^{(k)} \right\|} \right)^{\frac{2}{m-1}}} \tag{3}$$

At each iteration *k*, the algorithm updates a matrix $U^{(k)}$ whose columns refer to clusters and whose rows refer to items: $[U^{(k)}]_{ij} = u_{ij}^{(k)}$.

The fuzzy clustering algorithm stops when for each item *i* and for each cluster *j* the degree of membership is no longer updated relevantly from an iteration to the next. The prescribed level of relevance (accuracy) is taken to be $\varepsilon = 0.01$.

The defuzzification is originally performed according to the maximum membership procedure: that is, each cluster element is assigned to the cluster for which the degree of membership is the highest [20]. In the model, we take into consideration also lower degrees of membership, when searching for alternative clusters.

2.2 The second sub-problem: approximation and routing

In the second sub-problem, i.e. the delivery of goods from outside the city to the loading bay, we take advantage of the results obtained when solving the first sub-problem. Selection of the loading bay depends on the strategy of choosing the approximation method.

In the case of the first approximation method, the nearest loading bay is already the most optimal one. In the case of the second approximate method, the algorithm chooses among all the acceptable options of feasible loading bays considering their occupation and shortest possible path.

If approximation methods are not able to find a loading bay for all customers than the d_{max} is increased and clustering algorithm runs again. The procedure is repeating until all the customers are belonging to at least one (feasible) loading bay.

The routing is in both cases performed based on the well-known Dijkstra algorithm. The routing algorithm compares travel distances among origins (entrance points to the urban area) and destinations (potential loading bays). The most optimal (shortest/fastest) route is finally selected in combination with feasible and acceptable loading bays.

2.3 Outputs of the model

In output, the model provides positions of cluster centres, assignment of a particular delivery to the most optimal loading bay, optimal routing for each delivery, maximal/average time and distances needed for deliveries to and from loading bays.

3 Case study – evaluation of savings

To prove the validity of the model, the overall concept has been applied to the simulated case study of the historical city centre of Lucca, Italy.

Lucca city centre is a flat oval area, with the diameters of around 1.8 and 1.0 km. Access of commercial vehicles to the historical city centre is restricted, due to narrow streets and high pedestrian flows. Intensity of restrictions varies during the day as well as the demand.

The number of commercial activities in Lucca city centre is 1161. The average number of deliveries by day in Lucca city centre each day is 1272 and the number of freight vehicles entering in the city centre is 1058 (sales representative vehicles included), which results in around 1.2 deliveries performed by each vehicle.

The highest demand is recorded in three periods of the day: A: 8−10 a.m. (291 deliveries), B:10−12 a.m. (315 deliveries), and C: 4−6 p.m. (170 deliveries).

These three periods represent also three basically different situations in terms of congestion and restrictions.

For each of the three chosen periods of the day customer locations and their demand have been identified and the potential loading bays have been determined.

3.1 Environmental impact and energy savings

Environmental performances of the proposed last mile freight delivery system are compared with those of the existing scenario (without loading bays). The comparison includes only the freight vehicles travel time and distances. The main purpose of comparison of the two cases is to find out most environmently friendly option.

Environmental performance of the system is measured in travel times, travel distances, CO_2 emissions and fuel consumption. Our calculation considers deliveries performed with average light commercial vehicle (category N1 - up to 3,5 tons) with diesel engine. In urban areas, this kind of vehicles consume on average 11,4 litres of diesel per 100 km, which results approximately with 300 g/km CO_2 (taking into consideration conversion factor (1 litre/100km = 26.5 g/km CO_2) [23].

Table 1. Comparison of performance between existing scenario and two approximation methods

PERFORMANCE		tt_{max} [min/trip]	tt_{avg} [min/trip]	td_{max} [km/trip]	td_{avg} [km/trip]	td_{max} CO2 [kg/trip]	td_{avg} CO2 [kg/trip]	td_{max} fuel [liter/trip]	td_{avg} fuel [liter/trip]
Existing scenario	A	51	23,4	17,0	9,6	5,1	2,9	1,9	1,1
	B	51	23,2	15,9	9,5	4,8	2,9	1,8	1,1
	C	80	37,0	15,3	9,5	4,6	2,8	1,7	1,1
1st apr. method	A1	30	17,0	10,6	6,1	3,2	1,8	1,2	0,7
	B1	23	15,6	10,6	5,9	3,2	1,8	1,2	0,7
	C1	31	20,7	10,6	6,1	3,2	1,8	1,2	0,7
2nd apr. method	A2	30	15,4	10,6	5,6	3,2	1,7	1,2	0,6
	B2	23	14,5	10,6	5,5	3,2	1,7	1,2	0,6
	C2	31	18,6	10,6	5,5	3,2	1,7	1,2	0,6

The results, shown in Table 1, clearly reveal that the proposed optimisation methods highly improves performance of the last mile freight delivery system.

The most significant decrease, in commercial vehicles travel times, is shown in the afternoon period. Average travel time decreased from 37 to 20,7 minutes (44%), when the first approximation methods is applied, and to 18,6 minutes (50%) when the second approximation is applied; while the maximum travel time decreased from 80 to 31 minutes (61%) in both cases.

Better performance of the system is evident also from the travel distance point of view. Average distances decreased from 9,5 km to 6 km (36%), when the first approximation is applied and to 5,5 km (42%) in case of the second approximation method. In this case, maximum travel distance of 17 km is reported in the early morning period and it decreased to 10,6 (37%) in case of both methods.

Because of decreased distances, performance improvement can be observed also from the environmental impact point of view. The amount of CO_2 emissions for average distance trip decreased from 2,9 to 1,8 kg in case of first approximation method and to 1,7 kg in the case of second approximation method is applied. For the maximum distance trip, decrease from 5,1 kg to 3,2 kg is reported. The same results can be reported for fuel consumption. Average fuel consumption is decreased from 1,1itre to 0,7 litres/trip in the use of first approximation and 0,6 litres/trip in the case of second approximation method. For the maximum trip length, the fuel consumption decreased from 1,9 to 1,2 litres of diesel per trip in both cases.

4 Conclusions

The model developed in this article takes into consideration dynamically changing demand for urban freight deliveries and provides solution for defining optimal number, capacity and location of loading bays. Assignment of deliveries to loading bay is finnaly perfomed with the use of the vehicle routing algorithm.

The functioning of the model has been tested on the case of historical city centre of Lucca in Italy. Results clearly show that the proposed solution outerperform existing solution with: shorter delivery times and distances and considerable energy and CO2 savings.

The proposed last mile freight delivery system could be applied in any city. The success level of implementation depends highly upon booking and management information system and enforcement framework set by the city authorities.

References

[1] D. Huggins, *Panorama of transport*. 2009.
[2] European Commission, “Reducing CO2 emissions from passenger cars.” [Online]. Available: https://ec.europa.eu/clima/policies/transport/vehicles/cars_en.
[3] A. Nuzzolo, A. Comi, A. Ibeas, and J. L. Moura, “Urban freight transport and city logistics policies: Indications from Rome, Barcelona, and Santander,” *Int. J. Sustain. Transp.*, vol. 10, no. 6, pp. 552–566, 2016.
[4] E. Morganti, L. Dablanc, and F. Fortin, “Final deliveries for online shopping: The deployment of pickup point networks in urban and suburban areas,” *Res. Transp. Bus. Manag.*, vol. 11, 2014.
[5] J. Olsson and J. Woxenius, “Localisation of freight consolidation centres serving small road hauliers in a wider urban area: barriers for more efficient freight deliveries in Gothenburg,” *J. Transp. Geogr.*, vol. 34, pp. 25–33, Jan. 2014.
[6] S. Tadić, S. Zečević, and M. Krstić, “CITY LOGISTICS – STATUS AND TRENDS,” *Int. J. Traffic Transp. Eng.*, vol. 5, no. 3, pp. 319–343, 2015.
[7] MDS Transmodal Limited, “Study on Urban Freight Transport,” *DG MOVE*, 2012.
[8] S. Iwan, “Adaptative Approach to Implementing Good Practices to Support Environmentally Friendly Urban Freight Transport Management,” *Procedia - Soc. Behav. Sci.*, vol. 151, pp. 70–86, Oct. 2014.
[9] A. Domínguez, J. Holguín-Veras, Á. Ibeas, and L. dell’Olio, “Receivers’ Response to New Urban Freight Policies,” *Procedia - Soc. Behav. Sci.*, vol. 54, pp. 886–896, Oct. 2012.
[10] R. Bozzo, A. Conca, and F. Marangon, “Decision Support System for City Logistics: Literature Review, and Guidelines for an Ex-ante Model,” *Transp. Res. Procedia*, vol. 3, pp. 518–527, 2014.
[11] M. Tozzi, M. V. Corazza, and A. Musso, “Urban goods movements in a sensitive context:

The case of Parma," *Res. Transp. Bus. Manag.*, vol. 11, pp. 134–141, 2014.

[12] M. Roca-Riu and M. Estrada, "An Evaluation of Urban Consolidation Centers Through Logistics Systems Analysis in Circumstances Where Companies have Equal Market Shares," *Procedia - Soc. Behav. Sci.*, vol. 39, pp. 796–806, 2012.

[13] E. Taniguchi, R. G. Thompson, and T. Yamada, "Recent Trends and Innovations in Modelling City Logistics," *Procedia - Soc. Behav. Sci.*, vol. 125, pp. 4–14, 2014.

[14] W. Feng and M. A. Figliozzi, "Conventional vs Electric Commercial Vehicle Fleets: A Case Study of Economic and Technological Factors Affecting the Competitiveness of Electric Commercial Vehicles in the USA," *Procedia - Soc. Behav. Sci.*, vol. 39, pp. 702–711, 2012.

[15] Josh Sanburn, "Deliver a fix for traffic jams, 10 big ideas in transportation," *Time*, vol. March, no. 13, p. 40, 2013.

[16] J. Maes and T. Vanelslander, "The Use of Bicycle Messengers in the Logistics Chain, Concepts Further Revised," *Procedia - Soc. Behav. Sci.*, vol. 39, pp. 409–423, 2012.

[17] T. Cherrett, J. Allen, F. McLeod, S. Maynard, A. Hickford, and M. Browne, "Understanding urban freight activity – key issues for freight planning," *J. Transp. Geogr.*, vol. 24, pp. 22–32, 2012.

[18] A. R. Alho and J. de Abreu e Silva, "Analyzing the relation between land-use/urban freight operations and the need for dedicated infrastructure/enforcement — Application to the city of Lisbon," *Res. Transp. Bus. Manag.*, vol. 11, pp. 85–97, Jul. 2014.

[19] M.-S. Yang, "A survey of fuzzy clustering," *Math. Comput. Model.*, vol. 18, no. 11, pp. 1–16, 1993.

[20] T. J. Ross, *Fuzzy logic with engineering applications*. 2010.

[21] J. C. Bezdek, *Pattern Recognition with Fuzzy Objective Function Algorithms*. Springer Nature, 1981.

[22] F. K. Frank Hoppner, "Clustering with Size Constraints," in *Computational Intelligence Paradigms*, Studies in., C. A. Lakhami C Jain, Mika Sato-Ilic, Maria Virvou, George A Tsihrintzis, Valentina Emilia Balas, Ed. Berlin: Springer, 2008.

[23] G. Mellios, S. Hausberger, M. Keller, C. Samaras, L. Ntziachristos, S. Hausberger, C. Samaras, G. Mellios, and L. Nziachristos, *Parameterisation of fuel consumption and CO2 emissions of passenger cars and light commercial vehicles for modelling purposes*. 2011.

10TH INTERNATIONAL CONFERENCE ON SUSTAINABLE ENERGY AND ENVIRONMENTAL PROTECTION (JUNE 27TH – 30TH, 2017, BLED, SLOVENIA), ENERGY EFFICIENCY
J. Krope, A.Ghani Olabi, D. Goričanec & S. Božičnik

Energy Recovery Optimization of an Ammonia-Water Power Cooling Cycle Using Exergy-Pinch Method

JOUAN RASHIDI, CHANGKYOO YOO, POUYA IFAEI & JEONG TAI KIM

Abstract This study combines Pinch and Exergy approach to analyse a new combined power and cooling cogeneration with ejector absorption refrigeration cycle. The cycle, Kalina power-cooling with ejector (KPCE), combines Kalina cycle and ejector absorption refrigeration cycle with ammonia-water mixture as the working fluid to produce power and refrigeration outputs simultaneously. In this study inefficiencies and losses are identified through exergy and pinch analyses. The total exergy loss for the equipment is quantified to find the potential of equipment improvement. Additional losses of energy due to the inefficient heat recovery design of the system are then identified by cross pinch heat in the process. Evaporator, condenser, and the first flash tank preheater devoted the highest potential of improvement from exergy analysis and four preheaters showed inefficient design of the heat recovery through pinch analysis. After redesigning, the optimized KPCE showed 8% and 11% increase in power-cooling efficiency and exergetic efficiency, respectively.

Keywords: • Ejector • Energy recovery • Exergy • Kalina cycle • Pinch•

CORRESPONDENCE ADDRESS: Jouan Rashidi, Ph.D. student, Kyung Hee University, Department of environmental science and engineering, Suwon-si, Gyeongi-do, South Korea, e-mail: jouanra@khu.ac.kr. Changkyoo Yoo, Ph.D., Professor, Kyung Hee University, Department of environmental science and engineering, Suwon-si, Gyeongi-do, South Korea, e-mail: ckyoo@khu.ac.kr. Pouya Ifaei, Ph.D. student, Kyung Hee University, Department of environmental science and engineering, Suwon-si, Gyeongi-do, South Korea, e-mail: pooya_if@hotmail.com. Jeong Tai Kim, Ph.D., Professor, Kyung Hee University, Department of agricultural engineering, Suwon-si, Gyeongi-do, South Korea, e-mail: jtkim@khu.ac.kr.

https://doi.org/10.18690/978-961-286-050-9.38 ISBN 978-961-286-050-9

Available at: http://press.um.si.

1 Introduction

The low quality and free energy source such as industrial waste heat can be recovered and used in power as well as cooling production systems. Several researchers have studied the power production performance using low grade heat sources with concentrating on unconventional working fluids such as ammonia-water mixture in Rankine, Kalina or other cycles [1, 2]. Ammonia-water evaporates and condenses as a non-azeotropic mixture, over a range of temperature; therefore, it is enable to achieve a better temperature match between the working substance and the heat sources.

Kalina cycle (KC), introduced by Alexander Kalina, is a fairly new thermodynamic power cycle using ammonia-water mixture with potential to accomplish efficient energy conversion of the low-grade heat sources; Low-temperature geothermal energy [3], solar energy [4], and industrial waste heat [5].

Utilizing and recovering of low-grade heat for cooling purpose have been performed by various thermodynamic cycles, such as absorption, adsorption, desiccant and ejection cycles [6].

Power and cooling cogeneration systems utilizing low grade heat sources have been studied by various researchers. Rashidi et al., have introduced a high efficient power-cooling cycle integrating Kalina and absorption refrigeration cycles to produce both outputs simultaneously [7]. They reported a power-cooling efficiency of 18.8%. With the same propose the performance of a combined Rankine cycle with ejector has been investigated [8]. Dai et al., proposed a system combined the Rankine cycle and the ejector-refrigeration cycle by adding a turbine between the generator and the ejector [9]. The performance of different working fluids in a combined organic Rankine cycle and ejector refrigeration cycle has been studied [10]. Li et al. proposed a Kalina cycle where the ejector has been used to substitute for the throttle valve and the absorber [11]. The ejector could increase the pressure difference of working fluid; therefore, the cycle could obtain higher thermal efficiency.

Pinch Analysis (PA) and Exergy Analysis (EA), are two powerful analytical methods to identify and select concrete technical solutions for improving efficiencies and providing optimum manufacturing solutions [12]. Pinch analysis with the idea of setting targets prior to design were first introduced and developed in the late 1970s. It has reported significant changes in energy saving and several applications in chemical process industries [13]. Researchers have done studies on using PA in various power plants to simulate and modify the existing sites [14]. EA can obtain a deeper insight with regard to process efficiency and potential to improve energy utilization [15]. It has been applied since 1975 toward the design, modelling, simulation, and performance evaluation of systems [16-18]. Exergy can be a key parameter toward improving engineering systems by determining true efficiencies through consideration of the surroundings [19].

According to literature studies on performance of the combined Kalina and ejector cycle as a power-cooling cycle is rare. In this paper, we introduce the Kalina power-cooling cycle with ejector. The performance of the system is analysed using exergy analysis to find the total avoidable and unavoidable exergy losses. The equipment is quantified according to exergy losses to find the potential of equipment improvement. Additional losses of energy due to the inefficient heat recovery design of the system are identified through pinch analysis. According to losses which are identified by EA and PA the process is redesigned to improve the performance of equipment and eliminate the cross heat transfer.

2 Method and materials

2.1 System Configuration

Figure 1 shows a schematic of the proposed system, Kalina power-cooling cycle with ejector, KPCE. The cycle is a combination of KC and ejector absorption refrigeration cycle to produce power and cooling simultaneously. After the condenser the working fluid (stream 17) enters to the ejector to decrease the pressure drop inefficiencies and increase the cooling subsystem performance. Two inputs are considered to pass the ejector; primary flow which is a portion of condensed working fluid, and secondary flow which is a portion of evaporated working fluid in cooling subsystem. The output of ejector at state 18 generates cooling through the evaporator. Following cooling generation, the working fluid (state 31) is divided in two parts to be recycled in the system; one enters the ejector as the secondary flow (state 31) and the other one is absorbed by the absorber (state 33). The primary concentration (X_{ABS}) within an intermediate range (47%) at state 1 leaves the absorber and is separated through the flash tank to the highest (X_{TUR}) and lowest (X_{LOW}) concentration streams (step 4→5, 15). The solution with a concentration of X_{TUR} is divided into two portions to produce power and cooling through turbine and evaporator, respectively. Cycling the working fluid heat recovery happens in two heat exchangers (FTP1 and FTP2) before separation in the flash tank and in another heat exchanger (PH) after the before condensation.

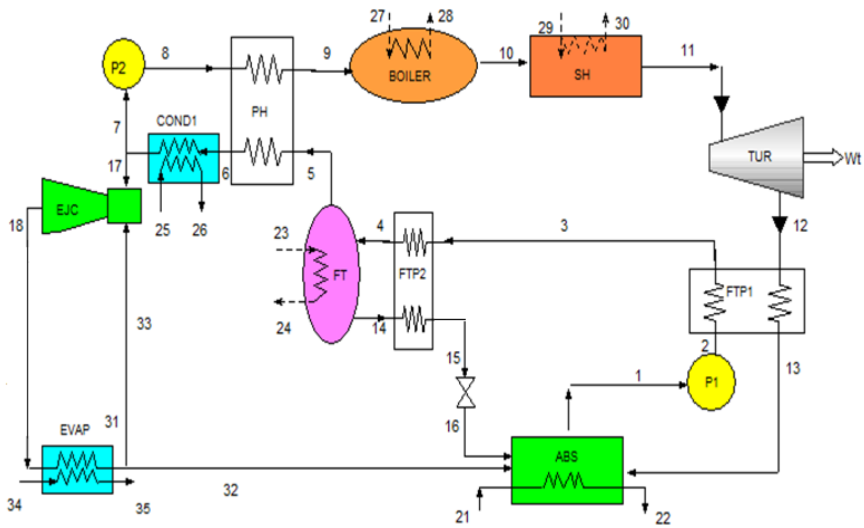

+

Figure 1. Schematic representation of Kalina power-cooling cycle with ejector (KPCE)

2.2 Exergy Analysis

The exergy of a system is the maximum work that can be performed by a system considering a specified reference environment as a dead state. The reference environment is assumed to be infinite, in equilibrium, and enclosed to all other systems [20]. Physical exergy is the maximum theoretical useful work that can be performed when the system is brought into physical equilibrium with the environment and chemical exergy is the separation of the chemical composition of a system from its chemical equilibrium [21]. Applying the first and second laws of thermodynamics, the following exergy balance is obtained:

$$\dot{E}x_Q + \sum_i \dot{m}_i ex_i = \sum_e \dot{m}_e ex_e + \dot{E}x_W + \dot{E}x_D \tag{1}$$

where subscripts e and i represent the inlet and outlet specific exergy of the control volume, respectively. $\dot{E}x_D$, $\dot{E}x_Q$, and $\dot{E}x_W$ are related to exergy destruction, exergy of heat transfer, and exergy of work which cross the boundary, respectively. $\dot{E}x_Q$ and $\dot{E}x_W$ are obtained from equations. (2) and (3):

$$\dot{E}x_Q = \left(1 - \frac{T_0}{T}\right) Q_i \tag{2}$$

$$\dot{E}x_w = \dot{W} \tag{3}$$

The term *Ex* is defined as follows:

$$\dot{E}x = \dot{E}x_{ph} + \dot{E}x_{ch} \tag{4}$$

$$\dot{E}x_{ph} = \dot{m}\cdot\left(h-h_0\right)-T_0\left(s-s_0\right) \tag{5}$$

where, $\dot{E}x_{ph}$ is the physical exergy, $\dot{m}$ is the mass flow rate (kg/s), h is the specific enthalpy, s is the specific entropy, T is the absolute temperature (K), and ($_0$) refers to the ambient state [21].

Since the concentration of NH3-H2O varies through the cycle, chemical exergy of working fluid also vary. It can be obtained as follows:

$$\dot{E}x_{ch} = x.\frac{ex_{NH_3}}{M_{NH_3}} + \left(1-x\right)\frac{ex_{H_2O}}{M_{H_2O}} \tag{6}$$

where ex_{NH3}, ex_{H2O}, M_{NH3}, and M_{H2O} are the standard molar specific chemical exergies and molecular mass of ammonia and water, respectively [22]. The exergy destruction and exergy efficiency of each component of the cycle can be obtained using equations (7) and (8), respectively[23].

$$\dot{E}x_{D,k} = F_k - P_k \tag{7}$$

$$\eta_{ex} = P_k / F_k \tag{8}$$

where *F*, *P*, and *K* refer to the fuel, products, and components. The overall exergetic efficiency and exergy loss of the cycle can be calculated as follows:

$$\eta_{ex,total} = E\dot{x}_w / E\dot{x}_Q \tag{9}$$

$$E\dot{x}_{loss} = E\dot{x}_Q - E\dot{x}_w \tag{10}$$

2.3 Pinch Analysis

PA has become a general methodology for the targeting and design of thermal and chemical processes, and associated utilities. When considering the energy efficiency of a process, pinch-based approaches target the identification of the possible energy recovery by heat exchange, and define the Minimum Energy Requirement (MER) of the process. The Composite Curves (CC) and the Grand Composite Curve (GCC) are two basic tools in PA, and they are constructed using temperature versus enthalpy axes[12]. The MER targeting procedure with CC is shown in Figure 2. The energy targeting in PA set by the CC and GCC are only in terms of heat loads. However, to deal with systems involving heat and power, the concepts of both the CC and the GCC should be extended.

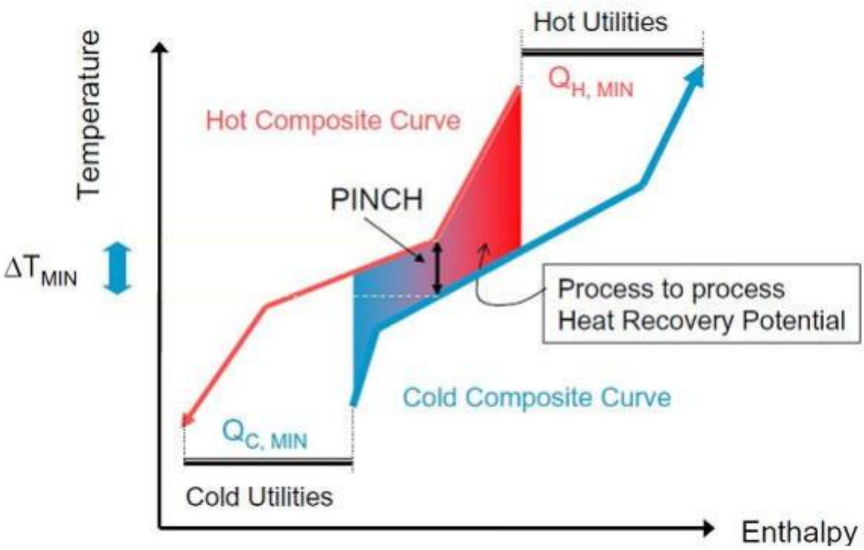

Figure 2. MER targeting procedure with cold and hot CC[12]

3 Result and discussion

Using the thermodynamic properties and definitions for fuel, product, and losses presented in equations (1)-(10), exergy analysis was performed to calculate the exergy destruction, exergetic efficiency, and total exergy loss of KPCE components. The input conditions for are shown in Table 1, including the ammonia mass fractions, mass flow rates, pressure and temperature levels, and mass ratios.

Table 1. Reference input condition of KPCE system

Parameter	Unit	Value
Turbine pressure (P_{TUR})	kPa	1500
Intermediate pressure (P_{FT})	kPa	470
Absorber pressure (P_{ABS})	kPa	80
Evaporator pressure (P_{EVAP})	kPa	200
Desorber pressure (P_{DES})	kPa	7.445
Turbine ammonia mass fraction (X_{TUR})	%	72
Absorber mass flow rate	Kg/s	4
Turbine temperature (T_{TUR})	ºC	280
Absorber temperature (T_{ABS})	ºC	20

The exergy destruction of components is demonstrated in figure 3. As can be seen FTP2, condenser, and evaporator have the major exergy destruction quantities among all components. The cycle showed the total exergy efficiency and the total exergy destruction equal to 20% and 972kw, respectively.

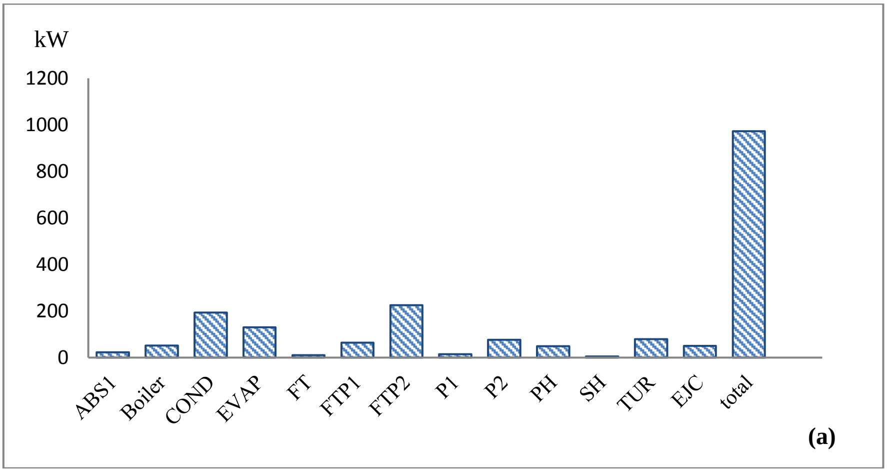

Figure 3. Exergy destruction of KPCE components

Figure 4 is a diagram of the system with the supply and target temperatures in degree of Celsius. C and H refer to cold and hot utilities which are cold water and steam. The figure also presents the streams with their numbers that have been described in Table 2.

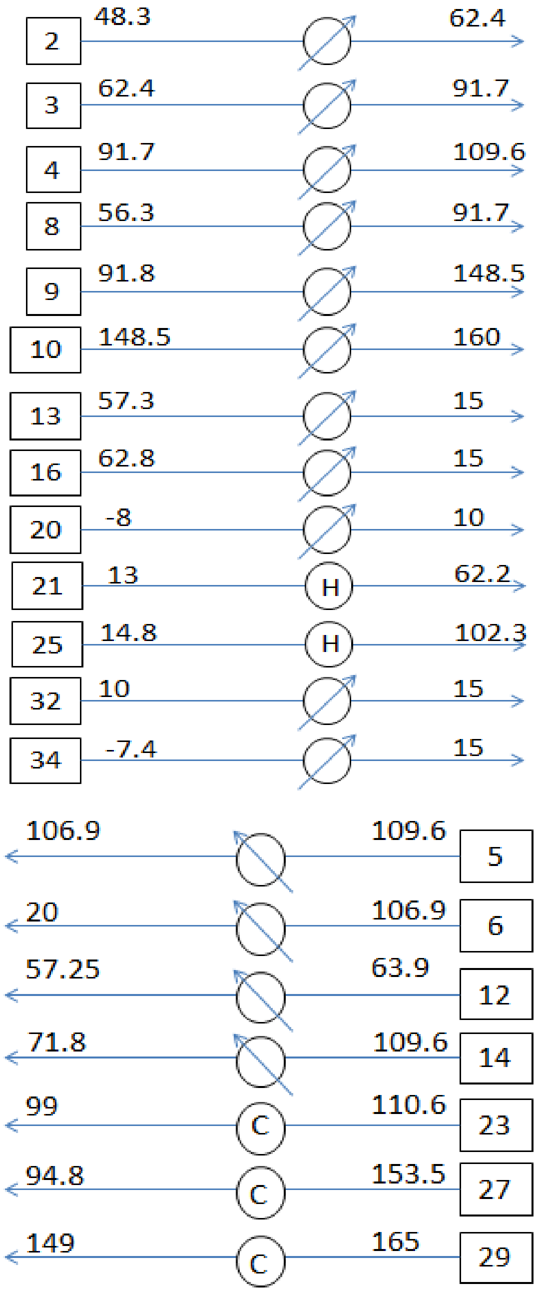

Figure 4. Diagram of the heat exchanger network of KPCE system

Table 2. Stream data of the heat exchanger network in the KPCE system

stream	type	ΔT	ΔH	C_p (kw/ºC)
2	cold	14.1	235.03	16.66879
3	cold	29.3	468.6	15.99317
4	cold	17.9	1146.5	64.05028
5	hot	-2.7	-101	37.40741
6	hot	-86.9	-1498	17.2382
8	cold	35.4	609.7	17.22316
9	cold	56.7	998.3	17.6067
10	cold	11.5	31	2.695652
12	hot	-6.67	-215	32.23388
13	hot	-42.3	-1225.1	28.96217
14	hot	-37.79	-162.1	4.289495
16	hot	-47.8	-84.6	1.769874
20	cold	18	388	21.55556
21	cold	49.2	885.3	17.9939
23	hot	-11.6	-2384	205.5172
25	cold	87.45	2618.6	29.9442
27	hot	-58.63	-2386	40.69589
29	hot	-15.7	-31	1.974522
32	hot	-3	-607.6	202.5333
34	hot	-22.37	-637	28.47564

Table 2 summarizes the target temperature difference (ΔT) of heat exchanger network streams as well as their corresponding enthalpy difference (ΔH). In the last column C_p is the ratio of ΔH to ΔT. to continue the pinch analysis the minimum temperature difference ΔT_{min} is set to 10ºC. After finding the pinch point and redesigning the heat exchanger network the required hot utility decreased from 4201 kw to 3300kw also the required cold utility dropped from 7594kw to 4910kw. The system before modification had several pinch problems where cold stream crossed hot stream in 4 points. Obtaining these results the modified KPCE system has been analysed from exergy point again. The new system demonstrates an exergy destruction decrease in all components especially for evaporator, condenser, and FTP2.

Figure 5a shows the comparison between exergy destruction of KPCE system before and after modification. As can be seen total exergy destruction has been dropped around 10%. Figure 5b compares the power-cooling and exergetic efficiencies of KPCE before and after optimization. It can be seen, power-cooling efficiency has increased by 8% and exergetic efficiency encounters an increment of 11%.

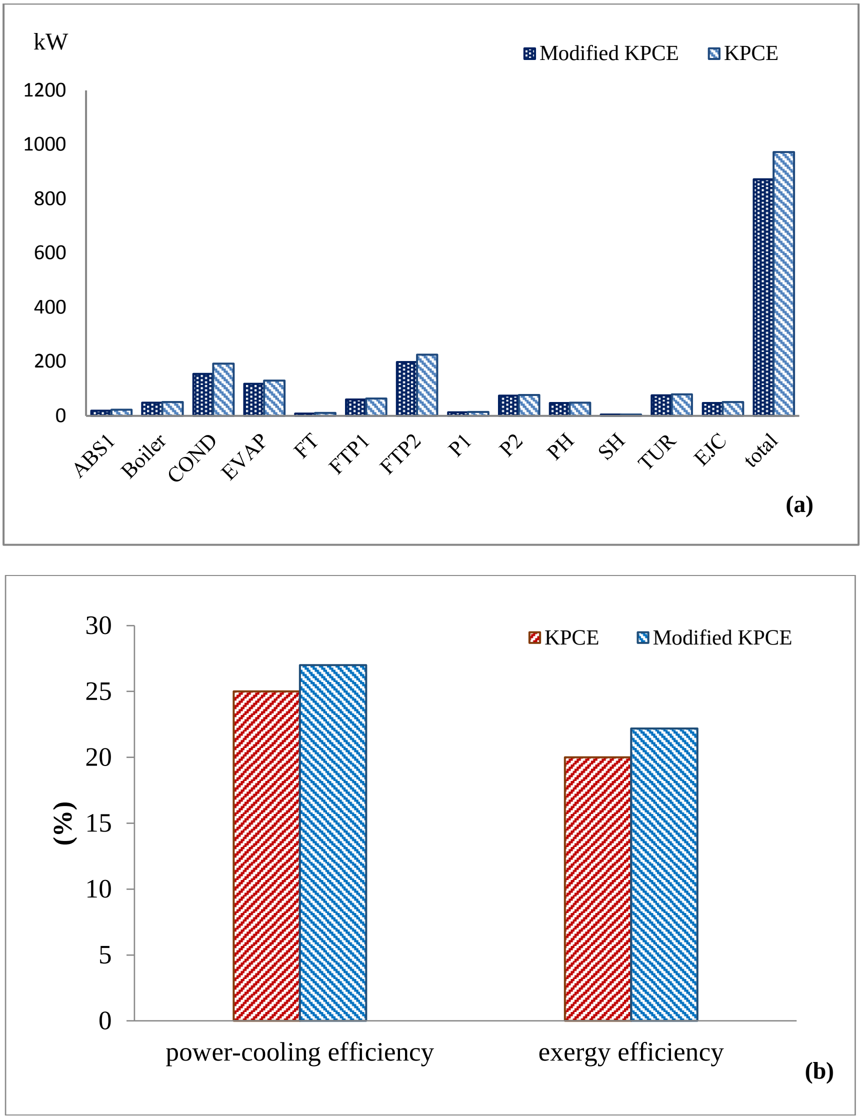

Figure 5. comparison between (a) component exergy destruction and (b) power cooling and exergy efficiencies of KPCE and modified KPCE system

4 Conclusion

Pinch and Exergy analyses are performed in this study to optimize the performance of a power and cogeneration system which combines Kalina cycle with and ejector absorption refrigeration cycle called KPCE, Kalina power-cooling cycle with ejector. The system uses ammonia-water mixture as the working fluid to produce power and refrigeration outputs simultaneously. Using both exergy and pinch analysis inefficiencies of components as well as heat exchanger network are identified. Exergy analysis identified three components including evaporator, condenser, and FTP1 corresponded with the highest exergy destruction among all components. Using pinch method, cross heat pinch points were detected and the heat exchanger network was redesigned in order to decrease losses through heat recovery in the cycle. By cycle modification and optimization, the optimized KPCE achieved 8% and 11% increase in power-cooling efficiency and exergetic efficiency, respectively.

Acknowledgements

This work was supported by a National Research Foundation of Korea (NRF) grant funded by the Korean Government (MSIP) (No.2015R1A2A2 A11001120).

References

[1] A. Nemati, H. Nami, F. Ranjbar, M. Yari, A comparative thermodynamic analysis of ORC and Kalina cycles for waste heat recovery: A case study for CGAM cogeneration system, Case Studies in Thermal Engineering, 9 (2017) 1-13.
[2] T. Eller, F. Heberle, D. Brüggemann, Second law analysis of novel working fluid pairs for waste heat recovery by the Kalina cycle, Energy, 119 (2017) 188-198.
[3] H. Saffari, S. Sadeghi, M. Khoshzat, P. Mehregan, Thermodynamic analysis and optimization of a geothermal Kalina cycle system using Artificial Bee Colony algorithm, Renewable Energy, 89 (2016) 154-167.
[4] F. Sun, Y. Ikegami, H. Arima, W. Zhou, Performance Analysis of the Low Temperature Solar-Boosted Power Generation System—Part II: Thermodynamic Characteristics of the Kalina Solar System, Journal of Solar Energy Engineering, 135 (2013) 011007.
[5] V. Zare, S. Mahmoudi, M. Yari, On the exergoeconomic assessment of employing Kalina cycle for GT-MHR waste heat utilization, Energy Conversion and Management, 90 (2015) 364-374.
[6] E. Aridhi, M. Abbes, A. Mami, Solutions based on renewable energy and technology to improve the performance of refrigeration systems, Journal of Renewable and Sustainable Energy, 8 (2016) 065906.
[7] J. Rashidi, P. Ifaei, I. JanghorbanEsfahani, A. Ataei, C.K. Yoo, Thermodynamic and economic studies of two new high efficient power-cooling cogeneration systems based on Kalina and absorption refrigeration cycles, Energy Conversion and Management, 127 (2016) 170-186.
[8] K. Zhang, X. Chen, C.N. Markides, Y. Yang, S. Shen, Evaluation of ejector performance for an organic Rankine cycle combined power and cooling system, Applied Energy, 184 (2016) 404-412.
[9] Y. Dai, J. Wang, L. Gao, Exergy analysis, parametric analysis and optimization for a novel combined power and ejector refrigeration cycle, applied thermal engineering, 29 (2009) 1983-1990.
[10] A. Habibzadeh, M. Rashidi, N. Galanis, Analysis of a combined power and ejector-refrigeration cycle using low temperature heat, Energy Conversion and Management, 65 (2013) 381-391.
[11] X.G. Li, Q.L. Zhang, X.J. Li, A Kalina cycle with ejector, Energy, 54 (2013) 212-219.

[12] A. Ataei, C. Yoo, Combined pinch and exergy analysis for energy efficiency optimization in a steam power plant, International Journal of Physical Sciences, 5 (2010) 1110-1123.
[13] R. Smith, Chemical process: design and integration, John Wiley & Sons, 2005.
[14] B. Linnhoff, F.J. Alanis, Integration of a new process into an existing site: a case study in the application of pinch technology, Journal of Engineering for gas turbines and power, 113 (1991) 159-169.
[15] R. Saidur, J. Ahamed, H. Masjuki, Energy, exergy and economic analysis of industrial boilers, Energy Policy, 38 (2010) 2188-2197.
[16] S.M. Sanaei, T. Furubayashi, T. Nakata, Assessment of energy utilization in Iran's industrial sector using energy and exergy analysis method, Applied Thermal Engineering, 36 (2012) 472-481.
[17] F. Zarifi, T. Mahlia, F. Motasemi, M. Shekarchian, M. Moghavvemi, Current and future energy and exergy efficiencies in the Iran's transportation sector, Energy Conversion and Management, 74 (2013) 24-34.
[18] Z. Rashidi, A. Karbassi, A. Ataei, P. Ifaei, R. Samiee-Zafarghandi, M. Mohammadizadeh, Power plant design using gas produced by waste leachate treatment plant, International Journal of Environmental Research, 6 (2012) 875-882.
[19] I. Dincer, M. Hussain, I. Al-Zaharnah, Energy and exergy utilization in transportation sector of Saudi Arabia, Applied Thermal Engineering, 24 (2004) 525-538.
[20] Ibrahim Dincer, M.A. Rosen, Exergy: energy, environment and sustainable development, Elsevier, 2007.
[21] P. Ahmadi, I. Dincer, Thermodynamic and exergoenvironmental analysis and multi-objective optimization of a gas turbine power plant, Applied Thermal Engineering, 31 (2011) 2529-2540.
[22] O.K. Singh, S.C. Kaushik, Reducing CO 2 emission and improving exergy based performance of natural gas fired combined cycle power plants by coupling Kalina cycle, Energy, 55 (2013) 1002-1013.
[23] P. Ifaei, J. Rashidi, C. Yoo, Thermoeconomic and environmental analyses of a low water consumption combined steam power plant and refrigeration chillers–Part 1: Energy and economic modelling and analysis, Energy Conversion and Management, 123 (2016) 610-624.

10TH INTERNATIONAL CONFERENCE ON SUSTAINABLE ENERGY AND ENVIRONMENTAL PROTECTION (JUNE 27TH – 30TH, 2017, BLED, SLOVENIA), ENERGY EFFICIENCY
J. Krope, A.Ghani Olabi, D. Goričanec & S. Božičnik

Ship Power Plant Environmental Impact and Costs Rationalization

ŽIGA SCHÄFFER, STOJAN PETELIN & IVAN BAJSIĆ

Abstract The world economy and environment awareness greatly effect on ship industry. Many of developed maritime countries already together with International Maritime Organization (IMO) adopted strict emission legislation. In one decade stronger limitations will take power on global maritime level where sustainable energy use and low exhaust gas print will be required. This study will be focused on harmonization of followed subject topic concerning: ship energetic sustainability, low emission print, introduction of low sulfur marine oil as only propellant and reincarnation of direct current (DC) power supply following the latest technology trends where DC systems are the only perspective.

Keywords: • waste heat • cogeneration • recuperation • low sulphur oil • DC systems •

CORRESPONDENCE ADDRESS: Žiga Schäffer, University of Ljubljana, Faculty of Maritime Studies and Transport Portorož, Pot pomorščakov 4, 6320 Portorož – Portorose, Slovenia, e-mail: dr.zigameister@gmail.com. Stojan Petelin, Ph.D., Full Professor, University of Ljubljana, Faculty of Maritime Studies and Transport Portorož, Pot pomorščakov 4, 6320 Portorož – Portorose, Slovenia, e-mail: stojan.petelin@fpp.uni-lj.si. Ivan Bajsić, Ph.D., Associate Professor, University of Ljubljana, Faculty of Engine Engineering Ljubljana,

https://doi.org/10.18690/978-961-286-050-9.39 ISBN 978-961-286-050-9

Available at: http://press.um.si.

1 Introduction

In today's society is high demand in goods transport which is still growing in world wide economy. Ship transport, where round 84% of total tonnage represents bulk, container carriers and tankers [6], is still the cheapest and most energy effective transport when comparing by energy consumption parameter according to t/km, bat very far from clean and sustainable if comparing by sulfur oxides (SO_x), nitrogen oxides (NO_x) and particle matters (PM) where comparing means of transport are electrified rail or on road transport with build in euro 6 internal combustion reciprocate diesel engines (ICD).

As main propellant heavy fuel oil (HFO), with 3.5% sulfur content, is still in use and propelling 98% ocean going vessels. [5] Some high developed countries already limited the use of HFO while sailing in their waters, global limitation is expected between years 2020-25 by IMO where HDO with 0.5% sulfur content will be only allowed. This limitation will offer us a chance to provide new standard for marine low sulfur oil (LSO) which is cleaner and caloric stronger. Implementation of modern technology from on road going vehicle engines and big stationary engines will be unavoidable in future to achieve together with new fuels higher standards by combustion and exhaust gasses emissions on one side and on another reducing heat emission together with heat reuse in cogeneration and recuperation. There is growing eligibility to implement again DC current system on ships due to the fact that most efficient electrical consumers today use DC power where also synchronization of DC power sources is easier and quicker in comparison with alternative current (AC) system. Although maritime ICD are high effective (50%), there are legitimate expectations and ongoing goals to improve energy efficiency index for 30% till 2025 by reduction of exhaust gas and heat emissions together with fuel consumption.

2 Diesel Fuels

In year 1903 was lunched first vessel "*Vandal*" with ICD. Since then ICD slowly take a lead and today is integrated on majority of ocean going vessels. With some innovations made on ICD it was possible to use HFO first on 2-stroke main engines later 4-stroke and even on 4-stroke auxiliary engines (AE). Since that time nothing was drastically changed by political decisions on global level to implement higher standards for marine fuels causing improvements in combustion and reduction of heat and exhaust gas emissions to environment.

2.1 Classical Maritime Fuels

First actual maritime fuel on today's market is still HFO. HFO contain predominantly residues from vacuum distillation or visbreaking where major part represents asphaltenes (aromatic hydrocarbons). Without dilution such residual fuel is useless. Dilution must be done with cycle-oils to prevent coagulation of aromats. Such residual fuels are also problematic in concentration aspect where impurities like are heavy metals and sulfur are 3 times more concentrated as in crudes. [1]

2.2 Near future diesel fuels

Near future marine fuel will have to meet three more parameters where one is environmental, another two are technical to reduce emissions. The primary environmental problem is sulfur and other impurities. Some see solution for this problem in scrubber technology where sulphur is washed away with sea water from exhaust gases. This technology is again very energy wasteful on one side and on another side we produce sulfuric acid together with carbon acid where both are washed back to sea. The acidity of sea is each year higher so this may not be a long term solution. Technical limitations will be, to reach higher emission and efficiency standards, in rise of injection pressure and installing the catalytic NO_x & particulate filters. HFO with its impurities and high viscosity will not be suitable any more for new task, where general pressure (15-35 MPa) injection nozzle will have to withdraw to high pressure nozzles (150-200 MPa) on common rail system on one side and sulfur will also have to be eliminated from fuel while clogging the catalytic NO_x & particle filters and causing sulfur acid with condensing water vapour in high efficiency condensing boiler if implemented (below 130 °C).

2.3 Fuel conclusion

There were several attempts to make some hybrids or to use another kind of fuel as HFO is, bat more or less without success. Vessels are huge energy consumer and need energy full source where renewable energy sources are far to meet demands, LPG is the most expensive fuel (safety), LNG is problematic for storing (cryogenic temperatures or high pressure, safety), only non-carbon source of energy is nuclear propulsion where the radiation safety is under big trial together with problematic issue of served out reactor storing. It is worthy to mention that Norwegians are designing short distances sea carriers where power will be stored in batteries.

Explosion safety will be also under big trial when using LPG or LNG (there are some trends to implement LNG on vessels as main propellant) on general cargo or passenger vessels. If this is specialised vessel for carrying gasses, where owners are reach and the proper maintenance is not question, where ports are out from cities, crew is well qualified and if something happens there are up to 30 well qualified people to be saved. It is hard to imagine what will happen if something goes wrong and LNG/LPG starts to leak on one cruiser with 4000 people on board at sea or in port… On cruisers there is also each cubic meter important and when placing the LNG tank, we will spend for the same amount of energy 2.3 times more space for storage in comparison to diesel fuel in practical meaning 3-4 times more. Also the weight can be problematic in connection with stability; LNG/LPG tanks are 1.5 times heavier than those for (H)DO. [4]

For cargo vessels the proper maintenance is general problem where ship owners are more or less short in money designated for proper maintenance and safety will be continuously on test. Also general personal from port stat control or from insurance companies are more or less not equal to deal with inspection of any kind design LNG/LPG propelled vessels. To inspect such a vessel special equipment, knowledge and familiarity is needed.

So, ultra-low sulfur marine diesel oil is seems to be only solution for now in blend where changing state of aggregate happens below 20°C to avoid needs for extensive heating where by HFO is unavoidable.

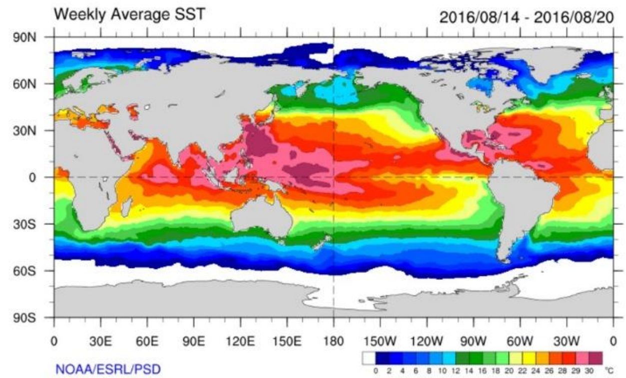

Figure 1, Summer Sea Temperatures [10]

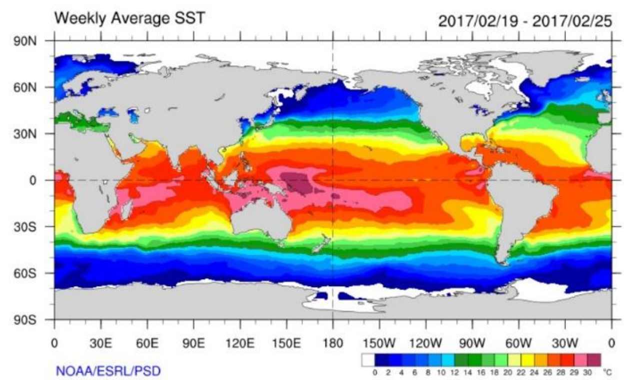

Figure 2, Winter Sea Temperatures [10]

Figure 3, Density on shipping routes [9]

When comparing figures no.: 1, 2 & 3 there we can see that there is no needed for extensive or even no need at all to heat LSO to keep it in liquid stat with normal transfer abilities. In this case the most valuable heat from exhaust gasses (300-400°C) can be instead for fuel heating used for indirect electrical power production & water making. The low temperature heat (95°C) from engine wetter cooling system can easily cover the heating needs for LSO if necessary.

Such a fuel can easily be prepared on land. If we would like to be low carbon society, then we can provide energy for preparing LSO from renewable sources of energy or nuclear power plants and there will be no need to consume the non-renewable sources, "waste" heat can be (re)used in further domestic or industrial objects from refineries. Separated sulfur can be later used in other production where needed. LSO contains also shorter CH-chains where carbon to hydrogen ratio is some lower else in HFO, what means few percent less CO_2 when burned.
The table 1 shows the comparison of energy density among different fissile fuel type. [11]

Table: 1 Energy density of fossil fuels

Fuel	Carbon content kg/kg	Energy density MJ/kg	t/t (CO_2)/fuel
Methanol	**0.3750**	**23.0**	**1.375**
Ethanol	**0.5217**	**29.7**	**1.913**
LNG*	**0.7500**	**43.0**	**2.750**
LPG	**0.8223**	**49.9**	**3.015**
HFO	**0.8493**	**43.0**	**3.114**
DO	**0.8744**	**44.8**	**3.206**

***** depends on source of exploitation

In table 2 comparisons are done among fuels counted in table 1 where final goal is the same amount of released heat. The least amount of CO_2 is produced when burning methanol bat also due to lower energy density twice amount has to be burned. Ethanol is better option just the question is where to obtain such amounts of alcohols. LPG and LNG are problematic for storing, so at the end again DO-LSO is the only solution.

Table: 2 Caloric comparison consumption table where LPG is base

Fuel	Energy density MJ/kg	kg/kg (CO_2)/fuel	kg (CO_2) produced to make 49.9 MJ	Cons.
CH_3OH	23.0	1.375	2.983	2.17
C_2H_7OH	29.7	1.913	3.266	1.68
LNG*	43.0	2.750	3.191	1.16
LPG	*49.9*	*3.015*	*3.015*	*1*
HFO	43.0	3.114	3.613	1.16
DO	44.8	3.206	3.579	1.11

* depends on source of exploitation

3 Heat

Heat is after metal second most important subject-meter on any vessel where HFO is in use and where main propulsion engine has to obtain stand-by temperature. In many working or operating conditions, we cannot obtain enough heat from main engine(s), so steam boiler has to be engaged to supply additional heat for engine system.

To fit technical, functional and operational needs the operation and stand-by temperatures are approximately the followed:

- main or auxiliary engines heating must obtain standby temperature (ca. 90°C),
- heavy fuel oil in liquid state (ca. 45°C),
- fuel and oil separators (ca. 100°C),
- heating settling tank (ca. 60°C)
- daily tank (ca. 95°C)
- before injection in fuel unit HFO is heated up to 145 °C,
- for heat-vacuum water maker (ca. 80°C),
- other technical and sanitary water etc.

From ME/AE we can obtain two qualities of heats divided in to temperature classes. First is high temperature water from engine cooling system (HT) reaching ca. 95°C and second is from exhaust system (EH) reaching 400 °C.

3.1 Current situation

To awaken ship from status of cold ship and to maintain ship in full operational condition, heat is produced in large steam boiler(s). If vessel is steaming enough fast the exhaust boiler (heat exchanger on exhaust system) can obtain enough heat from exhaust to reach the steam needs. In diagram 1 is presented general distribution of heat and steam flow.

Diagram: 1 Heat circulation from source to sink

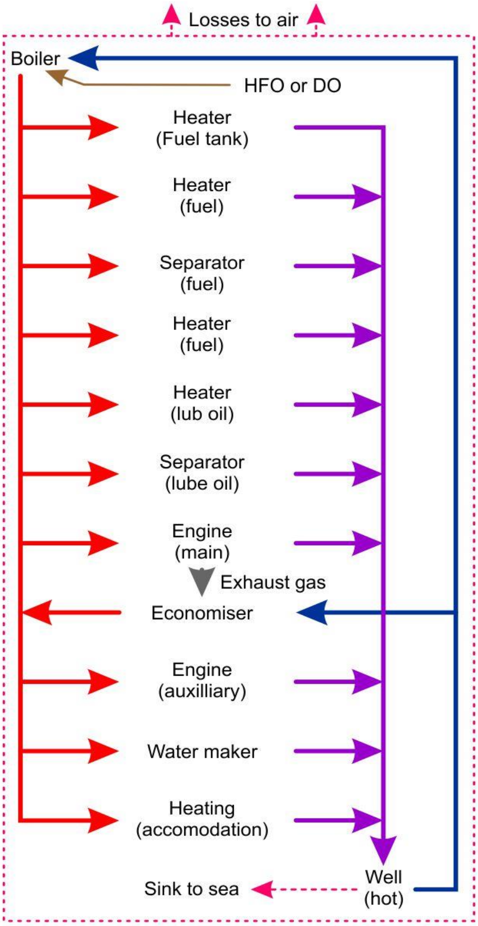

In many cases due to economic reasons vessels steams in economical speed where the support of steam boiler is still needed to maintain the vessel in full operational condition. The installed power of steam boilers can exceed MW! In the table 3 is presented one example from cargo vessel where MAN 6S70MC-C7-T1 engine is installed.

Table: 3 System heat needs table. [12]

	Consumed Energy $\dot{Q}(kW)$	HFO or lube oil ΔT (°C)
HFO storage tank	325	45 °C
HFO purifier	52	70 to 90
Lube Oil purifier	55	40 to 90
ME/AE module	196	up to 145
Accommodation heating	194	
Hot water	34.5	up to 60

As is evident from table 3, in this example the predominant heat is used for preparation and conditioning of the HFO. On passenger ship/cruiser (300m in length) while comfortably cruising between the destinations, with capacity of round 4.000 population units (PU) the lack of heat from main engines can easily happen and steam boiler has to be engaged. The minimum speed where main engines (MAN 12V46/60) diesel generators produce enough heat is 18 knots what means that 3 engines has to run on at least 75% load to supply enough heat to system that additional source of heat is not needed.

Diagram: 2, General heat balances for MAN engines 8-18V48/60.

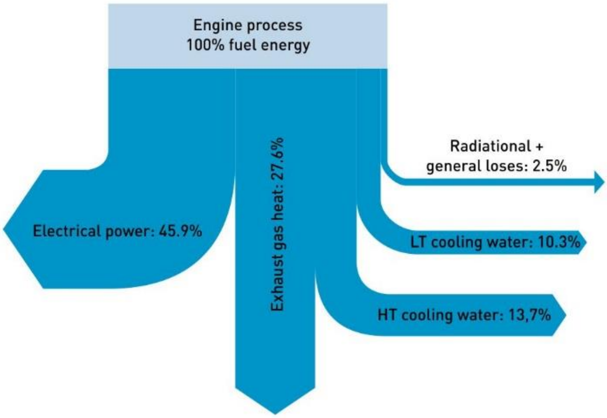

Each of MAN 12V46/60 has 14.4 MW, when loaded 75% there is theoretical round 10 MW heat released on each engine. To cover the heat needs, 30MW from three ICDs is minimum. In average 80% of cruising time the need of heat is not covered.

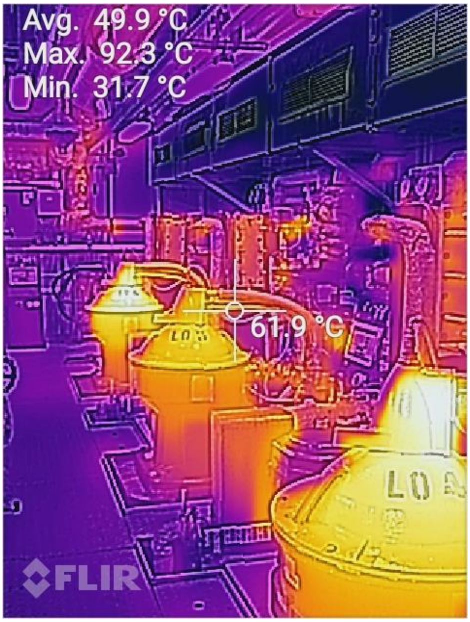

Figure 4, IR image of oil and fuel separators

The average temperature in separation room is 50 °C even there is intensive blowing with fresh air – heat losses are huge. Similar situation is round fuel heating station.

Image 5, IR image of daily and settling tanks

Behind the wall are two tanks. Primary is settling (60 °C) and another is daily tank (90 °C). Again huge amounts of heat are lost in to the space around the tanks.

Image 6, IR image of cylinder heads of MAN 12V46/60 with pick power 14.4 MW

3.2 Heat needs when LSO is the only fuel

When & if restrictions will become so rigorous that LSO with state of aggregate phase conversion (solid-liquid) between 15-20 °C will be the only allowed fuel for maritime vessels the need for heat will significantly drop. Beside where new materials are introduced we can also reduce stand-by heating temperatures on main and auxiliary engines from 90 to 70 °C. The heat from low pressure cooling system from ME will be enough to treat LSO and to maintain it at right temperatures for fuel transfer and separation (25-40°C). High quality temperature from exhaust can be used for electricity production, later for water making and then for other systems. The most important is that there is in use condensing economiser, where concentration of sulfur in exhaust gasses is so low that the production of sulfur acid is minor. Diagram 3 shows the situation where LSO is in use and how the heat can be transferred. Steam is only present in system for propelling the electrical power generation turbine; in other systems the water is present for heat transfer.

Diagram 3, of LSO heat cogeneration

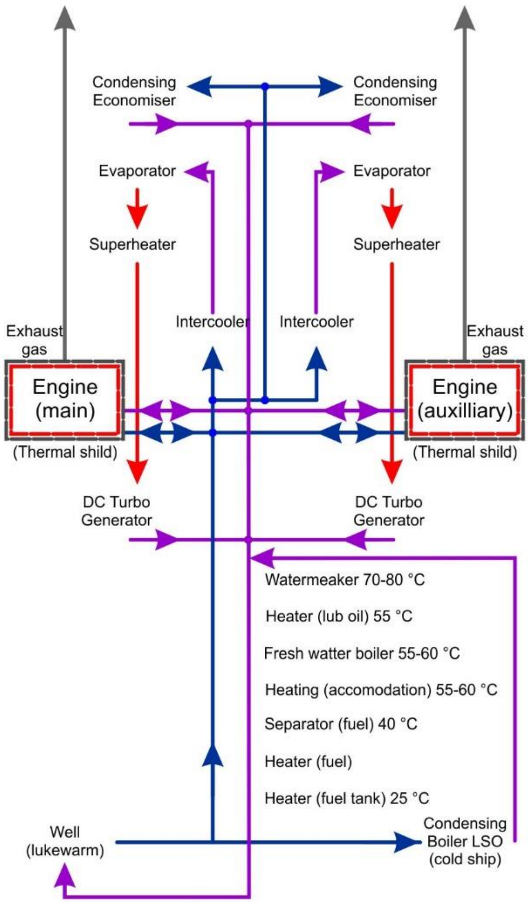

4 Electricity

On vessels we have bigger and bigger needs for electrical power which is running pumps, automation, navigation equipment, illumination, ventilation, accommodation equipment, galleys equipment, bow thrusters and systems maintaining the steady microclimate conditions for cargo if needed etc. The consumers are generally divided in to three categories where: low voltage (24V), medium voltage (110-230V) and high voltage systems are used (380-690V). If there is indirect propulsion in use such as “Azipod” drive, the voltage can rise 10kV and above. The supply is as usual AC 50/60Hz current transformed or converted on needed levels with classical cuprum transformer.

4.1 Production

The most common production of electricity on ships is from auxiliary engines, rear from shaft generators. On picture 7, 8 & 9 are presented three most common installations of power production on present vessels.

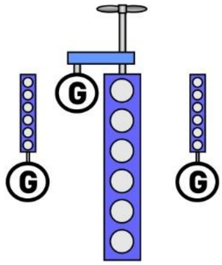

Image 7, most conventional power installation

Image 7 shows most common installation of main and auxiliary engines. Propulsion shaft is directly connected to the engine. AC shaft generator will be only engaged if the vessel is steaming full ahead to reach the working frequency.

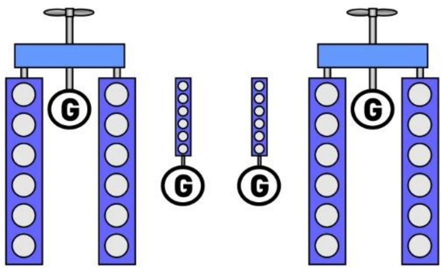

Image 8, installation with clutch and often with pitch propellers

Such installation on image 8 is typical for middle & short distance operating vessels, where is higher need in own manoeuvrability abilities. The AC shaft generators can be used only when sheep is steaming full ahead or engines are obtaining constant speed and the pitch propellers are engaged. It is impossible to keep working both AC shaft generators together on the same power bus due to unsteady condition while moving through the water/sea where maintaining synchronization is impossible.

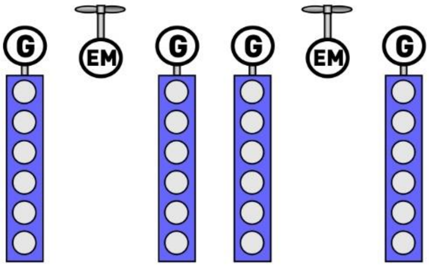

Picture 9, most conventional power installation

Installation on picture 9 is typical for vessels where space requirements are in front of economy or is requested perfect manoeuvrability. AC generators are obtaining constant speed due to frequency requirement.

So if AC electricity is produced from shaft generator the ship mast steam full ahead or if there is pitch propeller in use, the engines must run on designedted rounds per minute (RPMs) to maintain the frequency 50/60 Hz. Smaller percentage of ships use steam from exhaust gas boiler and produce the electricity from steam turbo generator. To fit the costs, ships are more or less running in economical speed what means that there is always need for auxiliary engines to operate and produce the necessary electrical power. If the vessel has two main propulsion shafts (with pitch propellers) – the synchronisation on AC system is impossible and when steaming in narrows or ports, there is always need for auxiliary engines to run and produce the electrical power.

4.2 Illumination

Illumination on vessel is very various there are mostly in use: neon tubes, compact fluorescent lights and in reflectors metal-halid or sodium bulbs and halogen lamps. In present time we find rarely classical incandescent bulbs. In illumination is future in light emitted diodes LED which are very versatile to serve as reflectors or corridor ceiling lights. The most important thing is proper cooling while LED diodes are sensitive to overheating. In table 4 is presented comparison among luminous bodies. [3] Table was updated with last LED values from Osram GmbH installed in tube T8. The values are interpolated to fit the table light output of round 1700 lumens.

Table 4, Comparison of luminous body

Lamp Type	Bulb	Tube	CFL	LED	LED (last)	Teor. limit
Power (W)	100	18	23	15	9	2.5
Operational Frequency (Hz)	AC/DC	AC/DC	50/60	DC	DC	/
Efficiency (%)	2,2	12	10	21	38	100
Efficiency (Lm/W)	17	94	74	113	205	683
Output (Lm)	1.700	1.692	1.702	1.700	1.700	1.700

4.3 E-Motors

Drive from electrical motors (EM) is very versatile and we use them for many purposes such are: ventilation, pumping, valve steering, compressing, lifting etc. On cargo ships the majority of consumption from EM falls on ventilation and fluid pumping, later illumination. Predominant share of electrical power can be consumed also from refrigeration compressors for maintaining constant temperature in cargo spaces where temperature sensitive goods are carried. This can be in ship holds, containers or semi-trailers. Most important fact is that in 90% + we will not need the full power of E-motor. The latest systems are capable to determine the actual need of E-drive power and savings can be significant. Due to that fact the variable speed drive (VSD) was introduced together with DC electro motor, where mentioned shows great potential by saving and some additional applicable properties over E-motor control like are: speed (it can hold constant speed even load is changing) , rotational force and start or working torque. [2] It is important to make accent on fact once again that DC electrical motors are capable to make heavy starts what is for AC electrical motors mission impossible.

Table 5, Potential energy savings by using VSD

Average percent speed reduction	Potential energy savings
10%	22%
20%	44%
30%	61%
40%	73%
50%	83%
60%	89%

4.4 Harmonization of electrical system

Harmonization of two or more DC power supply sources today is much easier and quicker as harmonization of two AC systems. The biggest problem in ship industry is if we have to steam in slow speed, then we cannot reach frequency 50/60Hz or if we have pitch propeller – engine has to run on nominal RPM (in most cases this speed is not economical) or two or more AC shaft generator where is impossible to maintain the constant speed on both shafts, so auxiliary engines has to run. By DC power supply the electronic can govern with extinction the voltage and current. The power output is only dependant to final RPM by DC power supply. So there is no need to use auxiliary engines (if we have two shaft generators) – even if we are approaching the port or sailing in waters with increased level of safe navigation. If anything happen auxiliary source of DC power is in les then 10 seconds in grid.

4.5 Why DC system

Now when the electronics is capable to meet high standards in power supply and on vessels we don't have a need for long distance power transport the answer is logic. Use of DC system on vessel, where more and more systems are working on DC current and where DC system can bring savings by generation of power and in consumption, is more & more logical. We can save a lot of cuprum where light energy efficient switchers replace huge transformers and the body of vessel can substitute one line. DC/DC converters are more efficient in cooperation with AC/DC converters where rectification is obligatory and where we lost 1 or 2 % of energy.

When there is no high power consumption the DC generator can work in lower rpm. For instance VW 2.0 TDI (2010) engine will consume 0.6l/h when running in idle speed, to obtain with no load 1.500 rpm the consumption will rise on 1,5l/h, and on 3.000 rpm already 3.6l/h just to maintain the speed! On the vessel with installed AC diesel generators, driven by MAN 12V46/60 and "Azipods" this can be seen on efficiency parameter where consumption by 75% of load is 198 kg/MWh and when reducing the load on 50% by same rpm it raise on 218 kg/MWh. So savings in combination with DC shaft generator can be significant.

5 Legislation

In short, maritime legislation is managing energetic systems and fuels in three main lows. IMO TIER exhausts standards where NO_x, SO_x and particle meters will have to be reduced, IMO fuel standards, where sulphur will have to be reduced until 2020, with possible extension to 2025 on level 0.5% or below worldwide and IMO energy efficiency standards where energy savings will have to be reduced for 30% by 2025 on new vessels.

6 Conclusion

A lot of effort will be needed to achieve the goal of 30% energy savings on ocean going vessels. The easiest problem seems to be savings by illumination where we can already today cut the consumption on half by installing LED in present illuminant housings. The quality of HDO or LSO is question of political will and how strong will the pressure be on refineries to build new facilities.

If political will is going to implement better fuel the ICD manufactures can start producing more sophisticated engines that will be even more energy efficient with less emissions in CO_2, NO_x & particle meters.

With implementation of DC system, we can save on non-renewable coper where metal vessel body can transport one power side and LSO. The any rpm on main engine with DC shaft generator can fit the need of electrical power, and if there are two on two or more ICDs with pitch propeller installation, there is no need for auxiliary engines while sailing. With isolation and lowering the ICDs temperatures when stand by, we can save another amount of heat and maintain the stand by temperature just with waste heat from ME or AE.

References

[1] M. B. Vermeire, Everything You Need to Know About Marine Fuels. Ghent: Chevron, 2012.
[2] R. Saidura, S. Mekhilefb, M.B. Ali, A. Safari, H.A. Mohammedc, “Applications of variable speed drive (VSD) in electrical motors energy savings,” Renewable and Sustainable Energy Reviews, vol. 16, p.p. 543– 550, 2012.
[3] N. Khan, N. Abas, “Comparative study of energy saving light sources” Renewable and Sustainable Energy Reviews vol. 15, p.p. 296–309, 2011.
[4] G. A. Livanos, G. Theotokatos, D. N. Pagonis, “Techno-economic investigation of alternative propulsion plants for Ferries and RoRo ships”, Energy Conversion and Management vol. 79, p.p. 640–651, 2014.
[5] M. E. Mondejar, F. Ahlgren, M. Thern, M. Genrup, Quasi-steady state simulation of an organic Rankine cycle for waste heat recovery in a passenger vessel, Applied Energy vol. 185, p.p. 1324–1335, 2017.
[6] D. V. Singh, E. Pedersen, A review of waste heat recovery technologies for maritime applications, Energy Conversion and Management vol. 111, p.p. 315–328, 2016.
[7] Module 2 – Ship Energy Efficiency Regulations and Related Guidelines, IMO, London, January 2016.
[8] Osram Trade Press, Research achievement means yet another innovation surge for LED products, May 2014
[9] https://people.hofstra.edu/geotrans/eng/ch1en/appl1en/maritimeroutes.html
[10] https://www.esrl.noaa.gov/psd/map/clim/sst.anim.year.html
[11] http://www.imo.org/en/OurWork/Environment/PollutionPrevention/AirPollution/Documents/245(66).pdf

[12] M. Grljušić, V. Medica, N. Račić, Thermodynamic Analysis of a Ship Power Plant Operating with Waste Heat Recovery through Combined Heat and Power Production, Energies, vol. 7, p.p. 7368-7394 (2014)

10TH INTERNATIONAL CONFERENCE ON SUSTAINABLE ENERGY AND ENVIRONMENTAL PROTECTION (JUNE 27TH – 30TH, 2017, BLED, SLOVENIA), ENERGY EFFICIENCY
J. Krope, A.Ghani Olabi, D. Goričanec & S. Božičnik

Double Stage High Temperature Heat-Pump for District Heating

IGOR IVANOVSKI, DARKO GORIČANEC, TINA ŽAGAR & SAŠA POZEB

Abstract High-temperature heat-pumps are devices that exploit a low-temperature heat source in order to produce hot water at high-temperatures. One of such sources can also be underground water with temperature of around 10 °C. This paper presents a comparison between two configurations of high-temperature heat-pumps for the purpose of district heating with temperatures between 70°C and 90°C. Ammonia was used as a refrigerant in high-temperature heat-pump. Theoretical calculations were based on the REFPROP property method within Aspen Plus software. The simulations showed that the double stage high-temperature heat-pump could be a feasible solution for exploiting low temperature sources. Including a flash unit into the double-stage heat-pump increases further increases the efficiency by up to 11.1% depending on the evaporation temperature and hot water temperature.

Keywords: • Heat pump • district heating • COP • simulation • REFPROP •

CORRESPONDENCE ADDRESS: Igor Ivanovski, M. Sc., Head of Centre for Ecology and Environmental Protection, Institute for Occupational Safety and Environmental Protection, Valvasorjeva ulica 73, 2000 Maribor, Slovenia, e-mail: igor.ivanovski@ivd.si. Darko Goričanec, Ph.D., Associate Professor, University of Maribor, Faculty of Chemistry and Chemical Engineering, Smetanova ulica 17, 2000 Maribor, Slovenia, e-mail: darko.goricanec@um.si. Tina Žagar, LL.M, Senior Adviser, Ministry of Economic Development and Technology, Trubarjeva 11, 2000 Maribor, Slovenia, email: tina.zagar@gov.si. Saša Pozeb, M. Sc., Ministry of Finance, Financial administration of the Republic of Slovenia, Titova cesta 10, 2000 Maribor, Slovenia, e-mail: sasa.pozeb@gov.si.

https://doi.org/10.18690/978-961-286-050-9.40 ISBN 978-961-286-050-9

Available at: http://press.um.si.

1 Introduction

Heat-pumps are devices that allow for a reduction in primary energy consumption, operating costs and CO_2 emissions according to EU climate package [1]. The heat-pump technology is well known for heating and cooling purposes. Over the last couple of years approximately 800,000 heat pumps were sold every year in the European Union alone [2]. Heat-pumps are usually electrically driven and low grade heat is lifted to a higher temperature by running a vapour compression cycle. The heat is taken from sources like outside air, underground water, or ground. Traditional heat-pumps are suitable for low-temperature heating systems such as underfloor heating, low-temperature radiators or fan convection heaters. On the other hand, district heating systems usually operate at higher temperature regimes. High-temperature heat-pump are suitable for those systems.

High-temperature heat-pumps are devices that exploit low-temperature heat sources such as geothermal water, waste heat of refrigerators, industrial sources, etc. in order to produce hot water that can be used for heating of buildings, production of sanitary hot water or in district heating systems.

There are many different refrigerants that are used in high-temperature heat-pumps. R-717 (ammonia) is perhaps the oldest of all the refrigerants and still widely used in the heat pump/refrigeration technologies [3]. It is also one of the more used refrigerants in high-temperature heat-pumps. There are a few publications regarding the application of ammonia high-temperature heat-pumps [3]–[7].

On the other hand, transcritical heat-pumps that use natural refrigerant carbon dioxide are getting an increasing attention [8]. However, those heat pumps don’t have a condenser. After the compression the supercritical CO_2 is cooled in a gas cooler. It is for this reason that supercritical heat pumps are suitable only for applications with high temperature lift of the heated fluid, for example preparing hot water in meat or diary industry.

It should also be noted that ammonia is considered a natural refrigerant, as it has zero GWP (global warming potential) as well as zero ODP (ozone depleting potential) [9]. Ammonia has an extremely high latent heat, and the acoustic velocity of ammonia is much higher than in any other refrigerant, which means that higher gas velocities can be used in the design of pipes, valves and fittings without incurring substantial pressure losses [10]. Other important advantages of ammonia are tolerance to normal mineral oil, low sensitivity for small amounts of water in the system, simple leak detection and low price. The disadvantages of ammonia are the facts that it is poisonous and it can burn in the air. However, these flaws have been often exaggerated. Ammonia is for example 10-50 times less toxic than chlorine [11]. Ammonia has an important advantage of smelling unpleasantly to most people. The gas can be easily smelled at 5 ppm in air, and according to European Commission Directive 2000/39/EC of 8 June 2000 [12] it has an occupational exposure limit values of 20 ppm and 50 ppm for eight-hour exposure and short term exposure, respectively.

The goal of this study is to compare two double-stage high-temperature heat-pumps for the purpose of district heating. Three heating regimes were observed during the simulations of both double-stage high-temperature heat-pumps. The comparison was based on COP values, which were calculated during theoretical simulations using Aspen Plus software.

2 Methods

Simulations of both high-temperature heat-pumps were performed using Aspen Plus software. The REFPROP Property method was used in all the simulations for all the process units. This method is one of the more accurate methods for pure fluid and mixture models currently available. It is based on three models for the calculation of the thermodynamic properties of pure fluids: equations of state explicit in Helmholtz energy, the modified Benedict-Webb-Rubin equation of state, and an extended corresponding states (ECS) model [13].

2.1 Double-Stage High-Temperature Heat-Pump – Principle of Operation

Double-stage high-temperature heat-pump consists of two compressors, with a cooler between them, condenser, expansion valve, and evaporator as shown in Figure 1. The vapour refrigerant is compressed to an intermediate pressure in compressor 1. After intermediate cooling it is further compressed to the condensation pressure. The vapour is superheated in stream 4 so it cools down to a condensation temperature, then it condenses and further cools down to an outlet temperature in point 5. The heat that is released during vapour cooling is transferred to a heating fluid that can be used in district heating or heating of greenhouses. The subcooled liquid refrigerant is conveyed to an expansion valve where it is reduced in pressure. After the expansion the refrigerant evaporates in the evaporator by exploiting a low-temperature heat source such as: underground water, heat of ambient air, etc.

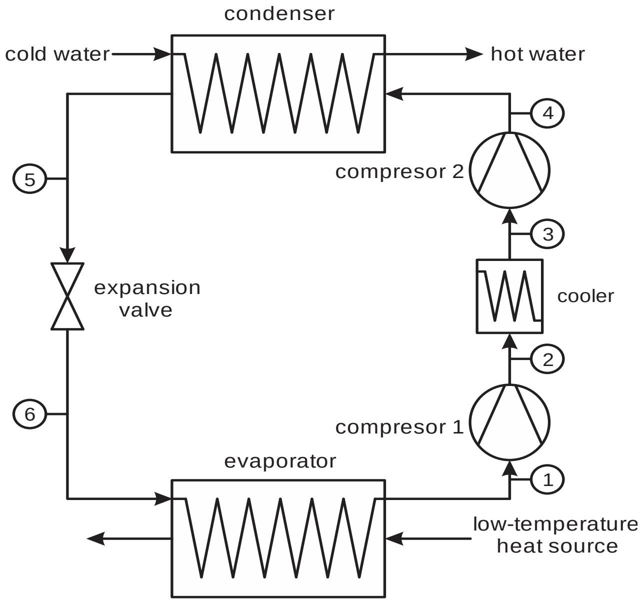

Figure 1. Double stage high-temperature heat-pump

2.2 Double-Stage High-Temperature Heat-Pump with a Flash Unit

Another configuration of a double-stage high-temperature heat-pump includes a flash unit and additional expansion valve in addition to other process units described in the previous chapter as shown in Figure 2. The subcooled refrigerant in point 5 is first expanded in the expansion valve 2 to an intermediate pressure, then the stream is flashed and the vapour phase is conveyed to the intermediate cooler. The liquid is flashed in the expansion valve 1 and evaporated in the evaporator.

2.3 Simulations

In the present study, the following simplifying assumptions were taken into account for the theoretical analysis of both configurations of high-temperature heat pump:

- Refrigerant at the evaporator outlet was specified as saturated vapour.
- Zero pressure drop was assumed in all heat exchangers (condenser, gas cooler, evaporators, and intermediate cooler) and connecting pipes.
- It was assumed that heat losses are negligible.
- An adiabatic, but non-isentropic compression process was assumed with isentropic efficiency 0.84 [2], [3] for ammonia compressor, whilst the mechanical efficiency was set to 0.97.

- The refrigerant temperature at the outlet of the condenser was set to 10°C above the inlet temperature of the heated water, which could be used for district heating.
- It was assumed that the low-temperature sources such as underground water would be available. It is for this reason that the evaporation temperatures were varied between -10°C and 10°C.
- The heating regime of a district heating was varied between 50/60°C, 60/80°C, and 70/90°C. The first number indicated the temperature of the return line and the second temperature of the heating fluid (water).

A design specification option was used during the simulations of both heat-pump cycles. It was set up to determine the pressure ratio of compressor 1 in order to achieve the logarithmic mean temperature difference of 20°C in the condenser in all simulation cases. The intermediate cooler was set to cool the refrigerant vapour to 3°C above the saturation temperature. COP values were calculated according to Equation (1).

$$\mathrm{COP} = \frac{\Phi}{W} \tag{1}$$

Where Φ is the rate of heat flow within the condenser (in W), and W is the work required to drive both compressor (in W). The calculations of COP values were done in an MS Excel spreadsheet. Afterwards graphs were drawn in the same program.

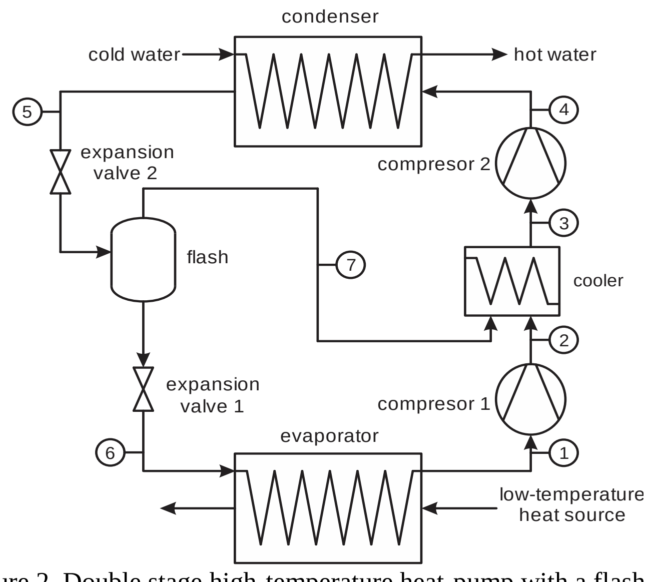

Figure 2. Double stage high-temperature heat-pump with a flash unit

3 Results and Discussion

The ammonia was subcooled in the condenser of both high-temperature heat-pumps during the simulations within Apsen Plus. Figure 3 shows an example of the temperature curves within the condenser of the double stage high-temperature heat-pump with a flash unit. Evaporation temperature (T_e) was set to -10°C, water was heated from 60°C to 80°C, which are the typical temperatures of a heating fluid during district heating. Pinch temperature was also monitored during the simulations. The logarithmic mean temperature difference was kept at 20°C. It is for this reason that the pinch temperature did not change much during the simulations. It was in the range between 11.2°C and 11.5°C during all the simulation cases.

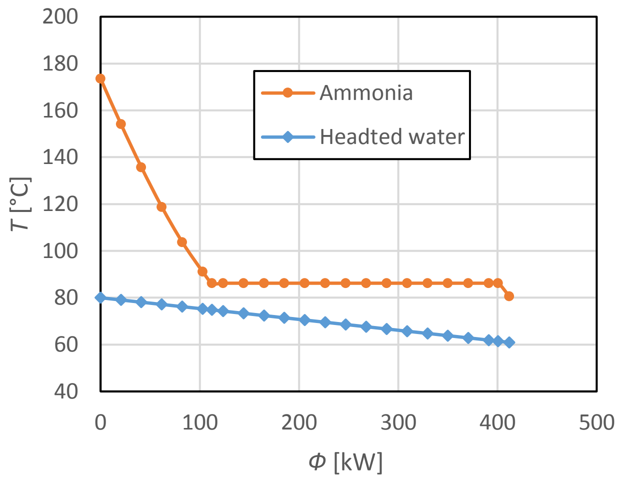

Figure 3. Temperature curves within the condenser of double-stage high-temperature heat-pump at T_e =-10°C; heating regime 60/80°C

Figure 4 presents the results of calculations of COP values dependent on the outlet temperatures of hot water for the double-stage high-temperature heat-pump without a flash unit. The inlet water temperatures (or the return line temperatures) were 20°C lower than the hot water temperatures in line with the above-mentioned temperature regimes. The simulations were undertaken at different evaporation pressures corresponding to temperatures from -10°C to 10°C with a step of 5°C. Figure 5 presents the results of COP values dependent on the hot water temperature for the double-stage high-temperature heat-pump with a flash unit. When comparing the results of both heat-pumps it can be concluded that the additional flash unit provides for a better COP of the double stage high-temperature heat-pump. Table 1 presents the increase of COP values of the double-stage high-temperature heat-pump with a flash unit in comparison to the double- stage high-temperature heat-pump without a flash unit. The highest increase of COP values was observed at low evaporation temperatures (-10°C), ranging from 6.6% and 11.1% and at high water temperature (90°C), ranging from 6.2% to 11.1%

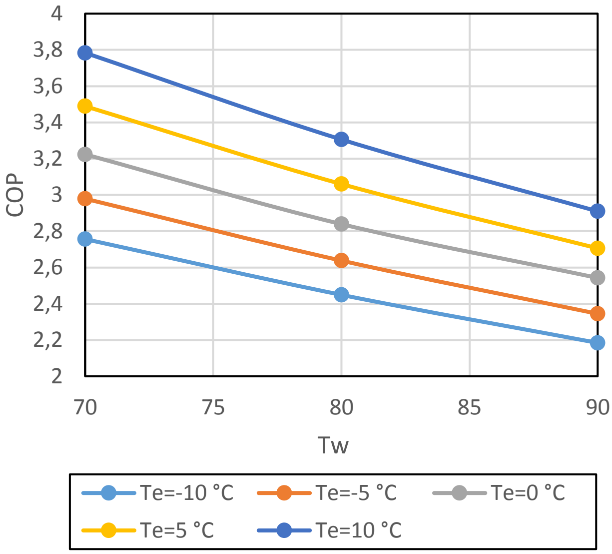

Figure 4. COP dependent on the hot water temperature for the double-stage high-temperature heat-pump without a flash unit

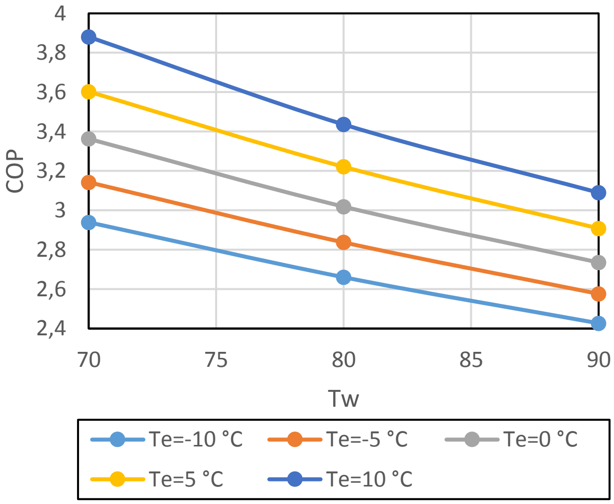

Figure 5. COP dependent on the hot water temperature for the double-stage high-temperature heat-pump with a flash unit

Table1. Increase of COP due to a flash unit.

T_e[°C] / T_w [°C]	-10 °C	-5 °C	0 °C	5 °C	10 °C
70	6.6%	5.5%	4.3%	3.3%	2.6%
80	8.6%	7.6%	6.3%	5.3%	3.9%
90	11.1%	9.9%	7.6%	7.5%	6.2%

4 Conclusions

The two configurations of double-stage high-temperature heat-pumps that use ammonia as a refrigerant were presented and compared during this research. The simulation models were designed in order to calculate the coefficient of performance at different evaporation temperatures and different heating regimes. This technology could be used for district heating by exploiting a low temperature heat source. It was observed that the COP values would increase if a flash unit were to be used in a double stage heat pump.

Flash units usually aren't expensive, so it is expected that including a flash unit would be economically feasible. However, if the evaporation temperatures were to be high and the demanded temperature of hot water low, the efficiency increase would be minor.

References

[1] G. Leonzio, "Mathematical modeling and environmental analysis of heat pumps integrated in aprocess to treat spent pickling liquors," *Journal of Cleaner Production*, vol. 133, pp. 835–849, Oct. 2016.
[2] D. Fischer and H. Madani, "On heat pumps in smart grids: A review," *Renewable and Sustainable Energy Reviews*, vol. 70, pp. 342–357, Apr. 2017.
[3] Z. Zhao, Z. Xing, F. Hou, Y. Tian, and S. Jiang, "Theoretical and experimental investigation of a novel high temperature heat pump system for recovering heat from refrigeration system," *Applied Thermal Engineering*, vol. 107, pp. 758–767, Aug. 2016.
[4] B. Kulcar, D. Goricanec, and J. Krope, "Economy of exploiting heat from low-temperature geothermal sources using a heat pump," *Energy and Buildings*, vol. 40, no. 3, pp. 323–329, 2008.
[5] D. Goričanec, V. Pozeb, L. Tomšič, and P. Trop, "Exploitation of the waste-heat from hydro power plants," *Energy*, vol. 77, pp. 220–225, Dec. 2014.
[6] A. Caf, D. Urbancl, P. Trop, and D. Goricanec, "Exploitation of low-temperature energy sources from cogeneration gas engines," *Energy*, vol. 108, pp. 86–92, Aug. 2016.
[7] M. B. Blarke, "Towards an intermittency-friendly energy system: Comparing electric boilers and heat pumps in distributed cogeneration," *Applied Energy*, vol. 91, no. 1, pp. 349–365, Mar. 2012.
[8] T. Bai, G. Yan, and J. Yu, "Thermodynamic analyses on an ejector enhanced CO2 transcritical heat pump cycle with vapor-injection," *International Journal of Refrigeration*, vol. 58, pp. 22–34, Oct. 2015.

[9] X. Li, M. Li, Y. Ma, and Q. Yan, “The influence of nitrogen on an expander in a carbon dioxide transcritical heat pump,” *Applied Thermal Engineering*, vol. 59, no. 1–2, pp. 182–188, Sep. 2013.

[10] A. Pearson, “Refrigeration with ammonia,” *International Journal of Refrigeration*, vol. 31, no. 4, pp. 545–551, Jun. 2008.

[11] G. Lorentzen, “The use of natural refrigerants: a complete solution to the CFC/HCFC predicament,” *International Journal of Refrigeration*, vol. 18, no. 3, pp. 190–197, Mar. 1995.

[12] “EUR-Lex - 32000L0039 - EN - EUR-Lex.” [Online]. Available: http://eur-lex.europa.eu/legal-content/EN/ALL/?uri=CELEX%3A32000L0039. [Accessed: 28-May-2017].

[13] Aspen Technology, Inc, *Aspen Plus V8.6*. 2015.

10TH INTERNATIONAL CONFERENCE ON SUSTAINABLE ENERGY AND ENVIRONMENTAL PROTECTION (JUNE 27TH – 30TH, 2017, BLED, SLOVENIA), ENERGY EFFICIENCY
J. Krope, A.Ghani Olabi, D. Goričanec & S. Božičnik

Linear Oscillatory Synchronous Generator Designed for a Stirling Engine

MIRALEM HADŽISELIMOVIĆ, GREGOR SRPČIČ, IZTOK BRINOVAR, ZDRAVKO PRAUNSEIS, SEBASTIJAN SEME & BOJAN ŠTUMBERGER

Abstract This paper presents a novel construction of a linear oscillatory synchronous generator designed to be used in a free-piston Stirling engine. High oscillation frequency and short displacement of linear movement present a challenge for the design of the linear oscillatory generator. This works proposes a novel construction of a modular linear synchronous generator. The novel modular linear synchronous generator consists of a basic stationary primary part with concentrated three-phase winding and a basic moving secondary part with permanent magnets. Modular topology of the proposed linear oscillatory synchronous generator enables assembly of different machine lengths according to the required power level by stacking together various numbers of basic primary and secondary modules. A prototype of the linear oscillatory synchronous generator was built and tested. This paper presents the electromagnetic design and the results of experimental testing in a laboratory environment..

Keywords: • Stirling engine • synchronous machine • linear oscillatory generator • permanent magnets •

CORRESPONDENCE ADDRESS: Miralem Hadžiselimović, Ph.D., Associate Professor, University of Maribor, Faculty of Energy Technology, Hočevarjev trg 1, SI-8270 Krško, Slovenia and Faculty of Electrical Engineering and Computer Science, Smetanova ulica 17, SI-2000 Maribor, Slovenia, e-mail: miralem.h@um.si. Gregor Srpčič, Master's Degree in Energy Technology, Assistant, University of Maribor, Faculty of Energy Technology, Hočevarjev trg 1, SI-8270, Krško, Slovenia, e-mail: grega.srpcic@um.si. Iztok Brinovar, Master's Degree in Energy Technology, Assistant, University of Maribor, Faculty of Energy Technology, Hočevarjev trg 1, SI-8270, Krško, Slovenia, e-mail: iztok.brinovar1@um.si. Zdravko Praunseis, Ph.D., Assistant Profesor, University of Maribor, Faculty of Energy Technology, Hočevarjev trg 1, SI-8270, Krško, Slovenia, e-mail: zdravko.praunseis@um.si. Sebastijan Seme, Ph.D., Associate Professor, University of Maribor, Faculty of Energy Technology, Hočevarjev trg 1, SI-8270, Krško, Slovenia and Faculty of Electrical Engineering and Computer Science, Smetanova ulica 17, SI-2000 Maribor, Slovenia, e-mail: sebastijan.seme@um.si. Bojan Štumberger, Ph.D., Professor, University of Maribor, Faculty of Energy Technology, Hočevarjev trg 1, SI-8270, Krško, Slovenia and Faculty of Electrical Engineering and Computer Science, Smetanova ulica 17, SI-2000 Maribor, Slovenia, e-mail: bojan.stumberger@um.si.

https://doi.org/10.18690/978-961-286-050-9.41 ISBN 978-961-286-050-9

Available at: http://press.um.si.

1 Introduction

Stirling engine was designed by Robert Stirling in 1821, and is one of the oldest machines with four-phase thermodynamic cycle operation [1-3]. Ever since its invention, researchers have been trying to improve it in terms of its construction, used materials, gases, and last but not least, application solutions, which would provide higher efficiency along with lower costs, leading to its use in daily life. Stirling engine is most often used in micro Combined Heat and Power (μCHP) applications [4-7], which are mostly based on renewable energy sources. Versions with mirrors [8-12], using solar energy, and versions with external combustion of e.g. biomass, are used.

Despite the large amount of research done in connection to Stirling engine, scientific literature does not include many works dealing with subject of appropriate electric generator design which can be used inside of Stirling engine. Electric generators are generally presented only as an addition to the operation description of the Stirling engine [8-10]. This paper focuses on novel construction of a linear oscillatory synchronous generator designed to be used in a free-piston Stirling engine. A review of existing electric generators used in Stirling engines showed that a modular energy-efficient low cost product needs to be designed for large-scale production.

2 Stirling Engine & Electric Generator

The basic topology of Stirling engine operation is presented in Figure 1, where the engine receives thermal energy and converts it into mechanical movement. Conversion is possible with three different types of Stirling engine, alpha, beta or gamma type [2, 3]. All three types need an external source of thermal energy. It can be provided by different conventional energy sources or renewable energy sources in applications with external combustion.

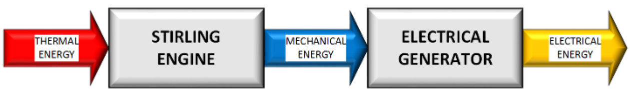

Figure 1. Energy conversion in a co-generator with a Stirling engine

A large number of applications also use solar energy directly, as is the case of our Institute of Energy Technology, where we use a 10 square meters large concentrator (Figure 2) with an installed beta type Stirling engine.

Figure 2. Solar concentrator with an installed Stirling engine

2.1 Stirling engine – types

The three basic types of Stirling engine are briefly described below [2, 3].

Alpha type

Alpha type Stirling engine consists of two cylinders. The expansion cylinder (hot piston) is maintained at a high temperature, while the compression cylinder (cold piston) is being cooled. A regenerator connects both cylinders, as shown in Figure 3.

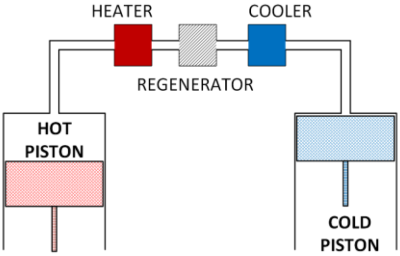

Figure 3. Presentation of alpha type mechanical configuration

Beta type

Beta type Stirling engine consists of one cylinder with a hot space and a cold space. A displacer moves the air between the hot space and the cold space. A power piston is at the end and moves the electrical generator.

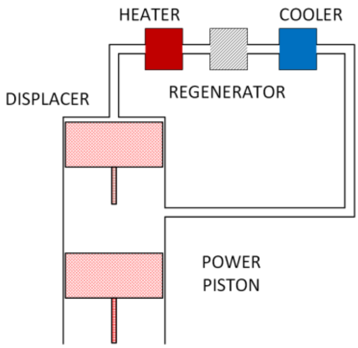

Figure 4. Presentation of beta type mechanical configuration

Gamma type

Gamma type Stirling engine is a modified beta type, in which the power piston is placed in a special cylinder next to the cylinder with the displacer. Both pistons are connected to the same flywheel. Gas can move between both cylinders (Figure 5).

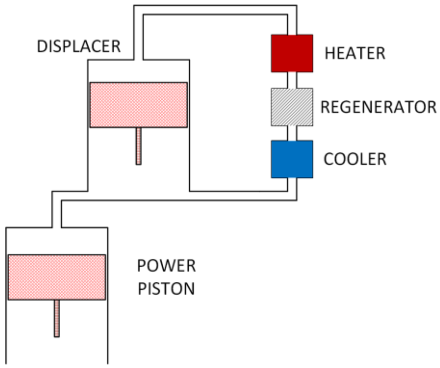

Figure 5. Presentation of gamma type mechanical configuration

2.2 Electric Generator Used in a Stirling Engine

Different electric generators can be found in scientific literature on Stirling engines, and they are briefly described below. Generators are usually linear to avoid unnecessary additional conversion of translational movement of pistons into rotation. The generator consists of a primary stationary part and a secondary moving part (mover).

Induction machines

In case of an induction machine, it is necessary to note that mechanical energy is converted to electric only if the speed of the mover is higher than synchronous speed. An induction machine also cannot generate reactive power, which can be solved with capacitors that maintain generator's voltage. Tubular versions with a simple secondary part in the shape of an aluminium cylinder [13, 14] or conventional rotational versions with a short-circuited squirrel cage [15] are mostly used.

Transverse flux machines

When designing the electric generator, it is necessary to take into account that Stirling engines are usually not self-started. It is well known that electric machines operate in generator or motor regime. Electric generator therefore needs to be designed in such a way that it can produce sufficient force/torque in the motor regime to start the Stirling engine. A solution for a linear generator with a transverse flux machine is presented in [16, 17].

Permanent magnet machines

Electric generators with permanent magnets are most commonly used in Stirling engines. The magnets are usually placed on the mover and the winding is placed in the cold space of the drive. Tubular generators [18-21] are usually installed in prototypes because of their small volume. To achieve higher power and better generator efficiency, ferromagnetic material needs to be installed on the mover next to permanent magnets. Because of the tubular form, soft magnetic composite (SMC) is usually chosen as ferromagnetic material, as it enables a more compact generator construction in comparison to conventional electrical steel, but leads to lower efficiency in the low-frequency area because of lower permeability of the SMC material [22, 23].

3 Modular Design of a Linear Oscillatory Generator

Stirling engines are produced in different size categories depending on the power of the application. This paper presents a modular design of a linear oscillatory generator with the intention of designing a module, which can be used as a basic element in all size categories of Stirling engines.

Figure 6. Stationary primary part with concentrated three-phase winding

This works presents a novel construction of the modular linear synchronous generator. The novel modular linear synchronous generator consists of a basic stationary primary part with concentrated three-phase winding (Figure 6) and a basic moving secondary part with permanent magnets (Figure 7).

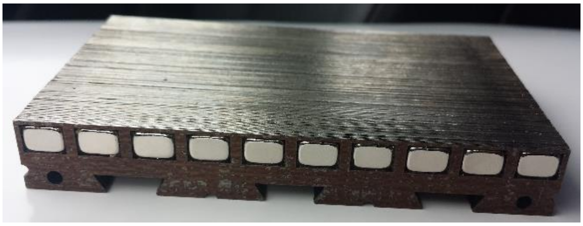

Figure 7. Moving secondary part with permanent magnets

Modular topology of the proposed linear oscillatory synchronous generator enables assembly of different machine lengths according to the required power level by stacking together various numbers of basic primary and secondary modules (Figure 8 and 9).

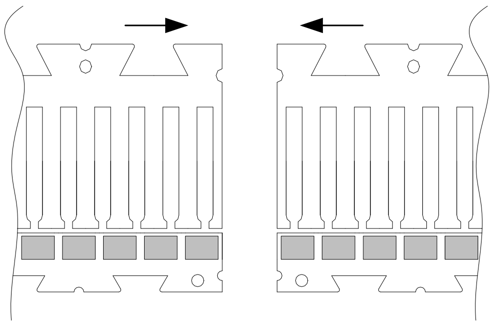

Figure 8. Modular topology – stacking concept

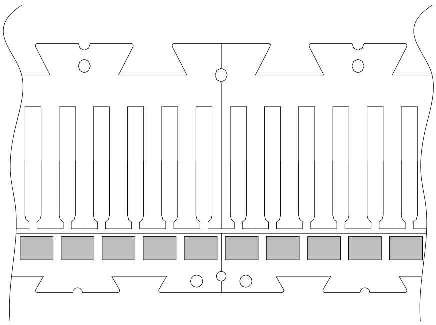

Figure 9. Joined modules

The basic generator segment is 102 mm wide and depends on the stroke length of the Stirling engine. The packet length (**l_{Fe}**) of the primary and the secondary part is 60 mm, meaning that they are both composed of 120 laminated plates with 0.5 mm thickness. Other data for the generator and permanent magnets are provided in Table 1.

Table 1. Generator data

Variable	Value
arrangement	linear
number of phases	3
output power of one module	75W
generator efficiency	$>$90%
coil resistance per phase	11.3 Ω
number of turns per phase	96
lamination length	60 mm
lamination width	102 mm
air-gap width	0.65 mm
oscillating piston stroke length	20 mm
permanent magnet material	NdFeB
remanence B_r	1.29 T
maximum temperature	180°C

Linear generator was constructed with a non-commercial software package TurboSolver, which is based on a finite element method (FEM). The basic discretization model of primary and secondary part is presented in Figure 10.

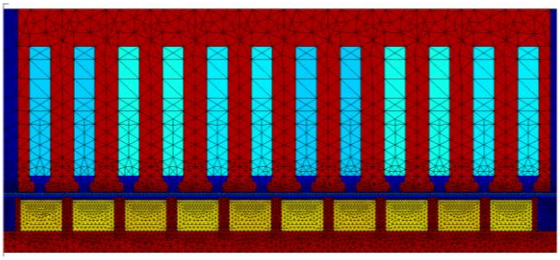

Figure 10. Discretization of primary and secondary generator part

In the design process of the electric generator geometry, it is necessary to select a correct air-gap dimension between the primary and the secondary. In the case that air-gap is to high this will results in the poor generator performance, while to small air-gap width might results in increased eddy current losses in permanent magnets. Figure 11 presents magnetic field distribution at load conditions.

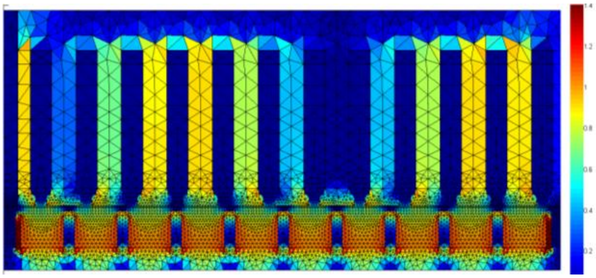

Figure 11. Magnetic field distribution at load conditions.

4 Experimental System and Results

The prototype of a linear oscillatory synchronous generator, presented in the previous section, was measured with an experimental system described below.

4.1 Experimental system

A measuring system which can drive a linear generator was constructed for verification of the constructed generator prototype. The core of the system is a controlled oscillatory drive, which can drive the test generator up to 4000 strokes per minute. Installation of the two modules of a linear generator inside the experimental system is shown in Figure 12. The instruments in the measuring system enable measurement of time-dependent values of individual mechanical and electric quantities: position and force needed to move the secondary part, and the current and voltage of individual phases.

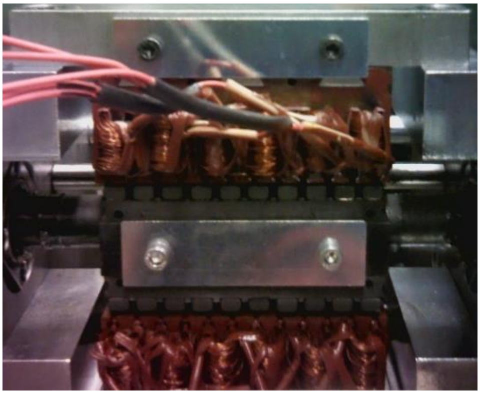

Figure 12. Two modules of linear electrical generator inside the experimental system

4.2 Results

Figure 13 shows the measured characteristics of the generated electric power in the case of resistive load for single generator module in dependency on different air-gap width between the primary and the stationary part of oscillatory generator.

The maximum achieved power with 0.65 mm air-gap width and 2000 strokes per minute was 75 W with the line-to-line voltage of 120 V. The target air-gap width in a Stirling engine is 0.25 mm, which equals to 100 W of target power of one generator module.

Generator current-voltage characteristic for different air-gap width are shown in Figure 14 and present the generator's load power ability given as a function of terminal voltage.

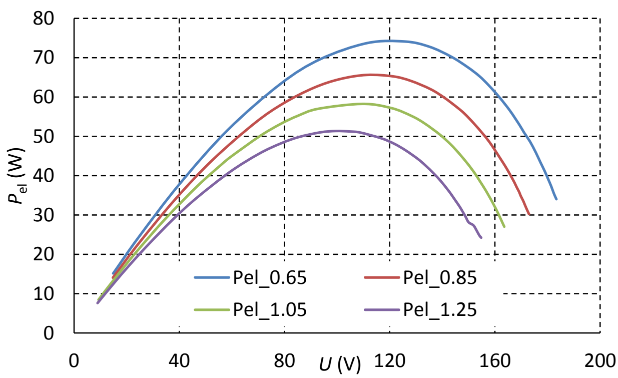

Figure 13. Generated electrical power in dependency of terminal voltage (single module, 2000 strokes per minute)

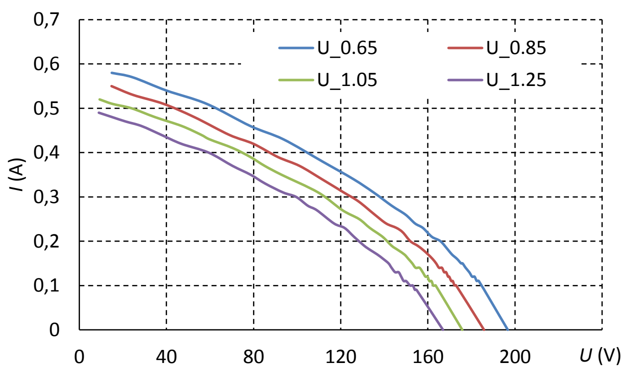

Figure 14. Current-voltage characteristics

During the movement of the secondary part with an oscillating free piston within one stroke (stroke length is 20 mm), the speed drops to almost zero in both end points. Induced voltage is zero at that point, and the electric power of the generator is consequently also zero (Figure 15).

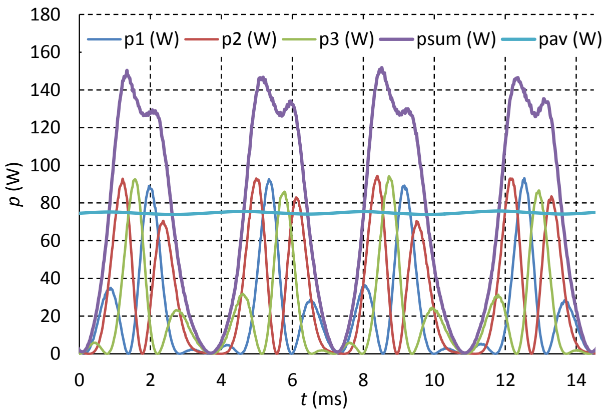

Figure 15. Time waveforms of phase, total and average electric power of the generator (single module, 2000 strokes per minute, air-gap width 0.65 mm)

When the secondary part is moving from one end point to the other, it accelerates to the highest speed and then decelerates to a full stop. The total time-dependent generated power p_{sum} is a sum of individual phase power values:

$$p_{\mathrm{sum}} = p_1 + p_2 + p_3 \tag{1}$$

where p_1, p_2 and p_3 are time-dependent individual phase power values. An average generating power p_{ave} can be calculated by integration of total power p_{sum} over the time period $T_2 - T_1$ (2):

$$p_{\mathrm{ave}} = \frac{1}{T_2 - T_1} \int_{T1}^{T_2} p_{\mathrm{sum}} \mathrm{d}t \tag{2}$$

For Stirling engine applications it is very important to select appropriate maximum working temperature of permanent magnets. In the temperature rise test with continuous electric load of 75 W, thermal equilibrium was reached after 45 minutes. The maximum temperature inside the generator (winding) was lower than 40 °C at ambient temperature 22 °C.

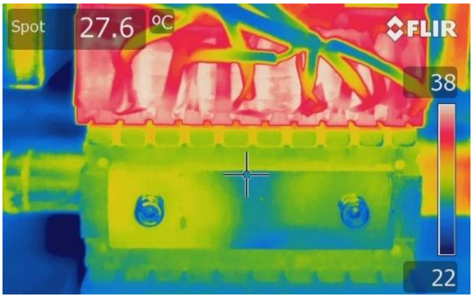

Figure 16. Temperature distribution inside the generator after the temperature rise test

The maximum temperature inside a Stirling engine housing, where the generator is installed, is limited to 120°C. At this limited ambient temperature the magnets and the winding permissible over-temperatures due to the electric load will be inside prescribed limits as well.

5 Conclusion

This paper deals with a three-phase twelve-slot/ten-pole linear oscillating generator. The measured results showed that the proposed design is suitable for free-piston Stirling engine applications. Permanent magnets are useful for oscillatory pistons with a short stroke in order to increase the power density and the overall efficiency of the generator. The results of the temperature rise test at nominal load confirmed that it is possible to use it inside a Stirling engine housing. Moreover, results in thermal equilibrium showed that the nominal load of the proposed generator could be increased. Finally, the modular design enables a cost-effective solution for integration into end-user applications with a Stirling engine.

References

[1] C. H. Cheng and H. S. Yang, "Analytical model for predicting the effect of operating speed on shaft power output of Stirling engines", *Energy*, vol. 36, pp. 5899-5908, 2011

[2] B. Kongtragool and S. Wongwises, "A review of solar-powered Stirling engines and low temperature differential Stirling engines", *Renewable and Sustainable Energy Reviews,* vol. 7, pp. 131-154, 2003

[3] D. G. Thombarea and S. K. Verma, "Technological development in the Stirling cycle engines", *Renewable and Sustainable Energy Reviews,* vol. 12, pp. 1-38, 2008

[4] W. Cho and K. S. Lee, "A simple sizing method for combined heat and power units", *Energy,* vol. 65, pp. 123-133, 2014

[5] A.D. Hawkes, M.A. Leach, "Cost-effective operating strategy for residential micro-combined heat and power", *Energy,* vol. 32, pp. 711-723, 2007

[6] L. F. Fuentes-Cortes, A. W. Dowling, C. Rubio-Maya, V. M. Zavala and J. M. Ponce-Ortega, "Integrated design and control of multigeneration systems for building complexes", *Energy,* vol. 116, pp. 1403-1416, 2016

[7] S. Karmacharya, G. Putrus, C.P. Underwood, K. Mahkamov, S. McDonald and A. Alexakis, "Simulation of energy use in buildings with multiple micro generators", *Applied Thermal Engineering*, vol. 62, pp. 581-592, 2014

[8] C. Toro and N. Lior, "Analysis and comparison of solar-heat driven Stirling, Brayton and Rankine cycles for space power generation", *Energy*, vol. 120, pp. 549-564, 2017

[9] G. Gavagnin, D. Sánchez, G. S. Martínez, J. M. Rodríguez and A. Muñoz "Cost analysis of solar thermal power generators based on parabolic dish and micro gas turbine: Manufacturing, transportation and installation", *Applied Energy*, vol. 194, pp. 108-122, 2017

[10] G. Barreto and P. Canhoto, "Modelling of a Stirling engine with parabolic dish for thermal to electric conversion of solar energy", *Energy Conversion and Management*, vol. 132, pp. 119-135, 2017

[11] A. Kaddour and B. Benyoucefa, "Simulation of a photo-solar generator for an optimal output by a parabolic photovoltaic concentrator of Stirling engine type," presented at the Seventh International Conference on Materials Science (CSM7) 20-22 May 2010 Beirut-Lebanon, *Physics Procedia*, vol. 21, pp. 140-145, 2011

[12] A. C. Ferreira, M. L. Nunes, J. C. F. Teixeira, L. A.S.B. Martins and S. F. C. F. Teixeira, "Thermodynamic and economic optimization of a solar-powered Stirling engine for micro-cogeneration purposes", *Energy*, vol. 111, pp. 1-17, 2016

[13] T. T. Dang, P. François, L. Prévond and H. Ben Ahmed, "Theoretical and experimental results of Tubular Linear Induction Generator for Stirling Cogenerator System", *International Conference on Electrical Machines*, pp. 1-7, 2010

[14] T. T. Dang, M. Ruellan, L. Prévond, H. B. Ahmed and B. Multon, "Sizing Optimization of Tubular Linear Induction Generator and Its Possible Application in High Acceleration Free-Piston Stirling Micro-cogeneration", *IEEE Transactions on Industry Applications*, vol. 51, No. 5, pp. 3716-3733, September/October 2015

[15] R. Beltrán-Chacon, D. Leal-Chavez, D. Sauceda, M. Pellegrini-Cervantes and M. Borunda, "Design and analysis of a dead volume control for a solar Stirling engine with induction generator", *Energy*, vol. 93, pp. 2593-2603, 2015

[16] W. M. Arshad, P. Thelin, T. Bäckström and C. Sadarangani, "Use of Transverse-Flux Machines in a Free-Piston Generator", *IEEE Transactions on Industry Applications*, vol. 40, No. 4, pp. 1092-1100, July/August 2004

[17] L.H. Joubert and J.M. Strauss, "Optimisation of a Transverse Flux Linear Oscillating Generator by Transient 3D Finite Element Analysis", *International Conference on Electrical Machines*, pp. 602-608, 2014

[18] Y. Huo, A. Zhang, X. Zhang, C. Yan, G. Yu, H. Chen and Z. Yang, "Research of Moving Magnet Linear Generator for Stirling Convertor" *International Power Electronics and Application Conference and Exposition*, pp. 1248 - 1252, 2014

[19] P. Zheng, C. Tong, J. Bai, B. Yu, Y. Sui and W. Shi, "Electromagnetic Design and Control Strategy of an Axially Magnetized Permanent-Magnet Linear Alternator for Free-Piston Stirling Engines", *IEEE Transactions on Industry Applications*, vol. 48, No. 6, pp. 2230-2239, November/ December 2012

[20] K. M. Nor, W. Arof and Wijono, "Design of a 5 kW Tubular Permanent Magnet Linear Generator", *39th International Universities Power Engineering Conference*, pp. 528- 532, vol. 1, 2004

[21] P. Zheng, B. Yu, S. Zhu, Q. Gong and J. Liu, "Research on Control Strategy of Free-Piston Stirling-Engine Linear-Generator System", presented at the 17th International Conference on Electrical Machines and Systems (ICEMS), Oct. 22-25, 2014, Hangzhou, China

[22] G. Cvetkovski and L. Petkovska, “Performance Improvement of PM Synchronous Motor by Using Soft Magnetic Composite Material”, *IEEE Transactions on Magnetics,* vol. 44, No. 11, pp. 3812-3815, November 2008

[23] G. Cvetkovski, L. Petkovska, M. Cundev, and S. Gair, “Improved Design of a Novel PM Disk Motor by Using Soft Magnetic Composite Material”, *IEEE Transactions on magnetics*, vol. 38, No. 5, pp. 3165-3167, September 2002

10TH INTERNATIONAL CONFERENCE ON SUSTAINABLE ENERGY AND ENVIRONMENTAL PROTECTION (JUNE 27TH – 30TH, 2017, BLED, SLOVENIA), ENERGY EFFICIENCY
J. Krope, A.Ghani Olabi, D. Goričanec & S. Božičnik

Energy Optimisation of Parallel Operating Processes for the Production of Formaldehyde

JÓZSEF MURSICS, TINA ŽAGAR & DARKO GORIČANEC

Abstract This article describes various combinations of parallel operating formaldehyde plants using different catalysts and analyses the energetic optimization of such combined operations. Excessive heat is transferred directly into electricity the formaldehyde production; innovative usage of off-gases form the formaldehyde production has been investigated. The efficiency of the various combinations of formaldehyde processes using various catalysts is evaluated by comparing the costs per mass unit of the produced formaldehyde (calculated as 37% concentration).

Keywords: • formalin production • parallel operating formalin processes • energetic efficiency • CO2 emissions • costs •

CORRESPONDENCE ADDRESS: József Mursics, M.Sc, Manager, FALCO Zrt. Zanati út 26, 9700 Szombathely, Hungary, e-mail: j.mursics@falco-woodindustry.com. Tina Žagar, LL.M., Ministry of Economic Development and Technology, Kotnikova 5, 1000 Ljubljana, Slovenia, e-mail: tina.krope@gmail.com. Darko Goričanec, Ph.D., Associate Professor, University of Maribor, Faculty of Chemistry and Chemical Engineering, Smetanova ulica 17, 2000 Maribor, Slovenia, e-mail: darko.goricanec@um.si.

https://doi.org/10.18690/978-961-286-050-9.42 ISBN 978-961-286-050-9

Available at: http://press.um.si.

1 Introduction

Formalin is a commercial name for aqueous solutions of formaldehyde and is one of the most important products in chemical industry in the category of high tonnage products [1] [2]. Despite such high and still increasing manufacturing capacities of formaldehyde, the proportion of international trading of formaldehyde is below 2%. This can be attributed mostly to formaldehyde's physical and chemical instability as well as to high transport costs for formaldehyde due to the relatively high concentration of water in the product [3] [4]. For these reasons, formaldehyde is usually used or processed at the site of production or in the nearby areas of production units. Taking into consideration the constant increases of energy expenses, an additional condition in the production of valuable products is the optimal use of by-product energy, based on off-gases from the production of formaldehyde from methanol [5] [6].

The production of formaldehyde has recently faced constant turmoil, which is evident by the following facts:

- Formaldehyde has been classified as a carcinogen;
- increasing ecological awareness, not only in the developed world, requires continuously lower emissions based on total off-gases: mg of chemical substances per cubic meter of gaseous emissions (mg/m^3) as well as total emission in kilograms of chemical substance per time unit (kg/day);
- high energy needs for the production of formalin lead to considerable costs, high CO2 emissions, and as a consequence formalin production processes create high amounts of unused by product energy;
- European legislation has significantly limited the degree of freedom for formaldehyde producers by regulating the permitted output of CO2 emissions. This has mostly affected the industry of high volume chemicals, which creates very low added value per unit of product and therefore the required quantity of CO2 coupons cannot be purchased in order to fulfil legally mandated and ever lower quotas.

Producers of formalin had to find solutions in a very short time (within three to five years), in order to address the following problems:

- compensation for negative effects of the reduction of annual CO2 quotas;
- adjustment of emissions according to regulations of legal values and acquisition of IPPC permission;
- preparation and execution of energy optimisation of the entire production process.;
- implementation of the »no waste« principle in production.

2 The Design of Formaldehyde Production Processes

There are two basic formaldehyde production processes:

- silver catalyst process, operating with methanol surplus and
- metal oxide catalyst process, operating with air surplus.

2.1 Formaldehyde production process on the basis of silver catalyst

Processes on the basis of silver as a catalyst burden the environment with gas emissions in the air, as well as with emissions of excess steam condensates, arising from the contact between the flows of products and steam as thermal energy carrier.

The energy flows of the two formaldehyde production processes F1 and F3 as a basis for the investigations reported here are presented in Fig. 1, where the red arrows shows the steam flow; black arrows the electrical energy flow; green arrows the off-gases from silver catalyst process (FOP), and the yellow arrows the natural gas flow for steam generation. The torch shows the emission to the environment.

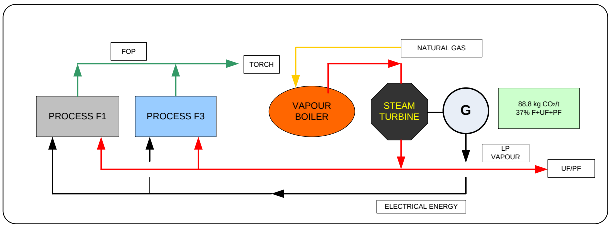

Figure 1: Gas and energy flows of the two formaldehyde production processes F1 and F3.

The process of catalytic oxidation and dehydration of methanol in silver catalyst carry out the synthesis. The process of catalysis is accomplished in two phases:

$$CH_3OH + 1/2\ O_2 \rightarrow CH_2O + H_2O \qquad -160\ \text{kJ/mol} \qquad (1)$$

alternatively:

$$CH_3OH \rightarrow CH_2O + H_2 \qquad -\ 84\ \text{kJ/mol} \qquad (2)$$

$$H_2 + 1/2\ O_2 \rightarrow H_2O \qquad +232\ \text{kJ/mol} \qquad (3)$$

Reaction (3) is exothermic; the thermal energy formed in this reaction maintains the temperature of the reactor and at the same time facilitates the shift of the equilibrium to the right side in reaction (2), which increases the formation of formaldehyde. Parallel to the main reactions (1, 2, and 3), some side reactions are carried out as well, and those reduce the efficiency of the process. Important side reactions are:

$$CH_2O \rightarrow CO + H_2 \quad (4)$$

$$CH_2O + 1/2\ O_2 \rightarrow HCOOH \text{ and } CO + H_2O \quad (5)$$

$$CH_2O + O_2 \rightarrow CO_2 + H_2O \quad (6)$$

In a following phase, the emission of off-gases from the formaldehyde process (FOP) into the air has been replaced with a technical solution in form of co-processing by burning these gases in a gas boiler and subsequent co-formation of electrical energy in a steam turbine (Fig.2).

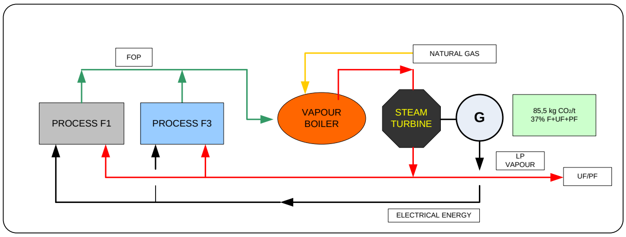

Figure 2: Gas and energy flows of the two formaldehyde production processes F1 and F3: this improved technical solution includes co-processing of the off-gases (FOP) for steam generation.

Average values for the composition of the gas mixture (FOP) are in following proportions (all numbers in vol. %):

$$N_2 : H_2 : CO_2 = 75\% : 21\% : 4\% \quad (7)$$

$$\text{Lower calorific value} = 2.7\ MJ/m^3 \quad (8)$$

2.2 Formaldehyde production process on the basis of metal oxide catalyst

During the production of formaldehyde on the basis of a metal oxide catalyst (process F2), formaldehyde is formed by partial oxidation of methanol with oxygen. Reactions are carried out on a metal oxide catalyst in a reactor with a static layer of catalyst for oxidation in gas phase (fixed-bed vapor phase oxidation reactor) and a cooling system, according to the reaction:

$$CH_3OH + ½\ O_2 \rightarrow CH_2O + H_2O \quad dH = -157 kJ/mol. \quad (9)$$

For the maintenance of the desired oxidation atmosphere, the required ratio between methanol and air is low; the content of methanol in the air is approximately 4 to 10 vol. %. Such high surplus of air is possible because a certain portion of the gas from the absorber is recycled, resulting in sufficient reduction in concentration of oxygen in order to avoid formation of explosive mixtures. The thermal energy released during the reaction is discharged from the reactor using thermal oil as liquid medium for the energy transfer, and used for the production of steam.

2.3 Work methods and data

Experimental work was based on measurements and analysis of data of various production sections for formaldehyde production processes F1, F2 and F3.

Data for the following factors have been collected:

- the origin of energy for production of water vapor for operation of the generator,
- production of electricity,
- consumption of electricity,
- withdrawal of vapor from turbine and
- use and production of vapor during processes.

Each experiment lasted for 24 hours. The preparation of each test run, during which the data for the further evaluations had been compiled however, lasted for several days; in order to obtain valid results, the system had to stabilise itself to achieve stationary state conditions for 3 days. The third day of the stationary state was chosen as a starting point for each individual collection of data.

Data collection was carried out with following devices:

- electricity: electrical consumption meters (kW/h),
- cooling power: digital meters for water consumptions (m^3/h) and on-line measurements of temperature increase between input and output,
- natural gas: digital consumption meter (m^3/h) with appropriate compensation for temperature fluctuations,
- off-gases from the formaldehyde production process (FOP): digital consumption meter (m^3/h),
- methanol consumption: flow meters at individual production units (t/h).

Utilized measuring technique had a ± 5% absolute deviation.

3 Optimization of Machinery for Formaldehyde Production

3.1 Formaldehyde production process on silver catalyst (processes F1 and F3) and on metal oxide catalyst (process F2): variation 2

After the implementation of the metal oxide process F2 into the total formaldehyde production, the parallel production was carried out with all three formalin production processes (F1, F3 and F2) system, together with co-generation of electricity from natural gas and the usage of the off-gases from the formaldehyde process (FOP) for additional steam generation.

The energy flows of the three formaldehyde plants F1, F2, and F3 (variation 2) are shown in Fig. 3.

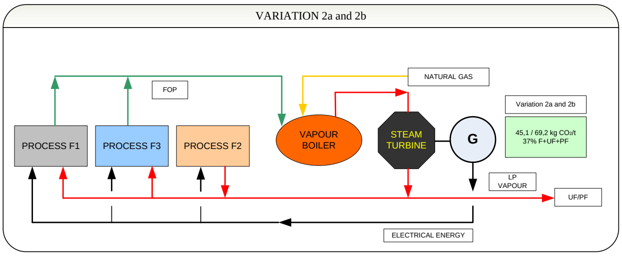

Figure 3: Gas and energy flows for variation 2a and 2b. Process F2 directly fuels other process with steam but still needs purchase of electrical energy from external network.

The mutual influences are the following: withdrawn quantity of steam from the turbine and used for the production of formalin is a function of capacity, ergo more FOP is available for production of steam or electricity.

This model is problematic in cases where the consumption of electricity for the processes falls below the minimal capacity of the turbine, generator or boiler. In such cases the consumption of natural gas increases because of insufficient available quantities of FOP in order to operate the generation of electric power; the excess of electrical energy (which, however, is not used in the small formaldehyde production) can be traded only for notably reduced end prices in comparison to production prices. Table 1 shows the influence of the produced quantity of products (formaldehyde + UF resin + PF resin) at the same operating regimes of the formaldehyde plants.

Table 1: CO_2 emissions for variation 2a and 2b

LABEL	TOTAL PRODUCTION F+UF+PF (t/day)	SPECIFIC CONSUPTION OF NATURAL GAS (Nm3/t)	SPECIFIC EMISSION OF CO_2 BASED ON PRODUCTS (kg/t)
V2a	894	15,9	45,1
V2b	771	31,2	69,2

The specific CO_2 emission has increased by 53% in variation V2b compared to variation V2a. Due to the low availability of FOP at low formaldehyde production but, on the other and due to the minimum allowed capacity of the turbine natural gas had to be used to keep the turbine above this lower operational level. Therefore the CO_2 emission increases due to the higher amount of natural gas in use, whereas the combustion of the FOP does not generate CO_2.

3.2 Variation 3

In variation 3 (V3) the process functionality of the model has been tested experimentally under the condition that the quantities of water vapor are limited as a function of capacity of formaldehyde line F2 (Fig.4). The weakness observed is that the production of formalin is relatively low in comparison to variation 2. Table 2 shows data for calculation of CO_2 emissions while taking into account emissions for purchased electricity as well.

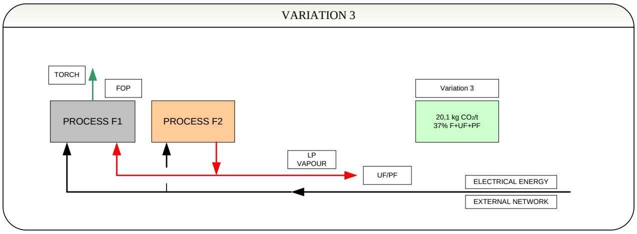

Figure 4: Gas and energy flows for variation 3. The parallel operation of the two formalin processes F1 and F2 enables the production of formalin, UF, and PF resins.

Table 2 shows data for calculation of CO_2 emissions under consideration of emissions due to the generation of the supplied electrical energy.

Table 2: CO_2 emissions for variation 3

LABEL	TOTAL PRODUCTION F+UF+PF (t/day)	SPECIFIC CONSUPTION OF NATURAL GAS (Nm3/t)	SPECIFIC EMISSION OF CO_2 BASED ON PRODUCTS (kg/t)
V3	649	0	20,1

4 Conclusion

The paper demonstrates that the possibilities of energetic integration and optimization of parallel running processes in the formaldehyde production are realistic and feasible. It also could be shown that a simultaneous reduction of environmental burden with special emphasis on reduction of CO_2 emissions is possible. Basic theoretical considerations as well as practical test runs enabled the further developments of the formaldehyde production process; this includes investments and processes for the transformation and use of excess thermal energy as well as the use of gaseous side streams (off-gases) of the formaldehyde process for direct generation of electrical energy during the formalin production processes.

References

[1] J Frederic Walker, Formaldehyde, New York: Reinhold Publ. Corp, 1964 3rd ed.

[2] Shaun M. Williams, Kenneth R. Rodriguez, Shannon Teeters-Kennedy, Amanda D. Stafford, Sarah R. Bishop, Ushani K. Lincoln, and James V. Coe, Use of the Extraordinary Infrared Transmission of Metallic Subwavelength Arrays To Study the Catalyzed Reaction of Methanol to Formaldehyde on Copper Oxide, The Journal of Physical Chemistry B 2004 108 (31), 11833-11837

[3] Ipatief, V.N., Monroe,G. S., J. Am. Chem. Soc., 1945, 67 , 2166-71.

[4] Newton, R. R., in Dodge, B. F., J. Am. Chem. Soc., 1933, 55, 4747.

[5] Rodney N. Hader, R. D. Wallace, R. W. McKinney, Formaldehyde from methanol, Ind. Eng. Chem., 1952, 44 (7), pp 1508–1518

10TH International Conference on Sustainable Energy and Environmental Protection (June 27TH – 30TH, 2017, Bled, Slovenia), Energy Efficiency
J. Krope, A.Ghani Olabi, D. Goričanec & S. Božičnik

Study of CNF Coating for Pool-Boiling and Condensation

Shoukat Alim Khan, Adnan Ali, Muataz A. Hussien & Muammer Koc

Abstract Condensation and boiling are effective phase change heat transfer processes with a wide range of application form daily life to industrial scale i.e. power generation, distribution, heating, cooling, refrigeration and air-conditioning; turbines/turbo-machinery, desalination, refinery, chemical/food processing, waste heat recovery; renewable energy technologies (concentrated photovoltaics, fuel cells, batteries, etc.). Copper (Cu) and Stainless steel are most common metals used for heat exchangers in industrial applications. Due to poor efficiency of condensation and boiling heat exchangers and its wide range of application a small enhancement in this area have significant impacts on energy efficiency. Both phenomena are surface based and depends on common surface properties i.e. thermal conductivity, wettability, porosity, roughness. Surface coating is an effective and robust solution for surface modification and Carbon nano fibers (CNF) have favourable properties to improve both boiling and condensation. In our study, CNF has coated on Cu, aluminium (Al) and stainless steel (SS 316) using electro-spinning technique. CNF has dispersed with PVA using ultrasonication in 4:1. Poor adhesion of resulted coating on substrate has been observed. This issue is overcome by incorporating metallic nano-particles into the solution. Solution has been modified with silver nano-particles which resulted in enhanced adhesion after heat treated at 500°C in inert environment. Both contact angle for the resultant surfaces were studied as wettability is the main parameter in boiling and condensation phenomena. Enhanced boiling and condensation heat transfer results are predictable due to combined effect of CNF/Ag nano-particles.

Keywords: • Carbon nano fibers • phase change • heat transfer • pool boiling •

Correspondence Address: Shoukat Alim Khan, Ph.D. Candidate, Hamad Bin Khalifa University (HBKU), Sustainable Development Division, Qatar Foundation, Education City, Doha, Qatar, e-mail: shokhan@hbku.edu.qa. Adnan Ali, Ph.D., Post-Doc, QEERI, Hamad Bin Khalifa University (HBKU), Qatar Foundation, Education City, Doha, Qatar, e-mail: adali@hbku.edu.qa. Muataz A. Hussien, Ph.D., Associate Professor and Senior Scientist, QEERI, Hamad Bin Khalifa University (HBKU), Qatar Foundation, Education City, Doha, Qatar, e-mail: mhussien@qf.org.qa. Muammer Koc, Ph.D., Professor, Hamad Bin Khalifa University (HBKU), Qatar Foundation, Education City, Doha, Qatar, e-mail: mkoc@hbku.edu.qa.

https://doi.org/10.18690/978-961-286-050-9.43 ISBN 978-961-286-050-9

Available at: http://press.um.si.

1 Introduction

Boiling is a multiphase and efficient energy transfer process and is used where a high amount of heat is used to be transferred in confined space [1]. Boiling heat transfer have a vast range of application such as desalination [2], [3], nuclear power plant [4], [5], thermal management data centers and electronic circuit cooling [6]–[8], and microfluidic systems [9]–[11]. Therefore, a small improvement in this area leads to high energy impacts. Heat transfer substrate, its surface, and working fluid are three main variables that can be modified to enhance the overall boiling heat transfer. In most of the cases such as desalination and steam power cycle, it is not possible to change the working fluid so surface modification remains as one of the main variables to enhance the overall process.

Compared to the subtractive modification techniques, the surface coating provides a robust and efficient solution to boiling heat transfer enhancement. Surface modification techniques for boiling can be classified as : (1) chemical processes (oxidation, etching and photochemical etching [12]–[15]) (2) mechanical shaping processes (machining and/or deforming using roughness tools, CNC, laser machining and sandblasting techniques (3) [16]–[18]), surface coating processes (CVD, PVD, spraying, plasma), and (4) MEMS/NEMS techniques [46–48].

Thermal conductivity, wettability and nucleation sites on the heating surface are three main variables in boiling heat transfer enhancement. Hydrophilic surfaces enhance the critical heat flux (CHF) of boiling surface by delaying its dry-out condition, while hydrophobic surface helps in starting of bubbles nucleation phenomena and work as nucleation points for bubbles generation [22]–[24]. Similarly, nanoparticles coating enhances the pool boiling phenomena by working as nucleation points for bubbles generation [25], [26].

This material has high potential in heat transfer research due to its high thermal conductivity [20], [27], [28]. Tuzovskaya et al. [29] measure the thermal conductivity for CNF coating on SS, and reported a range of enhancement from 30% to 75%. These properties make CNF a promising material for boiling heat transfer enhancement. Polymers coatings are usually hydrophobic in nature and have high thermal resistance, specifically at high thickness [30].

In order to modify surfaces of heat exchangers, according to the enhancement requirements of pool boiling phenomena, highly conductive CNF and PVA polymer have been coated on Cu, SS316, and Al substrates. To have thin film coating, electrospinning is used as the coating technique. Also, Silver nanoparticles have been added to PVA and CNF coating on the second step, as these Ag nanoparticles act as nucleation points for bubbles generation in nucleate pool boiling. In order to study the resultant wettability of the surface contact angle has been measured for these experiments.

2 Experiment

CNF (from sigma Aldrich) and PVA, in 1:4 by mass, has been dispersed in water using an ultrasonication probe, (vibra-cell) from Sonics&Materials, for 30 minutes at 60 kHz and 450 watts with a 3s pulse, 1s wait cycles. In another coating, AgNO3 has been added to the solution i.e. CNF: PVA: AgNO3 in 1:4:4 by mass and solution has been prepared by ultrasonication repeated above conditions. Thin Film of PVA: CNF has been achieved by electrospinning at the conditions of $\Delta V = -20.9$, volume flow rate of o.3 ml/hour, nozzle size of 80 μm and the distance between nozzle and substrate of 8 cm. For a thin film of PVA: CNF: AgNO3 these conditions were reported as $\Delta V = -21.4$, volume flow rate of 0.4 ml/hour, nozzle size of 80 μm and the distance between nozzle and substrate of 6 cm. To ensure uniform coating thickness, all three types of samples i.e. Cu, SS316 and Al, were placed for coating deposition for the same time in each run of the experiment. Although the coating thickness for both types of films is not comparable due to different coating time and coating conditions. CNF: PVA coating were performed for 10 minutes while CNF: PVA: AgNO3 coating time was performed for 2 minutes only due to frequent nozzle jam in the case of CNF: PVA: AgNO3 coating.

To perform thermal decomposition of AgNO3 to Ag, the samples were heated treated in a tube furnace under Nitrogen (N_2). The samples were first heated to 100 ^{0}C at the rate of 10^{0}C/min for 10 minutes to remove water by evaporation. And then heated to 460 ^{0}C at the rate of 10^{0}C/min and kept for 3 hours at this temperature, to ensure complete thermal decomposition of AgNO3.

3 Results

In order to investigate the wettability of these modified surface contact angle has been measured using rame'-hart, instrument co. as shown in Table 1. The contact angle and hence hydrophobicity can be observed to increase in both cases of PVA: CNF and PVA: CNF: Ag coating. Although the coating time and hence thickness of PVA: CNF: Ag is several times lower than PVA: CNF as observed from coating time and visual observation but the increase in contact angle PVA: CNF: Ag is almost equivalent. This indicates higher hydrophobicity of PVA: CNF: Ag coating as compared to PVA: CNF coating due to the presence of Ag nanoparticles. Strong adhesion was observed for PVA: CNF: Ag coating as compared to PVA: CNF, but no standard test was performed.

Table 1: Contact angle for Cu, SS316 and Al substrate after heat treated at 460 ^{0}C under inert condition.

Substrate	Uncoated surface	PVA:CNF coated samples	PVA:CNF:Ag coated samples
Cu	50.2	57.7	56.5
SS316	55.3	66.5	60.4
Al	61	73.2	66.5

4 Conclusion

Both enhancement in thermal conductivity and hydrophobicity were resulted from these coatings. Also, Ag particles act as nucleation source for bubble nucleation in pool boiling and hence enhanced the overall boiling phenomena. Keeping in view these behaviors of above coating, enhanced results are expected for pool boiling.

References

[1] A. R. Betz, J. Xu, H. Qiu, and D. Attinger, "Do surfaces with mixed hydrophilic and hydrophobic areas enhance pool boiling?," *Appl. Phys. Lett.*, vol. 97, no. 14, pp. 14–16, 2010.

[2] G. Hetsroni, J. . Zakin, Z. Lin, A. Mosyak, E. . Pancallo, and R. Rozenblit, "The effect of surfactants on bubble growth, wall thermal patterns and heat transfer in pool boiling," *Int. J. Heat Mass Transf.*, vol. 44, no. 2, pp. 485–497, Aug. 2001.

[3] C. Bartoli and F. Baffigi, "Effects of ultrasonic waves on the heat transfer enhancement in subcooled boiling," *Exp. Therm. Fluid Sci.*, vol. 35, no. 3, pp. 423–432, Apr. 2011.

[4] L. Zhang and M. Shoji, "Nucleation site interaction in pool boiling on the artificial surface," *Int. J. Heat Mass Transf.*, vol. 46, no. 3, pp. 513–522, Jan. 2003.

[5] D. Ciloglu and A. Bolukbasi, "A comprehensive review on pool boiling of nanofluids," *Appl. Therm. Eng.*, vol. 84, pp. 45–63, Jun. 2015.

[6] A. Jaikumar and S. G. Kandlikar, "Enhanced pool boiling for electronics cooling using porous fin tops on open microchannels with FC-87," *Appl. Therm. Eng.*, vol. 91, pp. 426–433, 2015.

[7] A. Kalani and S. G. Kandlikar, "Enhanced Pool Boiling With Ethanol at Subatmospheric Pressures for Electronics Cooling," *J. Heat Transfer*, vol. 135, no. 11, p. 111002, Sep. 2013.

[8] A. Schubert, M. Zinecker, M. Hackert-Oschätzchen, M. Lausberg, and A. Schulz, "Application of nucleate boiling with micro structured surfaces for electronic cooling," *PCIM Eur. Conf. Proc.*, no. May, pp. 1141–1148, 2014.

[9] H. A. Mohammed, G. Bhaskaran, N. H. Shuaib, and R. Saidur, "Heat transfer and fluid flow characteristics in microchannels heat exchanger using nanofluids: A review," *Renew. Sustain. Energy Rev.*, vol. 15, no. 3, pp. 1502–1512, Apr. 2011.

[10] T. Dixit and I. Ghosh, "Review of micro- and mini-channel heat sinks and heat exchangers for single phase fluids," *Renew. Sustain. Energy Rev.*, vol. 41, pp. 1298–1311, Jan. 2015.

[11] A. Mohammed Adham, N. Mohd-Ghazali, and R. Ahmad, "Thermal and hydrodynamic analysis of microchannel heat sinks: A review," *Renew. Sustain. Energy Rev.*, vol. 21, pp. 614–622, May 2013.

[12] H. S. Ahn, G. Park, J. M. Kim, J. Kim, and M. H. Kim, "The effect of water absorption on critical heat flux enhancement during pool boiling," *Exp. Therm. Fluid Sci.*, vol. 42, pp. 187–195, Oct. 2012.

[13] H. S. Ahn, C. Lee, J. Kim, and M. H. Kim, "The effect of capillary wicking action of micro/nano structures on pool boiling critical heat flux," *Int. J. Heat Mass Transf.*, vol. 55, no. 1–3, pp. 89–92, Jan. 2012.

[14] H. S. Ahn, C. Lee, H. Kim, H. Jo, S. Kang, J. Kim, J. Shin, and M. H. Kim, "Pool boiling CHF enhancement by micro/nanoscale modification of zircaloy-4 surface," *Nucl. Eng. Des.*, vol. 240, no. 10, pp. 3350–3360, Oct. 2010.

[15] S.-W. Chen, J.-C. Hsieh, C.-T. Chou, H.-H. Lin, S.-C. Shen, and M.-J. Tsai, "Experimental investigation and visualization on capillary and boiling limits of micro-grooves made by

different processes," *Sensors Actuators A Phys.*, vol. 139, no. 1–2, pp. 78–87, Sep. 2007.

[16] R. Jenkins, R. Lupoi, R. Kempers, and A. J. Robinson, "Heat transfer performance of boiling jet array impingement on micro-grooved surfaces," *Exp. Therm. Fluid Sci.*, vol. 80, pp. 293–304, Jan. 2017.

[17] J. Y. Ho, K. K. Wong, K. C. Leong, and C. Yang, "Enhanced Nucleate Pool Boiling From Microstructured Surfaces Fabricated by Selective Laser Melting," in *Volume 1: Micro/Nanofluidics and Lab-on-a-Chip; Nanofluids; Micro/Nanoscale Interfacial Transport Phenomena; Micro/Nanoscale Boiling and Condensation Heat Transfer; Micro/Nanoscale Thermal Radiation; Micro/Nanoscale Energy Devices and Systems*, 2016, p. V001T04A008.

[18] A. D. Sommers and K. L. Yerkes, "Using micro-structural surface features to enhance the convective flow boiling heat transfer of R-134a on aluminum," *Int. J. Heat Mass Transf.*, vol. 64, pp. 1053–1063, Sep. 2013.

[19] J. Mitrovic, "How to create an efficient surface for nucleate boiling?," *Int. J. Therm. Sci.*, vol. 45, no. 1, pp. 1–15, Jan. 2006.

[20] S. Launay, A. G. Fedorov, Y. Joshi, A. Cao, and P. M. Ajayan, "Hybrid micro-nano structured thermal interfaces for pool boiling heat transfer enhancement," *Microelectronics J.*, vol. 37, no. 11, pp. 1158–1164, Nov. 2006.

[21] M. Zhang and K. Lian, "Using bulk micromachined structures to enhance pool boiling heat transfer," *Microsyst. Technol.*, vol. 14, no. 9–11, pp. 1499–1505, Oct. 2008.

[22] J. S. Lee and J. S. Lee, "Conjugate heat transfer analysis for the effect of the eccentricity of hydrophobic dot arrays on pool boiling," *Appl. Therm. Eng.*, vol. 110, pp. 844–854, Jan. 2017.

[23] H. Bostanci and N. E. Joshua, "Nucleate Boiling of Dielectric Liquids on Hydrophobic and Hydrophilic Surfaces," in *Volume 8A: Heat Transfer and Thermal Engineering*, 2015, p. V08AT10A036.

[24] S. Gong and P. Cheng, "Lattice Boltzmann simulations for surface wettability effects in saturated pool boiling heat transfer," *Int. J. Heat Mass Transf.*, vol. 85, pp. 635–646, Jun. 2015.

[25] C. M. Patil and S. G. Kandlikar, "Pool boiling enhancement through microporous coatings selectively electrodeposited on fin tops of open microchannels," *Int. J. Heat Mass Transf.*, vol. 79, pp. 816–828, Dec. 2014.

[26] A. Jaikumar and S. G. Kandlikar, "Enhanced pool boiling heat transfer mechanisms for selectively sintered open microchannels," *Int. J. Heat Mass Transf.*, vol. 88, pp. 652–661, Sep. 2015.

[27] K.-J. Park and D. Jung, "Enhancement of nucleate boiling heat transfer using carbon nanotubes," *Int. J. Heat Mass Transf.*, vol. 50, no. 21–22, pp. 4499–4502, Oct. 2007.

[28] M.-S. Liu, M. Ching-Cheng Lin, I.-T. Huang, and C.-C. Wang, "Enhancement of thermal conductivity with carbon nanotube for nanofluids," *Int. Commun. Heat Mass Transf.*, vol. 32, no. 9, pp. 1202–1210, Oct. 2005.

[29] I. Tuzovskaya, S. Pacheco Benito, J. K. Chinthaginjala, C. Reed, L. Lefferts, and T. van der Meer, "Heat exchange performance of stainless steel and carbon foams modified with carbon nano fibers," *Int. J. Heat Mass Transf.*, vol. 55, no. 21–22, pp. 5769–5776, Oct. 2012.

[30] B. J. Zhang, C. Kuok, K. J. Kim, T. Hwang, and H. Yoon, "Dropwise steam condensation on various hydrophobic surfaces: Polyphenylene sulfide (PPS), polytetrafluoroethylene (PTFE), and self-assembled micro/nano silver (SAMS)," *Int. J. Heat Mass Transf.*, vol. 89, pp. 353–358, 2015.

10TH INTERNATIONAL CONFERENCE ON SUSTAINABLE ENERGY AND ENVIRONMENTAL PROTECTION (JUNE 27TH – 30TH, 2017, BLED, SLOVENIA), NUCLEAR ENERGY
J. Krope, A.Ghani Olabi, D. Goričanec & S. Božičnik

The Effects of Zirconium on the Microstructure and Mechanical Properties of FeCrAl Alloys For 4r Generation Nuclear Power Plants

VICTOR GEANTĂ, IONELIA VOICULESCU, ADRIAN DAN JIANU & HORIA BINCHICIU

Abstract FeCrAl alloys microalloyed with Zr can be regarded as potential materials for use in 4R generation nuclear power plants, operating in molten lead or lead-bismuth mixture. Limited quantities of Zr, Ti, Y, Hf, Ce in the range of 1-3 %wt. were introduced to improve the mechanical characteristics of the FeCrAl alloys and of the oxide layer. The effectiveness of Zr stems from the fact that it quickly penetrates the scale, by changing its morphology (the columnar structure is replaced by small equiaxed grains), while preventing the formation of chromium carbides located on grain boundaries. FeCrAl alloys microalloyed with Zr were prepared using a VAR (Vacuum Arc Remelting) unit, at 5 x 10-3 mbar and in high purity argon atmosphere. Four different experimental alloys were prepared using the metallic matrix of Fe-14Cr-5Al, by adding 0.5%wt Zr - 2%wt Zr. The microhardness values of the experimental alloys were in the range of 156 ... 166 HV0.2. The chemical composition on the oxide layer and the microstructural features were evidenced by EDAX-SEM analysis. The results showed the effect of Zr of forming a continuous oxide layer, Al and Zr-rich, on the surface of the FeCrAl alloy.

Keywords: • FeCrAl • zirconium • microstructure • • 4R generation nuclear • nuclear plant •

CORRESPONDENCE ADDRESS: Victor Geantă, Ph. D. Professor, University Politehnica of Bucharest, Faculty of Materials Science and Engineering, Splaiul Independenței 313, 060402, Bucharest, Romania, e-mail: victorgeanta@yahoo.com. Ionelia Voiculescu, Ph.D. Professor, University Politehnica of Bucharest, Faculty of Engineering and Management of Technological Systems, Splaiul Independenței 313, 060402, Bucharest, Romania, e-mail: ioneliav@yahoo.co.uk. Adrian Dan Jianu, Ph.D., Karlsruhe Institute of Technology, Institute for Pulsed Power and Microwave Technology (IHM), B630, Hermann-von-Helmholtz-Platz 1, 76344 Eggenstein-Leopoldshafen, Karlsruhe, Germany, e-mail: adrian.jianu@kit.edu. Horia Binchiciu, Ph.D., SUDOTIM AS, 300223 Bulevardul Mihai Viteazul, nr. 30, Timișoara, Romania, e-mail: sudotim_suport@yahoo.com.

https://doi.org/10.18690/978-961-286-050-9.44 ISBN 978-961-286-050-9

Available at: http://press.um.si.

1 Introduction

The change in the operating principle of generation IV nuclear power plants brought to the forefront the problem of more efficient metallic materials than the existing ones, and which can ensure high resistance to thermal stress, radiation and corrosive environments. Metals with low melting temperature (lead or lead-bismuth eutectic) were proposed as coolant fluids for the new types of nuclear power plants. In such conditions, the requirements for the set characteristics are stricter due to their erosive and corrosive effects on the superficial layers of metallic alloys composing the structure of the reactor. Since functional specifications stipulate operating periods of 25 to 30 years without any intervention, the new metallic materials must have a permanent capacity to form regenerative oxide layers on the surface that comes in direct contact with the metallic molten environment [1-5]. The results obtained in this area showed that stainless steels with Ni content (austenitic or ferritic/martensitic) do not behave sufficiently well in the new operating conditions, although they have the appropriate strength [6-7]. As a result, the specialists in the nuclear field opted for FeCrAl alloys, Ni-free and with low carbon content (less than 0.1 wt% C), which both behave well at high temperatures (400-800^{o}C) and meet the complex corrosion and erosion demands in a liquid metal environment [7-12]. An important issue in the development of new alloys is the establishment of optimal chemical compositions that ensure proper values for mechanical and corrosion resistance.

Therefore, compared with the usual ferritic stainless grades, in the FeCrAl alloys the aluminium content was increased to 6-8%wt Al, in order to form an oxide layer on the metallic surface, which ensures a good barrier against the specified operating conditions. There are known a lot of patents [U.S. Patent, 10] and papers [11-20] which present ferritic FeCrAl alloys with additions of rare earth and other alloying elements such as Mo, Si, Ti, Mn and with low content of impurities (C, N, O, S, P less than 0.05%) or alloying elements such as Ni, Cu (below 0.5%), Mg, Ca (below 0.005%). The low values of these alloying elements are required to avoid the negative influence on the oxide coating adhesion and to prevent the interference with the aluminium oxide surface, the formation of the alumina whiskers [16-18]. The addition of small amounts (<1wt%) of reactive elements, especially rare earths (Zr, Ha, Y), allows the increase of the chromium dioxide adhesion and of the oxidation resistance of these alloys by decreasing the oxidation rates [14, 18-20]. The most important effect of Zr in the FeCrAl alloy is the prevention of the Cr carbide formation on the grain boundaries and the suppression of the formation of oxides [19, 20].

Zr is probably responsible for the improvement of the oxide layer adherence on the FeCrAlY alloy during long term cyclic oxidation tests, allowing the extension of the lifetime in high temperature conditions [20].

The paper shows the microstructural features and mechanical properties of some experimental Fe14Cr5Al alloys by adding 0.5 wt% Zr to 2 wt% Zr. There was studied the microstructure of the oxide layer, the elemental distribution in the oxide layers and the micro-hardness values for different concentrations of Zr. The superficial oxide layers are alumina-rich and contain Zr-rich compounds that contribute to increasing their adhesion.

2 Designing and obtaining FeCrAl alloys microalloyed with Zr

The aims of the research were to design and obtain FeCrAl alloys microalloyed with zirconium as mini-ingot, using a VAR (Vacuum Arc Remelting) furnace, in order to analyse the microstructure and the mechanical characteristics. The samples were designed and manufactured in the ERAMET laboratory, at the Politehnica University of Bucharest, Material Science and Engineering Faculty using a MRF ABJ 900 furnace [14] (www.eramet.wix.com/eramet).

Four experimental FeCrAl alloys were obtained, with different contents of zirconium: 0.5%wt Zr, 1.0%wt Zr 1.5%wt Zr and 2.5%wt Zr, added into the same metallic matrix of the Fe14Cr5Al experimental alloy.

In order to obtain the high alloyed material, high purity alloying elements were introduced into the base material, high purity "extra soft" steel: metallic chromium 99.5 % Cr; electrolytic aluminium 99.4 % Al; 99.5 % pure zirconium.

The raw material on the plate of the VAR equipment is presented in fig. 1. After obtaining the stable vacuum of $1x10^{-4}$ mBar, the furnace chamber was filled with argon (Ar 5.3) to insure the electric arc stability. Each mini-ingot was remolten and solidified six times, in order to obtain the microstructural homogeneity (figure 2). The assimilation coefficient for this particular alloy class was over 99.75 %, due to the low vapour losses of the components in the electric arc remelting process. The mini-ingots had quasi-constant weight (39.83g – 39.97 g) (table 1).

Figure 1. Raw material on the plate of the VAR equipment

Figure 2. FeCrAl mini-ingot alloyed with Zr obtained in VAR equipment

Table 1. The assimilation efficiency and the weight values for each experimental batch and mini-ingot

Sample code	Initial batch weight, g	Mini-ingot weight, g	Assimilation efficiency, $(G_{ing.}/G_{ch.})$x100, %	Global efficiency, %
NUC 4 - Fe-14Cr-5Al-0.5Zr	40.0	39.97	99.92	99.75
NUC 5 - Fe-14Cr-5Al-1.0Zr	40.0	39.92	99.80	
NUC 6 - Fe-14Cr-5Al-1.5Zr	40.0	39.83	99.57	
NUC 7 - Fe-14Cr-5Al-2.5Zr	40.0	39.88	99.72	

3 Results and discussions

Each cross section cut from the mini-ingots was processed according to the metallographic procedure using abrasive grit paper, followed by a final polishing using alumina alpha powder. The metallographic analysis was performed with the aim of highlighting the microstructural characteristics of the experimental alloys, in order to estimate the distribution of the chemical elements in the superficial oxide layer [14, 18].

The microstructural analysis was conducted using a scanning electron microscope FEI QUANTA INSPECT F provided with an electron gun with field emission - EGF with a resolution of 1.2 nm and an X-ray spectrometer energy dispersive (EDS) with resolution of 133 eV at MnK [18].

3.1 Chemical composition and microstructural analysis

The chemical composition of the samples was determined by EDAX analysis in four successive zones (point 1 located on the surface layer, point 2 located at approximately 50 µm below the surface, point 3 located at approximately 90 µm and point 4 located in the middle of the sample), in accordance with figure 3. The chemical analysis values obtained for the four samples NUC 4 – NUC 7 in the centre zone (point 4) of the cross section samples are shown in Table 2.

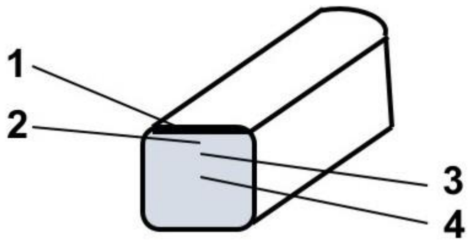

Figure 3. Location of chemical analysis in cross sections of FeCrAlZr alloys

Table 2. Chemical composition of alloying elements in the centre of the samples

Chemical composition, % wt							
NUC 4		**NUC 5**		**NUC 6**		**NUC 7**	
O K	0.7	O K	0.73	O K	0.65	O K	0.75
Al K	4.86	Al K	4.71	Al K	5,05	Al K	5.62
Cr K	14.69	Cr K	15	Cr K	14.66	Cr K	14.29
Fe K	79.75	Fe K	79.23	Fe K	78.17	Fe K	77.23
Zr K	-	Zr K	0.33	Zr K	1.47	Zr K	2.11

The concentration analysis of chemical elements in the centre of the samples (point 4) shows good concordance between the design of the FeCrAl alloyed with Zr and the chemical composition of each separate batch. The zirconium concentration of the sample NUC 4 is below the detection limit of the equipment used. Due to its strong affinity to oxygen, zirconium migrated into the surface layer of the mini-ingot. The increase of the Zr content in the composition of the batch leads to the increase of the Zr content in the centre of the sample. Table 3 shows the chemical compositions of the edge zone of the cross section for the four samples (point 1, figure 3). It is noted that the superficial layer contains high amounts of oxygen that will contribute to the formation of the regenerative alumina-rich layer, having beneficial influence on the behaviour of the material in the molten lead medium (figures 4-9).

Table 3. Chemical compositions in the edge zone of the cross section

Chemical composition, % wt							
NUC 4 (0.5%wt Zr)		**NUC 5** (1.0%wt Zr)		**NUC 6** (1.5%wt Zr)		**NUC 7** (2%wt Zr)	
O K	27.46	O K	38.37	O K	40.63	O K	36.08
Al K	58.43	Al K	40.11	Al K	35.7	Al K	30.34
Cr K	2	Cr K	0.36	Cr K	0.96	Cr K	0.63
Fe K	8.87	Fe K	0.73	Fe K	2	Fe K	1.71
Zr K	0.95	Zr K	20.43	Zr K	20.71	Zr K	31.24

The chemical composition of the edge zone of the samples microalloyed with zirconium indicates that the value of the Zr content increases with the increase of the zirconium amount in the alloy. This value decreases in the direction of points 1 to 4 due to the migration of this element towards the marginal zone, where it combines with the oxygen dissolved in the sample. Because of the simultaneous presence of the two elements with very high affinity for oxygen (aluminium and zirconium), complex oxides of Al and Zr are formed in the marginal crust and their share is given by the amounts of these elements in the alloy. For sample NUC 7, wherein the contents of Al and Zr are similar, the chemical element distribution is relatively similar. The superficial oxide layer, which contains mainly aluminium and zirconium, has different thicknesses. Thus, the thickness ranges from 4.668 μm for sample NUC 4 to 32.1 μm for sample NUC 5. The SEM images of the cross sections through the superficial layer for samples NUC 4 and NUC 7 are shown in figures 4 to 7. Depending on the amount of Zr, the oxide layer thickness is different.

The elemental distribution of the elements present in the surface layer shows the correlation between the amounts of elements present in the oxide layer for each sample separately, i.e. Fe, Cr, Al, Zr. Distribution image of X-radiation relative intensity for the main chemical elements detected by EDS analysis: AlKα, CrKα, FeKα, ZrKα and OKα (sample NUC 5) is shown in Figure 8.

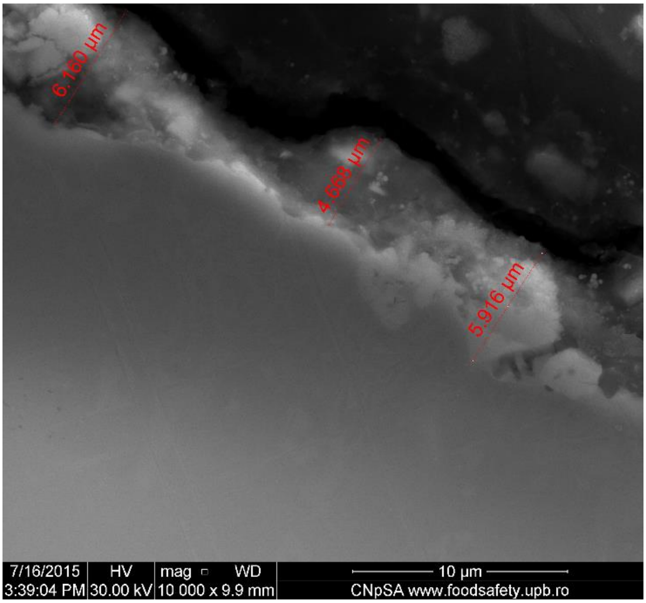

Fig. 4. Oxide layer for sample NUC 4

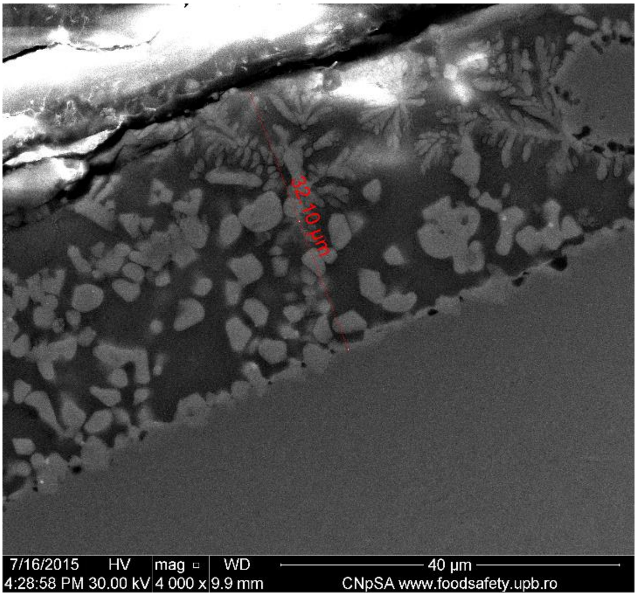

Fig. 5. Oxide layer for sample NUC 5

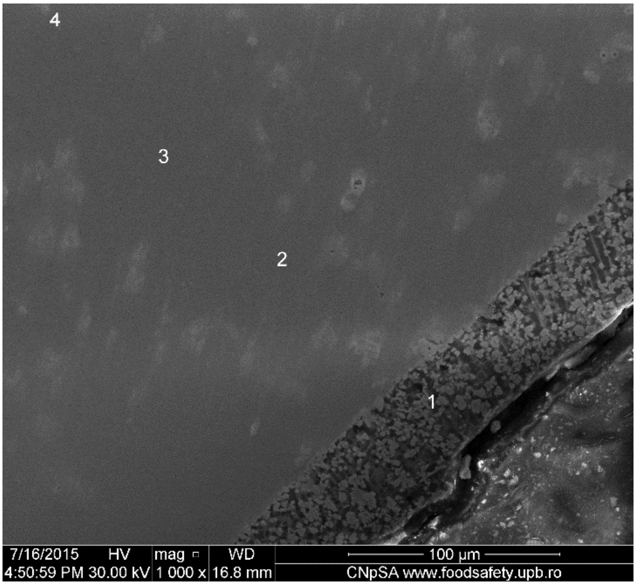

Fig. 6. Oxide layer for sample NUC 6

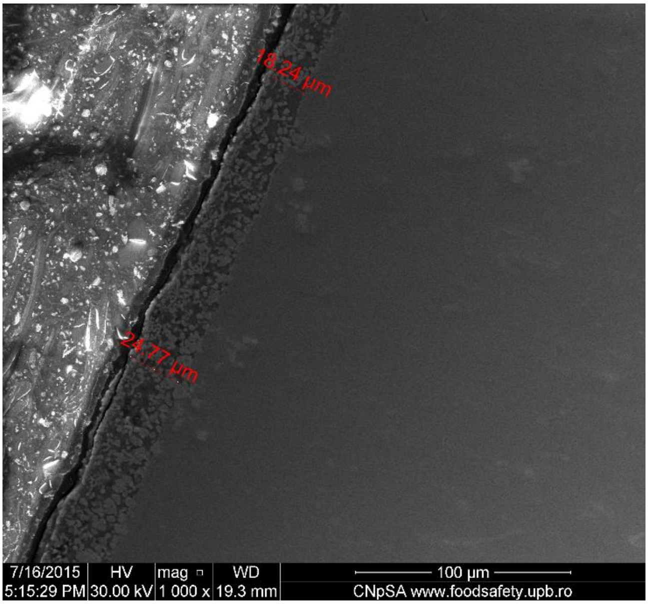

Fig. 7. Oxide layer for sample NUC 7

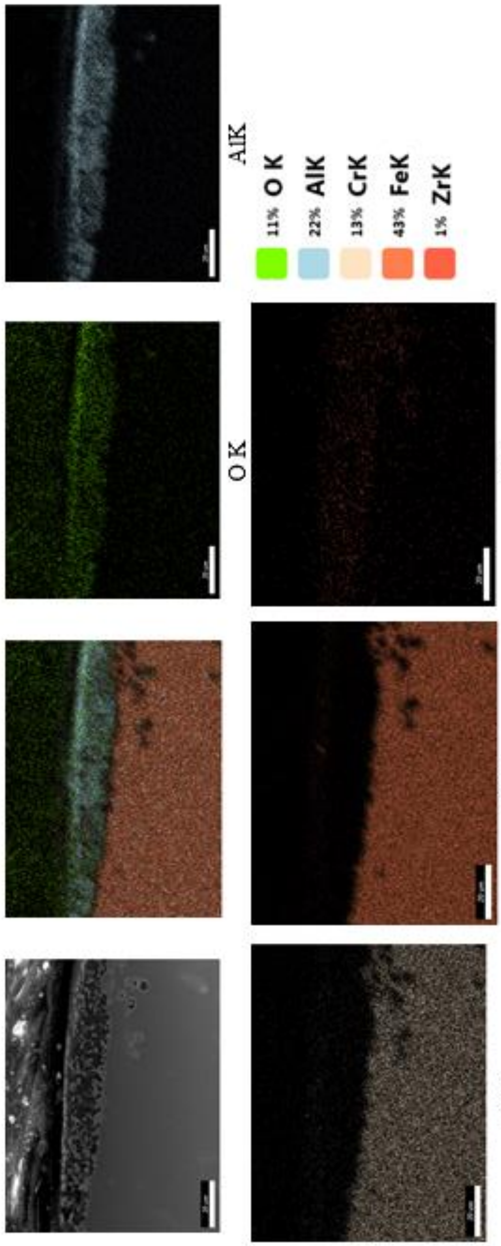

Figure 8. Distribution of the chemical elements in the oxide layer in the case of sample the NUC 5

3.2 Microhardness measurements

Microhardness measurements $HV_{0.2}$ were carried out using a Shimadzu HMV 2TE testing machine, with a measuring force of 1.9614 N, measurement duration of 10 seconds and an extended relative uncertainty of 1.2%. The microhardness measurement results for the four analysed samples are presented in Table 4.

Table 4. Microhardness values ($HV_{0.2}$)

Sample	Individual values*	Average value, $HV_{0,2}$
NUC 4 – Fe-14Cr-5Al-0.5Zr	160, 156, 162, 159, 156	159
NUC 5 – Fe-14Cr-5Al-1.0Zr	153, 155, 157, 161, 154	156
NUC 6 – Fe-14Cr-5Al-1.5Zr	158, 159, 160, 157, 168	160
NUC 7 – Fe-14Cr-5Al-2.5Zr	157, 170, 164, 171, 166	166

*The measurements were carried out on the cross sections of the mini-ingots, in diagonal line through the central zone, at distances of at least 1000 microns between indentations.

The primary analysis of the experimental data shows that there is a quasi-constancy of the microhardness values, which reflects an increased homogeneity of all samples obtained in the VAR equipment. There can be observed, for all the samples, that there is a narrow variation of the microhardness values, in the range of 156-166 HV0.2, solely due to the influence of the alloying elements in the metal alloy composition and to the uniform layout of the constituents in the metal matrix. The Vickers microhardness values of these alloys are similar to those of alloys microalloyed with hafnium, titanium and yttrium [14, 18]. Furthermore, there is a slight upward trend of the microhardness with the increase of the Zr content in the chemical composition of the alloy.

4 Conclusions

The research is aimed at obtaining and characterizing the FeCrAl alloys, microalloyed with zirconium, potentially usable in nuclear power plants (generation 4R, type LRF). To highlight the effect of alloying with zirconium on the mechanical and microstructural characteristics of the alloys, especially on the superficial oxide layers, four samples of FeCrAl alloys with variable content of zirconium (0.5 %wt Zr, 1.0 %wt Zr 1.5 % wt Zr and 2%wt Zr) were obtained. The distribution of Zr in the alloy is homogenous, the content in this element in the superficial layer of oxide increases with the increase of the Zr content in the alloy.

The micro-structural aspect of the superficial layer in the cross section shows the presence of two main oxides (alumina and zirconia) whose proportions are given by the concentration of these elements in the compositions of alloys. The general appearance of the oxide layer in the cross section indicates the presence of zirconium oxide formations in an amorphous matrix of alumina. The oxide thickness is variable, ranging from 4.668 μm in sample NUC 4 to 32.1 μm in sample NUC 5.

The micro-hardness values for FeCrAl alloys microalloyed with zirconium are within the range of 156-166 HV0.2, the normal limits for these materials. This value is mainly due to the influence of the alloying elements in the metal alloy composition and to the uniform distribution of the metallographic constituents in the metal matrix.

Acknowledgements

The research work was financially supported by the Romanian National Program for Research within the framework of the Project No.” PCCA 243/2014 Advanced Metallic Materials used for the New Generation of Nuclear Power Plant 4R – NUCLEARMAT.

References

[1] Caro, M., Woloshun, K., Rubio, F., Maloy, S. Materials Selection for the Lead-Bismuth Corrosion and Erosion Tests in DELTA Loop, Advanced SMR Materials Development, Small Modular Reactors Research and Development Program, Los Alamos National Lab. (2013);

[2] Kurata, Y., Saito, S. Temperature Dependence of Corrosion of Ferritic/Martensitic and Austenitic Steels in Liquid Lead-Bismuth Eutectic. Materials Transactions, Vol. 50, No. 10 (2009) p. 2410;

[3] Yaskiv, O.I., Fedirko, V.M. Oxidation/Corrosion Behaviour of ODS Ferritic/Martensitic Steels in Pb Melt at Elevated Temperature. International Journal of Nuclear Energy, Volume 2014;

[4] Allen, T. R., Crawford D. C. Lead-Cooled Fast Reactor Systems and the Fuels and Materials Challenges. Science and Technology of Nuclear Installations, (2007) Article ID 97486;

[5] M. Del Giacco, M.D. Weisenburger A., Spieler P., Zimmermann F., Lang F., Jianu A., Mueller G., Experimental equipment for fretting corrosion simulation in heavy liquid metals for nuclear applications, Wear 280– 281 (2012) p.46;

[6] Pillis, M.F., Correa, O.V., De Araújo E.G., Ramanathan, L.V. Oxidation Behavior of FeCr and FeCrY Alloys Coated with an Aluminium Based Paint, Materials Research, Vol. 11, No. 3, pp. 251-256, 2008;

[7] Lim, J., Nam, H.O., Hwang, I.S., Kim, J.H., A study of early corrosion behavior of FeCrAl alloys in liquid lead–bismuth eutectic environments, Journal of Nuclear Materials 407 (2010) p.205–210;

[8] Lim, J., Hwang, I.S., Kim, J.H. Design of alumina forming FeCrAl steels for lead or lead–bismuth cooled fast reactors. Journal of Nuclear Materials 441 (2013) p.650–660;

[9] Jianu, A., Weisenburger, A., Heinzel, A., Fetzer, R., Delgiacco, M., An, W., Mueller, G., Voiculescu, I., Geantă, V. Alumina scale formation on FeCrAl-alloys exposed to 400-600

^{0}C in oxygen containing liquid lead (E11-P-1-12 (1961/1/1), EUROMAT (2011) Montpellier, France;
[10] US3992161; US3837847; US 4414023; US5228932; US5866065; US6773660; EP0429793.
[11] M. Palm, Concepts derived from phase diagram studies for the strengthening of Fe–Al-based alloys, Intermetallics 13 (2005) 1286–1295;
[12] B.A., Pint, Y., Zhang, Performance of Al-rich content resistant coating for Fe based alloys, Materials and Corrosion, 2010, 61, no.9999;
[13] Hyo On Nam, Jun Lim, Dong Yoon Han, Il Soon Hwang, Dissolved oxygen control and monitoring implementation in the liquid lead–bismuth eutectic loop: HELIOS, Journal of Nuclear Materials 376 (2008) 381–385;
[14] V., Geantă, I., Voiculescu, R., Ştefănoiu, A., Jianu, Influence on Chemical Composition of FeCrAl Alloys on the Microhardness, *Metalurgia International*, vol.XVI Special Issue no. 5 (2011) p. 153-156;
[15] Amano, T., Takezawa, Y., Shiino, A., Shishido, T. Surface morphology of scale on FeCrAl (Pd, Pt, Y) alloys. Journal of Alloys and Compounds 452 (2008) p.16–22;
[16] Checmanowski, G.J., Szczygie, J., Effect of a ZrO2 coating deposited by the solegel method on the resistance of FeCrAl alloy in high-temperature oxidation conditions, Materials Chemistry and Physics 139 (2013) p.944-952;
[17] Pint, B., Garratt-Reed, A., Hobbs. L. The efect of Y and Ti on FeCrAl oxidation at 1400 ^{O}C. Journal de Physique IV, 1993, 03 (C9), pp.C9-247-C9-255;
[18] Geantă, V., Voiculescu, I., Stanciu, E.M., Hafnium influence on the microstructure of FeCrAl alloys, International Conference on Innovative Research, Euroinvent, Materials Science and Engineering, Vol. 133 (2016) Accession Number: WOS: 000391140000016;
[19] Naumenko, D., Coze, J.L., Wessel, E., Fischer, W., Quadakkers, W.J. Effect of trace amounts of carbon and nitrogen on the high temperature oxidation resistance of high purity FeCrAl alloys. *Materials transactions*, Vol. 43, No. 2 (2002) p.168-172;
[20] D. Naumenko @ all., Effect of Combined Yttrium and Zirconium Additions on Protective Alumina Scale Formation on High Purity FeCrAl Alloys During Oxidation in the Temperature Range of 1200 to 1300°C, *Materials Science Forum*, Vols. 461-464,(2004) p. 489-496.

METTLER TOLEDO

PRINSIS

energetika ljubljana

METTLER TOLEDO

PRINSIS

energetika ljubljana

METTLER TOLEDO

PRINSIS

energetika ljubljana

METTLER TOLEDO

PRINSIS

energetika ljubljana

METTLER TOLEDO

PRINSIS

energetika ljubljana

METTLER TOLEDO

PRINSIS

energetika ljubljana

METTLER TOLEDO

PRINSIS

energetika ljubljana

METTLER TOLEDO

PRINSIS

energetika ljubljana

METTLER TOLEDO

PRINSIS

energetika ljubljana

METTLER TOLEDO

PRINSIS

energetika ljubljana